Understanding Structure and Function in Semiarid Ecosystems: Implications for Terrestrial Carbon Dynamics in Drylands

Submitted by Andrew Michael Cunliffe to the University of Exeter as a thesis for the degree of Doctor of Philosophy in Physical Geography, May 2016

Supervisors: Professor Richard E. Brazier and Dr Karen Anderson

Volume 1 of 2

Abstract

This study advances understanding of how the changes in ecosystem structure and function associated with woody shrub encroachment in semi-arid grasslands alter ecosystem carbon (C) dynamics. In terms of both magnitude and dynamism, dryland ecosystems represent a major component of the global C cycle. Woody shrub encroachment is a widespread phenomenon globally, which is known to substantially alter ecosystem structure and function, with resultant impacts on C dynamics.

A series of focal sites were studied at the Sevilleta National Wildlife Refuge in central New Mexico, USA. A space-for-time analogue was used to identify how landscape structure and function change at four stages over a grassland to shrubland transition. The research had three key threads:

1. Soil-associated carbon: Stocks of organic and inorganic C in the near-surface soil, and the redistribution of these C stocks by erosion during high-intensity rainfall events were quantified using hillslope-scale monitoring plots. Coarse (>2 mm) clasts were found to account for a substantial proportion of the organic and inorganic C in these calcareous soils, and the erosional effluxes of both inorganic and organic C increased substantially across the vegetation ecotone. Eroded sediment was found to be significantly enriched in organic C relative to the contributing soil with systematic changes in OC enrichment across the vegetation transition. The OC enrichment dynamics observed were inconsistent with existing understanding (derived largely from reductionist, laboratory-based experiments) that OC enrichment is largely insignificant in the erosional redistribution of C.

2. Plant biomass: Cutting-edge proximal remote sensing approaches, using a remotely piloted lightweight multirotor drone combined with structure-from-motion (SfM) photogrammetry were developed and used to quantify biomass carbon stocks at the focal field sites. In such spatially heterogeneous and temporally dynamic ecosystems existing measurement techniques (e.g. on-the-ground observations or satellite- or aircraft-based remote sensing) struggle to capture the complexity of fine-grained vegetation structure, which is crucial for accurately estimating biomass. The data products available from the novel SfM approach developed for this research quantified plants just 15 mm high, achieving a fidelity nearly two orders of magnitude finer than previous implementations of the

method. The approach developed here will revolutionise the study of biomass dynamics in short-sward ecogeomorphic systems.

3. Ecohydrological modelling: Understanding the effects of water-mediated degradation processes on ecosystem carbon dynamics over greater than observable spatio-temporal scales is complicated by significant scale-dependencies and thus requires detailed mechanistic understanding. A process-based, spatially-explicit ecohydrological modelling approach (MAHLERAN - Model for Assessing Hillslope to Landscape Erosion, Runoff and Nutrients) was therefore comprehensively evaluated against a large assemblage of rainfall runoff events. This evaluation highlighted both areas of strength in the current model structure, and also areas of weakness for further development.

The research has improved understanding of ecosystem degradation processes in semi-arid rangelands, and demonstrates that woody shrub encroachment may lead to a long-term *reduction* in ecosystem C storage, which is contrary to the widely promulgated view that woody shrub encroachment increases C storage in terrestrial ecosystems.

Acknowledgements

My thanks are offered to my family, especially my parents, for their support over many years, and to all those, to many to name here, who have helped me on my journey. They contributed to the foundation upon which this thesis stands.

Throughout my doctorate I have been guided by two truly fantastic supervisors, Richard Brazier and Karen Anderson, to whom I am deeply indebted for their enduring support and positive feedback. I am very glad of the opportunity to work with these two academics. My predecessor Alan Puttock was extremely generous in sharing his knowledge, data and desert friends, without which it would have been difficult to undertake the work presented herein. Thanks to all those in Exeter and the desert who offered their valuable assistance and friendship.

This thesis and resultant publications have been supported by fruitful collaboration with John Wainwright and Laura Turnbull. My gratitude is also offered to several colleagues who generously gave offered their advice, particularly Jeroen Meersmans and Sankar Mariappan for stimulating discussions on soil science, Ian Vernon for advice on statistical approaches and Leon DeBell for facilitating my introduction to the world of drones. Joana Zaragoza-Castells and Natascha Steinberg provided essential assistance in the laboratory, Alain Plante and Felix Heitkamp kindly facilitated the inter-comparison of carbon determination methodologies, and Diane Fraser, Andrew Cowley and Rolf Aalto provided valuable computing support.

This research was supported by a NERC Doctoral Training Grant (NE/K500902/1), with additional funds from two research fellowships awarded by the NSF Long Term Ecological Research Program at the Sevilleta National Wildlife Refuge (DEB-1232294). Presentation of parts of this thesis at various conferences was supported by attendance grants awarded by the British Hydrological Society, the British Society for Geomorphology and the British Sedimentological Research Group.

List of Contents

List of Tables

List of Figures

Abbreviations

AGB	Aboveground biomass
amsl	Above mean sea level
AOI	Area of interest
ASM	Antecedent soil moisture
BEM	Bioclimatic envelope modelling
BGB	Belowground biomass
CDF	Cumulative distribution function
CHM	Canopy Height Model
CoV	Coefficient of variance
d	Monitored flow depth
DGPS	Differential global positioning system
DGVM	Dynamic Global Vegetation Model
EA	Elemental analyser
$\sum_{Obs}$	The observed size-specific OC event yield, determined by multiplying the observed OC concentration and mass of each particle size fraction eroded during each event
$\sum_{All}$	The expected OC event yield, calculated using the average OC concentration of the contributing soil multiplied by the mass of eroded sediment
$\sum_{PSD}$	The expected OC event yield, calculated by summing the average OC concentration of the contributing soil for each particle size fraction by plot multiplied by the eroded mass of that fraction
FC	Flash Combustion
GIS	Geographic information system
GNSS	Global navigation satellite system

GoF	Goodness of Fit
CoG	Centre of gravity
GIS	Geographic information system
GPS	Global positioning system
IC	Inorganic carbon
LIDAR	Light detection and ranging
LOI	Loss-on-ignition
LTER	Long term ecological research
MT-EGA	Multi-temperature evolved gas analysis
n	Number of samples/data points
OC	Organic carbon
OM	Organic matter
POM	Particulate organic matter
PSD	Particle size distribution
Q	Total event discharge
Q_H	Total runoff calculated from the observed hydrograph
Q_T	Total runoff calculated from the storage tank
q	Discharge per minute
RMSE	Root mean square error
RPAS	Remotely piloted aircraft system
SfM	Structure from Motion
SIC	Soil inorganic carbon
SNWR	Sevilleta National Wildlife Refuge
SOC	Soil organic carbon

SOM	Soil organic matter
SPT	Sodium polytungstate
TC	Total carbon

Statement of Contribution

I, Andrew Cunliffe, declare that the work presented in this thesis entitled *Understanding Structure and Function in Semiarid Ecosystems: Implications for Terrestrial Carbon Dynamics in Drylands*, is my own. I confirm that the work was undertaken while in candidature for a research degree at the University of Exeter. Where I have consulted the work of others the source(s) are always given. This thesis and the publications arising have been supported by contributions from various collaborators, where applicable these contributions have been clearly identified in the text. With the exception of such acknowledged contributions, this thesis is entirely my own work.

The list of published articles below summarises both the published parts of this thesis, and also that which has been co-authored as part of the wider development of the techniques. The papers included in this list have multiple co-authors, this is because this research has been supported by collaborators, particularly in providing samples and commenting on manuscripts after the initial draft was produced by me. Therefore a brief statement is given describing my contribution to each of these articles (published articles are included in Appendix 7, Appendix 8 and Appendix 9).

Published articles

Cunliffe, Andrew M., Alan K. Puttock, Laura Turnbull, John Wainwright, and Richard E. Brazier. (2016) 'Dryland, Calcareous Soils Store (and Lose) Significant Quantities of near-Surface Organic Carbon.' *Journal of Geophysical Research: Earth Surface*,121(4):684-702. doi:10.1002/2015JF003628.

- This article was based on Chapter 6. Initial design and construction of the runoff plots was by JW, LT and REB. Monitoring of runoff events was undertaken by LT and AKP. The research questions addressed in this article were developed by AMC, with input from REB and AKP. AMC collected characterisation samples, undertook all chemical and numerical analysis and wrote the manuscript with input from all co-authors.

Cunliffe, Andrew M., Richard E. Brazier, and Karen Anderson. (2016) 'Ultra-Fine Grain Landscape-Scale Quantification of Dryland Vegetation Structure with Drone-Acquired Structure-from-Motion Photogrammetry.' *Remote Sensing of the Environment*, 183:129-143. doi:10.1016/j.rse.2016.05.019

- This article was based on Chapter 8. The study was conceptualised by AMC, KA and REB. Method development and data acquisition and analysis was undertaken by AMC. The manuscript was written by AMC, with input from REB and KA.

Puttock, Alan K., **Andrew M. Cunliffe,** Karen Anderson, and Richard E. Brazier. (2015) 'Monitoring the Impact of Eurasian Beaver Reintroduction on Ecosystem Structure Using Aerial Photography Collected from a Multi-Rotor Drone.' *Journal of Unmanned Vehicle Systems,* 3(3):123–30. doi:10.1139/juvs-2015-0005.

- This article was based on the survey methodology developed in Chapter 8. AMC led the acquisition and analysis of the data, and AKP and AMC contributed equally to the study conceptualisation and writing of the manuscript, with input from REB and KA. This article exemplifies peer-acceptance of the methodological quality of the RPAS proximal remote sensing techniques presented in Chapter 8, and also the diversity of research applications to which these techniques are applicable.

Further work from this thesis is in preparation for publication

Cunliffe, A. M., Duffy, J., DeBell, L., and Anderson, K. (2016) *ESI DroneLab Operations Manual: Unmanned Aerial Systems for Environmental Research*.

- This 53 page technical manual describes the use of remotely piloted aircraft systems by the Environment and Sustainability Institute's DroneLab for environmental remote sensing. This document has been reviewed and approved by EuroUSC, an approved entity on behalf of the UK Civil Aviation Authority. This technical manual is in review for publication in *IEEE Robotics and Automation Society Letters*.

Cunliffe, Andrew M., Richard E. Brazier, Alan K. Puttock, Laura Turnbull, and John Wainwright. 'Shrub Encroachment Accelerates the Erosion of Inorganic Carbon from Semi-Arid Rangelands.' In Prep.

- This manuscript is based on Sections 3.2 and 7. The study was conceptualised by AMC. Erosional events were monitored by LT and AKP and all chemical and data analysis was undertaken by AMC. This manuscript was written by AMC, with comments from REB and AKP, and is in preparation for submission to *Geology*.

Cunliffe, A.M., Puttock, A.K., Turnbull, L., Wainwright, J., Brazier, R.E., Modelling the water erosion-induced redistribution of carbon across a semi-arid grass shrub ecotone. In Prep.

- This manuscript is based on Sections 3.4 and 9. Erosional events were monitored by LT and AKP. All chemical analysis, numerical modelling, and model analyses was undertaken by AMC. This manuscript will be written by AMC, with input from REB, JW, LT and AKP, and is planned for submission to *Earth Surface Processes and Landforms*.

Additional publications

During the course of my PhD research, I have also contributed to other research projects from my wider research group in recognition of which I am be included as a co-author. These papers do not form part of this thesis, but they are related to my understanding of the proximal remote sensing of ecosystem structure and function (Puttock et al., 2017) and erosional carbon dynamics (Mariappan et al., In Prep), and are therefore listed below.

Puttock, Alan K., Hugh Graham, **Andrew M. Cunliffe**, Mark Elliott, and Richard E. Brazier. (2017) 'Eurasian beaver activity increases water storage, attenuates flow and mitigates diffuse pollution from intensively-managed grasslands.' *Science of the Total Environment*, 576:430-443. doi:10.1016/j.scitotenv.2016.10.122.

- This study was conceptualised by REB, AKP and ME. AMC contributed to the instillation of monitoring equipment, produced RPAS-acquired georeferenced orthomosaic image products to monitor changes in biotic (vegetation) and abiotic (inundated extents, canal network extension, etc.) structure, and contributed to data interpretation and the production and revision of the manuscript.

Mariappan, Sankar, **Andrew M. Cunliffe**, Iain Hartley, Jennifer A. J. Dungait, and Timothy A. Quine. 'Erosion-induced redistribution of soil carbon and nutrients in agricultural landscapes of the Himalayan region.' *Geomorphology*, In Prep.

- This study was conceptualised by SM, IH, JAJD and TAQ. AMC contributed to statistical analysis and interpretation of results, and will contribute to the manuscript.

Contributions to scientific meetings

Parts of this thesis have also been presented at various national and international conferences, as listed below:

- **Cunliffe, Andrew M.**, Karen Anderson, and Richard E. Brazier. 'Soil Organic Carbon in Semiarid Rangelands.' Lancaster, (2013a)
- **Cunliffe, Andrew M.,** Alan K. Puttock, Karen Anderson, and Richard E. Brazier. 'The Distribution and Fluvial Redistribution of Soil Organic Carbon in Semiarid Rangelands.' In *Geophysical Research Abstracts*, 16 (EGU2014–2353), Vienna, Austria: EGU, (2014b).
- **Cunliffe, Andrew M.,** Richard E. Brazier, and Ian Vernon. 'Are We Overestimating Organic Carbon Concentrations in Soils Containing Inorganic Carbon?' In *Geophysical Research Abstracts*, 16 (EGU2014–4230). Vienna, Austria: EGU, (2014a).
- **Cunliffe, Andrew M.,** Richard E. Brazier, and Karen Anderson. 'Drones in the desert: characterising biotic structure in semiarid rangelands via drone-acquired SfM.' John Moores University, Liverpool, UK, (2015).
- **Cunliffe, Andrew M.,** Alan K. Puttock, Laura Turnbull, John Wainwright, and Richard E. Brazier. 'Erosion-Induced carbon fluxes from semiarid rangelands: implications of vegetation cover and enrichment dynamics for carbon inputs to aquatic systems.' In *Geophysical Research Abstracts*, Vol. 18 (2016–8621). Vienna, Austria: EGU, (2016c).
- **Cunliffe, Andrew M.,** Richard Brazier, and Karen Anderson. 'Drone-acquired structure-from-motion photogrammetry for high-precision measurements of biomass in semi-arid rangelands.' In *Geophysical Research Abstracts*, Vol. 18 (EGU2016–7888). Vienna, Austria: EGU, (2016a).
- Brazier, Richard E., Alan K. Puttock, Hugh Graham, Karen Anderson, **Andrew M. Cunliffe**, and Mark Elliot. 'Quantifying the multiple, environmental benefits of reintroducing the Eurasian beaver.' In *Geophysical Research Abstracts*, Vol. 18 (EGU2016–7243). Vienna, Austria: EGU, (2016).

1. Introduction and Research Context

1.1. Introduction

The global biogeochemical cycling of carbon (C) is an integral part of the Earth system, and is being significantly perturbed by anthropogenic activities, with major implications for the future state of the Earth climate system (IPCC, 2013). Knowledge of the physical science of the C cycle, including the efficacy of natural sinks, is essential to understand the effects of human perturbations, and to inform appropriate mitigation and adaptation strategies. Terrestrial ecosystems are the least understood component of the global C cycle (IPCC, 2013). Consequently, this thesis aims to advance process-based understanding of terrestrial C dynamics in spatially extensive dryland ecosystems using a combination of novel spatial and environmental modelling approaches.

Dryland ecosystems cover ca. 40% of the terrestrial surface and provide ecosystem services which directly support ~2.4 billion people. Although storage of highly dynamic forms of C per-unit-area is typically small in dryland ecosystems relative to other biomes (Thomey et al., 2014), their spatial extent means these environments play a significant role in the global C cycle (Ahlström et al., 2015; Poulter et al., 2014). Critically, dryland ecosystems are highly susceptible to change, due to variations in precipitation inputs, wildfire or dominant land cover, for example. Such changes can substantially alter the processing and storage of C in these ecosystems, with global-scale implications (Schlesinger et al., 1990).

One widespread example of dryland degradation in the southwestern USA is the encroachment of woody plants into semi-arid grasslands. Such encroachment significantly alters ecosystem structure and function, including the storage and processing of C, and is widely considered to result in an enhanced terrestrial C sink (Houghton et al., 1999; Houghton, 2003a; Liao et al., 2006a; Pacala et al., 2007; Barger et al., 2011; Petrie et al., 2015). The effects of shrub encroachment on ecosystem C dynamics are however known to vary across environmental gradients (e.g. aridity) (Conant et al., 1998; Klopatek et al., 1998; Jackson et al., 2002; Goodale and Davidson, 2002; Barger et al., 2011), and are highly uncertain (Brazier et al., 2013).

Improved mechanistic understanding of how dynamic dryland ecosystems function is valuable for improving assessments of landscape-scale C dynamics, including predictions of ecosystems responses to environmental changes, and may also help inform landscape management to optimise the provision of ecosystem services such as C sequestration. A key objective is to advance transferable, process-based understanding of C dynamics in semi-arid ecosystems. This is achieved through comparison of the differences in terrestrial C dynamics between vegetation communities across a grass-shrub ecotone, focussing on the interactions between ecosystem structure and function.

To this end, this study expands on recent research into C dynamics across a grassland (black grama, *Bouteloua eriopoda*) to shrubland (creosotebush; *Larrea tridentate*) vegetation transition in the southwestern USA (Brazier et al., 2013; Puttock et al., 2013, 2014). Four stages across a grass-shrub ecotone were examined to investigate:

(i) How soil organic and inorganic carbon was distributed relative to various components of ecosystem structure and redistributed by erosion during high-intensity rainstorm events
(ii) The extent to which drone-based structure-from-motion photogrammetry could be used to characterise ecosystem structure, including improved measurements of biomass C storage.
(iii) The extent to which deterministic ecohydrological modelling approaches can represent the redistribution of water and soil resoruces in degrading dryland environments.

A very wide range of methodologies have been employed, including soil characterisation, erosion flux monitoring, development of novel proximal remote sensing techniques for efficiently quantifying biomass C storage at unprecedented spatial resolutions and extents, and numerical modelling experiments to simulate the erosion-induced redistribution of C. The modelling component is valuable because scale-dependencies inherent in water-mediated erosional processes preclude simple extrapolation from plot-scale observations to landscape-scale estimates.

1.2. Terrestrial C Dynamics in the Global C Cycle

1.2.1. Overview

The global biogeochemical cycling of C has received significant scientific attention, in the context of major ongoing anthropogenic perturbations of this cycle and likely implications of these perturbations for the global climate system (IPCC, 2013). Better knowledge of terrestrial C cycling is valuable to improve the precision of global C budgets (Houghton, 2003a, 2003b, 2007; Le Quéré, 2010), improve prediction of the future global environment (Cao and Woodward, 1998; Sitch et al., 2008; Poulter et al., 2014; Ahlström et al., 2015; Atkin et al., 2015; Murray-Tortarolo et al., 2016) and inform efforts to mitigate the rate of greenhouse gas increase in the atmosphere (Lal, 2003, 2008; Metz et al., 2007; Follett and Reed, 2010) as well as to support societal adaptations to predicted environmental changes (IPCC, 2014).

Scientific understanding of the global C cycle has advanced dramatically in recent decades (IPCC, 1990, 1995, 2001, 2007, 2013), and the major stores and fluxes of this cycle are illustrated in Figure 1-1. The terrestrial C sink is believed to be increasing at a rate of between 0.8 to 2.0 Pg C yr^{-1} (Houghton, 2007; Denman et al., 2007), with top-down (atmospheric) indicators suggesting that this sink may be primarily located in northern, mid-latitude regions (Melillo et al., 1996; Fan et al., 1998; Houghton, 2003b). Soil is the largest component of the terrestrial C store, containing an estimated 2 350±1 300 Pg C (Kirschbaum, 2000; Lal, 2001a; Houghton, 2007). Soil C exists in both organic and inorganic physiochemical forms, accounting for an estimated ~2 450 Pg C and 750-1700 Pg C, respectively (Lal, 2001a; Thomey et al., 2014), although these estimates are highly uncertain. The soil C pool is larger than the atmospheric C pool, by a factor of 1.3 to 3.7 (Figure 1-1), so changes in the net flux of C between atmospheric and soil pools leading to relatively small changes in the magnitude of the soil C pool can equate to large changes in the magnitude of the atmospheric C pool (Lal, 2003). Globally the terrestrial-to-ocean C flux is estimated to be in the region of 0.4 - 0.9 Pg C yr^{-1}, ~90% of which is conveyed by rivers and the rest via aeolian transport (Ludwig et al., 1998; Holmén, 2000; Mackenzie et al., 2004; Ciais et al., 2013).

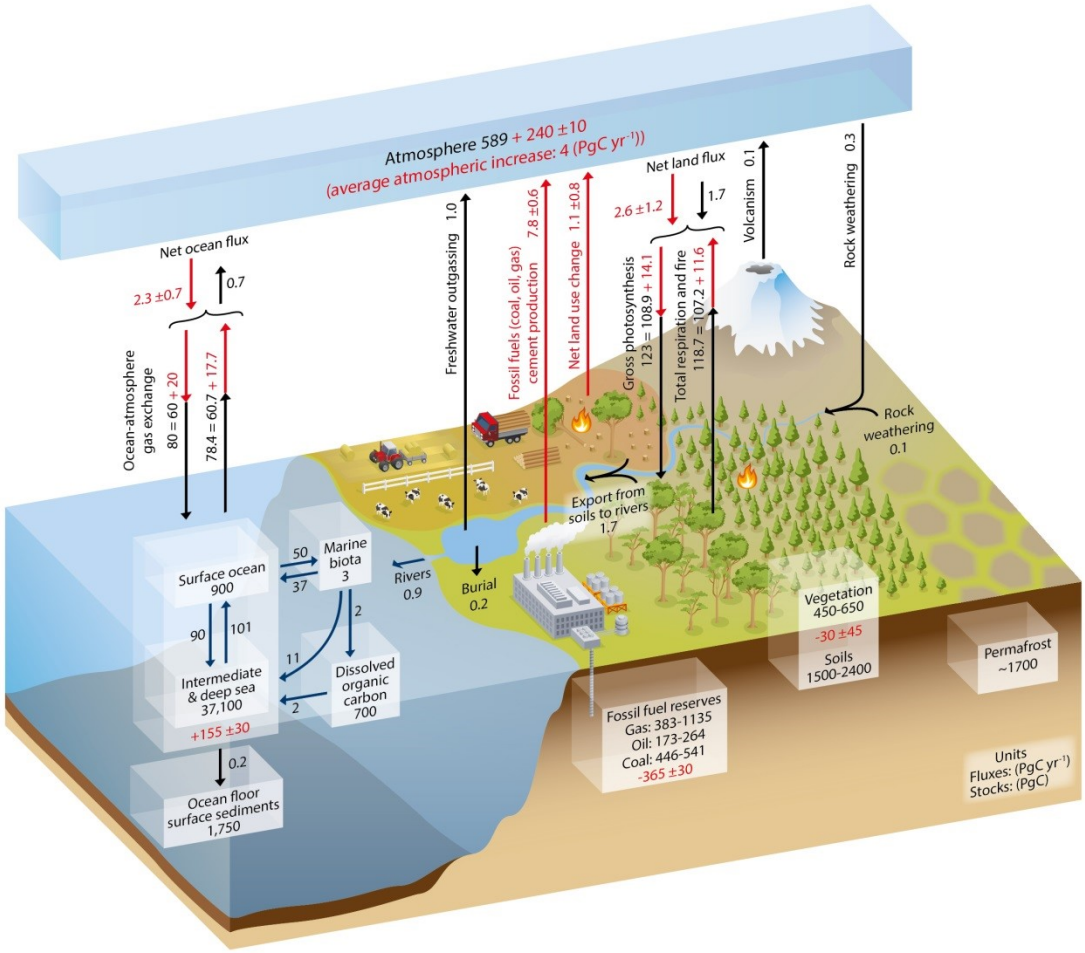

Figure 1-1. Simplified schematic of the global C cycle. Numbers represent C stocks in Pg C and annual C exchange fluxes in Pg C yr^{-1}. Black numbers and arrows indicate C stocks and exchange fluxes estimate for the time prior to the Industrial Era (ca. 1750). Red fluxes indicate annual anthropogenic fluxes averaged over the 2000-2009 period, while red stocks denote cumulative changes in reservoirs attributed to anthropogenic activity over the period 1750-2011. Positive changes indicate a gain in C stock, and uncertainties are reported as 90% confidence intervals. (From Ciais et al., 2013; IPCC, 2013).

Despite major advances in understanding, significant uncertainties remain with several components of the C cycle, particularly with regards to terrestrial components, where knowledge is hindered by heterogeneity in stocks and fluxes (cf. Schindler, 1999; Adams and Piovesan, 2002; Van Oost et al., 2007; Hill et al., 2013; IPCC, 2013; Brazier et al., 2013; Jandl et al., 2014). Terrestrial C dynamics can be significantly altered by changes in land-use, land-cover and climate (Melillo et al., 1996; McGuire et al., 2001; Lal, 2003; Schwendenmann and Pendall, 2006; Denman et al., 2007). Important climate-vegetation-C cycle

feedbacks are poorly represented in the current generation of global Earth surface models (Cox et al., 2000; Houghton, 2003b; Denman et al., 2007), and large uncertainties remain in scientific understanding of controls on soil C dynamics, such as the net effect of soil erosion on soil C pools, for example (Lal, 2003; Cole et al., 2007; Van Oost et al., 2007, 2008; Lal and Pimentel, 2008; Doetterl et al., 2012). These uncertainties limit confidence in model predictions of future environmental conditions, leading to continuing calls for research to constrain and reduce uncertainties in terrestrial C cycling (Holmén, 2000; Denman et al., 2007; Ciais et al., 2013).

1.2.2. Soil erosion: a source or a sink of atmospheric C?

Understanding of C transport across the landscape is very limited, largely due to significant spatial and temporal scale-dependencies (Van Oost et al., 2005; Nadeu et al., 2011, 2012). Understanding the ultimate fate of eroded soil C is one of the most pertinent questions in soil science, as there is considerable controversy even as to whether soil erosion represents a source or a sink of atmospheric C (Lal, 2004a; Lal et al., 2004a, 2004b; Van Oost et al., 2004; Renwick et al., 2004; Ciais et al., 2013; IPCC, 2013). Organic C (OC) is laterally redistributed across the landscape by a variety of processes, including: as dissolved forms of C (Grand-Clement et al., 2014) and erosion of particle-associated C via interrill (Brazier et al., 2013), rill/gully, bank and bed erosion (Nadeu et al., 2010, 2011, 2012), tillage (Van Oost et al., 2005, 2007) and aeolian (Zobeck and Fryrear, 1986; Zobeck et al., 1989; Leys and McTainsh, 1994; Sterk et al., 1996; Li et al., 2007) processes.

Proponents of the sink argument contend that the burial and re-aggregation of OC in often hypoxic depositional sites within lentic environments (reservoirs and lakes) (Ritchie, 1989), tilled arable land (Van Oost et al., 2004, 2005) and more widely across the landscape (Stallard, 1998; Smith et al., 2001) protects eroded OC from microbial decomposition and subsequent release to the atmosphere (Schimel et al., 1985; Gregorich et al., 1998; Stallard, 1998; Harden et al., 1999; Berhe et al., 2007; Quinton et al., 2010; Doetterl et al., 2012; X. Wang et al., 2014c, 2014a). An important component of the sink mechanism is the dynamic replacement of soil OC at eroding sites, via inputs from photosynthesis (Harden et al., 1999; Baisden et al., 2002; Van Oost et al., 2005; Quine and Van Oost,

2007; Li et al., 2007). Globally, soil erosion-driven sequestration has been estimated at ca. 1 Pg C yr^{-1} from the atmosphere (Smith et al., 2001), and has been proposed as the long-sought 'missing sink' in the global C cycle (Ritchie, 1989; Stallard, 1998; Smith et al., 2001; Liu et al., 2003).

Conversely, proponents of the source argument suggest that the breakdown of soil macroaggregates during mobilisation and transport exposes organic matter to microbial activity, increasing mineralisation rates (Gregorich et al., 1989; Sollins et al., 1996; Lal, 2003, 2005; Lal et al., 2004a; Polyakov and Lal, 2004a; Mora et al., 2007; Schiettecatte et al., 2008a; Jin et al., 2009). Furthermore, they suggest that in many ecosystems, erosion-driven removal of OC reduces soil fertility and thus net primary productivity, thereby restricting dynamic replacement of eroded OC (Schlesinger, 1995; Lal, 1999, 2001a, 2001b, 2003, 2004a, 2004b, Lal et al., 1999, 2004a, 2004b, 2007; McCarty and Ritchie, 2002; Lal and Pimentel, 2008; Quinton et al., 2010). Globally, soil erosion has been estimated to release ca. 1 Pg C yr^{-1} from the soil to the atmosphere (Lal, 2003).

An important part of the source versus sink debate is uncertainty regarding in-transit mineralisation rates, with estimates ranging from 0% to 100% mineralization of eroded C (Lal, 2003). For example, Smith *et al*. (2001) assume minimal mineralisation, Van Oost *et al*. (2005) assume mineralisation to be 10%, Lal *et al.* (Lal et al., 1998; Lal, 2003; Lal et al., 2004a) assume mineralisation to be 20%, Óskarsson *et al.* (2004) assume mineralisation to be 50% and Schlesinger (1995) suggested that nearly all OC is mineralised during transport. Simply assuming fixed proportions of mineralisation across different spatio-temporal scales is however highly problematic, as OC mineralisation depends on the physicochemical properties of the organic matter and environmental conditions during transport, such as temperature for example (Lal, 2003). Efforts to elucidate the OC mineralisation dynamics associated with erosion in natural systems are confounded by significant uncertainty around OC inputs to aquatic systems (Kuhn, 2007; Cunliffe et al., 2016d), in part due to poorly understood enrichment processes which are discussed further in section 3.1.

In summary, there is a very high degree of uncertainty regarding the long-term effect of soil erosion on global C dynamics (Follett et al., 2001; Lal, 2003; Ciais et al., 2013; IPCC, 2013). Whether soil erosion is a net source or a sink of atmospheric C depends on the balance between (i) increased mineralization of eroded SOC during and after transport, and (ii) the combination of reduced mineralisation in depositional sites and dynamic replacement at eroding sites (Van Oost et al., 2005; Berhe et al., 2007). At a global scale, Van Oost *et al.* (2007, 2008) consider soil erosion more likely than not to represent a source of atmospheric C, although the flux magnitude could potentially be insignificant in terms of the global C budget. Further field and modelling studies to better understand OC dynamics at eroding and depositional sites, and transport dynamics across different spatio-temporal scales (Lal, 2003; Van Oost et al., 2005).

Significantly, research into erosion-induced C fluxes has predominantly focused on intensively-managed agroecosystems in temperate environmental contexts (e.g. Lal, 2005; Quinton et al., 2006, 2010; Dawson and Smith, 2007; Beniston et al., 2015; Lacoste et al., 2015). As several workers have noted, process understanding from this work is not always directly transferable to less-intensively managed ecosystems in other environmental contexts (Schaefer et al., 1985; Parsons et al., 1990; Bryan, 2000; Mayeux, 2001; Liao et al., 2006b; Martinez et al., 2010). Therefore, it is appropriate to examine the transferability of process understanding by extending detailed study to unmanaged natural ecosystems.

1.3. Dryland Ecosystems

1.3.1. Overview

Drylands are globally important landscapes; ranging from hyper-arid to dry sub-humid environments and covering ca. 40% of the terrestrial surface (Safriel et al., 2005; Peters et al., 2006b). Dryland ecosystems provide services which directly support approximately 2.4 billion people; some of the key ecosystem services provided by drylands are listed in Table 1.1 (Adeel et al., 2005; Reynolds et al., 2007; Stringer et al., 2012). This study focuses predominantly on the supporting and regulating ecosystem services of C cycling and storage in dryland ecosystems. In drylands, primary productivity is generally limited by the availability of soil moisture, and secondly by bioavailable nitrogen (Fisher et al., 1988; Hooper and Johnson, 1999; Huenneke and Schlesinger, 2006).

In drylands, primary productivity is low relative to many other ecosystems, the lack of moisture also restricts microbial activity, slowing decomposition of organic matter. Per-unit-area, dryland ecosystems contain small quantities of OC compared with many other terrestrial ecosystems. For example, dryland soils typically comprise of less than 0.5% OC (Glenn et al., 1993) and dryland vegetation commonly stores $<50 \times 10^6$ g C ha^{-1}, although there are exceptions to this as shown in Figure 1-2. Nonetheless, their spatial extent means that drylands store globally significant amounts of C. For example, Thomey *et al*. (2014) estimates drylands store 19.9×10^{16} g C in vegetation and soil globally. Hyper-arid to dry sub-humid ecosystems contain an estimated >25% of the global terrestrial C sink (combined soil and biomass pools) (Adeel et al., 2005), with hyper-arid to semi-arid ecosystems estimated to contain >8% of the global terrestrial C sink (1.7% of the global biomass C and 9.5% of the global soil C) (Finch, 2012; after Jobbágy and Jackson, 2000) (Figure 1-3).

Table 1.1. Key dryland ecosystem services (adapted after Adeel et al., 2005)

Provisioning Services *Goods produced or provided by ecosystems*	• Provisions derived from biological productivity: food, fibre, forage, fuelwood, and biochemical • Freshwater
Regulating Services *Benefits obtained from regulation of ecosystem processes*	• Water purification and regulation • Climate regulation (local through vegetation cover effects on albedo and global through C storage) • Pollination and seed dispersal
Cultural Services *Nonmaterial benefits obtained from ecosystems*	• Recreation and tourism • Cultural identity and diversity • Cultural landscapes and heritage values • Indigenous knowledge systems • Spiritual, aesthetic, and inspirational services
Supporting Services *Services that maintain the conditions for life*	• Soil development (conservation, formation) • Primary production • Nutrient cycling

Dryland ecosystems are often described as marginal, as the limited water availability constrains the biotic processes that can occur in these landscapes. Drylands are also characteristically susceptible to change including degradation. Land degradation may be defined as a reduction in the biological or economic productivity of an ecosystem (Adeel et al., 2005), and in arid, semi-arid and dry sub-humid areas land degradation is often described as a process of desertification (UNCCD, 2000). Globally, 70% of dryland ecosystems, covering ca. 30% of the terrestrial surface are estimated to be moderately or severely degraded (Glenn et al., 1993; Maestre et al., 2006). Degradation of dryland ecosystems can influence the global environment via modification of regional albedo (Adeel et al., 2005) and biogeochemical cycles (Schlesinger et al., 1990), and may be one of the greatest environmental challenges confronting global society (Adeel et al., 2005; Reynolds et al., 2007). Degradation of dryland ecosystems can reduce their capacity to store C, resulting in estimated terrestrial-to-atmosphere C fluxes of 0.3 Pg C yr^{-1}, representing ~4% of the total global emissions from all sources combined (Adeel et al., 2005; after Dregne et al., 1991), although again this estimate is highly uncertain.

(a) Carbon Storage in Vegetation in Drylands

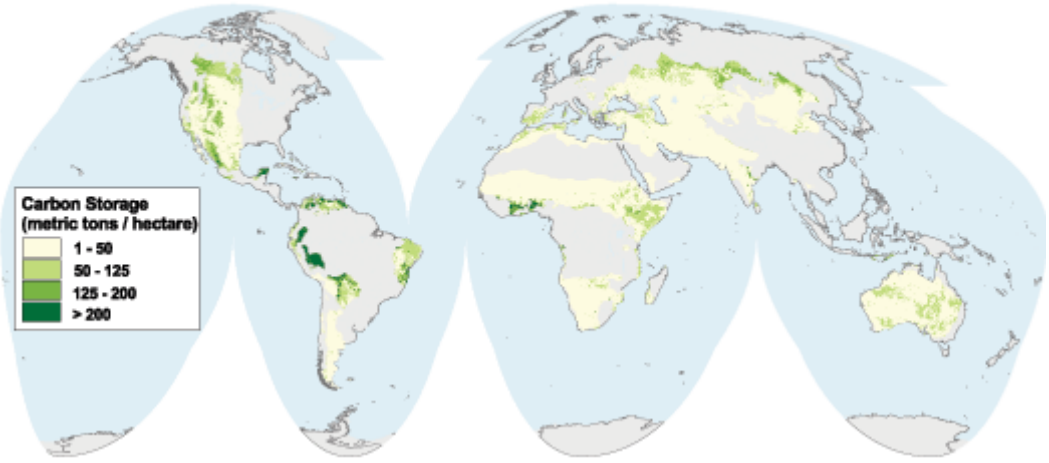

(b) Carbon Storage in Soils in Drylands

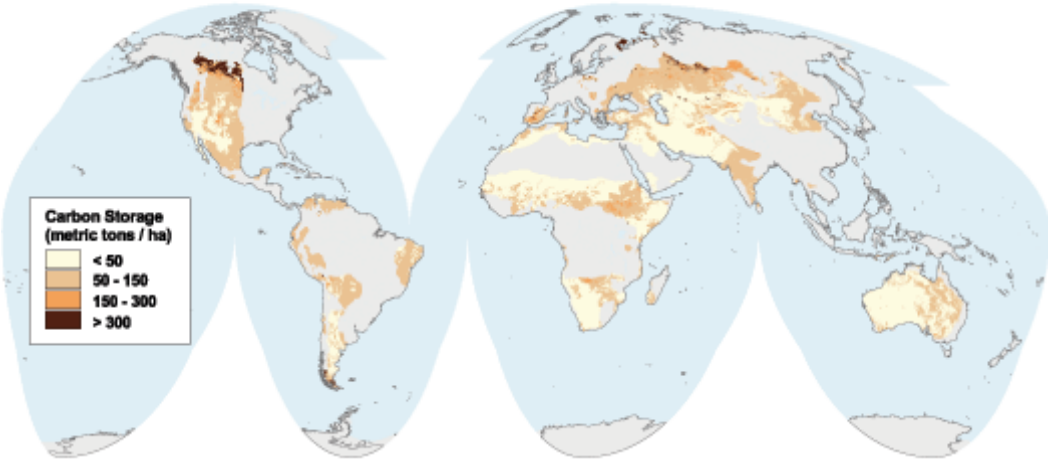

(c) Global Carbon Storage in Vegetation and Soils in Drylands

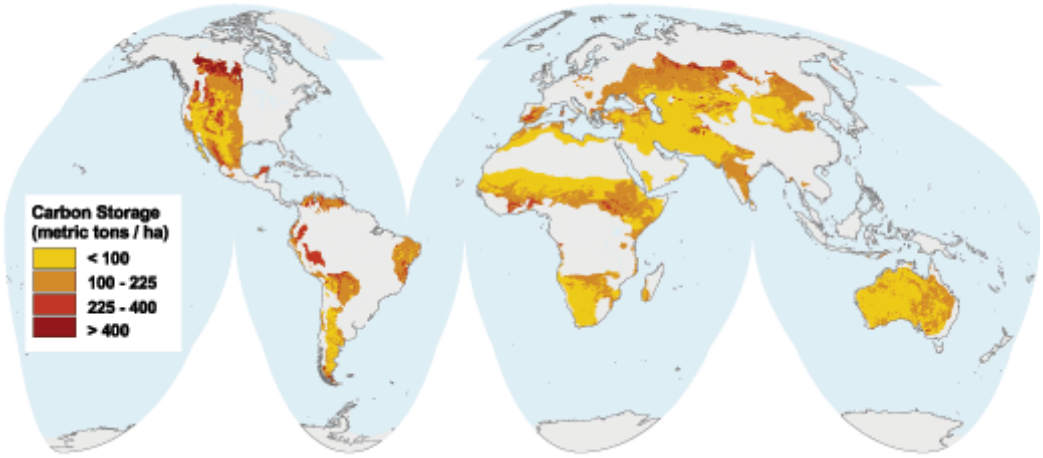

Figure 1-2. (a) estimated potential C storage in dryland biomass (above and below ground), (b) soil (principally the uppermost meter of soil, and (c) combined biomass and soils. Figure from World Resource Institute (www.wri.org/publication/content/8242).

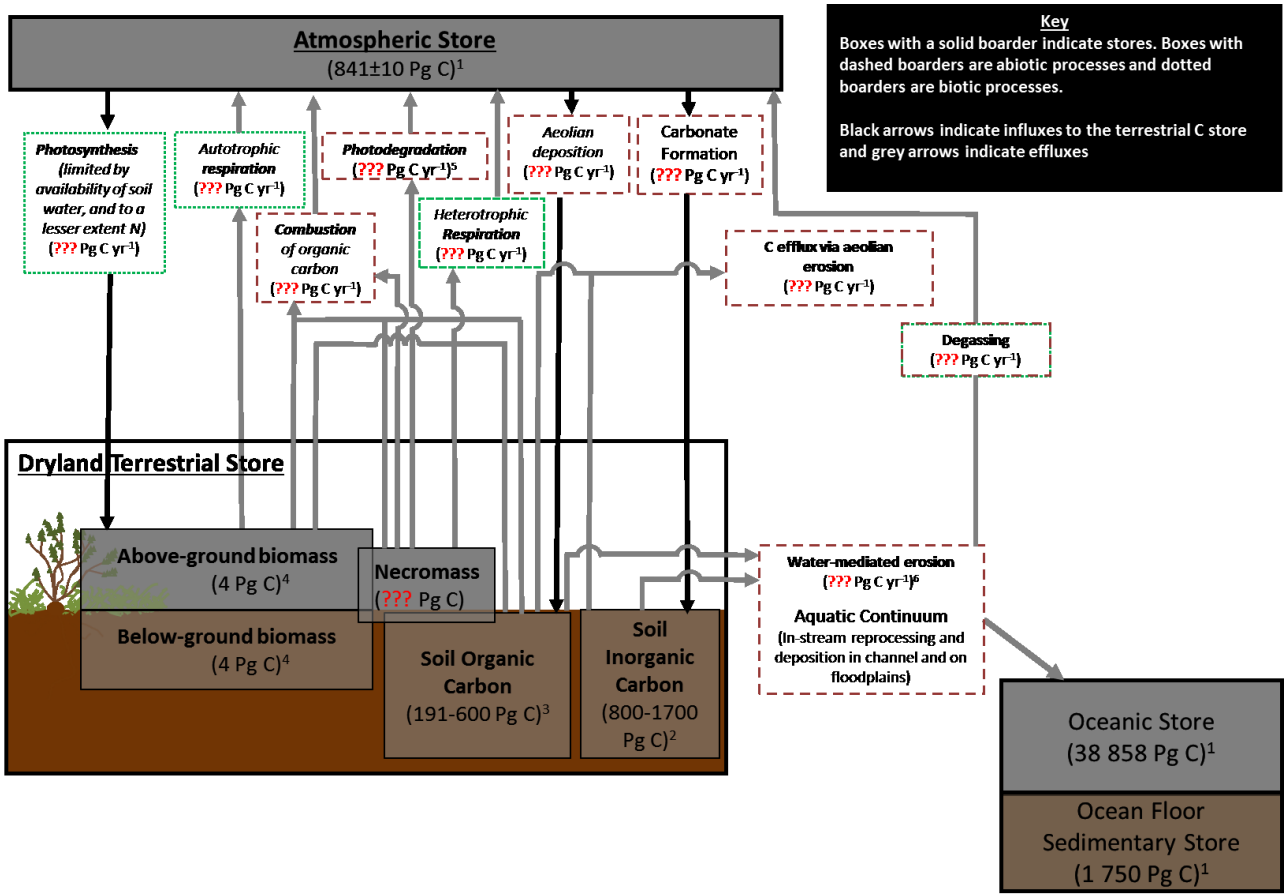

Figure 1-3. Outline of key carbon stocks and fluxes in dryland ecosystems. Note that all stock and flux, where available, are extreemly uncertain. [1](Ciais et al., 2013), [2](Thomey et al., 2014), [3](Janzen, 2004 (191 Pg C); Adeel et al., 2005 (600 PgC, as 25% of 2450 Pg C)), [4](based on estimated 8 Pg C biomass C stock and a root shoot ratio of 1 : 1, Janzen, 2004), [5](Rutledge et al., 2010; Petrie et al., 2015), [6](Meixner et al., 2012). Relevent references are suggested for flux pathways where information on fluxes is insufficient to support global extrapoliation.

1.3.2. Extent of woody shrub encroachment in former grasslands

Perennial grasslands and rangeland ecosystems comprise of ca. 60% of drylands, and are disproportionally important in the provision of ecosystem services from drylands globally. Importantly, vegetation communities in these ecosystems are susceptible to composition change, often with woody plants replacing previously dominant grasses (Van Auken, 2000, 2009; Briggs et al., 2005). This process is generally one of encroachment rather than succession or invasion, as the woody species have often been present in the community for long periods prior to the shift in community dominance (Archer et al., 1995; Van Auken, 2009).

Woody plant encroachment into former grasslands is a global phenomenon, observed on every continent apart from Antarctica (Archer et al., 1995; Archer, 2010; Myers-Smith et al., 2011; Eldridge et al., 2011, 2012; Elmendorf et al., 2012; Bestelmeyer et al., 2015; Masubelele et al., 2015), although the extent of shrub encroachment into former grasslands is not well quantified globally (Goodale and Davidson, 2002). Woody shrub encroachment has been extensively studied in the southwestern United States, where over the last 150 years creosotebush (*Larrea tridentate*) and mesquite (*Prosopis glandulosa*) shrubs have become the dominant species across 19 and 38 million ha, respectively, of formerly semi-arid grasslands (McCraw, 1985; Kieft et al., 1998; Van Auken, 2000; Biedenbender et al., 2004; Gibbens et al., 2005). By comparison, the land area of the UK is just 24.3 million ha.

Significant efforts have been made to understand woody shrub encroachment processes. Early work in this field was motivated principally by the desire to inform landscape management in order to prevent and, where possible, reverse grass-shrub transitions, in order to retain and regain the grazing potential that supported the economic productivity of affected ecosystems (e.g. Brown and Archer, 1999; Briggs et al., 2005; Rango et al., 2005; Peters et al., 2006b, 2012; Sankey et al., 2012). More recently, research has expanded to understand the effects of this change in community dominance on C dynamics, in order to understand the implications for the global climate system (e.g. Jackson et al., 2002; Barger et al., 2011; Friggens et al., 2012; Petrie et al., 2015) and inform land management to optimise C sequestration (Glenn et al., 1993; Bird et al.,

2001; Follett et al., 2001; Lal, 2001c, 2004c, Lal et al., 2004a, 2007; Follett and Reed, 2010; Brown et al., 2010; Finch, 2012; Meyer, 2012).

1.3.3. Controls on woody shrub encroachment

Extensive research has been undertaken to elucidate the drivers of woody shrub encroachment. This previous work has identified a variety of mechanisms which potentially alter the relative balance of competitive advantages between grass species and shrub species, and thus could contribute to a change in assembly composition; these mechanisms are briefly outlined below:

- Plant water use efficiency is important in water-limited ecosystems, and increased atmospheric CO_2 concentrations can improve water use efficiency by reducing transpiration losses via stomatal openings, thus increasing the photosynthesis : transpiration ratio. Under pre-industrial CO_2 concentrations, plants utilizing the C_4 photosynthetic pathway (e.g. many desert grasses such as Black and Blue Grama (*Bouteloua eriopoda* and *B. gracilis*)) use water more efficiently than plants utilizing the C_3 photosynthetic pathway (e.g. many desert shrubs, such as creosotebush and mesquite). Under elevated atmospheric CO_2 concentrations, due to anthropogenic emissions (IPCC, 2013), C_4 competitive advantage is diminished thus benefiting C_3 plants (Idso and Quinn, 1983; Mooney et al., 1991; Mayeux et al., 1991; Idso, 1992; Wolfe and Erickson, 1993; Knapp et al., 1996; BassiriRad et al., 1997; Bond et al., 2003; Ainsworth and Long, 2005; Ward, 2010). This hypothesis is attractive as a causal mechanism linking vegetation changes observed across disparate geographical areas, but it has been contested (Archer et al., 1995).
- Elevated levels of herbivory on grasslands due to grazing by commercial livestock are frequently cited as a cause of grass-shrub vegetation change (York and Dick-Peddie, 1969; León and Aguiar, 1985; Brown and Archer, 1987; Grover and Musick, 1990). Grasses are more palatable to cattle and therefore are subject to selective removal of aboveground biomass. This increases the availability of resources such as soil moisture and nitrogen available for other, less

palatable plants, such as shrubs. Recent modelling studies support overgrazing as a key trigger of woody shrub encroachment in semi-arid grasslands (Stewart et al., 2014; Caracciolo et al., 2016), although it is possible that these model structures reinforces existing beliefs. Furthermore, the movement of commercial livestock can transport shrub propagules, especially mesquite (Humphrey, 1958; Brown and Archer, 1987), thus accelerating dispersal relative to transport by other consumers such as Merriam kangaroo rats (*Dipodomys merriami*) (Reynolds, 1950). Some workers have also suggested that anthropogenic hunting pressures may alter herbivory by key mammalian herbivores (e.g. elephants in African Savannas), thus facilitating the increase of woody shrubs (Owen-Smith, 1992).

- The recruitment and survival of vegetation in semi-arid ecosystems can also be influenced by fire regimes (Hochstrasser et al., 2014; Ratajczak et al., 2014). Wildfire regimes have been perturbed by anthropogenic activities, due to deliberate fire suppression activities combined with reduction of fine fuel loads on grasslands due to elevated levels of herbivory. This has reduced burn frequencies, thus facilitating the establishment of shrubs species as, for example, creosotebush individuals are more susceptible to fire-induced mortality as juveniles than as mature plants, so reduced fire frequencies increase the likelihood of creosotebush recruitment (Humphrey, 1958; Briggs et al., 2002; Brown and Archer, 1999; Van Auken, 2000). Reduced grass cover also reduces fire connectivity, reducing fire pressures on shrubs (Ravi et al., 2010).
- Climate, particularly the amount and temporal distribution of precipitation inputs to water limited semi-arid rangelands, can differentially benefit particular plant functional types (Schlesinger et al., 1990; Archer et al., 1995; Moreno-de las Heras et al., 2016). Desert grasses and forbs typically have shallow root systems, this is in contrast to shrubs such as creosotebush which usually have more extensive root systems, enabling them to access moisture from deeper in the soil profile. These traits afford shrubs greater resilience to summer droughts, as shrubs are more able to utilize precipitation during winter periods which recharges deeper soil moisture stores.

Conversely, desert grasses may be more effective at utilizing shallow inputs of soil moisture, arising from smaller magnitude inputs of moisture during the growing season. Consequently, changes in precipitation regimes may confer a competitive advantage according to plant type and life history traits (Hastings and Turner, 1965; Neilson, 1986; Brown et al., 1997; Swetnam and Betancourt, 1998; Brown and Archer, 1999; Gao and Reynolds, 2003; Laliberte et al., 2004; Schwinning et al., 2005; Muldavin et al., 2008; Van Auken, 2009; Throop et al., 2012b; Báez et al., 2013; Cleland et al., 2013; Moreno-de las Heras et al., 2016).

- Changes in nutrient resource availability due to anthropogenic perturbations in nitrogen deposition have been postulated as another possible driver of woody shrub encroachment (Ehleringer, 2001; Köchy and Wilson, 2001; Báez et al., 2007). The C_4 photosynthetic pathway is more efficient in its use of nitrogen than C_3, so alleviating the nitrogen limitation reduces the competitive advantage of grasses.Perturbations of nitrogen deposition rates exhibit strong spatial relationships with anthropogenic emission sources, so the effect would be expected to be geographically limited.

In summary, several mechanisms have been identified which could drive woody shrub encroachment by altering the balance of competitive advantage between grass and shrub species in semi-arid rangeland ecosystems. Despite extensive ecological research characterising the physiological response of individual plants at leaf- and plant-scales (e.g. Smith et al., 2000; Throop et al., 2012b), upscaling this knowledge to explain and predict ecosystem responses to environmental change has proven challenging. This may be partly due to the slow pace of woody shrub encroachment over decadal to centennial timescales which are difficult to observe empirically (Jackson et al., 2000). Overgrazing is most commonly advanced as an explanation for woody shrub encroachment (cf. Archer et al., 1995; Gibbens and Lenz, 2001; Boardman et al., 2003; Müller et al., 2007a; Turnbull et al., 2008b). Numerous investigations have found that no single causal factor appears dominant, and it is likely the multiple interacting processes control the ecosystem state (Archer et al., 1995; Turnbull et al., 2008b; Van Auken, 2009; Throop et al., 2012b; Sala and Maestre, 2014). Various conceptual frameworks attempting to rationalise these interactions have been proposed (e.g. Turnbull et

al., 2008b; Soliveres et al., 2013). These usually consider the dominant vegetation type to result from an interplay of competitive advantages and disadvantages between different plants (D'Odorico and Porporato, 2006a). Considering the dominant vegetation type to result from an interplay of competitive advantage/disadvantage concurs with knowledge of how various environmental factors control the recruitment, survival and persistence of potentially dominant species through their various life stages (e.g. Brown and Archer, 1999; Huenneke et al., 2002; Peters et al., 2010; Moreno-de las Heras et al., 2016). Turnbull *et al*. (2008b) developed the cusp-catastrophe framework of Rietkerk et al. (1996), whereby broad-scale factors can influence ecosystem resilience to change (*e.g.* changes to precipitation, fire and grazing regimes) with other disturbances potentially triggering ecosystem change (*e.g.* wildfires, droughts etc.). This cusp-catastrophe framework could benefit from affording greater consideration to vegetation dispersal processes (cf. Peters et al., 2006a), though it is considered the most appropriate conceptual model for the study site considered herein. Once shrub encroachment is initiated, positive feedbacks in the redistribution of water, soil and soil-associated nutrient resources perpetuate woody plant encroachment in an autocatalytic process (Schlesinger et al., 1990; Müller, 2004).

1.3.4. Future projections of woody shrub encroachment

Three main approaches are used to project vegetation responses to changing environmental conditions: (i) experimental and observational studies (e.g. Collins et al., 2010; Ladwig et al., 2012), (ii) mechanistic modelling (e.g. Stewart et al., 2014; Caracciolo et al., 2016), and (iii) bioclimatic envelope modelling (BEM) developed using associations between vegetation communities and contemporary climate extended using future climate projections (e.g. Shafer et al., 2001; Rehfeldt et al., 2006). Perhaps the most widely employed approach is BEM, which was used by Rehfeldt *et al*. (2006) to predict the distribution of biotic communities across the semi-arid southwestern USA under future climate projections (Figure 1-4). Rehfeldt *et al.*'s analysis suggested that until 2060 the extent of Mojave, Sonoran and Chihuahuan Desert scrub vegetation dominated ecosystems will increase by 85%, 79% and 167%, respectively; subsequently Mojave and Sonoran scrub ecosystems will continue to expand while Chihuahuan Desert scrub ecosystems contract (Friggens et al., 2012). This concurs with the predictions of northward expansion of creosotebush by Shafer *et al.* (2001) and Neilson *et al.* (2005). Importantly, each of the three approaches listed above have significant limitations, and there is therefore scope for future research to better integrate these three approaches to derive more reliable predictions (Friggens et al., 2012). While mechanistic understanding of the controls of woody shrub encroachment is equivocal, it is sufficiently developed to assert that the observed trend of shifting plant functional type dominance is very likely to continue into the future, and may accelerate, due to continuation of CO_2 and nitrogen fertilization, commercial grazing, fire suppression and predicted climatic changes (Wilcox, 2010; Friggens et al., 2012; Bradford et al., 2014; Caracciolo et al., 2016).

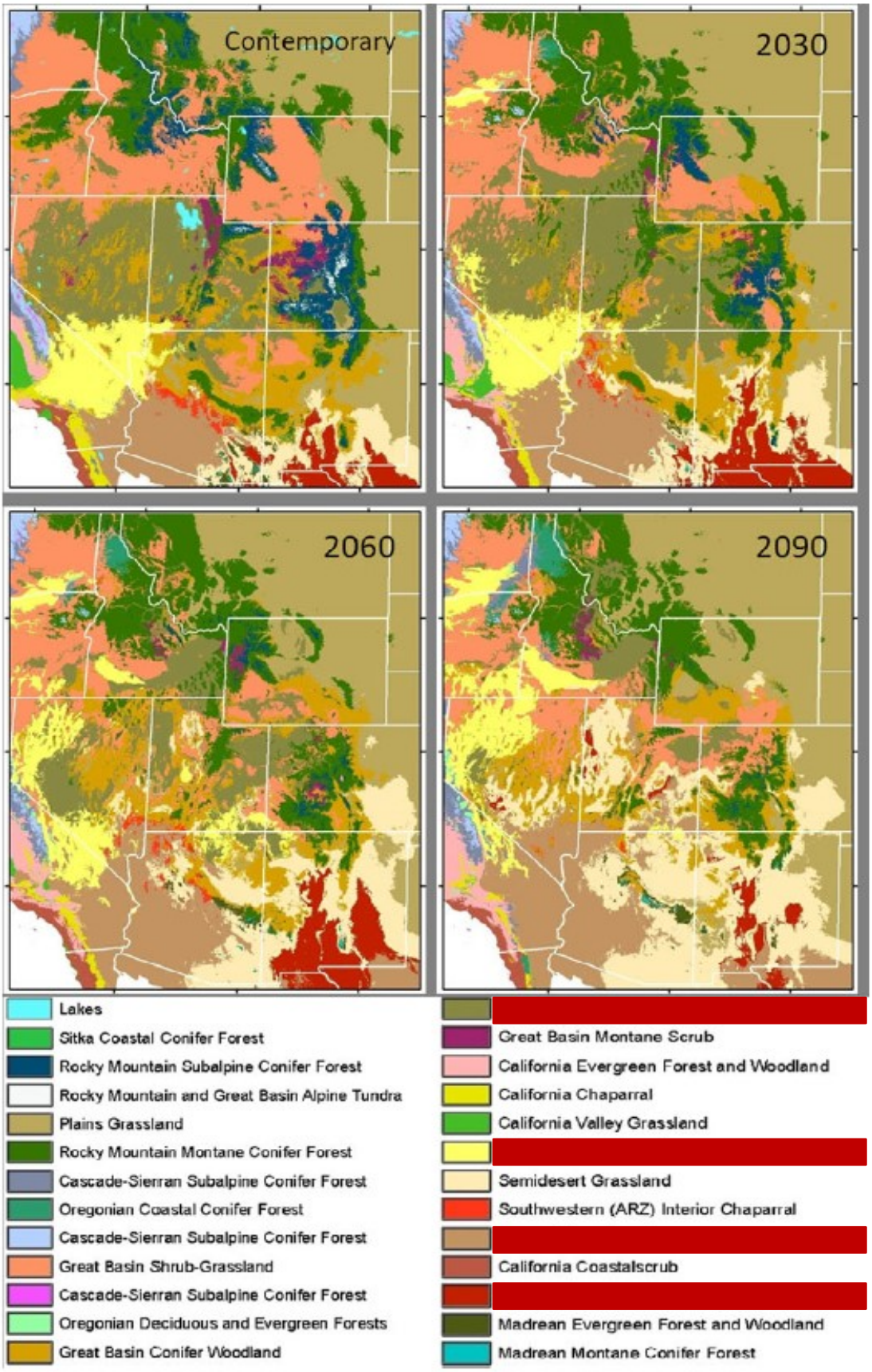

Figure 1-4. Biotic communities in the western United States, predicted using bioclimatic envelope models developed from contemporary climatic data and future climate projections (from Friggens et al., 2012; after Rehfeldt et al., 2006).

1.3.5. Consequences of woody shrub encroachment on ecosystem structure and function

The transition in community dominance from grass to shrub plant functional types results in major changes to both the structure and function of semi-arid ecosystems. These changes can have important implications for large-scale (regional to global) hydrological and biochemical processes (Schlesinger et al., 1990; Hibbard et al., 2001; Archer et al., 2001). The following discussion of the differences between grass- and shrub-dominated ecosystems focuses on the context of the semi-arid southwestern USA, and the limitations of this geographical focus are also considered.

The encroachment of woody plants increases competition for resources, principally soil moisture and nutrients, which typically reduces the net primary productivity of grass vegetation. This reduction in grass productivity can reduce biomass available to grass-eating livestock such as cattle and sheep and consequently decrease the ecosystem's herbivory value to such livestock (Quan et al., 1994; Eldridge et al., 2011). The impact of woody shrub encroachment on biodiversity is equivocal (Maestre et al., 2006). Inter-comparisons between studies are hindered by different metrics of biodiversity, but a global meta-analysis found no statistically significant difference in the species richness of vascular plants (n = 68 studies), vertebrates (n = 41 studies), ants (n = 14 studies) or trees (n = 9 studies) between grass- and shrub-dominated paired sites (Eldridge et al., 2011). Similarly, in the southwestern USA, the effect of shrub encroachment on biodiversity has been reported to have both negative (Jackson et al., 2002; Báez and Collins, 2008; Ratajczak et al., 2012) and positive effects, the latter increasing species richness of mammals (Whitford, 1997), birds (Pidgeon et al., 2001) and ants (Bestelmeyer, 2005).

While a global meta-analysis of the effects of shrub encroachment on bare ground cover shows no significant change (n = 28 studies) (Eldridge et al., 2011), in semi-arid ecosystems shrub-dominated areas have reduced overall foliar cover relative to grass-dominated ecosystems (Aguiar et al., 1996; Boardman et al., 2003; Müller, 2004; Turnbull et al., 2010c). This increase in bare ground increases regional albedo, which alters the radiative energy balance and increases regional air temperatures (Chopping et al., 2005, 2006).

The changes in ecosystem structure across grass-shrub ecotones can have major effects on the hydrological function of the ecosystem. The reduction in foliar cover reduces raindrop interception, increasing the delivery of kinetic energy to the soil surface (Wainwright et al., 1999a). This increased kinetic energy input increases detachment of soil particles (Wainwright et al., 1995) and development of impermeable surface seals (Baird, 2013). Relative to grasslands, there is an increase in the extent of bare soils in interplant areas, which have much lower infiltration rates compared with vegetated areas (Lister, 2007; Müller et al., 2007a). Consequently, there is much greater generation of overland flow during infrequent but high intensity rainstorm events (Parsons et al., 1996; Wainwright et al., 2000; Neave and Abrahams, 2002; Turnbull et al., 2010a; Puttock et al., 2013). Significantly, these runoff-generating bare areas are also more connected in shrub-dominated ecosystems (Parsons et al., 1997; Turnbull et al., 2010b, 2010a; Puttock et al., 2013). Together, this reduced infiltration and increased hydrological connectivity result in more runoff-per-unit-of-rainfall, resulting in significantly higher runoff coefficients from shrublands relative to grasslands (Schlesinger et al., 2000; Wainwright et al., 2000; Turnbull et al., 2010a; Puttock et al., 2013; Puttock, 2013). The differences in runoff coefficients is illustrated schematically in Figure 1-5.

The differences in hydrological function also have significant implications for erosional dynamics across grass-shrub ecotones. The increased runoff generation and higher hydrological connectivity results in increased overland flow velocities (Parsons et al., 1990; Parsons and Abrahams, 1992; Abrahams et al., 1996; Wainwright et al., 2000). The increased depths and velocities of overland flow, combined with greater delivery of raindrop kinetic energy to the soil surface, increases the detachment and transport of soil particles (Gile et al., 1981; Marion et al., 1990; Abrahams et al., 1994, 1995; Parsons et al., 1996; Schlesinger et al., 1999, 2000; Wainwright et al., 2000; Boardman et al., 2003; Turnbull et al., 2010a; Puttock, 2013). Accelerated soil erosion is often problematic, potentially reducing soil fertility and thus ecosystem productivity in degrading landscapes (Lal, 2001a). Increased sediment loading to fluvial systems can increase potable water production treatment costs and accelerate reservoir sedimentation (McCall et al., 1984; Walling, 1999; Walling and Fang, 2003). Aquatic ecosystems can be impacted through elevated turbitity, lowering primary productivity, reducing predation success, and through colmation of salmonid spawning redds (Bilotta

and Brazier, 2008). The differences in sediment yield are illustrated schematically in Figure 1-5.

Differences in the nutrient dynamics of grasslands versus shrublands are more complex than the sediment dynamics. A diverse range of methodological approaches have been employed across a range of different spatial and temporal scales (Table 1.2), making synthesis of the literature a challenging proposition. Generally, when both dissolved and particle-associated chemical species are considered, there is often an increase in the erosion-induced efflux from shrub-domianted sites relative to grass-dominated sites.

Table 1.2 Differences in water erosion induced nutrient fluxes across grass-shrub transitions.

Nutrient	Efflux	Notes	Reference
Nitrogen	Increase	Rainfall simulation	(Schlesinger et al., 1999)
	Increase (double)	Small plot (4 m^2), Natural rainfall, Jornada Dissolved species only	(Schlesinger et al., 2000)
	Increase	Large runoff plots (300 m^2), natural events, Sevilleta	(Turnbull et al., 2011).
	Increase	Small runoff plots (1.5 m^2), rainfall simulation, Jornada	(Michaelides et al., 2012)
Phosphorus	Minimal Change	Rainfall simulation	(Schlesinger et al., 1999)
	Increase	Dissolved P only, Small plot (4 m^2), Natural rainfall, Jornada	(Schlesinger et al., 2000)
	Increase	Large runoff plots (300 m^2), natural events, Sevilleta	(Turnbull et al., 2011).
	Increase	Small runoff plots (1.5 m^2), Rainfall simulation, Jornada	(Michaelides et al., 2012)
Potassium	Reduction	Small runoff plots (1.5 m^2), Rainfall simulation, Jornada	(Michaelides et al., 2012)

A valuable concept in understanding semi-arid shrubland ecosystems is Islands of Fertility, which recognises that in semi-arid ecosystems soil resources such as

fine particles and particle-associated nutrients are commonly concentrated in topographic mounds beneath plant canopies (Charley and West, 1975; Goldberg and Turner, 1986; Schlesinger et al., 1990; Schlesinger and Pilmanis, 1998; Titus et al., 2002). This concept was advanced by Schlesinger *et al*. (1990), who working in the southwestern USA suggested that (i) increased heterogeneity in soil resources is a characteristic of desertification, and (ii) increased heterogeneity of soil resources (principally nitrogen) can lead to strong positive feedbacks which perpetuate shrub encroachment. Such feedbacks include the inhibition of grass re-establishment in resource-poor intershrub areas following shrub emergence.

The concentration of soil resources beneath shrubs is attributed to the anisotropic redistribution of fines and associated nutrients from interplant areas through rainsplash (Parsons et al., 1992; Wainwright et al., 1999b) and aeolian transport processes (Coppinger et al., 1991). This resource redistribution hypothesis is supported empirically by observations that soil nutrient concentrations are spatially auto-correlated at similar distances to shrub spacing and therefore are inferred to be related to shrub vegetation structure (Schlesinger et al., 1996; Cross and Schlesinger, 1999; Turnbull et al., 2010c; Brazier et al., 2013). Even if individual shrubs die or are removed, the shrub-associated heterogeneity in soil resources can persist for many years (Schlesinger et al., 1996; Puigdefábregas et al., 1999).

Aeolian processes are another important vector driving the redistribution of soil resources in dryland environments, particularly in more arid contexts than those considered herein where mass transport due to aeolian processes can exceed transport by water (Larney et al., 1998; Okin et al., 2004; Cornelis, 2006; Li et al., 2007, 2008, Ravi et al., 2007, 2010; Field et al., 2010). In shrub-dominated landscapes, the reduction in vegetation cover enables increased entrainment of soil by aeolian processes; this increased entrainment accelerates the redistribution of soil resources from interplant areas to beneath shrub canopies (Harrison et al., 2001; Gillette and Pitchford, 2004; Li et al., 2007; Ravi et al., 2007, 2010). Increased dust loading can influence radiative balance, depending on its mineralogy and persistence in the atmosphere (Field et al., 2010; Harrison et al., 2001).

These substantial changes in ecosystem structure and function can result in land degradation, leading to desertification (Schlesinger et al., 1990). The paradigm that grass-shrub vegetation transitions are synonymous with land degradation is a conceptual model that has been widely adopted by the international community, for example the Millennium Ecosystem Assessment (Safriel et al., 2005; Adeel et al., 2005), the Intergovernmental Panel on Climate Change (Denman et al., 2007, p. 527) and the United Nations Convention to Combat Desertification (UNCCD, 2000). However, while this paradigm appears appropriate for the southwestern USA context, it originated from research examining a relatively narrow range of ecosystem services in a geographically-limited study region.

Evidence from other ecoregions suggests that when a larger range of ecosystem services are considered, shrub encroachment can have many positive effects of ecosystem services (Maestre et al., 2003, 2006, 2009; Eldridge et al., 2011; Sala and Maestre, 2014), challenging the ubiquity of the paradigm that shrub encroachment is synonymous with ecosystem degradation (Maestre et al., 2009; Eldridge et al., 2011). It is appropriate to advocate caution when extrapolating conceptual models developed in specific ecoregions, and further meta-analysis and global synthesis is necessary to fully elucidate the effects of shrub encroachment on the provision of ecosystem services in diverse ecoregions. Notwithstanding these limitations, given the present focus on grass-shrub transitions in the North American context, the ‘desertification’ paradigm remains the most appropriate conceptual framework for this study.

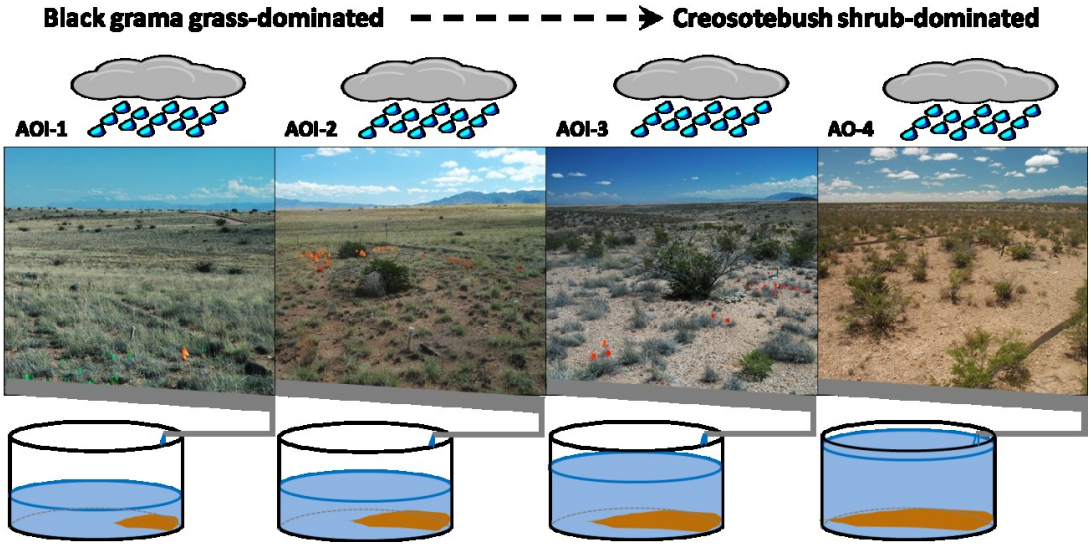

Figure 1-5. Schematic representation of the differences in runoff coefficients and sediment yield observed across a grass-shrub vegetation transition, from a black grama grass end-member, through grass-shrub and shrub-grass intermediary sites, to the creosotebush shrub end-member (based on findings by Turnbull et al., 2010a; Puttock et al., 2013). Blue and brown in the cylinders represents yield of runoff and sediment respectively, for the same magnitude of precipitation input. AOIs-1 to -4 refer to the grass-, grass-shrub, shrub-grass, and shrub- dominated sites, respectively.

1.4. Effects of Woody Shrub Encroachment on Ecosystem C Dynamics

The change in plant functional type resulting from woody shrub encroachment into former grasslands can significantly alter the C dynamics of these ecosystems. For convenience here, these differences will be considered broadly terms of (i) total ecosystem C storage, in both biomass and soil pools, (ii) the spatial distribution of C, and (iii) the movement of C through these ecosystems, though each of these components are deeply interrelated.

1.4.1. Ecosystem Carbon storage

In terms of (i) total ecosystem C storage, a global meta-analysis *of* all ecoregions indicated that woody shrub encroachment typically increases both the aboveground biomass (n = 14 studies) and soil OC pools (n = 67 studies), thus resulting in net increases in total ecosystem C storage (Eldridge et al., 2011). The total change in net C storage is potentially of sufficient magnitude to significantly influence continental-scale C budgets (Pacala et al., 2001, 2007; Schimel et al.,

2001; Gifford and Howden, 2001; Burrows et al., 2002; Henry et al., 2002; Houghton, 2003a; Barger et al., 2011).

For example, in the conterminous United States, woody plant encroachment over 220 X 10^6 ha of former grasslands was estimated to have sequestered 0.12-0.13 Pg C yr^{-1} between 1980 and 1990, comprising 18-34% of the total annual C sink (Pacala et al., 2001; after Houghton et al., 1999, 2000). A C sink of this magnitude is required to reconcile top-down (based on atmospheric observations) and bottom-up (based on terrestrial observations) estimates of the continental C sink in North America (Pacala et al., 2001).

More detailed studies comparing collocated paired grass- and woody shrub-dominated plots have indicated that the differences in ecosystem C dynamics between different plant functional types are complex, and can vary between different environmental settings (Jackson et al., 2002; Goodale and Davidson, 2002). Examining six pairs of sites across a gradient of mean annual precipitation (MAP), Jackson *et al*. (2002) found that shrub encroachment increased biomass C pools, particularly in wetter sites. The paired sites were selected to be comparable other than in terms of vegetation cover. Relative differences in SOC pools also varied with MAP, with dryer sites gaining and wetter sites loosing SOC following shrub encroachment (Figure 1-6a). Total ecosystem C storage increases in the dryer sites following shrub encroachment, principally due to increases in the SOC pool, but in wetter sites, decreases in SOC stocks outstripped gains in biomass C storage resulting in a net reduction in total ecosystem C storage (Goodale and Davidson, 2002) (Figure 1-6b). SOC pools represent the net balance between C inputs from plants against losses through erosion, leaching and microbial decomposition. The differences in SOC pools observed by Jackson *et al*. (2002) were suggested by Goodale and Davidson (2002) to originate from differences in plant-derived C inputs. In wetter sites, OC inputs are greater in grass-dominated ecosystems, because, relative to shrubs, grass vegetation has higher root : shoot ratios and productivity is more sensitive to precipitation (Sims and Singh, 1978). Importantly, all six sites examined by Jackson *et al*. (2002) have lower rates of C accumulation than the mean value presumed for conterminous USA non-forest, non-cropland areas used by Pacala *et al.* (2001), suggesting that the latter's estimate of the continental-scale shrub

encroachment-driven C sequestration is likely to be an overestimation (Goodale and Davidson, 2002).

Clearly, when evaluating the net effect of shrub encroachment on ecosystem C stocks, it is imperative to consider C storage explicitly in both above and belowground biomass, and the soil pools (Jackson, 2000; Jackson et al., 2000, 2002; Goodale and Davidson, 2002). Importantly, although Jackson *et al*.'s (2002) MAP control hypothesis did concur with empirical observations, it was constrained by just six data points (Figure 1-6a). Given understanding of the process governing ecosystem C dynamics, it is likely that the ratio of C storage in grassland or shrubland ecosystems may be more strongly predicted by measures of aridity, such as the ratio of annual average precipitation to potential evapotranspiration, rather than simply precipitation (although this still does not account for complexity induced by possible differences in OM inputs resulting from seasonality of precipitation inputs). The second driest site considered by Jackson *et al.* (2002) was the Sevilleta National Wildlife Refuge in central New Mexico (260 mm MAP), where recent investigation robustly (4 × 90 samples) demonstrated no significant differences in areally-averaged near-surface (0-0.05 m) SOC stocks between four sites across a grass-shrub ecotone (Brazier et al., 2013).

Understanding changes in ecosystem C dynamics following a shift in community dominance from one plant functional type to anther is further complicated by limited understanding of the time lags for SOC stocks to equilibrate (Connin et al., 1997a; Jackson et al., 2000; Denman et al., 2007), as it can take decades for SOC to equilibrate following grass-shrub transitions (Goodale and Davidson, 2002). Jackson *et al*. (2000) assumed SOC pools equilibrated within 30 years of shrub encroachment; however, SOC increases have been observed to continue until at least 130 years after shrub encroachment (Liao et al., 2006a). Elucidating these lag effects is particularly challenging in semi-arid environments, due to high degrees of spatio-temporal variability, compounded by a paucity of detailed long-term monitoring.

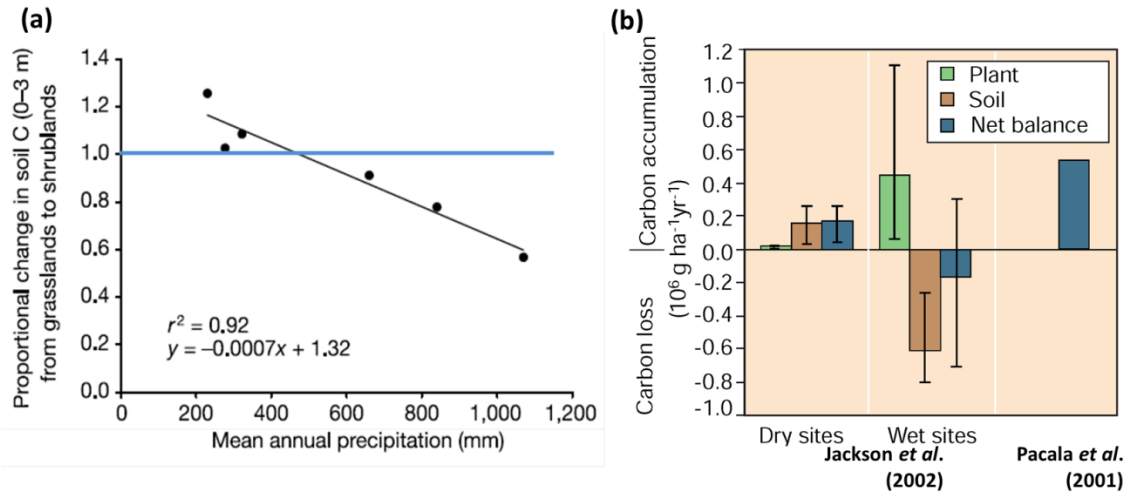

Figure 1-6. (a) The proportional change in soil organic C (SOC) (between 0 m down to 3 m depth) following woody shrub encroachment of native grasslands; values greater than unity indicate sites gaining SOC (from Jackson et al., 2002). (b) Changes in C storage resulting from shrub encroachment into grasslands. The left and centre panels show means (± ranges) of changes in plant, soil and total ecosystem C pools in three wetter sites versus three drier sites (data from Jackson et al., 2002), while the right panel shows the mean rate of total C accumulation used by Pacala *et al.* (2001) (modified from Goodale and Davidson, 2002).

The USA Geological Survey (USGS) publish a framework for national-scale assessments of North American ecosystem C storage, using process-based modelling to estimate baseline and future C stocks (Zhu and Reed, 2012). However, such numerical modelling approaches are often limited by inadequate process representation. For example, the study by Zhu and Reed did not represent changing vegetation dynamics – a key concern considering the widespread encroachment of woody shrub into former grasslands (Van Auken, 2000, 2009, Eldridge et al., 2011, 2012; Bestelmeyer et al., 2015) and the implications for ecosystem C dynamics (Pacala et al., 2001, 2007; Knapp et al., 2008; Eldridge et al., 2011; Brazier et al., 2013; Puttock et al., 2013, 2014; Petrie et al., 2015). Consequently, improving confidence in both current estimates and future predictions of terrestrial C dynamics requires substantial further work to better integrate large-scale empirical observations with numerical modelling approaches.

1.4.2. Distribution of Carbon

In terms of (ii) the distribution of C, woody shrub encroachment alters both the horizontal and vertical distribution of C in the ecosystem. Considering first the vertical distribution, shrubs generally have smaller root : shoot ratios relative to grasses, with a higher proportion of biomass allocated to aboveground pools (Chew and Chew, 1965; Barbour, 1973; Wallace et al., 1974; Ludwig et al., 1975; Sims et al., 1978; Miller et al., 1990; Krämer et al., 1996; Schlesinger and Pilmanis, 1998; Nowak et al., 1999; Mata-González et al., 2002; Goodale and Davidson, 2002; Mokany et al., 2006; Allen et al., 2008). Woody plants also usually have deeper rooting depths relative to grasses, resulting in C inputs at greater depths in the soil profile (Barth and Klemmedson, 1978; Connin et al., 1997a; Jackson et al., 1997, 2000; Jobbágy and Jackson, 2000); this is significant because differences in the vertical distribution of soil C can obfuscate comparisons between total soil C pools, unless the full soil profile depth is measured.

There are significant differences in the lateral distribution of C between grass- and shrub-dominated ecosystems, with much greater heterogeneity in both biomass and soil pools in semi-arid shrublands (Schlesinger et al., 1990, 1996; Kieft et al., 1998; Cross and Schlesinger, 1999; Bird et al., 2002; Titus et al., 2002; Brazier et al., 2013; Puttock, 2013; Puttock et al., 2013). This heterogeneity can be quantified using semivariograms, which describe the spatial pattern of, and autocorrelations, within spatial data (cf. Cross and Schlesinger, 1999; Müller et al., 2008; Turnbull et al., 2010c) (For a lucid description of semivariograms, see Dungan et al., 2002; Müller et al., 2008, p. 7). In rangelands, similarities in spatial autocorrelation lengths between the SOC and vegetation patterns have been inferred to indicate that the spatial distribution of SOC is dominantly controlled by ecosystem biotic structure (Schlesinger et al., 1990, 1996; Bird et al., 2002; Schlesinger and Pilmanis, 1998; Smith et al., 1994; Lett et al., 2004). Intriguingly, a detailed study across four stages of a grass–shrub ecotone recently found that the autocorrelation range of SOC was consistently greater than the autocorrelation range of the vegetation, which was argued to indicate that processes other than simple vegetation-soil feedbacks control the spatial distribution of SOC (Brazier et al., 2013). Brazier *et al*. (2013) suggest that the transport of soil resources by hydrological processes redistributes SOC around the landscape (cf. Connin et al., 1997b). Brazier *et al*. (2013) concluded that

abiotic processes may be as important as biotic controls relating to vegetation structure or size in determining the spatial distribution of soil OC in these ecosystem. This notion is supported by the observation that near-surface sediments in ephemeral preferential flowpaths are depleted in fine particles and soil organic matter compared with nearby microsites (Titus et al., 2002), and is also consistent with findings that biotic-abiotic feedbacks operate as the scale of individual plants and that the spatial distribution of vegetation alone does not explain the spatial distribution of soil nutrients (Schade and Hobbie, 2005; Turnbull et al., 2010c).

SOC concentrations are typically greatest in soils beneath shrub canopies, compared with sites beneath grass cover or in bare interplant areas (Bird et al., 2002; Titus et al., 2002; Schlesinger et al., 1996; Sankey et al., 2012; Brazier et al., 2013), due to complex interactions between the processes determining C influxes (e.g. litter inputs, deposition of soil) and effluxes (e.g. mineralisation, erosion, photodegradation) at any given point (Schlesinger et al., 1996; Titus et al., 2002; Petrie et al., 2015). Consequently, representative values of SOC contents are often calculated for each discrete surface type, which can be multiplied by the areal coverage of each surface type to obtain areally-weighted averages SOC contents over larger scales (e.g. Kieft et al., 1998; Brazier et al., 2013; Puttock et al., 2014).

Furthermore, abiotic controls can modulate biotic controls on SOC, both at plant-interplant (Brazier et al., 2013) and landscape scales (Bird et al., 2002). Such controls can include (a) soil mineralogy, which exerts a strong control on SOC turnover independently of vegetation structure (Torn et al., 1997), (b) slope, attributed to differences in soil fertility and consequently OM inputs to the soil (Rhoton et al., 2006), (c) aspect, due to differences in insolation and microclimate affecting net primary production (Rhoton et al., 2006), and (d) topographic position (Doetterl et al., 2012), although SOC does not always vary systematically with hillslope position (Rhoton et al., 2006). Investigating vegetation responses to precipitation in semi-arid grassland, Cervantes *et al.* (2012), found landscape morphology (relative topography) was a major control on grass productivity, and by extension, OM inputs to the soil. Calculation of SOC contents on the basis of ecosystem biotic structure alone therefore fails to account for these significant abiotic controls.

1.4.3. Carbon fluxes through grass and shrub ecosystems

Compared to C stocks and spatial distribution, even less is known about (iii) how C fluxes differ between grass- and shrub-dominated ecosystems. Fluxes matter, because the magnitude of C stocks change as a result of imbalance between influxes and effluxes (Holmén, 2000; Murray-Tortarolo et al., 2016). A range of techniques have been used to elucidate ecosystem C dynamics. For example, repeat monitoring of the magnitude of soil C stocks (e.g. Kieft et al., 1998), although high spatial variation adds significant uncertainty. Biomass C stocks can also be monitored for change over time, although again high levels of spatial heterogeneity and temporal dynamism can contribute significant uncertainty (e.g. Huenneke et al., 2001; Allen et al., 2008; Hill et al., 2013).

Using a chronosequence approach, Liao (2006b, 2006a) investigated changes in 0-0.15 m SOC stocks following woody shrub encroachment in a mesic grassland, and reported accrual rates of 10-30 g C m^{-2} yr^{-1} over 130 years since shrub encroachment. Vertical fluxes of gaseous C have been estimated using eddy covariance flux towers (e.g. Baldocchi, 2003; Petrie et al., 2015), which have been used to investigate differences in ecosystem sensitivity to precipitation inputs (Scott et al., 2009). Importantly, estimates of net ecosystem exchange (NEE) derived from eddy covariance towers are associated with high uncertainties, due in part to temporal variations in the footprint of the eddy covariance measurement and by spatial variability within that footprint (i.e. different vegetation types) (Twine et al., 2000; Finkelstein and Sims, 2001; Hollinger and Richardson, 2005; Oren et al., 2006).

Biogeochemical and stable radioisotope analysis (for example, stable C isotopes ($\delta^{13}C$)) have been used to discriminate between C originating from C4 and C3 vegetation types at locations with known history of vegetation change in order to providence OC (Boutton et al., 1998; Biggs et al., 2002; Krull et al., 2005; Turnbull et al., 2008a; Puttock et al., 2012b). N-alkyne lipid biomarkers have been used to discriminate SOC provenance to the species level (Puttock et al., 2012a, 2014; Puttock, 2013). Unstable radiocarbon dating techniques have been used to date C age since fixation, and to constrain turnover rates of OC in these ecosystems (Frank et al., 2012). Because shrub-dominated ecosystems typically have larger biomass C pools and a greater proportion of biomass in aboveground

components, the C stock's susceptibility to disturbances such wildfire may increase.

Relative to vertical C exchanges, much less is known about the lateral redistribution of C in both grasslands and shrublands. Aeolian and hydrological processes are both key vectors in the lateral redistribution of C. For example, monitoring aeolian erosion at the semi-arid Jornada Experimental Range in Southern New Mexico, USA, Li et al. (2007) found that up to 25% of the near-surface (0-0.05 m) soil OC stock was removed over three windy seasons, that wind erosion-induced OC fluxes were inversely related with vegetation cover and that airborne sediments were enriched in particle-associated OC by 3-6 times relative to the 0-0.05 m near-surface soil.

Monitoring erosion caused by overland flow following high-intensity rainstorm events from four 300 m^2 runoff plots across a grass-shrub ecotone in the central New Mexico, southwestern US, recent studies have shown that shrublands have significantly greater (i) runoff-per-unit-rainfall, (ii) erosion-per-unit-rainfall, and (iii) OC-per-unit-of-sediment which together results in much greater erosion-induced event-fluxes of OC from shrub-dominated ecosystems relative to grass-dominated ecosystems (Brazier et al., 2013; Puttock et al., 2013). Export of dissolved OC in runoff was negligible at these scales, due to limited production of DOC in the typically very arid soils (Puttock, 2013).

Further investigations at the same sites have used dual-proxy (lipid biomarkers and stable isotopes) biogeochemical tracing to provenance eroded organic matter during a dryer-than-average period. This tracing indicated that (i) across the grass-shrub ecotone eroded OM increasingly originated from shrub, (ii) large proportions of the OC eroded from shrub-dominated plots originated from bare interplant areas, where OC is older, legacy C from previously dominant grass vegetation (Puttock et al., 2014), and (iii) that the proportion of shrub-derived OC associated with the eroded sediment increased during larger magnitude events (Puttock, 2013), a trend considered likely to continue during wetter periods.

1.4.4. Effects of Woody Shrub Encroachment on Ecosystem Carbon

The differences in ecosystem C dynamics between grass- and shrub-dominated ecosystems are complex and not well understood, leading to high uncertainty regarding the effects of shrub encroachment on the biogeochemical cycling of C (Jackson et al., 2002; Goodale and Davidson, 2002; Denman et al., 2007). Many authors are of the view that woody shrub encroachment into former grasslands increases ecosystem C storage (e.g. Houghton et al., 1999, 2000, Pacala et al., 2001, 2007; Thomey et al., 2014; Petrie et al., 2015), although the consequences of shrub encroachment are recognised to represent the largest source of uncertainty in the North American C budget (Pacala et al., 2007).

As described in section 1.3.5, shrub encroachment generally significantly accelerates soil erosion, which degrades soil structure, selectively removes macronutrients and reduces soil water storage capacity. These changes can increase vegetation sensitivity to temporal variations in precipitation inputs and reduce soil fertility in these already marginal ecosystems, leading to degradation and desertification (Lal, 2001a; Safriel et al., 2005). Recruitment of new plants and primary productivity could be increasingly inhibited, reducing inputs of organic matter to the soil and resulting in a net loss of C from the ecosystem (Lal, 2001c; Quinton et al., 2010; Meyer, 2012). This process restricts dynamic replacement of eroded OC, and could conceivably lead to the near-total reduction in C stocks from both biomass and soil pools over long (centennial) timescales (Lal, 2001c).

Clearly, these two hypotheses are mutually inconsistent. Consequently, further research is needed to resolve this dichotomy, by advancing process-based understanding of how the C dynamics of these ecosystems change with dominant plant functional type (Jackson et al., 2002; Brazier et al., 2013; Puttock et al., 2014). This work should utilise both field and modelling approaches to develop mutually consistent mechanistic understanding, in order to improve predictions of how shrub encroachment is likely to influence landscape-scale C dynamics in rangelands over decadal and centennial timescales (Bird et al., 2002; Goodale and Davidson, 2002; Jackson et al., 2002; Pacala et al., 2007; Finch, 2012; Meyer, 2012).

2. Research Aims

The overall aim of this thesis is to advance quantitative understanding of the spatial distribution and erosion-induced redistribution of C in semi-arid rangelands, and how these dynamics change with woody shrub encroachment.

This aim is addressed through five related themes:

A. Across a vegetation ecotone from grass-dominated to shrub-dominated semi-arid ecosystems, characterise:
    i. The storage of OC in the near-surface soil, and
    ii. The water erosion-induced redistribution of OC via predominantly interrill erosion processes

B. Across a vegetation ecotone from grass-dominated to shrub-dominated semi-arid ecosystems, characterise:
    i. The storage of in IC in the near-surface soil, and
    ii. The water erosion-induced redistribution of in IC via predominantly interrill erosion processes

C. Develop new, scale-appropriate proximal remote sensing techniques to characterise the fine-grained biotic and abiotic structure of ecosystems to better quantify the storage and erosional redistribution of C in semi-arid ecosystems.

D. Advance the application of process-based numerical modelling approaches to simulate the erosion-induced redistribution of particle-associated organic and inorganic C in semi-arid ecosystems.

E. Synthesize process understanding to inform prediction of the possible long-term effects on terrestrial C dynamics of woody shrub encroachment into former grasslands.

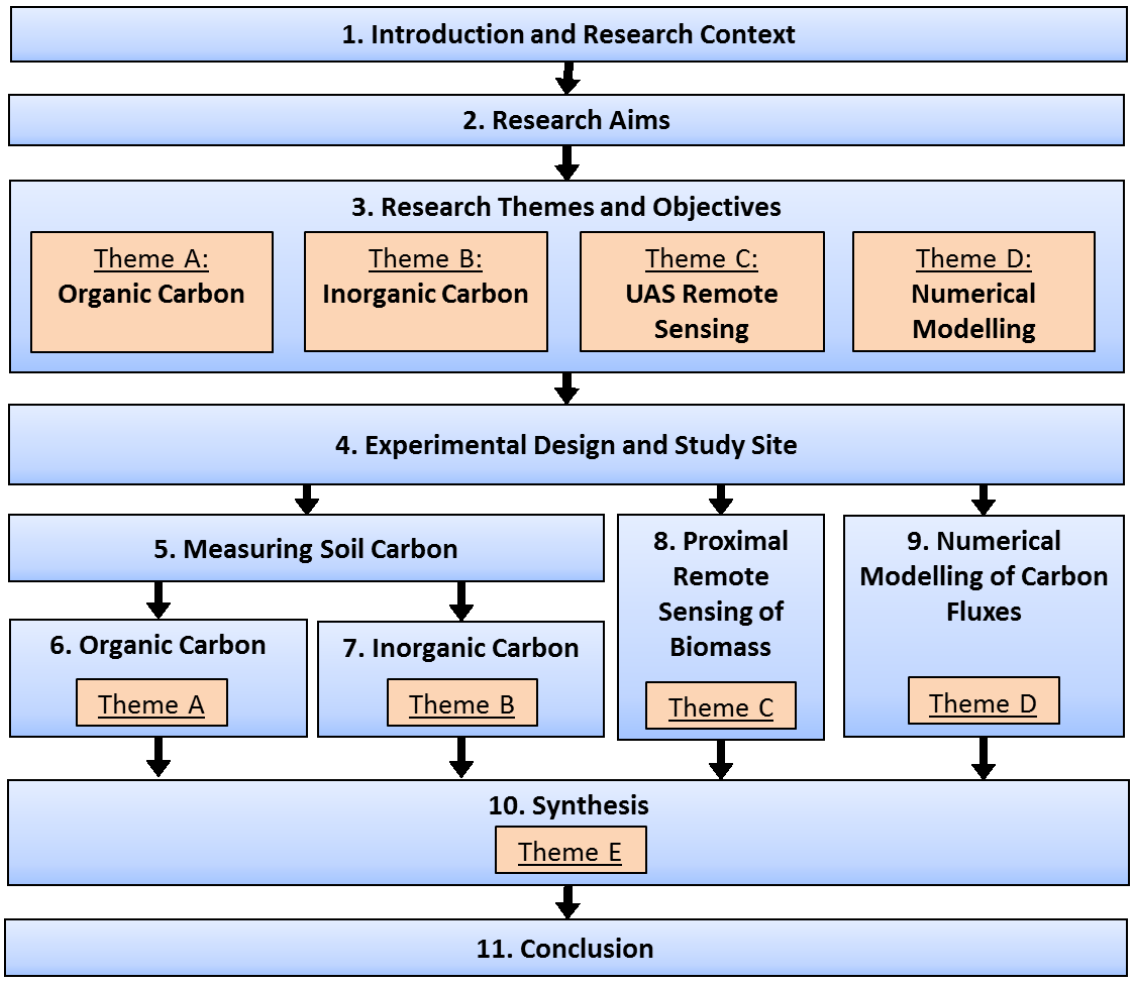

Figure 2-1. Illustration of the thesis structure (numbers correspond to Chapters). The overarching context for the research is presented in Chapter 1. The overall aim of the thesis and the five key research areas is outlined in Chapter 2. The detailed rationale and objectives for four of the themes are discussed and developed in Chapter 3. The focal sites and experimental design and methods subsequently employed are presented in Chapters 4 and 5, respectively. The findings of the soil stock and erosional dynamics of the soil organic carbon are presented in Chapter 6, and the related findings from the inorganic physiochemical form of inorganic carbon are presented in Chapter 7. Proximal remote sensing techniques for measuring ecosystem structure including aboveground biomass are presented in Chapter 8. Numerical modelling approaches are used in Chapter 9 to simulated the erosional redistribution of particule-associated carbon. The various strands of mechanistic understanding developed through Chapters 6~9 are synthesed in Chapter 10, supporting a hypothesis of the likely implications of woody shrub encroachment for terrestrial carbon storage in drylands. Finally, the overall conclusions are presented in Chapter 11.

3. Research Themes and Objectives

3.1. Soil Organic Carbon

3.1.1. Rationale

While much work has been undertaken to characterise C stocks in semi-arid grasslands and shrublands, the net C effect of the vegetation transitions varies with environmental context (Conant et al., 1998; Jackson et al., 2002; Barger et al., 2011) and significant uncertainty remains regarding the controls on the various C fluxes and pools in these ecosystems (Goodale and Davidson, 2002; Jackson et al., 2002; Pacala et al., 2007). Comparisons of the C budgets of grasslands and shrublands often assume that the lateral redistribution of C is insignificant (e.g. Petrie et al., 2015); however, it is well established that changes in ecosystem structure following shrub encroachment into semi-arid grasslands can accelerate the erosion of soil and soil-associated chemicals (Schlesinger et al., 2000; Wainwright et al., 2000; Ridolfi et al., 2008; Turnbull et al., 2010a, 2011; Brazier et al., 2013; Puttock et al., 2013, 2014). Recent work has indicated that the erosion-induced efflux of C from semi-arid shrublands may be substantially higher than that from co-located grasslands (Brazier et al., 2013; Puttock et al., 2013), and that this efflux includes the loss of previously stable legacy C (Puttock et al., 2014). Therefore, to constrain understanding of the impact of shrub encroachment on the C dynamics in semi-arid rangelands, it is useful is to examine the water erosion-induced redistribution of particle-associated OC at different sites across a semi-arid grass-shrub ecotone.

Most knowledge of SOC dynamics as impacted by erosion originates from studies in intensively-managed agro-ecosystems dominated by tillage erosion, often in temperate regions (e.g. Lal, 2005; Beniston et al., 2015; Lacoste et al., 2015). However, as several workers have noted, process understanding obtained from this work is not always directly transferable to less intensively managed ecosystems, in other environmental contexts (Parsons et al., 1991; Bryan, 2000; Mayeux, 2001; Yair and Raz-Yassif, 2004; Liao et al., 2006a; Martinez et al., 2010; Stringer et al., 2012). Therefore, it is important to extend detailed monitoring to unmanaged natural ecosystems, to evaluate transferability of existing process understanding.

Relative to contributing topsoils, eroded sediments are commonly enriched in particle-associated chemicals, such as OC (Jacinthe et al., 2001; Lal, 2005, 2003; Lal et al., 2004a). OC enrichment has been observed in laboratory simulations (Sharpley, 1985; Palis et al., 1997; Polyakov and Lal, 2004a; Kuhn, 2007; Jin et al., 2009; Hu et al., 2013), interrill erosion plots (Lal, 1976; Cogle et al., 2002; Quinton et al., 2006; Rumpel et al., 2006; Lister, 2007; Jin et al., 2008; Brazier et al., 2013; Puttock et al., 2013; Z. Wang et al., 2013; X. Wang et al., 2014c) and at catchment-scales (Starr et al., 2000; Owens et al., 2002; Rhoton et al., 2006; Wang et al., 2010; Nadeu et al., 2011, 2012; Meixner et al., 2012).

Enrichment of OC is important, because it precludes the accurate estimation of chemical fluxes on the basis of mass of sediment eroded and chemical concentration in the contributing soil. Organic C (OC) is typically associated with finer and less dense particles so OC enrichment is thought to depend on the selectivity of the dominant detachment, transport and deposition processes, which varies both spatially and temporally (Owens et al., 2002; Jacinthe et al., 2004; Schiettecatte et al., 2008a; Jin et al., 2008, 2009; Turnbull et al., 2010a; Nadeu et al., 2011, 2012; Hu et al., 2013; X. Wang et al., 2014c). For example, OC enrichment is thought to decrease during higher intensity and magnitude rainstorms, as the dominance of highly selective interrill erosion processes is exceeded by less-selective rill erosion processes (Schiettecatte et al., 2008a; X. Wang et al., 2014c).

Several workers have argued that OC enrichment is not significant as a long-term, large-scale phenomenon, on the basis that: (i) OC enrichment is thought to decrease over increasing spatial scales as the dominance of highly selective interrill erosion processes is surpassed by less selective concentrated flow erosion (Schiettecatte et al., 2008a; Van Oost et al., 2008), (ii) the OC mass balance in the contributing soil is preserved (Hu et al., 2013; Kuhn and Armstrong, 2012), and (iii) sedimentary deposits in lakes and reservoirs often contain OC concentrations near-parity with the contributing topsoils (Ritchie, 1989; Stallard, 1998).

These contentions are however challenged by the knowledge that: (i) rill erosion processes often exhibit at least some selectivity for particle size and density (Parsons et al., 1991, 1994; Malam Issa et al., 2006) and enrichment is observed at catchment-scales (Starr et al., 2000; Owens et al., 2002; Rhoton et al., 2006;

Wang et al., 2010; Nadeu et al., 2011, 2012; Meixner et al., 2012). (ii) The dynamic replacement of OM inputs to the soil surface (cf. Harden et al., 1999; Li et al., 2007; Berhe et al., 2008; Doetterl et al., 2012) could sustain preferential removal of particle-associated OC without depleting the contributing soil, preserving the mass balance. (iii) Without enrichment, deposited sediments should exhibit depletion in OC concentrations relative to the eroding soil. This is because C-rich particles are less likely to be deposited due to relatively low densities and small sizes (Starr et al., 2000; Jacinthe and Lal, 2001; Lal, 2003, 2005; Beuselinck et al., 2000; Schiettecatte et al., 2008b; Nadeu et al., 2011, 2012). Furthermore, the decomposition of mobilized OC is accelerated due to both aggregate disruption during erosion and transport reducing physical protection (Polyakov and Lal, 2004a; Lal et al., 2004a; Lal, 2005; Mora et al., 2007; Schiettecatte et al., 2008a; Jin et al., 2009) and also priming effects arising from the intermixing of younger labile OC with older more recalcitrant OC (Fontaine et al., 2003, 2007; Kuzyakov, 2010; Bianchi, 2011; Mariappan, 2016).

Numerical modelling approaches are a valuable tool to understanding the erosion-induced redistribution of OC over large spatial and temporal scales (Polyakov and Lal, 2004b; Schiettecatte et al., 2008a; Quinton et al., 2014), and are discussed in more detail in section 3.4. The belief that OC enrichment is insignificant has led to numerical model development which either ignores the process of OC enrichment (e.g. Voroney et al., 1981; Mitchell et al., 1998; Fierer and Gabet, 2002; Gabet et al., 2005; Quinton et al., 2014), or which represent it via a single, poorly validated coefficient (e.g. Bouwman, 1989; Lee et al., 1996; Starr et al., 2001). Clearly, there is a need to improve process representation of OC redistribution in numerical models; however, most information on the mechanisms of OC enrichment originates from highly reductionist experiments, often using small plots of homogenised repacked soils with synthetic structure, subjected to artificial rainfall (e.g. Ghadiri and Rose, 1991a, 1991b, Palis et al., 1990a, 1990b; Proffitt and Rose, 1991; Wan and El-Swaify, 1997, 1998; Kuhn, 2007; Schiettecatte et al., 2008a; Jin et al., 2009; Hu et al., 2013; Hu and Kuhn, 2014). Consequently, there are large uncertainties regarding the transferability of knowledge to the redistribution of soil-associated OC in natural ecosystems subject to natural rainfall events (Glenn et al., 1998; Lal et al., 2001a; Polyakov and Lal, 2004b; Kuhn, 2007; Nadeu et al., 2011, 2012; Doetterl et al., 2012). Although many studies have attributed OC enrichment predominantly to the

preferential erosion of fine, OC-rich particles (e.g. Nelson et al., 1994; Balesdent et al., 1998; Guibert et al., 1999; Rhoton et al., 2006; X. Wang et al., 2013), other work has suggested that the enrichment of fine particles alone often cannot explain observed OC enrichment (Sharpley, 1985; Z. Wang et al., 2010; 2013; Chartier et al., 2013). Consequently, there is a clear need for further information to inform mechanistic understanding of entrainment dynamics in a range of environmental settings (cf. Lal et al., 2001a; Polyakov and Lal, 2004b). Information on the distribution of OC across particle size fractions in the near-surface soil will be important for parameterising and evaluating numerical models of erosion-induced OC redistribution.

Standard protocols for measuring soil organic C (SOC) discard the coarse (>2 mm) particle size fraction, assuming it contains no OC (Robertson and Paul, 2000; Lal and Kimble, 2001; Ellert et al., 2001; Bird et al., 2002; Jackson et al., 2002; Lister, 2007; Ewing et al., 2007; Throop et al., 2012a; Sankey et al., 2012; Frank et al., 2012; De Baets et al., 2013; Brazier et al., 2013; Puttock et al., 2013, 2014; X. Wang et al., 2015). Yet work in a variety of environmental contexts has demonstrated that coarse (>2 mm) particles, can contain OC concentrations comparable to the fine (<2 mm) fraction, accounting for as much as 5% of the total SOC pool (Ugolini et al., 1996; Corti et al., 2002; Agnelli et al., 2000, 2002; Han et al., 2016). OC in coarse particles has been observed in both solid particles and stabilised aggregate structures.

In calcareous dryland soils, the precipitation of calcium carbonate can stabilize macro-aggregates (Bryan, 2000; Nash and McLaren, 2003; Alonso-Zarza and Wright, 2010). Such stabilized aggregates may incorporate OC associated with fine particles, or fine particulate organic matter (POM) (Duchaufour, 1976; Goudie, 1996; Baldock and Skjemstad, 2000), particularly as the biochemical actions of roots and fungi facilitate calcium carbonate precipitation in arid soils (Goudie, 1996; Alonso-Zarza and Wright, 2010; Gocke et al., 2011). Therefore, it seems appropriate to re-evaluate the assumption that all coarse (>2 mm) particles contain negligible OC concentrations, and assess whether this assumption may result in underestimation of SOC inventories in calcareous dryland soils.

Research into erosional-induced OC fluxes across the black grama grass to creosotebush shrub ecotone at the Sevilleta has previous reported on 17

rainstorm events during a wetter-than-average monsoon period (Brazier et al., 2013) and 19 events during a dryer-than-average monsoon period (Puttock et al., 2013, 2014). Hillslope processes in these semi-arid ecosystems exhibit high degrees of inter-event variability (cf. Turnbull et al., 2010a, 2011, 2013; Puttock et al., 2013; Brazier et al., 2013; Polyakov et al., 2016), due to sensitivity to temporal variations in factors such as antecedent soil moisture (Loague, 1992; Castillo et al., 2003; Wainwright et al., 2008a; Michaelides et al., 2009; Turnbull et al., 2010a, 2010b), soil surface crusting (Hoogmoed and Stroosnijder, 1984; Luk and Cai, 1990; Moore and Singer, 1990; Belnap, 2006; Baird, 2013) and precipitation characteristics (Wainwright and Parsons, 2002; Wainwright, 2005; Turnbull et al., 2013; Petrie et al., 2014). Therefore, to elucidate the emergent properties of resource redistribution processes in these complex ecosystems it is valuable to analyse large, multi-year assemblages of erosional events (a contention exemplified by Ewing et al., 2007; Raymond et al., 2008).

3.1.2. Objectives

The discussion in section 3.1.1 gives rise to four objectives:

A1 Characterise the distribution of OC across particle-size fractions, in order to:

- **(i) Assess potential OC storage in coarse (>2 mm) particles**
- **(ii) Parameterise a deterministic runoff/erosion model**

A2 Quantify differences in erosion-induced effluxes of OC across an ecotone of changing plant functional types from a grass-dominated to a shrub-dominated ecosystem over four monsoon seasons.

A4 Investigate controls on OC enrichment in natural ecosystems subjected to natural rainfall events, quantifying the extent to which particle size selectivity can explain observed OC enrichment

3.2. Soil Inorganic Carbon

3.2.1. Rationale

Soil inorganic C (SIC) accounts for most of the total C stock in dryland ecosystems (Schlesinger, 1982; Thomas et al., 2014), comprising an estimated 750 X 10^{15} g to 1 700 X 10^{15} g of C (Schlesinger, 1982, 1985; Sombroek et al., 1993; Batjes, 1996; Batjes and Sombroek, 1997; Adams and Post, 1999; Eswaran et al., 2000; Emmerich, 2003; Hirmas and Graham, 2011; Thomey et al., 2014). SIC is the second largest pool of terrestrial C and exists mainly as carbonates, most commonly as calcium carbonate ($CaCO_3$) (Schlesinger, 1982, p. 247; Serna-Pérez et al., 2006). Despite the greater magnitude of SIC relative to the soil organic C (SOC) stocks, SIC is more stable form of C with longer turnover time (Monger and Gallegos, 2000) and consequently the distribution, quantity and dynamics of SIC have historically been seen as less important for understanding contemporary perturbations to the C cycle and received much less attention than organic C (Holmén, 2000; Emmerich, 2003; Wu et al., 2009).

SIC can be classified as either lithogenic or pedogenic inorganic C. Lithogenic SIC is inherited from the parent material of the soil, such as limestone and alluvium. Pedogenic SIC forms in-situ through the precipitation of carbonate, which may in some cases have originated from dissolution of lithogenic carbonates (Emmerich, 2003). Measurements of soil profile ages and carbonate content indicate pedogenic accumulations of SIC in drylands can develop over thousands of years; however, this historical perspective does not provide information on contemporary dynamics (Emmerich, 2003). The formation of pedogenic SIC via carbonate precipitation is thought to be a contemporary process in desert regions receiving ca. < 500 mm of mean annual precipitation and a source of Ca or Mg from a non-carbonate source such as the weathering of Ca/Mg-bearing silicates (Emmerich, 2003; Breecker et al., 2009). However, estimated SIC sequestration rates in dryland soils are extremely uncertain, ranging from 0.1 to 622 g C m^{-2} yr^{-1}, and thus have to potential to represent a substantial global C sink (Gile, 1970; Schlesinger, 1982, 1985; Marion, 1989; Reheis et al., 1995; Stone, 2008; Xie et al., 2009; Breecker et al., 2009). Significant uncertainty persists in fundamental mechanistic understanding of SIC dynamics in dryland soils, particularly with regard to the relative significance of different processes for ecosystem C budgets (Emmerich, 2003; Stevenson and

Verburg, 2006; Stone, 2008; Breecker et al., 2009; Wu et al., 2009; Xie et al., 2009; Schlesinger, 2016).

Globally, the transfer of IC in fluvial runoff represents a small but significant component of the global biogeochemical C cycle, producing a net flux of C from terrestrial to oceanic systems which acts as a sink of atmospheric C (Lal et al., 1999; Holmén, 2000; Mackenzie et al., 2004; Pacala et al., 2007, p. 36; Cai et al., 2008, p. 1539; Raymond et al., 2008; Liu et al., 2010; Ciais et al., 2013). Indeed, increasing the terrestrial-to-ocean carbonate flux has been proposed as a possible geo-engineering solution to sequester atmospheric CO_2, thus mitigating anthropogenic emissions (Archer and Maier-Reimer, 1994; Archer et al., 1998). Liu *et al*. (2010) have argued that inorganic C dynamics play a much greater role in modulating atmospheric C dynamics than is apparent from analysis of riverine effluxes alone, and that carbonate dissolution is more important than silicate weathering as a sink of atmospheric CO_2. Liu *et al*. (2010) also suggest that the magnitude of the CO_2 sink in the global water cycle is likely to increase in the future.

Fluvial transport of IC from terrestrial ecosystems is primarily controlled by drainage basin mineralogy, but other factors such as surficial deposits and pedogenic carbonates are also important. Critically, fluvial transport of IC from terrestrial ecosystems can be substantially altered by changes in precipitation and land-use in river catchments (Cai, 2003; Raymond and Cole, 2003; Oh and Raymond, 2006; Cai et al., 2008; Raymond et al., 2008; Gislason et al., 2009). For example, Raymond *et al*. (2008) found that the hydrogencarbonate flux from the Mississippi, North America's largest river, increased by 46% over the last century, from 0.01 to 0.0146 Pg C yr^{-1}, which they attributed primarily to anthropogenic changes in land use and management. Yet the implications of altered IC fluxes in runoff for oceanic systems are poorly understood. Because the ocean is generally saturated with respect to carbonate above the calcrete saturation depth (typically ~4 km depth), in shallow coastal waters increased influx of carbonate is likely to increase precipitation of carbonate and therefore may not significantly affect the thermodynamic equilibrium of the oceanic carbonate cycle (Holmén, 2000; Sigman and Boyle, 2000; Zeebe and Wolf-Gladrow, 2001; Bianchi, 2007; Engel et al., 2009b, 2009a; Borges, 2011; Zeebe, 2012).

Several workers have argued that inorganic C can be lost from dryland ecosystems subjected to land degradation, through the erosion of topsoil exhuming the carbonate-rich sub-soil (known as caliche, calcretes or a petrocalcic horizon) (Kieft et al., 1998; Lal, 2003; Emmerich, 2003; Adeel et al., 2005, p. 18; Quinton et al., 2010; Thomey et al., 2014). Exhumed SIC may be lost via three potential pathways: (i) carbonates exposed to subaerial processes may react with naturally acidic precipitation, resulting in emission of CO_2 to the atmosphere and (ii) increased production of dissolved inorganic carbon (DIC) exported to fluvial systems. (iii) IC may also be exported in particulate form, via the erosion of particle-associated inorganic C (PIC).

Several studies have sought to test the hypothesis that exhumed calcretes release more gaseous C. Working to understand gaseous C exchanges at grass- and woody shrub-dominated semi-arid sites in Arizona, Emmerich (2003), found a net flux of CO_2 to the atmosphere which was attributed to the large SIC pool. Emmerich (2003) also found indications of a seasonal signal in CO_2 emissions from abiotic processes although this signal was not strong. A detailed subsequent study by Serna-Pérez *et al.* (2006) found no significant differences in the fluxes or $\delta^{13}C$ of emitted CO_2 between sites with relatively 'intact' soils and those with exhumed calcrete horizons, and thus concluded that there was no support for the hypothesis that exhumation accelerates degassing. Stevenson and Verburg (2006) investigated gaseous fluxes of C in Mojave desert soils, and suggested that up to 13% of gaseous C emissions from these soils originated from abiotic processes. In terms of testing the hypothesis that exhumation of carbonates accelerates IC loss from these ecosystems, these studies are equivocal, particularly as all three focus on only the gaseous pathway (acknowledged by Emmerich, 2003; Stevenson and Verburg, 2006).

It is possible, and indeed likely, that some eroded PIC will be subsequently acidified resulting in gaseous C emissions further along the aquatic continuum. There is limited empirical evidence to constrain this process in natural fluvial systems, but Quinton *et al*. (2010) estimated that 10% of the carbonates eroded from Canadian prairies may be acidified releasing a gaseous flux of ca. 0.12 to 1.2 Mg C ha^{-1} yr^{-1}. Many workers have called for more empirical information constraining the stocks and fluxes of soil IC and the processes controlling the transfers of IC between different components of the Earth system, particularly

how SIC is affected by erosional dynamics (Follett et al., 2001; Lal et al., 2001b, 2001a; Lal, 2003; Ogrinc et al., 2002; Emmerich, 2003; Polyakov and Lal, 2004b; Liu et al., 2010; X. J. Wang et al., 2014). There is a paucity of empirical information on the erosion-induced fluxes of IC from dryland ecosystems. As woody shrub encroachment is associated with a significant acceleration in erosion rates (as described in section 1.3.5), it was therefore considered constructive to investigate how the erosion-induced efflux of IC changes across a grass-shrub vegetation transition.

3.2.1. Objectives

B1 Characterise the distribution of IC across particle-size fractions, in order to

(i) Assess potential IC storage in coarse (>2 mm) particles

(ii) Parameterise a deterministic runoff/erosion model

B2 Quantify differences in erosion-induced effluxes of IC across an ecotone of changing plant functional types from a grass-dominated to a shrub-dominated ecosystem over four monsoon seasons.

3.3. Measuring Structure in Semi-arid Rangeland Ecosystems

3.3.1. Rationale

Work across diverse environmental contexts has repeatedly demonstrated the multifaceted interconnections between ecosystem structure and function (Anderson et al., 2010; Turnbull et al., 2010a, 2010c, 2011; Puttock et al., 2013; Luscombe et al., 2014; Grand-Clement et al., 2014). For example, the (abiotic) topographic structure of the land surface and the (biotic) vegetation influences functions such as overland flow routing with implications for runoff generation and associated erosion. The (biotic) vegetation biophysical structure influences functions such as biomass C storage and forage potential (Ludwig et al., 1975; Rango et al., 2006; Muldavin et al., 2008; Allen et al., 2008). Vegetation cover is a major control on the erosion-induced redistribution of soil and associated chemicals, and pertubations in vegetation cover can lead to land degradation (Abrahams et al., 1995; Parsons et al., 1996; Wainwright et al., 1999a, 2000; Müller et al., 2007a; Turnbull et al., 2010a, 2011; Michaelides et al., 2012; Baird, 2013; Puttock et al., 2013, 2014). Detailed mechanistic knowledge of these structural-functional interactions is critical in furthering understanding of both the current services provided by these ecosystems, and improving predictions of how these services may change in the future in response to changes in climatic conditions or community assemblage, for example.

Carbon stored in dryland vegetation represents a globally significant store of C (Rango et al., 2006; Mirik et al., 2013a; Poulter et al., 2014; Ahlström et al., 2015). As discussed in section 1.4, historic changes in biotic structure associated with woody thickening are widely considered to have sequestered globally important, but highly uncertain, quantities of C (Pacala et al., 2001, 2007; Schimel et al., 2001; Gifford and Howden, 2001; Burrows et al., 2002; Henry et al., 2002; Houghton, 2003a; Thomey et al., 2014). Semi-arid vegetation exhibits high levels of inter- and intra-annual variability in aboveground biomass (AGB). For example, AGB has been measured in the spring and autumn at three sites at the Sevilleta LTER, using species-, site-, year-, and season-specific volume-biomass allometric models derived from destructive harvesting (Moore, 2015; Scott Collins, pers. comm. 2015) (Figure 3-1). These data exemplify the necessity for frequent surveys for ecologically useful monitoring of these ecosystems; overall, coefficient of variance (CoV) was 65.3%, 77.5% and 103.8% for the

creosote-dominated, black grama-dominated and blue grama-dominated sites, respectively. Note the period between spring 2011 and spring 2013, during which total AGB remained well below typical levels for a sustained period, due to below average precipitation restricting primary productivity (Petrie et al., 2015). Recent modelling studies have highlighted the highly dynamic role of semi-arid vegetation in the global C cycle, accounting for as much as half of the observed inter-annual variation in the strength of the terrestrial C sink (Poulter et al., 2014; Ahlström et al., 2015). This dynamic role appears to be underrepresented in the state-of-the-art dynamic global vegetation models (DGVM) used in the current generation of Earth surface models (Poulter et al., 2014; Ahlström et al., 2015).

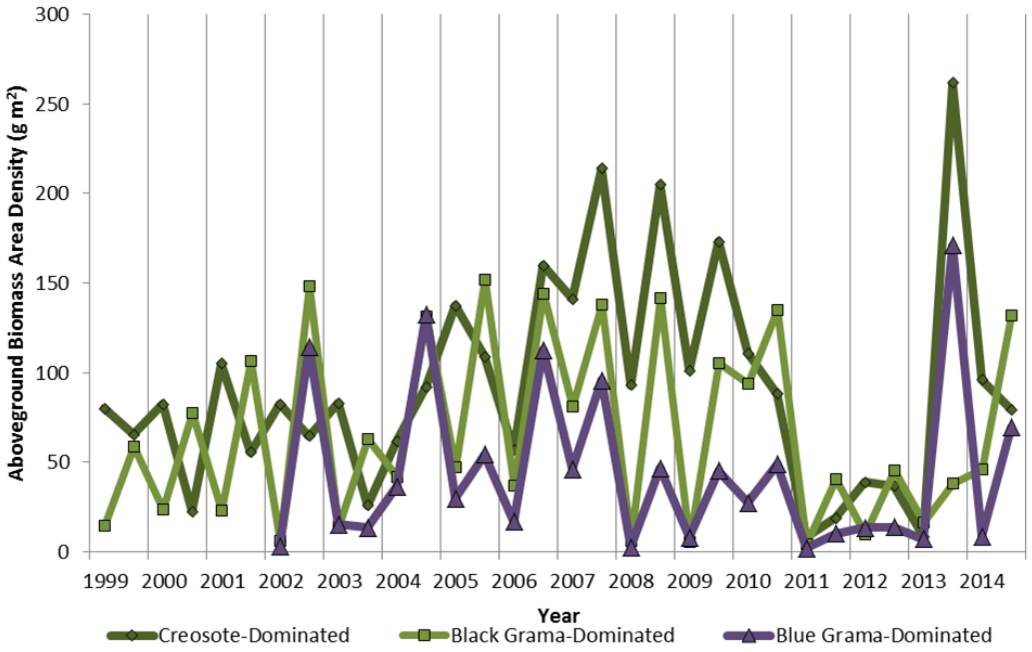

Figure 3-1. Area density of aboveground biomass observed in the spring and autumn at three core monitoring sites at the Sevilleta long-Term Ecological Research Site in central New Mexico (Data from Moore, 2015; Scott Collins, pers. comm. 2015).

The following discussion concentrates on the characterisation of biotic structure in order to infer biomass and associated C storage, but it is constructive to note that information products characterising ecosystem structure can be used for an extensive range of applications, including, but not limited to:

(i) Parameterising and evaluating deterministic models of resource redistribution by runoff and aeolian processes (Parsons et al., 1997; Wainwright et al., 2008a; Turnbull et al., 2010b; Stewart et al., 2014).

(ii) Quantifying ecological responses to changes in temperature, precipitation, fire, grazing or nutrient regimes (Thomas et al., 2008; Zhao and Popescu, 2009; Warne et al., 2010; Antonarakis et al., 2011; Dandois and Ellis, 2013; Petrie et al., 2015; Masubelele et al., 2015).

(iii) Mapping habitat quality and biodiversity (Hansen and Rotella, 2000; Goetz et al., 2007; Vierling et al., 2008; Bergen et al., 2009; Jung et al., 2012; Davies and Asner, 2014; Getzin et al., 2012, 2014; Zahawi et al., 2015; Puttock et al., 2015; Gonçalves et al., 2015),

(iv) Modelling fire behaviour (Akay et al., 2008; Erdody and Moskal, 2010),

(v) Predicting soil properties (Müller et al., 2008; Turnbull et al., 2010c; Croft et al., 2012),

(vi) Investigating concepts of connectivity (McGlynn and Okin, 2006; Mayor et al., 2008; Puttock et al., 2013; Kollongei and Lorentz, 2014; Wester et al., 2014),

Consequently, there is a scientific imperative to quantify biotic structure in semi-arid rangeland ecosystems, in order to elucidate the spatial and temporal dynamics of functions such as biomass C storage. Acquisition of scale-appropriate (*sensu* Asner et al., 2012; Hill et al., 2013) information describing ecosystem structural attributes is essential to develop and validate process understanding, which in turn can support conceptual advances in broad-scale understanding of complex environments (Stewart et al., 2014; Li et al., 2015). For example, by providing new spatial insights useful for evaluating the information content of coarse grained satellite-derived Earth observations. Such information is needed to support sensitive quantification of changes in biomass C stocks following the changes in community dominance associated with woody shrub encroachment.

Direct quantification of AGB via destructive sampling is extremely time and labour intensive, and causes major disturbance which is particularly problematic in marginal semi-arid ecosystems characterised by low recruitment rates (Huang et al., 2007). Therefore, AGB is commonly estimated using allometric size/biomass regression models, derived using observations from limited campaigns of

destructive sampling (e.g. Burk and Dick-Peddie, 1973; Ludwig et al., 1975; Huenneke et al., 2001; Allen et al., 2008; Muldavin et al., 2008). Ground-based monitoring programs employing species-, site-, and year-specific size-biomass relationships (e.g. Huenneke et al., 2001; Herrick et al., 2005; Yao et al., 2006; Allen et al., 2008; Muldavin et al., 2008) can be very accurate, but are labour-intensive and susceptible to under-sampling in spatially heterogeneous ecosystems such as semi-arid rangelands (Elmore et al., 2000; Huenneke et al., 2001; Rango et al., 2006; Allen et al., 2008; Muldavin et al., 2008; Nafus et al., 2009). For example, investigating similar ecosystems in the Jornada, southern New Mexico, USA, Huenneke *et al*. (2001) found that it was necessary to survey 50 quadrats per site to arrive at any confidence in estimate of average above-ground properties, and criticized the paucity of discussion around the adequacy of sample sizes. Comparisons between sites are challenging because there is little by way of standardisation in the techniques for monitoring biomass in drylands, compared with forested ecosystems, for example (Thomey et al., 2014).

Due to these limitations in the coverage extent and comparability of on-the-ground approaches, remotely sensed multispectral image data has been widely employed to characterise ecosystem attributes such as cover and community composition over large extents (Zhang et al., 2003; White et al., 2009). Deriving information on ecosystem structure in drylands from spectral reflectance is complicated by high proportions of high reflectance bare ground, and spectral heterogeneity in the reflectance of low density vegetation cover (Chopping et al., 2006; Huang et al., 2007; Turnbull, 2008; Hufkens et al., 2008; Puttock, 2013; Bryson et al., 2014). Consequently, various classification approaches have been applied, including manual digitisation (Turnbull et al., 2010c; Puttock et al., 2013), object-based (Rango et al., 2006, 2009; Dunford et al., 2009) and supervised machine learning (Mirik et al., 2013b, 2013a), for example. Such spectral classification approaches have fostered new understanding of ecosystems pertaining to hydrological connectivity (McGlynn and Okin, 2006; Puttock et al., 2013), community composition (Ansley et al., 1995; Asner et al., 2003) and AGB estimation for specific species (Ansley et al., 2012; Mirik et al., 2013a). Importantly however, the spectral properties of the ecosystem yield only limited information on many important biophysical attributes, which severely constrains functional inferences (Lisein et al., 2013; Krofcheck et al., 2014; Li et al., 2015). For example, spectral signatures often have only limited correlation with AGB

(Roderick et al., 2000; Friedel et al., 2000; Huang et al., 2007; Meyer et al., 2016). Huang *et al.* (2007) demonstrated that the relationship between canopy cover and AGB can be very sensitive to disturbance history (e.g. grazing or fire), but that this was poorly represented in spectral products which are primarily sensitive to canopy chemistry rather than structure.

Monitoring changes and patterns in three-dimensional (3D) vegetation structure can be more informative to derive functional understanding of ecosystems (Huenneke et al., 2001; Dandois and Ellis, 2010; Vierling et al., 2013; Calders et al., 2015; Cunliffe et al., 2016a). 3D measurements of biotic structure have been widely used to infer biomass and associated C storage (Wang and Glenn, 2008; Thomas et al., 2008; Zhao et al., 2009; Asner, 2009; Frolking et al., 2009; Houghton et al., 2009; Goetz and Dubayah, 2011; Yao et al., 2011; Asner et al., 2012; Hill et al., 2013; Tilly et al., 2015b). Although there have been some attempts to quantify 3D plant structure from spectral radiance (e.g. Chopping et al., 2003, 2004, 2005, 2006), this has proven challenging to interpret and most attempts to characterise ecosystem biotic structure have employed LiDAR technology. A diverse and growing range of LiDAR systems exist, but for the present application a useful distinction can be drawn between two groups of systems, those mounted on the ground and those designed for use on airborne platforms. Ground-based LiDAR systems can only survey a limited spatial coverage (Vierling et al., 2013; Soulard et al., 2013; Sankey et al., 2013, 2015; Olsoy, 2013; Olsoy et al., 2014; Tilly et al., 2015b; Li et al., 2015). Manned aircraft are commonly used as platforms for airborne laser scanners (ALS), which generally yield with typical point densities of < 10 points per 1 m^2 (Rango et al., 2000; Mundt et al., 2006; Streutker and Glenn, 2006; Glenn et al., 2011; Sankey and Bond, 2011; Sankey et al., 2013; Li et al., 2015). Both the spatial resolution (point density) and support (footprint) of ALS are important limitations when characterising the sparse, short-sward vegetation communities which dominate dryland ecosystems. Typical ALS have a support (footprint) of ~0.3 m, which is similar to the crown area of many plants, so individual plants are represented by a small number of points, each with a relatively large degree of uncertainty (Dungan et al., 2002). This is illustrated by the comparisons between estimates of canopy cover derived using ALS versus ground-based LiDAR in a sagebrush dominated system, which revealed that ALS has greatly reduced sensitivity to vegetation below a canopy height threshold of 0.25 m (Li et al., 2015).

Importantly, LiDAR data is also relatively expensive to acquire, which significantly limits its availability (Huang et al., 2009; Erdody and Moskal, 2010; Hellesen and Matikainen, 2013). This cost restricts the spatial extent, spatial resolution and temporal resolution of the available data, which are important limitations because biotic structure in dryland ecosystems is both spatially and temporally highly variable (Huenneke et al., 2001; Hulet et al., 2014; Ahlström et al., 2015). Consequently elucidating complex ecosystem dynamics across vegetation transition zones requires accurate fine-scale data over large spatial extents with multiple observations per year (House and Hall, 2001; House et al., 2003; Huang et al., 2009).

Dryland ecosystems are typically sparsely vegetated, with potential for large changes in vegetation structure over relatively short temporal scales due to wildfires, intensive herbivory or rapid growth following infrequent rainfall events (Friedel et al., 2000; D'Odorico and Porporato, 2006b; Huang et al., 2007) (e.g. Figure 3-1). This ecological dynamism contributes to very large, scale-dependent uncertainties associated with estimates of terrestrial C stocks (Huenneke et al., 2001; Hill et al., 2013) and constraining these uncertainties requires the development of new techniques to measure terrestrial biomass efficiently and accurately at time-steps that are able to capture this dynamism (Strand et al., 2008; Hill et al., 2013; Murray-Tortarolo et al., 2016). Remote sensing approaches to quantifying ecosystem biomass and associated C stocks are subject to significant sources of error, yet these often receive inadequate consideration, leading to high levels of disagreement between remotely sensed estimates of AGB (Chave et al., 2004; Asner et al., 2012; Thomas and Martin, 2012; Hill et al., 2013).

Understanding and reducing the overall uncertainty in the estimated biomass and C stocks requires work to constrain and propagate the various sources of error inherent within each approach, thus informing prioritization of efforts to reduce overall uncertainty by elucidating which sources of error contribute the most to overall uncertainty (Chave et al., 2004; Hill et al., 2013). One component of this is the requirement for cost-effective techniques to quantify ecosystem biotic structure with high sensitivity and temporal frequency, which can be implemented over meso-scale spatial extents, including transitional ecotones between vegetation communities. There is a clear need to refine techniques for accurate

determinations of biophysical ecosystem structure at appropriate measurement scales, which capture the ecological dynamism.

Remotely piloted aerial systems (RPAS) have been heralded as potentially revolutionary tools for ecological surveying, due to their low deployment costs which facilitates the acquisition of fine grain data over substantial spatial extents (Rango et al., 2006, 2009; Anderson and Gaston, 2013; Browning et al., 2015). Despite these claims, there have been surprisingly few demonstrations of RPAS as a *quantitative* survey or monitoring tool, presumably because these technologies are still relatively immature.

One significant development supporting this approach has been the advent of structure-from-motion (SfM) photogrammetry, arising from technological advances in low-cost consumer cameras, RPAS technology and computer vision algorithms (Westoby et al., 2012). SfM can reconstruct 3D models from convergent image data, and scientific understanding of the information content of SfM-derived point clouds is rapidly developing (e.g. James and Robson, 2012, 2014; Dandois and Ellis, 2013; Tonkin et al., 2014; Smith and Vericat, 2015; Tuominen et al., 2015; Nouwakpo et al., 2015). Environmental applications of RPAS SfM have mostly been limited to surveying abiotic structure, such as bare surfaces for geomorphological analysis (e.g. James and Robson, 2012; Westoby et al., 2012; Mancini et al., 2013; Kaiser et al., 2014; McShane et al., 2014; Hackney and Clayton, 2015; Smith and Vericat, 2015). In contrast, the potential for RPAS SfM to characterise ecosystem biotic structure has received relatively little attention. Indeed, to date most SfM practitioners have actively avoided vegetation, due to the perceived difficulties associated with producing and analysing SfM-derived points clouds of scenes containing vegetation (e.g. Remondino et al., 2014).

Although the potential of RPAS-acquired SfM to survey vegetation has been demonstrated for tree-dominated ecosystems (Dandois and Ellis, 2010, 2013; Lisein et al., 2013; Zahawi et al., 2015; Dandois et al., 2015; Puliti et al., 2015), previous work has suggested that SfM modelling of RPAS-acquired image data was not yet suitable for measuring the structure of small plants, such as grasses, due to limitations with the accuracy of the derived canopy height models (CHMs) (Zahawi et al., 2015). Errors in SfM-derived models depend greatly on the quality of geometric control constraining the reconstruction (Puliti et al., 2015; Shahbazi

et al., 2015), and further refinement of the technique was needed to improve measurement accuracy of RPAS SFM approaches to support application to ecosystems dominated by short-sward vegetation (cf. Lisein et al., 2013; Zahawi et al., 2015). Applications of RPAS SfM have generally sought to acquire nadir image data, which is often suggested to reduce distortion (e.g., Dandois and Ellis, 2010, 2013; Dandois et al., 2015; Tonkin et al., 2014; Zahawi et al., 2015). While the acquisition of nadir image data may be necessary for particular applications, such as correcting for refraction in the production of bathymetric maps (Woodget et al., 2015), the inclusion of convergent (non-nadir) image data has recently been shown to significantly improve the accuracy of SfM photogrammetric reconstructions (James and Robson, 2014; Smith and Vericat, 2015; Shahbazi et al., 2015).

Consequently, it is both timely and highly appropriate to investigate whether the data acquisition and SfM modelling workflow could be improved to characterise the biotic structure of short-sward ecosystems at hitherto inaccessible combinations of spatial extent and grain. Workflows demonstrating the efficient acquisition such spatially explicit data products will provide an essential foundation for efforts to better understand drylands ecosystems in a variety of ways. This includes better knowledge of the sensitivities of dryland ecosystems to various environmental drivers, and better knowledge of the information content of coarse grained but globally available observations from space-borne Earth observation sensors. Such knowledge can support the robust evaluation and development of more accurate models of the C dynamics of these ecosystems, suitable for application at global scales.

3.3.2. Objectives

C1 Develop RPAS SfM remote sensing techniques to measure the abiotic and biotic biophysical structure of semi-arid rangeland ecosystems

C2 Estimate biomass and associated C storage at measurement scales which bridge the gap between on-the-ground and satellite-based measurements

C3 Produce fine-scale digital maps describing topography and vegetation cover to parameterise spatially-explicit process-based numerical models

3.4. Modelling the Redistribution of Particle-Associated Carbon

3.4.1. Rationale

As has been discussed in the preceding chapters, the C dynamics of dryland ecosystems are controlled by a range of different processes, which interact in a myriad of complex ways. One important area of uncertainty in terrestrial C dynamics pertains to the effects of land degradation particularly through soil erosion on C stocks and fluxes (Polyakov and Lal, 2004b; Quinton et al., 2006). Substantial non-linear scale dependencies in water-mediated hillslope erosion processes preclude simple extrapolations from plot-scale observations to landscape-scales (for further discussion of these scaling issues, see Parsons et al., 2006; Brazier et al., 2007, 2011; Cerdà et al., 2013). Improving understanding the net influence of erosion on terrestrial C dynamics requires better understanding of these individual processes, their interaction across different spatial and temporal scales, and how they differ with environmental setting (Lal, 2003; Van Oost et al., 2005, 2008; Lal and Pimentel, 2008).

Numerical modelling approaches offer a valuable means of formalising these process interactions into a useful framework, and are essential for developing robust understanding of how ecosystems are likely to respond to future changes in environmental conditions (Polyakov and Lal, 2004b; Wainwright and Mulligan, 2013a). Numerical modelling approaches can take a variety of forms, with process-based models valued for their capacity to support the development and testing of hypotheses regarding such process interactions in complex ecogeomorphic systems and across spatio-temporal scales that are challenging to observe directly (Post et al., 2001; Michaelides et al., 2009; Turnbull et al., 2010b, 2014a; Beven and Brazier, 2011; Wainwright and Mulligan, 2013b). In contrast to modelling approaches which focus more on prediction, the capacity of deterministic models to support explanation has been argued to support better mechanistic understanding of environmental systems (Wainwright and Mulligan, 2013a).

This theme of this thesis contributes towards the ongoing development and evaluation of spatially-explicit process-based modelling approaches which integrate hydrological, geomorphological and ecological processes (*sensu* Nouvellon et al., 2001; Turnbull, 2008; Turnbull et al., 2014a). Significant progress has been made with developing such integrated models, which are

being used for a range of numerical experiments to better understand the likely implications of environmental change (e.g. Stewart et al., 2014; Müller et al., In Review).

The model selected for use in this experiment was MAHLERAN, a deterministic hydrologic, soil erosion and chemical transport model developed by John Wainwright and various collaborators (Wainwright et al., 2008b, 2008a, 2008c). A full description of this model structure and its development is presented in Section 9.4. It is constructive to note that MAHLERAN and its constituent routines are being used by a number of researchers internationally for investigations into hydrology, geomorphology, ecology and long-term environmental change (e.g. Wainwright et al., 2008a, 2008b, 2008c; Tatard et al., 2008; Turnbull et al., 2010b, 2014a, 2014b; Cooper et al., 2012; Stewart et al., 2014; Müller et al., 2007a, In Review; Hewett et al., In Prep). Consequently, advancing understanding of the capabilities and limitations of this particular model structure with regards to simulating the redistribution of soil C in drylands is of benefit to a wide community of scientific users.

MAHLERAN's structure has been evaluated against a number of observational datasets quantifying the movement of (i) water (Wainwright and Parsons, 2002; Wainwright et al., 2008a, 2008b; Turnbull et al., 2010b), (ii) sediment (Wainwright et al., 2008a, 2008b; Tatard et al., 2008; Turnbull et al., 2010b; Cooper et al., 2012), and (iii) nutrients in dissolved and particle-associated forms (Turnbull et al., 2010b). These evaluations have shown that MAHLERAN's hydrological component generally performs reasonably well. The sediment transport component usually predicts sediment yields of the correct order of magnitude and relative magnitude between different events, although the predictions of particle size distributions of eroded material are often poor. The predictive accuracy of the particle-associated chemical transport component depends greatly on the accuracy of the sediment transport component, when the letter performs well, so does the former. The dissolved chemical transport model, used to simulate the transport of nutrients such as nitrogen and phosphorous, performs poorly (Turnbull et al., 2010b).

An essential first step in understanding the impact of erosion on soil C dynamics is understanding the erosion-induced transport of soil-associated C, and several workers have called for efforts to improve numerical representations of C erosion

by interrill processes (e.g. Polyakov and Lal, 2004b; Kuhn et al., 2009). Investigations into the impact of soil erosion on terrestrial C dynamics have predominantly focused on intensively-managed landscapes, where soil erosion rates are often accelerated through anthropogenic activities (e.g. Bauer and Black, 1981; Gregorich, 1996; Gregorich et al., 1998; Manies et al., 2001; Van Oost et al., 2004, 2005, 2007; Jarecki et al., 2005; Quinton et al., 2006, 2010; Meersmans et al., 2009; Viaud et al., 2011; Zhang and Li, 2013). This focus has perhaps been the result of a combination of accessibility to researchers, history of perturbation and potential for better process understanding to inform future landscape management practices to control SOC dynamics. The focus on this environmental context has also been reflected in efforts to represent the effects of soil erosion on soil C dynamics in numerical models (e.g. Andrén and Kätterer, 1997; Govers et al., 1999; Harden et al., 1999; Van Oost et al., 2005; Quinton et al., 2006; Lacoste et al., 2015), although see Fierer and Gabet (2002) and Gabet *et al.* (2005) for examples from a semi-natural dryland ecosystem. Most of the terrestrial surface is however, not intensively cultivated, and understanding of key processes is not always directly transferable between environmental contexts (Parsons et al., 1991; Bryan, 2000; Mayeux, 2001; Liao et al., 2006a; Martinez et al., 2010). Therefore, it is valuable to evaluate the transferability of mechanistic understanding of C redistribution by interrill processes to more natural ecosystems.

The primary objective of this modelling exercise is to evaluate the capacity of MAHLERAN's model structure to simulate the erosional redistribution of inorganic and organic forms of particle-associated C in drylands. While earlier applications of this model structure have included simulation of the erosional redistribution of total C (Turnbull, 2008), observational data was not previously available to evaluate the model performance. Carbon storage in dryland ecosystems is dominated by the IC pool, which is generally more stable than organic physiochemical forms of C (Batjes, 1998; Eswaran et al., 2000; Lal, 2004c). Mechanistic understanding of IC dynamics is more limited relative to OC, but IC dynamics may also partly mediate OC dynamics in drylands (as discussed in sections 3.1.1 and 3.2.1) and several workers have suggested that soil erosion may substantially influence IC dynamics (e.g. Lal, 2001d; Emmerich, 2003).

Within MAHLERAN's structure, the erosional redistribution of IC and OC is calculated as a function of simulated sediment flux, which in turn depends on the simulated hydrology. Predictions of OC flux on the basis of sediment flux are often poor, because eroded sediments are usually enriched in OC relative to the contributing soil (discussed in detail in sections 3.1 and 6.5). OC enrichment is often ignored in numerical models (e.g. Voroney et al., 1981; Mitchell et al., 1998; Fierer and Gabet, 2002; Quinton et al., 2014), or is sometimes represented via a single poorly validated coefficient (e.g. Bouwman, 1989; Lee et al., 1996; Starr et al., 2001; Quinton et al., 2006). Inadequate representation of OC enrichment in erosion models is problematic because it can lead to underestimation of both erosion-induced OC effluxes from terrestrial ecosystems, and inputs of C to aquatic ecosystems and depositional sites. These shortcomings can make it difficult to reconcile knowledge of various components of the C cycle. This numerical experiment will qualify the extent to which the current model structure represents OC enrichment due to particle size selectivity, and reproduces observed OC yields at hillslope scales.

Simulated C fluxes within MAHLERAN's structure depend on simulated sediment fluxes, which in turn depend on the simulated hydrology. Given this chain of dependency, it is important to understand the performance of each of the preceding component(s). As described above, MAHLERAN's structure has been extensively evaluated by others. However, it is constructive to ensure that modelling approaches are continually confronted with the best available empirical information (Brazier et al., 2000).

Hillslope processes during rainstorm events are highly sensitive to temporally-variable conditions including the antecedent soil moisture (ASM) content, soil structure (including crusting) arising from previous precipitation events and thermal cycling, and the precipitation intensity (Wainwright and Parsons, 2002; Castillo et al., 2003; Turnbull et al., 2010b). These conditions can result in substantial temporal variations in the dynamics of (i) runoff hydrology (Hoogmoed and Stroosnijder, 1984; Martinez-Mena et al., 2001; Wainwright and Parsons, 2002; Yair and Raz-Yassif, 2004; Bochet et al., 2006; Parsons and Stone, 2006; Truman et al., 2007; Lister, 2007; Turnbull, 2008; Turnbull et al., 2010a, 2010b, 2013; Puttock, 2013), (ii) erosion processes (Martinez-Mena et al., 2001, 2012; Bochet et al., 2006; Parsons and Stone, 2006; Truman et al., 2007; Turnbull,

2008; Turnbull et al., 2010a; Puttock, 2013; Ziadat and Taimeh, 2013), and (iii) erosion-induced transport of particle-associated chemicals such as C (Quinton et al., 2006; Truman et al., 2007; Jin et al., 2009; Turnbull et al., 2011; Martinez-Mena et al., 2012; Hu et al., 2013; Brazier et al., 2013; Cunliffe et al., 2016d).

This variability in hillslope response is an important consideration when evaluating model structures, as evaluation against a single rainstorm can only reveal the model performance under a single set of specific conditions. The inherent variability in hillslope response means that using larger and more representative assemblages of rainstorm events yield more robust evaluations of model structures (sensu Turnbull et al., 2010b). Meta-analysis of model performance against an assemblage of varied events elucidates model performance under a wider range of conditions, which may (or may not) provide confidence in the capacity of the model structure to produce predictions that are behavioural across the range of conditions likely to be encountered in a natural environment. Multi-event evaluations will normally yield more sensitive and nuanced appraisals as to the strengths and weaknesses of model structures.

Consequently, it is desirable to evaluate model performance with regards to observational data from the largest and most representative assemblages of rainstorm events which can be obtained. Using data from previous monitoring (Turnbull, 2008; Puttock, 2013), an assemblage of up to 59 rainstorm events from both wetter- and dryer-than-average monsoon periods is available. This new assemblage is 55% larger than the largest previous event assemblage used to evaluate MAHLERAN's model structure (Turnbull et al., 2010b).

Across vegetation transition from grass-dominated to shrub-dominated ecosystems there are significant differences in the hydrological and erosional responses to rainstorm events, which result in large differences in erosion-induced fluxes of IC and OC (Brazier et al., 2013; Cunliffe et al., 2016d) (chapters 1.4, 6 and 7). MAHLERAN will be evaluated against observations of hydrological, erosional and carbon flux data from four sites across a grass-shrub ecotone, using data and samples collected by previous monitoring (as described in section 4.3.4). This experimental design supports testing of the model structure under different conditions and as erosion rates increase (Turnbull, 2008; Turnbull et al., 2010b).

An important motivation for this evaluation exercise was to improve confidence of the capacity of MAHLERAN's deterministic process representations to reproduce hillslope processes over the observable spatial (hillslope) and temporal (event) scales considered herein. While it is well understood that models which perform well at one spatio-temporal scale are no guarantee of model performance at other spatio-temporal scales, such appraisals provide an important foundation to the application of these process representations over greater spatio-temporal scales (Müller et al., 2014b). This is particularly valuable given growing appreciation that erosion during discrete, runoff-producing rainfall events is an important component of long-term landscape evolution which is poorly reproduced by generalised geomorphic transport laws (Michaelides and Martin, 2012). A continuous version of MAHLERAN is already being used for such spatio-temporally upscaled ecogeomorphic modelling experiments (Stewart et al., 2014; Müller et al., In Review).

An final noteworthy limitation of deterministic modelling approaches is their typically high requirements for parameterisation data, and MAHLERAN is no exception to this (Merritt et al., 2003; Brazier et al., 2003; Hairsine and Sander, 2009; Smith et al., 2010; Nunes and Nearing, 2011). This limitation, at least for topographic, surface cover and biomass parameters, is partly addressed through the development of a novel approach using proximal remote sensing to efficiently acquire spatially-explicit parameterisation data in chapter 8 (Cunliffe et al., 2016b).

3.4.2. Objectives

D1 Evaluate MAHLERAN's simulation of the hydrology of natural runoff events at hillslope-spatial and event-temporal scales.

D2 Evaluate MAHLERAN's simulation of the erosion of sediment during natural runoff events at hillslope-spatial and event-temporal scales.

D3 Evaluate MAHLERAN's simulation of the erosion of particle-associated IC during natural runoff events at hillslope-spatial and event-temporal scales.

D4 Evaluate MAHLERAN's simulation of the erosion of particle-associated IC during natural runoff events at hillslope-spatial and event-temporal scales.

4. Conceptual Approach and Study Site

This chapter describes the conceptual approach and study sites used to investigate the objectives identified in Chapter 4.

4.1. Conceptual approach: Ergodic hypothesis

The slow rate of processes responsible for differences in C dynamics between grass- and shrub-dominated ecosystems, operating over multi-decadal timescales, means that it is difficult to undertake fully longitudinal research on the ecogeomorphic implications of woody shrub encroachment. Consequently, "space-for-time" substitutions using an ergodic hypothesis are frequently used to overcome the disparity between long (decadal-centennial) ecological timescales and short (annual to sub-decadal) observational timescales (e.g. Wainwright et al., 2000; Lett et al., 2004; Liao et al., 2006b, 2006a; Turnbull, 2008; Turnbull et al., 2010c, 2010a, 2011, Puttock et al., 2013, 2014; Jandl et al., 2014). Under the assumption that chronosequence sites differ only by age and are otherwise identical, chronosequences allow for the effect of time on selected properties to be investigated. For further discussion of the implications of such space-for-time substitutions, see Forester and Tilman (2000), Walker *et al.* (2010) and Jandl *et al.* (2014).

4.2. Vegetation Communities Studied

Grass- and shrub-dominated rangelands are the most prevalent land cover in the Western United States, together occupying ca. 60 % of the total area (Zhu and Reed, 2012). Black grama (*Bouteloua eriopoda*) is a typical perennial bunchgrass, common on rocky or sandy mesas with well-drained coarse soils (Humphrey, 1958) and is dominant over many of the hot desert grasslands of the southwestern USA including much of the Chihuahuan desert (Nelson, 1934; Paulsen and Ares, 1962; Smith et al., 1996; Peters, 2002; Yao et al., 2006). Black grama grass is a particularly important species providing forage for livestock in the semi-arid southwestern USA (Nelson, 1934; Canfield, 1939; Paulsen and Ares, 1962).

Creosotebush (*Larrea tridentata*) is a drought-tolerant evergreen shrub, found throughout the Mojave, Sonoran and Chihuahuan deserts of North America (Barbour, 1969), where it is often the dominant or co-dominant species

(Humphrey, 1958; Chew and Chew, 1965; Huenneke et al., 2001; Allen et al., 2008; Muldavin et al., 2008). Creosote generally occurs in sparsely vegetated areas, but also occurs as a transitional species in desert grassland communities (Humphrey and Mehrhoff, 1958), commonly growing on calcareous, sandy soils that are underlain by a caliche hardpan (Went and Westergaard, 1949). Creosotebush is a long-lived species (ca. 400 years) (Moreno-de las Heras et al., 2016) and there are at least three distinct chromosomal races of creosotebush: *diploids* in the Chihuahuan Desert, *tetraploids* in the Sonoran Desert, and *hexaploids* in the Mojave desert (Yang and Lowe, 1968; Barbour, 1969; Yang, 1970; Hunziker, 1975; Laport et al., 2012). Creosotebush canopies frequently grow in the form of an inverted cone (Chew and Chew, 1965; Ludwig et al., 1975; De Soyza et al., 1997; Wainwright et al., 1999a; Abrahams et al., 2003; Dodson, 2012), particularly in more arid environmental settings such as the Chihuahuan desert where the redirection of stemflow following raindrop interception is thought to optimise the acquisition of limited water resources (De Soyza et al., 1997).

Piñon-Juniper (P-J) woodland is the third most extensive biome in the United States (Huang et al., 2009; Hulet et al., 2014). Piñon-Juniper are dynamic ecosystems, thought to be highly sensitive to climatic changes (Krofcheck et al., 2014), and have been widely observed to be undergoing range expansion and woody thickening over the last 150 years. This woody thickening has important implications for both forage potential (Pieper, 1990) and ecosystem C storage (Strand et al., 2008; McKinley and Blair, 2008; Huang et al., 2009; Sankey et al., 2013).

4.3. Study Area: Sevilleta National Wildlife Refuge

4.3.1. Locational and historical context

This study was undertaken at the Sevilleta National Wildlife Refuge (SNWR), situated in central New Mexico (34°19' N, 106°42' W), at the northern margin of the Chihuahuan desert, which is the largest desert region of North America (Aide and Van Auken, 1985). The SNWR encompasses a transition zone between several major biomes: Chihuahuan Desert warm-temperate desert grassland and shrubland to the south, Great Plains cool shrub steppe to the north, Piñon-Juniper woodland in the upper elevations of the neighbouring mountains, Colorado Plateau shrub-steppe to the west, and riparian vegetation along the middle Rio Grande Valley.

The SNWR was grazed by cattle for at least 37 years prior to its designation as a wildlife refuge in 1973. In 1988 it was established as a Long Term Ecological Research (LTER) site run by the University of New Mexico (UNM) in partnership with the USA Fish and Wildlife service (Gosz, 1993). As an LTER site for 30 years, the SNWR has been subject of extensive research activity, affording a wealth of knowledge which supports the present study[1].

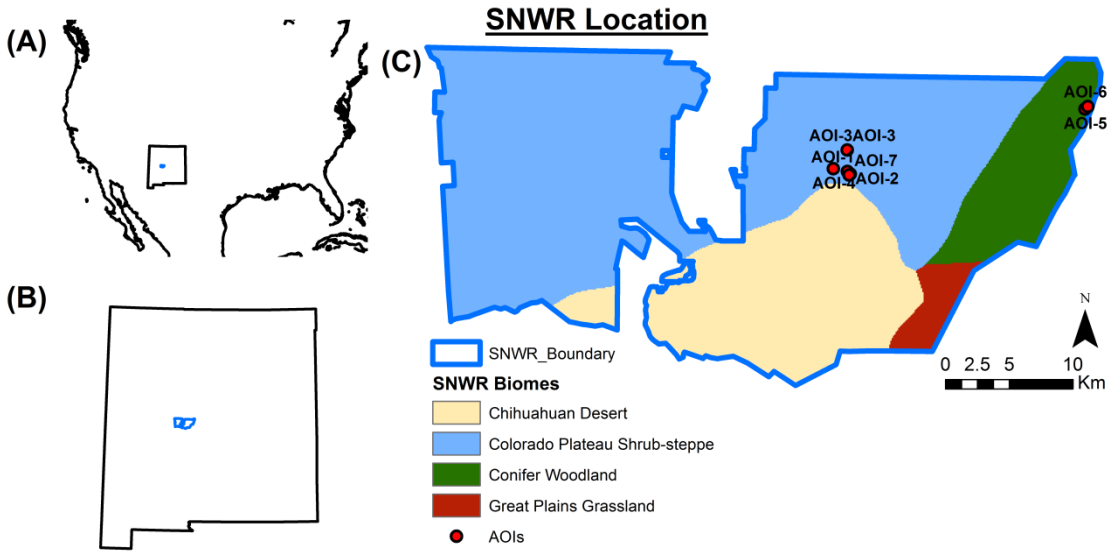

Figure 4-1. Location of the study sites: (A) locations of the Sevilleta National Wildlife Refuge (SNWR) within the USA and (B) New Mexico. (C) Location of the seven AOIs within the SNWR and coarse map of vegetation cover, Derived from 0.5 ha NDVI Thematic mapper image data 1987-1993 (http://sev.lternet.edu).

[1] Although note the SNWR is scheduled to be discontinued from the LTER network from 2017.

4.3.2. Climatic context

The SNWR experiences a semi-arid climate, with hot summers and cold winters. Around 60% of the precipitation falls as intense convectional rainfall in a summer monsoon period (late-June to September), and in the McKenzie Flats mean annual precipitation (MAP) is ca. 250 mm, although this is highly variable though time and space (Dahm and Moore, 1994; Turnbull et al., 2010c; Petrie et al., 2014). As is typical for drylands, precipitation follows a gamma distribution, meaning that most years are dryer than the arithmetic mean (Ehleringer, 2001). The main limiting resource on ecological processes in this setting is water availability (Puttock, 2013).

Over southwestern North America, there is high temporal variability in precipitation over seasonal, annual and decadal time-scales. This variability exhibits spatial correlation, with large regions experiencing broadly similar precipitation patterns. Central New Mexico is affected by three major climate cycles: (i) North American Monsoon (NAM), (ii) El Niño Southern Oscillation (ENSO), and (iii) Pacific Decadal Oscillation (PDO) (Cable, 1975; Ropelewski and Halpert, 1986; Dahm and Moore, 1994; Reynolds et al., 2000; Gutzler et al., 2002; Milne et al., 2003; Wainwright, 2005; Petrie et al., 2014). NAM regulates summer monsoonal rainfall, which is delivered by convective cells as high-intensity, short-duration spatially localised events (Adams and Comrie, 1997; Stursova et al., 2006; Wainwright, 2005; Petrie et al., 2014). ENSO regulates variability in winter precipitation, typically as frontal systems. ENSO events typically occur event 3-4 years, usually last only through one inter-season, and winter precipitation is higher and lower during El Niño and La Niña periods, respectively (Ropelewski and Halpert, 1986; Dahm and Moore, 1994; Schubert et al., 2004, 2010; Wainwright, 2005; Seager et al., 2005; Herweijer et al., 2006). Oscillating on approximately 50-year cycles, the PDO modulates the magnitude of ENSO events and may cause periodic, extended, severe regional droughts (Latif and Barnett, 1996; Cayan et al., 1998; Gutzler et al., 2002; Milne et al., 2003).

Environmental proxies (mineralogy, pollen and charcoal) from the mid-Holocene indicate drought cycles with a 100-130 year periodicity in the southwestern USA, causing periodic vegetation change (Clark et al., 2002). The most extreme drought in the 300 year proxy records at the Sevilleta occurred between 1942 and 1957, and resulted in broadscale plant mortality (Petrie et al., 2014). Petrie

et al. (2014) analysed historical patterns of monsoon precipitation in the Northern Chihuahuan Desert around the SNWR from 22 climate stations over the past 100 years. Over this time frame they found a slight increase in precipitation frequency, a slight decrease in mean event size, and no change in MAP regionally. At the local scale, spatial variability in precipitation totals is about 50% from place to place, and the difference between very wet and very dry monsoon seasons typically resulted from a small number of large events. The longest dry periods are increasing (from 38 days in 1910 to 46 days in 2010). Petrie *et al*. suggested that this high degree of spatial variation in precipitation is likely to mean that these ecosystems are probably more resilient to climate change projections than commonly thought, because they are already frequently subjected to the degrees of aridity projected by climate models.

Looking forward, climate models generally predict that the southwest USA will become hotter than present, in terms of average, maximum and minimum temperatures (Seager et al., 2007; Gutzler and Robbins, 2011; Deser et al., 2012). Projections of precipitation are more uncertain than temperature, but the models consistently predict that the southwest USA will become dryer and received more variable precipitation (Seager et al., 2007, 2013; Seager and Vecchi, 2010; Gutzler and Robbins, 2011; Deser et al., 2012; Mearns et al., 2012). Modelling work has also predicted a substantial shift in the seasonal distribution of precipitation, with reduced winter and early monsoon precipitation and increased late monsoon precipitation inputs (Seager and Vecchi, 2010; Cook and Seager, 2013). Such changes in the seasonality of precipitation would have substantial biological impacts in these water-limited ecosystems, particularly given the differences in water utilization between different plant functional types (Cook and Seager, 2013).

4.3.3. Shrub encroachment at the SNWR

Long-term ecological monitoring in the Rio Grande basin around the SNWR has indicated large areas which were formerly dominated by perennial bunchgrass, mainly black and blue grama (*B. eriopoda* and *B. gracilis*) but which are now dominated by woody shrubs, particularly creosotebush (*L. tridentata)*. These changes have occurred over the last 150 years, and are inferred from several lines of evidence:

(i) anecdotal evidence of change in community dominance in historical accounts from 1858 to 1963 (Buffington and Herbel, 1965);

(ii) aerial photographs show expansion and consolidation of shrubs into grasslands between 1935 and 1984 (Gosz, 1993);

(iii) differences in carbon fractionation between the C4 photosynthetic pathway used by grama grasses and the C3 photosynthetic pathway used by creosotebush shrubs means SOC $\delta^{13}C$ carbon signatures can be used to provenance OM. Analysis of samples from several stages across grass-shrub ecotone supports the interpretation that creosotebush occupies soils that were once dominated by grasses (Turnbull et al., 2008a; Puttock et al., 2012b);

(iv) inferences from the $\delta^{13}C$ analyses have been corroborated by recent work using n-alkane lipid biomarkers (Puttock et al., 2014).

Although some workers have suggested that woody shrub encroachment at the Sevilleta is an ongoing process (e.g. Gibbens et al., 1992; Beck et al., 1999), it appears to be highly episodic and non-continuous, depending on specific climatic conditions for seedling recruitment (Moreno-de las Heras et al., 2016).

4.3.4. Study sites

The grass-shrub ecotone investigated for the soil OC and IC and modelling components of this study is located within the Five Points area of the McKenzie Flats (34°19’ N, 106°42’ W). The McKenzie Flats is a large area of ~50 km^2 in the eastern SNWR, located between the Los Piños Mountains and the Rio Grande to the east and west respectively, and Highway 60 and Palo Duro Canyon to the north and south respectively. The McKenzie Flats have an average slope gradient of 1%, and drain into Palo Duro Canyon, an ephemeral tributary of the Rio Grande (Puttock, 2013).

Soils at all sites are classified as Turney Loams. They are shallow, alkaline sandy loams with <10% clay content (Moreno-de las Heras et al., 2016), overlying a well-developed calcium carbonate horizon typically 0.2 to 0.45 m below the soil surface (Kieft et al., 1998; Rawling, 2005; Turnbull et al., 2008a), although in places this horizon has been exhumed by erosion (Buxbaum and Vanderbilt, 2007). Less-cemented layers are known as caliche or calcic horizons while highly indurated layers are referred to as calcrete or petrocalcic horizons (Schlesinger, 1982). At Deep Well, the nearest meteorological station to the study area, the mean July maximum and mean January minimum temperatures are 33.6°C and -7.1°C, respectively (Turnbull, 2008).

Investigations of differences in structure and function between plant functional types (PFT) have commonly only compared end-member vegetation assemblages. An important limitation of such binary approaches is that they fail to elucidate the nature of the transition between dominant PFTs, which impedes examination of feedbacks potentially controlling the vegetation transition (Martinez-Meza and Whitford, 1996; Wainwright et al., 2000; Turnbull et al., 2008b). Investigating intermediary plots in addition to end-member sites supports more nuanced understanding of how ecosystem structure and function changes across ecotones (Neave and Abrahams, 2002; Turnbull, 2008; Turnbull et al., 2011, 2010a, 2010c; Brazier et al., 2013; Moreno-de las Heras et al., 2016).

For the lateral redistribution of IC and OC, four sites were examined across a grass-shrub ecotone from black grama (*B. eriopoda*) dominated communities to creosotebush (*L. tridentata*) shrub dominated communities. These sites were selected to examine interactions between surface vegetation cover and ecosystem functioning, so were selected to be topographically similar, with planar slopes (Turnbull et al., 2010b). Figure 4-2 illustrates the sites, where area of interest (AOI)-1 corresponds to the ‘grass’ site, AOI-2 corresponds to the ‘grass-shrub’ site, AOI-3 corresponds to the ‘shrub-grass’ site, and AOI-4 corresponds to the ‘shrub’ site. The vegetation transitions zones characterised at these sites are representative of the grass-woody transitions occurring across large swathes of the basin and range topography of the semi-arid southwest USA.

At each site, a 300 m^2 (30 m × 10 m) runoff plot was constructed by Dr Laura Turnbull in 2005 as part of her doctoral research into changes in ecosystem structure and function across this grass shrub ecostone (Turnbull, 2008). These

runoff plots were then monitored over four summer monsoon seasons, during rainstorm events which resulted in runoff and erosion (Turnbull, 2008; Puttock, 2013). Previous work across this same grass-shrub ecotone has examined differences in abiotic and biotic ecosystem structure (Turnbull et al., 2010c; Puttock et al., 2013), hydrology and sediment dynamics (Turnbull et al., 2010a, 2010b), nitrogen and phosphorus dynamics (Turnbull et al., 2011), seed banks and seedling recruitment dynamics (Moreno-de las Heras et al., 2016) and some investigation of C dynamics (Turnbull et al., 2008a; Puttock et al., 2012b, 2013, 2014; Brazier et al., 2013). Working at these sites provides an opportunity to build upon knowledge previously obtained about the relationships between ecosystem structure and function at this location.

This experimental design enables comparison of key features of ecosystem structure and functions across the grass-shrub ecotone and thus investigation into the patterns and processes. Inherent scale-dependencies of water, sediment and nutrient fluxes mean that the erosion-induced C yields observed from these runoff plots cannot be linearly extrapolated between spatial scales without a very high degree of uncertainty (Parsons et al., 2006; Brazier et al., 2007; Wainwright et al., 2008c).

For the remote sensing component of this study, seven areas of interest (AOIs) were examined, covering a combined area of 9.8 ha within the SNWR. AOIs-1 to -4 correspond to each site across the grass shrub ecotone, encompassing the (300 m^2) runoff plots but also but also ca. 2000 m^2 of their surrounding landscape in order to obtain a more representative characterisation of the ecosystem structure at these sites. AOIs 5 and 6 are situated in piñon-juniper (P-J) woodland on the Los Pinos Mountain range, and are dominated by an overstory of one-seed juniper (*Juniperus monosperma*) with black grama-dominated understory. These sites have a MAP of 326 mm (Gaylord et al., 2013; Plaut et al., 2013; Pangle et al., 2015), and are described further by Puttock (2013; Puttock et al., 2013, 2014). AOI-7 is a larger site of mixed grass-shrubland, adjacent to AOI-2, which encompasses a boundary of a historic wildfire (discussed further in section 8.6).

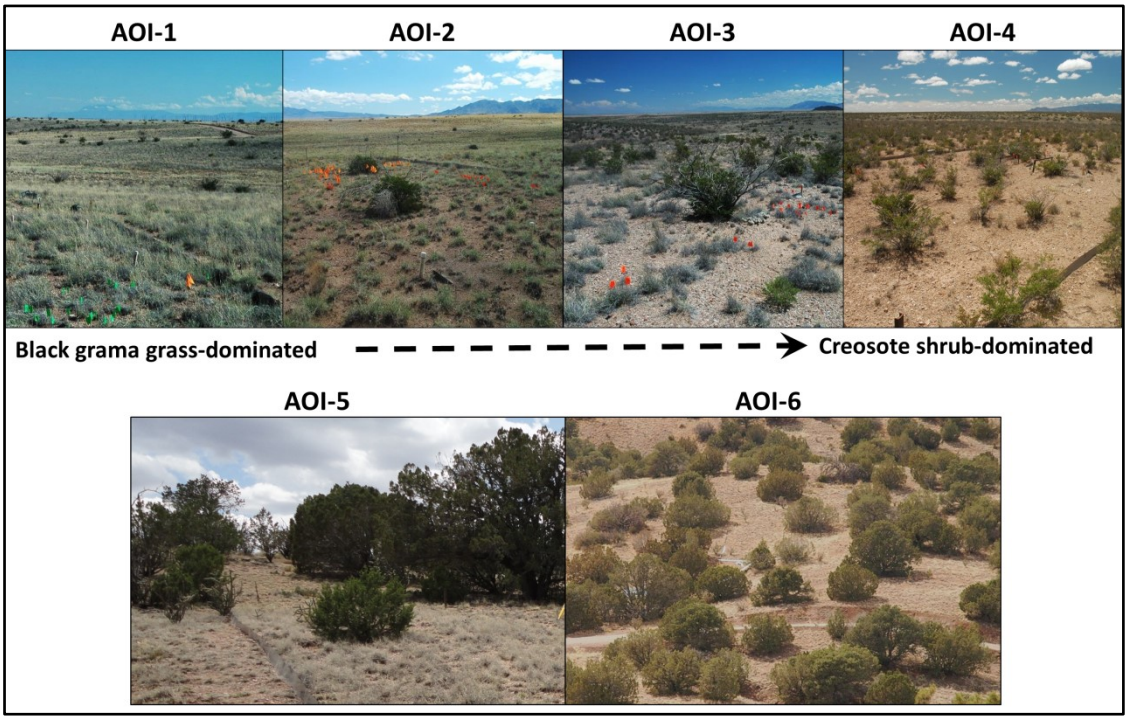

Figure 4-2. Photographs of the community assemblage at each AOI. AOIs-1 to -4 illustrate the change in biophysical structure over a grass-shrub ecotone, from black grama-dominated grassland to creosotebush-dominated shrubland. AOI-7 (not shown) is similar to AOI-2.

The sandy soils characterising these locations have relatively high infiltration rates. Measurments on infiltration rates at the Sevilleta are limited, but one study suggests that they may be as high as 0.4 m hr^{-1} on the basis of single ring infiltration measurments in areas beneath and between plant canopies (Furbish et al., 2009), although such instruments are prone to significant errors compared with rainfall simulation type methods (Lister, 2007; Turnbull, 2008). High infiltration rates have been argued to preclude to occurrence of infiltration excess overland flow in these landscapes (e.g. Furbish et al., 2009; Taube and Furbish, 2010). This suggestion that overland flow does not occur is at least partly responsible for the oft-repeated contention that the erosion-induced lateral redistribution of soil resources in these landscapes only occurs over spatial scales of up to ~3-5 m, i.e. sufficient only to contribute to the development of Islands of Fertility (Schlesinger et al., 1990) (Section 1.3.5). However, the high precipitation rates associated with the infrequent but high-intensity convectional rainstorms during the summer monsoon periods do often exceed infiltration into the soil, resulting in the generation of infiltration-excess overland flow (Wainwright et al., 2000; Turnbull et al., 2010a; Puttock, 2013; Puttock et al., 2013). Such

infiltration excess overland flow and the general structure of the shrub-dominated ecosystems is illustrated in Figure 4-3. Such overland flow results in infrequent, episodic transfers of material into aquatic systems.

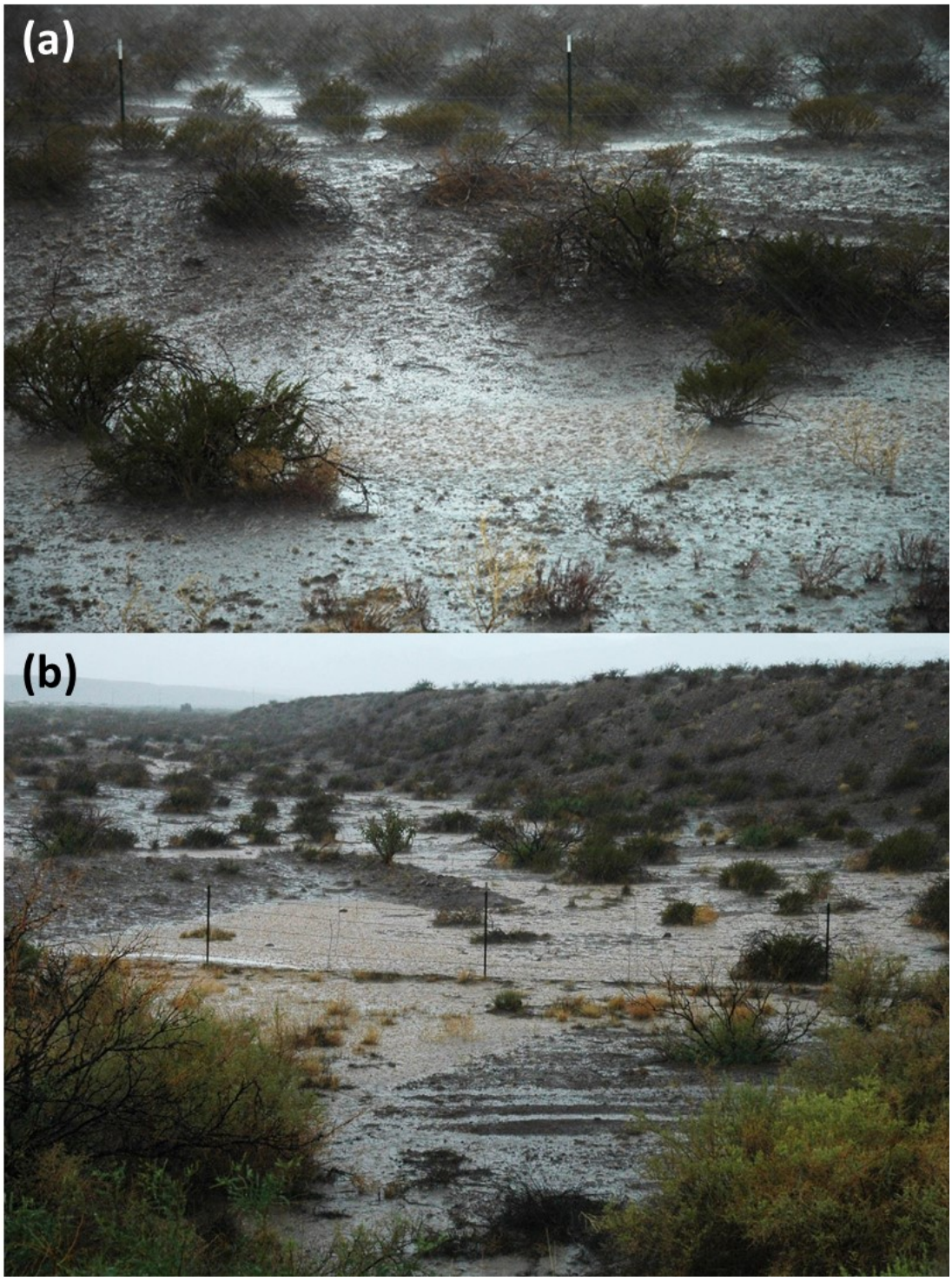

Figure 4-3. Photographs illustrating overland flow during a high-intensity rainstorm event (2013-09-07) in a creosotebush shrub-dominated landscape in the Sevilleta National Wildlife Refuge.

5. Methodology

5.1. Chapter Overview

This chapter presents the methodologies underpinning the findings presented in Chapters 6, 7 and 9. The detailed exposition is necessary to underpin the robustness of the presented findings, which in some cases differ substantially from previous work. Note that for clarity of presentation, the methodology for chapter 8 is presented within that chapter.

5.2. Acquisition of Soil and Sediment Samples

5.2.1. Near-Surface Soil

Within the runoff plots at the grass, grass-shrub, shrub-grass and shrub sites, five 236 cm^3 samples of soil were collected from random locations beneath each surface cover type (bare soil and, where present, grass and shrub), totalling 10-15 samples per plot. A cylindrical ring sampler (0.0775 m diameter × 0-0.05 m depth) was driven into the soil. In the few occasions where large stones prevented the full insertion of the sampler, the sampler was moved to the nearest possible undisturbed visually similar soil surface, which was always less than 40 mm away from the original sample location. For further discussion of the methodological implications of using small samplers in rocky ground, see Throop *et al*. (2012a, p. 67).

The surrounding soil was excavated from around the tin and a pointing trowel was used to separate the sample from the underlying soil, keeping the soil surface flush with the tin. The 0-0.05 m soil sampling depth was selected because this near-surface layer is highly susceptible to interaction with surface-transport processes at hillslope scales and attempting to sample at discrete finer depth intervals is extremely challenging in these unconsolidated, gravel-rich soils; this 0.05 m depth is in accordance with similar research undertaken in these environments (e.g. Wainwright et al., 2000; Yoo et al., 2005; Rhoton et al., 2006; Li et al., 2007; Turnbull et al., 2010a, 2010c, Puttock et al., 2012b, 2013, 2014; Brazier et al., 2013). The number (n = 50) of near-surface soil samples was appropriate for the present study, which required a fine-resolution (in terms of

particle size fractions) dataset to study the distribution of OC and IC concentrations across particle size fractions, in order to elucidate the role of particle size selectivity in contributing to OC enrichment in eroded sediments.

5.2.2. Runoff plots and erosion-induced fluxes

The design and operation of these plots is reported here to contextualise the presentation of new results arising from new chemical analysis of archived sediments and meta-analysis of the aggregated four-year assemblage of erosion events. For further description of the design, instrumentation and characterisation of the plots, see Turnbull *et al.* (2010a, 2010c, 2011), Puttock *et al.* (2012b, 2013, 2014) and Brazier *et al.* (2013).

Each experimental site consisted of a 30 m long by 10 m wide, planar, runoff plot, bounded on three sides by metal flashing to isolate overland flow within the plot. Parsons *et al.* (1990) argued that to be representative of interrill erosion processes on semi-arid hillslopes, experimental plot dimensions must exceed 20 m in length and 5 m in width, in order to minimise the effects of plot boundaries on the hydrology and erosional dynamics. The runoff plots employed herein were designed to be sufficiently large so as to minimise these possible boundary effects (cf. Parsons et al., 1990; Poesen et al., 1996; Boix-Fayos et al., 2006; Turnbull, 2008; Turnbull et al., 2011). The bordering flashing was installed to a shallow soil depth to minimise alteration of infiltration rates. The downslope end of each plot was bounded by a gutter, which directed all runoff through a super-critical flume and into storage tanks (2120 litre capacity). Runoff depth through the flumes was measured using a bubbler module (ISCO 730) at 1-minute intervals, and converted to discharge using calibrated depth/discharge rating relationships (discussed in detail in section 5.8). Flume-derived hydrographs were scaled linearly to match tank-observed total runoff; this treatment increases the accuracy of the discharge measurements and is explained in detail in section 5.8 (after Turnbull, 2008; Turnbull et al., 2010a, 2010b). Rainfall was monitored using a tipping-bucket precipitation gauge connected to a data logger that recorded data at 1-minute intervals, with total rainfall validated using two independent rain gauges at each plot. An example of the monitoring equipment is depicted in Figure 5-1.

Overland flow and associated eroded sediment was captured in the runoff tanks. These runoff tanks contained all runoff and sediment in 84% (31/37) of the events analysed for carbon yields. This (mostly) total capture is important because partial sampling of eroded material via pump samplers, bedload traps or natural sediment deposits risks being non-representative of the eroded material, due to selectivity in transport and deposition processes (Beuselinck et al., 2000; Owens et al., 2002; Nadeu et al., 2011, 2012). Interrill erosion processes dominated sediment transport during the events, and are described in detail in Turnbull *et al*. (2010a). When the stock tank capacity was exceeded, there may have been an unquantified loss of fine particles carried in suspension (Turnbull et al., 2010b).

Nevertheless, the main conclusions presented here are unlikely to have been significantly undermined by these potential losses for several reasons: (i) Occurrences of stock tank exceedance were evenly distributed across the four plots (two events in the grass plot, one event in the grass-shrub plot, one event in the shrub-grass plot and two events in the shrub plot), so between-site bias should be minimal. (ii) Of the six occurrences of exceedance, the smaller two only resulted in the loss of 3% and 8% of the total runoff, and therefore potential losses of eroded material would be relatively small. (iii) There was no appreciable evidence of the potential loss of fines altering the PSD of eroded sediment, as in all six occurrences of exceedance, the enrichment of the finest (<0.0625 mm) particle size fraction was greater than the average enrichment for that size fraction, for each plot. (iv) The potential loss of low-density OC-rich fines in suspension would underestimate overall OC enrichment in eroded sediment, which is found to be much higher than is commonly reported in the literature.

The erosional C dynamics of the four sites were examined for 37 discrete rainstorm events over the four summer monsoon periods, covering both wetter- and drier-than-average monsoon seasons (Petrie et al., 2014). These storm events were monitored by Drs Laura Turnbull and Alan Puttock (Turnbull, 2008; Puttock, 2013), and archived samples of eroded sediment were analysed as part of the present project. Although archived eroded sediment was not available for the remaining erosion events, in terms of total rainfall, total runoff, runoff coefficients and total sediment event-flux, the 37 events analysed for C content were representative of all of the events observed over the four monsoon periods, albeit with some larger differences in the shrub-grass plot due to the small sample

size analysed for C fluxes (n = 4) (discussed further in Section 5.7). Dried and sealed samples of eroded sediment were archived for a maximum of eight years, and were believed to have undergone negligible change in C in this time; no systematic decrease in OC concentration (indicating possible mineralisation of OC) was observed in the 29 samples where some analysis was undertaken prior to archiving, and far older samples subjected to less controlled storage conditions have been similarly analysed (e.g. Torn et al., 2002).

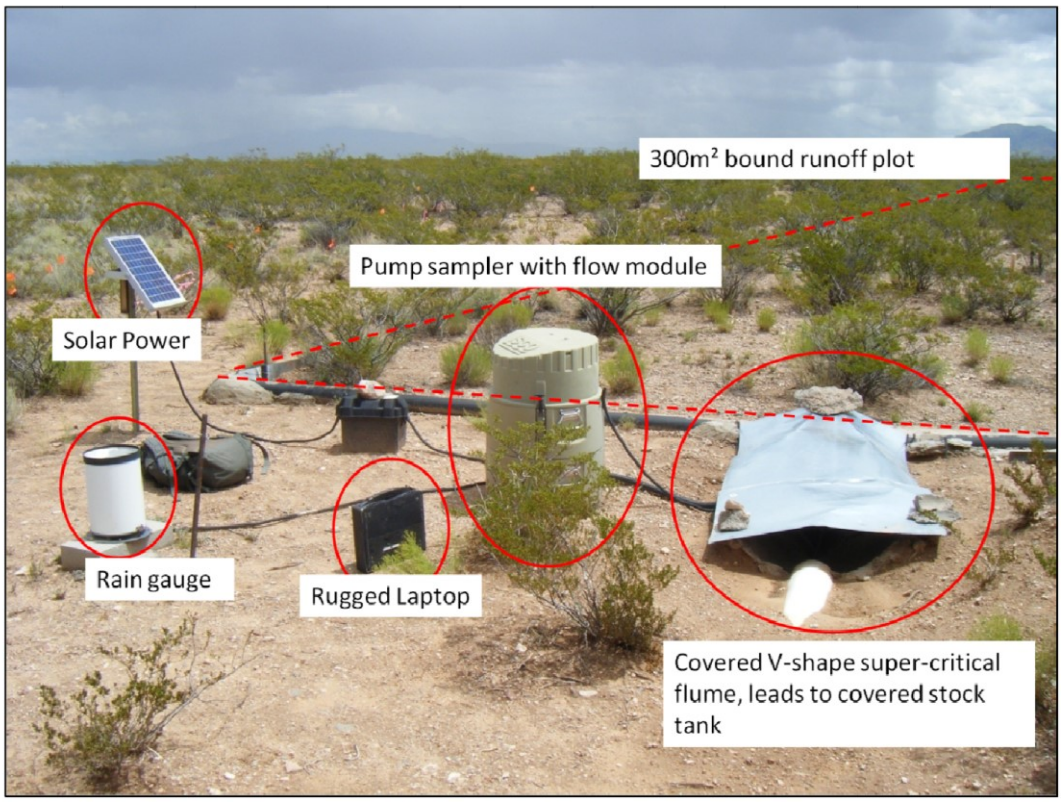

Figure 5-1. A labelled example of the experimental runoff monitoring plot and monitoring equipment at the shrub-dominated site (Figure from Puttock, 2013, p. 81).

5.3. Sample Preparation

5.3.1. All Samples

Investigations characterising the chemistry of soil fractionated by particle size commonly undertake deliberate dispersion of aggregates (e.g. Quiroga et al., 1996; Six et al., 2002; von Lützow et al., 2007; Marzaioli et al., 2010). Nevertheless, the concept of primary particles as a measurable unit is challenged by detailed investigations showing that solid mineral and organic matter are broken apart before aggregate structures are fully dispersed (Chenu and Plante,

2006). Depending on the nature of the precipitation event and soil characteristics, significant proportions of soil can be eroded in aggregate forms (Alberts and Moldenhauer, 1981; Loch and Donnollan, 1983; Egashira and Nakai, 1987; Walling, 1988; Martinez-Mena et al., 1999; Slattery and Burt, 1997; Beuselinck et al., 2000; Hu and Kuhn, 2014).

In calcareous soils, precipitation of calcium carbonate can bind soil particles, stabilising aggregate structures (Bryan, 2000; Nash and McLaren, 2003; Alonso-Zarza and Wright, 2010). The occurrence of this stabilization mechanism in the present study was supported by observations that small aggregates were often covered by calcium carbonate deposits, and that some eroded particles were stable in water and during dry sieving, but dispersed following acid treatment, apparently due to the removal of calcium carbonate. The likely occurrence of calcium carbonate stabilization suggests that further artificial disaggregation would be inappropriate when investigating particle-associated chemical transport in this highly calcareous environmental context. Therefore, particles were fractionated by effective particle size, in accordance with previous investigations into the erosion-induced redistribution of particulate-associated chemicals (Egashira and Nakai, 1987; Slattery and Burt, 1997; Lister, 2007; Lister et al., 2007; Nadeu et al., 2011).

Bulk samples of near-surface soil were fractionated by density using flotation-sedimentation density separation in a 1 g cm^{-3} medium (deionised water), and the >1 g cm^{-3} fraction was dried at 60°C for >48 hours to a constant weight. 60°C was used because a pilot trial of drying at 90°C was observed to result in blackening of organic matter, interpreted as indicating partial combustion. Samples were then divided into eight effective particle size classes by dry-sieving at one ϕ (Wentworth phi) intervals, of: >4, 4-2, 2-1, 1-0.5, 0.5-0.25, 0.25-0.125, 0.125-0.0625, <0.0625 mm. Evaluating discrete physical fractions increases sensitivity to changes compared to whole-soil analysis (Dalal and Mayer, 1986; Six et al., 2002), facilitating detection of subtle differences between samples or over shorter monitoring periods following changes to influx or stability of OC (Smith, 2004). Dry sieving was employed to minimise potential losses of soluble OC arising from wet sieving (Beauchamp and Seech, 1990; Sainju et al., 2003, 2011; Lister, 2007); such losses could be significant given the very low OC concentrations indicated by previous work (Lister, 2007; Puttock, 2013; Puttock

et al., 2012b; Brazier et al., 2013). Dry sieving was undertaken using mechanical shaking in a sieve stack for 10 minutes. Increasing shaking duration (up to 30 minutes) showed no further changes in gravimetrically-determined PSD, indicating that 10 minutes of shaking had disaggregated all loosely aggregated particles. This treatment helps to reduces problems with possible re-aggregation due to wetting and drying during sample preparation. The largest size class was selected because particles >4 mm have been observed to erode from these hillslopes during high-energy erosional events. The minimum particle size threshold of <0.0625 mm was considered appropriate for undispersed particles (Lister, 2007; Michaelides et al., 2012) and to parameterise numerical simulations given current limitations in the representation of detachment, transport and deposition of cohesive silt and clay particles (Wainwright et al., 2008c; Turnbull et al., 2010b). To quantify loss of material during dry sieving, the mass of each particle size fraction was measured and summed; recovery rates ranged from 97.1% to 100.8%, with a mean of 99.6%, indicating minimal loss of loss of material due to inhalation during dry sieving.

Following each rainstorm event, all eroded sediment was recovered from the runoff tanks, dried at 60°C to a constant weight and subsampled by means of a riffle splitter (De Zorzi et al., 2005). The sediment was fractionated via dry sieving to gravimetrically determine effective PSD for five size classes (>2, 2-0.5, 0.5-0.25, 0.25-0.0625, <0.0625 mm). Relative to the eight particle size classes employed for the characterisation of near-surface soil, eroded sediment was fractionated at a coarser resolution to correspond with the PSD resolution originally recorded for sediment eroded during all monitored events (by Turnbull, 2008; Puttock, 2013). Each size fraction was subjected to flotation-sedimentation density separation in a 1 g cm^{-3} medium (deionised water), and the >1 g cm^{-3} fraction was again dried at 60°C.

Particle size fractions larger than 0.125 mm were homogenised manually, and all fractions larger than 0.25 mm were ground manually so as to pass through a 0.25 mm sieve. This homogenisation treatment increases the likelihood that the combusted aliquots will be representative of the rest of the sample (Chichester and Chaison, 1992; Sainju et al., 2003; Lukasewycz and Burkhard, 2005; Wang et al., 2012; X. J. Wang et al., 2014; X. Wang et al., 2015).

5.3.2. Multi-density fractionation

As an exploratory analysis, sediment eroded from one rainstorm event was subjected to additional fractionation on the basis of density prior to analysis of C contents. The idea that particle density may contribute to OC enrichment in erosion is supported by recent findings of significant co-variance between OC concentrations with settling velocity, a function of density (Hu and Kuhn, 2016). This pilot study may help inform parameterisation of future numerical modelling approaches to simulate the mobilization of multiple particle fractions with different densities.

Sub-samples of (unground) material from each particle size fraction eroded from the grass-shrub plot (rainstorm on 2010-07-25) were subjected to additional floatation-sedimentation density separation in a sodium polytungstate (SPT) ($Na_6(H_2W_{12}O_{40}).H_2O$)) solution with a specific gravity of 1.8 g cm^{-3}. 1.8-1.85 g cm^{-3} mediums are commonly used for separating of soil particles into light (1-1.8 g cm^{-3}) and dense (>1.8 g cm^{-3}) fractions, which are generally described as POC and mineral components, respectively (Lal, 2003; Liao et al., 2006a, 2006b; Zimmermann et al., 2006; Conen et al., 2008). A small quantity (~10 g, in order to minimise the amount of heavy liquid required) of each particle-size class was measured into a centrifuge tube and ~50 ml of heavy liquid was added. To increase separation efficacy the sediment was agitated in the separating medium by shaking the sealed container, reducing the occurrence of heavy particles trapping light particles and light particles suspending heavy particles. The light fraction was scooped off into a fine (<0.0225 mm) sieve and rinsed with deionised water, and the heavy fraction was scooped out into a fine (<0.02 mm) sieve and rinsed with deionised water (Zimmermann et al., 2006). Consequently, it is possible that some of the <0.02 mm particles will have been lost from the <0.0625 mm fraction during the rinsing phase, and therefore the results from the <0.0625 mm fraction should be treated with caution in this pilot dataset. Each rinsed fraction was placed in a suitably heatproof pre-weighted container and oven dried at 60°C to a constant weight, allowing determination of the dry mass and calculation of recovery ratios. The number of samples which could be separated into multiple density fractions was limited by the high-cost of tungstate-based heavy liquids, as well as the additional time taken to process samples in this manner.

5.4. Determination of Carbon Contents

A range of analytical techniques are available to quantify TC, IC and OC concentrations in soils. For an introduction to analytical methods for OC please see Schumacher (2002) and Bisutti *et al*. (2004), although recent developments in this field should be noted, particularly with regards to the limitations of the Walkley-Black method for determining OC, and the proper use of acidic pre-treatments to remove IC (Harris et al., 2001; Lukasewycz and Burkhard, 2005; Komada et al., 2008; Walthert et al., 2010; Meersmans et al., 2009; Ramnarine et al., 2011; Wang et al., 2012; Brodie et al., 2011b, 2011a). As $TC = OC + IC$, to determine the concentrations of IC and OC in a sample it is possibly to determine the concentration of any two of TC, IC or OC, and to simply infer the third, unknown component from the two known components (Kimble et al., 2001; Schumacher, 2002; Bisutti et al., 2004).

While organic forms of C can be sub-divided into pools on the basis of their functional attributes (Cheng and Kimble, 2001), given the objectives of the current study – namely to further understanding of the role of ecosystem structure in influencing the distribution and erosion-induced redistribution of OC and IC across the landscape – it was appropriate to consider total pools of OC and IC. As is common for alkaline dryland soils (Schumacher, 2002; Ewing et al., 2007), IC, predominantly in the form of calcite ($CaCO_3$), comprises 70-80% of total C in near-surface (0-0.05 m) soils of the McKenzie Flats (Puttock, 2013).

Dry combustion is an accurate and efficient means of determining elemental TC (Kimble et al., 2001; Schumacher, 2002; Bisutti et al., 2004), and therefore this method was employed for the present study. Aliquots of 12-20 mg dried homogenised sample were weighted into tin (Sn) capsules. Capsules were flash combusted at 900°C in an elemental analyser (Flash 2000, Thermo Scientific) and the evolved CO_2 was measured chromatographically using a thermal conductivity detector. The thermal decomposition temperature of calcium carbonate can be above 848°C (Halikia et al., 2001), so a copper oxide reaction catalyst was used to increase the efficacy of C decomposition. The helium (He) carrier gas flow rate was 130 ml min^{-1} and oxygen (O2) flow was 250 ml min^{-1} (injection time 5 seconds). Ethylenediaminetetraacetic Acid (EDTA) (41.1% C

and 9.59% N) was used as a check standard. Each sample run was interspersed with standard reference materials, analysed as unknown samples. A tolerance threshold of ±0.5% C concentration was used to evaluate check standards, and only samples bracketed by in-range check standards were accepted as valid. Samples rejected due to out-of-range bracketing check standards were reanalysed. This ±0.5% tolerance threshold is more conservative and robust than the ±1% threshold more commonly used for this kind of analysis. Chromatograph outputs were analysed using the program EAGER EXPERIENCE FOR FLASH (v1.3) (Thermo Scientific). Defining chromatograph peak end points mathematically is challenging, leading to errors in the automated identification of peak endpoints, which often result in substantial errors in estimating evolved CO_2. Therefore, automatically identified peak endpoints were manually validated for every sample. Somewhat surprisingly, such manual validation of peaks is not standard practice in dry combustion analysis. Gravimetric loss-on-ignition (LOI) has a low accuracy in samples with low OC (Schumacher, 2002), such as those investigated by the present study (Kieft et al., 1998; Brazier et al., 2013; Puttock et al., 2014).

To quantify OC, IC was first removed via acid digestion. Five g of each particle size fraction was digested in 75 ml of 2M HCL for seven days, stirred once, and then filtered through a 0.45 µm glass microfiber filter using a Büchner setup and triple rinsed with 100 ml of deionised water to remove the HCL (Turnbull et al., 2008a; Puttock et al., 2012b; Puttock, 2013; Brazier et al., 2013; Puttock et al., 2014). The strong acid was thought necessary to ensure complete removal of inorganic carbon; however, a yellow-brown colouration of the acid solution following the acid treatment indicated some solubilisation loss of OC (cf. Chenu and Plante, 2006). The reliability of the OC and IC determinations was therefore investigated further, as described in Section 5.5. Acid-treated samples were analysed via dry combustion in an elemental analyser as described above, giving the elemental OC content of each aliquot.

While IC concentration can be directly determined using pressure calcimeter-type methods (e.g. Rhoton et al., 2006; De Baets et al., 2013) or heating in ortho-phosphoric acid (e.g. Lister, 2007), for convenience it was calculated as

$$IC = TC - OC \qquad \textit{Equation 5-1}$$

In total, 592 unique samples were analysed for total C and OC. Losses of volatile organic compounds due to drying (Schumacher, 2002) were expected to be negligible in samples from these frequently desiccated dryland soils. For elemental analysers, absolute instrument precision is usually defined as the standard deviation of replicate analysis of standard reference materials (Brodie et al., 2011a); for in-range check standards the standard deviation of standard reference materials was ±0.22%. Errors in check standards were parametrically distributed. Error in determining the mass of the combusted aliquot contributes to error in measured C concentrations. Consequently, a sensitivity analysis was undertaken, which showed that absolute C concentrations are fairly insensitive to small differences (<0.1%) in mass determination; a mass error of 0.01%, 0.05% and 0.1% increases *relative* C concentration by only 0.54%, 0.58% and 0.63%, respectively (Dr. Natascha Steinberg, pers. comm.).

Dry combustion only quantifies the C content of a small aliquot, therefore insufficiently homogenised samples risks analysing non-representative aliquots. To evaluate the assumption of sample homogeneity, replicate analysis was undertaken on 11.3% of all samples (n = 138). The *absolute* difference between maximum and minimum C concentrations (range) and *relative* difference (absolute difference divided by the mean C concentrations) is summarised in Table 5.1. Note that differences between replicates are only really noteworthy if both absolute and relative differences are high; i.e., relative error of 100% is not very significant if the absolute 0.1% increases to 0.2%, and similarly an absolute increase of 0.5% is not very meaningful if the relative increase is only 5%. The replicate analysis yielded a median relative difference in C concentration of just 6.1%, and indicated that combusted aliquots were generally representative of the sample.

Table 5.1. Results from replicate analysis of samples for carbon concentration.

Absolute Maximum Difference		Difference relative to mean	
Mean	0.42%		15.34%
Median	0.17%		6.05%
Maximum	5.45%		119.93%
SD	0.69%		21.71%
SE	0.06%		1.85%
n	138		138
n >1%?	16	**n >50%?**	8
n >2%?	5	**n >75%?**	5
n >3%?	2	**n >100%?**	2
n >4%?	1		

5.5. Validation of OC and IC Determinations

5.5.1. Problem Statement

As noted above, the concentrations of TC, OC and IC in soils can be quantified using several diverse approaches. The results obtained from these different methods are often considered interchangeable; however, there is limited validation of the accuracy of these determinations, particularly in calcareous soils with very high IC/OC ratios. There were several concerns regarding potential inaccuracies in OC determinations using the acid pre-treatment and dry combustion approach described in section 5.4.

While a strong acid digestion was used and no effervescence was observed at the end of the digestion period, this endpoint is somewhat subjective (Lukasewycz and Burkhard, 2005; Brodie et al., 2011b), and the efficacy of carbonate removal by the acidic pretreatment had to be assumed. Incomplete carbonate removal would overestimate OC concentrations and underestimate the IC concentrations, so validating the efficacy of carbonate removal was desirable.

Very fine colloids can be lost, either through the filter or when the supernatant is decanted off; in extreme cases, these can account for as much as 78% of the OC present in a sample (Brodie et al., 2011b) and thus their loss could potentially underestimate sample OC concentrations.

During acid treatment the removal of IC and associated elements such as evolved oxygen and solubilised Ca reduce the sample mass. This is potentially significant because the adhesion of some sample material to filtering equipment precludes the accurate determination of sample mass prior to acid treatment, and weighing

aliquots after the acid treatment does not account for this mass reduction, potentially introducing a systematic bias which could overestimate the concentration of remaining (organic) C (Brodie et al., 2011b). This bias is greatest in samples with a high concentration of IC, particularly when the ratio of IC to OC is high. This source of error can be avoided for acid treatments applied to aliquots within the combustion capsule, for example acid fumigation type treatments. Acid fumigation techniques can have other issues, such as higher risk of incomplete carbonate removal, degradation of combustion capsule integrity, and potential contamination of sensitive analytical equipment with corrosive chloride ions.

Some organic compounds can be solubilised by reaction with acids, particularly strong acids, resulting in their loss during subsequent rinsing (Midwood and Boutton, 1998; Harris et al., 2001; Kimble et al., 2001; Schumacher, 2002; Chenu and Plante, 2006; Galy et al., 2007). This may be indicated by discolouration of the acid supernatant (Chenu and Plante, 2006), which was observed during the acid pre-treatment undertaken herein. While the removal of more mobile organic compounds can be desirable to remove potential contaminants (such as fulvic acids) when investigating the isotopic properties of OC (e.g. Boutton et al., 1998; Turnbull et al., 2008a; Puttock et al., 2012b), it is undesirable when seeking to quantify OC concentrations for estimating the magnitude of pools and erosion-induced fluxes (e.g. Brazier et al., 2013; Puttock, 2013; Puttock et al., 2013, 2014). A further point of interest here is that although there have been suggestions acid pre-treatments cause minimal changes in $\delta^{13}C$ (e.g. Midwood and Boutton, 1998; Torn et al., 2002), there is growing evidence that both the pre-treatment method and reagent can substantially influence not only the determination of OC concentration, nitrogen concentration and CN ratio, but also the stable isotopes ratios of $\delta^{13}C$ and $\delta^{15}N$ (Komada et al., 2008; Walthert et al., 2010; Brodie et al., 2011a, 2011b; Plante, 2013). Indeed, the changes to C/N and stable isotope ratios induced by different acidic pre-treatments can be sufficient to significantly alter inferences regarding the provenance of organic matter (e.g. as having been fixed by vegetation employing C3 versus C4 photosynthetic pathways) (Brodie et al., 2011a). While this potential error does not significantly influence the present study, it may have implications for the interpretation of previous analysis. The NERC Radiocarbon Facility at East Kilbride normally uses liquid acid to remove carbonates (Mark Garnett, pers. comm. 2014) and the Arizona Accelerator Mass Spectrometry Lab usually remove carbonates with an

acid digestion (85% phosphoric) followed by rinsing (Jull, 2007; Timothy Jull, pers. com. 2014).

To constrain the potential errors arising from these sources, the TC, OC and IC concentrations determined using flash combustion (FC) of paired untreated and acid-treated aliquots (described in section 5.4) were compared to analysis of CO_2 evolved during multi-temperature combustion of single aliquot.

Multi-temperature combustion of a single sample has been described using many different names in the literature, but here will simply be referred to multiple-temperature combustion (MTC). MTC makes use of the fact that OC combusts at substantially lower temperatures than IC, allowing evolved CO_2 to be accurately apportioned between physiochemical forms on the basis of decomposition temperature; a thermal threshold of 600°C is widely accepted to differentiate between organic and inorganic forms (Rabenhorst, 1988; Chichester and Chaison, 1992; Bisutti et al., 2007; Maharaj et al., 2007; Fernández et al., 2012; Vuong et al., 2013).

For evolved gas analysis (EGA), samples can be heated to either (i) a single temperature of ~550-600°C, allowing the more accurate determination of OC concentration than gravimetric loss-on-ignition (e.g. Hu et al., 2013), (ii) dual-temperature combustion (e.g. 515°C and 925°C Bisutti et al., 2007), or (iii) progressively increasing temperatures as high as 1,000°C (e.g. Vuong et al., 2013), possibly with isothermal pauses in order to better isolate thermally distinct C fractions (e.g. Fernández et al., 2012). MTC alleviates the need for multiple determinations of different aliquots from each sample to quantify TC, OC or IC, avoiding the multiplication of uncertainty due to analytical error following multiple determinations and reducing operator time requirements (Chichester and Chaison, 1992; Vuong et al., 2013). MTC also helps avoid other problems such as the potential loss of volatile organic carbon due to acid pre-treatments or the introduction of corrosive halide residues to analytical instruments (Vuong et al., 2013). MTC typically has a lower sample throughput than single-temperature FC, but with appropriate autoloaders throughput can be upwards of 50 samples a day.

While thermal gradient-EGA yields a richer source of information which can be used to apportion CO_2 between different forms of OC on the basis of decomposition temperatures (Fernández et al., 2012) and to study the isotopic

properties of the thermally distinct forms of carbon (Plante, 2013), for simple determinations of OC and IC concentrations dual-temperature combustion is generally more appropriate as this is simpler and faster than thermal gradient approaches. MTC-EGA it has been in existence for several years and, although it is still somewhat developmental with some problems around incomplete gas recovery and specification of optimum thermal gradient profiles, many researchers consider MTC-EGA it to be a 'gold standard' for the accurate determination of TC, OC and IC concentrations (Vuong et al., 2013; Alain F. Plante, pers. comms. 2014).

5.5.2. Method of C determination evaluation

A subset of 13 pairs of control (untreated) and acid-treated samples were selected for MTC-EGA analysis at partner laboratories. The selected samples included a full set of eight particle-size fractions from one near-surface soil characterisation site, and several other samples with OC concentrations somewhat uncharacteristic of the particle-size fraction, as these anomalies were thought to possibly highlight errors in the previous OC determinations. One of the samples selected for further investigation (Sample #C) had one of the highest OC concentrations out of all of the samples analysed.

Two different progressive heating thermal regimes were employed. Samples A, B and C were heated from ambient to 105°C at 10°C min^{-1}, with an isothermal pause for 15 min, before being heated at 10°C min^{-1} to 900°C. Evolved CO_2 was measured between 120°C to 900°C and apportioned between two phases, OC (<600°C) and IC (>600°C). Each sample run took ca. 90 minutes. Samples D to M were analysed using a multiphase C determinator (RC-412, Leco, St. Joseph, MI, USA) heated from 138°C to 900°C, at ~35°C min^{-1} with several isothermal pauses. The isothermal pauses were used to separate the several peaks in OC decomposition, in an effort to characterise different thermal fractions of OC (Felix Heitkamp, pers. comm.). Evolved CO_2 was quantified using an infrared detector (3 measurements per second) and apportioned between two phases, OC (<600°C) and IC (>600°C), and each sample run took ca. 22 minutes.

Absolute differences were calculated as

$$\boldsymbol{Absolute\ difference} = \boldsymbol{OC\%_{FC}} - \boldsymbol{OC\%_{MTC}} \qquad \textit{Equation 5-2}$$

Where the subscripts FC and MTC indicate flash combustion and multitemperature combustion repsectivly. Relative differences were calculated as

$$\boldsymbol{Relative\ differences} = \frac{|\boldsymbol{OC\%_{FC}} - \boldsymbol{OC\%_{MTC}}|}{\left(\frac{\boldsymbol{OC\%_{FC}} + \boldsymbol{OC\%_{MTC}}}{2}\right)} \qquad \textit{Equation 5-3}$$

Each analytical approach has an precision (±0.22% for the FC) and different aliquots of the same sample were combusted, so some degree of variance in measured C concentrations was inevitable. Information on the analytical precision of the MTC was not available from the partner laboratories. Concordance correlation coefficients (CCC) are a robust statistical measure of agreement for two methods of measuring the same continuous variable (Lin, 1989, 1992, 2000; Lin et al., 2012; Steichen and Cox, 2002; McBride, 2005), and were used to evaluate the concordance between the various methods. CCC is robust to small sample sizes (n ≥10), and is calculated using,

$$\boldsymbol{CCC} = \boldsymbol{\rho\ C_b} \qquad \textit{Equation 5-4}$$

where ρ is the Pearson correlation coefficient which measures how far each observation deviates from the best-fit line and is a measure of precision, and C_b is a bias correction factor that measures how far the best-fit line deviates from the 45° line through the origin and is a measure of accuracy (Lin, 1989, 1992, 2000; Steichen and Cox, 2002; McBride, 2005; Lin et al., 2012).

The evolution of CO_2 can be plotted against decomposition temperature/time. These thermograms are not central to the findings of this section, and therefore are presented in Appendix 2. The thermograms presented there illustrate the efficacy of carbonate removal (indicated by the absence of a CO_2 signal in acid-treated samples heated above 600°C). Differences in the *shape* of the thermograms during the low temperature (<600°C) combustion phase can potentially indicate altered thermal decomposition temperatures due to changes of the physiochemical structure of the organic component arising from the acid pretreatment, as the thermograms to the left of the 600°C threshold should be extremely similar *if the aliquot mass was identical* for two homogenised samples (which was rarely the case).

5.5.3. Findings of C determination evaluation

There was generally very good agreement in TC concentrations determined using FC and multi-temperature combustion (MTC). The CCC was 0.985 (95% CI 0.995 to 0.949), indicating substantial agreement (McBride, 2005), illustrated by Figure 5-2. The mean actual difference and mean relative difference was just 0.09% and 14.7%, respectively. Discrepancy between TC determinations was dominated by a single sample, Sample #C. Replicate FC determinations were undertaken on Sample #C, which yielded TC concentrations of 2.6%, 4.9%, 5.9% and 10.1%. This variance was extremely high and indicative of substantial inhomogeneity in the sample, but replicate testing of 11.3% of the total samples indicated that this degree of inhomogeneity was very infrequent (described in Section 5.4 and Table 5.1). Because this high level of inhomogeneity was not representative of the sample set, Sample #C was excluded from the method inter-comparison as an outlier.

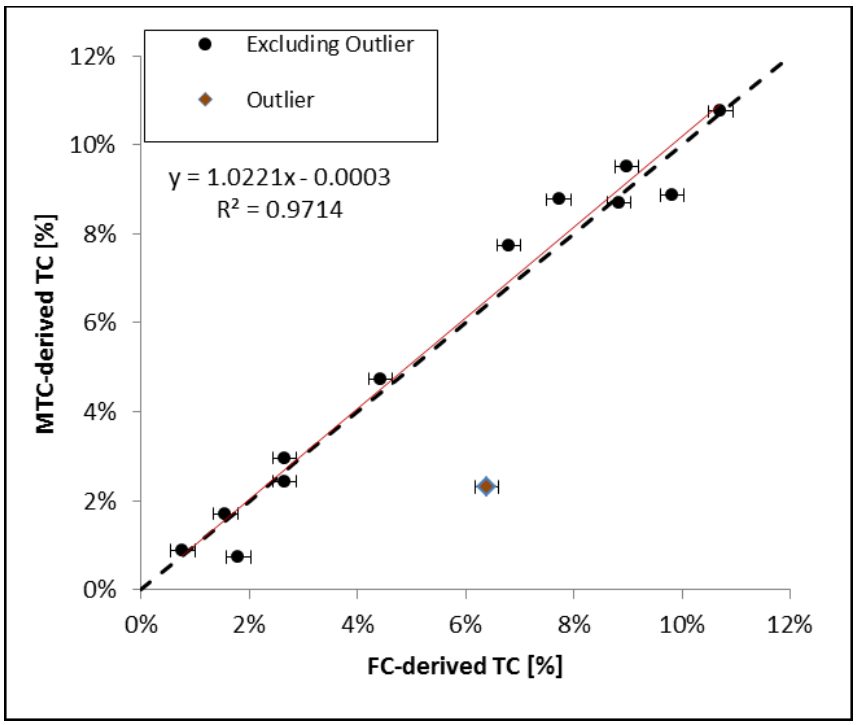

Figure 5-2. Comparison of total carbon (TC) concentrations determined using flash combustion (FC) and multi-temperature combustion (MTC) analytical techniques. Error bars represent standard deviations of the check standards (±0.22 %).

The FC and MTC methods both yielded very similar values of IC concentration in the untreated control samples. The CCC was 0.987 (95% CI 0.995 to 0.964),

indicating substantial agreement (McBride, 2005), illustrated by Figure 5-3. The mean actual difference and mean relative difference was -0.03% and 27.2%, respectively. This offers strong confidence in the determination of IC using the approach described in Section 5.4. The MTC analysis indicated that IC concentration of acid-treated samples was consistently <0.035%, demonstrating that the acid pretreatment employed was highly effective at removing carbonates (as illustrated by the thermographs in Appendix 2).

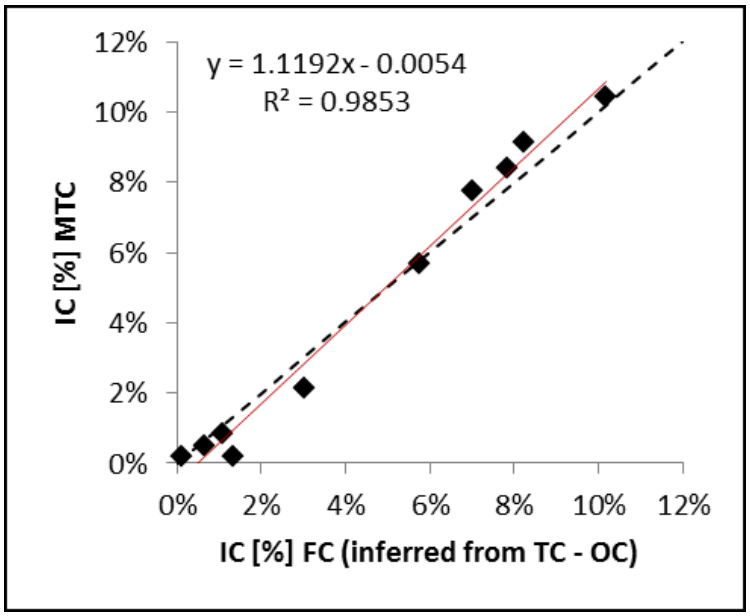

Figure 5-3. IC inferred from flash combustion (TC-OC), versus IC measured using multi-temperature combustion (MTC) evolved gas analysis.

Comparison was made between three sets of OC determinations. The MTC method allowed quantification of OC in both untreated and acid-treated samples, so it was possible to evaluate whether the acid pretreatment introduced any systematic bias in OC concentrations, as discussed in section 5.5.1. This comparison between MTC-determined OC in control and acid-treated samples yielded a CCC of 0.776 (95% CI 0.916 to 0.469), indicating poor agreement (McBride, 2005) (Figure 5-3). Actual and relative mean difference was -0.05% and 44.9%, respectively (Figure 5-4a). This degree of dissimilarity was due to a comparatively high degree of variance around the 1:1 line, but there were no evidence of systematic difference (either shift or drift) between OC concentrations determined for the acid-treated and control samples using the MTC approach.

OC concentrations were compared between the FC and MTC of acid-treated samples. The CCC was 0.508 (95% CI 0.720 to 0.210), indicating poor agreement (McBride, 2005) (Figure 5-4b). Actual and relative mean differences were -0.19% and 0.1%, respectively. Critically, there was some weak indication of systematic drift, with increasing deviation from the 1:1 line at higher OC concentrations (Figure 5-4b). OC concentrations were also compared between the FC and MTC of (untreated) control samples. This yielded a CCC of 0.673 (95% CI 0.847 to 0.369), indicating poor agreement (McBride, 2005). Again there was some weak indication of systematic drift between measures, with increasing deviation from the 1:1 line at higher OC concentrations (Figure 5-4c).

There was some limited evidence of systematic difference in OC concentrations determined using FC versus MTC methods, with MTC predicting higher OC concentrations than FC at higher concentrations. Nevertheless, this difference was very small considering the analytical error associated with these methods, the actual difference only exceeds ±0.3% in 25% of samples considered. High IC/OC ratios reduce the accuracy of MTC determinations of OC concentration, due to higher signal-to-noise ratios when measuring small amounts of CO_2 evolved from <600°C phase when much more CO_2 is evolved at >600°C (Felix Heitkamp, pers. comm.). This was likely to contribute to the larger differences observed between FC and MTC concentrations in the untreated samples relative to the acid-treated samples. MTC methods have not been widely employed for samples with very high IC/OC ratios, but for simple apportioning evolved CO_2 between OC/IC phases, it may be more precise to not use multiple isothermal steps in the organic phase (Felix Heitkamp, pers. comm.). Furthermore, it is conceivable that, due to the sensitivity of infrared detectors to chloride (Cl), incomplete removal of Cl ions from some samples may have interfered with the quantification of evolved CO_2 during MC of acid-treated samples. In summary, there was minimal evidence of any systematic bias in OC concentration. The finding that some of the highest OC concentrations (e.g. sample #C) were due to inhomogeneous samples yielding non-representative aliquots supports targeted replicate analysis on samples with anomalously high OC concentrations.

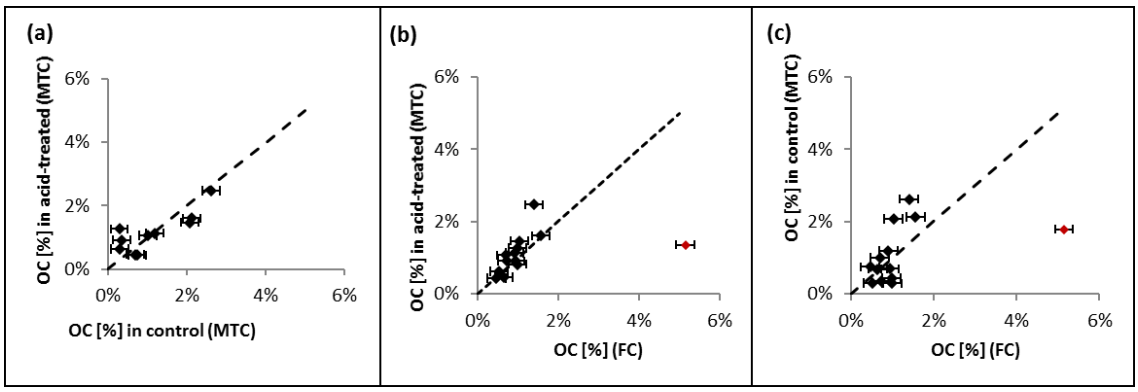

Figure 5-4. Comparison of organic carbon (OC) concentrations as determined using multi-temperature combustion (MTC) of untreated control samples and acid-treated samples (a), MTC and flash combustion (FC) of acid-treated samples (b), and MTC and FC of control (non-acid treated) samples.

Table 5.2. Analytical costs of OC and IC determinations using flash combustion.

	Step	**FC** (Two aliquots)
Operator Time (Minutes per sample)	Acid-pretreatment	34
	Packing Capsules	10
	Locating analyser	4.8
	Data Processing	4
	Total	**52.8**
Fiscal Cost (£ per sample)	Analyser	£0.54
	Consumables	£1.80
	Total	**£2.34**

5.5.4. Summary of C determination evaluation

Multi-temperature combustion enables evolved CO_2 to be apportioned between organic and inorganic physiochemical forms according to decomposition temperature. Comparison between the FC methods and MTC methods revealed extremely good agreement in both TC and IC measurements, and minimal evidence of any systematic error in OC determinations. The poorer correlation in OC observations may be explained by the very low concentration of OC in the examined samples, compounded by reduced accuracy of OC determinations with MTC when IC/OC ratios are very high. This methodological comparison (i) upholds OC and IC determinations made using combustion of paired untreated and acid-treated samples, and (ii) supports the direct comparison between IC and OC concentrations determined using the two methods. Furthermore, MTC approaches are considered to likely to be a more time- and cost-efficient means

of determining OC and IC compared with FC of paired untreated and acid-treated aliquots (information on the anlaysical costs associated with FC is presented in Table 5.2). Therefore, where available, MTC methods are considered preferable for future work.

5.6. Statistical Analysis

Soil bulk density was calculated as the mass of soil divided by the volume of the sampling ring, and soil bulk densities are reported in Appendix 1. Using size-sorted samples for measuring total sediment-bound chemical pools has been suggested to be more accurate than bulk samples when only small aliquots are analysed (Michaelides et al., 2012). Whole-soil OC concentrations were calculated by multiplying size-specific OC or IC concentrations by the fractional mass of particles in each size class and summing values across sizes. Average OC or IC concentrations [mass/mass, expressed as a %] and PSD for each surface cover (bare, grass, shrub) were weighted by fractional canopy cover (Table 5.3) to derive areally-weighted values for each site (after Müller et al., 2007b). Near-surface (0-0.05 m) OC or IC stocks [g m^{-2}] were calculated using the areally-weighted OC or IC concentration for each site (expressed as a proportion), multiplied by areally-weighted bulk density [g m^{-3}] and sample depth [0.05 m].

Table 5.3. Fractional canopy cover for all sites, derived from manual classification of near-ground aerial imagery (after Turnbull et al., 2010c; Puttock et al., 2013). Photos by the author (July 2013).

Surface Cover	Site			
	Grass	Grass-Shrub	Shrub-Grass	Shrub
Bare	45.46%	57.00%	73.80%	79.35%
Grass	54.54%	38.60%	14.30%	0.00%
Shrub	0.00%	4.40%	11.90%	20.65%
Slope	4%	5%	7%	3%
Site Photo				

Because of the variations in event characteristics, such as the antecedent soil moisture and the timing, magnitude and duration of precipitation inputs, it was not possible to directly compare the hydrological and erosional response of the four plots to the same rainfall events. Therefore, each rainstorm event over each site was treated as an independent event, and the general trends in hydrological and erosional response in relation to controlling factors over each site were investigated (after Turnbull et al., 2010a).

OC or IC event yields were determined by multiplying the observed particle size-specific OC or IC concentration by mass of that particle size eroded for each event (*sensu* Michaelides et al., 2012). Although the near-surface soil samples contained the full particle size range, 19/37 of the eroded sediment subsamples contained no coarse (>2 mm) particles; arising from the low abundance of this size fraction in the original material and the limited subsample size. Because hillslope processes in these semi-arid ecosystems exhibit substantial degrees of inter-event variability (Turnbull et al., 2010a, 2011, 2013; Puttock et al., 2013;

Brazier et al., 2013), large assemblages of events are valuable to improve signal-to-noise ratios to support inferences regarding the mechanistic functioning of these ecosystems (as demonstrated by Petrie et al., 2015). To best use the available event assemblage, the 19 missing >2 mm OC or IC concentrations were replaced with median >2 mm OC or IC concentrations derived from each plot. This error introduced by this substitution was likely to be very small, because (i) particles of this size fraction comprised a small proportion (median 5%) of the overall PSD of eroded material, and (ii) variance in observed OC or IC concentrations of this particle size fraction within each plot was not large (coefficient of variation ~30% and ~9% for OC and IC, respectively). The interpolated datasets are used to calculate overall OC and IC event-fluxes and enrichment, but they are not be used for examining OC and IC fluxes and enrichment dynamics of individual particle size fractions.

OC enrichment (ER_{OC}) can be expressed as the ratio of OC concentration in eroded soil (ES_{OC}) to that in the contributing soil (CS_{OC})

$$\boldsymbol{ER_{OC} = \frac{ES_{OC}}{CS_{OC}}} \qquad \textit{Equation 5-5}$$

IC enrichment (ER_{IC}) can be expressed as the ratio of IC concentration in eroded soil (ES_{IC}) to that in the contributing soil (CS_{IC})

$$\boldsymbol{ER_{IC} = \frac{ES_{IC}}{CS_{IC}}} \qquad \textit{Equation 5-6}$$

OC enrichment ratios were calculated for each particle size fraction and the total mass of eroded sediment for each event. It is reasonable to compare OC concentrations in non-concurrently acquired samples because previous work has found very low temporal variation in soil OC concentrations in this semi-arid ecosystem (Kieft et al., 1998).

To examine the extent to which particle size selectivity explains observed OC enrichment in eroded sediment, three OC event yields were calculated: (i) $\sum_{Obs}$ is the observed size-specific OC event yield, determined by multiplying the observed OC concentration and mass of each particle size fraction eroded during each event, (ii) $\sum_{All}$ is the expected OC event yield, calculated using the average OC concentration of the contributing soil multiplied by the mass of eroded sediment, and (iii) $\sum_{PSD}$ is the expected OC event yield, calculated by summing the average OC concentration of the contributing soil for each particle size

fraction by plot multiplied by the eroded mass of that fraction (Palis et al., 1990a). Assuming OC enrichment due to size selectivity *within* particle size fractions is minimal compared with OC enrichment due to size selectivity *between* particle size fractions, calculation of $\sum_{Obs}$, $\sum_{All}$ and $\sum_{PSD}$ enables calculation of the proportion of OC enrichment due to size selective transport (ER_{OC_PSD}), which can be expressed as

$$ER_{OC\_PSD} = \frac{\sum_{Obs} - \sum_{All}}{\sum_{PSD} - \sum_{All}} \qquad \textit{Equation 5-7}$$

Equation 6-7 is the ratio of observed enrichment to the enrichment predicted due to particle size selectivity. I also explored whether ER_{OC} was related to overall sediment concentration (e.g. X. Wang et al., 2014c), were the total sediment concentration during each event (C_{event}) [g l^{-1}] was calculated as the total sediment yield (S_{event}) [g] normalised by the total runoff (Q_{event}) [l]

$$C_{event} = \frac{S_{event}}{Q_{event}} \qquad \textit{Equation 5-8}$$

Statistical analyses were conducted using R (R Core Team, 2015), and unless otherwise stated all errors are standard errors (SE). Results from the two grass-dominated and the two shrub-dominated sites were combined for heteroscedastic *t*-tests (see discussion in Brazier et al., 2013).

5.7. Evaluating Representativeness of Rainstorm Event Assemblages

As discussed in section 3.4.1, hillslope processes during rainstorm events are highly sensitive to temporally-variable conditions. It is therefore valuable to examine the (dis)similarities in key parameters between the various assemblages of rainstorm events considered in different parts of this thesis (Figure 5-5). For each runoff plot, seven metrics characterising the rainstorm events were examined: (i) total rainfall, (ii) peak rainfall, (iii) total runoff, (iv) peak runoff, (v) runoff coefficient, (vi) antecedent soil moisture, and (vii) sediment event flux). The five event assemblages were: (i) all events observed over the four monsoon seasons, (ii) all events observed over the initial two wetter-than-average monsoon seasons and reported in Turnbull *et al*. (2010a), (iii) events analysed for erosion-induced carbon fluxes and reported in Chapter 6 (Cunliffe et al., 2016d) and Chapter 7, (iv) events previously used to evaluate MAHLERAN performance (by Turnbull et al., 2010b), and (v) events modelled herein, presented in Chapter 9.

Considering each parameter in isolation, this approach offers a first-order approximation of the (dis)similarity between the various assemblages, focusing on three comparative questions described below. Although more complex treatment is possible, for example, considering the multi-dimensional parameter space occupied by these summary metrics in each assemblage, such treatment is unlikely to be much more informative given the presently available data support, and was therefore considered to be beyond the scope of this project.

- **How (dis)similar are the full, four-season event assemblages to the partial, two-season assemblages reported by Turnbull *et al*.** (2010a)**?**

Whereas the full four-season assemblages encompasses two wetter-than-average seasons and two dryer-than-average seasons, only the two wetter seasons were represented in the assemblages reported in Turnbull *et al*. (2010a). Consequently, as one would expect for the seven metrics considered, the full assemblage exhibited lower average values and (typically) a greater range of values. The full assemblage was therefore considered to be more representative of the average response of these ecosystems.

- **How (dis)similar are the full four-season event assemblages to the assemblages analysed for carbon dynamics?**

The assemblages available for analysis of C fluxes are broadly representative the full event assemblages across all seven metrics considered, with generally similar median values, particularly in total rainfall, peak rainfall intensity, runoff coefficient and sediment flux. The C assemblage typically exhibits larger interquartile ranges, attributed to greater variance in the smaller sample sizes, and typically exhibits a slight negative bias in antecedent soil moisture, with similar but consistently lower median values to the full assemblage. The C assemblage exhibits a slight positive bias in total runoff and peak runoff.

- **How (dis)similar are the assemblages used to evaluate model performance herein from the full, four-season event assemblages, and are they more (or less) representative than the assemblages previously used to evaluate model performance?**

The assemblages of events used to evaluate MAHLERAN'S performance in the present work are considered to be representative of the full assemblage of observed events, with similar median and interquartile ranges across all seven descriptors (Figure 5-5). Relative to the assemblages previously used to evaluate MAHLERAN (Turnbull et al., 2010b), the new assemblages available for the present model evaluation (chapter 9) exhibit better correspondence with the observed event characteristics, particularly in terms of total rainfall, peak rainfall intensity, total runoff, runoff coefficient, and sediment event flux.

Events were unevenly distributed among the plots, but as each event was evaluated separately, this lack of synchronicity (which is common in convective events in dryland regions) does not materially affect the conclusions (sensu Wainwright et al., 2008b, p. 1114).

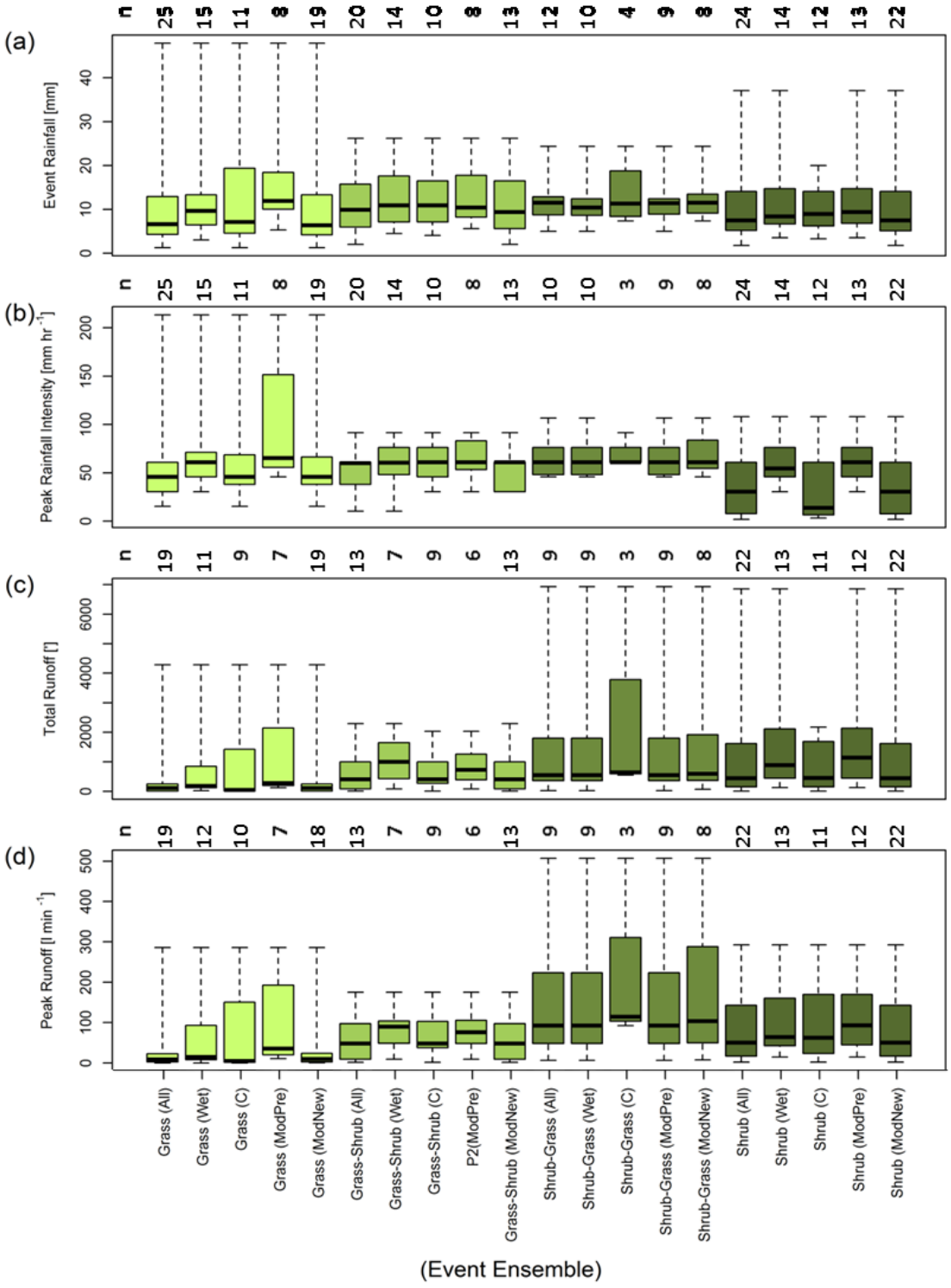

Continued overleaf.

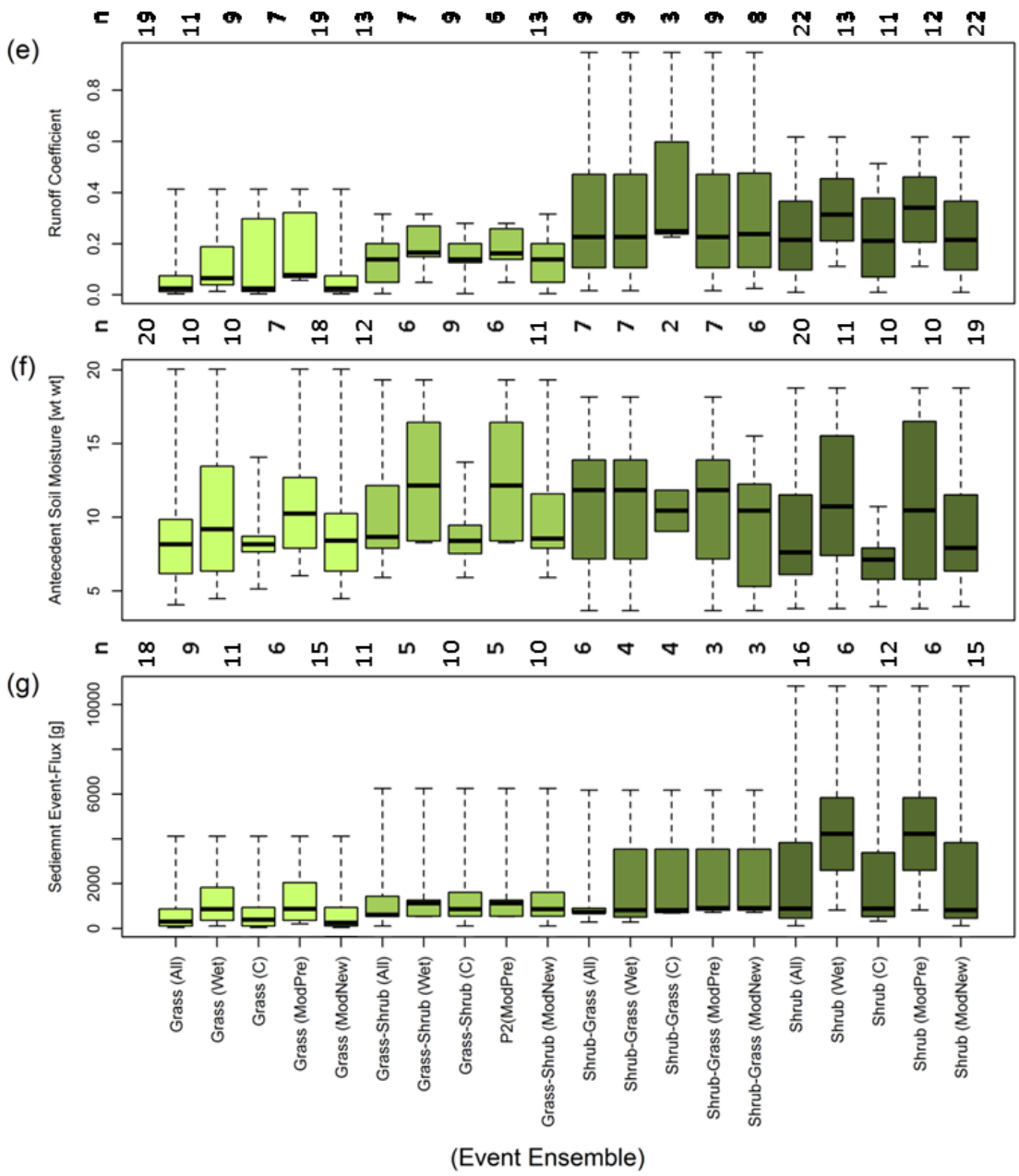

Figure 5-5. (Dis)Similarity of event metrics between different assemblages of rainstorm events. Each panel depicts one metric: (a) total rainfall, (b) peak rainfall, (c) total runoff, (d) peak runoff, (e) runoff coefficient, (f) antecedent soil moisture, and (g) sediment event flux. For each of the four plots, the five assemblages presented are: (i) all events observed over the four monsoon seasons ("All"), (ii) all events observed over the initial two wetter-than-average monsoon seasons (reported in Turnbull et al., 2010a) ("Wet"), (iii) events analysed for erosion-induced carbon fluxes ("C"), (iv) events previously used to evaluate MAHLERAN performance (by Turnbull et al., 2010b) ("ModPre"), and (v) events modelled herein ("ModNew"). From top to bottom, horizontal bars represent the maximum, upper quartile, median, lower quartile, and minimum values. The number of observation (n) for each dataset is presented in above each plot.

5.8. Observational Data for Model Evaluation

Observational data describing the runoff and sediment dynamics of the monitoring plots were originally collected by Drs Alan Puttock (2013; Puttock et al., 2013) and Laura Turnbull (2008; Turnbull et al., 2010a, 2010b). In order to integrate these observational data into a new model evaluation and to support the best possible evaluation of whether model predictions are behavioural (sensu Krueger et al., 2010; Goldstein et al., 2013), it was necessary to re-analyse the original observational data to standardise and refine the methodologies previously employed.

Depth discharge rating functions were recalculated from the original observations of flow depth (*d*) and discharge (*q*) through the supercritical flume, using 2nd degree polynomial models fitted using the least squares approach with intercepts constrained to zero (appropriate for physical reasons). This yielded Equation 5-9, where *d* is flow depth [mm], q is discharge [l s^{-1}], and *a* and *b* are coefficients for each site as specified in Table 5.4. The 95% CI error term for each polynomial model was calculated using all observations, which is considered to be a more appropriate statistical treatment than that employed previously (when observations were simply divided into higher and lower sets each fitted with a polynomial model to estimate upper and lower uncertainty bounds Turnbull, 2008; Puttock, 2013).

$$q_{(d)} = a \times d^2 + b \times d \qquad \text{Equation 5-9}$$

In addition to the uncertainty arising from the depth-discharge relation, additional uncertainty arises from measurement error associated with the depth observations. For the bubbler modules employed, this was considered to be ±0.002 m (Turnbull, 2008). To further constrain uncertainty associated with discharge observations, storage tanks were used to collect the runoff from each plot to independently measure the total runoff (Q_T), along with associated upper and lower bounds (Q_{TMax} and Q_{TMin}, respectively). The results of this comparison are shown in Figure 5-8, and are much more informative than the more limited analysis undertaken previously (e.g. Turnbull, 2008 especially Figure 3.21 therein). Generally there is acceptable agreement between Q_T and total runoff calculated from the hydrograph (Q_H), with the 1:1 line intersecting the 95% CI uncertainty bounds in nearly all cases.

Table 5.4. Parameters for depth/discharge models, and goodness-of-fit metrics

	Grass	Grass-Shrub	Shrub-Grass	Shrub
a	0.0009215	0.0009448	0.001283	0.00107
95% CI	*(0.000807, 0.001036)*	*(0.0008855, 0.001004)*	*(0.001226, 0.001341)*	*(0.0009692, 0.00117)*
b	0.0176	0.02283	0.01175	0.01387
95% CI	*(0.01283, 0.02238)*	*(0.02015, 0.0255)*	*(0.009123, 0.01437)*	*(0.009116, 0.01863)*
Depth-Discharge Model Goodness-of-Fit (GoF)				
SSE	5.854	6.103	5.960	11.300
R^2	0.966	0.982	0.987	0.967
Adjusted R^2	0.966	0.982	0.987	0.966
RMSE	0.206	0.163	0.173	0.259

Where CI is confidence interval, SSE is the sum of squared errors and RMSE is root mean square error.

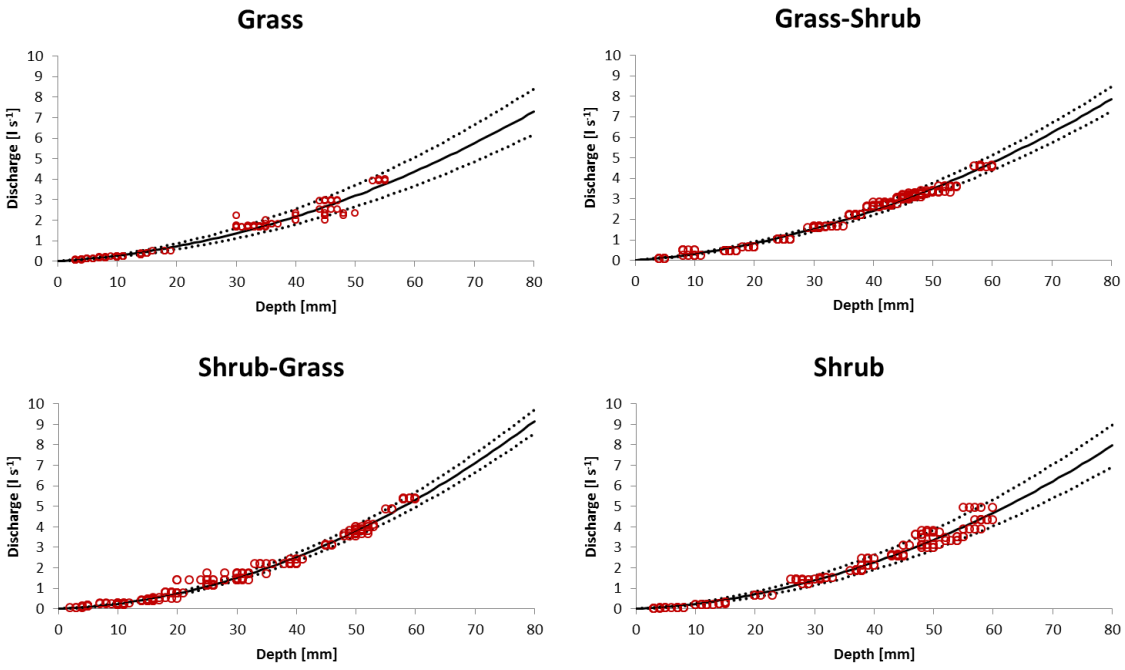

Figure 5-6. Recalculated rating curves (solid lines) with upper and lower uncertainty bounds (dotted lines). Note that uncertainties are calculated differently to previous work (Turnbull, 2008; Turnbull et al., 2010a, 2010b; Puttock, 2013), and are now more robust statistically and larger.

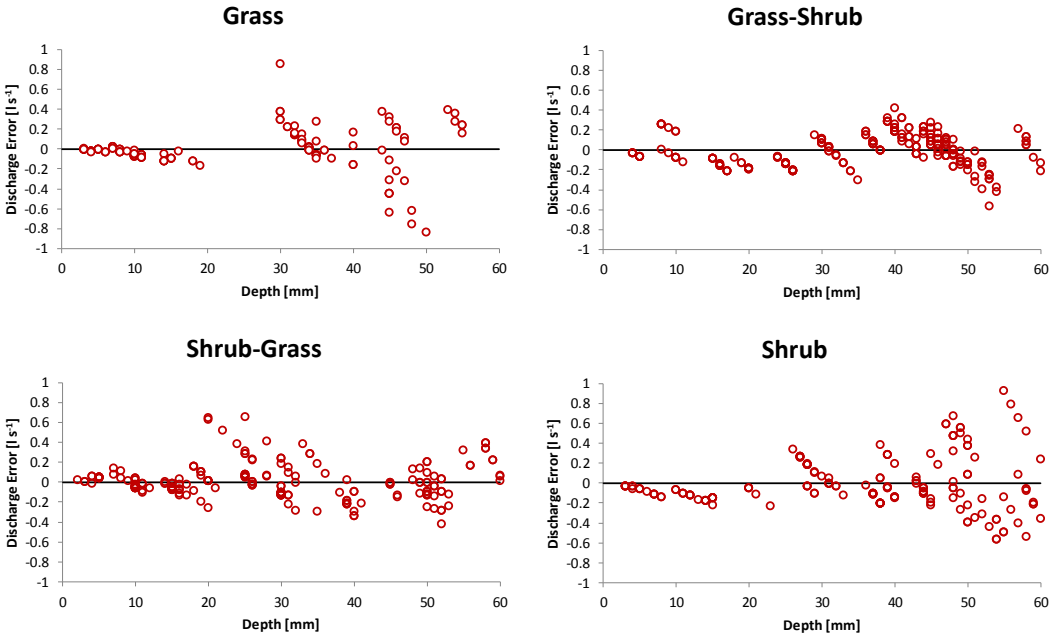

Figure 5-7. Residuals between observed depth-discharge values and the derived rating curve models. The worsening fit at greater depths indicates a positive relationship between flow depth and model uncertainty.

Where Q_T was available, event hydrographs were scaled linearly using coefficients derived from Equation 5-10, where Q_H is the total event discharge derived from the raw hydrograph (Q_H) (after Turnbull, 2008; Turnbull et al., 2010a; Puttock, 2013). The hydrographs were also scaled to the upper and lower uncertainty bounds (@95% CI) of the tank observations (Q_{Tmax} and Q_{TMin}, respectively), using Equation 5-11 and Equation 5-12, respectively, thus constraining uncertainty. Scaled hydrographs usually, but not always, fell within the uncertainty bounds calculated for the unscaled hydrographs. The number of event hydrographs which could be scaled using this approach is given in Table 5.5. Unfortunately, due to operational limitations such as consecutive events and exceedance of the runoff tank capacities, Q_T values are only available to constrain 47 of the 62 observed event hydrographs.

$$S = \frac{Q_T}{Q_H} \qquad \textit{Equation 5-10}$$

$$S_{Max} = \frac{Q_{TMax}}{Q_H} \qquad \textit{Equation 5-11}$$

$$S_{Min} = \frac{Q_{TMin}}{Q_H} \qquad \textit{Equation 5-12}$$

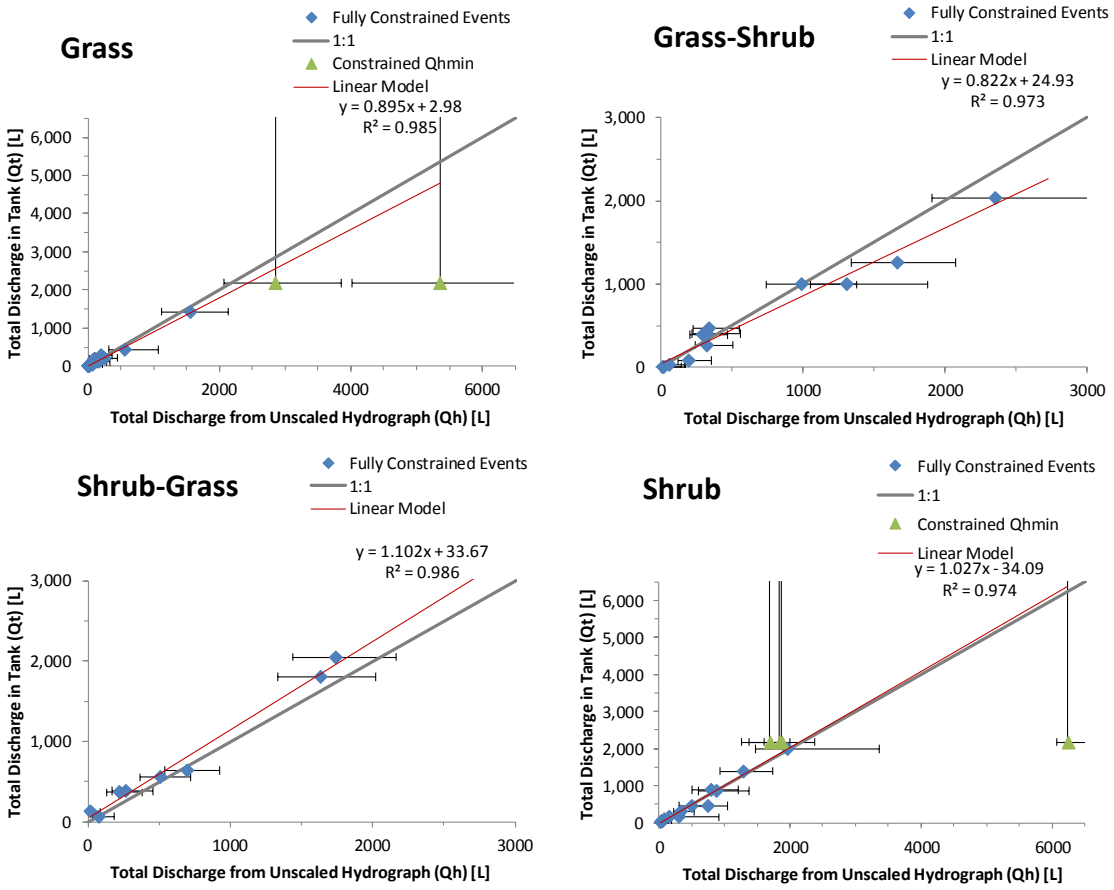

Figure 5-8. Relationship between total discharge calculated from unscaled hydrographs (Q_H) plotted against total discharge measured in the runoff tanks (Q_T), in litres. The grey line denotes 1:1. Note that 95% CI error bars are plotted on both the x and y axes, but are very small in the y axis in the events which did not exceed the tank capacity. The magnitude of the uncertainty bound derived from each hydrograph is sensitive to the shape of that hydrograph.

Table 5.5. Scaled and potentially-scalable hydrographs.

	Grass	Grass-Shrub	Shrub-Grass	Shrub	All
Scaled hydrographs	15	12	7	13	47
Unscaled hydrographs	4	1	2	9	15
***N* available with scaling extrapolation**	19	13	10	21	62
% increase in *n* if scaling relationships were extrapolated	27%	8%	25%	61%	32%

The events which were not constrained by runoff tank observations and thus have unscaled hydrographs included all events yielding more than 2181 litres of runoff. These largest events are likely to be highly significant in terms of erosion-induced redistribution of sediment and associated chemicals, including C (Martinez-Mena et al., 2001; Howes and Abrahams, 2003; Turnbull et al., 2010a, 2010b; Puttock et al., 2013). Furthermore, as discussed in sections 3.4.1 and 5.7, it is desirable to consider large assemblages of natural rainfall events when evaluating whether model predictions are behavioural in comparison to natural events. Consequently, it was useful to consider the transferability of observed scaling relationships to unscaled events.

Previous workers have used linear regression models to predict Q_T from Q_H, Q_{TMax} from Q_{HMax}, and Q_{TMin} from Q_{HMin}, before calculating scaling coefficients accordingly (Turnbull, 2008; Turnbull et al., 2010a). This approach was supported by the high coefficients of determination shown in Figure 5-8 (r^2 0.97 to 0.99); however, it has several significant limitations: (i) linearity is assumed in the relationship between Q_H and Q_T, (ii) the models are only constrained by a limited number of observations (n = 15 to 13), and (iii) linear models are extended far beyond the constraining observations.

The observed scaling coefficients (S) were plotted relative to Q_H for each of the four runoff plots (Figure 5-9). As each of the four plots, scaling coefficients were highly variable when Q_H was low, to trend towards unity around the maximum observed values of Q_H up to the limit of 2120 l (imposed by the capacity of the runoff tank). Where available, runoff events which exceed the tank capacity are also plotted, as the full tank constrains the minimum amount of runoff that rasults from the event (shown by the green triangles in Figure 5-9). Importantly, Q_H was found to be a very poor predictor of S, as illustrated by the poor correspondence between the linear regression models and S ($R^2 < 0.03$).

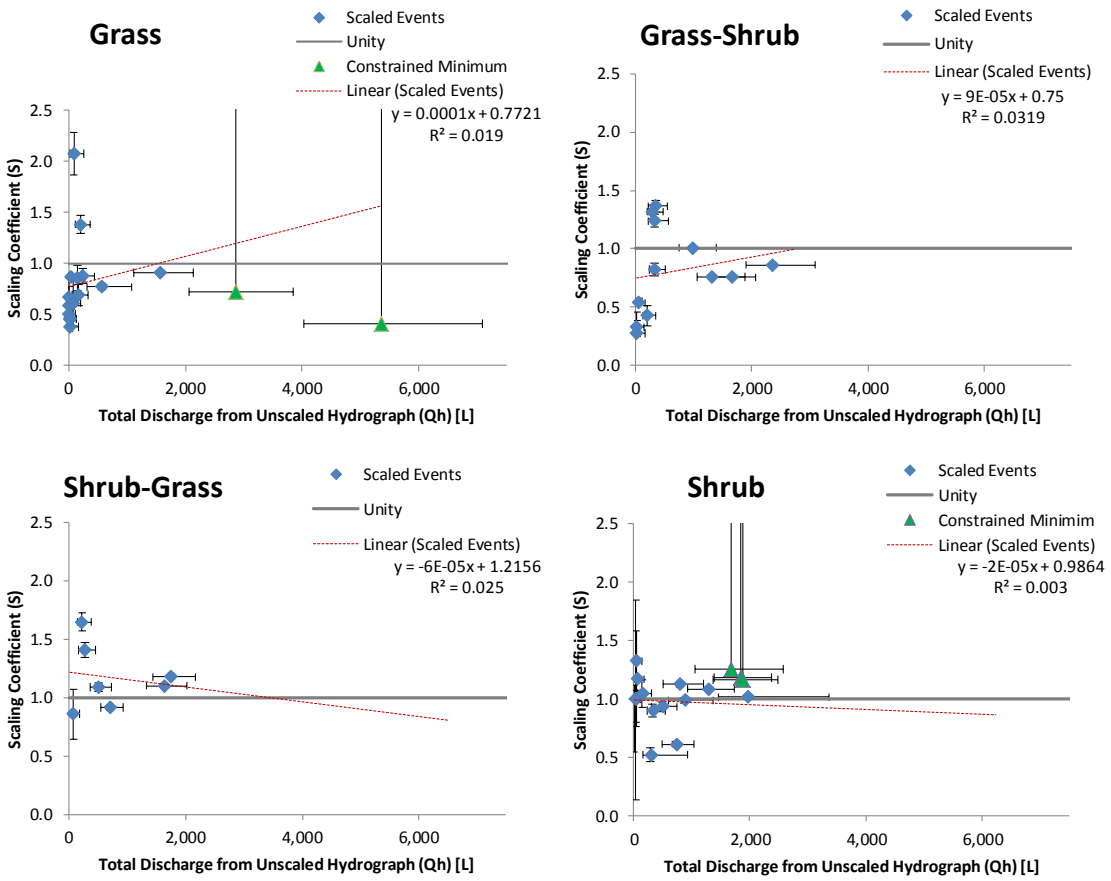

Figure 5-9. Relationship between total discharge calculated from unscaled hydrographs (Q_H) and the scaling coefficient (S). Unity is indicated by the grey line, and linear regression models by the red dashed line. In five events which exceeded the runoff tank capacities which therefore only constrains the minimum runoff, the minimum scaling coefficient is indicated by the green triangle. The magnitude of the uncertainty bounds around the Q_H is strongly influenced by the shape of each hydrograph.

The available information supports the following statements.

- At the grass-dominated plot, hydrographs are likely to overpredict discharge during smaller magnitude events, resulting in a mean scaling coefficient of ~0.80 when Q_H < 1000 l (*n* = 14). When Q_H > 1000 l, scaling coefficients are likely to be ~1 (insufficient observations to average).
- At the grass-shrub-dominated plot, hydrographs are likely to overpredict discharge during smaller magnitude events, resulting in a mean scaling coefficient of ~0.73 when Q_H < 500 l (*n* = 7). When Q_H > 500 l scaling coefficients are likely to be ~0.84 (mean of five highest observations).

- At the shrub-grass plot, hydrographs are likely to underpredict discharge during low magnitude events, resulting in a mean scaling coefficient of ~1.18 when Q_H < 500 l (n = 5). When Q_H > 500 l scaling coefficients are likely to be ~1.07 (mean of four highest observations).
- At the shrub plot, hydrographs are generally fairly accurate, particularly during smaller magnitude events so scaling coefficients are considered to be most likely to be 1 when Q_H < 1000 l. Runoff tank observations can constrain the minimum total runoff; in three events Q_H under-predicted Q_T, requiring scaling coefficients of 1.18, 1.16 and 1.25 for the scaled hydrographs to exceed the observed minimum discharge. Therefore, reconciling the available information, these estimated scaling values were used for these three events, and when Q_H is > 1000 l scaling coefficients are considered to be most likely to be 1.1.

Consequently, in an effort to minimise systematic bias in the observational data, hydrographs unsupported by independent Q_H observations were adjusted using the scaling coefficients as described in the preceeding statements. Figure 5-10 illustrates the distributions of the estimated scaling coefficients and resultant estimates of Q_H.

This approach is considered to represent the most robust, data-based method to derive the best possible observational datasets to evaluate whether MAHLERAN's predictions are behavioural. Figure 5-10 also exemplifies some of the limitations with the previous approach of extrapolating linear regression models, which could *increase* hydrograph error, particularly in larger events as illustrated in the case of the grass-dominated plot. Note that it is not considered appropriate to use estimated scaling coefficients to scale the upper and lower uncertainty bounds, and consequently events which are scaled using estimated coefficients only have a 'best estimate' hydrograph, without uncertainty bounds. With the benefit of hindsight, if these experimental plots were being constructed afresh it would be desirable to install an additional runoff tank to capturing a known fraction of the total runoff, in order to support hydrograph scaling for large events which may exceed the capacity of the primary tank.

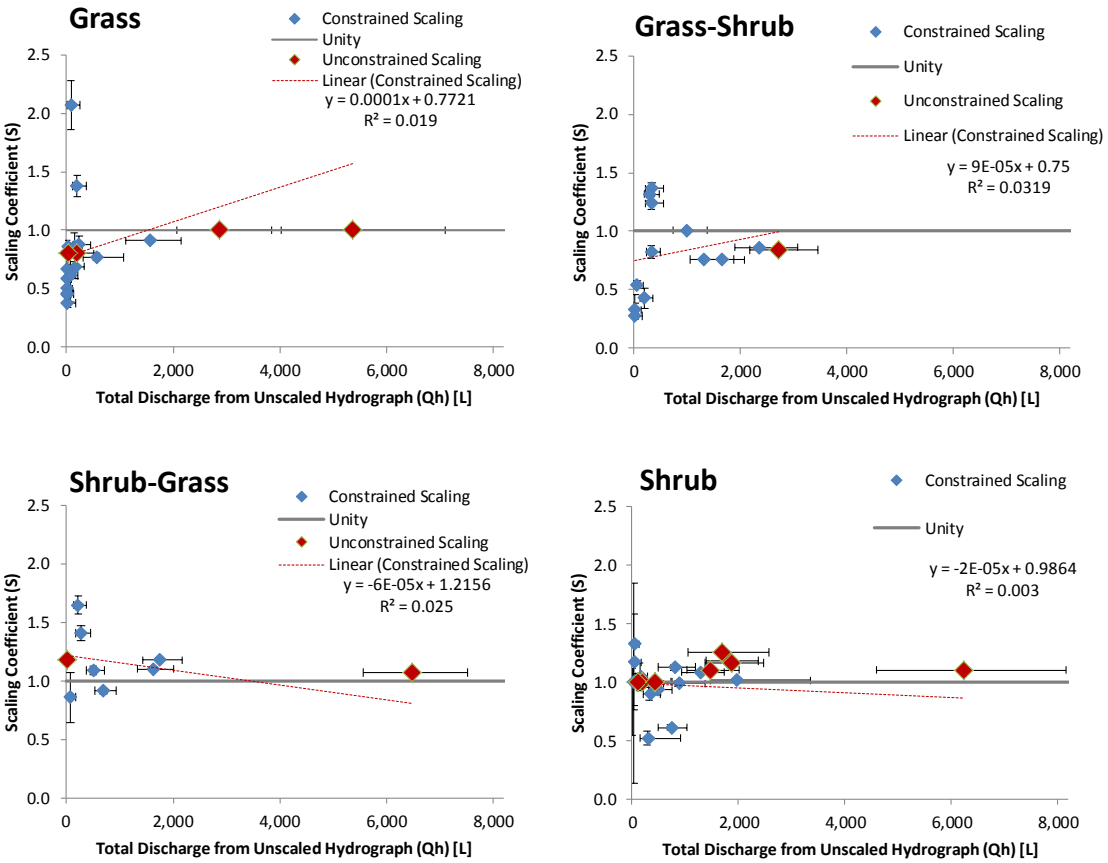

Figure 5-10. Relationship between total discharge calculated from unscaled hydrographs (Q_H), and the observed and best-estimates of scaling coefficients (S). Unity is indicated by the grey line, and (previously used) linear regression models are shown by the red dashed line. This illustrates where estimation of S was necessary relative to available observations. Note that the magnitude of the uncertainty bounds is strongly influenced by the shape of each hydrograph, and that is was not appropriate to estimate uncertainty bounds associated with estimated scaling coefficients.

6. Organic Carbon

6.1. Chapter Overview

This section examines soil organic carbon (OC) dynamics across the ecotone from grass-dominated to shrub-dominated sites. Particular focus is on the distribution of OC between particle size fractions and the erosion-induced redistribution of OC. The rationale leading to the objectives listed below is described in section 3.1.

The material presented in this chapter has been published in ***Cunliffe, Andrew M., Alan K. Puttock, Laura Turnbull, John Wainwright, and Richard E. Brazier. 'Dryland, Calcareous Soils Store (and Lose) Significant Quantities of near-Surface Organic Carbon.' Journal of Geophysical Research: Earth Surface, 2016. doi:10.1002/2015JF003628***, and a copy of this article is included in Appendix 7.

6.2. Objectives

A1 Characterise the distribution of OC across particle-size fractions, in order to:

- **(i) Assess potential OC storage in coarse (>2 mm) particles**
- **(ii) Parameterise a deterministic runoff/erosion model**

A2 Quantify differences in erosion-induced effluxes of OC across an ecotone of changing plant functional types from a grass-dominated to a shrub-dominated ecosystem over four monsoon seasons.

A4 Investigate controls on OC enrichment in natural ecosystems subjected to natural rainfall events, quantifying the extent to which particle size selectivity can explain observed OC enrichment

6.3. Key Findings

- Coarse (>2 mm) clasts can contain relatively significant amount of organic carbon, accounting for ca. 20-30 percent of total soil organic carbon in the near-surface soil.
- Erosion-induced yields of organic carbon are higher from shrublands relative to grasslands, with average event yields four times higher from the shrub-dominated site.
- Sediment eroded from shrub-dominated sites exhibited significantly greater enrichment in organic carbon relative to sediment eroded from grass-dominated sites.

6.4. Results

6.4.1. Organic carbon in the near-surface (0-0.05 m) soil

Four hundred aliquots were analysed to characterise OC concentrations in the near-surface soil. There was a bimodal distribution in OC concentrations across particle size fractions, consistent in the average values for each surface cover type at all sites (data not shown), with peaks in both the finest (<0.0625 mm) and some sand (1-0.5 mm and 2-1 mm) fractions (Figure 6-1). Across the grass-shrub ecotone, there was generally an overall decrease in the proportion of particles smaller than 0.125 mm and an increase in the proportion of particles larger than 0.25 mm (Figure 6-1, Table 6.1). One hundred >2 mm aliquots were analysed, revealing OC concentrations ranging from 0.2% to 3.7% and <0.1% to 1.1% for the >4 mm and 4-2 mm fractions, respectively. The areally-weighted average OC concentration was very similar to the average OC concentrations of the fine (< 2 mm) fraction (Figure 6-2a). These averages represent a wide range of concentrations, and are not an artefact caused by the lower detection limit of the elemental analyser.

The areally weighted, whole-soil, near-surface (0-0.05 m) OC stock is 275.8±24.0, 315.5±34.6, 390.5±60.8 and 327.7±36.3 g OC m^{-2}, in the grass-, grass-shrub-, shrub-grass- and shrub-dominated sites, respectively (Figure 6-2b). Coarse (>2 mm) particles contribute 24% to 38% of these overall SOC stocks, mainly due to the abundance of these fractions (20% to 37% by weight)

(Figure 6-1c). The proportion of the total SOC stock associated with the coarsest (>4 mm) fraction increases across the grass-shrub ecotone, mainly due to changes in PSD (Figure 6-1b and c). Despite its relatively low OC concentration, the 0.125-0.0625 mm fraction contributes substantially (18% to 22%) towards the whole-soil SOC stock, primarily due to the abundance of particles in this size-fraction (21% to 33% by weight) (Figure 6-1b and c). Across the grass-shrub ecotone, there was generally an overall decrease in the proportion of particles smaller than 0.125 mm and an increase in the proportion of particles larger than 0.25 mm (Figure 6-1b).

Table 6.1. OC concentrations [%] in near-surface (0-0.05 m) soil (Errors are SE).

	Site			
Particle Size Fraction [mm]	**Grass**	**Grass-Shrub**	**Shrub-Grass**	**Shrub**
<0.0625	0.71±0.04	0.72±0.06	0.73±0.08	0.69±0.06
0.125-0.0625	0.28±0.02	0.31±0.03	0.46±0.06	0.31±0.03
0.25-0.125	0.25±0.03	0.26±0.04	0.44±0.12	0.27±0.05
0.5-0.25	0.39±0.05	0.38±0.07	0.54±0.12	0.31±0.06
1-0.5	0.70±0.12	0.65±0.11	0.89±0.20	0.61±0.10
2-1	0.55±0.11	0.59±0.11	0.81±0.21	0.60±0.11
4-2	0.41±0.02	0.35±0.05	0.41±0.07	0.39±0.04
>4	0.47±0.09	0.47±0.11	0.53±0.15	0.58±0.15

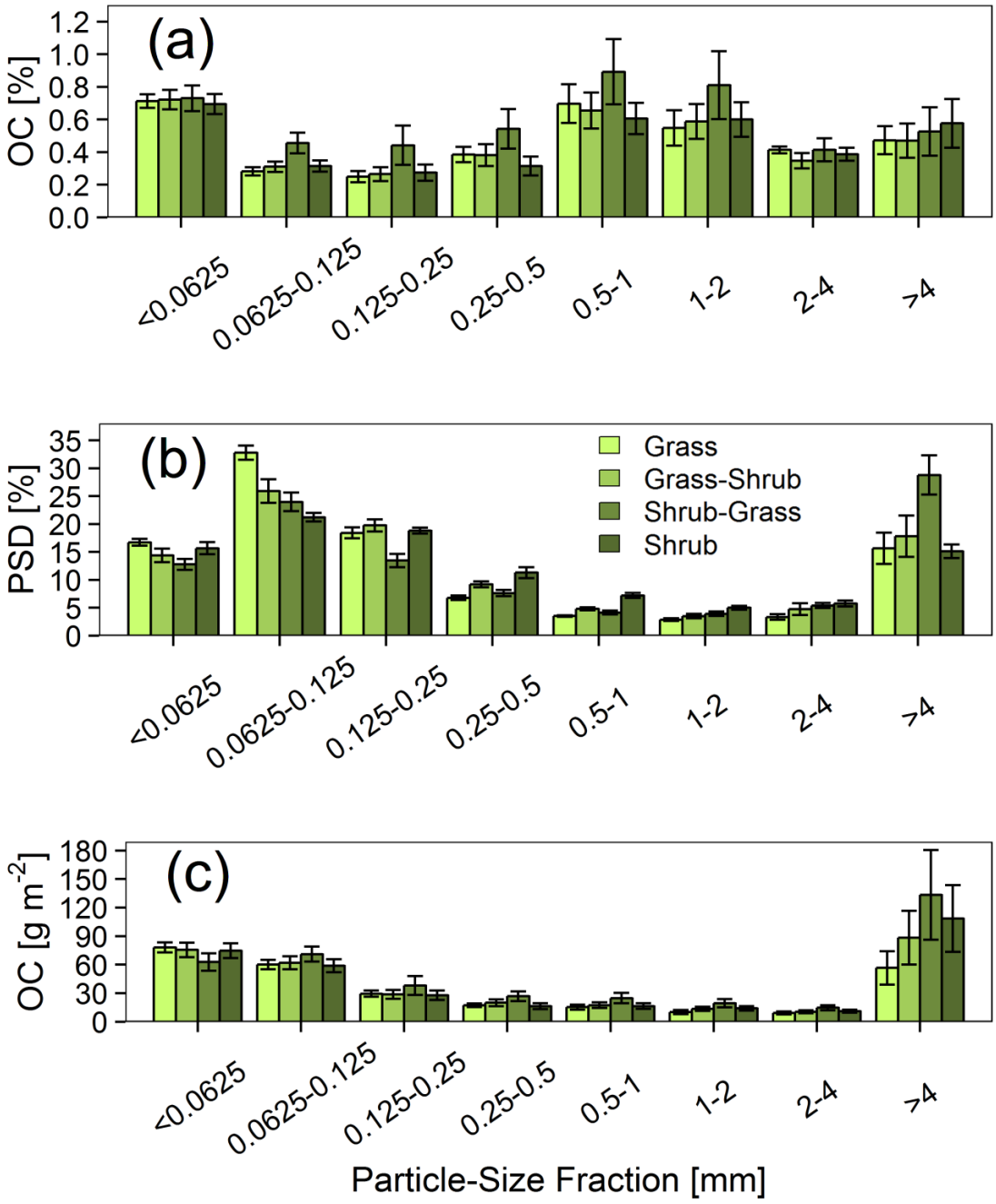

Figure 6-1. For each study site across the grass-shrub ecotone: (a) areally-weighted organic carbon (OC) concentrations observed in each particle size fraction, (b) areally-weighted particle size distribution (PSD), and (c) areally-weighted OC concentration in each particle size fraction in near-surface (0-0.05 m) soil [g m-2] (weighted by the fractional mass of each particle size fraction). Bar colours correspond to sites across the grass shrub ecotone (as shown in Table 1 and Table 6.1). Values are means ± standard error.

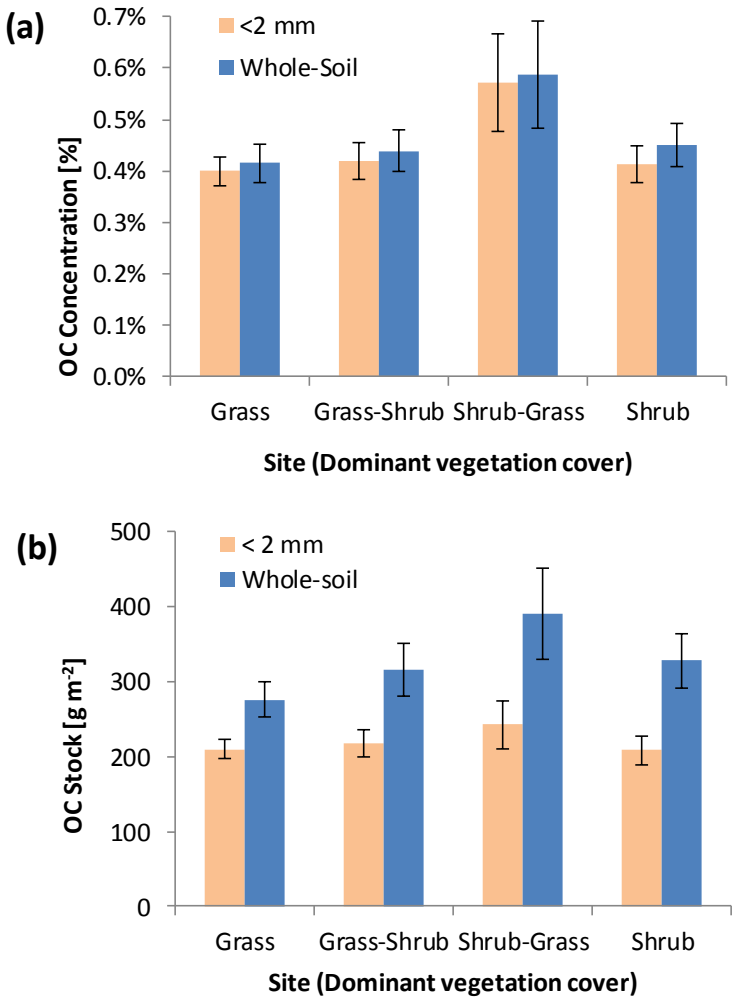

Figure 6-2. (a) Areally-weighted near-surface (0-0.05 m) average organic carbon (OC) concentrations in the <2 mm fraction and whole soil. (b) Areally-weighted near-surface soil OC stocks for each site, calculated for the <2 mm fraction, and with the whole-soil OC concentration (including the >2 mm fractions). Values are means ± standard error.

6.4.2. Erosion-induced OC event yields and enrichment dynamics

Observed OC event yields greatly exceeded those predicted using the average OC concentrations of the contributing surface soils, indicating substantial OC enrichment. The magnitude of the under-prediction error is correlated with event yield magnitude, and the median underestimate was 65% (±4.9%). It is more appropriate to report mean event yield (± standard error) of OC rather than the total mass of eroded organic C for two reasons:

(i) The convective rainfall which drives these erosion events is characteristically highly variable in both space and time (Wainwright, 2005; Petrie et al., 2014). Establishing these runoff plots across a vegetation ecotone in a natural ecosystem meant that the runoff plots could not be located immediately adjacent to one another, and while they were located within just a few km of each other the different sites experienced different storm events over the monitoring periods and therefore total yields are not directly comparable (Turnbull, 2008; Turnbull et al., 2010a).

(ii) Due to equipment limitations in these very harsh environments, it was not possible to measure the erosion-induced OC yields resulting from all erosion events. Critically however, in terms of total rainfall, total runoff, runoff coefficients and total sediment event yield, the 37 events presented herein are representative of all of the events observed over the four monsoon periods, albeit with some larger differences in the shrub-grass site due to the small sample size analysed for OC yields ($n = 4$) (assemblage representativeness was evaluated in section 5.7).

Mean OC event yield increased substantially across the grass-shrub ecotone, from 15.3, 22.2, 49.7 and 83.3 g from the grass, grass-shrub, shrub-grass and shrub dominated sites, respectively. The six-fold increase was caused by both increasing erosion and increasing OC enrichment in the eroded sediment. A heteroscedastic t test suggested that the difference in OC event yield between the two combined grass-dominated sites (Mean = 18.65, SD = 25.57) versus the two combined shrub-dominated sites (Mean = 74.87, SD = 108.26) was only statistically significant to the 6% level ($t = 2.034$, $df = 16.28$, $p = 0.059$). OC event yields were variable, both between events and between sites, with the standard error of the mean increasing across the grass-shrub ecotone from 7.8, 7.9, 24.5

and 36.7, for the grass, grass-shrub, shrub-grass and shrub sites respectively (Figure 6-3a).

The <0.25 mm particle size fractions contributed an average of 85.1% (±1.6%) of the total OC event yield over all events. Considering all sites together, event ER_{OC} values ranged from 1.0 to 10.2, and were greater than unity in 97% of the events, >2 in 68% of events, and >6 in 24% of events (Figure 6-3b). Overall, ER_{OC} was statistically significantly >2 (Wilcoxon one-sample signed rank test; V=551, p<0.001). Stratifying by site reveals a substantial increase in mean OC enrichment across the grass-shrub ecotone, with mean ER_{OC} increasing from 2.74, 3.36, 4.89 and 5.16 for the grass, grass-shrub, shrub-grass and shrub dominated sites, respectively (Figure 6-3b).

Variation in ER_{OC} also increased across the grass-shrub transition, with SE increasing from 0.51, 0.73, 0.74 and 1.13 for the grass, grass-shrub, shrub-grass and shrub dominated sites, respectively. A heteroscedastic t test indicated that the difference in ER_{OC} between the two amalgamated grass-dominated (M = 3.04, SD = 2.07) and the two amalgamated shrub-dominated sites (M = 5.09, SD = 3.42) was statistically significant (t = 2.126, df = 23.17, p = 0.044). OC enrichment was observed in all five particle size fractions during nearly all events, and across the grass-shrub ecotone, there was an increase in ER_{OC} in all particle size fractions smaller than 2 mm. In events showing overall OC enrichment (36/37), changes in PSD were found to explain a median average of 6% and up to 67% of observed OC enrichment.

ER_{OC} was plotted against metrics of event intensity and magnitude: total rainfall, peak rainfall intensity, runoff coefficient, peak runoff, total runoff, total sediment event yield, total event sediment concentration (Figure 6-4). ER_{OC} generally exhibited weakly positive correlations with most metrics (with the exception of total event sediment concentration), and there was some indication for steepening of the relationships across the grass-shrub ecotone. However, these relationships were not strong and and further statistical analysis is hindered by the nonparametric data distributions and limited degrees of freedom ($n \leq 12$). Stratified by site, ER_{OC} was also plotted against the chronological order of the events over the monitoring period; revealing no evidence of systematic change in ER_{OC} values through time, particularly given the high degree of variation between the precipitation event characteristics (data not shown).

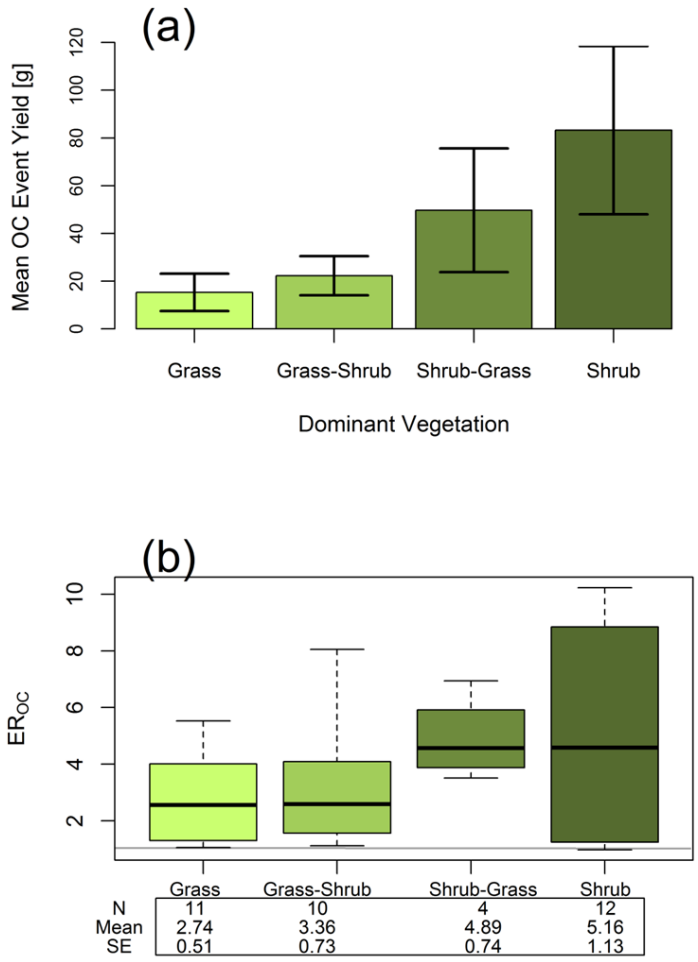

Figure 6-3. (a) Mean organic carbon (OC) event yield (± standard error) and (b) OC enrichment ratios and summary statistics, stratified by site. Where N is number of rainfall events, and SE is standard error. Bar colours correspond to sites across the grass shrub ecotone (as shown in Table 5.3). In the boxplots, from top to bottom, horizontal bars represent the maximum, upper quartile, median, lower quartile, and minimum values. The grey line in (b) denotes unity.

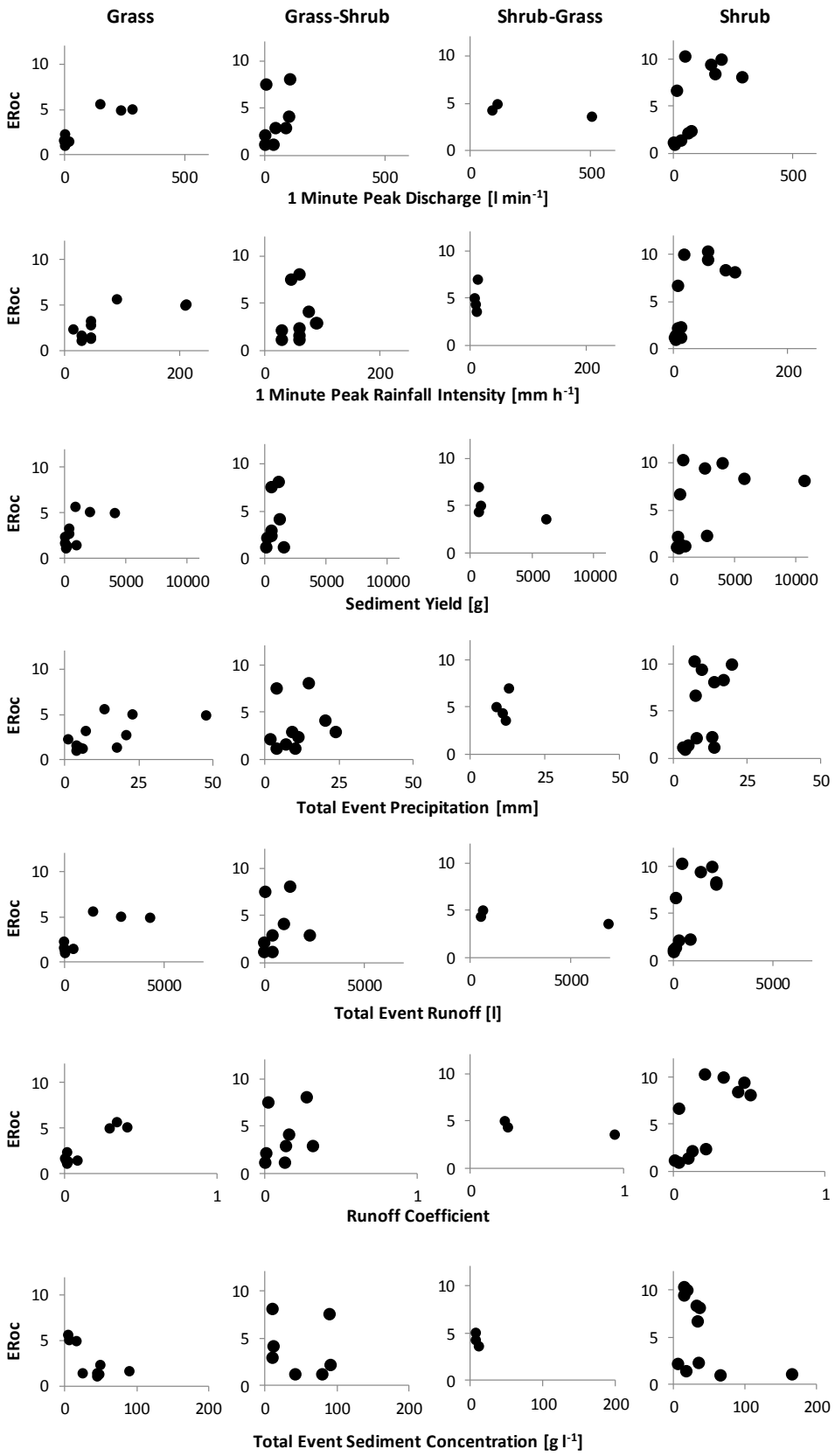

Figure 6-4. Relationships between the organic carbon enrichment ratio (ER_{OC}) and metrics of event intensity and magnitude: 1 minute peak discharge, 1 minute peak rainfall intensity, sediment yield, total event precipitation, total runoff, runoff coefficient, and total event sediment concentration (Cevent = S_{event} / Q_{event}).

6.5. Discussion

6.5.1. Particle Size Distribution

Across the grass-shrub ecotone there was a decreasing proportion of <0.125 mm particles and an increasing proportion of >0.25 mm particles remaining in the near-surface soil. If it is assumed that changes in PSD observed in space across the grass-shrub ecotone represent change through time, this finding is consistent with the progressive degradation of the soil resource and development of stone pavement cover concomitant with vegetation change in this desert landscape (Wainwright et al., 1995, 1999b, 2000; Turnbull et al., 2008b; Rieke-Zapp et al., 2007; Michaelides et al., 2009; Brazier et al., 2013; Puttock et al., 2014).

6.5.2. OC stocks in the near-surface soil

The relationships between particle size and OC concentration were broadly consistent across all sites – and also microsite surface cover at each site (data not shown) – showing relatively subdued variation in OC concentration between particle size classes (Figure 6-1, Table 6.1). This subdued variation in OC with particle size is similar to the relationships reported by Lister (2007) from the slightly dryer Long Term Ecological Research (LTER) site at the Jornada in southern New Mexico, although that dataset was truncated due to an assumption that >2 mm particles contained no OC (shown in Figure 6-5). The two studies were very similar with sampling of near-surface soil from 0-0.01 m depth, three replicates from three microsites (grassland, bare interplant, and beneath creosotebush (*L. tridentata*) shrubs, particle fractionation by dry sieving. There was no evidence of a peak in OC concentrations around the coarse sand fraction (0.5-2 mm) in the dataset from the Jornada. The meticulous cross-validation of OC determinations described in section 5.5 affords high confidence in the data presented in the present study.

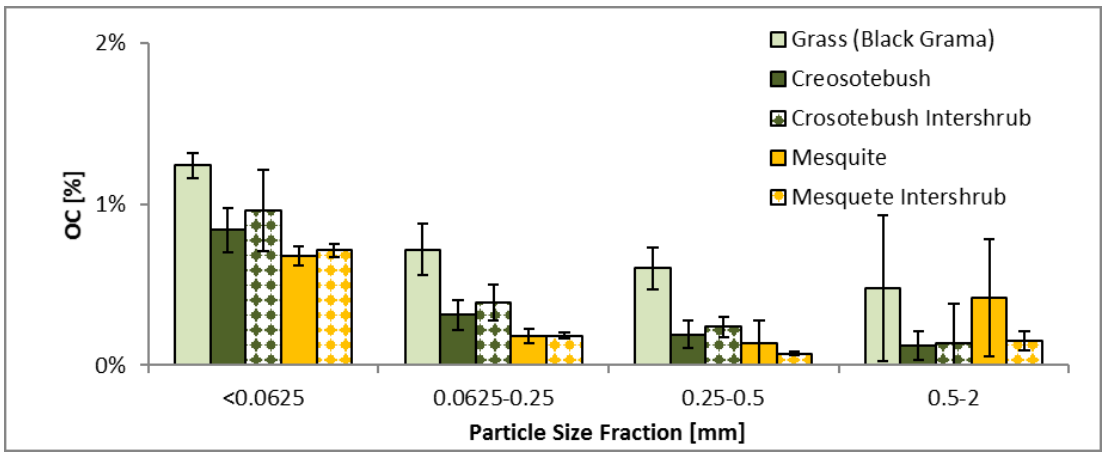

Figure 6-5. Concentration of OC concentration across particle size fractions for sites at the semi-arid Long Term Ecological Research site at the Jornada in southern New Mexico (after Lister, 2007). Note that these data pertain to microsites either beneath shrub canopies or in intershrub areas, rather than areally-weighted averages).

Both of the coarse (>4 mm and 4-2 mm) particle size fractions contained mean OC concentrations similar to the fine (<2 mm) fraction (Figure 6-2a), and accounted for 24% to 38% of the total near-surface SOC stocks (Figure 6-1c). The proportion of the near-surface SOC stocks associated with the coarse particles cannot be simply extrapolated to deeper soil layers because erosion of fine particles by aeolian and fluvial processes can increase the relative abundance of coarse particle in the near-surface soil (Larney et al., 1998; Wainwright et al., 1999b, 2000). Critically, widely used standard protocols discard the >2 mm clasts, assuming they contain no SOC (e.g. Robertson and Paul, 2000; Lal and Kimble, 2001; Ellert et al., 2001; Bird et al., 2002; Jackson et al., 2002; Ewing et al., 2007; Throop et al., 2012a; Sankey et al., 2012; Frank et al., 2012; De Baets et al., 2013; Brazier et al., 2013; Puttock et al., 2013, 2014; X. Wang et al., 2015). Ignoring OC in the coarse fraction of these calcareous soils therefore risks substantial underestimation of SOC stocks in C inventories (*sensu* Agnelli et al., 2002; Corti et al., 2002).

Noteworthy concentrations of organic C in >2 mm clasts have been reported by Corti *et al*. (2002) and Agnelli *et al.* (2002) for a variety of environmental contexts, which they attributed to a combination of organic particles incorporated during the formation of sedimentary rocks and to subsequent infilling of porous rock

fragments by soil solutions containing organic substances. These rock fragments contributed up to 4.5% of the total SOC in a forest soil, and were found to be chemically and biologically active in the soil, forming what was described as a continuum with the fine earth (<2 mm particles) (Agnelli et al., 2002).

In calcareous soils, the precipitation of calcium carbonate is known to stabilize soil aggregates (Bryan, 2000; Nash and McLaren, 2003; Alonso-Zarza and Wright, 2010), and in the present study substantial disaggregation was frequently observed in both soil and eroded sediment samples following the acid pre-treatment, resulting in particle size reductions of up to five ϕ intervals in individual aggregates. Such stabilized aggregates are likely to include OC associated with fine particles, or fine particulate organic matter (POM) (Duchaufour, 1976; Goudie, 1996; Baldock and Skjemstad, 2000), particularly as the biochemical actions of roots and fungi can facilitate the formation of pedogenic (secondary) carbonates in arid soils (Klappa, 1980; Wullstein and Pratt, 1981; Wright et al., 1995; Goudie, 1996; Alonso-Zarza and Wright, 2010; Gocke et al., 2011; Schlesinger and Bernhardt, 2013a). Therefore, it is suggested here that the relatively substantial OC concentrations observed in coarse (>2 mm) particles are likely due to the stabilization of soil aggregates by precipitated calcium carbonate (Duchaufour, 1976; Oyonarte et al., 1994; Goudie, 1996; Baldock and Skjemstad, 2000). Calcium carbonate precipitation in calcareous dryland soils may contribute to the physical protection of OM from decomposition, both by forming thin coatings of pedogenic (secondary) carbonate on OM, and by stabilizing aggregates (Duchaufour, 1976; Oyonarte et al., 1994; Olk et al., 1995; Baldock and Skjemstad, 2000; Clough and Skjemstad, 2000; Lopez-Sangil and Rovira, 2013).

Consequently, it appears appropriate to recommend a re-evaluation of the ubiquitous assumption that the coarse (>2 mm) fraction of the soil is free of OC, particularly in environments with stabilised aggregates such as calcareous soils. While there is an extensive literature on many aspects of carbonate formation (see Breecker et al., 2009; Alonso-Zarza and Wright, 2010) and several studies mention the mechanisms by which precipitated calcium carbonate physically protects OC (e.g. Duchaufour, 1976; Oyonarte et al., 1994; Olk et al., 1995; Baldock and Skjemstad, 2000; Clough and Skjemstad, 2000; Lopez-Sangil and Rovira, 2013), there appears to be something of a knowledge gap regarding the

full implications of calcium carbonate precipitation for soil OC dynamics in drylands. This mechanism may contribute to the characteristically high mean residence times of soil OC in dryland ecosystems (Frank et al., 2012), and radioisotope analysis could be utilised to determine whether OC in the coarse (>2 mm) particle fraction is chemically and biologically active, as found by Agnelli *et al.* (2000, 2002) in a temperate forested environmental context.

6.5.3. Erosion-induced OC event yield and enrichment dynamics

This section describes the predominantly interrill erosion-induced efflux of OC from four large (300 m^2) runoff sites during 37 rainstorm-runoff events over a four year period. The analysis expands upon previous investigations into erosional C dynamics at these sites (Puttock et al., 2012b, 2013, 2014; Brazier et al., 2013) by quantifying the temporally-variable OC event yield through both wetter- and drier-than-average monsoon seasons (Petrie et al., 2014). This data set is believed to represent the largest plot-scale characterisation of erosion-induced OC yields from any dryland ecosystem. This information is valuable because it represents total capture of sediment eroded from unperturbed sites during natural rainfall events for 31/37 erosion events, and substantial capture of sediment eroded during the other six events. Consequently, these data afford a more accurate representation of erosion-induced redistribution of OC in semi-arid natural landscapes than is possible using the predominantly laboratory-scale, reductionist experiments undertaken to date. The relatively long period of monitoring is valuable in that it yields assemblages of natural erosion events, analyses of which helps to elucidate emergent properties of resource redistribution processes in these ecosystems.

The six-fold increase found in average erosion-induced OC yields across the grass-shrub ecotone was consistent with earlier, less comprehensive, analysis (Brazier et al., 2013; Puttock et al., 2013, 2014), and was driven predominantly by greater soil erosion (~3.5 fold increase) (for further discussion see Jin et al., 2008, 2009; Turnbull et al., 2010a). This increase in soil erosion has been largely attributed to reduced vegetation cover, increased runoff generation and greater hydrological connectivity in the shrublands (Turnbull et al., 2010a; Puttock et al., 2013). Importantly, eroded sediments were also significantly enriched in OC relative to the contributing near-surface soil, and OC enrichment increased

significantly across the grass-shrub ecotone, almost doubling from the grass-dominated site to the shrub-dominated site.

Because OC concentrations usually decrease rapidly with depth (Charley and West, 1975; Bird et al., 2002; McClaran et al., 2008), ER_{OC} values are sensitive to the sampled depth of the contributing surface soils (Cogle et al., 2002; Li et al., 2007). The 0-0.05 m depth considered herein is shallower than is often considered (e.g. Quinton et al., 2006), which should increase the OC concentration of the contributing soil (CS_{OC}) relative to the OC concentration of the eroded soil (ES_{OC}), and therefore reduce ER_{OC} values (although this hypothesis was not corroborated by Cogle et al. (2002)). In contrast to this expectation, observed ER_{OC} were often found to be far greater than the highest values previously reported in the literature (e.g. ≤3.0 Palis et al., 1997; Cogle et al., 2002; ≤5 Lal, 2003, 2005; ≤3 Rhoton et al., 2006; ≤5.5 Quinton et al., 2006; ≤2.2 Truman et al., 2007; ≤2.2 Jin et al., 2008; ≤3.9 X. Wang et al., 2014c).

OC enrichment is commonly attributed to the selective detachment and transport of fine OC-rich particles (e.g. Nelson et al., 1994; Balesdent et al., 1998; Guibert et al., 1999; Rhoton et al., 2006; X. Wang et al., 2013). Although the interrill erosion from the study sites was strongly size-selective with preferential transport of fractions smaller than 0.25 mm (Turnbull et al., 2010a; Puttock, 2013), differences in OC concentration between particle size fractions in the contributing soil were fairly small (Figure 7-1a). Particle size selectivity was found to only explain an average of 6% of observed OC enrichment across the assemblage of events; indicating changes in particle size selectivity do not significantly drive the significant, systematic change in ER_{OC} observed across the grass-shrub ecotone. This insensitivity of OC enrichment to particle size distribution is strikingly different to findings from a similar semi-arid site at the Jornada that the erosional redistribution of sediment bound nitrogen and phosphorus was highly sensitive to particle size distribution (Lister, 2007; Michaelides et al., 2012).

Relative to black grama grasses, creosotebush shrubs produce more litter (Liao et al., 2006a). Long-term decomposition experiments have shown that *L. tridentata* litter decomposes much more rapidly than *B. eriopoda* and *B. gracilis*. litter in this environmental setting (Vanderbilt et al., 2008), in contrast to predictions based on the litter biochemistry (Liao et al., 2006b). Despite these differences in decomposition rate, it is hypothesized here that the observed

increase in ER_{OC} across the grass-shrub ecotone may arise from differences in the biotic processes continually contributing OC to the soil surface, which may not be incorporated evenly throughout the 0-0.05 m layer, causing an increased availability of OC in the uppermost surface soil of shrublands relative to grasslands.

Previous understanding arising from reductionist experimental work predicts that enrichment ratios should decrease over time towards unity, due to depletion of OC-rich fines in the source soil (e.g. Polyakov and Lal, 2004a; Jin et al., 2009; Hu et al., 2013). However, there was no evidence of decreasing enrichment ratios over the four year study period, indicating that the previous finding may be an artefact of the experimental designs deployed in lab-based studies. The results presented herein suggest that OC enrichment can be an enduring phenomenon, at least at hillslope scales in semi-arid rangelands, and the preferential removal of OC may be sustained long-term by the dynamic replacement of OM via litter inputs via the soil surface (Harden et al., 1999; Li et al., 2007; Berhe et al., 2008; Doetterl et al., 2012). This interpretation is consistent with monitoring of eight 875 m^2 runoff plots in an intensively managed temperate agro-ecosystem, which also found no decreasing trend in OC enrichment in the eroded sediments over a ten-year monitoring period (Quinton et al., 2006).

OC enrichment dynamics in eroded sediment may also be a function of event intensity. Prior work suggests that OC enrichment will decrease during higher intensity events, due to the increasing dominance of less-selective detachment and transport processes (Ghadiri and Rose, 1991a; Truman et al., 2007; Schiettecatte et al., 2008a; Jin et al., 2009; Wang et al., 2010; X. Wang et al., 2014c; Kuhn et al., 2012), as discussed earlier (Section 3.1.1) and illustrated as Model 1 in Figure 6-6a. However, in these semi-arid ecosystems, changes in particle size selectivity are not so simply related to event magnitude, as larger rainstorm events produced smaller proportions of sand and a higher proportion of silt in eroded sediment (Turnbull, 2008; Puttock, 2013), and the results reported above show that size-selective transport plays a minor role in OC enrichment. Instead, I hypothesize that the effect of rainfall event intensity on OC enrichment can be modulated by spatial heterogeneity of soil characteristics, due to the concentration of fine and OC-rich particles in areas of higher topographic relief beneath vegetation, particularly shrubs (Barth and Klemmedson, 1978;

Schlesinger et al., 1990, 1996; Parsons et al., 1996; Kieft et al., 1998; Wainwright et al., 2000; Turnbull et al., 2010c; Brazier et al., 2013; Puttock et al., 2014; Harman et al., 2014).

Previous work at these sites found that OC event yield was correlated with total event runoff and that the slope of this relationship steepened over the grass-shrub ecotone, indicating greater sensitivity of OC event yield to event runoff in shrub-dominated sites (Brazier et al., 2013). Biogeochemical tracing of sediment eroded during a dryer-than-average period indicated that large proportions of the OC eroded from shrublands originated from bare interplant areas, where OC is older, legacy C from previously dominant grass vegetation (Puttock et al., 2014), but that the proportion of shrub-derived OC associated with the eroded sediment increased during larger magnitude events (Puttock, 2013), a trend considered likely to continue during wetter periods.

Based on the above understanding, I propose refined conceptual models for OC enrichment as a function of rainfall event intensity for grass-dominated (Model 2) and shrub-dominated (Model 3) hillslopes (Figure 6-6a). In grasslands, the (relatively) homogeneous distribution of OC results in low sensitivity of ER_{OC} to rainfall event intensity. ER_{OC} is inversely related to rainfall event intensity due to changes in the selectivity of dominant erosion processes; but was always enriched, in contrast to Model 1. OC enrichment therefore occurs mainly due to the vertical gradient in OC concentrations within natural, non-homogenised soils (Model 2 (Grass) in Figure 6-6a). In shrublands, during low intensity rainfall, erosion predominantly occurs in the bare interplant areas which have low soil OC concentrations relative to areas of micro-topographic relief beneath vegetation (Kieft et al., 1998; Wainwright et al., 2000; Brazier et al., 2013; Harman et al., 2014) (Figure 6-6b). Consequently eroded sediment may initially be depleted in OC relative to the aerially-weighted average OC concentrations ($ER_{OC} < 1$ in Figure 6-6a). As rainfall event intensity increases, areas of topographic relief become inundated (Figure 6-6b), with greater erosion of material from these OC-rich areas enhancing OC enrichment in the eroded sediment (Model 3 in Figure 6-6a). The variable source areas caused by co-variation of topography and OC concentrations are hypothesised to produce a positive relationship between ER_{OC} and rainfall event intensity, in contrast with understanding obtained from work in

other, simpler, environmental contexts (cf. Ghadiri and Rose, 1991a; Truman et al., 2007; Schiettecatte et al., 2008a; Wang et al., 2010; X. Wang et al., 2014c).

The interpretation that differences in spatial distribution of OC concentrations across the grass-shrub ecotone (Brazier et al., 2013) influence the OC concentration of eroded sediment and thus OC enrichment is consistent with the observation that inter-event variation in ER_{OC} increases across the grass-shrub ecotone (Figure 6-3b). ER_{OC} was generally weakly positively correlated with most metrics of rainfall event intensity (total rainfall, peak 1-minute rainfall intensity, runoff coefficient, peak 1-minute runoff, total runoff, total sediment event yield) (Figure 6-4). However, further analysis of these relationships was not supported by the available data, due to small sample sizes which were unbalanced and non-parametrically distributed.

Therefore, limited support was found for any of the three conceptual models described above. This finding appears to reflect the low signal-to-noise ratios arising from the complex erosional dynamics of these natural ecosystems (see also Hu et al., 2013). Variation in ER_{OC} is probably also partly caused by factors such as the quality of litter accumulated prior to each rainstorm event, which will be a function of litter production rates, the interval since last rainstorm event and the magnitude of the last rainstorm event.

Further elucidating mechanistic controls on the OC enrichment dynamics of these complex natural hillslopes may require rainfall simulation experiments on natural hillslopes in order to increase control over variables such as antecedent conditions and rainfall intensities (e.g. Parsons et al., 1997; Truman et al., 2007; Lister, 2007; Michaelides et al., 2009, 2012). The complex relationships demonstrate the need for caution when extrapolating understanding from reductionist experiments to multifaceted real world environments (as acknowledged by X. Wang et al., 2014c).

OC enrichment dynamics are a critical aspect of erosion-induced OC redistribution, and must therefore be represented in numerical models to accurately simulate erosion-induced OC fluxes (see Polyakov and Lal, 2004b; Schiettecatte et al., 2008a). While OC enrichment is typically attributed to size-selective detachment and transport, this process was negligible at my sites. Instead, I suggest that improvements in the predictive accuracy of deterministic

models may require explicit consideration of topographic variation in OC concentration as influenced by surface cover (Figure 6-6) and differences in transport dynamics associated with the lower density of OC-rich fractions. The appraisal that the role of density in OC enrichment is under-appreciated is consistent with recent findings of co-variance between OC concentrations with settling velocity, a function of density (Hu and Kuhn, 2016).

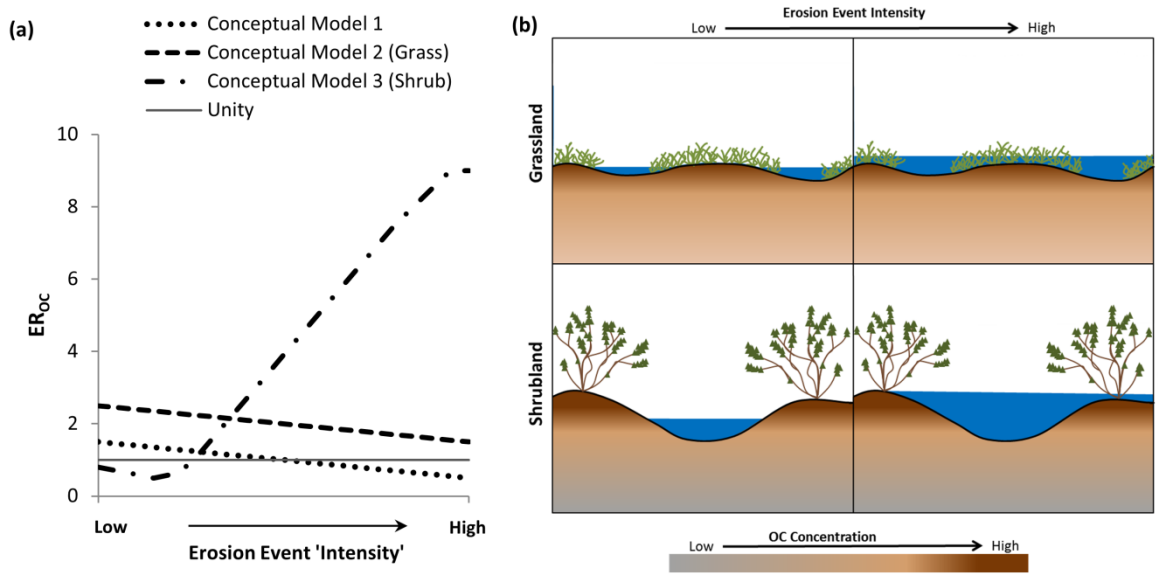

Figure 6-6. (a) Conceptual models of the relationship between event intensity and the enrichment ratio of organic carbon (ER_{OC}). Conceptual Model 1 reflects understanding from previous laboratory experiments documenting changes in sediment source areas (interrill vs. rill) and associated degree of size-selective transport of OC-rich fines with increasing rainfall intensity (discussed in Schiettecatte et al., 2008a). Conceptual Model 2 (Grass) is the authors' expectation for these grass-dominated ecosystems based on understanding of the (relatively) homogeneous distribution of OC and topography. Conceptual Model 3 (Shrub) is the authors' expectation for these shrub-dominated ecosystems based on understanding of the heterogeneous, co-varying distribution of OC and topography. (b) Schematic representation of how differences in the microtopography and spatial distribution of OC between grass-dominated ecosystems (upper panel) and shrub-dominated ecosystems (lower panel) influence the availability to erosion of soil OC arising from different depths of overland flow – higher OC concentrations are indicated by darker brown shading.

While this study focuses on the erosion-induced redistribution of OC by overland flow processes, aeolian processes are acknowledged to be another key vector driving the redistribution of soil resources in dryland environments (Larney et al.,

1998; Okin et al., 2004; Li et al., 2007, 2008, Ravi et al., 2007, 2010; Field et al., 2010). For example, monitoring aeolian erosion at the semi-arid Jornada Experimental Range in Southern New Mexico, USA, *Li et al.* (2007) found that up to 25% of the near-surface (0-0.05 m) soil OC stock was removed over three windy seasons, and that wind erosion-induced OC fluxes were inversely related with vegetation cover, due to accelerating erosion rates with reducing vegetation cover. They reported airborne sediments were enriched in OC by 3-6 times relative to the contributing (0-0.05 m near-surface) soil, although further comparisons are hindered by the fact that their monitoring plots were somewhat disturbed by the vegetation removal treatments. Aeolian processes clearly play an important role in the redistribution of soil resources in semi-arid environments, and there is a need for co-located empirical studies to quantify concomitant fluxes arising from aeolian and fluvial processes (Field et al., 2009; Ravi et al., 2010). Advancing mechanistic understanding of the interactions between aeolian and fluvial abiotic vectors will support their representation in numerical models used to elucidate emergent dynamics of complex ecosystems (see Stewart et al., 2014 for an example of such an experiment).

Monitoring net ecosystem exchange of gaseous C has suggested shrub-dominated ecosystems may take up significantly more C than grass-dominated ecosystems at this study site (Petrie et al., 2015). However, despite the higher rates of litter inputs to the soil surface from shrubs suggested by Liao *et al.* (2006a), no meaningful difference in areal average, near-surface OC stocks across the grass-shrub ecotone was observed, in agreement with previous studies (Brazier et al., 2013; Puttock et al., 2013). The results presented here demonstrate that the erosion-induced OC yield is nearly six times higher from shrub-dominated sites relative to grass-dominated sites. Together, these findings indicate that these shrub-dominated ecosystems appear to have a much quicker throughput of near-surface SOC relative to grass-dominated ecosystems. The substantial increase found in the erosion-induced yield of OC from shrub-dominated ecosystems compared with grass-dominated ecosystems implies that the higher net ecosystem exchange of gaseous C in shrublands relative to grasslands (Petrie et al., 2015) does not invariably lead to increased sequestration of C in these terrestrial ecosystems (Gabet et al., 2005; Brazier et al., 2013).

Understanding the C sequestration potential of woody shrub encroachment requires comprehensive comparison of the C dynamics of grasslands versus shrublands (Pacala et al., 2007; Barger et al., 2011). In addition to existing monitoring of gaseous fluxes (e.g. Scott et al., 2009, 2016; Petrie et al., 2015), this requires detailed understanding of erosion-induced C fluxes (Gabet et al., 2005; Li et al., 2007; Brazier et al., 2013). For example, *Wolkovich et al.* (2009) looked at C dynamics following grass encroachment into semi-arid shrubland, but acknowledged that their findings did not quantify potential changes in erosional fluxes arising from the changes in vegetation structure. The <1 g cm^{-3} fraction of eroded material, including most leaf litter, may also comprise a substantial proportion of the total OC efflux arising from runoff (Bianchi, 2011), and should be considered in future work monitoring lateral transfers of C in these ecosystems.

6.6. Summary

Coarse (>2 mm) particles can contain substantial amounts of OC, accounting for up to 38% of the total SOC stock in the semi-arid soils studied; this is likely to be due to the incorporation of organic C into macro-aggregates stabilized by precipitated calcium carbonate into water stable forms. Standard soil analysis protocols assume that the >2 mm “mineral” fraction contains no OC, which may be causing significant underestimation of SOC stocks.

OC enrichment can increase the erosion-induced redistribution of OC by up to an order of magnitude at hillslope-scales, and average enrichment increases significantly across the ecotone from grass-dominated to shrub-dominated communities. Predictions of OC enrichment dynamics based on reductionist experiments appeared to transfer poorly to complex, real-world environments, and OC enrichment appeared to be an enduring feature of uncultivated semi-arid ecosystems. OC enrichment is often attributed to particle size selectivity, yet changes in PSD explained very little of the observed OC enrichment.

Across the transition from grass-dominated to shrub-dominated ecosystems there was a six-fold increase in the erosion-induced OC yields, due to both accelerated erosion and increased OC enrichment. Shrub-dominated ecosystems may have a quicker throughput of near-surface SOC relative to grass-dominated ecosystems, which suggests that higher net ecosystem exchange of gaseous C in shrublands relative to grasslands may not necessarily lead to increased sequestration of C in these ecosystems.

7. Inorganic Carbon

7.1. Chapter Overview

This chapter presents findings of the investigation into the distribution of SIC across particle size fractions and the erosion-induced redistribution of PIC across the grass-shrub ecotone. The rationale for the objectives listed below is presented in section 3.2, and the material in this chapter is being prepared for submission for publication.

7.2. Objectives

B1 Characterise the distribution of IC across particle-size fractions, in order to:

(iii) Quantify IC storage in coarse (>2 mm) particles

(iv) Parameterise a deterministic runoff/erosion model

B2 Quantify differences in erosion-induced effluxes of IC across an ecotone of changing plant functional types from a grass-dominated to a shrub-dominated ecosystem over four monsoon seasons.

7.3. Key Findings

- Coarse (>2 mm) clasts account for most of the inorganic C in these near-surface soils, and should be considered when investigating spatial controls on the distribution of soil inorganic C.
- Erosion-induced yields of inorganic C are higher from shrublands relative to grasslands, with average event yields four times higher from the shrub-dominated site due to increased erosional yields.
- Unlike organic C, eroded sediment was depleted in IC relative to contributing soils.
- The accelerated erosional flux of IC associated with shrub dominated landscapes may have significant implications for the transport of IC from terrestrial to aquatic systems and consequently large-scale cycling of C.

7.4. Results

IC concentrations were positively correlated with particle size (Figure 7-1), and coarse (>2 mm) clasts accounted for 67-76% of the SIC stocks in the near-surface soil (Figure 7-2a). Across the grass-shrub ecotone, there was minimal change in the IC concentration within each individual particle size fraction; however, there was a large change in bulk soil IC concentration, due to changes in the particle size distribution (PSD) (shown in Figure 6-1b). Total SIC stocks in the near-surface soil increased by ca. 47% across the grass-shrub ecotone, from 1492.0±241.6, 1941.2±227.5, 2436.9±330.6 and 2178.7±196.1 for the grass, grass-shrub, shrub-grass and shrub dominated sites, respectively.

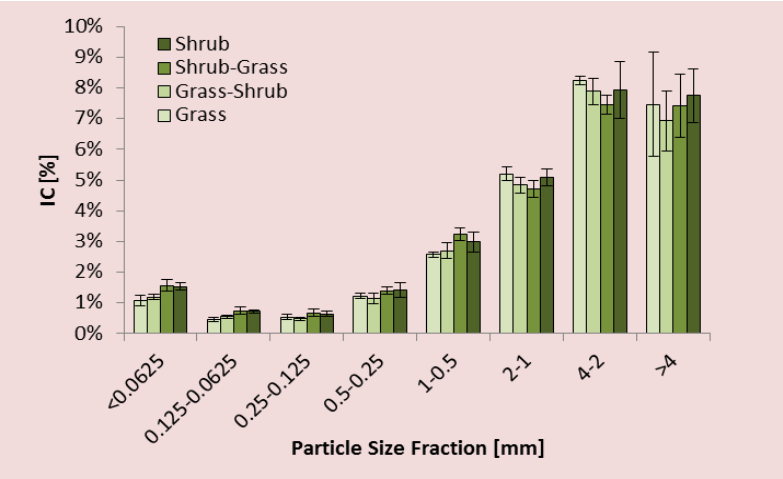

Figure 7-1. Concentration of inorganic carbon (IC) for each particle size fraction in the near-surface soil, stratified by dominant vegetation cover. Errors bars denote standard errors.

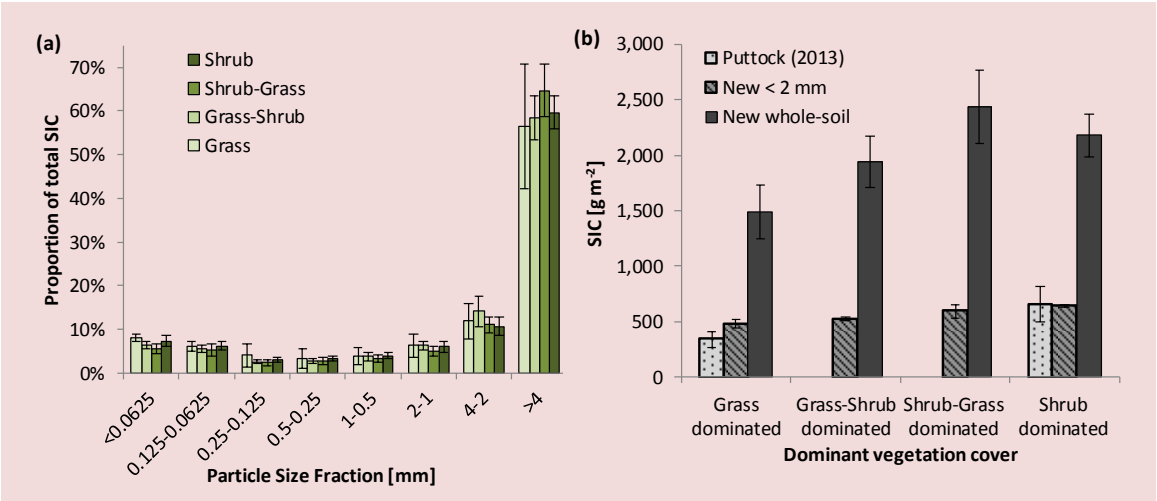

Figure 7-2. (a) Proportion of total SIC content associated with each particle size fraction in the near-surface soil, stratified by site. (b) Total SIC stock estimated by

previous work, calculated for the <2 mm particle size fraction and calculated for the whole soil. Errors bars denote standard errors.

There was a three-fold increase in mean erosion-induced event yields of IC across the ecotone from grass- to shrub-dominated ecosystems (Figure 7-3a). This systematic increase in average IC yield was controlled by erosion rates, as there was no systematic difference in the IC concentrations of eroded sediment across the grass-shrub ecotone.

Erosion-induced IC fluxes were dominated by contributions from the finer (<0.25 mm) particle size fractions (Figure 7-3b). Eroded sediments were substantially depleted in IC relative to the contributing near-surface soil (Figure 7-4a) with overall ER_{IC} was statistically significantly <0.57 (one sample t-test, *df* = 36, *t* = -1.69, *p* = 0.05). Across the particle size classes, eroded sediment generally had IC concentrations similar to the contributing source soil, with IC enrichment ratios (ER_{IC}) near unity within each individual size fraction, although IC appeared slightly enriched in the fine sand particle size classes (0.5-0.0625 mm) (Figure 7-4b).

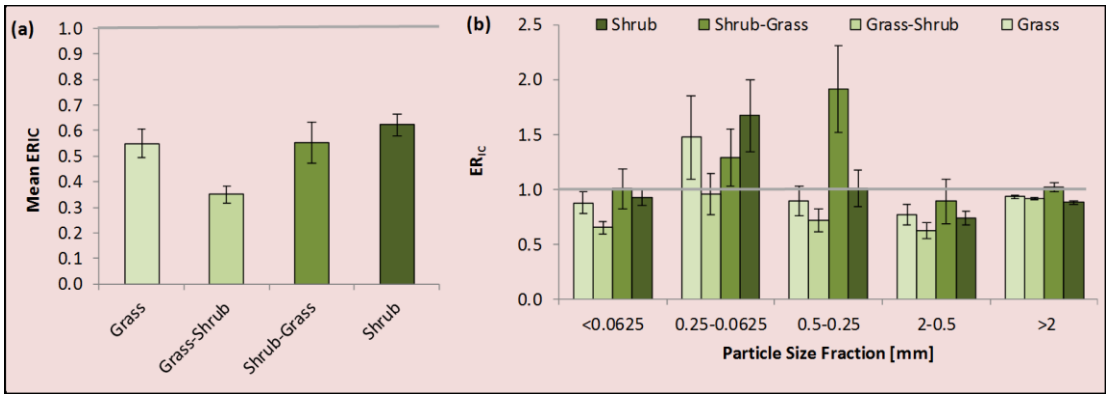

Figure 7-3. (a) Mean event yields of IC across the grass-shrub ecotone. (b) Mean event yields of IC across the grass-shrub ecotone, stratified by particle size fraction. Errors bars denote standard errors and the grey.

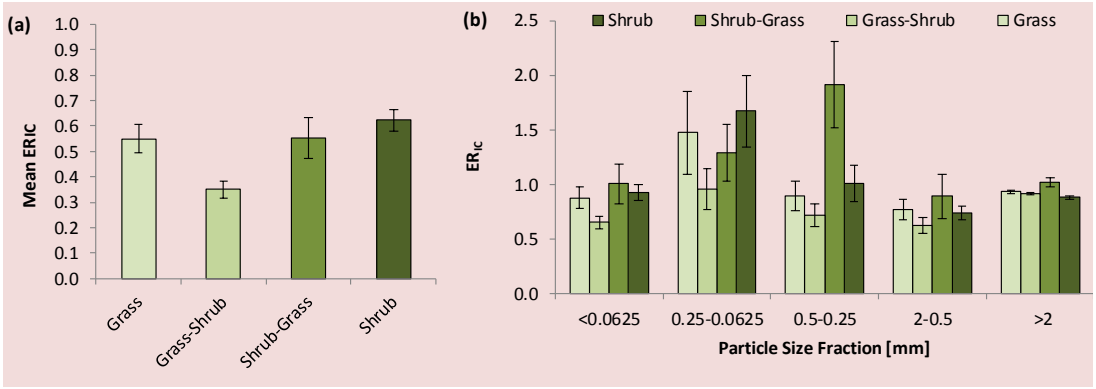

Figure 7-4. (a) Mean IC enrichment ratio by site, and (b) Mean ER_{IC} for sediment eroded stratified by particle size and site. Error bars denote standard errors.

7.5. Discussion

The positive relationship between IC concentrations and particle size combined with the high proportion of coarse (>2 mm) particles means that around two thirds of the total IC content of these near-surface soils is associated with coarse (>2 mm) particles. This distribution is meaningful because the >2 mm particle size fraction is often simply assumed to contain no SIC and discarded (e.g. Bird et al., 2002; Rhoton et al., 2006; Ewing et al., 2007; Puttock, 2013; X. Wang et al., 2015).

Analysis of incomplete samples therefore has potential to introduce substantial errors in estimates of the magnitude and distribution of SIC stocks, and therefore the processes controlling SIC dynamics. Exemplifying this point, Figure 7-2b illustrates how SIC inventories calculated for the <2 mm particle size fraction were consistent with previous estimates by Puttock (2013), but greatly underestimated the *total* SIC stocks calculated for the whole soil. Most of the difference in total SIC stocks found across the grass-shrub ecotone was associated with changes in the abundance of coarse (>2 mm) particle size fractions, rather than changes in IC concentrations associated with individual particle size fractions.

SIC stocks were found to be far higher in bare interplant microsites relative to vegetated grass and shrub microsites (Figure 10-2). This findings is contrary to the findings of Puttock (2013) for the same four study sites, who reported that SIC concentrations were significantly lower in bare interplant microsites relative to vegetated microsites. In accordance with widely employed protocols (e.g. Bird et al., 2002; Ewing et al., 2007; Sankey et al., 2012), Puttock (2013) only measured the IC content of the <2 mm particles. Consequently, although the soil sampling of 360 discrete locations by Puttock (2013) was more spatially representative compared with the present sampling of 50 discrete locations, the n = 400 samples analysed in the present study provide a more accurate representation of the true distribution of IC in the near-surface soils at these sites. The disparity is again attributed to the differences in the particle size distribution examined for IC concentration between the current and previous studies. This

exemplifies the necessity of robust analytical approaches when collecting empirical data from which to derive inferences about the process controlling the spatial distribution of SIC. Because analysis of the <2 mm fraction alone can lead to erroneous inferences, it was not considered constructive to undertake further comparisons with other studies which employed incomplete sampling protocols.

The positive relationship between particle size and IC concentrations combined with particle size selectivity in detachment, transport and deposition processes (discussed in chapter 6) means that relatively IC-poor particles are more likely to be eroded from the landscape. Consequently, eroded sediments are expected to be depleted in IC relative to the contributing near-surface soil, and more degraded sites would be predicted to exhibit elevated SIC concentrations in the near-surface soils. Elevated SIC concentrations in degraded sites subject to greater erosion are also expected due to the gradual exhumation of the $CaCO_3$-rich horizon (Kieft et al., 1998; Lal et al., 1999; Emmerich, 2003; Turnbull, 2008). These predictions are supported by the finding of (i) coarsening of PSD (Figure 6-1b) and (ii) IC enrichment ratios which were consistently sub-unity and overall significantly < 0.57 (Figure 7-4a), and (iii) generally increasing SIC stock across the grass-shrub ecotone (Figure 7-2b).

Overall, there was a positive relationship between particle size and IC concentration, although the finest (<0.0625 mm) fraction had approximately double the IC concentrations observed in the fine sand fractions (0.0625 mm to 0.25 mm) (Figure 7-1). These relationships were broadly consistent across all sites, and also in the microsite surface cover at each site (data not shown). The positive relationship between IC concentrations and particle-size is consistent with the hypothesis that $CaCO_3$ precipitation may be an important stabilization mechanism for organic matter in alkaline dryland soils, as postulated in Chapter 6 (Cunliffe et al., 2016d). Such a stabilization mechanism is also consistent with the positive correlation between SOC and SIC in arid soils in northwest China (X. Wang et al., 2015).

Intriguingly, the positive relationship observed between IC concentration and particle size is diametrically opposed to that previously found at similar semi-arid sites at the Jornada LTER in southern New Mexico (Lister, 2007) (Figure 7-5). The cause of the differences between these two datasets is unclear, as sample collection, preparation and analysis was similar between both studies. The

Jornada samples were collected from near-surface soil (0-0.01 m depth) with three replicates from three microsites (grassland, bare interplant, and beneath creosotebush shrubs), particle fractionation by dry sieving and IC determination via FC. The mean values and associated errors for each microsite are shown in Figure 7-5. The meticulous cross-validation of IC determinations described in section 5.5 affords high confidence in the data presented in the present study.

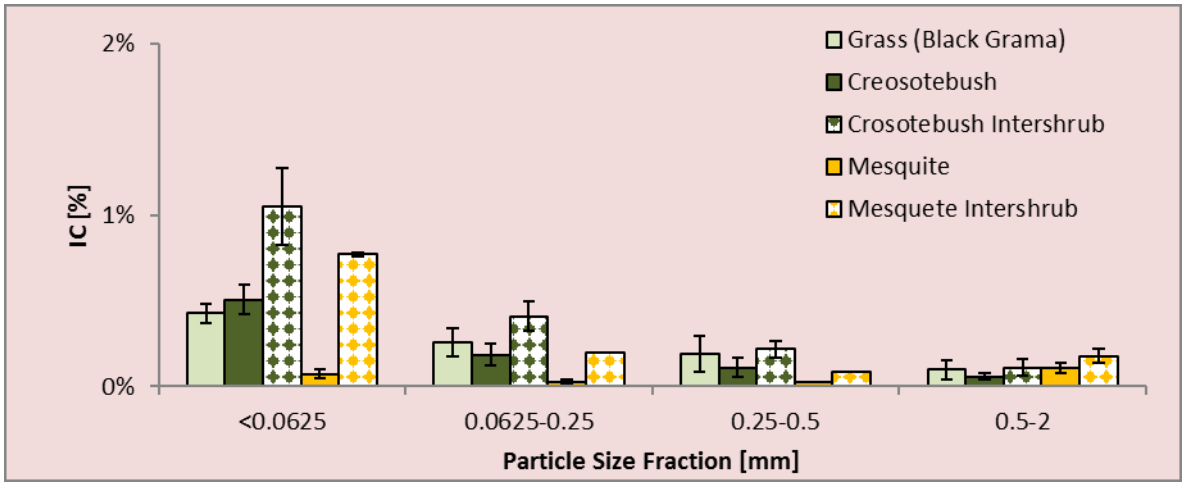

Figure 7-5. Concentration of IC concentration across particle size fractions for sites at the semi-arid Long Term Ecological Research site at the Jornada in southern New Mexico (data from Lister, 2007). Note that these data pertain to microsites either beneath shrub canopies or in intershrub areas, rather than areally-weighted averages).

The substantial, three-fold increase in the yield of PIC eroded from the runoff plots across the ecotone from grass- to shrub-dominated ecosystems was primarily caused by increased erosion and, to a lesser extent, increased availability of PIC in the surface soil across the grass-shrub ecotone. Although only one pathway is characterised, these findings are nonetheless useful empirical information. When seeking to understand the effects of land degradation (such as the woody shrub encroachment described herein) on ecosystem carbon dynamics, in addition to organic C in biomass and soil pools it is appropriate to also consider the implications for IC dynamics. Such holistic consideration challenges the perception that dryland IC pools are simply stable and inert (as argued by Serna-Pérez et al., 2006; Petrie et al., 2015).

The depletion of eroded sediments in IC relative to the contributing near-surface soil was explained by changes in the PSD of eroded sediment, due to the

selective detachment, transport and non-deposition of IC-poor finer particles (Figure 7-4a). In contrast to the present findings that eroded sediments are depleted in IC relative to the contributing source soils, previous analysis of the erosional dynamics of IC at these sites suggested eroded sediments were enriched in IC (Puttock, 2013). This discrepancy was due to incomplete characterisation of the near-surface soils in the previous work.

Research conducted by Rhoton *et al*. (2006) at (small) catchment-scales in similar semi-arid landscapes at the Walnut Gulch Experimental Watershed in Arizona found that bedload and suspended sediments had typical IC concentrations of 1.03% and 1.55%, respectively. Relative to the contributing soils (typically 1.09% IC), the bedload and suspended sediments were depleted (ER_{IC} = 0.94) and enriched (ER_{IC} = 1.42), respectively (Rhoton et al., 2006). The analysis of IC enrichment presented in section 7.4 was based on total sampling of eroded material, not separated by mode of transport. Unfortunately, the data reported by Rhoton *et al*. does not allow calculation of an overall enrichment ratio for PIC, and therefore is not directly comparable with the findings reported herein. Furthermore, the analysis undertaken by Rhoton *et al*. excluded PIC associated with clasts >2 mm, and therefore cannot be directly compared with the findings presented herein.

7.5.1. Implications for global biogeochemical cycling of carbon

The dissolution and precipitation of carbonate involves two main reactions

$$CO_2 + H_2O \leftrightarrow HCO_3^- + H^+ \qquad \text{Equation 7-1}$$

$$Ca^{2+} + 2HCO_3^- + \leftrightarrow CaCO_3 + H_2O + CO_2 \qquad \text{Equation 7-2}$$

When there is enough H^+ to create acidic conditions, for example, during rainfall events in this region (Vet et al., 2014, p. 76), carbonate dissolution may occur taking up atmospheric CO_2. The resulting hydrogencarbonate[2], is transported via rivers, to the oceanic reservoir (Adams, 1993; Adams and Post, 1999). The dissolution of carbonate takes up an equimolar quantity of gaseous C (Adams

[2] Note that hydrogencarbonate is the correct nomenclature to describe what was formerly often known as 'bicarbonate' (IUPAC, 2005).

and Post, 1999). Critically, this reaction is two-way, and depending on the fate of the carbonate-derived hydrogencarbonate precipitation of HCO_3 as calcareous sediments or accumulations on near-shore coral reefs (for example) can release sequestered CO_2.

PIC in fluvial systems buffers low pH and causes more alkaline/basic conditions in aquatic environments. In-stream dissolution of PIC will utilise dissolved CO_2, decreasing the partial pressure of CO_2 in the surface water and thus drawing down atmospheric CO_2 (Liu et al., 2010). As shown here, woody shrub encroachment can accelerate the influx of PIC into fluvial systems. Depending on the available hydrogen which controls subsequent dissolution (and riverine connectivity to the ocean), this accelerated input of carbonate could potentially accelerate the sequestration and transfer of atmospheric C to the oceanic system.

However, despite regional precipitation being mildly acidic (typically pH 4.8-5.4) (Vet et al., 2014, p. 76), the major catchment draining this region, the Rio Grande, has a carbonate-rich geology and therefore typically has a high alkalinity with very high $CaCO_3$ concentrations resulting in typical stream pH of ca. 8 (7.8-8.4) (Carter and Porter, 1997; Brown, 2004; Rios-Arana et al., 2004). Therefore, it is perhaps most likely that PIC eroded from these sites may have a long residence time in the catchment, remaining in solid form rather than undergoing dissolution and moving episodically in response to rainfall-driven flow events. Sediments in the Rio Grande fluvial system have been reported to comprise of ~24-50% $CaCO_3$ (Scott and Slater, 1987).

7.6. Summary

In summary, it is very important to avoid arbitrarily curtailing the particle size distributions of samples when analysing SIC stocks and subsequent dynamics, as most IC can be associated with coarse particles. This finding has implications for understanding of how SIC stocks are mobilised by the episodic rainfall/runoff events that characterise these dryland systems.

Changes in the IC concentration of eroded sediments are mainly due to changes in PSD, suggesting that with particle-size specific parameterization of IC concentrations, it may be straightforward to simulate the lateral redistribution of IC in a process based model.

Several findings were inconsistent with other reports of the distribution and erosion-induced redistribution of IC in similar environmental settings; the cause of these inconsistencies is presently unclear, but suggests caution is appropriate when seeking to generalise understanding of IC dynamics in dryland ecosystems.

This contribution increases empirical knowledge of the redistribution of IC due to erosion by water in semi-arid landscapes. The implications of this IC redistribution for large-scale C dynamics depends on the chemical status (hydrogen availability) of the fluvial systems draining these landscapes.

8. Measuring Abiotic and Biotic Ecosystem Structure

8.1. Chapter Overview

This chapter presents a novel methodology, advancing the application of remotely piloted aerial systems (RPAS) to acquire aerial image data with structure-from-motion (SfM) photogrammetry to obtain 3D models representing ecosystem structure at very fine (cm^2) spatial resolutions over landscape (~10 ha) spatial extents. The rational for developing these objectives were described in section 3.3. The resultant information products are highly sensitive to changes in biotic ecosystem structure, and were used to estimate vegetation biomass and C stocks as well as spatially explicit parameterisation of the deterministic modelling work undertaken in Section 10.

The material in this chapter has been published in ***Cunliffe, Andrew M., Richard E. Brazier, and Karen Anderson 'Ultra-fin grain landscape-scale quantification of dryland vegetation structure with drone-acquired structure-from-motion photogrammetry' (2016) Remote Sensing of Environment, 183:129-143. doi:10.1016/j.rse.2016.05.019***, a copy of which is included in Appendix 8.

The method developed for this chapter also informed the approach used in ***Puttock, Alan K., Andrew M. Cunliffe, Karen Anderson, and Richard E. Brazier. 'Monitoring the Impact of Eurasian Beaver Reintroduction on Ecosystem Structure Using Aerial Photography Collected from a Multi-Rotor Drone.' Journal of Unmanned Vehicle Systems 3, no. 3 (2015): 123–30. doi:10.1139/juvs-2015-0005***, a copy of which is included in Appendix 9.

8.2. Objectives

C1 Develop RPAS SfM remote sensing techniques to measure the abiotic and biotic biophysical structure of semi-arid rangeland ecosystems

C2 Estimate biomass and associated C storage at measurement scales which bridge the scale gap between on-the-ground and satellite-based measurements

C3 Produce fine-scale digital maps describing topography and vegetation cover to parameterise spatially-explicit process-based numerical models

8.3. Key Findings

- When optimally implemented, drone-based survey methods can be used to quantify ecosystem structure at ultrafine spatial resolutions (cm^2) over landscape extents (10s of ha).
- The implementation of the method developed in this chapter produced information products with a fidelity nearly two orders of magnitude better than has been possible using previous implementations of these inexpensive survey techniques.
- Available information products are sensitive to subtle changes in ecosystem structure across the grass-shrub ecotone, and include spatially-explicit maps of topography, canopy height and volume, aboveground biomass, estimated belowground biomass, and associated C stocks.
- The derived information products are highly complementary to existing survey approaches, and have significant potential to revolutionise the study of spatial ecology in short-sward dominated ecosystems.

8.4. Methodology

8.4.1. Overview

Figure 8-1 presents a graphical overview of the technical workflow for this section, which includes the capture, processing, and validation of spatial data for describing landscape-scale C distribution.

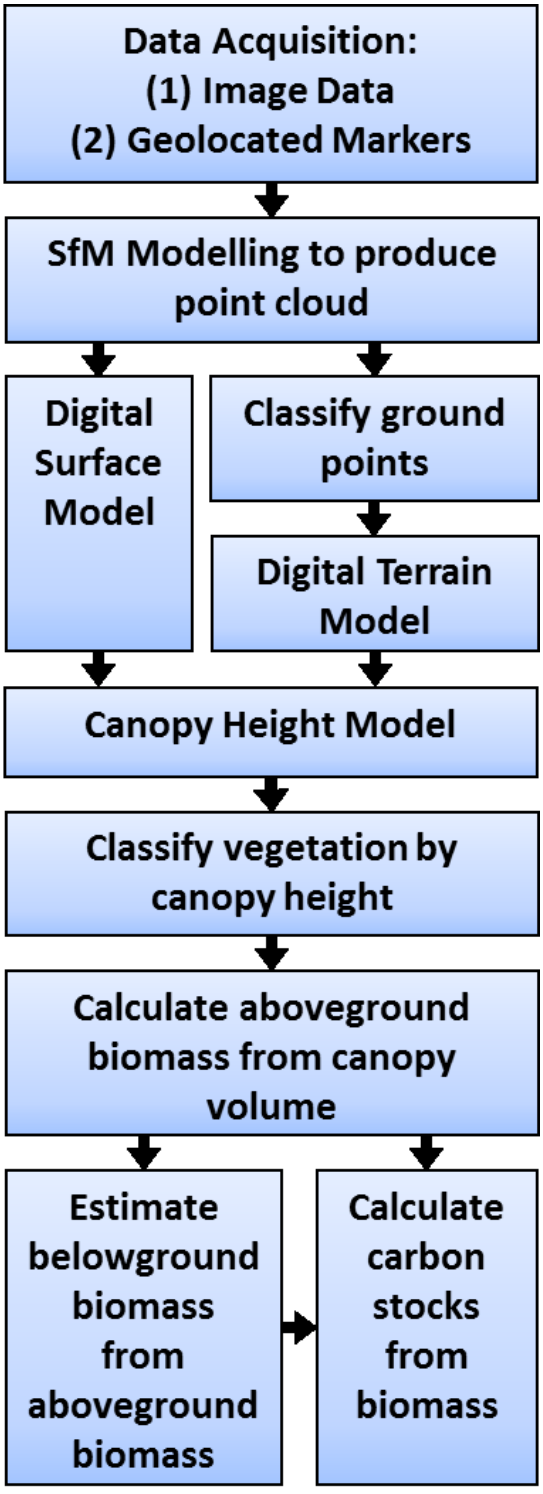

Figure 8-1. Outline of workflow for ecosystem characterisation.

8.4.2. Acquisition of Aerial Image Data

Consistent with other non-profit environmental research surveys (e.g. McGwire et al., 2013; Christian, 2015), RPAS flight operations were conducted in USA Federal Aviation Authority (FAA) airspace in compliance with hobby-grade exemptions which included maintaining line-of-sight of the aircraft, operating within 400 feet (121 m) of ground level, and not operating within restricted airspace (FAA, 1981, 2005, 2007, 2010, 2011, 2013).

All image data were acquired by RPAS overflights in October 2014, following the summer monsoon season when the increased availability of soil moisture allowed vegetation biomass to 'green-up' (Huenneke and Schlesinger, 2006; Muldavin et al., 2008). This maximised spectral and structural contrast in the ecosystem, facilitating the application and analysis of SfM photogrammetry. The remotely piloted aerial system used was a 3D Robotics Y6 hexacopter (Figure 8-2), equipped with an AMP2.6 flight controller running open source ArduCopter (V3.2; http://copter.ardupilot.com) software, and sensors included a GNSS receiver (3DR Ublox LEA-6 GPS+Compass) and low cost (ca. £200), consumer-grade camera (Canon Powershot S100). This UAV had a take-off weight of less than 2.5 kg, and cost less than $3,000 USD and was chosen because of its modular nature, allowing in-field repairs and modifications to be carried out easily.

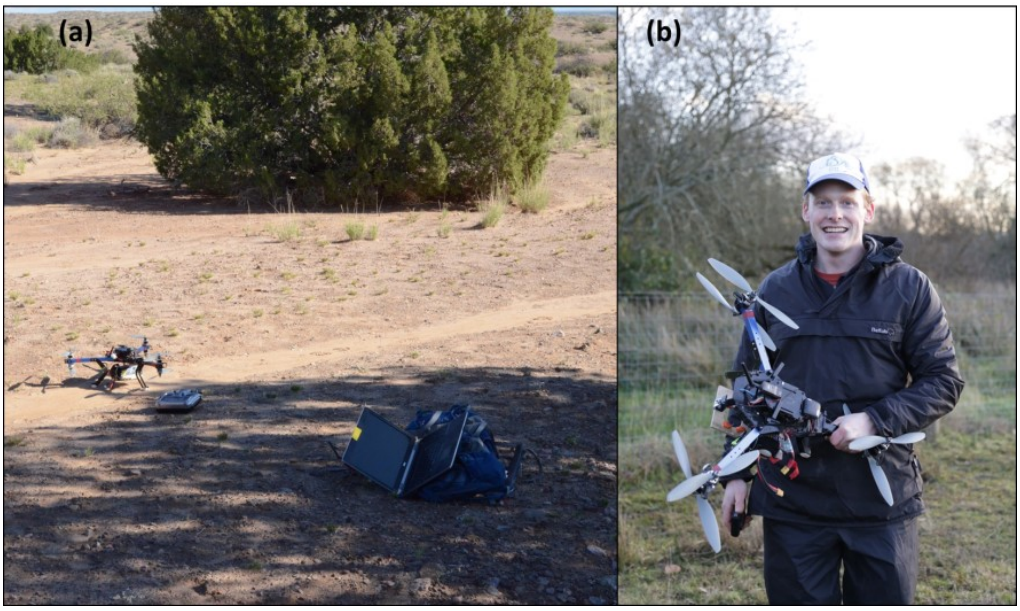

Figure 8-2. (a) Photograph of 'Yoda', the remotely piloted aircraft used to acquire image data for the present study (taken in the semi-arid rangeland), (b) photograph of the author with 'Yoda' (taken in Devon).

This RPAS was assembled, programmed and operated by the author, and included several custom modifications to optimise the quality of data acquisition. One such modification was the development of a custom-made camera mounting system, to dampen the camera sensor from airframe vibrations (Figure 8-3). The operating software on many Canon cameras has been reverse-engineered (Canon Hack Development Kit, CHDK, http://chdk.wikia.com/wiki/CHDK), which enables users to install programmable scripts to improve the sensor capabilities for specific applications such as aerial photography. Therefore, Canon cameras were selected for the present application. Canon's Powershot cameras now include vibration reduction technology, designed to dampen low frequency vibrations associated with handheld operation. Unfortunately, this vibration reduction system accentuates high frequency vibrations, such as those associated with the motor rotations on UAV airframes. Efforts to reduce the generation of vibrations included meticulously balancing the propellers and buffering motor mounts from the airframe, but still image quality was significantly affected by excessive vibrations, with only ca. 1/70 images being useable. Therefore, a custom made camera mounting system was constructed in order to dampen the camera sensor from airframe vibrations. This consisted of a combined camera and battery tray, mounted beneath the airframe by springs. This design leverages the (ca. 500 g) mass of the flight battery to dampen the camera from the high frequency vibrations from the airframe, with a secondary buffer provided by the earplugs upon which the camera itself is installed. This design was inspired by examples and discussions on the DIY Drones community forum (http://diydrones.com/), and using this mounting system nearly all photos were of sufficient quality for contribute to the SfM modelling process.

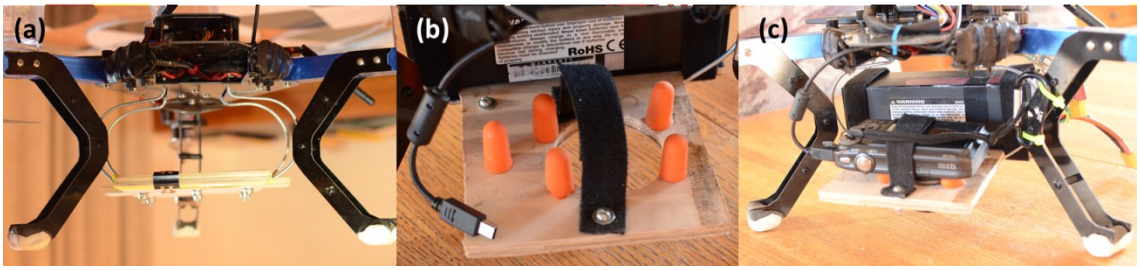

Figure 8-3. Photographs illustrating the custom-made camera mount for isolating the camera sensor from airframe vibrations. (a) camera/battery tray mounted on springs beneath the airframe, (b) secondary vibration dampening barrier consisting of ear-plugs, and (c) with the camera and flight battery installed.

Each part of each AOI was surveyed with two fully automatic overflights designed using Open Source Mission Planner (V1.3) software (http://planner.ardupilot.com/). One flight acquired nadir (parallel) image data and a second acquired convergent (~45° from nadir) image data (Figure 8-4). The two flights followed perpendicularly-aligned 'lawnmower' survey patterns at ca. 15-20 m altitude, yielding an effective ground sampling distance of 0.004 to 0.007 m per pixel. The effective base-to-height ratio, the distance on the ground between the centres of overlapping photos, divided by camera altitude, was ca. 0.15. The intersecting acquisition angles mean that this ratio is not directly comparable with equivalent values for solely nadir image data, but low values are considered favourable for improving the accuracy and density of points identified with SfM-MVS photogrammetry (Haala, 2011).

The inclusion of convergent (non-nadir) image data is important to constrain estimation of both extrinsic (position and orientation) and intrinsic (lens calibration) parameters estimated during the bundler adjustment step, which significantly influences the reconstruction accuracy of SfM modelling (James and Robson, 2014; Smith and Vericat, 2015; Shahbazi et al., 2015). Convergent image data affords another significant advantage because creosotebush canopies frequently grow in the form of an inverted cone (Singh, 1964; Chew and Chew, 1965; Ludwig et al., 1975; De Soyza et al., 1997; Wainwright et al., 1999a; Abrahams et al., 2003; Dodson, 2012), particularly in more arid environments such as the Chihuahuan desert (De Soyza et al., 1997) (Figure 8-5). Consequently, the oblique perspective improves the observation of the terrain surface beneath creosotebush canopies, yielding additional ground points which better constrain the digital terrain model (DTM) generation in these locations and thus increase confidence in the resulting canopy height models (CHM).

The camera was triggered by the autopilot according to distance travelled, attaining 70% forward overlap and 65% sidelap, which combined with the dual flights, meant every part of the AOI was captured in ≥18 photographs. The platform flying speed was varied to ensure a minimum interval between two consecutive images of 2.5 seconds. Camera shutter speed (Tv) was faster than 1/1250th second, which was sufficient to minimise motion blur at the low flying speeds possible using multi-rotor drones. Camera ISO (Sv) was 200, aperture (Av) was f3.5 and focus was set at infinity.

Flights were completed within a few hours of solar midday to minimise shadowing (Quilter and Anderson, 2001; Rango et al., 2006; Puttock et al., 2015). Sky conditions were generally clear, with some image data acquired during overcast conditions. All seven AOIs were surveyed during 11 days over one month, though it would be straightforward to streamline data acquisition for this combination of spatial extent, spatial resolution and UAV platform to ≤6 days, under good weather conditions. Each image was geotagged with the platform's GNSS-derived location, and 10-18 'iron-cross' markers were deployed across each AOI as GCPs and geolocated using differential GNSS [Leica GS08] to a relative spatial accuracy (95% confidence) of 0.015 m in x, y and z (Puttock et al., 2015).

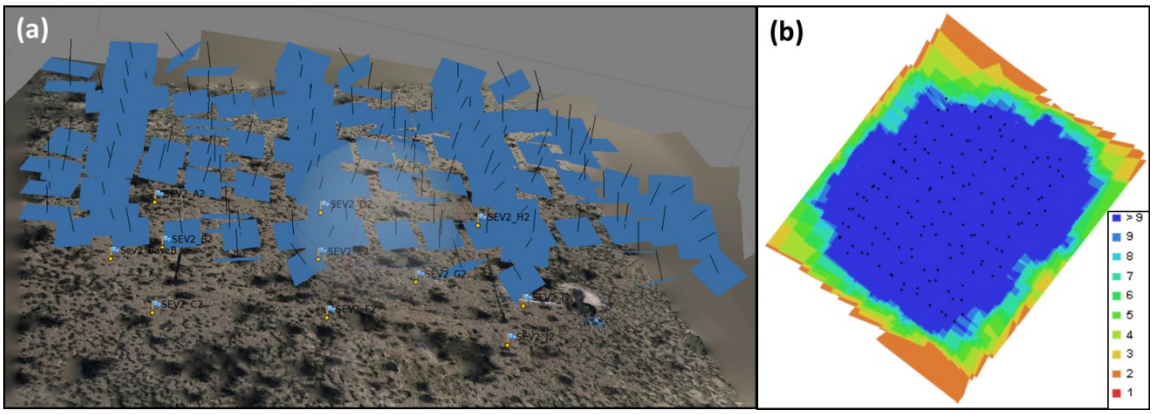

Figure 8-4. Configuration of data acquisition at AOI-1. (a) The distribution of ground control points (yellow dots) and camera positions and orientations (blue squares, with normal indicated by black lines). (b) Camera locations and image footprints of the source image data.

Figure 8-5 Photograph of creosotebush (*Larrea tridentata*) at AOI-3, illustrating the 'inverted cone' typical growth form. Photograph by Alan Puttock.

Deploying RPAS for low-altitude ecosystem surveying in the Chihuahuan Desert entailed some particular challenges not commonly encountered in other environmental contexts. As awareness of these challenges is valuable for supporting successful data acquisition in future RPAS surveys, these challenges are briefly described here.

Air density is fundamental to the flight operation of aerial vehicles (e.g., the generation of thrust by propellers and lift by wings), and is inversely related to both altitude and air temperature. This survey in the Chihuahuan desert involved flight missions at up to 1800 m above mean sea level (amsl), with ground level air temperatures reaching in excess of 45°C. The reduced air density under these conditions reduces the performance envelope of aerial vehicles, reducing flight endurance, manoeuvrability and payload capacity, for example, and should be considered when planning missions.

Deserts can be subject to extreme localised heating of the ground surface, which can give rise to vertically-orientated rotating columns of high-intensity wind, colloquially known as dust devils. These localised wind systems can catastrophically interfere with flight operations, but are often visible approaching survey areas; consequently, to support the pilot it can be valuable to utilise a spotter to keep a lookout for these highly localised weather phenomena.

Dust is somewhat pervasive in dryland ecosystems (cf. Field et al., 2010), particularly when performing near-ground operations (*i.e.,* take-off and landing) with a multi-rotor aircraft (Rodgers, 1968; Wadcock et al., 2008; “Making Landings Safer,” 2011). Dust ingress into the lens retraction mechanism caused the catastrophically failure of several camera sensors, and consequently necessitated the careful sealing of cameras into dust-proof casing prior to every flight (see Figure 8-6). For work in similarly dusty or sandy environments, such as drylands ecosystems and beaches, it would be appropriate to investigate the use of camera sensors with sealed lens units, such as the Canon Powershot D30, for example. Additionally, all six motor bearings exhibited signs of severe wear much more rapidly than motors used in other, less dusty environments, which was attributed to mechanical erosion by particulate matter (Rodgers, 1968; Wadcock et al., 2008; “Making Landings Safer,” 2011).

Figure 8-6. Camera sensor sealed in dust-proof protective casing.

During two of the survey flights, the hexacopter attracted the undesirable close attentions of large birds of prey, believed to be Ferruginous Hawks (*Buteo regalis*). In both cases, it was possible to abort the survey mission and land the aircraft before any contact occurred, and to wait until the birds had vacated the areas before resuming flight operations. It appeared that the hexacopter was perceived to be an intruder incurring into the hunting territory of the raptors. Clearly there are legitimate concerns regarding the potential impact of RPAS operations on fauna, which may be intensified in ecologically sensitive or protected sites, such as the Sevilleta National Wildlife Refuge (SNWR). Until very recently, very little has been known about the impacts of RPAS on wildlife, although this knowledge gap is rapidly being addressed (e.g. Sardà-Palomera et al., 2012; NPS, 2014; Schiffman, 2014; Ditmer et al., 2015; Moreland et al., 2015; Pomeroy et al., 2015; Vas et al., 2015; Ratcliffe et al., 2015; Chabot et al., 2015; Dulava et al., 2015; Goebel et al., 2015; Smith et al., 2016). Researchers using RPAS technologies should be transparent about their experiences of wildlife/drone interactions, in order to provide reliable information to inform the development of appropriate guidance for the responsible use of RPAS around wildlife. It may be appropriate for such guidance to reflect the purpose of the flights, for example, surveying flights supporting environmental research which yield ecological benefits in contrast to purely recreational flying (Chabot and Bird, 2015). As noted in several recent reviews, relative to other methods of data acquisition such as on-the-ground surveying, environmental surveying using RPAS often causes less disturbance to wildlife (Chabot et al., 2015; Chabot and Bird, 2015; Linchant et al., 2015).

8.4.3. Structure-from-Motion (SfM) Modelling

SfM and multi-view stereopsis modelling was undertaken on a high performance computer (4 x 16 core AMD Opteron 6276, 512GB 1600MHz RAM), although the memory requirements for SfM modelling are high, a lower specification computer can be used if scene areas are modelled in discrete chunks. A range of computer software tools for implementing SfM are available (e.g, Snavely et al., 2008), but for this work Agisoft's PhotoScan (V1.1.0) (http://www.agisoft.com/) was used because it compares favourably with other software in terms of reconstruction detail and accuracy as well as computational efficiency (Verhoeven, 2011; Dandois and Ellis, 2013; Gini et al., 2013; Turner et al., 2014; Sona et al., 2014; Remondino et al., 2014; Dandois et al., 2015).

The structural complexity of vegetation raising particular challenges for SfM photogrammetry. First of these is aligning source imagery using feature matching algorithms in order to back-calculate camera exterior orientations. Depending on the canopy structure, identifying sufficient tie-points can be nontrivial due to similarity of textures across the scene and potentially high parallax between adjacent images. This was overcome using high overlap (≥18 photos of every location), considering high numbers (>80,000) of candidate tie-points in each image, and using geotagged images to constrain tie-point search areas to neighbouring images.

All processing was undertaken using highest quality settings, to maximise retention of spatial detail (see Table 8.1 for details). More than 98.8% of the source image data were aligned and used in the reconstruction for each AOI; alignment of the remaining images was not possible due to insufficient identification of tie points by the image feature descriptor algorithms, and unaligned images were not used in the subsequent modelling. Direct georeferencing of the image data substantially improves the image alignment process by allowing comparisons between only nearby images (Agisoft, 2014). This increases computational efficiency, which also enables searching for higher numbers of tie-points and consequently improves the likelihood of successful image alignment (Turner et al., 2014), particularly in texturally complex, vegetated scenes (Lisein et al., 2013; Puttock et al., 2015). SfM reconstruction geometric accuracy was optimised through full photogrammetric bundle adjustment, using both direct georeferencing of image data and GCPs in order to refine estimation

of the extrinsic (positon and orientation) and intrinsic (lens calibration) parameters of all images. Error terms were specified for both directly georeferenced camera positions (±15 m) and GCPs (±0.015 m). The lens calibration model distortion plot is shown in Figure 8-7a, and the average vector of the reprojection error in tie points remaining after the lens model was applied is shown in Figure 8-7b. Although some systematic residual errors are apparent in the residual plot, *average* uncorrected distortion was less than a pixel in all areas of the photograph.

Table 8.1. Settings used for Structure-from-Motion modelling in Agisoft PhotoScan (v1.1.0). Note that the user-control on these parts of the PhotoScan processing workflow has been expended in subsequent versions.

Step	Parameter	Setting
Camera alignment	Accuracy	High
	Pair-preselection	Reference
	Key points limit	80,000
Dense cloud build	Quality	Ultra-high
	Depth filtering	Mild

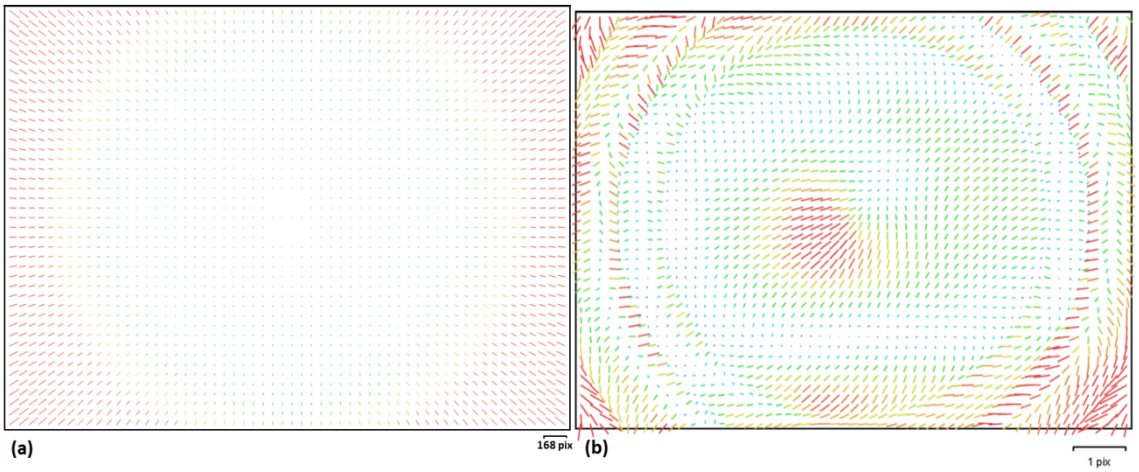

Figure 8-7. Lens model calibration quality for AOI-7. (a) distortion plot, illustrating the distortions modelled by the lens calibration model, and (b) image residuals plot, illustrating the average vector of the reprojection error for the pixels in the corresponding cells (i.e. the uncorrected error remaining). Note the change in scales between the two plots.

Dense point clouds were produced using multi-view stereopsis to estimate points with both spatial (x, y, z) and spectral (red, green, blue) attributes. Mild-depth filtering was used to reduce erroneous points the dense point cloud while retain points associated with small features of interest such as vegetation elements (Puliti et al., 2015). The seven resultant point clouds each comprised of 41 million to 415 million points. Point cloud renderings were produced using the open source software CloudCompare (V2.6.1) (http://www.danielgm.net/cc/). Orthomosaics were produced in PhotoScan; where image overlap occurs the 'mosaic' parameter ensures that the source images with pixels closest to the image centre are used preferentially for orthophoto generation and colour correction was employed to reduce variations in illumination in the orthomosaic (Agisoft, 2014).

8.4.4. Digital Terrain, Surface and Canopy Height Model Generation

Digital Surface Model (DSMs) were obtained by applying 10 mm *x*,*y* grids to the dense point clouds; the highest point in each cell was identified and interpolated linearly (Delaunay triangulation) to a triangular irregular network, which was then sampled regularly at 10 mm spatial resolution. Delaunay triangulation uses a triangular net where the acuteness of the triangles is minimized, i.e., the triangles are as close as possible to equilateral. Although more statistically sophisticated interpolation approaches are available, such as inverse distance weighting (e.g., Tilly et al., 2015a) or kriging (e.g., Luscombe et al., 2014), for example, more complex approaches require additional assumptions about the surface being modelled. Furthermore, Delaunay triangulation is computationally very efficient which was an important consideration given the extent and resolution of the datasets (Williams et al., 2013). The 1 cm^2 grid size was selected to maximise utilization of the detail available in the spatially variable point cloud densities, and is supported by the average point densities as reported in Table 8.3.

To produce Digital Terrain Models (DTMs) from point clouds it was necessary to identify a subset of points representing true ground returns and interpolate between these ground points to produce a continuous surface. The dense point clouds were classified as ground or non-ground, using the two-step classifier implemented in PhotoScan. Firstly, a regular *x,y* grid of a prescribed spatial resolution ('cell size') is applied to the point cloud, the lowest point in each cell is identified and classified as an initial ground point, and these initial ground points

are interpolated using Delaunay triangulation to produce an approximate initial terrain model. Secondly, all remaining unclassified points are evaluated, and added to the ground class if they meet both of two conditions: (i) They lie below a threshold maximum distance above the initial terrain surface, and (ii) the difference in angle between the closest ground point and the initial terrain surface and the closest initial ground point and the point under evaluation is less than a threshold maximum angle (Agisoft, 2015, 2014). This classification process is illustrated schematically in Figure 8-8.

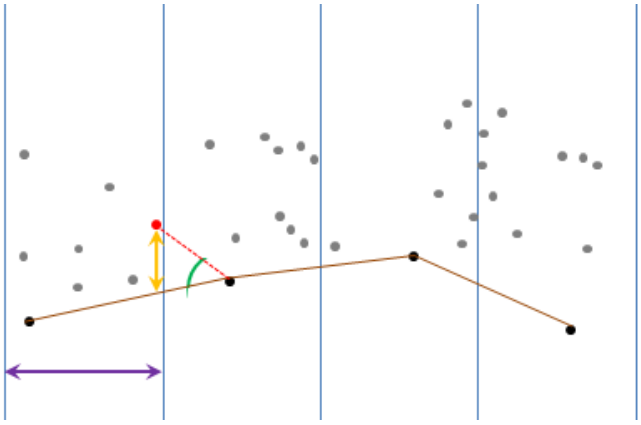

Figure 8-8. Schematic representation of the ground/non-ground point classifier implemented in Agisoft PhotoScan. This is a 2D cross section, looking sideways through the ground surface. The regular grid has a spatial resolution ('cell size') equivalent to the purple arrow, and is shown in the x axis by the blue lines. The lowest point in each x domain (shown in black) is assigned to the ground class. These points are interpolated to an initial terrain model (shown as the brown line). Unclassified points (shown in grey) are evaluated to see whether they fit the two conditions of being less than a threshold distance ('maximum distance', shown as the yellow arrow) above the initial terrain model AND the angle of the terrain slope to connect the evaluated point to the closest ground point is less than a threshold number of degrees ('maximum angle', shown as the green arc).

This treatment works well for classifying ground points in point clouds with spatially variable density, compromising between accuracy and topographic detail. The cell size parameter is contingent on the minimum density of true ground returns, and should allow every cell to contain at least one ground point. Maximum distance and maximum angle depend on the degree of topographic variation within each cell; maximum distance represents the maximum permitted maximum variation in Z within any cell and thus is contingent upon the topography and cell size, maximum angle should approximate the maximum gradient of the

ground within the AOI. Identifying appropriate parameter values required an iterative trial and error process, tuning the parameters in order to filter non-ground (vegetation) points while maximising retention of topographic detail. The optimised values identified for these ecosystems are reported in Table 8.2.

In these grassland and shrubland ecosystems, the micro-topographic relief associated with the shrub 'islands' is very similar in scale to that of the grass tussocks. Consequently, as any given set of parameters used for the classification of points as ground/non-ground results in some errors of either commission (with grass tussocks classed as ground) or omission (with shrub 'island' mounds classed as vegetation), no single optimum parameter set was completely accurate for classifying points as ground/non-ground. The DTMs will be used to characterise ecosystem structure in two distinct ways: (i) modelling canopy height models and (ii) hydrological flow-path routing. It was therefore appropriate to derive two parameter sets, yielding DTMs optimised for each application.

- For hydrological routing it was considered preferable to err on the side of commission, correctly representing shrub mounds while also representing some grass tussocks as areas of topographic relief, because functionally the grass tussock structures impede overland flow (Parsons et al., 1997; Müller et al., 2007b).

- For modelling canopy heights, it was considered preferable to err on the side of omission, correctly characterising grass patches as non-ground at the risk of misclassifying some ground returns associated with the shrub mounds as non-ground; this will yield more accurate overall estimation of canopy volume because grass vegetation often covers a larger extent than shrub vegetation and the relative error will be very small relative to the total shrub volume.

Table 8.2. Parameter sets used for classification of points as ground/non-ground for the production of digital terrain models (DTM) and canopy height models (CHM).

	Parameter	AOI-1						
		1	**2**	**3**	**4**	**5**	**6**	**7**
DTM for CHM	Cell Size [m]	0.4	0.4	0.4	0.4	3	3	0.9
	Max Distance [m]	0.05	0.05	0.05	0.05	0.03	0.03	0.06
	Max Angle [°]	3	3	3	3	1	1	3
DTM for hydrological modelling	Cell Size [m]	0.4	0.4	0.4	0.4	3	3	NA
	Max Distance [m]	0.1	0.1	0.1	0.1	0.04	0.04	NA
	Max Angle [°]	4	4	4	4	1.5	1.5	NA

Potentially negative outliers (also known as “sinkers”) are automatically identified by PhotoScan’s ground point classifier according to the number of points present in an inverted cone above the potential outlier, and assigned to a ‘Low Points (noise)’ class; further information on this step was not available for this ‘black box’ proprietary software. Visual examination indicated that this filter performed fairly well, with most apparent negative outliers and few valid ground points removed. 1 cm^2 *x,y* grids were applied to each point cloud, the highest ground point in each domain identified, and a surface interpolated between them (using Delaunay triangulation); this surface was than sampled at a spatial resolution of 1 cm^2.

Orthomosaic, DSM and DTM were compiled in a Geographic Information System (GIS) (ArcMap V10.2.2, developed by Environmental Systems Research Institute, Redlands, California, USA). Limited image coverage beyond the AOI resulted in poor quality SfM reconstructions, with limited density and accuracy of points in these distal areas (Dandois and Ellis, 2010). Consequently, each SfM reconstruction was subset to the AOI which was fully captured by the survey imagery, excluding distal areas only represented by a limited number of oblique images.

CHMs were produced through surface differencing, by subtracting DTMs from DSMs, which yielded top-of-canopy heights (Dandois and Ellis, 2010, 2013, Chang et al., 2012, 2015; Greaves et al., 2015). Despite average-area-per-TIN-facet of between 1 cm^2 and 5 cm^2, subtle differences in the TIN interpolation of DTM and DSM m resulted in physically impossible negative

canopy heights in less than 0.2% of cells. As negative canopy heights are physically impossible, negative values were corrected to zero (after Dandois and Ellis, 2013). These CHMs do not represent sub-canopy vegetation, and no further smoothing of the CHMs was undertaken.

8.4.5. Structural Classification of Surface Cover

The surface cover of each 10 mm cell in the CHM was classified structurally. Modelled canopy heights were used to differentiate bare ground from vegetated cells, with <0.015 m taken to represent bare surfaces, and ≥0.015 m to represent vegetated areas. Because of the error inherent in SfM-derived models, a threshold >0.01 m was necessary to minimise commission errors when classifying domains as vegetated; comparison of 0.010 m, 0.015 m, 0.020 m, and 0.025 m indicated very low classification sensitivity around this parameter value (data not shown). The accuracy of the bare versus vegetated classification was assessed at 1,000 random locations across AOI-7, using photointerpretation of the orthomosaic image as reference data; where surface cover was indistinguishable, points were replaced with other randomly selected locations (~4% of original points).

Vegetated cells were further apportioned between a grass vegetation class and a woody (either shrub or juniper, according to their presence in the AOI) vegetation class, using a threshold canopy height of 0.2 m to differentiate between grasses (<0.2 m) and woody plants (>0.2 m). While such height-based distinction between plant functional types is a simplification, as the boundary is fuzzy, such approximation is physically reasonable and appropriate in ecosystems where the botanical composition is dominated by differently sized species (Féret and Asner, 2012; Hellesen and Matikainen, 2013). Selection of the 0.2 m threshold was also informed by the natural break in the slope of the canopy height frequency distribution for grass-dominated AOI 1 (depicted in Figure 8-18).

8.4.6. Estimation of Plant Biomass from Canopy Volume

Commonly measured plant dimensional attributes such as plant height or canopy area are usually non-linearly related to AGB, which necessitates the identification and measurement of individual plants prior to estimation of AGB (e.g., Ludwig et al., 1975; Gholz, 1980; Smith and Brand, 1983; Cleary et al., 2008; Lufafa et al., 2009; Ansley et al., 2012; Mirik et al., 2013a; Li et al., 2015; Berner et al., 2015). However, for all three vegetation classes considered herein, canopy volume is linearly related to AGB, with an intercept at zero. This linear relationship is fundamental to this approach, as it obviates the need to identify discrete individual plants prior to measuring the volume associated with that class and thus circumvents challenges such as differentiating between neighbouring plants with coalesced canopies, a common occurrence in natural ecosystems (Neufeld et al., 1988; De Soyza et al., 1997).

Canopy volume was calculated from CHM, using a foliar canopy approach. For each vegetation class (grass, and shrub or juniper) the volume beneath the ultra-high spatial resolution CHM was summed (Huenneke et al., 2001; Allen et al., 2008; Muldavin et al., 2008; Ladwig et al., 2012; Berner et al., 2015). Foliar canopy approaches to estimating canopy volume are sensitive to subtle differences in plant biophysical structure which do not influence overall plant dimensions (such as maximum height or canopy area); this is particularly important in semi-arid rangeland community assemblages (Neufeld et al., 1988; De Soyza et al., 1997; Rango et al., 2006, 2009). By definition, the grass vegetation class volume was therefore limited to ≤0.2 m^3 m^{-2}.

AGB was predicted from canopy volume, using linear regression models developed from published datasets with strong coefficients of determination ($P < 0.001$; $r^2 \geq 0.64$). These published datasets are described below; for the grass and shrub classes these datasets were collected at the same SNWR site as the present study, while the juniper class used datasets from other sites. The intercepts were constrained through the origin as plants with a canopy volume of zero have no AGB (Ludwig, 1977; Brisson and Reynolds, 1994; Muldavin et al., 2008; Ansley et al., 2012); in all cases constraining the intercept made minimal difference to the regression slope parameters.

Canopy volume is very strongly correlated with AGB in semi-arid woody plants (Huenneke et al., 2001; Cleary et al., 2008; Allen et al., 2008; Ansley et al., 2012;

Mirik et al., 2013a). The biomass of grasses such as black grama is strongly correlated with basal diameter and, to a lesser extent, average height, with residual variation attributed to differences in stem density (Andariese and Covington, 1986; Guevara et al., 2002; Nafus et al., 2009; Muldavin et al., 2008). The CHM-derived estimates of grass canopy volume obtained herein integrate the basal area, average height and density of each grass plant, so the estimates of grass canopy volume presented herein would be expected to be more strongly correlated with biomass than either basal area or average height alone. At the Sevilleta LTER, between 8 and 44 samples of black grama grass and partial creosote shrubs have been destructively harvested three times each year in winter (February), spring (May) and autumn (September) between 1999-2014 (Moore, 2015). To optimise temporal transferability, all available observations were used when producing regression models[3].

Despite extensive literature examining the quantification of juniper biomass on the basis of plant dimensions (e.g., Meeuwig, 1979; Meeuwig and Cooper, 1981; Miller et al., 1981; Ambrosia et al., 1983; Smith and Brand, 1983; Chojnacky, 1985; Grier et al., 1992; Chojnacky and Moisen, 1993; Huang et al., 2009; Starks et al., 2011; Ansley et al., 2012; Sankey et al., 2013; Chojnacky et al., 2014; Hulet et al., 2014), there has been limited whole-tree destructive sampling for accurate biomass determination of juniper and where destructive sampling has been undertaken, measured attributes rarely include canopy volume. To the best of my knowledge, there is no published data on the relationship between canopy volume and AGB for Oneseed Juniper (*J. monosperma*), the juniper species present at AOI-5 and AOI-6. In the absence of species-specific information,

[3] Any method of biomass estimation has the two central objectives of accuracy and transferability (across space, time, and/or species); to an extent, these are mutually exclusive, As canopy volume-biomass models are more accurate (with higher coefficients of determination) when developed for specific species, sites, seasons and years (Huenneke et al., 2001; Jenkins et al., 2003; Muldavin et al., 2008). The present treatment adopted an intermediate approach, using species-specific data gathered across a large environmental gradient but across multiple seasons and years. Thus, if greater accuracy was desired additional destructive sampling could be used to derive more specific models. Conversely, to extend this technique to sites with more diverse vegetation communities, it would be appropriate to utilise generalised, multi-species canopy volume-biomass models. Such models have been found to be moderately successful for species with similar growth forms (Enquist, 2002; Chojnacky et al., 2014), such as woody plants (Singh, 1986; Buech and Rugg, 1989; Tietema, 1993; Jenkins et al., 2003; Lambert et al., 2005) and semi-arid grasses (Ares and Fownes, 2000; Nafus et al., 2009). Interestingly, compared to previous efforts using other plant dimensions, such as basal area alone, it is conceivable that foliar canopy volume-biomass relationships may be more transferable. If transferability is preferred, it may also be appropriate to utilise universal scaling theories to obtain root : shoot coefficients (e.g. Robinson, 2004; Cleary et al., 2008).

volume-biomass regression model were examined for other species of the *Juniperus* genus, in order to (I) examine whether canopy volume is a good predictor of AGB, and (II) assess similarities between volume-biomass models for different species of the same genus to evaluate their applicability to *J. monosperma*. Working in semi-arid rangeland in nearby Texas, Ansley *et al*. (2012) found that canopy volume is a very strong predictor of AGB in redberry juniper (*J. pinchotii*) (r^2 = 0.95, *n* = 40, AGB ranged from 9 kg to 688 kg) reporting an relationship of: AGB [g] = 23360 + 2350 × Volume [m^3]. Miller et al. (1981) reported size and biomass measurements for Utah Juniper (*J. osteosperma*). Due to the commonly apical dominance (for example, see Figure 4-2, Figure 8-2a and Figure 8-12d) and for equivalence with canopy volume as measured by RPAS-SfM, *J. osteosperma* canopy volume was calculated as a domed cylinder (Figure 8-9), using Equation 9-1

$$\boldsymbol{V} = \frac{\left(\frac{\pi \times a \times b \times c}{4}\right)}{2} + \frac{\left(\frac{4}{3} \times \pi \times A \times B \times \frac{B}{2}\right)}{2} \qquad \textit{Equation 8-1}$$

where V = volume [m^3], A = radius of the longest canopy axis [m], B = radius of the perpendicular canopy axis [m], and C = height [m] (adapted from Cleary et al., 2008; Ansley et al., 2012). This yielded a relationship of AGB [g] = 2149.25 × Volume [m^3] (r^2 = 0.954, P<0.000001, *n* = 33, AGB between 12 kg to 956 kg) for *J. osteosperma*. The similarity in slopes between the regression models for these two Juniperus species offers some support for the transfer of the derived relationship between *Juniperus* species with similar growth forms, such as *J. monosperma*, in order to explore the potential of this approach. Reconciling these two models, a coefficient of 2250 was used for the Juniper vegetation class. All regression models are presented in Table 8.7. More powerful predictive models can be developed if size-biomass relationships are calibrated to the site, year and even phenological stage of dominant plants (’t Mannetje, 2000; Huenneke et al., 2001; Allen et al., 2008; Muldavin et al., 2008), but the combined relationships are considered to be more transferable spatially and temporally, and were considered appropriate for the present study.

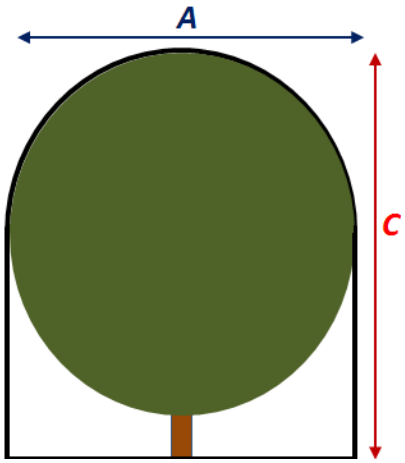

Figure 8-9. Schematic representation of the domed cylinder geometry (black line) used to calculate juniper canopy volume (where A = radius of the longest canopy axis and C = height).

Belowground biomass (BGB) is an important component of ecosystem C dynamics (Marshall, 1977; Sims et al., 1978; Richter et al., 1990; Holland et al., 1992; Jackson, 2000; Jackson et al., 2000; Schenk and Jackson, 2002; Scurlock et al., 2002, 2002), and it is appropriate to include this component in C inventories. BGB can be estimated from AGB using root : shoot ratios, defined as root biomass divided by shoot biomass (Mokany et al., 2006). Species-specific root : shoot ratios are generally good predictors of BGB (Mokany et al., 2006), although this trait can exhibit some plasticity, for example due to removal of AGB by herbivory or combustion (Burnett et al., 2012), differences in the availability of moisture and nutrients in the soil (Ludwig, 1977; Brisson and Reynolds, 1994), soil bulk density (Goodman and Ennos, 1999), the shape of soil particles (Lipiec et al., 2016) and the necessity for anchoring to resist wind-induced mechanical stresses (Goodman and Ennos, 1996).

A meta-analysis of published root : shoot ratios was undertaken, summarised in Figure 8-10. Representative values for each vegetation class were selected using expert judgement, with credence weighted according to sample size, methodological rigour (treatment of fine roots, etc.) and similarity of environmental context to the Sevilleta NWR. This treatment makes best use of the information in the literature and is considered to be more robust process than simply using a value based on a single study (this appraisal was supported by a pers. comm. from Dr Adrian Goodman).

Creosote shrub root : shoot ratios are independent of plant size (Wallace et al., 1974; Allen et al., 2008) and although AGB is a good predictor of BGB for juniper (Krämer et al., 1996; Rozas et al., 2009), no published information could be found describing root : shoot ratios for Oneseed Juniper (*J. monosperma*), so other similar species in the *Juniperus* genus were considered. The uncertainty associated with each vegetation class was conservatively estimated, based on expert judgement of the variance indicated by meta-analysis (Figure 8-10).

This yielded root : shoot ratios of 2±0.6 for the semi-arid grass class (Sims et al., 1978; Schlesinger and Pilmanis, 1998; Mata-González et al., 2002; Corkidi et al., 2002; Peters, 2002; Mokany et al., 2006), 0.45±0.2 for the creosotebush shrub class (Singh, 1964; Chew and Chew, 1965; Barbour, 1973; Wallace et al., 1974; Ludwig et al., 1975; Ludwig, 1977; Allen et al., 2008), and 1±0.5 for the juniper vegetation class (Miller et al., 1990; Krämer et al., 1996; Nowak et al., 1999; Gentine et al., 2015). The use of logarithmic scales is necessary to visually compare relative differences between ratios above and below unity (Michaelides et al., 2012; Cunliffe et al., 2013b).

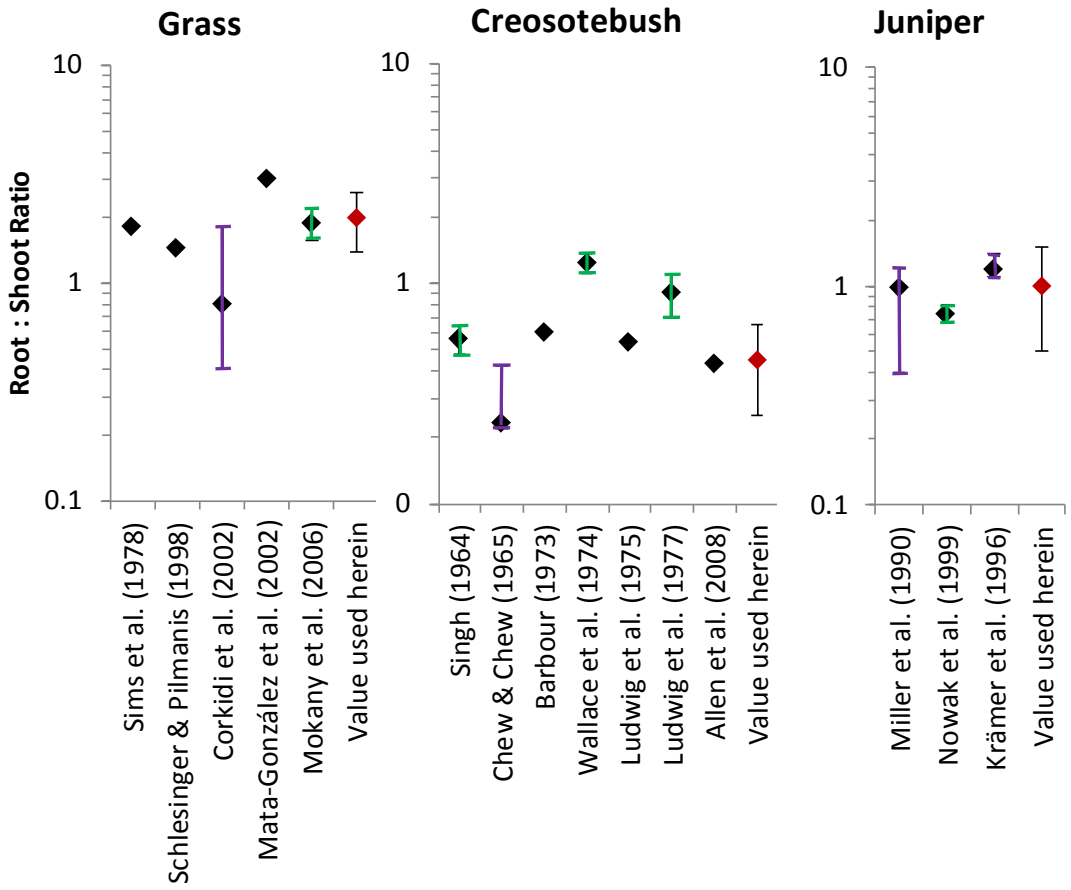

Figure 8-10. Meta-analysis of published root : shoot ratios for juniper, creosotebush shrubs and black grama. Note that logarithmic scales are necessary to correctly represent relative differences between ratios above and below unity (Michaelides et al., 2012; Cunliffe et al., 2013b). Where available, uncertainties are presented in preference of SD (Black) > SE (Green) > range (Purple). Values assumed in modelling studies referred to in the text are not plotted.

8.4.7. Estimation of Carbon Stocks from Biomass

The carbon stock of each vegetation class was estimated as a fraction of dry biomass weight. Biomass-carbon conversion coefficients were selected using expert judgement based on published C coefficients, which represent the proportion of biomass which is C (Figure 8-11). These values were 0.45±0.03 for grasses (Lieth, 1975; Puttock, 2013), 0.48±0.03 for shrubs (Schlesinger, 1997; Puttock, 2013), and 0.50±0.03 for juniper (Norris et al., 2001; Pregitzer et al., 2002; Strand et al., 2008; Huang et al., 2009; Puttock, 2013). Although biomass-carbon coefficients are likely to differ slightly between AGB and BGB (see Figure 8-11), insufficient empirical evidence was available to contain these differences

so the same C coefficients were applied to both AGB and BGB. For comparability with other published assessments, vegetation volume, biomass and C stock estimates were normalised by area to m^2.

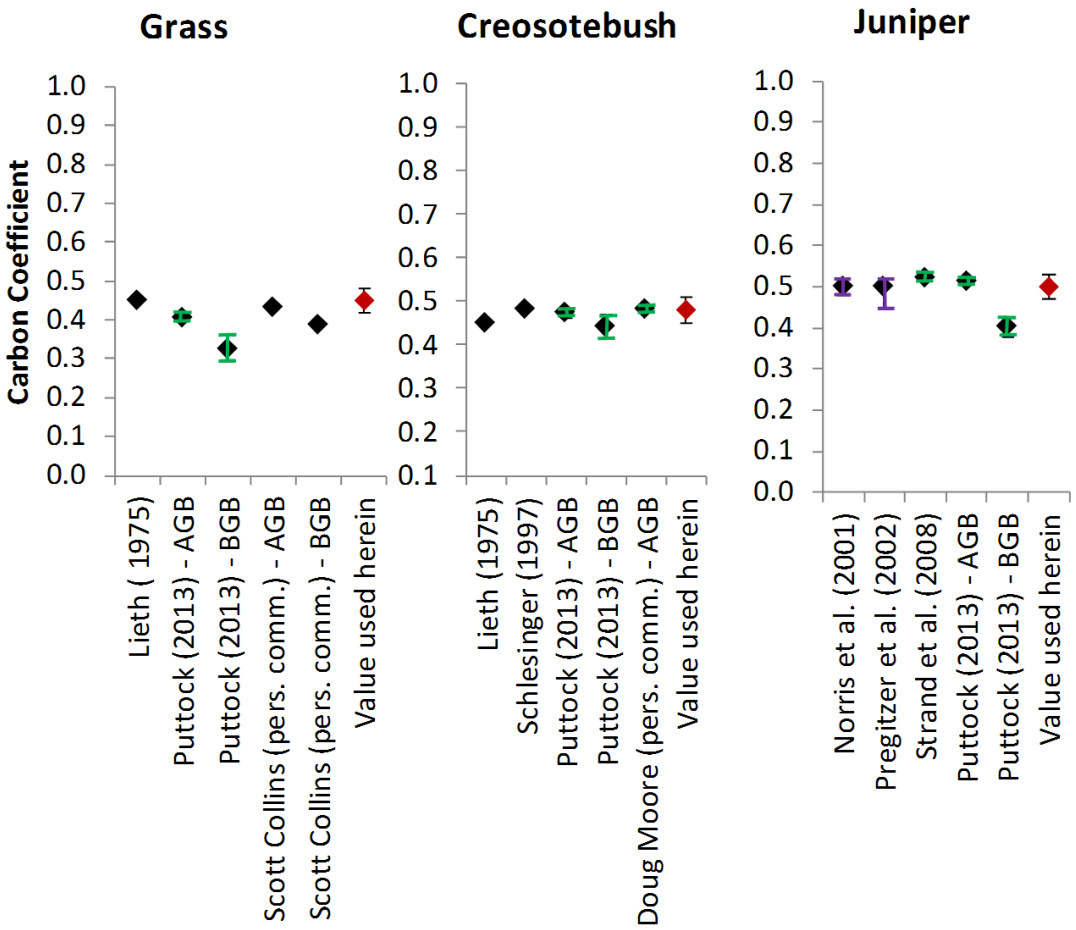

Figure 8-11. Meta-analysis of published carbon coefficients for grass, shrub and juniper biomass. Where available, uncertainties are presented in preference of SD (Black) > SE (Green) > range (Purple). Values assumed in modelling studies referred to in the text are not plotted.

8.4.8. Treatment of Uncertainty

Four main sources of error contribute to the cumulative uncertainty in summary metrics of ecosystem biomass and vegetation C stocks.

(i) Minimal empirical information is currently available to constrain error in SfM-derived canopy height models (although see Dandois et al., 2015), but underestimation of canopy volume is more likely so a asymmetric error of -5%/+20% was conservatively estimated.

(ii) Allometric volume-AGB conversion error was estimated as the 99% confidence interval of the regression error (*i.e.*, three times the standard error of the slope) (Figure 8-22).

(iii) Prediction of BGB from AGB is likely to be one of the largest sources of overall uncertainty in total C stock estimation because of plasticity in root : shoot ratios in response to soil medium, nutrient and water availability, plant age, and reduction of AGB through herbivory, fire or frost damage (Wallace et al., 1974; Holland et al., 1992; Goodman and Ennos, 1996, 1999; Mokany et al., 2006; Strand et al., 2008; Padilla et al., 2009; Epron et al., 2012; Schlesinger and Bernhardt, 2013b, 2013a). Uncertainty in root : shoot ratios associated with each vegetation class was conservatively estimated, based on variance observed in meta-analysis of published data (Figure 8-10).

(iv) Errors in the biomass C content are usually ignored but can be significant, particularly as models are applied over larger spatial extents (Jenkins et al., 2003; Lamlom and Savidge, 2003; Thomas and Martin, 2012; Hill et al., 2013). Therefore, an estimated error of ±0.03 was specified for the biomass C coefficient for all three vegetation classes (Figure 8-11).

Estimated errors were assumed to be independent and parametrically distributed, and so were propagated using the quadratic approach (Equation 9-2), as the square root of the sum of all squared errors (Taylor, 1997; Asner et al., 2012). Relative to the propagated overall uncertainty, total biomass and total C stock estimates were insensitive to differences in the proportion of canopy volume assigned to grass versus shrub/juniper classes. This is important, because it indicates that these metrics are insensitive to variations in the 0.2 m canopy height threshold used to differentiate grasses from the two woody plant classes.

$$\boldsymbol{Relative\ Error} = \frac{\Delta z}{z} = \sqrt{\left(\frac{\Delta x}{x}\right)^2 + \left(\frac{\Delta y}{y}\right)^2 + \cdots} \qquad \textit{Equation 8-2}$$

8.5. Results

8.5.1. RPAS Survey and SfM reconstruction

Further details of the source image data and SfM reconstruction for each AOI are given in Table 8.3. The overall root mean square error (RMSE) of the GCPs for the six smaller AOIs (AOI 1 to AOI 6) is <0.04 m, and for the much larger AOI 7 is 4.86 m. Note that the overall RMSE is generally dominated by the z component, and because GCPs are used by the bundle adjustment to optimise both exterior (position and attitude) and interior (lens calibration model) camera parameters, this RMSE was not an independent measure of model accuracy.

8.5.1. SfM derived point clouds

Point-clouds derived using SfM processing of RPAS-acquired image data yielded detailed photorealistic representations of these ecosystems with a high degree of fidelity and spatial accuracy. Although there are some instances where individual plants were poorly represented in the point cloud and subsequent CHM, both abiotic and biotic features were usually very well represented across a range of scales, from grass tussocks 20 mm high to trees several meters high. Figure 8-12 shows example renderings of the point clouds representing individual black grama grass, creosotebush shrub and Oneseed juniper plants. The representation of abiotic structure, particularly microtopography associated with the bare areas dominated by stone pavement cover is illustrated in Figure 8-13. The limited canopy penetration of SfM-derived point clouds results in a ‘shell’ of the vegetation (*sensu* Greaves et al., 2015), illustrated in Figure 8-14, with few ground returns beneath the dense juniper canopy. Because the creosotebush shrub canopies often exhibited patchy canopy structure and typically grow in the form of an inverted cone (Chew and Chew, 1965; Ludwig et al., 1975; Wainwright et al., 1999a; Abrahams et al., 2003; Dodson, 2012) (Figure 8-5), ground points were frequently generated beneath at least part of the canopy extent (e.g. Figure 8-13b and c), constraining the DTM interpolation, thereby improving confidence in both the DTMs and subsequent CHMs in systems with creosotebush shrubs.

Table 8.3. Details on source data and reconstruction parameters for SfM reconstructions.

Parameter		AOI						
		1	2	3	4	5	6	7
Vegetation type		Grass Dominated (*Bouteloua eriopoda*)	Grass-Shrub (*B. eriopoda* and *Larrea tridentata*)	Shrub-Grass (*L. tridentata and B. eriopoda*)	Shrub-dominated (*L. tridentata*)	Shrub-Grass (*B. eriopoda*, *Pinus edulis*, and *Juniperus monosperma*)	Grass-Shrub (*B. eriopoda*, *Pinus edulis*, and *Juniperus monosperma*)	Grass-Shrub (*B. eriopoda* and *Larrea tridentata*)
Source Images		135	149	121	253	159	216	2518
% used in reconstruction [%]		99.3	100.0	100.0	100.0	98.7	100.0	98.8
Average GSD [m]		0.004	0.005	0.006	0.004	0.006	0.004	0.007
Coverage [m^2]		4,259	4,552	7,520	4,875	10,328	3,467	68,222
Number of points [$\times 10^6$]		170.3	172.8	139.0	339.7	101.1	41.3	415.4
Point density [points cm^{-2}]		4.00	3.80	1.85	6.97	0.98	1.19	0.61
GCPs		10	10	10	10	10	10	18
Each GCP visible in *n* images	Range (mean)	11-19 (14.6)	16-28 (20.4)	13-24 (18.5)	12-23 (16.7)	9-41 (22.5)	13-24 (18.3)	20-87 (44.4)
GCP estimated error	Average Pixels	0.18	0.36	0.25	0.23	0.23	0.22	1.97
	Overall RMSE [m]	0.019	0.024	0.041	0.023	0.016	0.026	4.858
	X RMSE [m]	0.005	0.011	0.038	0.013	0.012	0.023	1.301
	Y RMSE [m]	0.011	0.010	0.014	0.018	0.011	0.012	0.751
	Z RMSE [m]	0.015	0.019	0.003	0.006	0.003	0.005	4.620

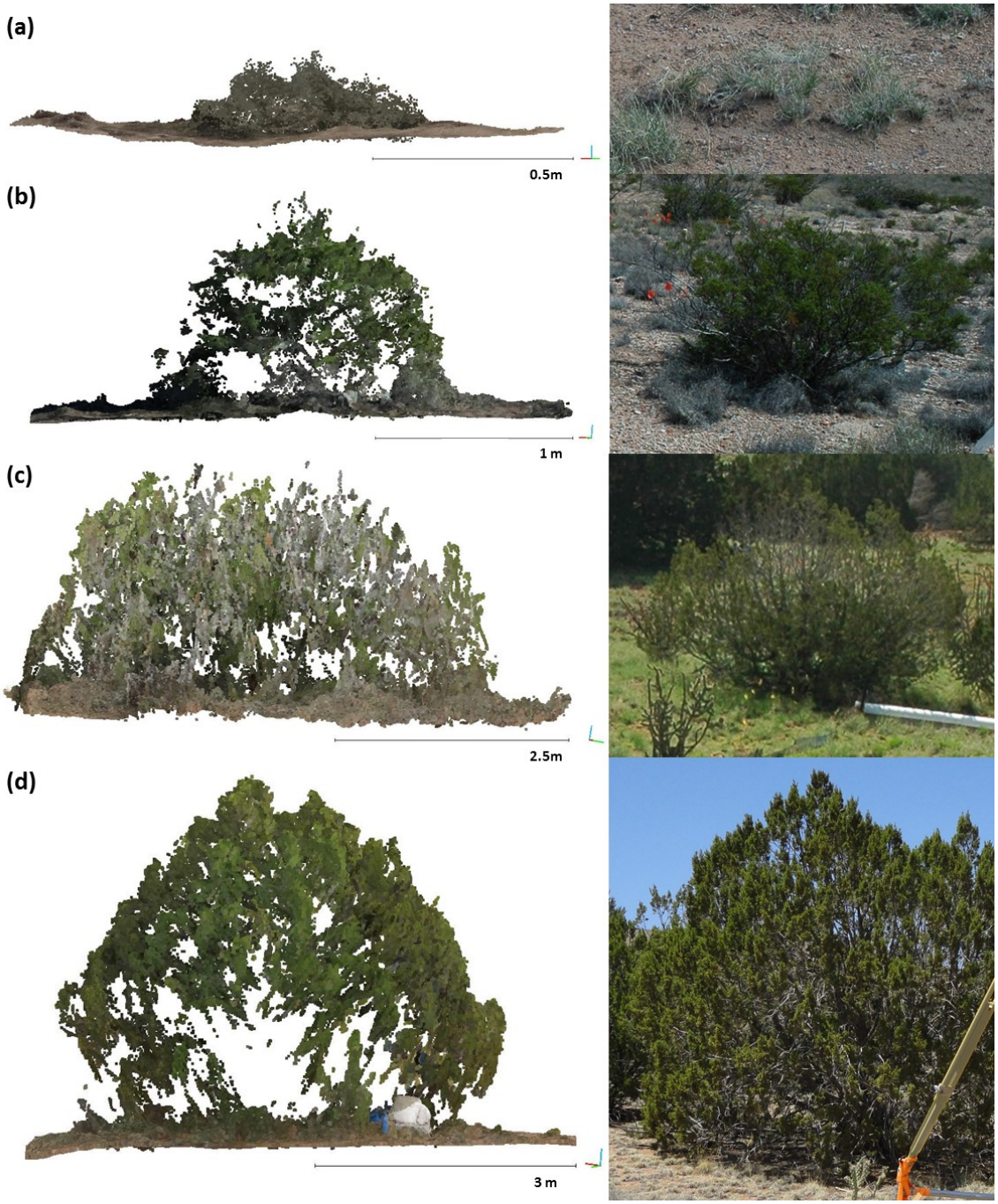

Figure 8-12. Renderings of the point clouds representing individual plants: (a) black grama grass (*Bouteloua eriopoda*) (~72,000 points from AOI-2), (b) creosotebush shrub (*Larrea tridentata*) (~250,000 points from AOI-3), (c) and (d) oneseed Juniper trees (*Juniperus monosperma*) (~640,000 points and ~713,000 points from AOI-6). Accompanying photographs of each plant individual were taken from slightly different viewpoints to the point cloud renderings.

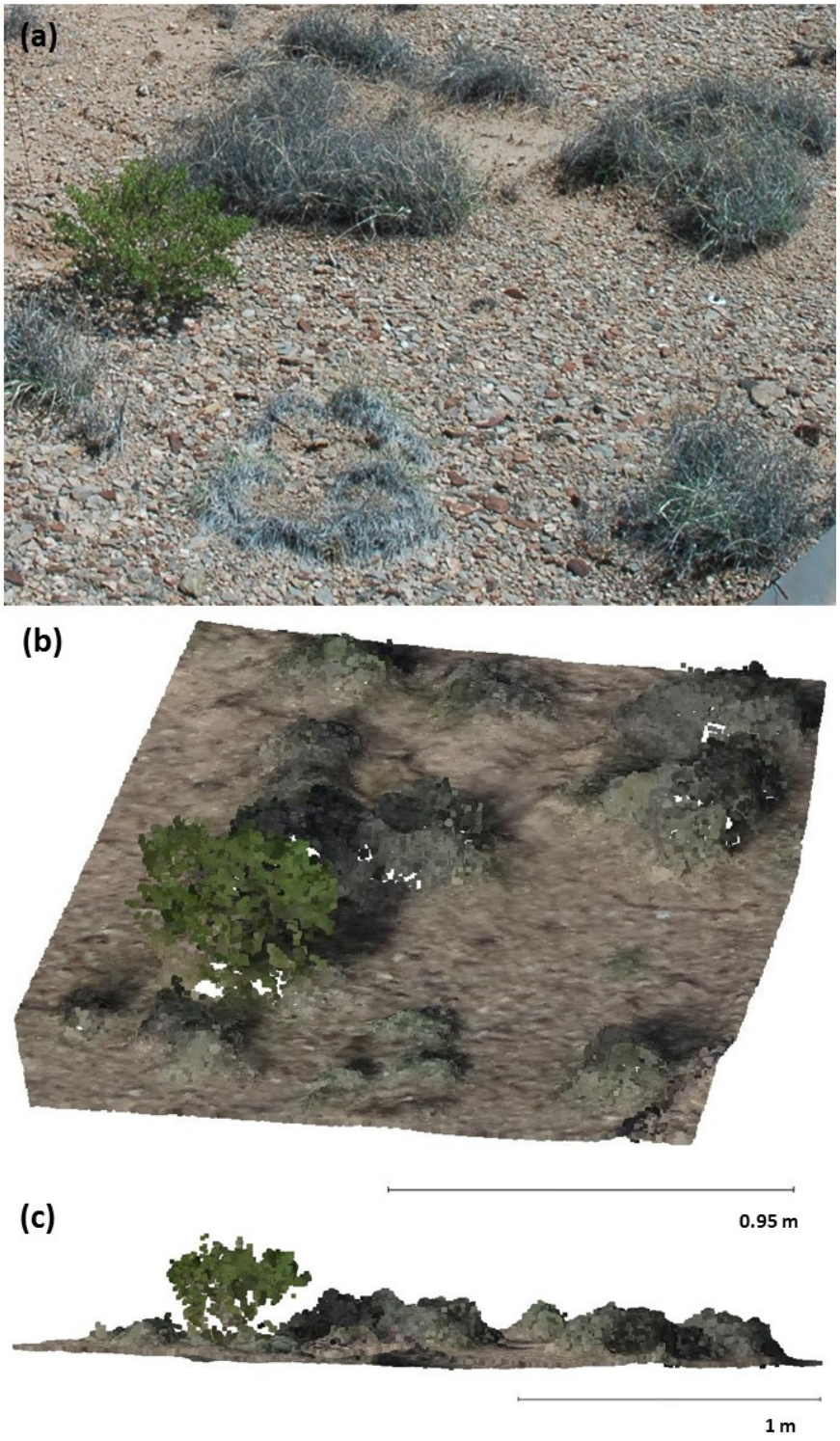

Figure 8-13. (a) photograph of mixture of black grama grass (*B. eriopoda*) and one small creosotebush shrub (*L. tridentata*) taken in July 2013. (b) point cloud rendering of the same scene surveyed in October 2014 (~178,000 points from AOI 3). (c) cross section of through the point cloud.

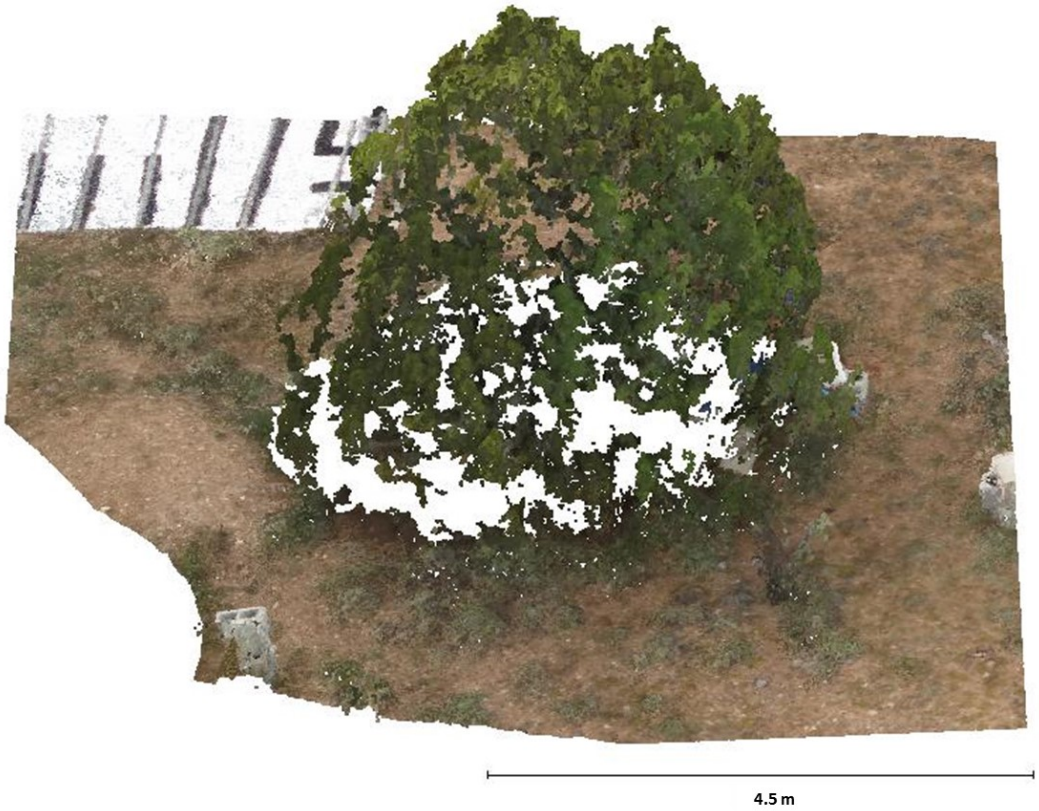

Figure 8-14. Point cloud rendering from AOI-6, exemplifying the limited canopy penetration of SfM, with no ground returns beneath the canopy of a oneseed Juniper (*Juniperus monosperma*) tree.

8.5.2. Digital Surface Models and Digital Terrain Models

All the DSMs and DTMs were free of noticeable doming effect indicative of systematic geometric error in the SfM reconstruction (James and Robson, 2014; Remondino et al., 2014). At AOIs 1 to 6, DTM vertical spot height accuracy was assessed against n = 78-89 independent GNSS-RTK observations (Figure 8-15) (Table 8.4). Different locally coordinated benchmarks were employed for the GCPs used to constrain the SfM reconstruction and the separate topographic survey; the DGPS instrument (Leica GC08) had an absolute accuracy of ±0.05 m (95% CI) and a relative accuracy of ±0.015 m (95% CI). The residuals generally have a leptokurtic distribution, with SDs of less than 0.031 m (five of the six AOIs had SD <0.016 m), indicating internal consistency which translates as good relative accuracy. Mean absolute error (MAE) ranges between -0.077 m to +0.084 m for the six AOIs, this is not significantly greater than the absolute error associated with the benchmarks, indicating no evidence of meaningful error in absolute terms (see further discussion in Turner et al., 2016).

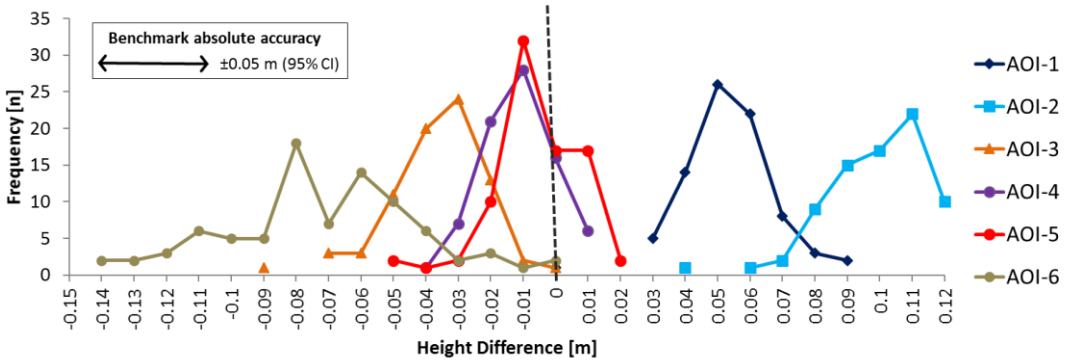

Figure 8-15. Residual Z elevations in m from the SfM-derived DTM and the GNSS-RTK observations. Frequencies are absolute counts [n] and zero dissimilarity is denoted by the dashed line.

Table 8.4. DTM vertical spot height accuracy assessment.

	AOI					
Parameter	**1**	**2**	**3**	**4**	**5**	**6**
n	83	78	78	79	83	87
Mean Absolute Error [m]	0.048	0.084	-0.042	-0.016	-0.011	-0.077
Standard deviation [m]	0.016	0.015	0.015	0.011	0.014	0.031
Standard error [m]	0.002	0.002	0.002	0.001	0.002	0.003
Maximum error [m]	0.080	0.107	-0.007	0.008	0.018	-0.004
Minimum error [m]	-0.027	0.030	-0.095	-0.040	-0.058	-0.149

8.5.3. Canopy Height Models

The bare-vegetated height threshold of 0.015 m is an order of magnitude smaller than the 0.15 m threshold use for analysing similar point clouds derived from ground-based LiDAR systems (Li et al., 2015), and is thus significantly more sensitive to low stature, short sward vegetation. Modelled canopy heights were consistent with knowledge of the vegetation structure obtained from both site visits and photointerpretation of the ultra-fine spatial resolution orthomosaics. Figure 8-16 depicts the grass-dominated ecosystem at AOI-1, and the CHM illustrates spatial variation in modelled grass heights that is not apparent in the orthomosaic image. Figure 8-17 depicts correct identification of bare ground in a darkly shadowed area next to a creosotebush shrub at AOI-3, demonstrating that the SfM-derived CHM is insensitive to variations in illumination. Full-page illustrations of all (i) orthophoto, (ii) DSM, (iii) DTM, (iv) CHM, and (v) Classified surface cover for all seven AOIs are included in Appendix 3.

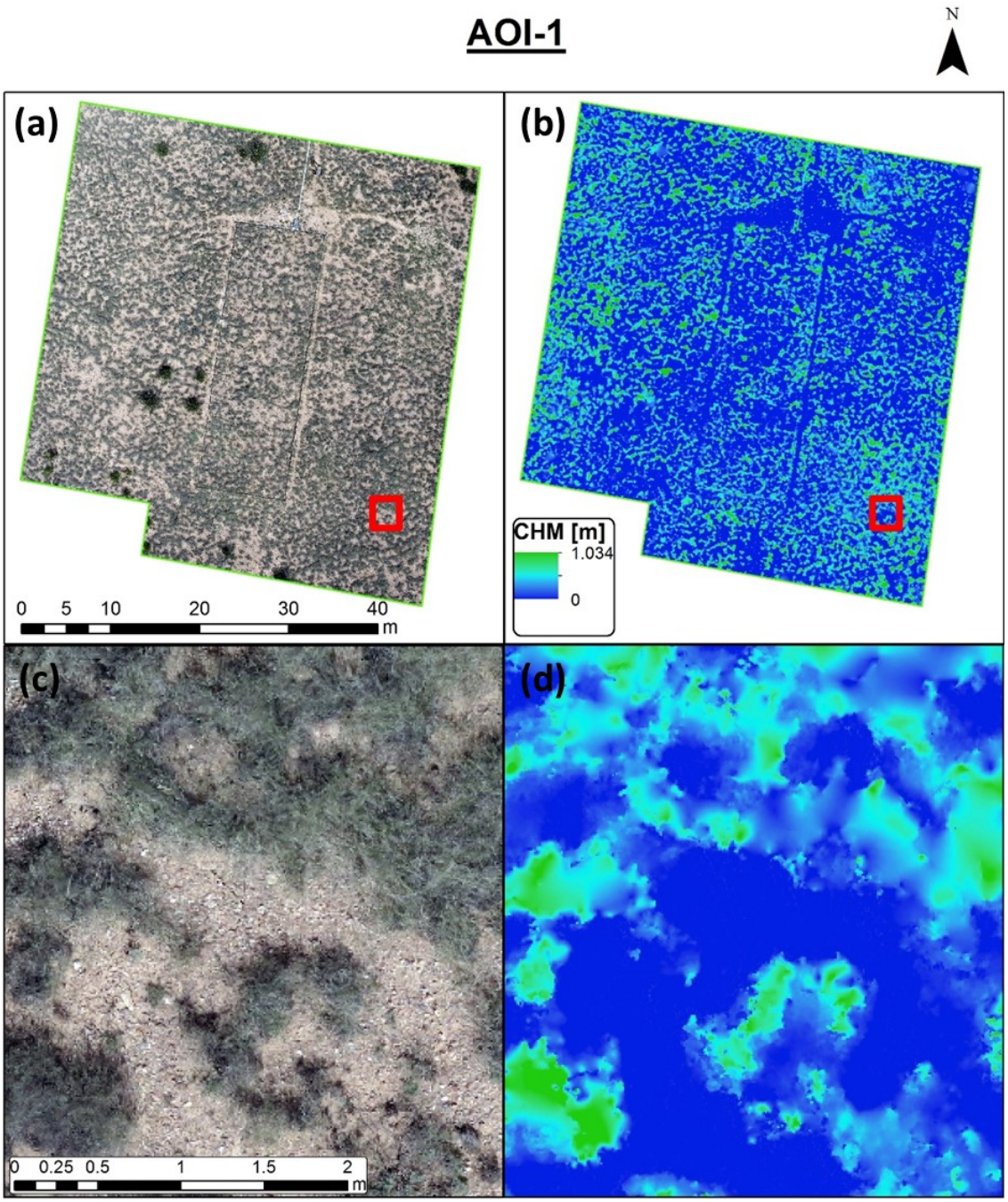

Figure 8-16. AOI-1: orthomosaic (a) and canopy height model (CHM) (b), (c) and (d) are close-ups of (a) and (b), respectively, as indicated by the red boxes.

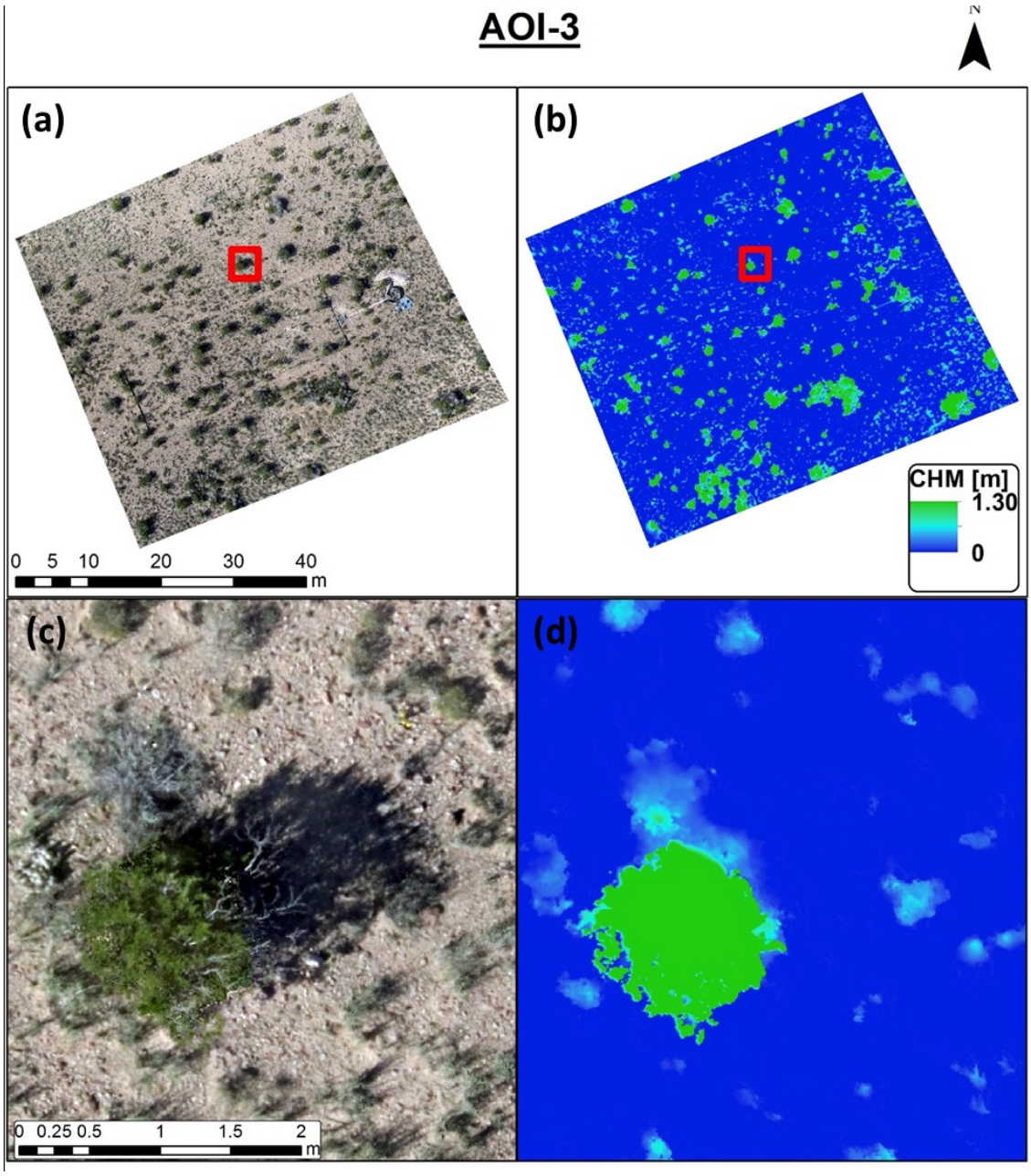

Figure 8-17. AOI-3: orthomosaic (a) and canopy height model (CHM) (b), (c) and (d) are close-ups of (a) and (b), respectively, as indicated by the red boxes.

Canopy height cumulative distribution functions are a powerful way of summarising the information content of these CHMs, and illustrate several functionally significant differences in ecosystem biophysical structure. To exemplify this, canopy height cumulative distribution functions are compared across the ecotone from grass- to shrub-dominated vegetation communities, AOI-1 to AOI-4 (Figure 8-18). AOIs 1 to 4 each comprise of between 19-20 × 10^6 one cm^2 domains. Because each AOI included at least a few individual creosote shrubs, maximum canopy heights were 1.03 m, 1.38 m, 1.30 m and 1.36 m for AOI-1, AOI-2, AOI-3 and AOI-4, respectively. The median canopy height of vegetated cells increased from 0.06 m, through 0.07 m, 0.09 m to 0.11 m, for AOI-1 - 4, respectively.

These graphical summaries demonstrate that the CHMs all had modal values of zero, indicating bare ground. Across the grass-shrub transition, the proportion of bare surface cover increased from 52% (grass-dominated site) to 89% (shrub-dominated site). Across the grass-shrub ecotone, there was an increase in the gradient of the canopy height cumulative distribution functions, indicating decreasing prevalence of low-height vegetation. Across the grass-shrub ecotone there was a substantial increase in the proportion of bare domains, as indicated by canopy heights <0.015 m. Another attribute demonstrated by the height cumulative distribution functions were the differences in the change in slope across the grass-shrub ecotone. There was a natural break in the slope of the grass-dominated AOI-1 canopy height cumulative distribution function at ca. 0.2 m, indicating that in the canopy heights of vegetated domain are predominately less than 0.2 m; 99.5% of the total area of AOI-1 had a canopy height <0.2 m (Figure 8-18). The severity of this inflection becomes less pronounced across the grass-shrub ecotone. Comprising of 267 million observations, the canopy height cumulative distribution functions for AOI-7 plots between AOI-1 and AOI-4 (Figure 8-19). This is as expected from field observations of the vegetation community composition, and 70% and 99% of domains have canopy heights of <0.01 m and <0.21 m, respectively.

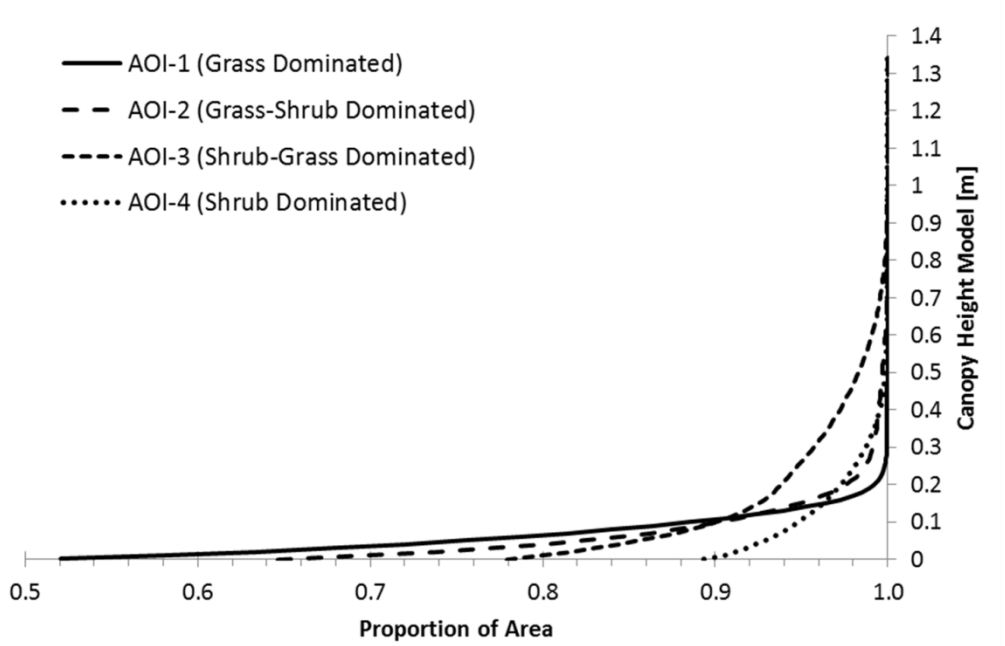

Figure 8-18. Canopy height cumulative distribution functions for AOI 1 to AOI 4, across the ecotone from grass-dominated to shrub-dominated vegetation communities.

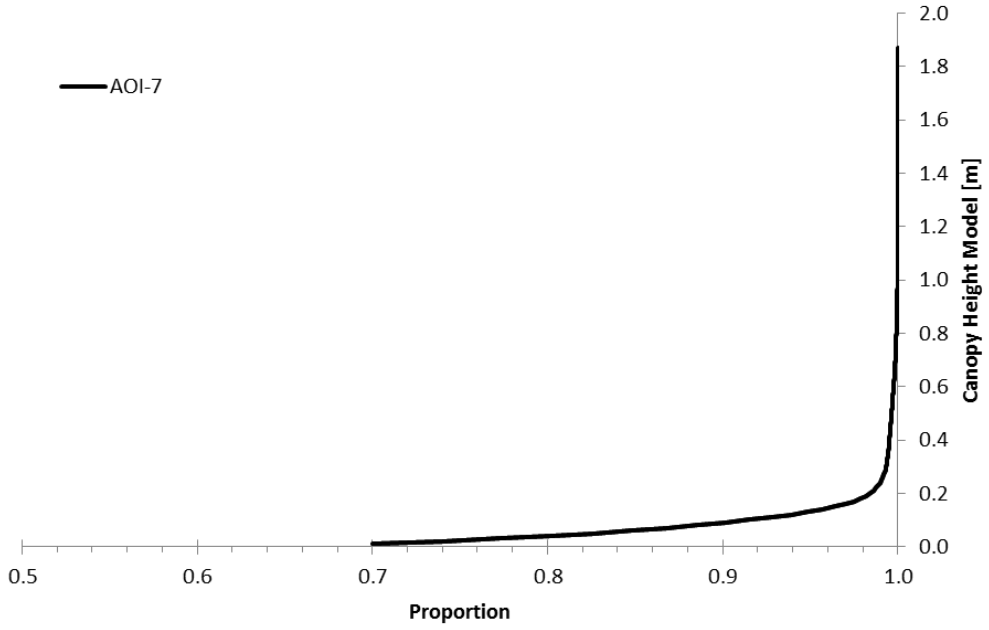

Figure 8-19. Canopy height cumulative distribution functions for AOI-7.

Table 8.5. Median modelled canopy height of vegetated domains

AOI	1	2	3	4	5	6	7
Median canopy height [m]	0.06	0.07	0.09	0.11	0.42	0.15	0.06

Structural classification of surface cover between bare and combined vegetated classes exhibited high correspondence with spatial patterns observed in all seven orthomosaics. Comparison with photointerpretation at 1000 randomly selected points across AOI-7 indicated overall accuracy >90% and kappa coefficient of 0.79 (Table 8.6). Kappa coefficients express the proportionate reduction in error generated by a classification process compared with the error of a completely random classification, and can range from -1 to + 1. The kappa value of 0.79 implies that the classification process avoided 79% of the errors that a completely random classification would generate (Cohen, 1960; Congalton, 1991), and can be considered to indicate excellent classifier performance (Landis and Koch, 1977). Errors of omission (proportion correctly classified / total identified in orthomosaic) and commission (proportion correctly classified / total allocated to class) were calculated, which indicated the most dominant classification error was vegetated domains being misclassified as bare. This was attributed to underestimation of canopy heights when vegetation was of very low density and, to a lesser extent, small area (ca. <7 cm^2).

CHM-inferred classifications of vegetation class (grass versus shrub or juniper) usually agreed with surface cover depicted in the orthomosaic images. Note that for the present study, it was not constructive to extend this accuracy assessment of surface cover classification to evaluate assignment between vegetation classes. The use of the 0.2 m threshold for differentiating between grass and shrub or juniper vegetation classes was acknowledged to be an imperfect approximation (section 8.4.5), and qualitative evaluation of digital maps (Appendix 3) highlights several areas where the classification of vegetation type performs well, and also several areas where it performs poorly. Calculation of Kappa coefficients requires a random (non-stratified) distribution of assessment points, so obtaining sufficient sampling of minority classes across all seven AOIs would require manual checking of several thousand additional points. This task would be very labour intensive and would not be valuable for the present application because sensitivity analysis indicated that, in both grass-shrub and grass-juniper vegetation systems, relative to other sources of error, total vegetation biomass and total vegetation C stock were relatively insensitive to variations in the assignment of canopy volume between vegetation classes (Figure 8-23).

Table 8.6. Error matrix evaluating surface cover classification by canopy height.

Predictions (Canopy height)	Reference Observations (Orthomosaic) Bare	Vegetated	Row Total	Commission Accuracy
Bare	**600**	64	664	90.4%
Vegetated	32	**304**	336	90.5%
Column Total	632	368	**1000**	
Omission Accuracy	94.9%	82.6%		
Overall Accuracy:	90.04%	**Kappa coefficient:**	0.79	

Bare surface cover was dominant in all seven AOIs, accounting for over half of the surface area in all five McKenzie Flats sites (AOI-1 to AOI-4, and AOI-7). There was an increase in proportion of bare cover across the ecotone from grass-dominated to shrub-dominated vegetation communities (AOI-1 to AOI-4) (Figure 8-20). To enable direct comparison with previous studies, percentage bare cover was also calculated for smaller 300 m^2 sub-AOIs at AOI-1 to AOI-6 that were consistent with earlier work by Turnbull *et al*. (2010c) (AOIs 1, 2, 3 and 4) and Puttock *et al.* (2013) (AOIs 1, 4, 5, and 6).

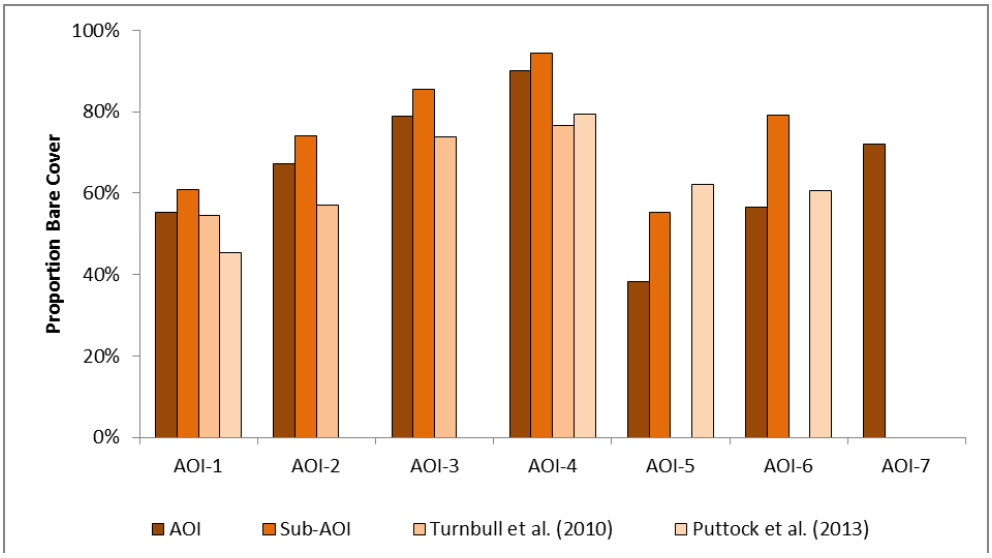

Figure 8-20. Estimated of bare cover. Structural classification (canopy height <0.015 m) of the whole AOI and (for comparison with previous studies) a 300 m^2 sub-AOI. Turnbull *et al.* (2010c) and Puttock *et al*. (2013) used manual digitisation classification of spectral images obtained in July 2006 (pre-monsoon) and August 2010 (mid-monsoon), respectively.

An example of the fine grain orthomosaics and digital maps of CHM and surface cover are shown for AOI-7 (Figure 8-21). The northern area of AOI-7 was burnt by wildfire on 4th August 2009, five years prior to the present survey (Figure 8-21a) and the persisting spatial changes in vegetation can be clearly seen.

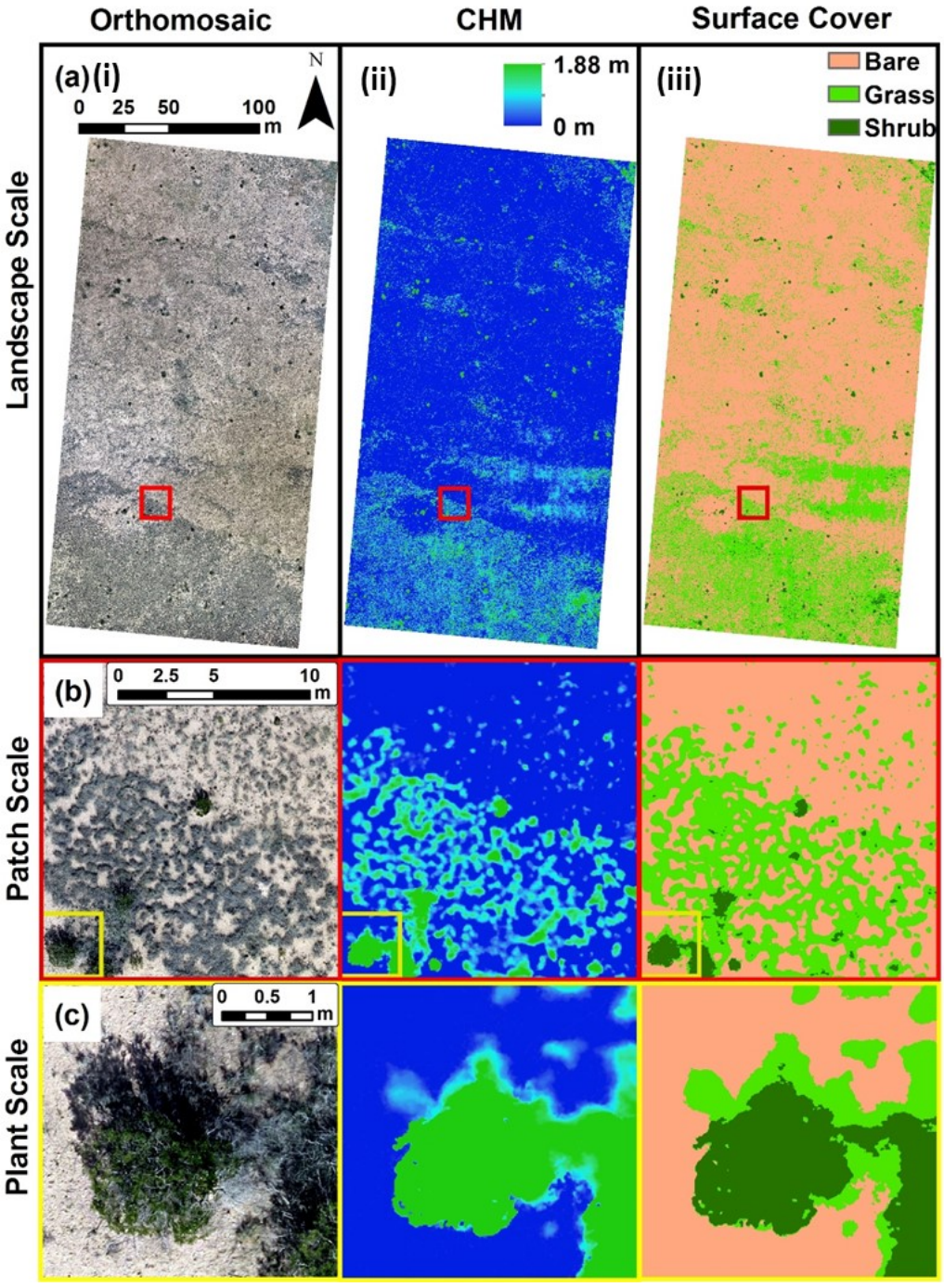

Figure 8-21. Three scales of AOI-7 are displayed: (a) landscape (~68,000 m^2), (b) patch (~250 m^2), and (c) plant (~10 m^2). The columns are (i) orthomosaic photograph, (ii) scalar CHM, and (iii) surface cover classified according to modelled canopy height. Magnification increases down through the rows, with the extent each zoom map indicated on the preceding map.

8.5.4. Plant Volume and Inferred Biomass and Carbon Stocks

Across the grass-shrub ecotone, total foliar canopy volume decreased from 0.0315 m^3 m^{-2} to 0.0148 m^3 m^{-2} from AOI-1 to AOI-4, respectively (Figure 8-24a). This decrease in total foliar canopy volume was largely controlled by a linear decline in the canopy volume associated with grass (canopy heights <0.2 m). The concomitant increase in canopy volume associated with woody vegetation (canopy heights >0.2 m) was more complex, increasing dramatically at AOI-3 before decreasing at AOI-4. Canopy volume in the juniper-dominated AOIs (5 and 6) was dominated by Juniper vegetation class (making up 96.3% and 93.1% of canopy volume, respectively), and was an order of magnitude larger than the volumes observed at the five McKenzie Flats sites (AOI-1 to AOI-4, and AOI-7).

From the available data on all three vegetation classes, there was no evidence for systematic change in either the slope of the relationship or the variance between canopy volume and biomass (Miller et al., 1981; Ansley et al., 2012). The consistency of the relationships supports the present analytical treatment, which implicitly assumes that the volume-biomass relationship is independent of volume. There is no indication of un-modelled nonlinearity (Figure 8-22) and the linear model is necessarily extrapolated beyond the range of calibration observations; such extrapolation is a common issue for allometric modelling (Chave et al., 2004; Calders et al., 2015). Future work should seek to increase the size range of destructively harvested plants, in order to better constrain the volume-AGB models (Chave et al., 2004; Ansley et al., 2012).

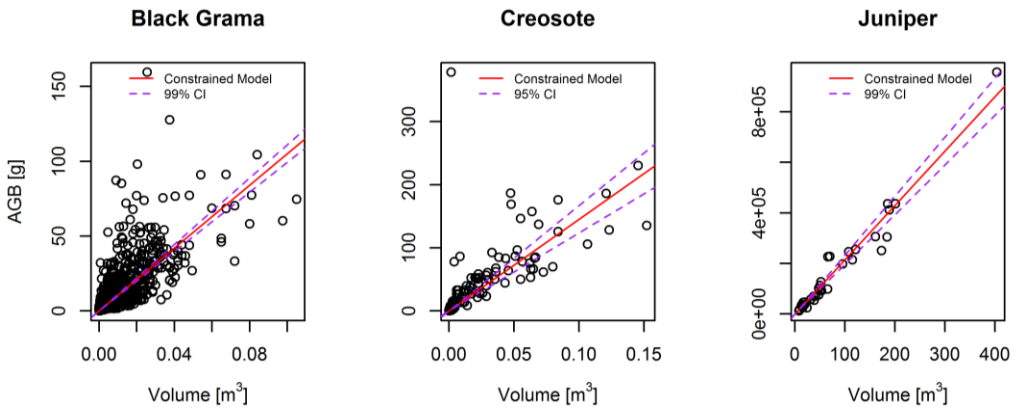

Figure 8-22. Canopy volume-aboveground biomass (AGB) relationships for grass (*B. eriopoda*), shrub (*L. tridentata*) and juniper (*J. osteosperma*), illustrating constrained regression models (intercept forced through the origin) and 99% confidence intervals (CI).

Table 8.7. Linear regression models obtained from canopy volume versus AGB.

Vegetation Class (*Species*)	*n*	AGB Range [g]	Intercept	Slope	SE	r^2	*P*
Grass	1383	1-160	2.092	979.099	21.87	0.592	$<1e^{-10}$
(*B. eriopoda*)			0	1053	19.60	0.676	$<1e^{-10}$
Shrub	228	1-380	6.825	1346.952	79.27	0.559	$<1e^{-10}$
(*L. tridentata*)			0	1453	72.13	0.640	$<1e^{-10}$
Juniper[1]	33	12,000-	-10002.823	2210.071	87.21	0.954	$<1e^{-10}$
(*J. osteosperma*)		956,000	0	2149.248	61.51	0.954	$<1e^{-10}$

Where SE is the standard error of the regression slope, representing the average distance observed points fall from the linear model in units of the response variable (AGB). [1] Note that the relationship for juniper was modified as explained in the text, to reconcile with the relationship reported in Ansley *et al.* (2012).

Although biomass density did vary between the three vegetation classes, with Juniper (2.25 kg m^3) greater than Creosotebush (1.45 kg m^3) greater than Grass (1.05 kg m^3), trends in AGB across the AOIs reflect those observed in canopy volume. Estimated AGB was 17.7 g m^2, 28.4 g m^2, 31.5 g m^2, 33.4 g m^2, 45.7 g m^2, 731.0 g m^2, and 1337.4 g m^2, for AOI-4, AOI-7, AOI-2, AOI-1, AOI-3, AOI-6 and AOI-5, respectively. Total biomass (AGB and BGB for all vegetation classes) decreases across the grass-shrub ecotone (AOI-1 to AOI-4). Across AOI-7, grass vegetation (canopy height <0.2 m) accounts for 78.0% of the total

canopy volume, 84.2% of the total biomass and 83.3% of the total biomass C stock.

BGB was dominated by the grass vegetation in the Mackenzie Flats (AOIs-1 to 4 and 7) and Juniper vegetation at the Los Piños Mountains (AOIs 5 and 6), and is subject to higher levels of relative uncertainty due to uncertainty in root : shoot ratios. Similar biomass-carbon coefficients between vegetation classes mean that the relative C stocks associated with AGB and the total biomass paralleled AGB and total biomass, respectively (Figure 8-24d and Figure 8-24c).

Table 8.8. Coefficients used to predict AGB, BGB and C stocks for each vegetation class.

Grass	$AGB_{Grass} = V_{Grass} \times 1053 \pm 58.80$
	$BGB_{Grass} = AGB_{Grass} \times 2 \pm 0.6$
	$C_{Grass} = (AGB_{Grass} + BGB_{Grass}) \times 0.45 \pm 0.03$
Creosote	$AGB_{Shrub} = V_{Shrub} \times 1453 \pm 216.39$
	$BGB_{Shrub} = AGB_{Shrub} \times 0.45 \pm 0.2$
	$C_{Creosote} = (AGB_{Shrub} + BGB_{Shrub}) \times 0.48 \pm 0.03$
Juniper	$AGB_{Juniper} = V_{Juniper} \times 2250 \pm 184.53$
	$BGB_{Juniper} = AGB_{Juniper} \times 1 \pm 0.5$
	$C_{Juniper} = (AGB_{Juniper} + BGB_{Juniper}) \times 0.50 \pm 0.03$

Where subscript denotes vegetation class, V is plant volume [m^3], AGB is aboveground biomass [dry weight, g], BGB is belowground biomass [dry weight, g] and C is carbon stock [g].

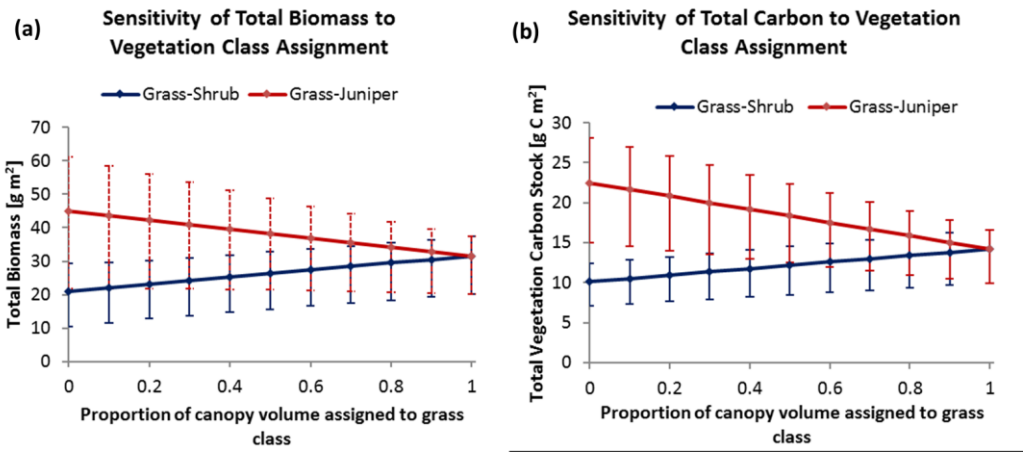

Figure 8-23. Sensitivity analysis for total vegetation biomass (a) and total vegetation carbon stock (b) to allocation of canopy volume (0.01 m^3) between vegetation classes.

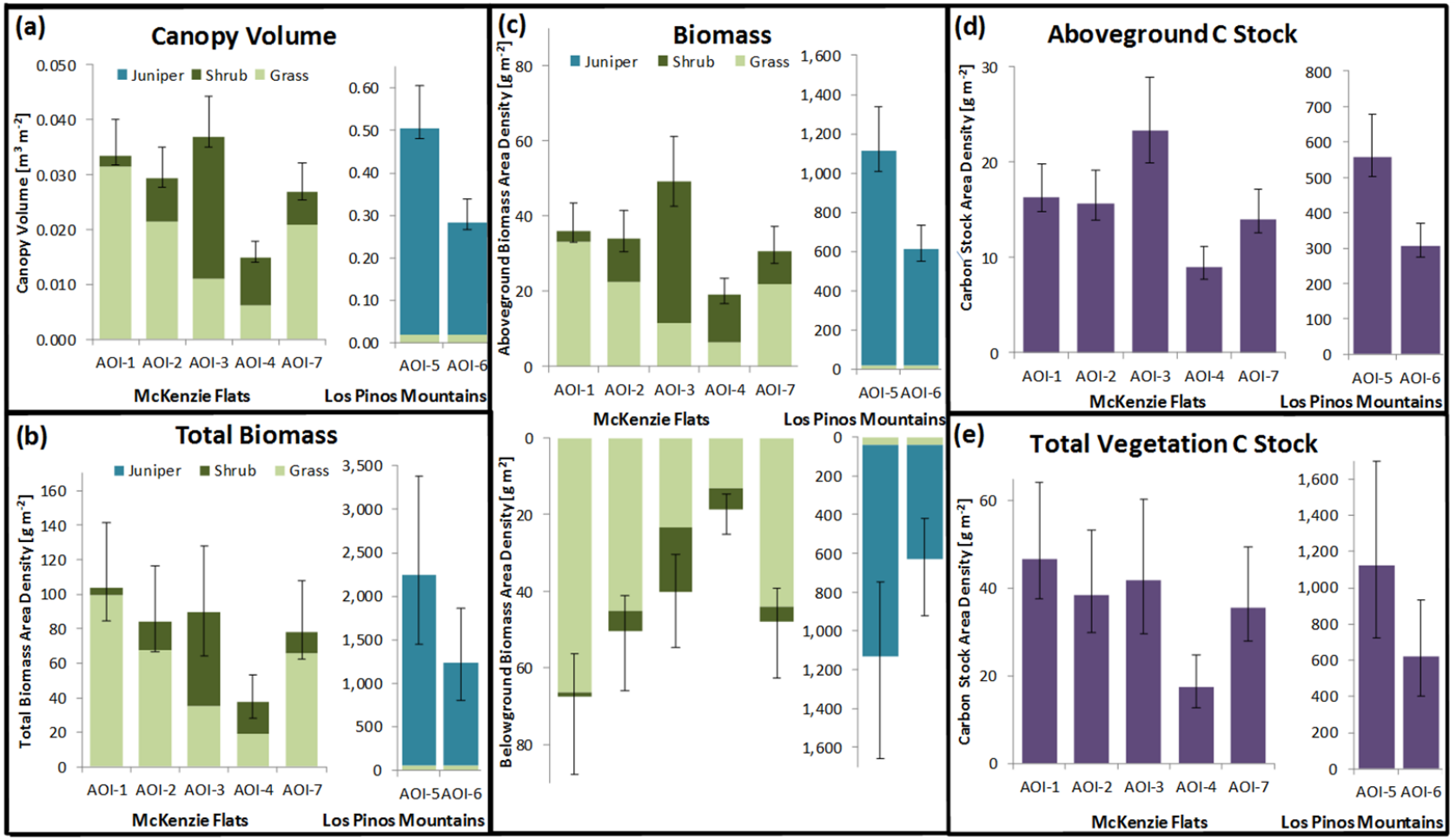

Figure 8-24. (a) Measured canopy volumes, (b) total biomass, (c) inferred aboveground biomass (AGB) and belowground biomass (BGB) for each vegetation class, and estimated (d) aboveground and (e) total vegetation carbon stocks.

Table 8.9. Propagated relative errors depicted in Figure 8-24.

AOI	Canopy Volume [%]	AGB [%]	BGB [%]	Total Biomass [%]	Aboveground C stock [%]	Belowground C stock [%]	Total Biomass C stock [%]
AOI-1	-0.5 to +20.0	-8.1 to +21.1	-16.8 to +30.0	-18.7 to +36.7	-8.6 to +21.5	-17.3 to +30.5	-19.3 to +37.3
AOI-2	-0.5 to +20.0	-10.2 to + 22.2	-18.4 to +31.3	-21.1 to +38.3	-10.8 to +22.6	-19.0 to +31.8	-21.8 to +39.0
AOI-3	-0.5 to +20.0	-13.8 to +24.0	-24.5 to +36.1	-28.1 to +43.3	-14.3 to +24.4	-25.2 to +36.7	-29.0 to +44.1
AOI-4	-0.5 to +20.0	-12.9 to +23.5	-22.3 to +34.3	-25.7 to +41.6	-13.4 to +24.0	-22.9 to +34.9	-26.6 to +42.4
AOI-5	-0.5 to +20.0	-9.6 to +21.6	-33.0 to +46.0	-35.3 to +50.2	-9.9 to +22.0	-34.4 to +46.5	-35.8 to +51.4
AOI-6	-0.5 to +20.0	-9.5 to +21.6	-33.4 to +45.5	-34.8 to +49.7	-9.9 to +22.0	-33.9 to +46.0	-35.3 to +51.0
AOI-7	-0.5 to +20.0	-9.8 to +21.9	-18.0 to 31.0	-20.5 to +37.9	-10.3 to +22.4	-18.6 to +31.5	-21.2 to +38.6

8.6. Discussion

8.6.1. Advances in RPAS SfM Quantification of Ecosystem Structure

This study is the first to demonstrate how SfM photogrammetry to process aerial photographs acquired using a lightweight RPAS to efficiently quantify ecosystem biotic structure at cm grain over landscape extents. Individual plants just a few cm^3 in volume were resolved over areas of ca. 10 ha, which is a level of detail hitherto unobtainable with previous implementations of the RPAS-acquired SfM approach.

Dandois *et al.* were the first to demonstrate the capacity of RPAS-acquired SfM to characterise vegetation structure at low cost (Dandois and Ellis, 2010, 2013). Work to date has focused on application in forest ecosystems (Dandois and Ellis, 2010, 2013; Lisein et al., 2013; Dandois et al., 2015; Zahawi et al., 2015; Puliti et al., 2015), and had indicated that SfM modelling of aerial image data was not yet able to resolve smaller vegetation, such as grasses, due to limitations in the precision of SfM modelling approaches as previously implemented (Zahawi et al., 2015). The present study demonstrates that, with appropriate source data to constrain the SfM reconstructions, it is possible to overcome this scale limitation. The SfM reconstructions presented herein resolve biotic structure with a fidelity nearly two orders of magnitude finer than previous implementations of this approach (Dandois and Ellis, 2013; Dandois et al., 2015; Zahawi et al., 2015).

Canopy volumes derived from the CHMs can be used to infer aboveground biomass (AGB), and subsequently belowground biomass and associated C stocks. The measurements are sensitive to subtle spatio-temporal changes in biophysical structure and could be acquired at daily timesteps over extents of ~1-5 ha. Using this RPAS-acquired SfM approach, ultra-fine grain CHMs can be obtained at much lower cost than comparable, on-the-ground LiDAR datasets. Compared to on-the-ground surveys, this coverage yields more spatially-representative assessments of ecosystem state at landscape-scales, facilitating the extraction of subtle signals that elucidate mechanistic controls on biophysical and ecohydrological processes.

The technique will revolutionise monitoring of biophysical structure over landscape-levels (*sensu* Anderson and Gaston, 2013). Such data would reduce uncertainty in biomass inventories, and allow previously unfeasible experiments on process interactions in a range of environmental contexts. For example, the capacity to survey areas diametrically equivalent to coarse-grain information products such as

Moderate Resolution Imaging Spectroradiometer (MODIS) at spatial resolutions comparable to on-the-ground monitoring will facilitate upscaling studies, vegetation responses to precipitation inputs in water-limited ecosystems could be characterised at landscape-levels on very short timesteps and the impact of different intensities of herbivory on AGB under various environmental conditions could be quantified. The inexpensive approach presented herein is highly complementary to existing approaches for monitoring biophysical structure, and represents an appreciable advance in the tools available to geoscientists.

8.6.2. Constraining SfM Modelling

Reducing the error in SfM-derived reconstructions to produce accurate and precise information products requires SfM models are appropriately constrained by high quality image and GCP data (James and Robson, 2014; Smith and Vericat, 2015; Shahbazi et al., 2015). To achieve this requirement, this this study systematically acquired convergent (non-nadir) image data, in addition to parallel (nadir) image data and high-precision GCPs. This approach yielded high-precision models, but necessitated multiple overflights of the study areas, doubling field survey effort and also increasing the subsequent computational effort. While the inexpensive sensors employed herein produced reconstructions of sufficient quality to be ecologically informative, greater coverage efficiency and reconstruction accuracy could be supported through the use of higher spatial resolution sensors employing static (‘prime’) lenses, although such equipment is more expensive.

It is hypothesized that there may be an optimum acquisition angle which provides sufficiently convergent image data to adequately constrain SfM modelling, while being sufficiently close to nadir to alleviate the need for additional acquisition of nadir images to ensure sufficient similarity between adjacent images for successful matching. Optimal image acquisition angles will be influenced by the nature of the canopy structure; i.e., the perspective required to obtain multiple images of the ground surface through small gaps in high canopies will require near-nadir view angles and high levels of overlap. Furthermore, there are some suggestions that both feature matching and multi-view stereopsis is hindered if view angles exceed 20° (Lowe, 2004; Dandois et al., 2015), although again such a limitation is likely to be sensitive to scene structure and complexity. I speculate that an optimum

acquisition angle for the biotic structures observed in the rangeland ecosystems studied herein may be around 15-25°; although, robustly testing this hypothesis will require a large, multifactorial experiment (e.g. Dandois et al., 2015).

8.6.3. Quantification of Topography

There was very good agreement between the spot heights of 488 DGPS observations and the SfM-derived DTMs (described in section 8.5.2, Figure 8-15), indicating good relative accuracy and no evidence for significant error in absolute position. This level of agreement is nearly an order of magnitude better than the correspondence between LiDAR and SfM-derived DTMs reported by Dandois and Ellis (2013). This improvement is predominately due to improvements in the constraint of SfM reconstructions and is expected to continue with ongoing refinements to SfM approaches (e.g. direct georeferencing incorporating information on camera attitude) which will see continuing improvements to the quality of SfM-derived data products (Turner et al., 2016).

The DTMs produced from the RPAS-SfM survey were used to parameterise the deterministic modelling exercise undertaken in Chapter 9. In this application, these fine-grain products were degraded to a spatial resolution of 0.5 m, but the fine-grain DTMs will be valuable for supporting planned future investigations into model sensitivity to parameter scale (described further in section 9.10).

8.6.4. Quantification of Canopy Heights

The CHM obtained are physically meaningful and straightforward to interpret, in contrast to some more complex descriptions of canopy structure derived from information obtained by space-borne sensors (e.g. Chopping et al., 2003, 2006). This is because CHMs represent a direct measurement of vegetation structure, which is a critical parameter in defining vegetation function, rather than optical space-borne measurements which are indirect and thus require a greater degree of modelling to relate measured attributes to the process of interest.

Foliar canopy approaches to estimating canopy volume are sensitive to subtle differences in plant biophysical structure which do not influence overall plant dimensions (such as maximum height or canopy area). Consequently, foliar volume

is frequently a more accurate predictor of AGB than maximum plant height (Neufeld et al., 1988; De Soyza et al., 1997; Huenneke et al., 2001; Rango et al., 2006, 2009; Allen et al., 2008; Muldavin et al., 2008; Ladwig et al., 2012), particularly in semi-arid rangeland community assemblages (Neufeld et al., 1988; De Soyza et al., 1997; Rango et al., 2006, 2009).

It is constructive to reflect on the use of maximum point elevations within each *x*,*y* cell when interpolating surfaces, as the approach used herein diverges somewhat from the approaches adopted in similar studies of vegetation structure using RPAS-SfM products. It has often been advocated to use the elevation of a particular percentile within a cell to obtain more representative measurements of canopy height which are less sensitive to possible high outlier points (colloquially described as 'flyers') (e.g. Jung et al., 2012; Dandois and Ellis, 2013; Zahawi et al., 2015). These percentile approaches are sensible when characterising large plants at spatial resolutions of >1 m^2, when many points exist within a cell (Dandois and Ellis, 2013; Zahawi et al., 2015). My use of ultra-fine, cm^2 x,y spatial resolution offers an alternative approach to averaging canopy heights across an AOI, as this similarly restricts the influence of possible outlier points on estimates of overall canopy volume. Using an ultra-fine spatial resolution better utilizes the information content in the millions of point observations comprising each point cloud, while affording greater sensitivity to fine-scale spatio-temporal differences in vegetation biophysical structure which are critically important in grass-shrub ecosystems where plants are low and have a small footprint. Furthermore, the maxima height approach employed herein is also consistent with the approaches developed for on-the-ground monitoring of canopy volumes and inferred aboveground biomass and associated C stocks in these ecosystems (e.g. Huenneke et al., 2001; Yao et al., 2006; Allen et al., 2008; Muldavin et al., 2008; Ladwig et al., 2012).

There was good agreement between modelled canopy heights versus knowledge of the vegetation structure derived from many site visits and subsequent photointerpretation of the ultra-fine spatial resolution orthomosaics. The absence of highly implausible CHM values indicates the efficacy of the workflow for avoiding outlier points ('flyers' and 'sinkers') in the final point clouds; maximum canopy heights were 1.88 m and 6.89 m in the Grass/Shrub-dominated sites (AOIs 1-4 and 7), and Juniper-dominated sites (AOIs 5 and 6), respectively. The reconstructions supported a threshold height value of 0.015 m to differentiate vegetated from bare

cells, which was two orders of magnitude lower than the equivalent value of 2 m employed for this parameter by Dandois and Ellis (2013). The lower value supported by the SfM reconstructions presented herein illustrates the benefit of highly constrained SfM reconstructions for precise and sensitive quantification of vegetation structure in short sward systems.

Collecting *appropriate* reference data with which to evaluate RPAS SfM-derived CHMs is extremely challenging (Lisein et al., 2013; Dandois et al., 2015; Puliti et al., 2015), a problem compounded by difficulties obtaining spatially referenced canopy height observations commensurate with very fine grain CHMs. Previous applications of RPAS SfM-derived CHMs have concentrated on silviculture and have typically considered dominant canopy heights for CHM evaluation, using field observations of the average *maximum* height of dominant plants within plots (Dandois and Ellis, 2010, 2013; Lisein et al., 2013; Zahawi et al., 2015; Puliti et al., 2015; Dandois et al., 2015). Metrics of dominant canopy height are however less appropriate in the rangeland ecosystems studied herein, due to the important contribution of low stature plants to overall ecosystem AGB and the complexity of the shrub canopy architecture (Lisein et al., 2013).

Field measurements of grass sward height are multifarious (’t Mannetje, 2000), but what is measured poorly represents what SfM captures. For example, the highest extremities of grass plants are generally too small and mobile to be represented in RPAS SfM-derived canopy height models, while drop-disk approaches alter sward height through compression as well as covering a much larger extent than the centimetre grain size of the CHMs employed herein (Friedel et al., 2000; ’t Mannetje, 2000). Field measurement of shrub canopies is no less problematic, as shrubs such as creosotebush are characterised by complex canopy architecture (Wardley et al., 1987; Neufeld et al., 1988; Wilson, 1995; De Soyza et al., 1997) (Figure 8-5, Figure 8-12), and therefore using a single, maximum height as validation will rarely provide good correspondence.

Plant extremities are often underrepresented in photogrammetric reconstructions (Dandois and Ellis, 2010, 2013; Lisein et al., 2013; Gillan et al., 2014; Zahawi et al., 2015; Dandois et al., 2015), as well as LiDAR surveys (Lefsky et al., 2002; Glenn et al., 2011; Mitchell et al., 2011; Sankey et al., 2013; Li et al., 2015). Even when the

average height is well represented SfM-derived CHMs will often underestimate *maximum* canopy height of individual plants (Dandois et al., 2015).

Therefore, the *maximum* height of individual plants is suggested not to be the best metric for evaluating CHM quality, particularly in rangeland ecosystems. To address these important considerations, this study used spatially distributed canopy heights to characterise ecosystem structure, with a conservatively estimated asymmetric error term of -5%+20% for the modelled canopy heights. Critically, these uncertainties do not mask the main vegetation patterns, and they do not prohibit meaningful estimates of biomass in these ecosystems (as discussed in section 8.6.6).

Compared to spectral reflectance, CHMs (and the derived surface cover maps discussed in section 8.6.5 and Figure 8-21a) can be more informative with regards to biologically important differences in ecosystem structure. While the enduring effect of historic fire can be faintly observed in the orthomosaic through reduced vegetation cover, delineation of the burn extent is much more apparent in the CHM and derived surface cover maps (Figure 8-21a). Spatial differences in vegetation structure across the burn boundary differ between the orthomosaic and the CHM-derivatives due to the similarity of spectral (RGB) reflectance between mature and immature vegetation regrowth, in contrast to dissimilarities in biophysical structure (Huang et al., 2007). The spatial differences in vegetation structure are functionally significant, for example in terms of C storage and biomass available for herbivory by livestock, and exemplify one limitation using 2D image data to monitor biotic structure (Huang et al., 2007).

The patch scale (Figure 8-21b) depicts this ecological frontier between unburnt and burnt areas, and the spatial patterns of surface cover portrayed at these patch scales are major controls on the distribution and erosion-induced redistribution of ecosystem resources in semi-arid landscapes, including water, soil and associated chemicals which influence the provision of ecosystem services (Müller, 2004; Müller et al., 2007b, 2007a; Turnbull et al., 2010a; Stewart et al., 2014; Cunliffe et al., 2016d). The plant-scale panels depict a *L. tridentata* individual, illustrating the correspondence between the orthomosaic and surface cover classification (Figure 8-21c). Figure 8-21c exemplifies how CHM-derived classifications are robust against variable illumination (e.g. deep shadowing) which can be problematic for

spectral classification approaches, particularly in fine resolution image data (Popescu et al., 2003; Adeline et al., 2013; Gini et al., 2013; Puttock, 2013). The 'patchy' shrub canopy shows detail resolved by the ultra-fine spatial resolution which is not resolved in coarser-scale surveys, for example in larger ca. 30 cm footprint airborne LiDAR products.

The canopy height distribution functions presented in Figure 8-18 and Figure 8-19 are more informative than simpler summary metrics such as average canopy height, elucidating functionally-significant differences in community-level ecosystem structure across the ecotone from grass- to shrub-dominated ecosystems. The spatial patterns observed in canopy height distributions across this grass-shrub are consistent with existing understanding of changes in biophysical structure across this ecotone derived from 2D remote sensing (Turnbull et al., 2010c; Puttock et al., 2013). Critically, because of the spatially contiguous nature of this surveying technique, these cumulative distribution functions summarise upwards of 42 million cells over spatial extents of >4000 m^2 (though these extents could easily be increased). Such averaging of large numbers of remotely sensed observations is believed to improve accuracy and sensitivity when measuring community-level traits over large extents (Gobakken and Næsset, 2004; Huang et al., 2009; Puliti et al., 2015; Greaves et al., 2015).

This quantitative approach is sensitive to subtle spatial or temporal differences in biotic structure, yet can rapidly survey relatively large (several ha) spatial extents (Anderson and Gaston, 2013). It can therefore be used to quantify comparatively subtle changes in vegetation structure with small effect sizes, for example in response to herbivory, fire or rainfall. Such information can support experiments to advance mechanistic understanding of vegetation dynamics at landscape-levels (e.g. Brisson and Reynolds, 1994; Friedel et al., 2000; L. Wang et al., 2015). For example, it could be used to investigate the precipitation thresholds required to elicit vegetation response, including differences between different plant functional types (PFTs) (Huxman et al., 2004; Thomey et al., 2014). Better knowledge of how different PFTs respond to different amounts of precipitation will inform understanding of competitive advantages between different plants, and thus support more accurate predictions of how plant communities may respond to changing precipitation regimes. Alternatively, spatially distributed information on AGB dynamics could be used to better understand the impact of herbivory on grass

biomass. *B. eriopoda* (black grama) communities are readily damaged by overgrazing, particularly during the summer growing season (Canfield, 1939; Nelson, 1934; Paulsen and Ares, 1962). Better knowledge of grazing patterns could be used to optimise the utilisation of grama-dominated grasslands by livestock, potentially simultaneously improving both the profitability and sustainability of cattle ranging activities.

8.6.5. Classification of Surface Cover

Classification of surface cover between bare and combined vegetated classes on the basis of modelled canopy height exhibited excellent discriminatory accuracy (overall accuracy = 90%, Kappa coefficient = 0.79) (after Landis and Koch, 1977), indicating that the extent of vegetated cells was well characterised on the basis of modelled canopy heights. This demonstrated that modelled canopy heights were accurate, at least around the height threshold used to differentiate bare ground from vegetated cells. The <10% errors in the bare versus vegetated classification were predominantly due to incorrect assignment of sparsely vegetated domains to the bare class, overestimating bare cover; this error had little impact on the utility of the bare/vegetated surface cover digital maps, as sparsely vegetated cells are relatively insignificant in terms of several key ecosystem functions, such as their contribution to AGB and grazing potential, modification of raindrop kinetic energy and subsequent particle detachment, or impedance of overland flow (Parsons et al., 1990; Abrahams et al., 1994; Wainwright et al., 1999a, 2000; Michaelides et al., 2009).

The CHMs represent foliar cover, which is strongly interconnected with the interception of rainfall and resultant dissipation of raindrop kinetic energy. Raindrop kinetic energy is a significant control on the detachment of soil particles and the subsequent erosion of soil and associated chemicals including particulate organic and inorganic C, as described in chapters 6 and 7, respectively (Abrahams et al., 1995; Parsons et al., 1996; Wainwright et al., 1999a, 2000, 2008a; Bochet et al., 2006; Baird, 2013). The canopy height cumulative distribution functions illustrate an increase in bare surface cover from ca. 50% to ca. 90% (Figure 8-20), which concurs with the relative spatial tends across this grass-shrub ecotone reported previously

following manual digitisation of three band (RGB) optical aerial image data (Turnbull et al., 2010c; Puttock et al., 2013).

Compared to the previously reported values, bare ground measured using the structural approach presented herein is ca. 5-20% greater for 5 of the 6 same sub-AOIs. Some of this increase may arise from the underrepresentation of vegetation canopy in the SfM-derived CHM; however, the differences cannot be conclusively attributed to the survey and classification approach as vegetation is highly variable through time (Figure 3-1) and the surveys were conducted up to eight years apart. Furthermore, part of this difference likely arises from the mismatch of scales when describing the very patchy surface cover between the current classification of domains at 1 cm^2 scale and the previous manual digitisation at scales of ~5 cm^2. Given these unknown potential differences, further temporal comparisons between the classification maps produced by the different survey approaches would not be appropriate.

Increased bare cover is associated with decreased infiltration and increased runoff generation during infrequent but intense rainfall events (Scoging et al., 1992; Müller et al., 2007b; Turnbull et al., 2010a; Puttock et al., 2013, 2014). The mediation of runoff and redistribution of soil resource by vegetation can give rise to powerful ecogeomorphic feedbacks, which govern the overall ecosystem state (Wainwright et al., 2000, 2001; Müller et al., 2007a; Turnbull et al., 2008b). Consequently, digital maps of fine-scale spatially distributed information characterising vegetation cover can be used to parameterise and evaluate process-based numerical models. Such numerical models are vital tools for advancing multi-scale understanding of multiple interacting ecological and geomorphic processes (e.g. Müller et al., 2007a, 2007b, 2009, 2013; Michaelides et al., 2009; Wainwright et al., 2008c, 2008a, 2008b, Turnbull et al., 2010b, 2014b; Stewart et al., 2014; Moreno de las Heras et al., 2015).

Qualitative evaluation indicated that assignment of vegetated domains between grass and woody (creosotebush or juniper) vegetation classes was slightly less accurate, compared to the structural classification of cells as vegetated or bare. Maps of the surface cover classifications, and concomitant orthomosaic photos, are included in Appendix 3. Errors in discriminating between plant functional types (PFTs) included the occasional mis-assignment of grass vegetation to woody plant classes (see, for example, AOI-1 and AOI-5) and underestimation of shrub extents

(see, for example, AOI-1 and AOI-4). The former error is considered indicative of overly low threshold canopy height, as grass heights was occasionally observed in the field to exceed 0.2 m, while the latter is considered to result from underrepresentation of patchy, shrub extremities in the SfM-derived point clouds.

Assignment of vegetated domains between grass and woody classes was more variable in the juniper-dominated sites, compared to the grass- and creosote-dominated sites. AOI-5 was subject to more noticeable errors in PFT assignment, particularly in the northern corner of the AOI where a few large patches of grass had modelled canopy heights of ca. 0.3 m and so were assigned to the juniper vegetation class. Grass vegetation in this area was particularly dense and high, so the modelled canopy heights in excess of 0.2 m may reflect the true vegetation heights, although the DTM at the juniper-dominated sites was also probably less accurate due to less-frequent true ground returns in the point clouds characterising these sites. PFT discrimination was good in AOI-6, with spatial variations in grass cover density also well characterised and all nine mature juniper trees correctly identified with several juvenile juniper trees and other plants (notably large cacti) also assigned to the juniper class.

Over largest spatial extent (AOI-7), PFT assignment between grass and shrub appears very good; shrubs are well characterised and spatial variations in grass cover are also well reflected. These errors in discrimination between PFT mainly reflect the limitations of using a simple height threshold as the sole discriminator. Importantly, as explained above, errors in discriminating between PFTs do not meaningfully alter estimates of overall biomass or overall C content in these ecosystems.

8.6.6. Quantification of Aboveground Biomass

Critically for biomass estimation, foliar volume is linearly related to AGB and, for all three plant functional types considered in the present study, has an intercept of zero. Consequently, it was not necessary to isolate individual plants using object-based classification approaches, in contrast to when measured plant attributes are non-linearly related to AGB (e.g. Ludwig et al., 1975; Gholz, 1980; Smith and Brand, 1983; Northup et al., 2005; Cleary et al., 2008; Lufafa et al., 2009; Ansley et al., 2012; Mirik et al., 2013a; Sankey et al., 2013). Avoiding the requirement of identifying individual plants is valuable in structurally complex natural ecosystems,

where the canopies of neighbouring plants commonly coalesce confounding distinction between individuals (Ffolliott and Gottfried, 2002; Strand et al., 2008; Starks et al., 2011; Ansley et al., 2012). Similar linear relationships between AGB and foliar volume have also recently been reported for several species of shrubs in the Arctic (Greaves et al., 2015), supporting the contention that this allometric approach is very likely to be widely applicable across environmental contexts.

Furthermore, this approach can be applied across a very wide range of plant sizes (spanning three orders of magnitude), alleviating the need to exclude biomass associated with smaller plants from C accounting (Strand et al., 2008; Asner et al., 2012; Sankey et al., 2013). Note that the biomass density may vary to some extent with phenological state (Allen et al., 2008; Huenneke et al., 2001; Muldavin et al., 2008; Yao et al., 2006); consequently, care should be taken to evaluate the temporal stability of the relationship between canopy volume and AGB if this approach is employed to characterise AGB of an ecosystem during different phenological states.

The values of AGB estimated for each AOI (presented in Figure 8-24) are all consistent with the magnitudes of AGB stocks expected for similar ecosystems (e.g. Barbour et al., 1977; Sims et al., 1978; Grier et al., 1992; Huenneke et al., 2001; Muldavin et al., 2008; Ansley et al., 2012; Sankey et al., 2013; Krofcheck et al., 2015; Moore, 2015). The shrub volume at AOI-3 is much larger in volume than shrub individuals at AOI-4 (Figure 8-18 and Figure 8-24) because the shrubs were much taller at this intermediary site; this was because other ecosystems attributes (such as slope gradient, and the spatial extent of bare, grass and shrub cover, etc.) were afforded greater precedence during initial site selection (see Turnbull, 2008; Puttock, 2013).

The Mackenzie Flats sites (AOIs-1, 2, 3, 4 and 7) can be likened with AGB estimated from on-the-ground observations of quadrats at the LTER core monitoring site (Figure 8-25 and Figure 3-1). However, while surveys were almost concurrent, they were not co-located so spatial heterogeneity in community composition means that these estimates cannot be compared like-for-like. At the more arid Jornada LTER, ca. 140 km south of the Sevilleta LTER, black grama–dominated communities typically have AGB of between 50 g m^2 to 300 g m^2 (Sims et al., 1978; Huenneke et al., 2001) and creosote-dominated communities typically have AGB <25 g m^2, but range up to 142 g m^2 (Huenneke et al., 2001). The two Juniper-dominated AOIs,

containing an estimated 1008-1338 and 554-735 g m^2 of AGB, were in extremely good agreement with the estimate of 1260 g m^2 AGB for an adjacent AOI (Krofcheck et al., 2015), and were consistent with typical AGB for these ecosystems (Grier et al., 1992).

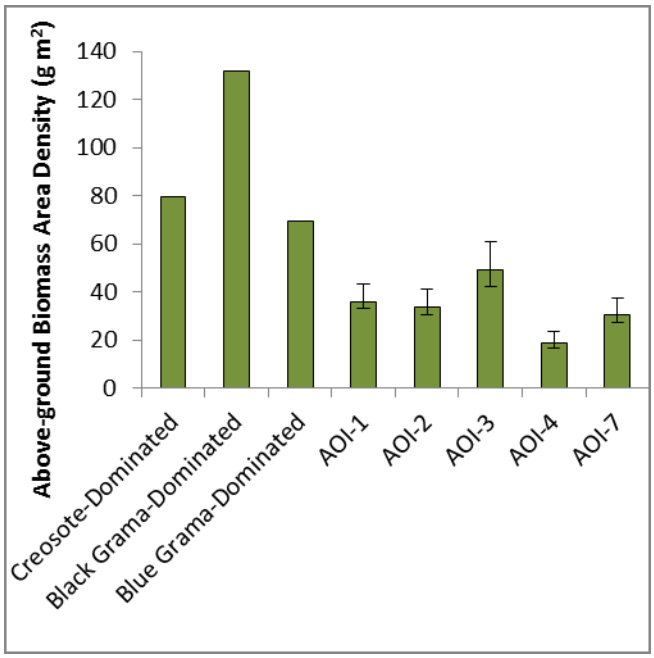

Figure 8-25. Aboveground biomass observed in the spring and autumn at three core monitoring sites (Creosotebush-, Black Grama-, and Blue Grama-dominated) across the Sevilleta LTER (Moore, 2015; Scott Collins, Pers. Comm.), and the five Mackenzie Flats sites surveyed herein.

For greater transferability to apply these methods in more complexly structured ecosystems, such as those likely to be encountered over larger spatial extents, it may be desirable to further refine the allometric approach employed herein. Foliar volume was assigned to for three specific vegetation classes on the basis of threshold canopy height, and then AGB was estimated on the basis of this foliar volume. While distinguishing vegetation classes on the basis of canopy height was broadly successful, and total biomass and total C stock are relatively insensitive to differences in assignment of canopy volume between the types of flora, because each vegetation class is associated with a different biomass density (g m^3) this treatment results in an artificially 'stepped' transition that was somewhat simplistic compared to the more gradual transition observed in nature.

Intriguingly, for the three vegetation types considered herein, biomass density (g m^3) is greater for the taller plants (Figure 8-22, Table 8.7 and Table 8.8). This suggests

that the relationship between canopy volume and AGB may be contingent on the height of the canopy and consequently that by using a non-linear equation it may be possible to develop a unified allometric model. Such a model would enable a single function to be used to estimate AGB from canopy height across a range of plant types, as demonstrated in Figure 8-26. Regrettably, development of this more sophisticated approach was not possible in the present work, due to limitations in the empirical data available to appropriately constrain such a modelling exercise. On biological grounds, it would still be appropriate to constrain the intercept to zero (Ludwig, 1977; Brisson and Reynolds, 1994; Muldavin et al., 2008; Ansley et al., 2012).

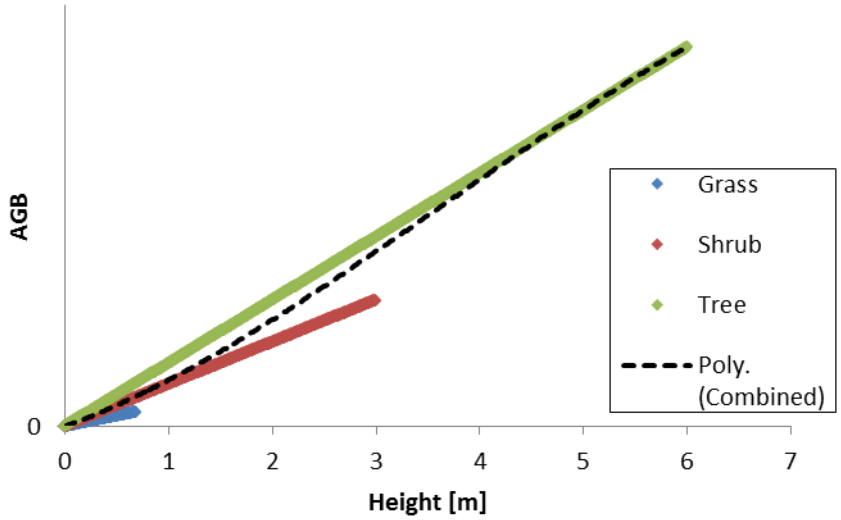

Figure 8-26. Conceptual illustration of how a non-linear function could be used to reconcile the canopy height/AGB relationships observed in the linear models derived for the three vegetation classes considered herein.

More work is needed to refine validation of this approach in short sward ecosystems, which should include more destructive sampling of individual plants whose canopy volume has first been measured using RPAS SfM under field conditions. It is also pertinent to exercise caution when evaluating estimates of AGB obtained from RPAS SfM CHMs against estimates of AGB derived from other forms of allometry (e.g., AGB estimated from breast height diameter), as both forms of allometry have uncertainties which should be explicitly considered (Puliti et al., 2015). Spatially-distributed, fine grain data describing AGB are invaluable for evaluating models used to test hypotheses regarding complex ecosystem dynamics over a wide variety

of spatial and temporal scales (e.g. Peters, 2002; Stewart et al., 2014; Poulter et al., 2014; Ahlström et al., 2015).

8.6.7. Limitations of RPAS-SfM

While the natural colour attributes of SfM-derived point clouds facilitate visual interpretation, this technology has limited penetration through vegetation canopies which restricts the number of ground points beneath vegetation canopies (Dandois and Ellis, 2010; Lisein et al., 2013; Dandois et al., 2015). Consequently, RPAS-acquired SfM alone may be most usefully applied in ecosystems with spatially or temporally discontinuous vegetation cover, as is common in dryland ecosystems. Alternatively, hybrid approaches have been proposed combining SfM-derived DSMs with DTMs derived from other survey techniques, such as LiDAR (Dandois and Ellis, 2013; Lisein et al., 2013; Dandois et al., 2015; Puliti et al., 2015) or GNSS observations (Zahawi et al., 2015). Such hybrid approaches are promising, although the measurement-scale of CHMs derived using such approaches is limited by the co-registration accuracy of SfM-derived DSMs with the DTMs.

8.6.8. Applications of RPAS-SfM in Short-Sward Systems

Herein, I answer the call for new techniques to measure aboveground biomass (Hill et al., 2013) and demonstrate how an emerging technology can fulfil the need for scale-appropriate (fine-resolution and large spatial extent) measurements. Such quantitative descriptions of plant architecture at centimetre scales are essential to elucidate the dynamics of ecosystems subject to significant environmental change (Getzin et al., 2014; Stewart et al., 2014; Poulter et al., 2014; Ahlström et al., 2015).

Foliar volume measurements from RPAS-acquired SfM are of comparable measurement-scale to data obtained from on-the-ground surveying (Yao et al., 2006; Muldavin et al., 2008; Huenneke et al., 2001; Allen et al., 2008), facilitating both validation and integration of ecosystem knowledge derived from these two complementary approaches. Although direct estimation of AGB on the basis of foliar volume is a well-established technique in on-the-ground monitoring of rangeland vegetation dynamics (Huenneke et al., 2001; Herrick et al., 2005; Allen et al., 2008), foliar volume measured using remote sensed fine grain CHMs has not been widely

used to predict AGB (although see Greaves et al., 2015). Because ultra-fine grain CHMs have not previously been widely available there has been limited research on their utilisation. However, because high-precision, fine grain CHMs directly account for some variation in growth form between plant individuals, these approaches are likely to be more accurate and sensitive predictors of AGB than simpler metrics such as maximum plant height or canopy area. Spatially explicit quantification of AGB can be used to evaluate deterministic simulations of vegetation in these environments (Tietjen et al., 2009; Turnbull et al., 2014a).

Spatially explicit fine grain CHMs are valuable to a diverse array of ecological research applications, for example to better understanding the interactions between biotic and abiotic controls on intraspecific trait variables in semi-arid ecosystems {Citation}. For example, fine grain CHMs could be applied to advance understanding of vegetation self-organization in 2.5D, progressing beyond the insights supported by 2D approaches. Although most plant species exhibit no orientation relative to azimuth (Kimes, 1984; Falster and Westoby, 2003; McNeil et al., 2016), creosotebush branches and canopies are sometimes orientated to face the southeast (Neufeld et al., 1988; Whitford et al., 1995). This orientation in creosotebush is hypothesised to optimise water use efficiency by maximising interception of insolation earlier in the day when air temperatures are lower, as when air temperatures rise during each day stomatal closure to reduce transpiration losses limits gas exchange and thus photosynthesis (Neufeld et al., 1988; Whitford et al., 1995). RPAS-SfM could be used to efficiently characterise creosotebush canopies, for example across the climatic range of this species, and thus could further elucidate the mechanistic controls on orientation in vegetation canopies.

RPAS-acquired SfM approaches can be used to survey extents diametrically equivalent to coarse-grain, satellite-derived, globally-available products describing vegetation structure, at least at the scale of several ha (Dandois and Ellis, 2013; Browning et al., 2015). Therefore, fine grain, spatially distributed datasets quantifying spatio-temporal variations in AGB could be used to facilitate scaling studies to understand the accuracy and sensitivity of globally-available information products used for biomass estimation in drylands globally, such as MODIS (Zhang and Kondragunta, 2006; Muukkonen and Heiskanen, 2007; Baccini et al., 2008) or vegetation optical depth (VOD) (Owe et al., 2001; Liu et al., 2013a, 2013b; Murray-Tortarolo et al., 2016). For example, MODIS pixels cover an area ~20,000 times

greater than that observed by cameras typically installed on eddy covariance flux towers, hindering comparisons of vegetation phenology observed at these measurement scales (Balzarolo et al., 2016). Hierarchal modelling approaches (e.g. Wilson et al., 2011) are particularly promising for such upscaling efforts.

High quality datasets describing spatial and temporal changes in AGB are also needed to critically evaluate the performance of dynamic vegetation models (Chave et al., 2004), particularly in dryland regions (Tietjen et al., 2009, 2009; Stewart et al., 2014; Poulter et al., 2014; Ahlström et al., 2015). Dynamic vegetation models are an important component of the Earth System Models used to simulate global scale phenomenon and investigate possible future states of the Earth System. Consequently, improving the empirical foundation of these vegetation models is therefore essential to improve understanding of the role of dryland ecosystems in both long term trends and interannual variability in the global land C sink (Poulter et al., 2014; Ahlström et al., 2015). New, high-quality datasets describing temporal vegetation dynamics in grass and shrub dominated rangeland ecosystems are particularly required because recent studies have highlighted significant disagreements between current dynamic vegetation model predictions and the limited empirical observations, indicating the need for further model refinement in these ecosystems (Murray-Tortarolo et al., 2016).

8.7. Summary

This study is the first to demonstrate how ecosystem biotic structure can be efficiently characterised at cm grain over landscape extents, by using SfM photogrammetry to process aerial photographs captured from a lightweight RPAS costing less than $3,000 USD. The well-constrained SfM reconstructions resolved individual plants just a few cm^3 in volume over areas of 10 ha, a level of detail hitherto unobtainable using the RPAS-acquired SfM approach. Using this RPAS-acquired SfM approach, ultra-fine grain CHMs can be obtained at much lower cost than comparable LiDAR datasets.

Canopy volumes derived from the CHMs can be used to infer aboveground biomass, and subsequently belowground biomass and associated C stocks. The measurements are sensitive to subtle spatio-temporal changes in biophysical structure, as demonstrated by the survey over a historically burned area and could easily be acquired at daily timesteps over extents of ~1-5 ha. Compared to on-the-ground surveys, this coverage yields more spatially-representative assessments of ecosystem state at landscape-scales, facilitating the extraction of subtle signals that elucidate significant controls on biophysical and ecohydrological processes.

The technique has the potential to revolutionise monitoring of biophysical structure over landscape-levels in ecosystems with spatio-temporally discontinuous canopy covers. Such data could reduce uncertainty in biomass inventories, and allow previously unfeasible experiments on process interactions in a range of environmental contexts. For example, the capacity to survey areas diametrically equivalent to coarse-grain information products such as MODIS at spatial resolutions comparable to on-the-ground monitoring would facilitate upscaling studies, the impact of different intensities of herbivory on AGB under various environmental conditions could be quantified, and vegetation responses to precipitation inputs in water-limited ecosystems could be characterised at landscape-levels on very short timesteps. The inexpensive approach presented herein is highly complementary to existing approaches for monitoring biophysical structure, and represents an appreciable advance in the tools available to geoscientists.

9. Modelling the Redistribution of Carbon by Runoff

9.1. Chapter Overview

This section presents the results of a series of experiments to simulate the redistribution of runoff, sediment and particle associated inorganic and organic C. MAHLERAN (model for assessing hillslope erosion, runoff and nutrients; Wainwright et al., 2008a, 2008c, 2008b), is evaluated against the largest monitoried group of natural rainstorm events in a dryland ecosystem. The rationale for developing the objectives described below was presented in section 3.4, and suggestions for future work in this area are presented in section 9.10.

9.2. Objectives

D1 Evaluate MAHLERAN's simulation of the hydrology of natural runoff events at hillslope-spatial and event-temporal scales.

D2 Evaluate MAHLERAN's simulation of the erosion of sediment during natural runoff events at hillslope-spatial and event-temporal scales.

D3 Evaluate MAHLERAN's simulation of the erosion of particle-associated IC during natural runoff events at hillslope-spatial and event-temporal scales.

D4 Evaluate MAHLERAN's simulation of the erosion of particle-associated IC during natural runoff events at hillslope-spatial and event-temporal scales.

9.3. Key Findings

- New information sources were used to parameterise and evaluate a spatially-explicit ecohydrological modelling approach, enabling one of the most comprehensive evaluations to date of any process-based model structure against a large number of natural rainstorm events in a dryland ecosystem.
- The comprehensive evaluation enabled refinement of priorities for the future development of such process-based modelling approaches.
- When the erosional component was behavioural, the model structure was able to reproduce the erosion-induced redistribution of sediment associated inorganic C.
- Even when the erosional component was behavioural, the current model structure was unable to reproduce the erosion-induced redistribution of sediment associated organic C, due to underrepresentation of processes leading to OC enrichment.

9.4. Numerical Model Structure

9.4.1. Model Basis

The following sections present a brief description of constituent submodels for MAHLERAN (Version 1.2.1):

MAHLERAN's hydrology component

MAHLERAN's hydrological component is based on a lineage tracing back through Scoging (1992), Scoging *et al.* (1992), Parsons *et al.* (1990, 1997), Wainwright and Parsons (2002), and Wainwright *et al.* (2008c). An infiltration model simulates the generation of infiltration- and saturation-excess overland flow, based on the Smith and Parlange (1978) approach to the Green and Ampt model

$$f = \frac{K_s e^{\frac{F}{B}}}{e^{\frac{F}{B}} - 1} \qquad \textit{Equation 9-1}$$

where f is the infiltration rate [mm min^{-1}], K_s is the saturated hydraulic conductivity [mm s^{-1}], F is the cumulative infiltration to present [mm s^{-1}] , and B is a soil storage parameter that account for capillary suction and antecedent soil moisture conditions. This representation explicitly considers infiltration of runon.

Overland flow is routed using a continuity equation of the kinematic wave approximation of the Saint Venant (2D shallow water) equations (Wainwright and Parsons, 2002), with all flow assigned to the direction of steepest descent in cardinal directions (D4) on a simple finite difference grid (Scoging et al., 1992)

$$\frac{\partial q}{\partial x} + \frac{\partial d}{\partial t} = r - i \qquad \textit{Equation 9-2}$$

where q is the discharge per unit width [mm^2 s^{-1}], *d* is the flow depth [mm], *r* is the rainfall rate [mm s^{-1}], *I* is the infiltration rate [mm s^{-1}] and *∂x ∂t* are space and time increments. Flow routing uses a Crank-Nicolson with Newton-Raphson solution (Hewett et al., In Prep) (although other solutions are also available within the model structure). Flow velocity is determined dynamically as a function of flow depth and surface roughness using the Darcy-Weisbach flow equation

$$v = \sqrt{\frac{8gds}{f}} \qquad \textit{Equation 9-3}$$

where *v* is the flow velocity [mm s^{-1}], *g* is the acceleration due to gravity [mm s^{-2}] , and *s* is the surface slope [m m^{-1}]. This approach differs from most kinematic wave implementations, which typically assume a fixed rating function which poorly represents feedbacks of flow hydraulics with runoff and infiltration (Wainwright et al., 2008c). Drainage from the base of the soil profile (*b)* [mm hr^{-1}] is modelled using an empirical relationship (Wainwright and Parsons, 2002)

$$b = a\left(1 - e^{b'\left[\frac{St_{max}}{St_{now}}\right]}\right) \qquad \textit{Equation 9-4}$$

where *b'* [dimensionless] reflects the rate of convergence from unsaturated to saturated drainage conditions, St_{max} is the total available soil-water storage [mm] and St_{now} is the current cumulated depth of water stored in the soil [mm]. Lateral movement of water in the subsurface and possible return flow due to rising water tables is uncommon in semi-arid hillslopes, especially during short-term runoff events (Michaud and Sorooshian, 1994; Michaelides and Wainwright, 2008), and is not represented in the present model structure.

MAHLERAN's sediment transport component

MAHLERAN's sediment transport component is described in Parsons *et al*. (2004, 2006), Wainwright *et al.* (2008c) and Cooper *et al.* (2012). The process representation in MAHLERAN realizes a conceptualization of soil-erosion processes

which takes account of the fact that interrill erosion on hillslopes is dominated by rolling or sliding along surfaces or in short steps akin to movement of bedload (Wainwright, 2016). MAHLERAN employs an approach to modelling erosion that is based upon the concept of entrainment and travel distances of particles from six particle size classes in order to account for differing behaviour of particles of different size (Table 9.1). Explicitly representing the interactions between concentrated and unconcentrated erosion processes is imperative because the relative balance of different processes is a critical control on the resulting erosion patterns (Wainwright et al., 2008c, 2008b; Turnbull, 2008). Explicit treatment of discrete particle size classes has been argued to be an essential component of simulating the differences between transport-limited movement of coarse particles from the (generally) supply-limited movement of fines (Kirkby, 2010). Each size class is simulated separately using a form of the continuity equation, in which sediment belonging to different size classes (Table 9.1) is simulated seperatly (Wainwright et al., 2008c)

$$\frac{\partial h_{s,\varphi}}{\partial t} + \frac{\partial q_{s,\varphi}}{\partial x} - \varepsilon_{\varphi} + dep_{\varphi} = 0 \qquad \textit{Equation 9-5}$$

where h_s is the equivalent depth of sediment transport [m], q_s is the unit discharge of sediment ($m^2\ s^{-1}$), ε is the rate of erosion of the surface [$m\ s^{-1}$], *dep* is the rate of deposition [$m\ s^{-1}$], φ is an index relating to a specific size class of sediment, *t* is time [s] and *x* is location in space [m].

Table 9.1. Particle size classes in MAHLERAN.

Particle size class (φ)	*[mm]*
1	*<0.0625*
2	*0.0625-0.25*
3	*0.25-0.5*
4	*0.5-2*
5	*2-12*
6	*>12*

The modelling of sediment transport based on particle travel distances scales poorly with time, and as model time steps decrease, sediment transport may be significantly overestimated depending on the velocity of sediment movement and value *∂t* (Wainwright et al., 2008c; Turnbull, 2008, p. 147). To account for the temporal scaling characteristics of this model structure, $q_{s,\varphi}$ is defined as

$$q_{s,\varphi} = h_{s,\varphi} v_{p,\varphi} \qquad \textit{Equation 9-6}$$

where $v_{p,\varphi}$ is the virtual velocity of sediment of particle size class φ [m s^{-1}], which can be derived empirically from observations of sediment transport distance per-unit-time or by theoretical calculation by differentiation of transport distance per unit-of-time (Wainwright et al., 2008c; Turnbull et al., 2010b). MAHLERAN simulates four conditions of sediment erosion (for further details see Wainwright et al., 2008c; Turnbull et al., 2010b):

(i) Erosion as a function of raindrop detachment, with transport by splash when no surface flow is present

$$\varepsilon_{r,\varphi} = \alpha_\varphi K E^{b_\varphi}, \qquad Sl = 0 \qquad \textit{Equation 9-7}$$

$$\varepsilon_{r,\varphi} = \alpha_\varphi K E^{b_\varphi}, Sl^{c_\varphi} \qquad Sl > 0 \qquad \textit{Equation 9-8}$$

where $\varepsilon_{r,\varphi}$ is raindrop detachment for particle size class φ [m s^{-1}], KE is rainfall kinetic energy per unit area per unit precipitation [J m^{-2} mm^{-1}], *Sl* is surface slope [m m^{-1}] and α_φ, b_φ $c_\varphi$are empirical parameters that are a function of particle size and density.

(ii) Erosion as a function of raindrop detachment modified to account for the shielding effects of the surface water layer, with transport by overland flow

$$\varepsilon_{u,\varphi} = \varepsilon_{r,\varphi} e^{-\beta_\varphi h} \qquad \textit{Equation 9-9}$$

Where $\varepsilon_{u,\varphi}$ is unconcentrated flow detachment rate for a particle of size class φ [m s^{-1}] and β_φ is an empirical parameter reflecting the changing energy arriving at the surface with increasing flow depth (relative to the diameter of a particle of size class φ).

(iii) Transport by mixed unconcentrated and concentrated flow (500 ≤ *Re* ≤ 2000) (where *Re* is the flow Reynolds number)

$$\varepsilon_{c,\varphi} = P_\varphi \delta_{\varepsilon_c,\varphi} \qquad \textit{Equation 9-10}$$

where $\varepsilon_{c,\varphi}$ is detachment rate by concentrated flow for particles of size class φ [m s^{-1}], P_φ is the probability that a particle will be entrained

(described further in Wainwright et al., 2008c), and $\delta_{\varepsilon_c,\varphi}$ is the effective detachment rate of sediment of size class [m s^{-1}].

(iv) Erosion as a function of detachment and transport by turbulent concentrated flow (*Re* > 2000).

Note that these numerical representations do not currently account for differences in particle submergence, which may be a significant control on particle detachment on hillslopes (Michaelides and Martin, 2012).

MAHLERAN simulates particle deposition using a transport-distance approach, based on the transport mechanism. Given the estimated amount of detachment and knowledge of the distribution function of travel distances of particles under specific transport mechanisms, deposition rates can be estimated for each location along the transport pathway (Wainwright et al., 2008c). Travel distances are assumed to be described by exponential distribution functions, which represents the declining probability of particle movement with distance from the source (Wainwright et al., 2008c; after Hassan et al., 1992). These exponential distribution functions can be fitted using a single, physically meaningful parameter that describes the average empirically-observed travel distance. Other, more complex distribution functions may potentially better describe the actual distribution of transport distances, but limited empirical information is available to constrain such functions (Wainwright et al., 2008c). This representation of deposition is relatively efficient, but is limited by its inability to consider variations in the forces influencing the likelihood of a particle deposited at different points in space.

To improve the accuracy of process representation within the model and support future numerical investigations into the role of particle density on particle mobility, MAHLERAN's sediment transport component was modified to make the detachment, transport and deposition functions explicitly depended on a user-specified sediment density parameter, $\rho_{Sediment}$. To represent the effect of density on particle transport by unconcentrated flow, the unconcentrated flow component was modified by scaling median transport distances for each model size class by S_b

$$S_b = \frac{\rho_{Sediment\_Original}}{\rho_{\_Sediment\_New}} \qquad \textit{Equation 9-11}$$

To represent the effect of density on particle detachment and transport by concentrated flow, these components were modified to explicitly consider particle excess density in the fluid medium, as suggested by Bagnold (1980)

$$S_c = \frac{P_{Excess\_Original}}{P_{Excess\_New}} = \frac{\left(\frac{\rho_{Sediment\_Original}}{\rho_{Fluid}}\right)}{\left(\frac{\rho_{Sediment\_New}}{\rho_{Fluid}}\right)} \qquad \textit{Equation 9-12}$$

MAHLERAN'S carbon transport component

Carbon fluxes are calculated as a function of sediment transport, which assumes that the chemical content of each particle size class is the same as that in the contributing near-surface soil (Fierer and Gabet, 2002; Turnbull et al., 2010b). The flux of particulate-bound chemicals is modelled as

$$q_{c,\varphi} = q_{s,\varphi} \cdot c_{c,\varphi} \qquad \textit{Equation 9-13}$$

The flux of carbon (organic or inorganic), bound with sediment in each particle-size class per time-step is a function of the discharge of sediment ($q_{s,\varphi}$) and the carbon concentration of sediment in each particle-size class ($Cc_{,\varphi}$)

Eroded particulate-associated inorganic and organic C is routed conservatively. While conservative behaviour is known to be an incomplete process representation (as discussed in sections 1.2.2, 3.1 and 3.2,), conservative treatment is suggested to be a reasonable assumption at the spatial (hillslope) and temporal (rainstorm event) scales of interest here. At present there is insufficient empirical information to represent non-conservative behaviour in this modelling approach (*sensu* Quinton et al., 2006), although significant efforts are ongoing to understand non-conservative transport of C through terrestrial and aquatic systems (discussed further in section 10.3) which will support the representation of non-conservative transport in process-based modelling approaches in the future.

9.4.2. Model Parameterisation

Consistent with most previous implementations of MAHLERAN, the model was implemented on a 0.5 m^2 spatial resolution grid. A significant novelty introduced by this research was that topography and surface cover (bare versus vegetated) were parameterised using digital maps derived from structure-from-motion (SfM)

photogrammetry of image data acquired using an remotely piloted aerial system (RPAS), as described in chapter 8 and Cunliffe *et al.* (2016b). Using SfM-derived digital terrain models (DTMs) to parameterise hydrologic and erosion models has been proposed in a number of remote sensing publications (Laliberte and Rango, 2009, 2011; Rango et al., 2014), but to the author's knowledge, this application was the first time that RPAS-acquired SfM-processed data have actually been used to parameterise a process-based erosion model. As discussed in section 8.5.2, relative errors in these DTMs are low and are negligible at the 0.5 m^2 spatial resolution used for the current modelling exercise.

DTMs often contain local minima, also known as 'pits', 'sinks' or 'depressions'. Although such features have often been described as 'errors' or 'artificial depressions' ascribed to survey errors (e.g. Grimaldi et al., 2007; Zhu et al., 2013; ESRI, 2016) such depressions can also reflect the true topography which can result in the hydrologically significant surface storage of water in puddles, ponds and lakes (Wang and Liu, 2006). Advances in survey accuracy increases confidence that depressions are genuine features in the landscape, and finer grid resolution DTMs typically have a greater number of local minima (Grimaldi et al., 2007; Zhu et al., 2013). However, like most hydrologic models (Zhu et al., 2013), MAHLERAN's routines cannot automatically overtop local minima (although this functionality is under development, Hewett et al., In Prep). Consequently, it was necessary to eliminate local minima in the DTM. This step should be considered as necessary to meet the requirements of imperfect models, rather than as 'correcting' errors in the DTM.

Eliminating topographic depressions is a non-trivial task (Planchon and Darboux, 2001). Common practice is to detect depressions and fill them up to the elevation of the surrounding pixels, although this can introduce errors such as systematic reduction of average slopes which are often important parameters in hydrologic models (Wang and Liu, 2006; Grimaldi et al., 2007; Zhu et al., 2013) and over-estimation of hydrological connectivity (Turnbull et al., 2010b). Nonetheless, to meet current model requirements, local minima in a D4 (Von Neumann) neighbourhood were filled. As most sink eliminating utilities consider a D8 (Moor) neighbourhood (see Zhu et al., 2013), this necessitated development of a bespoke program in collaboration with Professor Rolf Aalto (pers. comm.). Rainfall inputs were simulated at 1-minute temporal resolution, and the model was implemented at 1-second timesteps.

Parameterisation of the hydrology component

The hydrological component was parameterised broadly following Wainwright *et al.* (2008a) and Turnbull *et al*. (2010b). Infiltration and roughness parameters are fully distributed spatially, and key parameters are summarised below. The final infiltration rate, K_{sat} (mm min^{-1}), was parameterised as

$$K_{sat} = 0.351 + 0.01\,rain - 0.006P\% \qquad \textit{Equation 9-14}$$

Where *rain* is the event average rainfall intensity (mm hr^{-1}) and P% is the percentage of the ground surface covered by desert pavement [%] (after Abrahams et al., 1989; Parsons et al., 1996; Wainwright et al., 2008a; Turnbull et al., 2010b). As noted by Turnbull *et al*. (2010b), there are limitations in using this relationship to estimate K_{sat} as it was developed for a different, albeit similar, field site; however, it was the preferred option as it accounts for the effect of varying stone-pavement cover and rainfall intensities on K_{sat}. Where pavement cover (P%) was very high, this function can yield negative values of K_{sat}, as negative K_{sat} is not physically possible, negative K_{sat} values were truncated to zero. While infiltration rates are related to vegetation cover and type, as discussed further in section 9.10.1 (Abrahams et al., 2003; Neave and Abrahams, 2002; Müller, 2004; Müller et al., 2007b; Miller et al., 2007) modelled infiltration rates do not currently explicitly consider spatial differences in vegetation cover and type (Wainwright et al., 2008a, 2008c; Turnbull et al., 2010b).

As a first order approximation, the Darcy-Weisbach friction factor, *ff*, (dimensionless) was parameterised using the simple depth feedback relationship of Scoging *et al*. (1992)

$$ff = 14 - 0.008\,h \qquad \textit{Equation 9-15}$$

Where h is the depth of water flow [m]. While a variety of functions exist for predicting *ff* (Parsons et al., 1994; Abrahams et al., 1995, 1996, Wainwright et al., 2000, 2008a), this simple approximation generally performs best in this environmental context (Turnbull et al., 2010b; John Wainwright, pers. comm.).

The depth to wetting front must be known *a priori*, and is a difficult parameter to measure (Wainwright et al., 2008b). Soil thickness represents effective depth to wetting front, which was thus estimated to be 0.35 m, based on reports of depth to

the caliche horizon (Kieft et al., 1998; Turnbull et al., 2010b). The wetting front suction parameter was estimated to be 5 cm, and the saturated soil-moisture content was set uniformly to 39% (after Turnbull et al., 2010b).

The kinetic energy (*KE* in J m^{-2} mm^{-1}) of rainfall impacting the ground surface is mediated by vegetation cover (Wainwright et al., 1999a; Baird, 2013). To represent this mediation, raindrop *KE* was modified using the following function (after Wainwright et al., 1999a)

$$\boldsymbol{KE_v = KE\left(1 - 8.1 \times 10^{-3} V\%\right)} \qquad \textit{Equation 9-16}$$

where KE_v (J m^{-2} mm^{-1}) is the *KE* of rainfall arriving to the ground that is adjusted to account for the vegetation cover and V% is the percentage vegetation canopy cover (%) (for further discussion see Turnbull et al., 2010b). V% was determined using the high grain canopy height models developed in chapter 8 and Cunliffe *et al.* (2016b). As described in sections 9.5.3 and 9.6.5, this characterisation of surface cover was 90% accurate with most of the classification error due to misclassification of sparsely vegetated areas as being bare (unvegetated). This error is considered insignificant, as sparse vegetation cover has limited capacity to modify raindrop kinetic energy.

ASM content is a critical control on runoff generation at fine temporal and spatial scales (Cammeraat, 2002), and is a key parameter in MAHLERAN's infiltration component. Spatio-temporal analysis has shown that there are often significant differences in the soil moisture content between bare and vegetated soils (Turnbull, 2008; Turnbull et al., 2010c; Peter Biro, unpublished data). Therefore, ASM was parameterised using spatially distributed maps, using observed ASM values for each surface cover (bare and vegetated) (Turnbull et al., 2010c; Peter Biro, unpublished data) combined using an area-weighted approach based on the percentage of vegetation cover in each cell (V%)

$$\boldsymbol{ASM = \left((1 - V\%) \times ASM_{Bare}\right) + \left(V\% \times ASM_{Veg}\right)} \qquad \textit{Equation 9-17}$$

where ASM is antecedent soil moisture content, V% is the percentage of vegetation cover in each cell, ASM_{Bare} is the ASM observed for the bare surface cover and ASM_{Veg} is the ASM observed for the vegetated surface cover (after Turnbull, 2008; Turnbull et al., 2010b). This approach is a simple yet effective way to account for the spatial variability in this influential input parameter (Müller et al., 2007b; Turnbull, 2008; Turnbull et al., 2010b). Appropriate parameterisation of ASM can be

challenging due to difficulties in quantifying this parameter in the field; however, when not directly observed, ASM can also be reasonably predicted from climatic variables (e.g. Tietjen et al., 2009, 2009).

Parameterisation of the erosion component

Soil particle size distribution was spatially distributed, using digital maps based on the proportion of stone-pavement cover (made up of φ = 5 and φ = 6) assessed using near-ground aerial image data (Turnbull et al., 2010b, 2010c). The proportion of sediment in the remaining particle size classes (1 to 4) was also spatially distributed, based on the particle size characteristics of the soil measured over each plot (Turnbull et al., 2010c). The values of sediment detachment and transport parameters for each φ class are given in Table 9.2, and active layer sensitivity (controlling detachment by concentrated flow) was 0.000152 (after Wainwright et al., 2008b, 2008a; Turnbull et al., 2010b).

Table 9.2. Parameter values for MAHLERAN's detachment and transport routines

Particle size class (φ)	*a*	*b*	*c*	*d*
1	0.000035	1.20	0.23	14.49275
2	0.000665	1.08	0.21	10.98901
3	0.000420	0.79	0.11	12.04819
4	0.000665	0.75	1.06	12.34568
5	0.000665	0.75	0.10	40.00000
6	0.000007	0.50	0.10	1000.00000

To support future numerical experiments into the influence of particle density on simulated erosion dynmaics, the parameters for the splash detachment component, *a*, and the splash transport component, *d*, for each particle size class should be scaled by S_a and S_d, respectively, using

$$S_a = \left(\frac{\rho_{Sediment\_New}}{\rho_{Sediment\_Original}}\right)^{-0.5} \qquad \textit{Equation 9-18}$$

$$S_d = \frac{\rho_{Sediment\_New}}{\rho_{Sediment\_Original}} \qquad \textit{Equation 9-19}$$

where $\rho_{Sediment\_Original}$ is the original density of the eroding material (2.65 g cm^{-3}) and $\rho_{Sediment\_New}$ is the new density of the eroding material [g cm^{-3}].

Parameterisation of carbon component

The concentration of IC and OC associated with each particle size class was parameterised using the areally-weighted average concentration for each site reported in Chapter 6 (Cunliffe et al., 2016d) and Chapter 7 (Table 9.3).

Table 9.3. Concentrations of inorganic (IC) and organic (OC) carbon determined for each modelled particle size class. Values calculated from data presented in Chapter 6 (Cunliffe et al., 2016d) and Chapter 7.

		Particle size class					
		1	**2**	**3**	**4**	**5**	**6**
	[mm]	*<0.0625*	*0.0625-0.25*	*0.25-0.5*	*0.5-2*	*2-12*	*>12*
IC	**Grass**	1.083	0.487	1.229	3.760	7.678	7.678
	Grass-Shrub	1.174	0.514	1.155	3.633	7.457	7.457
	Shrub-Grass	1.575	0.723	1.396	3.963	7.401	7.401
	Shrub	1.516	0.675	1.436	3.858	8.043	8.043
OC	**Grass**	0.712	0.270	0.385	0.630	0.469	0.469
	Grass-Shrub	0.722	0.294	0.381	0.626	0.458	0.458
	Shrub-Grass	0.730	0.452	0.542	0.863	0.535	0.535
	Shrub	0.695	0.300	0.315	0.606	0.556	0.556

9.5. Approach to Model Evaluation

This modelling exercise is intended to improve knowledge of the process representation currently implemented in MAHLERAN, in order to better understand the capabilities of this modelling approach and where future refinements may be valuable (Wainwright and Mulligan, 2013b; Turnbull et al., 2014a). Comprehensive evaluations are constructive because the more aspects of ecosystem dynamics a model can reproduce, the greater the confidence that the model encapsulates a plausible representation of system behaviour (*sensu* Popper, 1959; Baird, 2013; Young and Leedal, 2013, p. 114).

MAHLERAN is a modular model, with the sediment transport component dependent on the hydrology component, and the C component dependent on the sediment transport component. Therefore, while redistribution of C was of primary concern in the present study, it was constructive to consider the extent to which the hydrology component was behavioural, i.e. the extent to which predictions reflected the observed reality (Brazier et al., 2000; Turnbull et al., 2010b). Note that it is valuable

to use a variety of measures to obtain a comprehensive assessment of model performance, as different statistical measures are sensitive to different attributes of model behaviour (Michaelides and Wainwright, 2008).

MAHLERAN was evaluated over a number of runoff events at four sites with different levels of vegetation cover, supporting examination of how well this model performs under a range of conditions. Full descriptions of the measurements of inputs of rainfall and plot outputs of runoff, sediment yield, and inorganic and organic carbon yield are provided in Chapter 5. A large group of natural rainfall events was collated to evaluate model predictions (Table 9.4), and the representativeness of these assemblages with regards to observed rainstorm events was analysed in Section 5.7. The runoff events occurred due to natural rainfall, and consequently were of varying intensity and duration (Turnbull, 2008; Turnbull et al., 2010b, 2010a; Puttock, 2013). Evaluation of model performance against a group of natural rainfall events (e.g., Turnbull et al., 2010b) affords a much more robust evaluation compared to appraisal against either a single event or simulated rainfall events (e.g. Parsons et al., 1997; Hessel, 2005).

The hydrologic, sediment and nutrient predictions of MAHLERAN have been evaluated previously (Wainwright et al., 2008c, 2008b, 2008a; Turnbull, 2008; Turnbull et al., 2010b; Cooper et al., 2012; Hewett et al., In Prep). This study extends on existing work by evaluating MAHLERAN against $n \leq 59$ natural rainfall events, a much larger group than has previously been considered (n = 38, Turnbull et al., 2010b), including for the first time appraisal of the modelling approach's capacity to predict the transfer of particle-associated inorganic and organic C. Furthermore, re-analysis of the observational hydrological datasets supports more accurate and robust evaluations then were previously implemented (discussed further in section 5.8).

As discussed in section 5.7, the event assemblages considered herein are both larger and more representative of the observed rainstorm characteristics events than previous evaluations of this model structure. Given the sensitivity of the hillslope processes to differences in antecedent conditions and event characteristics (discussed further in sections 3.1.1 and 3.4.1), the present assemblage of rainstorm events supports a much more robust evaluation of the model behaviour than was previously possible. Consequently, the present evaluations are argued to support

more accurate inferences regarding the capacity of this model to represent the emergent properties of resource redistribution in these ecosystems.

Note that these assemblages do not include events which could be simulated if ASM were back-calculated through calibration of the hydrologic model (after Wainwright et al., 2008b). In the present analysis, the hydrology, erosion and C components of MAHLERAN are only evaluated against data at the plot outlet. For spatially distributed (internal) evaluation of MAHLERAN's hydrology and erosion components, please see Wainwright *et al*. (2008a and references cited therein) and Turnbull *et al*. (2010b).

Table 9.4. *n* of events available for model evaluation per assemblage.

Component	Grass	Grass-Shrub	Shrub-Grass	Shrub	Total
Hydrologic Yield	20	8	9	22	**59**
Erosion Yield	19	6	4*	14*	**43**
Carbon Yield	10	5	3	10	**28**

*combined events counted as one.

A number of metrics were calculated to summarise the goodness-of-fit (GoF) between observations and model predictions, including the Index of Agreement (IoA) (Willmott, 1981), Spearmans correlation coefficient, root mean square error (RMSE) and normalised RMSE (NRMSE) and Nash-Sutcliffe efficiency (NSE) coefficients (Nash and Sutcliffe, 1970; calculated using the method of Zambrano-Bigiarini, 2014). These various GoF metrics have different degrees of sensitivity to different attributes of the data (For further discussion of the (de)merits of various GoF metrics, please see Legates and McCabe, 1999; Willmott and Matsuura, 2005; Krause et al., 2005; Michaelides and Wainwright, 2008; Krueger et al., 2010; Goldstein et al., 2013; Zambrano-Bigiarini, 2014).

Undertaking the modelling exercise described herein required troubleshooting to identify several issues with the model and subsequent refinements to the code, which has resulted in improvements to both model stability and versatility. These changes include the addition of explicit consideration of particle density during the

detachment and transport routines, and the resolution of several ‘bugs’ in the routines for reading in spatial data, for example.

9.6. Evaluation of Hydrological Component

The present evaluation of MAHLERAN’s hydrological component suggests that predictions were often highly plausible (*sensu* Goldstein et al., 2013) but that accuracy was quite variable across the range of runoff events, and typically was worse in relative terms during smaller magnitude events. These findings corroborate earlier evaluations of the model against smaller assemblages of simulated and natural rainstorm events (Wainwright et al., 2008b; Turnbull et al., 2010b). The present evaluation was able to refine previous understanding of shortcomings in the hydrological component, informing prioritization of future efforts to further refine this model structure.

Comparative hydrographs for all available simulated events are included in Appendix 4 and the hydrological characteristics of the runoff events used to evaluate MAHLERAN’s hydrological component are shown in Appendix 5. Note that, due to equipment malfunctions, observed hydrographs were not available for all events in the assemblage; in such cases the available hydrometrics (total discharge (Q) and runoff coefficients (RC)) were used for the evaluations.

Example comparisons of observed and modelled hydrographs for hydrologically simple, uni-modal runoff events are depicted in Figure 9-1, each of which yielded a goodness-of-fit (GoF) Nash-Sutcliffe Efficiency coefficient of ≥0.79. Example comparisons of observed and modelled hydrographs for four hydrologically complex, multi-modal events are depicted in Figure 9-2, these four events yielded GoF NS coefficients ranging from -0.21 to 0.45. Multi-modal runoff events such as these are a regular occurrence in natural precipitation regimes (Wainwright and Parsons, 2002; Wainwright, 2005; Brazier et al., 2016; Puttock et al., 2017), comprising for around a fifth of the total assemblage considered here, and are a more challenging test of model performance than uni-modal events.

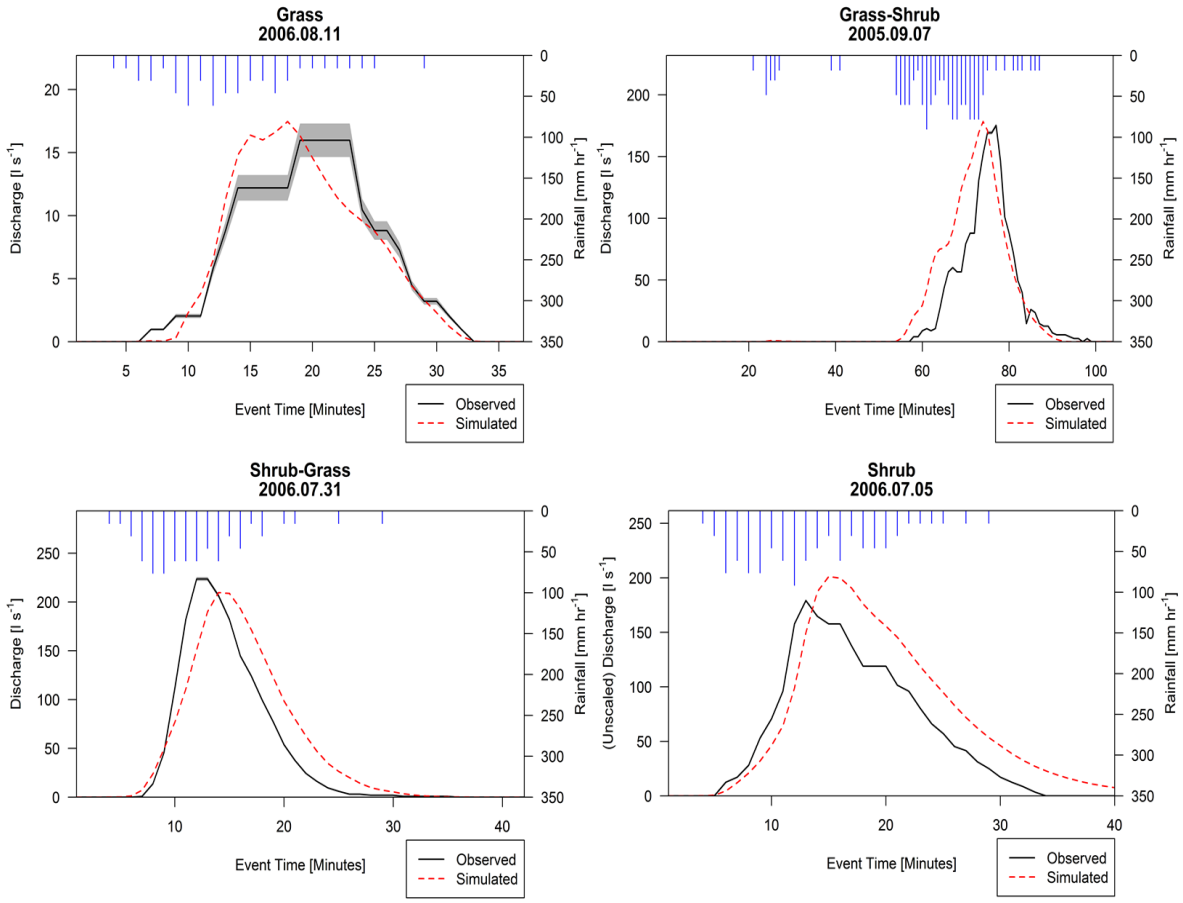

Figure 9-1. Examples of observed and modelled hydrographs for simple, essentially uni-modal events with model goodness-of-fit Nash-Sutcliffe Coefficients of ≥0.79. The blue bars indicate rainfall inputs, the red line shows the simulated hydrograph and the black line shows the observed hydrograph. Where available (i.e. for events where total discharge did not exceed the tank capacity of 2181 l), the grey shading indicates the uncertainty band around the observed hydrographs.

Comparison of observed and predicted hydrographs (Appendix 4, Figure 9-1, Figure 9-2) indicated that predictions of runoff were generally fairly good, affording confidence in the process representation of infiltration and the parameterisation of soil moisture in the present model structure. Although the hydrology of smaller magnitude events was occasionally simulated very well (e.g. Grass 2006-08-04 and Grass 2006-07-28, Shrub 2006-09-29 and Shrub 2011-08-19), smaller events were generally prone to larger relative errors than larger magnitude events. For the shrub-dominated site, although the rising limb of the hydrograph was occasionally well modelled (e.g. the Shrub 2006-07-05 event shown in Figure 9-1), the steepness of the rising limb was generally underestimated resulting in the simulated peak discharge (q_{Max}) lagging behind the observed q_{Max} in 19/21 events.

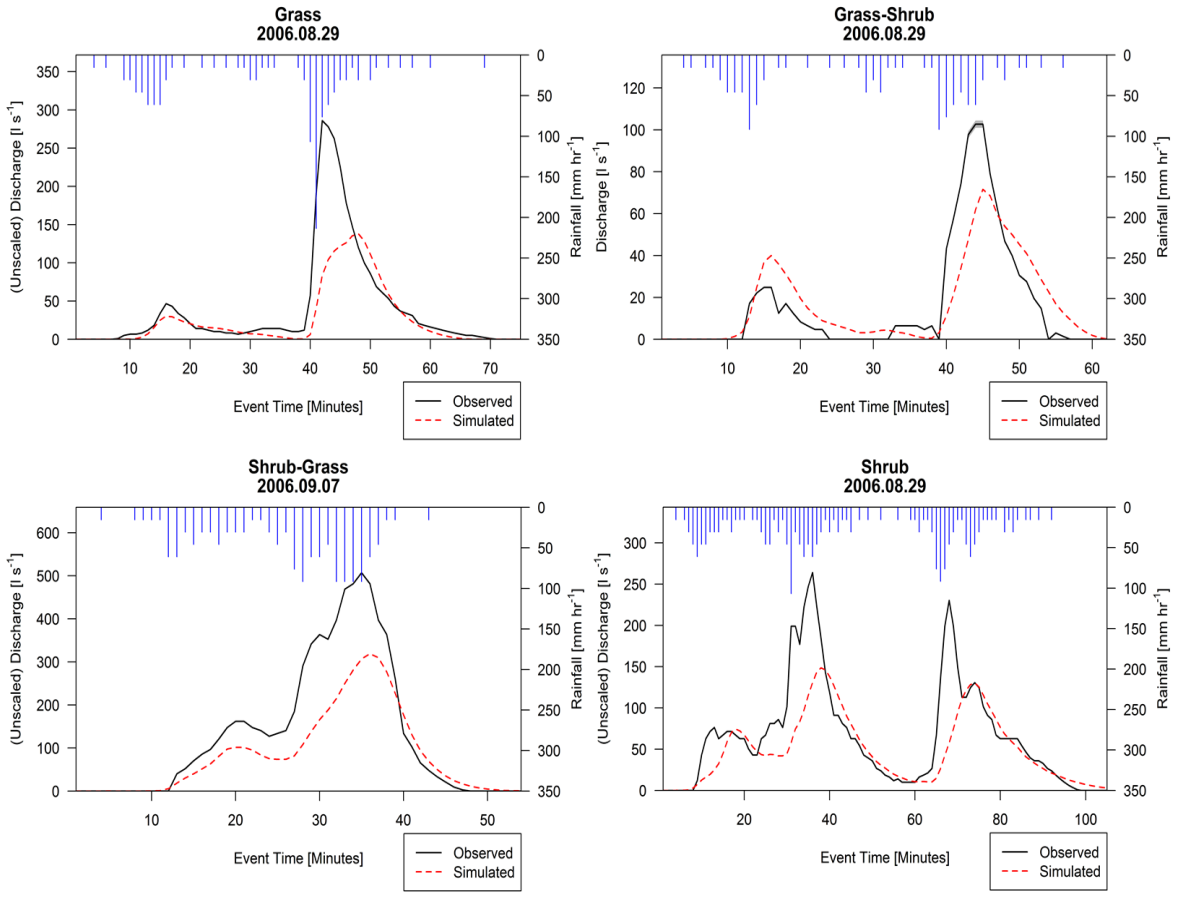

Figure 9-2. Examples of observed and modelled hydrographs for hydrologically complex, multi-modal events with goodness-of-fit Nash-Sutcliffe Coefficients ranging from 0.45 to -0.21. The blue bars indicate rainfall inputs. The red line shows the simulated hydrograph, the black line shows the observed hydrograph, and the grey shading indicates the uncertainty band around the observed hydrographs.

Comparison of observed versus modelled total discharge (Q) for all events simulated over each site (Figure 9-3a) shows that while there are some discrepancies the simulation of Q is generally in fairly good agreement with observed values. The best agreement (indicated by closest alignment of the fitted linear model with the 1:1 line), is found for the two end member sites, which also have the greatest *n*. Modelled total discharge was significantly correlated with observed total discharge ($p \leq 0.05$, $Rho \geq 0.65$) demonstrating that overall the model simulates the correct rankings of total discharge (

Table 9.5). Nash-Sutcliffe Efficiency (NSE) coefficients were >0 for all four sites, indicating that the model was a better predictor of total runoff that the mean of the observations and performed particularly well at the two end member sites (

Table 9.5). The greatest systematic dissimilarity between observed and modelled Q is found on the shrub-grass site, where runoff from <1000 l events was systematically overestimated and the runoff from the single large event (Q_{Obs} 6539 l) was underestimated.

Compared to the previous model evaluation, the present assemblages of runoff events include a greater number of small magnitude events (Figure 5-5). For example, across the four sites, in the new assemblage 19 and 38 events yielded ≤100 l and ≤500 l of runoff, respectively, compared with just 3 and 19 events previously (Turnbull et al., 2010b). Evaluation of this more comprehensive dataset broadly refutes an earlier previous finding that runoff was over-predicted for smaller events (Turnbull et al., 2010b). As illustrated in Figure 9-3, there are cases of both over- and under-prediction of runoff, and the only strong bias in prediction of runoff from smaller magnitude events exists in the shrub-grass dominated site. This systematic overestimation of runoff arising during smaller magnitude events at this site reflects underestimation of infiltration, possibly due to over-estimation of stone pavement cover and/or overestimation of the control of stone pavement cover on K_{Sat} (Equation 10-2).

Comparison of observed versus modelled runoff coefficient (RC) for all events simulated over each site is similar to the relationships observed for Q, but with a generally greater variance (Figure 9-3b). RCs were generally lower in both grass-dominated sites relative to the shrub-dominated sites. Modelled RC was significantly correlated with observed RC ($p \leq 0.05$) in three out of four sites, demonstrating that overall the model generally simulates the correct rankings of RC (

Table 9.5). Compared to total discharge, NSE coefficients were lower for observed versus modelled RC with only the two grass-dominated sites attaining positive values, indicating that the mean of the observed RC was a better predictor of RC than the model for the two shrub-dominated sites. This apparent inversion from the findings from the evaluation of total discharge was attributed to the influence of poorly simulated smaller events in the case of the shrub site, and systematic error in the predictions of the infiltration component in the shrub-grass site. These discrepancies between the evaluations of total discharge compared with the evaluations of RC illustrate the importance of multi-criteria evaluations of model performance. The dissimilarities between observed and modelled values in the shrub-grass site are even more pronounced for RC, though the fairly tight grouping around the fitted linear model is again interpreted as indicative of systematic miss-parameterisation of the infiltration component at this site rather than under-representation of temporally variable processes, such as precipitation inputs or soil crusting. In both shrub-dominated sites, RCs were systematically over-predicted for events producing smaller observed RCs, and under-predicted of RC for events producing large RCs. The degree of variance in paired observed-simulated RC values around the fitted linear model for the shrub-dominated plot (Figure 9-3b) indicates both the underrepresentation of temporally variable processes in controlling hillslope hydrology in the current model structure, and consequently also the value of large, multi-event assemblages for elucidating the emergent behaviour of hillslope hydrogeomorphic process (see sections 3.1.1 and 6) (Cunliffe et al., 2016d).

Comparison of observed versus modelled peak discharge (Q_{Max}) [l min^{-1}] for all events simulated over each site (Figure 9-3c) is a more specific metric of model performance than total discharge or RC. Although individual events were occasionally over or under estimated, overall, modelled Q_{Max} exhibited excellent agreement with observed values at the grass and grass-shrub dominated sites, and good agreement at the shrub dominated site. Modelled peak discharge was very strongly correlated with monitored discharge ($p \leq 0.0001$, $Rho \geq 0.83$), demonstrating that overall the model simulates the correct rankings of peak discharge (

Table 9.5). NSE coefficients for modelled and observed peak discharge were consistently >0, and were >0.7 for three of the four sites (

Table 9.5), indicating that overall the model was a strong predictor of peak discharge. The lower NSE coefficient for the grass-dominated site was attributed to the cluster of smaller magnitude events in this site's assemblage. Again, the shrub-grass site exhibited the greatest dissimilarity with observed values, with systematic over-prediction during smaller (<150 l min^{-1}) events and under-prediction during larger (>150 l min^{-1}) events.

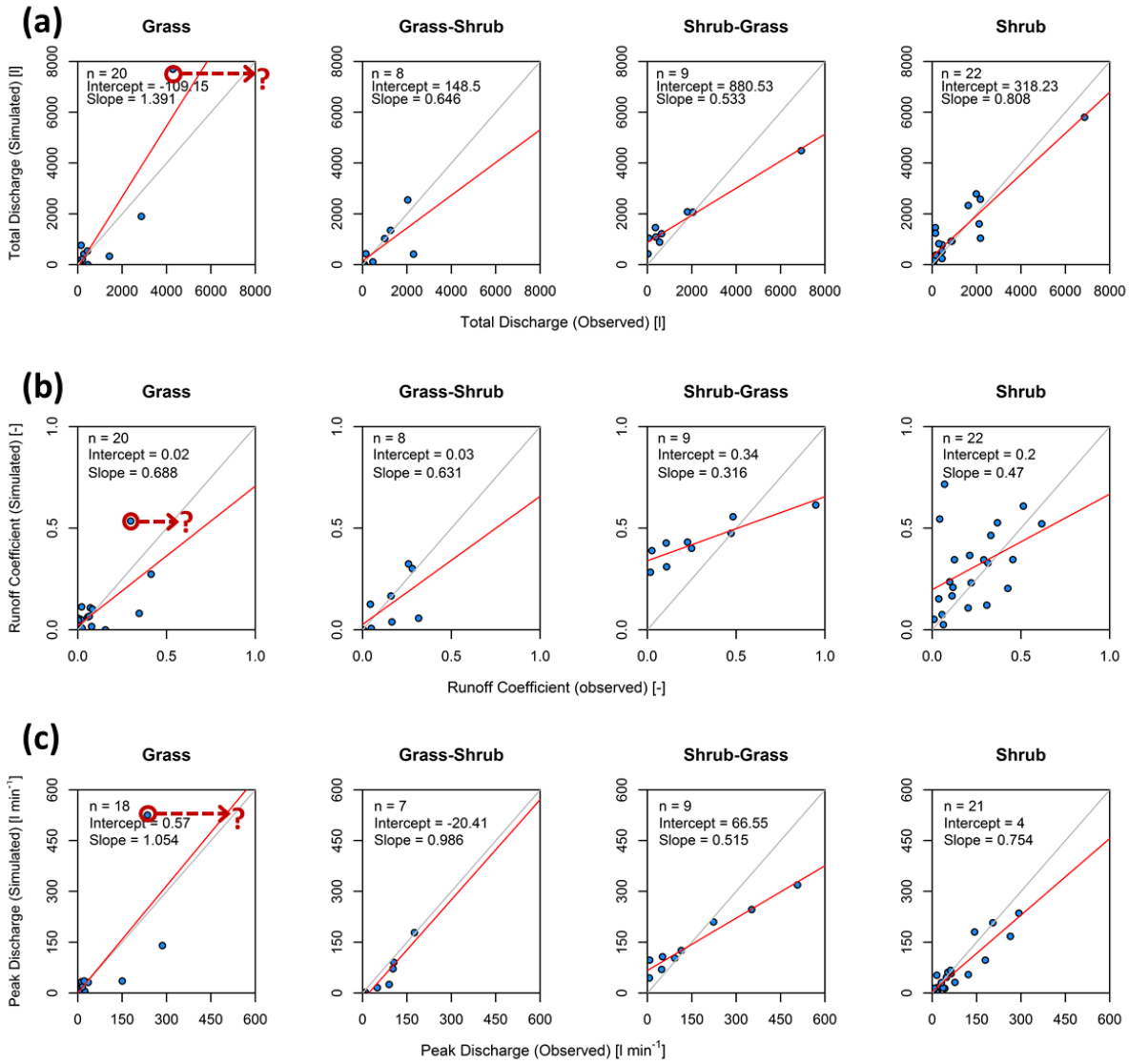

Figure 9-3. Comparisons of observed and modelled (a) total discharge [l], (b) runoff coefficient [-], and (c) peak discharge (q_{Max}) [l min^{-1}]. 1:1 is represented by the grey lines and the red lines are linear models fitted using least squares approach (see discussion of circled event in the text).

The largest magnitude (Q) event on the Grass-dominated site (Grass 2005-09-07), attained a depth of 64 cm in the measuring flume. Importantly, the depth-discharge rating curve for this site was poorly constrained at this depth (Figure 5-6) and this depth may have overtopped the installed flume. Consequently, between the fairly flat-topped hydrograph (Figure 9-4a) and surprisingly low runoff coefficient for an event of this magnitude (measured rainfall = 47.9 mm, RC = 0.298), it is considered likely that the observed hydrograph for this particular event is a significant underestimate. This event was believed to be the only one affected by exceedance of the measurement flume, and this event was circled in red in Figure 9-3a, b and c.

Issues with large, geomorphically significant events exceeding the measurement range of instillations are a common limitation of this kind of field-based experimental work (*sensu* Michaelides and Wainwright, 2008).

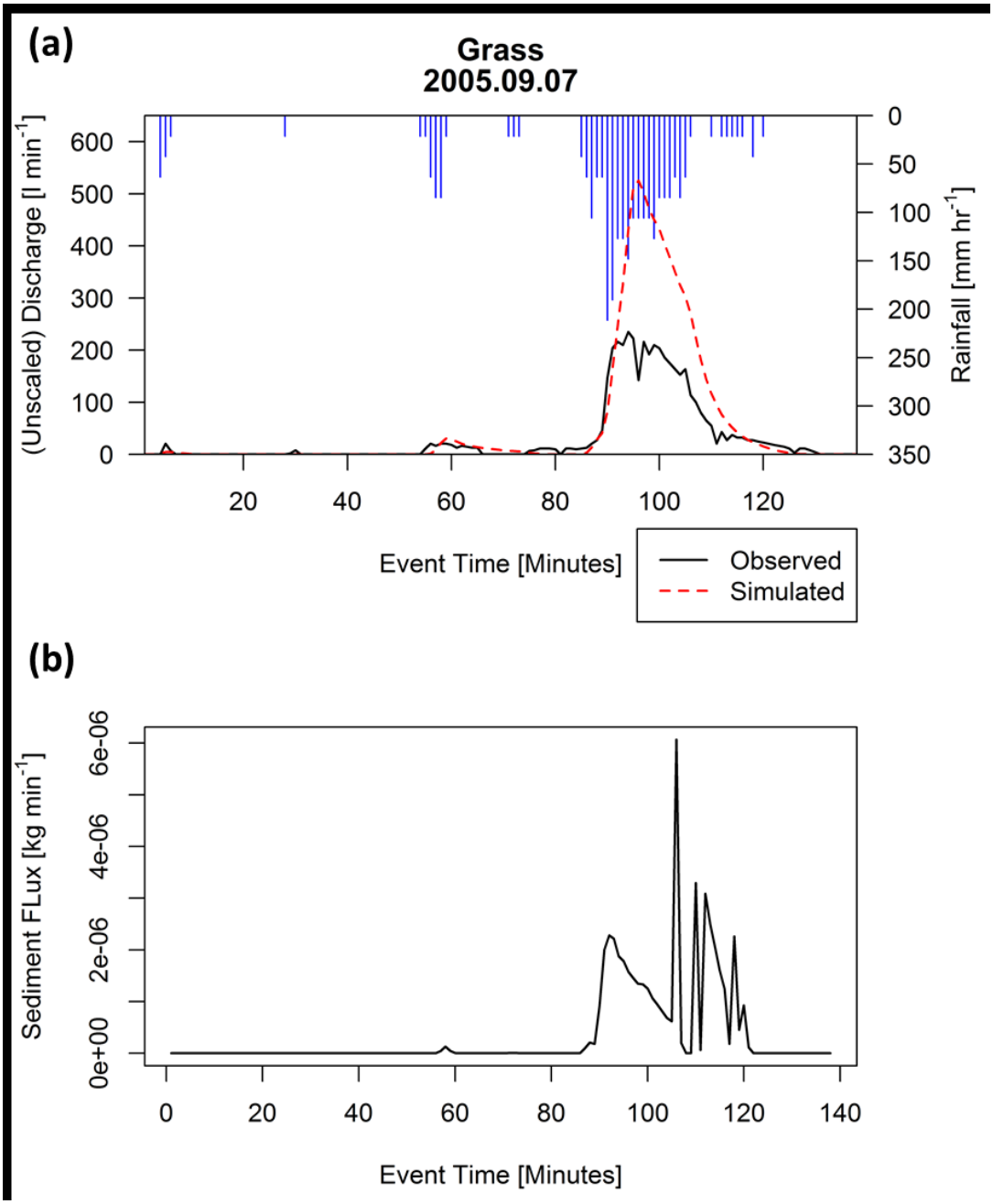

Figure 9-4. (a) Comparative hyetograph, observed hydrograph, simulated hydrograph and (b) simulated sedigraph for the anomalous Grass 2005-09-07 event.

Table 9.5. Correlation analysis of observed versus predicted hydrometrics and antecedent soil moisture (ASM) versus hydrograph goodness-of-fit (GoF-IoA).

		Site			
Parameter		**Grass**	**Grass-Shrub**	**Shrub-Grass**	**Shrub**
Q_{Obs} vs. Q_{Sim}	***Rho***	**0.645**	**0.714**	**0.817**	**0.800**
	p	0.0022	0.0465	0.0072	<0.0001
	NSE	0.75	0.26	0.18	0.80
RC_{Obs} vs. RC_{Sim}	***Rho***	**0.470**	**0.548**	**0.883**	**0.455**
	p	0.0365	0.1600	0.0016	0.0336
	NSE	0.36	0.15	-4.88	-0.21
q_{Max_Obs} vs. q_{Max_Sim}	***Rho***	**0.833**	**1.000**	**0.967**	**0.869**
	p	<0.0001	<0.0001	<0.0001	<0.0001
	NSE	0.05	0.70	0.75	0.80
ASM vs. GoF (IoA)	***Rho***	**0.509**	**0.883**	**0.200**	**0.474**
	p	0.0311	0.0085	0.606	0.0299

In total, 55 events were described by observed hydrographs which could be compared to modelled hydrographs. Several GoF metrics, including IoA, Spearmans correlation coefficient, root mean square error (RMSE) and normalised RMSE (NRMSE) are plotted on Figure 9-5. The GoF metrics calculated are presented with regards to observed total discharge (Q_{Obs}) in Figure 9-5, as infrequent but larger magnitude rainstorm events contribute disproportionately to the redistribution soil resources in these environments (Wainwright, 1996; Martinez-Mena et al., 2001; Lane and Kidwell, 2003; Howes and Abrahams, 2003; Nearing et al., 2007; Michaelides et al., 2009; Turnbull et al., 2010a; Nearing and Hairsine, 2011; Puttock, 2013). NSE coefficients comparing observed against modelled hydrographs for individual events are reported in Appendix 5.

All GoF metrics examined indicated hydrograph similarity broadly increased with observed Q, and the positive relationships between accuracy of hydrograph prediction and observed total discharge (Q_{Obs}) concurs with earlier findings (Turnbull et al., 2010b). The positive relationship between GoF and event magnitude results from the greater sensitivity to errors in infiltration simulation when rainfall rates are close to infiltration rates (Wainwright et al., 2002; Turnbull et al., 2010b), compounded by shorter duration (typically smaller) events being more sensitive to errors in the timing pf simulated runoff (discussed further in section 9.7 and Figure

9-7). The NSE coefficients indicated limited performance of the hydrological component on the overall event assemblage, as just 44% (24/55) events had positive NSE coefficients and 20% (11/55) events have NSE coefficients >0.5.

There is no evidence of systematic changes in site average hydrograph GoF across the grass-shrub ecotone (Table 9.6, Appendix 5). This finding of no systematic change in site-average hydrograph GoF across the ecotone contrasts with earlier investigations, which found that found that average NSE increased from -0.09, -0.49, 0.81 and 0.73 for the grass, grass-shrub, shrub-grass, and shrub dominated sites, respectively (Turnbull et al., 2010b). Turnbull *et al.* interpreted this as suggesting MAHLERAN's hydrological component performed worst when simulating runoff events over the two grass-dominated plots, and suggested a need for improved derivation of empirical relationships for grass-dominated sites (Turnbull et al., 2010b).

This discrepancy in findings between different event assemblages is quite interesting. The presently considered assemblage of events was large relative to those typically employed for such evaluations of physically-based models (e.g. Wainwright et al., 2008a; Turnbull et al., 2010b), and was representative of the rainstorm events experienced at each site (See section 5.7). However, simple measures of central tendency afford equal credence to smaller runoff events which are hydrologically and geomorphically less significant than larger runoff events. Smaller events typically have poorer GoF metrics (Figure 9-5) and thus the absence of systematic trends in hydrograph GoF metrics across the grass-shrub ecotone may be caused partly by the 'noise' resulting from the inclusion of a greater number of small events in the assemblage. The highest average GoF values are reported for the shrub grass site, but this may be an artefact of this site also having the largest average runoff (see Appendix 5).

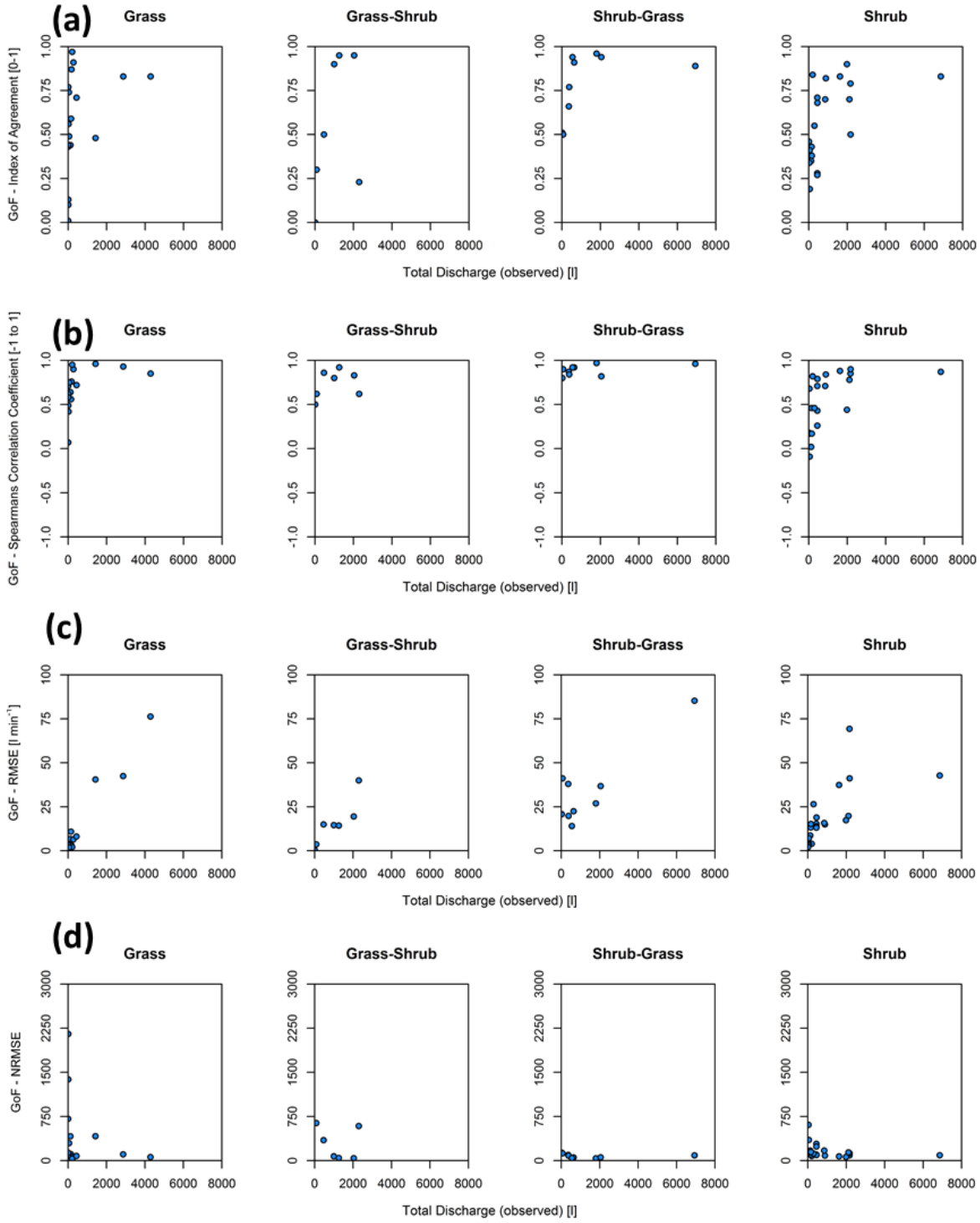

Figure 9-5. Goodness of Fit (GoF) metrics stratified by site and plotted against total observed discharge. (a) Index of Agreement (Willmott, 1981), (b) Spearman's correlation coefficient, (c) root mean square error, and (d) normalised root mean square error.

These considerations again raise the question of how robustly average GoF metrics can be compared between sites. Again, this issue substantiates the desirability of larger, more representative assemblages of rainstorm events, but also suggests that

comparing site averages in this way offers only limited insights. Possible avenues for further investigation into this aspect of the evaluation are discussed further in section 9.10.1.

Table 9.6. Mean (and median) average GoF metrics for each site.

	Site			
	Grass	**Grass-Shrub**	**Shrub-Grass**	**Shrub**
Nash-Sutcliffe Efficiency	-42.60	-1262855.48	0.23	-3.23
	(-0.22)	(-11.34)	(0.30)	(-0.56)
Index of Agreement	0.54	0.55	0.78	0.57
	(0.58)	(0.50)	(0.89)	(0.65)
Spearmans CC	0.67	0.74	0.89	0.54
	(0.68)	(0.80)	(0.90)	(0.68)

As MAHLERAN's infiltration component was sensitive to antecedent soil moisture (ASM) (Wainwright et al., 2008a; Turnbull et al., 2010b), the relationships between ASM and the accuracy of modelled Q, RC and hydrographs were also investigated (Figure 9-6). No trends were apparent in the relationship between ASM and either Residual Q or Residual RC, indicating that error in these summary metrics of total runoff was insensitive to ASM. In contrast, there were strong positive correlations between ASM and hydrograph goodness-of-fit (GoF index of agreement) at all four sites, which were statistically significant ($p \leq 0.05$) at three of the four sites (

Table 9.5). This positive correlation was most robust in the two sites representing vegetation end-members, which each had $n \geq 19$ events. To an extent, this positive correlation was expected because when ASM is high, infiltration into the unsaturated soil is less significant, and infiltration into unsaturated soils well known to be particularly difficult to predict (John Wainwright, pers. comm.). However, the correlation between ASM and hydrograph GoF was considered to be surprisingly strong, given that there was no normalisation by event magnitude. It is possible that there may be some temporal autocorrelation in rainstorm events, with the co-

occurrence of larger (better simulated) events causing wetter ASM for the next event. Larger magnitude events may overwhelm the possible influence of ASM on model performance; however, the *n* of each assembalge was not felt to be sufficient to support three-dimensional analysis of GoF, ASM and event magnitude.

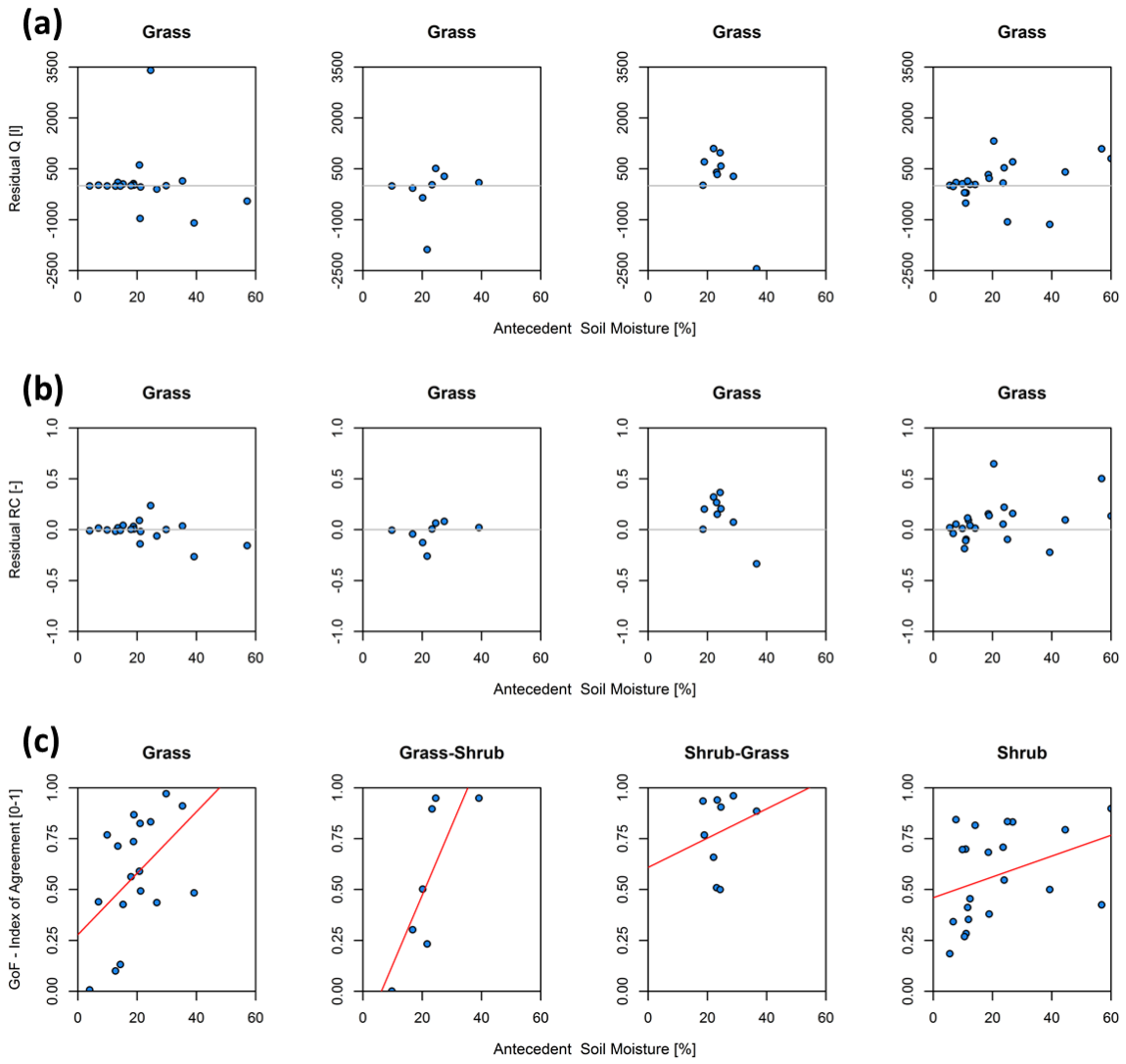

Figure 9-6. (a) Residual Q ($Q_{Sim} - Q_{Obs}$) plotted against antecedent soil moisture (ASM). (b) Residual RC ($RC_{Sim} - RC_{Obs}$) plotted against ASM. (c) Relationship between hydrograph goodness of fit and ASM. The red lines are linear models fitted using a least squares approach.

The systematic delay in predicted peak discharge for the shrub-dominated site, and the associated underestimated gradient of the rising limb and lagged recessional limb concurs with the earlier finding of Turnbull *et al*. (2010b). Lagged recessional limbs are characteristic of models implementing kinematic wave theory (Singh,

1996, 2001). Turnbull *et al*. posited that the delay in peak discharge may have been caused by underrepresentation of processes such as sub-minute variation in rainfall (e.g. Wainwright and Parsons, 2002) or soil surface crusting (after Luk and Cai, 1990; Luk et al., 1993). However, the prevalence of this systematic error in hydrograph timing within the much larger assemblage examined herein is suggested to be more indicative of errors in model parameterisation, most likely overestimation of *ff* and/or infiltration, rather than under-represented temporally variable processes.

9.7. Evaluation of Erosion Component

The erosion component of MAHLERAN was evaluated against the total sediment yield and particle size distribution observed at the plot output for each event, and monitored and modelled values are reported in Appendix 6. There is widespread recognition that when dependent models are evaluated, it is generally preferable to employ multi-function criteria to ensure that dependent model components are only evaluated when the predictions of the preceding model components can be considered 'reasonable' (Brazier et al., 2000; Wainwright et al., 2008a; Turnbull et al., 2010b). This logic is applicable to the present case, where the erosion component is dependent on the hydrologic component. Because of error propagation, no process-based erosion model can be better than the hydrology and hydraulics upon which it is founded (Wainwright et al., 2008a; Turnbull et al., 2010b).

Hydrograph goodness-of-fit (GoF) metrics are often used for such multi-function criteria, for example erosion components have been evaluated when preceding hydrological components yield NSE scores of >0.5 (Quinton, 1997; Morgan and Quinton, 2001), >0.65 (Turnbull et al., 2010b) or >0.725 (Wainwright et al., 2008b). However, GoF metrics such as NSE are sensitive to timing errors and therefore can underestimate model performance even when the magnitude and form of the simulated hydrograph is similar to the observed hydrograph (Jachner et al., 2007; Müller et al., 2009). This is exemplified by the Grass 2006-08-04 event, where the simulated hydrograph was very similar to the observed hydrograph in terms of total and peak discharge, and the steepness of the rising and falling limbs, but where a ca. 5 minute timing offset resulted in a NSE of just -0.48 (Figure 9-7). As the simulated hydrograph should result in similar geomorphic work to the observed hydrograph, it is consequently preferable not to rely solely on hydrograph GoF scores when evaluating whether hydrological component predictions are

behavioural for the present application. Therefore, simulations were considered to be hydrologically behavioural if either GoF-NSE was >0.5, or the simulated total discharge was within 30% of the observed total discharge. This dual criterion also allows MAHLERAN's erosion component to be evaluated for events when the hydrograph was not monitored fully, but where simulated total discharge was in agreement with observed total discharge.

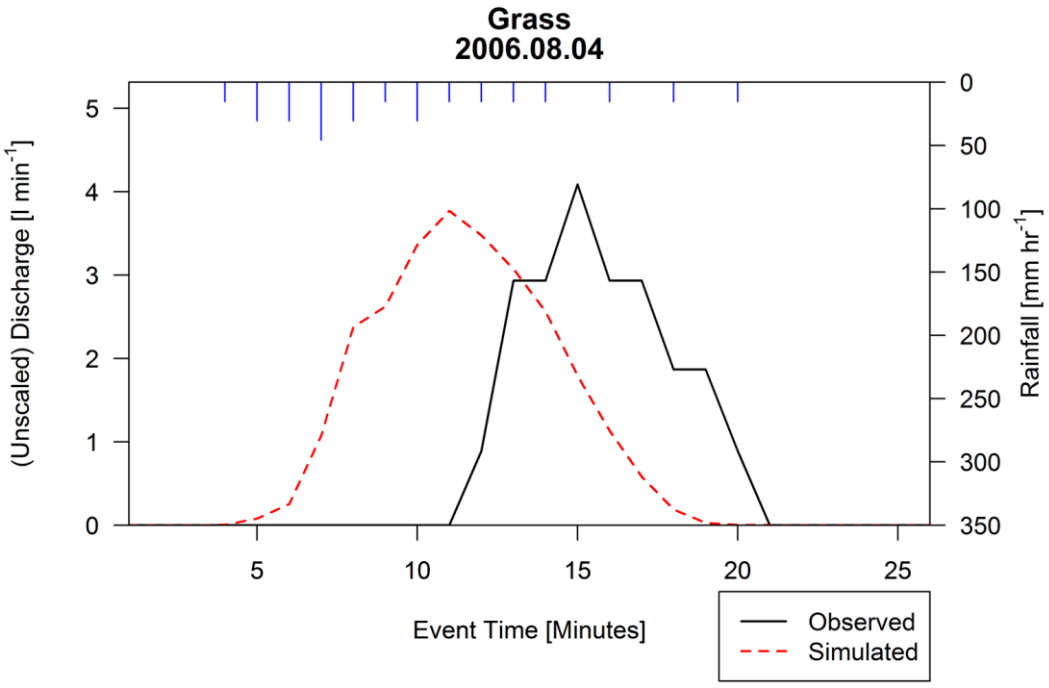

Figure 9-7. Example of timing error in hydrograph, resulting in poor goodness-of-fit metrics, when the overall hydrology influence on sediment transport was represented well (Q_{Obs} = 21.3 l vs. Q_{Sim} 26.4 l; Q_{Max_Obs} = 4.1 l min^{-1} versus Q_{Max_Sim} = 3.8 l min^{-1}) but NSE was -0.48.

Relative to the hydrological assemblages, observational data were only available for a smaller number of events, limiting evaluation of the erosional component. There was also an unquantifiable loss of fine material during runoff events which exceed the runoff tank capacities (Turnbull et al., 2010a, 2010b). Comparison of the particle size distribution of recovered sediment suggests that any such loss was not strongly selective of fines, as the finest (<0.0625 mm) particle size fraction was generally more enriched during tank-exceedance events compared to the average for all events (Cunliffe et al., 2016d), although this inference is complicated by the possible greater contribution of fine material from the microtopographic 'islands' during larger

magnitude events (see Figure 6-6) (Wainwright et al., 1995; Michaelides et al., 2012).

Simulated versus observed total sediment yields are compared in Figure 9-8, which suggests that excluding events which were not hydrologically behavioural did not substantially alter the correspondence between observations and simulations. Total sediment yield was best predicted at the Shrub-Grass site, followed by the Grass-Shrub site, and was systematically underestimated at the Shrub site (Figure 9-8). For all of the sites, simulated sediment yields were generally of the correct order of magnitude (Figure 9-8b), although an exception to this general conclusion is seen in the Grass 2005-09-07 event (discussed below). Modelled sediment yields were strongly and significantly correlated with observed sediment yields ($p \leq 0.02$, $Rho \geq 0.75$) demonstrating that the model generally simulates the correct rankings of sediment yield (Table 9.7). Nash-Sutcliffe Efficiency (NSE) coefficients were generally poor, usually below zero (Table 9.7), demonstrating that there is still considerable room for improvement (sensu Turnbull et al., 2010b).

One anomalous event (Grass 2005-09-07, Figure 9-4) had a simulated sediment yield of 46.91 kg, which far exceeded the observed sediment yield of 4.11 kg. As discussed in section 10.6, this event probably greatly exceeded to limits of the monitoring instillation, so there is limited confidence in the observed sediment yield, which must be viewed as an unquantifiable underestimate. The predicted sediment flux is consistent with the process representation of erosion in the model structure, with the large changes caused by activation of simulated flow detachment, due to simulated stream power in excess of the Bagnold threshold. This process-representation resulted in the particularly 'spiky' sedigraph, with a 10-minute lag between simulated peak discharge and simulated peak sediment flux, a function of the virtural velocity of the eroded sediment (Figure 9-4b). While this erosional behaviour is plausible (*sensu* Goldstein et al., 2013), it represent the limits of conditions under which the current model structure has been evaluated.

Simulated PSD was evaluated against observed PSD to support a more nuanced evaluation of MAHLERAN's erosion component than evaluation of total sediment yields alone, which is valuable given that sediment observations are already time-integrated from a single outlet location. Note that observed versus simulated sedigraphs for some of these rainstorm events were evaluated by Turnbull *et al*.

(2010b). The proportions of simulated and observed sediment in each model size class were compared for all events (Figure 9-9) and those events with hydrologically behavioural simulations (Figure 9-10).

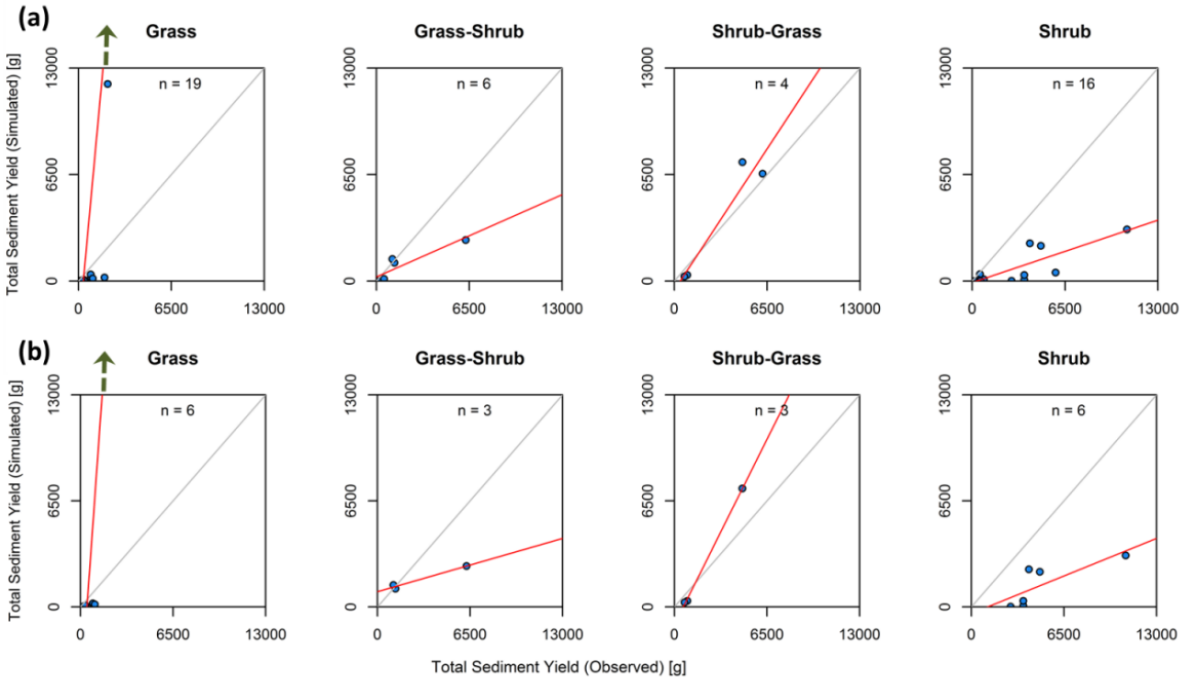

Figure 9-8. Comparisons of observed and modelled total sediment yield for (a) all events and (b) those with behavioural hydrological predictions. Note that axis scales are limited to 13 kg for visual presentation, excluding one anomalous event (Grass 2005-09-07, Figure 9-4) which is discussed further in the text.

Table 9.7. Statistical comparisons of modelled and observed sediment yields.

		Site			
Sediment yield		**Grass**	**Grass-Shrub**	**Shrub-Grass**	**Shrub**
All events	***n***	19	5	4	16
	Rho	**0.751**	**0.886**	**1.000**	**0.855**
	p	0.0002	0.0189	<0.0001	<0.0001
	NSE	0.102	-1.839	0.976	-7.034
Hydrologically behavioural events	***n***	6	*3*	*3*	6
	Rho	**0.943**	*Insufficient n*	*Insufficient n*	**1.000**
	p	0.0048	*Insufficient n*	*Insufficient n*	<0.0001
	NSE	-0.004	-11.666	-120.895	-9.854

MAHLERAN's erosion component generally over-estimated the proportion of finer particles (model size classes 1 and 2), under-estimated the erosion of coarse particles (model size classes 3, 4 and 5), and correctly simulated the absence of erosion of the coarsest (>12 mm) particle size fraction. Consequently, the simulated range of particle size classes eroded was narrower than the observed range. There was often compensatory error in the simulated proportion of material eroded in model size classes 1 and 2, with a large variance between the two classes.

Comparison of observed and simulated proportions of model size classes 1 and 2 exhibits less scatter around the 1:1 line for the hydrologically behavioural events (Figure 9-10) relative to all simulated events (Figure 9-9). This suggests that the erosion component is more behavioural when the hydrological component is more behavioural, although simulated PSD still exhibited limited correspondence with observed PSD. The model tends to overpredict the proportion of Phi 1 and underpredict the proportion of Phi 2 in the grass dominated plot, and underpredict the proportion of Phi 1 and overpredict the proportion of Phi 2 in the grass-shrub, shrub-grass and shrub dominated sites.

These PSD errors concur with previous evaluations of this modelling approach at sites at the Walnut Gulch Experimental Watershed in southern Arizona and at these same sites as studied herein (Wainwright et al., 2008a; Turnbull et al., 2010b). The PSD errors were likely caused by errors in the detachment and transport parameters, due to limited empirical information on these properties for discrete particle size classes (Wainwright et al., 2008a, 2008b, Turnbull et al., 2010b, 2014a). To address this knowledge gap, ongoing laboratory-based experimentation is being undertaken to continually refine the parameterisation of erosion models such as MAHLERAN (Turnbull et al., 2014a; e.g. Cooper et al., 2012; Long et al., 2014).

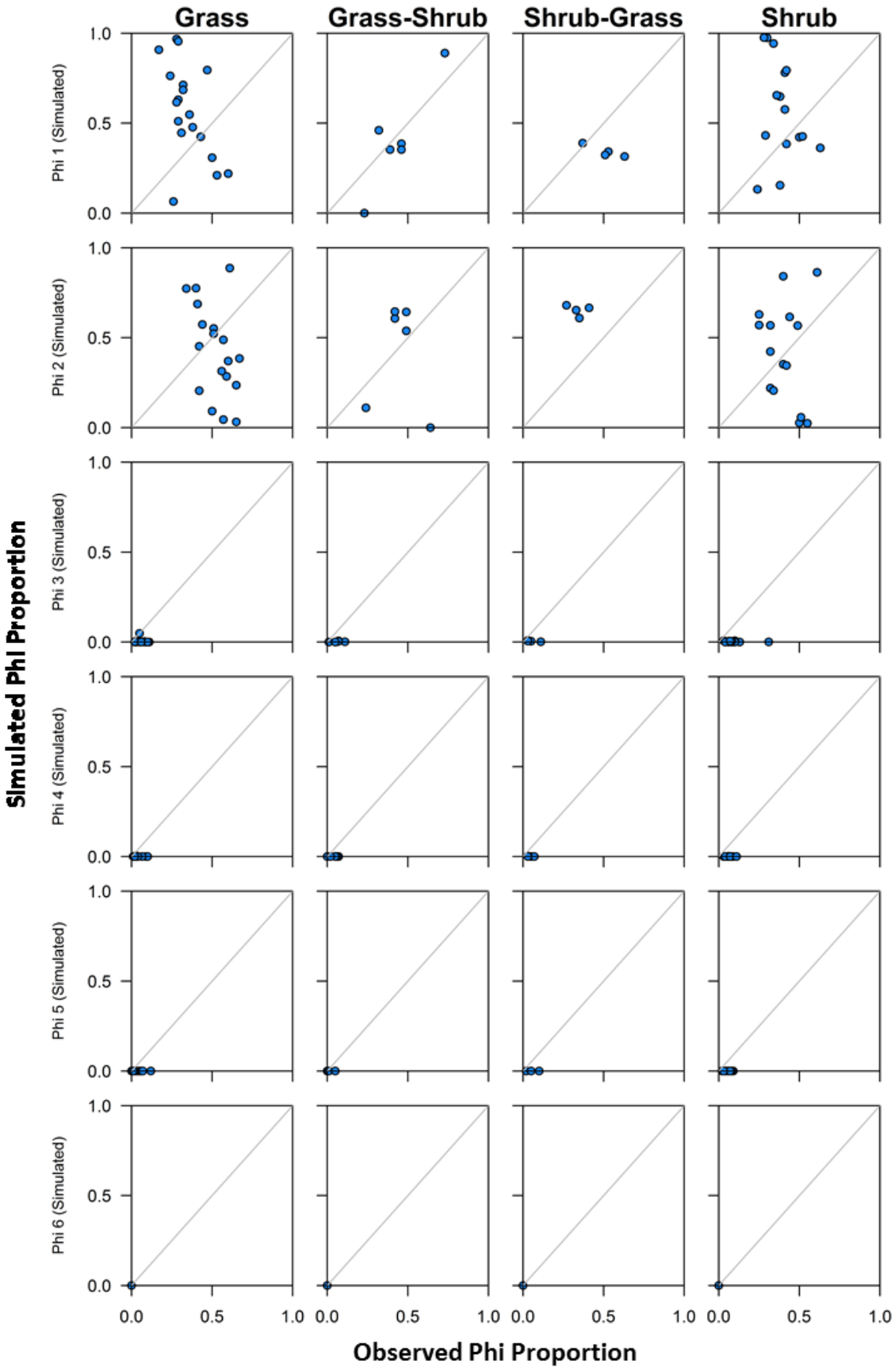

Figure 9-9. Comparisons of observed and modelled particle size distributions for all available events.

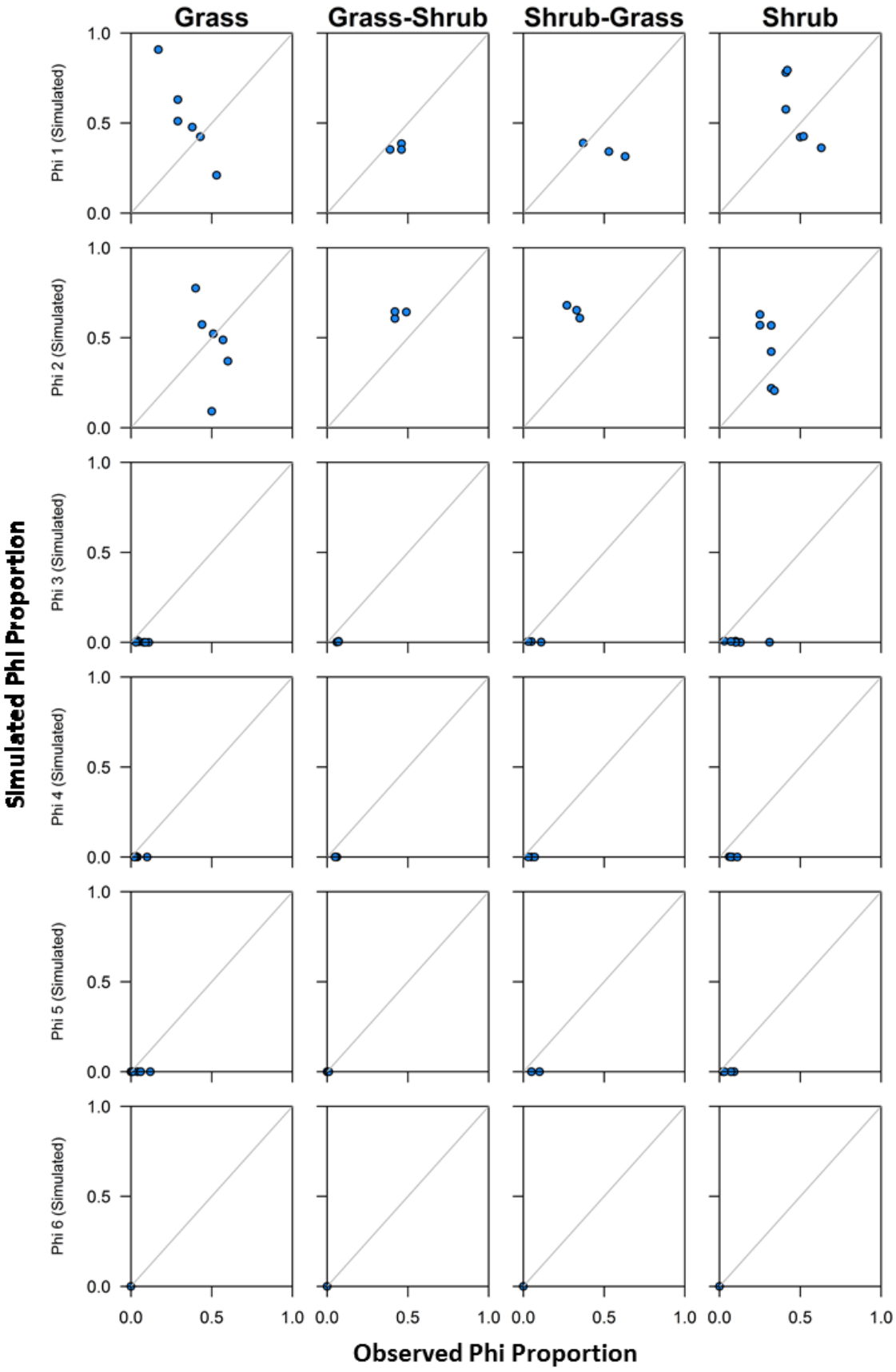

Figure 9-10. Comparisons of observed and modelled particle size distributions for available events where the hydrological component predictions were behavioural.

9.8. Evaluation of Carbon Component

To the author's knowledge, this is the first evaluation of the capacity of a physical process-based model such as MAHLERAN to simulate the redistribution of particulate inorganic and organic C in a dryland environmental context. This evaluation represents an important first step towards expanding the capacity to simulate these important processes within an existing integrated ecogeomorphic modelling framework.

To evaluate the *potential* capacity of this modelling approach to predict IC and OC fluxes, if the detachment, transport and deposition of sediment is modelled perfectly, modelled yields of IC and OC were compared to yields calculated using the observed sediment fluxes and the C content of the contributing near-surface soil for 37 erosion events (listed in Table 9.4). This calculated yield is equivalent to $\sum_{PSD}$ (described in section 6.5 and Cunliffe et al., 2016d), and was calculated for both IC and OC. This analysis was constructive as the intention of this modelling exercise was to evaluate the potential of this modelling approach as well as to simply test the predictive capacity of the current model (sensu Wainwright et al., 2008a; Turnbull et al., 2010b).

To evaluate the *current* capabilities of the modelling approach, the event yields of eroded IC and OC were compared against 27 discrete runoff events (see Table 9.4 for breakdown). Evaluation of model predictions against observed data represents a significant advancement compared to previous efforts to simulate erosional fluxes of particulate C in drylands, which have in some cases simply been unvalidated modelling exercises (e.g. Gabet et al., 2005; Turnbull, 2008).

9.8.1. Inorganic C

Figure 9-11 illustrates observed and calculated ($\sum_{PSD}$) IC yields (the latter the sum of the product of the each eroded mass and IC concentrations from the contributing topsoil of each particle size fraction). For all four sites, events plot reasonably close to the 1:1 line, indicating that erosional yields of IC can be simulated fairly well if the detachment, transport and deposition of eroded sediment is correctly predicted. This demonstrates the validity of this modelling approach to predict the erosional dynamics of IC at these spatio-temporal scales.

Particle size-specific parameterisation of erosion models used to simulate IC erosional dynamics is necessary because of the large differences in IC concentration between different particle size fractions (Figure 7-1). Notably, calculated ($\sum_{PSD}$) IC yields consistently overestimate observed IC yields (Figure 9-11). This over-estimation was by a constant factor, as evidenced by the low variance around the linear best-fit models and the similarity in the slopes of these linear models across all four sites. The consistency of this relationship is indicative that the over-estimation is caused by a mechanism that is not represented in the current implementation of the model. Several possible mechanisms contributing to this discrepancy are listed below, but it is not possible to differentiate between these with the present empirical support:

- IC-rich particles are less mobile (less readily detached and transported) compared to IC- poor particles; however, IC has a lower density to mineral soil (section 7).
- IC could be less readily available on the soil surface, due to translocation downwards within the soil profile (Breecker et al., 2009)
- Even at these spatio-temporal scales, the transport of IC may be non-conservative. Although previous monitoring at these sites found negligible DIC fluxes (Puttock, 2013) gaseous pathways are also possible, and this could indicate that this C pool is dynamic than commonly thought (see sections 3.2 and 7 for further discussion).

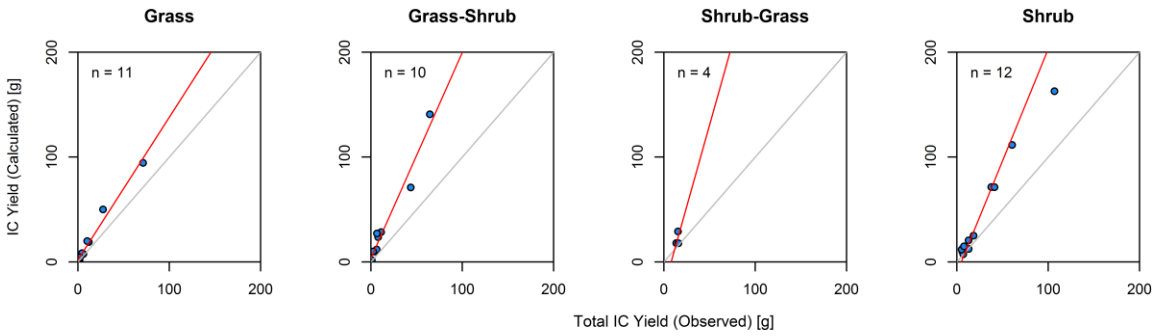

Figure 9-11. Comparison of observed and calculated IC event yields (the latter the sum of the product of the each eroded mass and IC concentrations from the contributing topsoil of each particle size fraction). Grey lines indicate 1:1 and red lines are linear best fit models.

Observed and simulated IC yields are compared in Figure 9-12. Model performance was generally poor, particularly in the two end-member sites with the largest number of events (≥9). Modelled IC yield was correlated with observed IC yield ($p \leq 0.04$, *Rho* ≥ 0.85), demonstrating that the model generally simulated the correct rankings of IC yield (Table 9.8). As within this model structure erosion dynamics are the primary control over particular-bound chemical export, simulated IC dynamics broadly mirror the erosional dynamics. When the erosion component is behavioural, the IC component is also behavioural. This finding is similar to previous evaluations of particle-associated nitrogen and phosphorus (Turnbull, 2008, p. 144; Turnbull et al., 2010b), and supports further efforts to refine MAHLERAN's erosional component. Even though a large assemblage of 37 discrete rainstorm events was analysed for IC dynamics, it was not considered a constructive exercise to investigate the small subset of IC events where the hydrologic and erosional components were both behavioural.

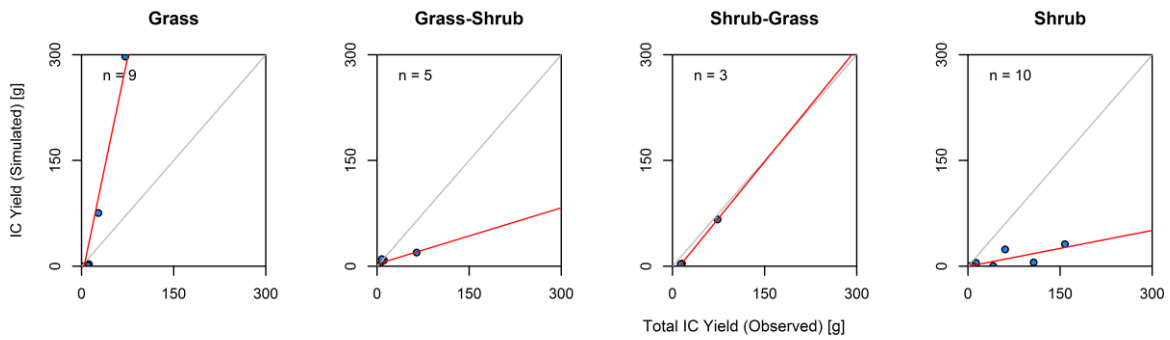

Figure 9-12. Comparison of observed and modelled total particulate-associated IC yield [g]. Grey lines indicate 1:1 and red lines are linear best fit models.

This evaluation contributes towards addressing the calls for improved capacity to model the redistribution of C by interrill erosion processes (Kuhn et al., 2009). The erosional dynamics of IC was previously simulated with MAHLERAN by Turnbull (2008), but no observational data were available then to evaluate predictions from those simulations. Furthermore, MAHLERAN's C component was parameterised using data from the Jornada research site (Lister, 2007), which has been found here to be very different from the present study sites (see section 7.5 and Figure 7-5 for further discussion).

Table 9.8. Statistical comparisons of calculated, modelled and observed IC yields.

		Site			
IC yield		**Grass**	**Grass-Shrub**	**Shrub-Grass**	**Shrub**
Calculated vs. observed	***Rho***	**0.973**	**0.988**	**0.400**	**0.944**
	p	<0.0001	<0.0001	0.600	<0.0001
	NSE	0.855	0.523	0.311	0.568
Modelled vs. observed	***Rho***	**0.979**	**0.900**	*Insufficient n*	**0.845**
	p	<0.0001	0.0374	*Insufficient n*	0.0021
	NSE	0.316	-7.269	0.888	-25.034

9.8.2. Organic C

This evaluation contributes towards addressing the calls for improved capacity to model the redistribution of C by interrill erosion processes (Kuhn et al., 2009). As with IC, observed OC yields were compared against calculated OC yields to evaluate the potential of the modelling approach to simulate the redistribution of OC if the sediment dynamics were predicted perfectly. Figure 9-13 illustrates observed and calculated ($\sum_{PSD}$) OC yields (the latter the sum of the product of the each eroded mass and OC concentrations from the contributing topsoil of each particle size fraction). The information presented in Figure 9-13 is similar to Figure 6-3b, which has been extensively discussed in chapter 6 and Cunliffe *et al.* (2016d). To recap briefly, even if the erosion dynamics of sediment were predicted perfectly, predictions of OC yields will be substantially underestimated due to OC enrichment in the eroded material. This OC enrichment is likely due to selectivity in detachment, transport and deposition processes, and the magnitude of the enrichment-induced error increases systematically across the grass-shrub ecotone.

Models such as MAHLERAN, which simulate the erosion of discrete particle size classes, represent OC enrichment due to particle size selectivity (assuming that selectivity *within* modelled particle size classes is negligible). However, recent work has demonstrated that the enrichment of fine particles alone cannot explain observed OC enrichment (Z. Wang et al., 2010; 2013; Chartier et al., 2013); for example, on average particle size selectivity alone only explains and average of 6% (maximum of 67%) of OC enrichment observed in sediment eroded from these sites (chapter 6) (Cunliffe et al., 2016d). This suggests that the role of particle size selectivity in explaining observed OC enrichment may be overstated. Consequently, the assumption that all particles within a discrete particle size class have identical OC concentrations and transport characteristics is invalid. Within particle size fractions these attributes co-vary, commonly attributed to the low density of OC relative to mineral soil which results in OC-rich particles being more readily detached and transported, and less likely to be deposited (Lal, 2005; X. Wang et al., 2014c; Cunliffe et al., 2016d). The selectivity for OC-rich particles in the present study is thought to be caused by differences in particle density (chapter 6) (Cunliffe et al., 2016d).

The current model structure can only represent OC enrichment caused by particle size selectivity, but this mechanism only accounts for a tiny fraction of the observed

OC enrichment. Because differences in OC concentration between particle size classes were relatively small (Figure 6-1a), particle size class specific parameterisation of OC concentrations will not make much difference to the accuracy of simulated OC dynamics. The finding that OC enrichment varies systematically and significantly between vegetation communities suggests that better simulating OC enrichment dynamics across the grass-shrub ecotone may also require the representation of enrichment to account for differences between vegetation type (Cunliffe et al., 2016d). Vegetation type is not currently considered by MAHLERAN's model structure.

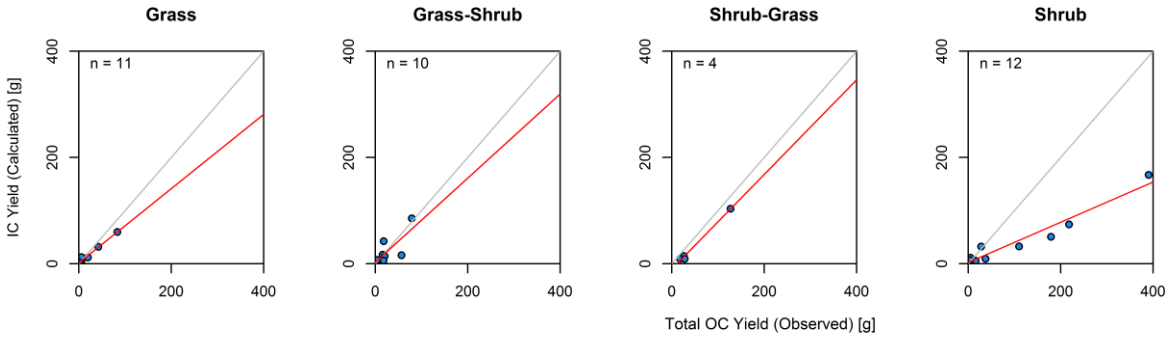

Figure 9-13. Comparison of observed and calculated OC event yields (the latter the sum of the product of the each eroded mass and OC concentrations from the contributing topsoil of each particle size fraction). The assemblages include all events with quantified OC fluxes, grey lines indicate 1:1 and red lines are linear best fit models.

As with the IC evaluation, because within MAHLERAN's model structure erosion dynamics are the primary control over particular-bound chemical export, simulated OC dynamics broadly mirror the erosional dynamics. Modelled OC yield was correlated with observed IC yield ($p \leq 0.04$, $Rho \geq 0.85$), demonstrating that the model generally simulated the correct rankings of OC yield (Table 9.9). However, as discussed above, even when the erosion component is behavioural, the OC component is not behavioural, due to unrepresented processes leading to OC enrichment. This relationship is fundamentally different to the findings for the IC component (9.8.1) and that previously found for particle associated nitrogen and phosphorus (Turnbull, 2008, p. 144; Turnbull et al., 2010b). This finding suggests that to simulate the erosional dynamics of OC this model structure must be

expanded to include more explicit representation of enrichment processes, and some suggestions on implementing this are offered in section 9.10.3.

Even though a large assemblage of 37 discrete rainstorm events was analysed for OC dynamics, it was not considered a constructive exercise to investigate the small subset of IC events where the hydrologic and erosional components were both behavioural.

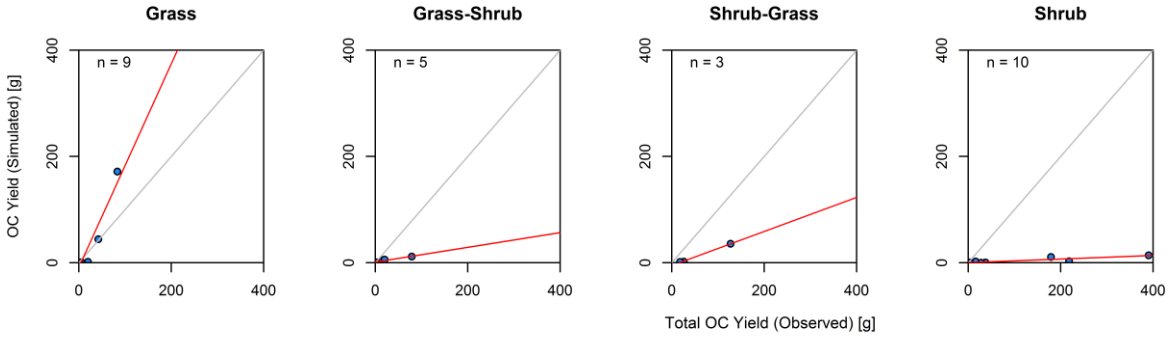

Figure 9-14. Comparison of observed and modelled total particulate-associated OC yield [g]. Each group includes all modelled events with quantified OC fluxes. Grey lines indicate 1:1 and red lines are linear best fit models.

Table 9.9 Statistical comparisons of calculated, modelled and observed OC yields.

		Site			
OC yield		**Grass**	**Grass-Shrub**	**Shrub-Grass**	**Shrub**
Calculated vs. observed	***Rho***	**0.946**	**0.721**	**0.400**	**0.923**
	p	<0.0001	0.019	0.600	<0.0001
	NSE	0.767	0.577	0.824	-2.692
Modelled vs. observed	***Rho***	**0.850**	**1.000**	*Insufficient n*	**0.927**
	p	0.0037	<0.0001	*Insufficient n*	0.0001
	NSE	0.688	-54.832	-11.088	-954.619

9.9. Summary

Numerical modelling approaches are an essential tool for understanding the effects of vegetation change on ecosystem C dynamics over greater than observable spatio-temporal scales. This chapter seeks to refine, extend and evaluate a process-based modelling approach, contributing towards the combination of erosion modelling with biogeochemical cycling modelling in a fully-integrated, spatially-explicit modelling approach.

In one of the most comprehensive evaluations to date, the event-based version of MAHLERAN was evaluated against detailed field measurements of water, sediment and C fluxes, measured at the outlets of four runoff plots each with different types and amounts of vegetation cover. A large number (n = 59) of natural rainstorm events with varied antecedent soil moisture and precipitation characteristics enabled evaluation of the model across a wide range of conditions, supporting a more robust evaluation than has previously been possible.

An important motivation for this evaluation exercise was to improve confidence of the capacity of MAHLERAN's deterministic process representations to emulate the behaviour of the processes over the observable spatial (hillslope) and temporal (event) scales considered herein. While it is well understood that models which perform well at one spatio-temporal scale are no guarantee of model performance at other spatio-temporal scales, such appraisals provide an important foundation to the application of these process representations over greater spatio-temporal scales (Müller et al., 2014b). Versions of MAHLERAN are already being used for such upscaled ecogeomorphic modelling efforts (sensu Stewart et al., 2014; Müller et al., In Review). A number of minor refinements to the model code were also made, improving both the stability and versatility of the model and thus supporting a wider research community.

Evaluation of the hydrological component found that the hydrological predictions were generally plausible across a wide range of conditions, such as antecedent soil moisture contents and rainfall inputs. Simpler summary descriptors of prediction accuracy (*i.e.* total discharge, runoff coefficient, peak discharge) typically indicated better performance than more discerning goodness-of-fit evaluations of the predicted hydrographs. Meta-analysis of the simulation of a larger number of separate rainstorm events allowed refinement of several previous findings, for

example indicating that errors in the hydrological predictions obtained for the Shrub-Grass site are more likely due to issues with spatial parameterisation rather than under-representation of temporally-variable processes in the model structure.

Evaluation of MAHLERAN's erosion component showed that over all four sites the model is generally able to reproduce the observed order of magnitude of sediment yield, and reproduces the relative order of the observed sediment yields. The evaluation of predicted particle size distributions indicates greater errors, with over-estimation of the erosion of fines and under-estimation of coarser particles. This finding corroborates earlier studies, and reinforces calls for ongoing empirical work to better parameterise the detachment, transport and deposition characteristics of discrete particle size classes.

This chapter represents the first effort to evaluate the representation of the erosional dynamics of C in this process-based model. This evaluation increases understanding in the capability of MAHLERAN to reproduce the erosional dynamics particle-associated C redistribution in semi-arid landscapes. When sediment dynamics are predicted well, IC fluxes were predicted well, although there was a small but consistent over-estimation of IC yields by the model, indicating that the present model structure is not a complete representation of IC redistribution.

Comparison of the calculated and simulated OC yields indicated that even when sediment dynamics were predicted well, OC dynamics would be predicted poorly. This was due to under-representation of OC enrichment, which results from selectivity in detachment, transport and/or deposition processes. The current model structure does represent selectivity due to particle *size*, but this explains only a small fraction of the observed enrichment. Differences in particle density between OC-rich and OC-poor particles are thought likely to be significant in enrichment processes (discussed further chapter 6 and Cunliffe *et al.* (2016d)).

In summary, the modelling work undertaken in this chapter has supported valuable advances in understanding the present and potential capabilities of such modelling approaches. Evaluation of the larger number of events has enabled more nuanced evaluation of the model components than has previously been possible, and refinements to the model code will support other users of this research model. Deterministic modelling approaches are often limited by their high requirements for parameterisation data (section 3.4.1). The proximal remote-sensing approaches

developed in this thesis contribute to alleviating this limitation, at least for topographic, surface cover and vegetation /biomass parameters (chapter 8) (Cunliffe et al., 2016b). Possible avenues for future modelling work are explored in section 9.10.

9.10. Future Modelling Work

This section outlines some possible avenues for future work to advance the modelling approach promulgated above:

9.10.1. Refining Hydrological Component Evaluation

The evaluation of MAHLERAN's hydrological component indicated no systematic differences in predictive accuracy across the grass-shrub transition (section 9.6), which was contrary to previous findings that there were systematic differences with worse model performance in the grass-dominated sites (Turnbull et al., 2010b). The previous finding had been interpreted as indicating limitations of the model structure when applied to grass-dominated landscapes (Turnbull et al., 2010b). As discussed in section 9.6, the present null finding may arise from the site averages being skewed through the inclusion of a greater number of smaller rainstorm events in the assemblages, which typically have poor hydrograph GoF (Figure 9-5). Consequently, it could potentially be constructive to subset events by magnitude of total discharge prior to calculating site average GoF metrics for classes of event magnitude, which could support more nuanced inferences about when the current model structure was more or less behavioural and thus inform future efforts to refine the hydrological component of MAHLERAN. However, this must be done carefully to ensure that there are sufficient events within each magnitude class for such an exercise to be informative.

A further, complex but likely constructive line of enquiry could be to undertake an in-depth investigation of the sensitivity of MAHLERAN's hydrological component to the spatial grain of parameterisation data. Numerical simulations of the movement of water over hillslopes are usually highly sensitive to the parameterisation of (i) topography, (ii) infiltration rate, and (iii) surface roughness. Hydrological prediction depends strongly on accurate characterisation of spatial patterns in these surface properties (Merz and Plate, 1997; Michaelides and Wainwright, 2002; Calvo-Cases

et al., 2003; Michaelides and Wilson, 2007). Therefore, improving the spatially-explicit representation of surface properties would improve the accuracy of hydrological predictions and consequently the representation of bio-geomorphic processes arising from hydrological predictions.

Topography influences both the routing and velocity of overland flow (Zhang and Montgomery, 1994; Parsons et al., 1997). Coarser resolution topographic representations reduce flowpath lengths (Garbrecht and Martz, 1994; Yin and Wang, 1999; Rojas et al., 2008), influencing represented hydrological connectivity and the timing of runoff arrival at a catchment outlet (Parsons et al., 1997; Hessel, 2005). Velocity is sensitive because roughness coefficients such as the Darcy-Weisbach friction factor (*ff*) are highly sensitive to slope (Parsons et al., 1997; Müller, 2004; Müller et al., 2007b; Tatard et al., 2008), and slope values decrease at coarser cell resolutions (Zhang et al., 1999; Yin and Wang, 1999; Hessel, 2005; Rojas et al., 2008; Hutton, 2012). Infiltration rate is an essential parameter for calculating runoff generation caused by infiltration-excess mechanisms, and, in more sophisticated model structures, unsatisfied infiltration capacity can be deducted from runon flow to represent transmission loss (e.g., Wainwright et al., 2008c). Surface roughness, represented via parameters such as friction factors (*ff*) is important for hydraulic calculations controlling flow velocity (Scoging, 1992), and is inherently scale-dependent.

The premise here is to utilise newly available, accurate data sources for spatially explicit parameterisation of the model structure. Such investigation is only possible because of the large advances in efficiently acquiring parameterisation data at fine spatial grains developed in Chapter 8 (Cunliffe et al., 2016b). Readily available spatially explicit products now include digital maps of topography, and vegetation cover and type at 1 cm^2 grain (Appendix 3). Furthermore, given the inherent variability in the hydrological responses to natural rainstorm events, the large assemblage of natural rainfall events compiled herein is invaluable for evaluating such investigations into model parameterisation scale against observed reality.

Sensitivity to grid resolution is a fundamental property of finite difference modelling approaches; however, despite a number of investigations (e.g. Parsons et al., 1997; Wainwright et al., 2008b), the influence of grid resolution on the predictions of hydrological/hydraulic models is often not well understood, especially in the case of

spatially distributed, process-based models. While increasing the complexity of parameterisation can increase model uncertainty, understanding how the hydrologic component's capability to reproduce natural rainfall events varies with the spatial grain of key parameters potentially offers valuable insights into the process-basis of models such as MAHLERAN. Insights from such work would help to address calls for efforts to better understand the complex interactions between multiple, simultaneous spatially varying parameters with hydrological models (Michaelides and Wilson, 2007).

Readily measured surface properties include topography, vegetation cover and type (Chapter 8) (Cunliffe et al., 2016b). Although infiltration rates and roughness factors are not directly observed, these properties differ significantly between surface covers (Tromble et al., 1974; Abrahams and Parsons, 1991; Bhark, 2002; Bhark and Small, 2003; Müller, 2004; Müller et al., 2007a, 2007b) and therefore could be predicted using empirical relationships (e.g. Table 9.10). Note however that further empirical investigations may be appropriate to better understand the variance in these relationships between observable surface cover and inferred roughness and infiltration (e.g. Neave and Abrahams, 2002).

Table 9.10. Empirically-derived estimates of *ff* and K_{sat} values for different surface covers (from Müller, 2004; Müller et al., 2007a, 2007b).

Surface Cover	*ff*	K_{sat} [mm hr^{-1}]
Bare	1	11
Creosotebush shrub	20	33
Black Grama grass	114	106

The sensitivity of hydrologic predictions to parameterisation scale is likely to vary systematically across the grass-shrub ecotone, with less sensitivity at very fine grains in shrub-dominated landscapes. The sensitivity of hydrologic predictions is also likely to vary with event magnitude, with less sensitivity in larger magnitude events (as micro-topographic controls on overland flow are inundated). The rationale for this hypothesis is complex, and space limitations mean that it is not possible to offer a detailed exposition here.

Critically, to be constructive, such a sensitivity experiment requires unfilled topographic models (see section 9.4.2 for discussion), which in turn requires an

overland flow routing function capable of dynamic overtopping local minima. Although such overland flow routing functions exist, they have not yet been implemented in MAHLERAN. Therefore, integrating automatic overtopping routines should be a priority for the future development of this modelling approach.

9.10.2. Refining Sediment Component Evaluation

As described in section 9.7, MAHLERAN's erosion component performs poorly in terms of predicting the particle size distribution of eroded material. This is attributed to errors in the detachment and transport parameters for different particle size classes, and resolving this empirical knowledge gap requires further laboratory-based experimentation (e.g. Cooper et al., 2012; Long et al., 2014). Note that scale-dependencies in the current sediment transport component (Wainwright et al., 2008b) mean that the investigation into model sensitivity to parameterisation scale described in section 9.10.1 cannot yet be extended to the sediment transport component.

9.10.3. Improving Representation of OC Enrichment

As described in section 9.8.2, simulating the erosion-induced redistribution of OC will require refinement to MAHLERAN's model structure, in order to represent the processes leading to OC enrichment in eroded material. Such refinements are essential if these modelling approaches are to be applied over a greater range of spatial and temporal scales (Nadeu et al., 2011, 2012). OC enrichment is caused by selectivity in detachment, transport and deposition processes. This selectivity has frequently been attributed to particle size selectivity (e.g. Nelson et al., 1994; Balesdent et al., 1998; Guibert et al., 1999; Rhoton et al., 2006; X. Wang et al., 2013); however, empirical evidence suggests that particle size selectivity alone accounts for a small proportion of overall OC enrichment (Sharpley, 1985; Wang et al., 2010; Z. Wang et al., 2013; Chartier et al., 2013; Cunliffe et al., 2016d) (sections 6.4.2 and 6.5.3). OC is commonly associated with lower density particles relative to the mineral rock, causing them to be more readily detached, transported and less readily deposited (Cambardella and Elliott, 1994; Quiroga et al., 1996, 1998, Lal, 2001c, 2003; Wang et al., 2010; Meixner et al., 2012; Z. Wang et al., 2013; X. Wang et al., 2014c).

Such density-mediated selectivity could be represented in a process-based model such as MAHLERAN. Therefore, some first steps were taken towards implanting such process representation by modifying MAHLERAN's sediment transport component to explicitly consider differences in the user-specified particle density (as described in section 9.4.1). Preliminary testing indicated that these modifications functioned as expected, with lower density parameters resulting in greater predicted sediment yields. This is promising as it offers a process-based means of representing OC enrichment due to density-driven selectivity, rather than simple empirical coefficients which scale poorly (e.g. Bouwman, 1989; Lee et al., 1996; Starr et al., 2001; Post et al., 2001).

The revised version of MAHLERAN will therefore support future numerical experiments exploring the influence of variable particle density in explaining observed OC enrichment. For example, multiple density classes could be simulated, including a lighter OC-rich and heavier OC-poor cases, with the OC contribution from both classes combined to estimate a plot yield. Such explicit treatment of different density classes is supported by the findings of Wang *et al*. (2014b), who demonstrated that low density OC-rich particles were preferentially eroded. Such discretisation is a simplification, but may be sufficient to account for much of the processes leading to OC enrichment. Another attractive aspect of this approach is that it could also be extended in the future to incorporate the transport of a third class of particle, the low (<1 g cm^3) density organic matter (including leaf litter) which potentially accounts for a substantial proportion of the OC laterally redistributed on semi-arid hillslopes (section 6) (Cunliffe et al., 2016d; Lister, 2007). Such exploratory numerical experiments could inform future empirical monitoring in a two-way dialogue between modelling and empirical approaches (*sensu* Grayson et al., 1992; Bras et al., 2003; Epstein, 2008; Wainwright et al., 2010; Turnbull et al., 2014a).

Parameterisation of the multi-density simulation experiments outlined above would require three additional model parameters: the (i) density and (ii) OC concentration of the OC-rich sediment class, and (iii) the scaling factor used to scale the event OC fluxes from each simulation. To inform the possible parameterisation of such an exploratory modelling experiment, a provisional pilot study was undertaken characterise OC concentrations of multiple density fractions for sediment eroded during one event (Grass-Shrub 2010-07-25). Density fractionation was undertaken using sodium polytungstate (SPT), with a density of 1.8 g cm^{-3} (described in section

5.3.2). Recovery ratios for each size fraction ranged from 72-95%, and, of the recovered material, 76-90% by mass was denser than 1.8 g cm^{-3} (Figure 9-15). The OC concentration of the lighter 1-1.8 g cm^{-3} fractions were >25 times that of the dense >1.8 g cm^{-3} fraction in ¾ cases. The much smaller difference in OC concentrations between the light and dense fractions observed in the finest (<0.0625 mm) particle size fraction may reflect incomplete separation of fine particles by density and/or the possible loss of very fine (<0.02 mm) particles.

Following this pilot study, a modelled OC-rich fraction could have a density of 1.40 g cm^{-3} and an OC concentration of 25 times that observed in the 'normal' fraction. A scaling parameter could be 4:1; i.e., the combined OC flux would comprise of 80% of the OC flux associated with the 'normal' fraction and 20% of the OC flux associated with the 'OC-rich fraction'. More complex approaches to combine modelled OC fluxes are not readily supported by the currently available empirical data. Time constraints meant that it was unfortunately not possible to develop this line of inquiry further in the present study.

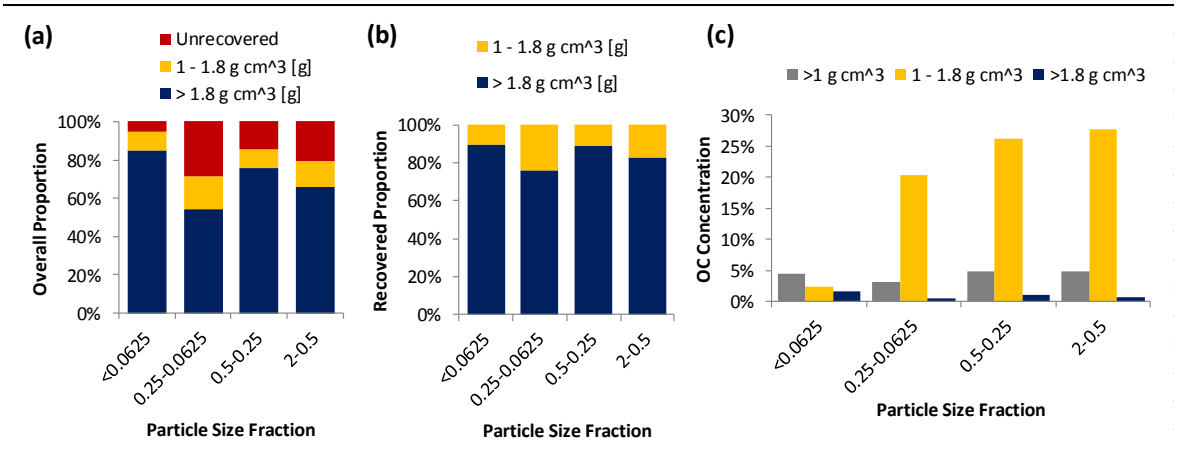

Figure 9-15. Results from multi-density fractionation experiment. (a) Proportion of recovered light (1-1.8 g cm^3) and dense (>1.8 g cm^3) mass relative to original mass. (b) Proportion of light (1-1.8 g cm^3) and dense (>1.8 g cm^3) mass recovered (assuming material loss was independent of density) (c). OC concentrations for each size/density fraction.

10. Synthesis

10.1. Chapter Overview

Terrestrial ecosystems are changing in a variety of ways, altering the provision of ecosystem services which support human activities at a variety of spatial scales. These services include the storage and sequestration of atmospheric C in the terrestrial ecosystem (CCSP, 2007; Stringer et al., 2012; IPCC, 2013). It is necessary to understand how these ecosystems function in order to predict how they and the services they support may change in the future, in response to chances in land management strategies, climate or regimes, for example (Thomey et al., 2014).

This chapter synthesises the collective findings from the preceding chapters to develop mutually consistent understanding of C dynamics in these dryland ecosystems. This synthesis contributes to calls for efforts to better understand the influence of degradative processes on C dynamics (Lal et al., 2001a; Brazier et al., 2013), and achieves the overall aim of this thesis of advancing quantitative understanding of the spatial distribution and erosion-induced redistribution of C in semi-arid rangelands. The measured stocks and fluxes of C are presented in sections 10.2 and 10.3, respectively. An evaluation of the overall stability of the ecosystem state with regards to data-based mechanistic understanding is presented in section 10.4, and finally thoughts on future research directions are presented in section 10.5.

10.2. Comparison of Carbon Pools

10.2.1. Intra- and Inter-Site Carbon Pools

The most important finding with regards to C pools is that the widespread assumption that >2 mm clasts contain insignificant amounts of SOC is not valid in these calcareous dryland soils. Coarse (>2 mm) clasts accounted for 24~38% of the SOC and 67~76% of the SIC stocks in the near-surface soil (Chapters 6 and 7). Critically, standard protocols for SOC analysis assume that coarse (>2 mm) clasts are free of SOC (see discussion in Chapter 6). Investigations using these protocols are therefore are likely to substantially underestimate SOC stocks in similar dryland

environments. These same sampling/analysis protocols have sometimes been applied to the study of SIC (e.g. Bird et al., 2002; Rhoton et al., 2006; Lister et al., 2007; Ewing et al., 2007; Puttock, 2013; X. Wang et al., 2015), which has potential to result in an even larger underestimate of SIC stocks relative to the underestimate of SOC stocks (Chapters 6 and 7). Such omissions can potentially lead to misleading conclusions regarding the storage and movement of C through these systems (Cunliffe et al., 2016d).

The combined total C stock in the three pools (biomass, SOC and SIC) ranges from 1815~2869 g C m^2. Although the inventory presented herein is more comprehensive and accurate than previous efforts (e.g. Puttock, 2013; Puttock et al., 2014; Brazier et al., 2013), it should be noted that these inventories of C stocks are not all-inclusive. Measured stocks did not include either necromass (e.g. leaf litter) (Encinales, 2016) or the full soil profile, as accurate information on soil depth is difficult to obtain in these dryland soils which are frequently characterised by hardened caliche layers. The exclusion of possible C storage in deeper soils likely accounts for much of the discrepancy with the average C stock for warm deserts of 6700 g C m^2 suggested by Zhu and Reed (2012, p. 9).

There are significant differences in chemical kinetics between organic and inorganic forms of soil C (Holmén, 2000), which were therefore considered seperatly thoughout this thesis. Because of these differences, investigations into spatial patterns of total soil C (e.g. Turnbull, 2008, pp. 77–78) can offer only limited insights into the mechanisms controlling the dynamics of these C pools. Of the three C stocks considered in this analysis, organic C in biomass, and organic and inorganic C in the near-surface (0~0.05 m^{-1}) soil, the overall C stock is dominated by the SIC stock (Figure 10-1). SIC and SOC account for 82~86% and 13~15%, respectively, of the total C stock in these three pools. The proportion of total C in the biomass pool decreases systematically across the grass-shrub ecotone, from 2.6%, 1.7%, 1.5% and 0.7% of the total C stock in the grass, grass-shrub, shrub-grass and shrub dominated plots respectively.

Measurements of terrestrial C stocks, particularly C associated with biomass, are often characterised by high, poorly constrained, uncertainties caused by spatial heterogeneity compounded by limitations in measurement techniques (Hill et al., 2013) (see section 3.3.1 for further discussion). Herein, a novel, inexpensive

technique for biomass estimation was developed, using consumer grade cameras and lightweight drones, which is highly complementary to existing monitoring programs (Chapter 8) (Cunliffe et al., 2016b). Importantly, this method quantifies biomass associated with both large and small plants, and careful treatment of errors affords high confidence in the estimates of biomass C stocks presented herein, within the stated uncertainties.

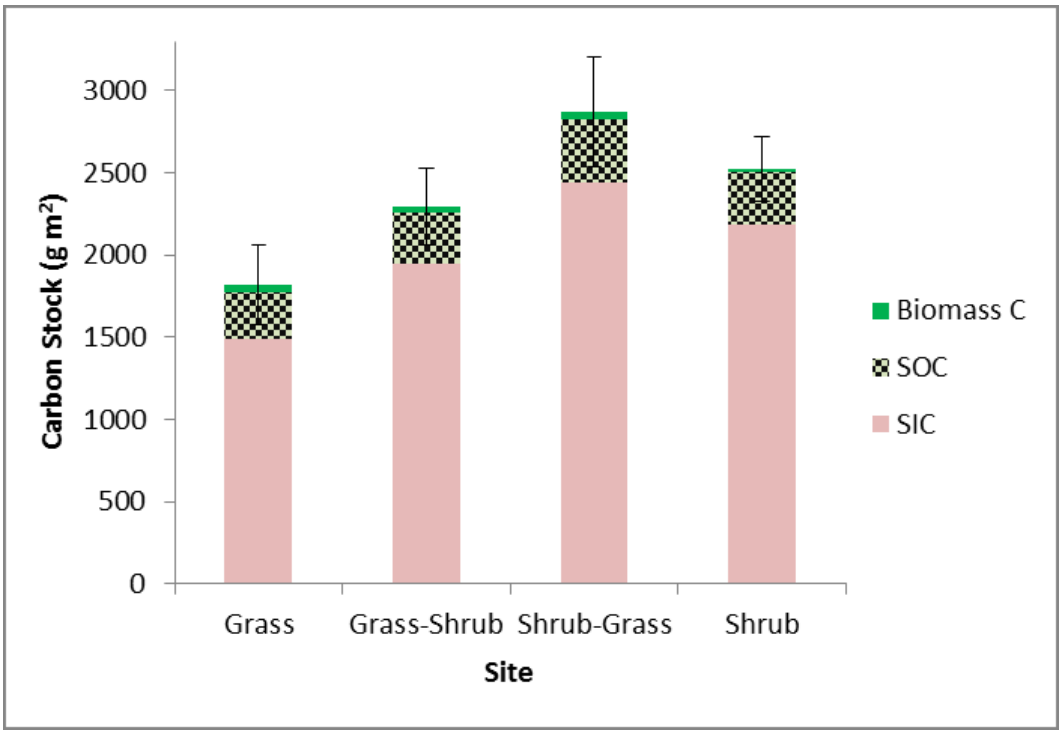

Figure 10-1. Carbon inventory of the three C stocks considered in this analysis, biomass, near-surface SOC and near-surface SIC. Error bars represent the cumulative uncertainty, propagated in quadrature. For the uncertainties associated with individual components, please refer to chapters 6, 7 and 8.

The distribution of C between different pools does contrast with observations from similar semi-arid sites. For example work at the Jornada in southern New Mexico, USA reported soil OC stocks were higher than IC stocks in non-calcareous soils (Lister, 2007), although again detailed comparisons are impeded as that study assumed that there was no OC or IC in coarse >2 mm particles. Although the biomass C pool is small relative to the soil C stocks, it is important to the C dynamics of these landscapes, as water-limited photosynthesis mediates the biotic inputs of OC into these soils. Biomass C stocks in drylands are highly dynamic (e.g. Figure 3-1) (Poulter et al., 2014; Ahlström et al., 2015; Cunliffe et al., 2016b), due to the

high variability in rainfall and episodic destruction of biomass though combustion, as well as longer term phenomena such as changes in dominant plant functional type, for example woody shrub encroachment (Pacala et al., 2007) (discussed further in Section 3.3.1). These processes can result in large relative changes in biomass C stocks, across a range of spatial and temporal scales. Indeed, as described in Section 3.3.1, global modelling studies have suggested that vegetation change in dryland ecosystems is the largest control on both long term trends and interannual variability in the global terrestrial C sink (Poulter et al., 2014; Ahlström et al., 2015; Murray-Tortarolo et al., 2016), although it must be noted that the empical basis for these model predicitons is limited.

10.2.2. Differences in Soil C Pools Between Individual Surface Covers (Microsites: *i.e.* bare soil, grass-covered or shrub-covered)

Stocks of inorganic and organic C were compared for all surface cover microsites (bare interplant, grass-covered and shrub-covered). SIC stocks were much greater than SOC stocks for all three microsites considered, with SOC accounting for ca. 12~13%, 17~25% and 23~54% of total soil C in the bare interplant, grass and shrub covered microsites, respectively (Figure 10-2). Bare, interplant microsites contained 2213 ± 140 g C m^2 of IC and 368 ± 20 g C m^2 of OC. Grass-covered microsites contained 1131 ± 121 g C m^2 of IC and 279 ± 16 g C m^2 of OC. Shrub-covered microsites contained 1271 ± 112 g C m^2 of IC and 469 ± 53 g C m^2 of OC.

These differences in SIC and SOC stocks between microsites were investigated for statistical significance. To maximise statistical power, observations for each microsite were combined from the sites across the grass-shrub ecotone, yielding $n = 15$ or $n = 20$ observations per microsite (although the same relative patterns were also observed within each of the four sites across the grass-shrub ecotone). As microsite C stocks were not all parametrically distributed, a one-way ANOVA on ranks (Kruskal-Wallis) test was used to determine whether the differences between microsite C stocks were statistically significant, which indicated that there was a statistically highly significant difference between some of the medians (chi-squared = 80.15, $df = 5$, $p < 0.00001$). Following this result, a Dunn post-hoc multiple comparison test was undertaken; the Dunn test is appropriate for unbalanced samples (Zar, 2010) and familywise error was corrected using the Bonferroni

method (p = 0.05). The comparison of SIC and SOC stocks between microsites indicated that there was no statistically significant difference in IC concentrations between the three surface cover microsites or in OC concentrations between the three microsites, but that there was a significant difference between OC and IC stocks within each microsite (Figure 10-2).

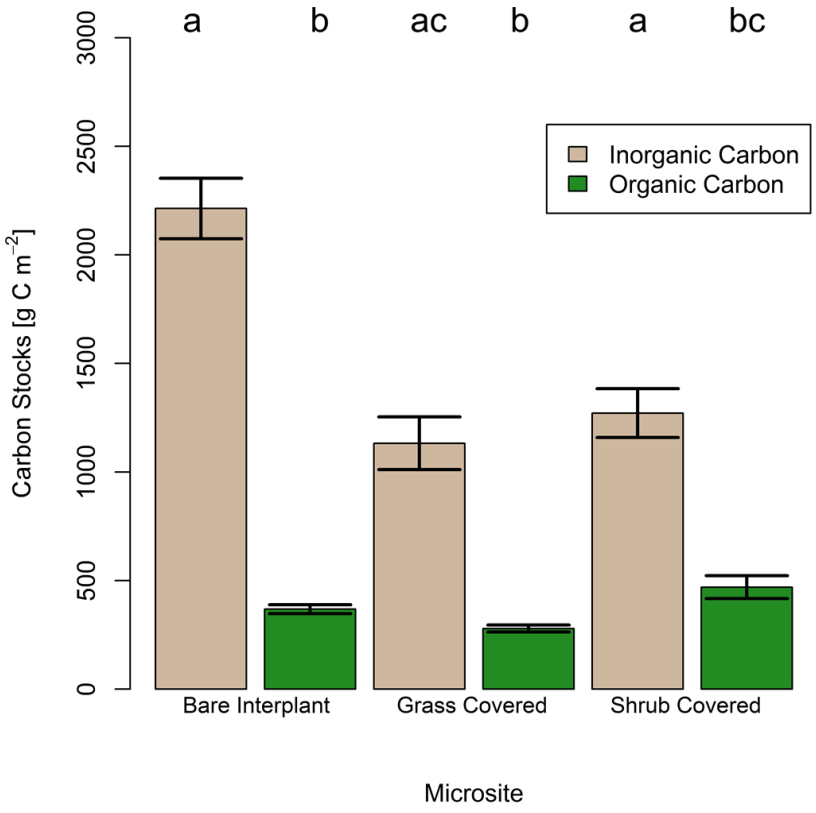

Figure 10-2. Comparison of mean inorganic and organic carbon stocks in the near-surface soil per unit area for each microsite (surface cover: bare, grass, shrub). Error bars denote standard errors and columns sharing the same letter code are not significantly different (p > 0.05, statistical methodology described in the text).

The distribution of near-surface SOC and SIC between microsites found herein was broadly similar to the findings of Ewing *et al*. (2007), who investigated soil properties around creosotebush shrubs in the Mojave Desert and found that SOC accounted for over half of the total soil C beneath shrub canopies whereas in the bare interplant areas virtually all soil C was SIC. It should be noted however that the analysis by Ewing *et al.* (2007) was not comprehensive, as they only quantified SOC and SIC associated with <2 mm clasts. Combined with the data presented in Chapters 6 and 7, these results demonstrate that the increase in total soil C

stocks in the soil reported across the grass-shrub ecotone by Turnbull (2008, p. 84) is predominantly caused by differences in SIC, rather than SOC.

10.3. Evaluation of C Fluxes

This section synthesises the new insights derived from Chapters 6 and 7, and compares them with existing knowledge of other aspects of C dynamics in these dryland ecosystems. The importance of lateral transfers to the global biogeochemical cycling of C is now widely recognised (Smith et al., 2001; Lal, 2003; Chaplot et al., 2005; Van Oost et al., 2007, 2008; Cole et al., 2007; Gomez et al., 2010; Aufdenkampe et al., 2011; Bianchi, 2011; Chaplot and Poesen, 2012; Mutema et al., 2015; Sutfin et al., 2015; Chappell et al., 2016), with some workers estimating the lateral transport of carbon to equate to ca. 10% of the total amount of C sequestered in the terrestrial environment (Pacala et al., 2001; Zhu and Reed, 2012). Understanding these lateral transfers and representing these processes in Earth system models is imperative to understanding the present and future behaviour of the terrestrial ecosystem C sink (Cole et al., 2007). While understanding of these lateral transfers is advancing with useful conceptualisations such as the Land-Ocean aquatic continuum (LOAC), empirical understanding of C transport through aquatic systems remains challenging to upscale, due to spatial heterogeneity in landscape properties, non-linear scale dependencies in erosional processes and non-conservative biogeochemical kinetics.

This study helps to address the paucity of published information on the erosional yields of particle associated C from semi-arid environments (*sensu* Gabet et al., 2005). To re-iterate from chapters 2 and 3, this study sought to advance knowledge of the initial mobilisation of C from the landscape and thus C inputs to aquatic systems. It was not the aim of the present work to quantify the ultimate fate of eroded material through possible mineralisation while in transit and subsequent depositional sites.

Across the grass-shrub ecotone, there was a systematic, five-fold increase in the average erosional event yield of total C (Figure 10-3). This increase in total C flux was caused by changes in the erosional dynamics of both IC and OC. IC mean event yield increased three-fold across the grass-shrub ecotone, due to a three-fold

increase in erosion rates (chapter 7). OC mean event yield increased six-fold across the grass-shrub ecotone, due to increases in both erosion rates and OC enrichment (chapter 6) (Cunliffe et al., 2016d). Mean erosion-induced yields of OC were consistently greater than erosion-induced yields of IC across all four sites (Figure 10-3). The significant increase in OC enrichment in eroded sediments across the grass-shrub ecotone meant that the mean proportion of total C in the form of IC in the decreased systematically from 45.5%, 40.9%, 37.2% and 32.3%, for the grass-, grass-shrub-, shrub-grass- and shrub-dominated sites, respectively. The finding that water erosion mediated effluxes of particle-associated C was dominated by organic forms of C is consistent with work on small scale (1.5 m^2) rainfall simulation plots at a similar semi-arid site at the Jornada (Lister, 2007). However, the present finding that the erosional fluxes of particle-associated C increase across the grass-shrub ecotone is contrary to the findings of Lister (2007). In that study, erosion-induced C fluxes were found to be higher from grass-dominated plots relative to plots situated either beneath or between the canopies of creosotebush or mesquite shrubs (Lister, 2007 especially Figure 7.10 therein). The reasons for these differences in findings are unclear, but may possibly relate to the spatial scale of investigation.

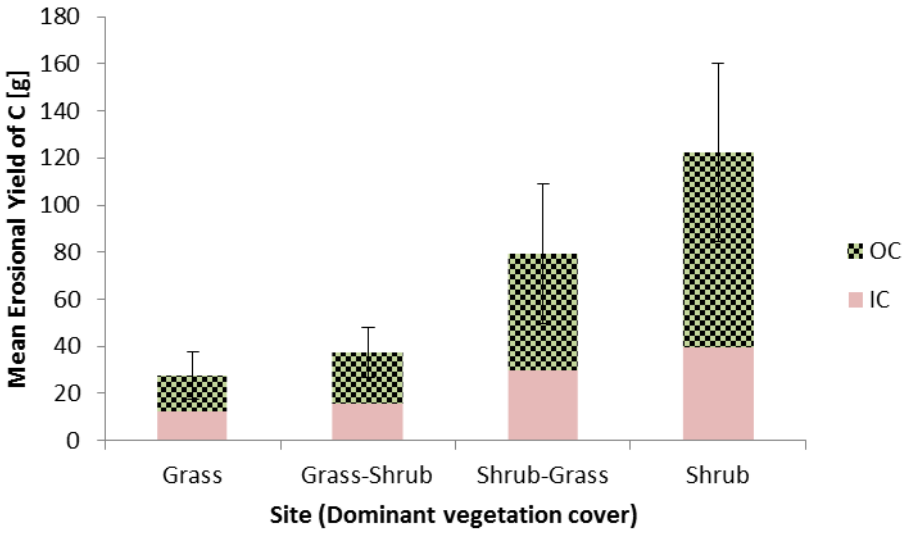

Figure 10-3. Comparison of mean erosion-induced yields of inorganic (IC) and organic (OC) across the grass-shrub ecotone. Error bars represent the cumulative uncertainty, propagated in quadrature. For uncertainties associated with individual components, please refer to chapters 6 and 7 (Cunliffe et al., 2016d).

IC was found to be not significantly enriched in eroded sediment (Chapter 7). This result contrasts with findings of enrichment in IC from work with small scale (1.5 m^2)

rainfall simulator plots at the similar semi-arid Jornada site (Lister, 2007), although that study did not quantify IC associated with the coarse >2 mm particles, which can substantially affect calculated enrichment ratios (as discussed in Chapter 7).

Eroded sediment was consistently enriched in OC relative to the contributing soils, OC enrichment appeared to be an enduring phenomenon sustained through the dynamic replacement of preferentially eroded particulate OC (chapter 6) (Cunliffe et al., 2016d). Advancing mechanistic understanding of OC enrichment is valuable because ignoring OC enrichment risks greatly underestimating the magnitude of C transfer from terrestrial to aquatic systems, increasing the likelihood of erroneous inferences regarding the lateral redistribution of C across these systems and of the magnitude and stability of terrestrial C sinks.

The lateral redistribution of C is rarely considered when comparing the C dynamics of different plant functional types, such as grass and shrubs. This is problematic because although these semi-arid shrubs sometimes appear to fix more gaseous C than grasses (Muldavin et al., 2008; Petrie et al., 2015), the differences in erosional effluxes will offset, and possibly even exceed, the differences in C fixation, potentially resulting in a net loss of OC from the terrestrial ecosystem (Meyer, 2012; Brazier et al., 2013; Puttock et al., 2013, 2014; Cunliffe et al., 2016d). Note also that the measured erosional effluxes of OC did not include C associated with the low density (<1 g cm^3) fraction, which includes necromass such as leaf litter. This fraction potentially comprises of a substantial proportion of the total OC flux from terrestrial to aquatic systems, and is also likely to be in a more bioavailable form, and therefore should be explicitly quantified in future work in these ecosystems (Cunliffe et al., 2016d). The (im)balance between influxes and effluxes of C must be understood to predict the long-term implications of wide-spread woody shrub encroachment on ecosystem C dynamics in these dynamic semi-arid ecosystems (*sensu* Gabet et al., 2005; Brazier et al., 2013; Puttock et al., 2014).

10.3.1. Integration with C budgets

It is constructive to consider to what extent the runoff-induced erosional effluxes of C can be compared with knowledge of other flux pathways in these ecosystems, for example, aeolian and gaseous exchanges. Several workers have sought to compare the relative importance of erosion-induced C fluxes for ecosystem C

budgets (e.g. Jacinthe et al., 2001, pp. 435–436; Quinton et al., 2006). Such comparisons are however difficult, due to nontrivial differences in spatio-temporal scales of measurement.

Aeolian processes can be an important vector for the lateral redistribution of soil resources, including SOC, in drylands, as has been discussed in sections 1.3.5, 1.4.2 and 6.5.3. However, reconciling empirical observations of aeolian fluxes with in a spatio-temporally normalised way is challenging,. Here it is sufficient to note that the relative dominance of aeolian versus fluvial transport generally depends on the aridity of the environment with wind playing a greater role in dryer locales, aeolian redistribution of soil and associated chemicals is typically accelerated in shrub-dominated sites relative to grass dominated sites, and that more co-located studies are needed to obtain spatially and temporally comparable measurements of aeolian C fluxes (Li et al., 2007; Ravi et al., 2007, 2010).

The measurements obtained in Chapter 6 (Cunliffe et al., 2016d) and Chapter 7 are considered to be very robust characterisations of the water-mediated redistribution of OC and IC *at these spatial scales* (300 m^2), which are dominated by interrill erosion processes (Turnbull et al., 2010a). Although it is numerically possible to normalise the erosional transport of OC and IC spatially and temporally, many water-mediated hillslope erosion processes are non-linear. Such normalization therefore necessitates several, non-trivial assumptions, which result in high and poorly understood uncertainty in the estimated fluxes. These scaling limitations are discussed further in sections 1.2.2 and 3.4, and Parsons *et al.* (2006), Brazier *et al*. (2011) and Cerdá *et al*. (2013). Consequently, these scaling issues make it challenging to directly compare gaseous and aeolian flux estimates derived for different measurement scales.

At the Sevilleta National Wildlife Refuge, eddy covariance towers have been used to investigate the net ecosystem exchange (NEE) of gaseous C for grama grass- and creosotebush shrub-dominated ecosystems (e.g. Petrie et al., 2015). Constrained with additional measurements of soil moisture, and above- and belowground biomass, Petrie *et al*. (2015) reported on five years (2007-2011) of NEE dynamics, and concluded that a grass-dominated site was a net source of 31 g C m^{-2} yr^{-1} to the atmosphere, while a shrub-dominated site sequestered an average of 49 g C m^{-2} yr^{-1}. Importantly however, estimates of NEE derived from

eddy covariance towers are associated with very poorly constrained uncertainties, particularly in dyland ecosystems (Stringer et al., 2012; Schlesinger, 2016). This is partly due to temporal variations in the footprint of the eddy covariance measurement and by spatial variability within that footprint (i.e. different vegetation types) (Twine et al., 2000; Finkelstein and Sims, 2001; Hollinger and Richardson, 2005; Oren et al., 2006). Furthermore, gas flux observations are not made during precipitation events (e.g. Petrie et al., 2015), yet there is a large body of empirical evidence demonstrating precipitation inputs to water-limited ecosystems cause rapid release of gaseous C over timescales of minutes to hours (e.g. Austin et al., 2004; Huxman et al., 2004, pp. 255–256; Sponseller, 2007; Borken and Matzner, 2009; Stringer et al., 2012). There are significant concerns regarding the spatial representativeness of eddy covariance-derived measurements (Twine et al., 2000; Baldocchi, 2003; Kanda et al., 2004; Schlesinger, 2016). Notably, there was no assessment of uncertainty in the NEE values estimated by Petrie *et al.* (2015).

While the new insights developed in this thesis are therefore highly complementary to research into the other components of the terrestrial and aquatic C budget by others working at the SNWR, given the available data, I suggest that it is not yet possible to calculate a comprehensive C budget for these dryland grass or shrub ecosystems. Currently, the uncertainties associated with estimates of each flux pathways are simply insufficiently constrained for direct comparisons to be either meaningful or informative. One further component to this uncertainty is that the length of the monitoring periods (e.g. five years Petrie et al., 2015; and four monsoon seasons Cunliffe et al., 2016d), is short relative to the high degree of climatic variability experienced by these ecosystems (Wainwright, 2005; Petrie et al., 2014).

More work is needed to constrain these uncertainties further to reconcile knowledge of different components of the C dynamics in these dryland ecosystems. In order to transcend the space and time scale-dependencies that inhibit extrapolation of empirical observations, it is likely that this future work will involve a significant modelling component, building upon the kind of process-based approaches advanced in chapter 9. The evaluation presented in chapter 9 demonstrated that MAHLERAN's hydrological component often performs very well, but that the sediment transport component requires further refinement, particularly with regards to the particle size distribution. Erosional redistribution of IC can be fairly well represented

by the model structure employed herein, but representing redistribution of OC will require further work to improve the representation of processes leading to OC enrichment. Detailed suggestions for developments the modelling approach further are presented in section 9.10.

10.4. Long-Term Effects of Semi-Arid Woody Shrub Encroachment on Carbon

Based on the mechanistic understanding developed throughout this thesis, supported by existing literature, I suggest that the even if woody shrub encroachment causes a short-term *increase* in C uptake and storage by a terrestrial system, over longer timescales, degradation of the soil resource and reduction in water availability will lead to a *reduced* uptake and storage of C in these dryland landscapes.

Woody shrub encroachment into former grasslands is a global phenomenon (Van Auken, 2000, 2009). The change in dominant plant functional type can alter ecosystem C dynamics (Pacala et al., 2001, 2007; Knapp et al., 2008; Eldridge et al., 2011; Barger et al., 2011; Brazier et al., 2013; Puttock et al., 2013, 2014; Petrie et al., 2015; Cunliffe et al., 2016d), and the extent of the change is sufficient to impact global-scale C cycling (Pacala et al., 2001, 2007).

The replacement of grasses by woody plants has generally been thought to increase ecosystem C storage, in both biomass and soil pools (Barth and Klemmedson, 1978; Connin et al., 1997b; Houghton et al., 1999; Houghton, 2003a; Jackson, 2000; Jobbágy and Jackson, 2000; Jackson et al., 2002; Liao et al., 2006a; Pacala et al., 2007; Eldridge et al., 2011; Barger et al., 2011; Petrie et al., 2015). This hypothesis has prompted assessments regarding large-scale changes in the terrestrial C pools (Pacala et al., 2001, 2007; Schimel et al., 2001; Gifford and Howden, 2001; Burrows et al., 2002; Henry et al., 2002; Houghton, 2003a; Barger et al., 2011). In the conterminous United States, for example, woody shrub encroachment into more than 220 million ha of former grasslands has been estimated to have sequestered 0.12-0.13 Pg C Yr^{-1} between 1980 and 1990 (Pacala et al., 2001; after Houghton et al., 2000).

However, as discussed in section 1.4, it is apparent that differences in C dynamics between grass-dominated and shrub-dominated ecosystems vary between different

environmental contexts, such as aridity (Conant et al., 1998; Klopatek et al., 1998; Jackson et al., 2002; Goodale and Davidson, 2002). For example, Jackson *et al*. (2002) investigated six paired grass- and shrub-dominated plots across a gradient of mean annual precipitation (MAP) and found that while the biomass C pool was greater in shrub-dominated ecosystems, relative differences in SOC pools vary systematically with MAP with dryer sites appearing to gain SOC and wetter sites losing SOC following the grass-shrub transition (Figure 1-6). Indeed, uncertainty around the effects of woody shrub encroachment on ecosystem C storage has been acknowledged to be the greatest single source of uncertainty in the North American C budget (Pacala et al., 2007).

In semi-arid environments, it is well demonstrated that significant changes in ecosystem structure associated with grass-shrub transitions result in significant changes in ecosystem function, many of which can be considered effectively irreversible (Sankey et al., 2012; Turnbull et al., 2012; Moreno-de las Heras et al., 2016). These changes include an increased loss of water via overland flow, and increased erosion of soil and soil-associated nutrients transported via both aeolian and runoff from shrub-dominated ecosystems (Parsons et al., 1996; Schlesinger et al., 1999; Wainwright et al., 2000; Safriel et al., 2005; Li et al., 2007; Ravi et al., 2007, 2010; Turnbull et al., 2010a; Meyer, 2012; Puttock et al., 2013, 2014; Cunliffe et al., 2016d). The loss of resources includes a reduction in the availability of macro- (N and P) and micro-nutrients needed for plant growth, and also a loss of soil, particularly fine (<0.0625 mm) particles, which reduces soil water holding capacities (Quinton et al., 2010). These resource losses are significant in these ecosystems which are already water-limited with low availability of important plant nutrients (Huenneke et al., 2002; Schlesinger et al., 2006; Huenneke and Schlesinger, 2006; Turnbull et al., 2011). Consequently, plant primary productivity is negatively impacted, with reduced rates of recruitment and growth in degraded areas (Lal, 2001c; Rhoton et al., 2006; Burg et al., 2015), which in turn leads to a positive feedback whereby the reduced foliar cover perpetuates the loss of soil resources from the landscape (Schlesinger et al., 1990; Turnbull et al., 2008b; Puttock et al., 2013; Burg et al., 2015).

Soil as a medium for sustaining vascular plants can be considered analytically in terms of mass balance. Inputs include pedogenesis of the underlying regolith and accretion from transport processes such as runon from upslope positions and

aeolian deposition. Outputs include wind- and water-mediated erosion. If inputs equal outputs, the mass balance remains constant, whereas if inputs are less than outputs the soil mass will decrease. Burg *et al*. (2015) developed a mathematical model of the two-way interactions between soil and vegetation in drylands, with plants controlling erosion and soil availability controlling primary productivity. The study by Berg *et al*. focused on wildfire perturbations to vegetation structure, but their treatment is equally applicable to other mechanisms of changing vegetation structure which lead to accelerated erosion rates, such as changing community dominance. Burg *et al*. found that for some ranges of parameter values their model predicted systems would reach one of two steady states, either fully vegetated or fully degraded. For another range of parameter values, bi-stability emerged. Importantly, both sets of parameter values examined by Burg *et al.* were plausible in semi-arid landscapes.

These changes in ecosystem structure and function have multifaceted implications for ecosystem C dynamics. Reduced resources (water, nutrient and growth medium) restrict primary productivity, which results in reduced storage of C in biomass (Huenneke et al., 2002; Huenneke and Schlesinger, 2006). Reduced primary productivity results in reduced inputs of OC to the soil, reducing dynamic replacement of selectively eroded SOC stocks (Lal, 2001a; Rhoton et al., 2006; Quinton et al., 2010; Cunliffe et al., 2016d). Selective erosion of fine particles (Li et al., 2007; Turnbull et al., 2010a) reduces both the capacity and stability of OC in the soil (Wiesmeier et al., 2015), reducing potential C storage. Another, oft overlooked, component to this complex story is that accelerated erosion in drylands can exhume inorganic C (calcretes), potentially leading to their destabilization (discussed further in sections 3.2 and 7) (McAuliffe, 1994; Follett et al., 2001; Emmerich, 2003; Thomey et al., 2014).

Together, this process understanding suggests that woody shrub encroachment in semi-arid rangelands is *likely* to lead to a long term reduction in the amount of C stored in the terrestrial environment. A schematic illustration of this degradation process is presented in Figure 10-4. While this hypothesis of continuing degradation is controversial, it is consistent with many independent lines of empirical observations, discussed below. Understanding terrestrial C dynamics and predicting future changes in these dynamic landscapes requires mechanistic understanding, particularly given the significant challenges associated with longitudinal monitoring

at landscape-scales. Developing mechanistic understanding of these complex eco-hydro-geomorphic systems requires truly interdisciplinary approaches, fostering dialogue between empirical observations and numerical modelling to develop mutually consistent understanding (Wainwright et al., 2000; Sankey et al., 2013; Müller et al., 2014b). This thesis contributes towards such an approach.

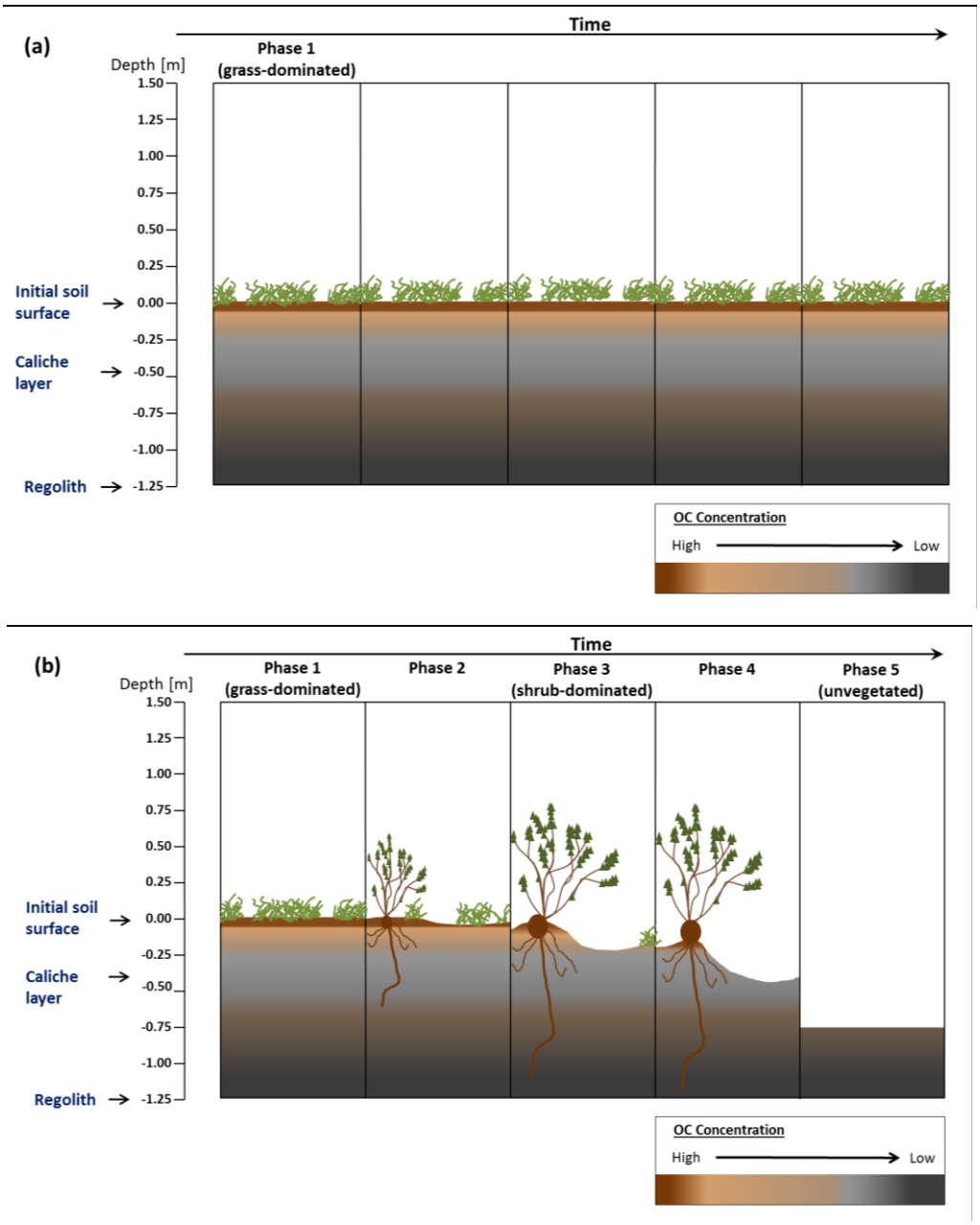

Figure 10-4. Conceptual model depicting: (a) a stable grass-dominated ecosystem, and (b) possible changes in ecosystem structure following woody shrub encroachment into former grassland. Note that phases of degradation portrayed in Figure 10-4 cannot be considered directly comparable to the focal sites studied in this thesis, as it is not appropriate to make necessary assumptions such as uniformity in antecedent soil depth.

The timescales of the degradation process depicted in Figure 10-4 are highly uncertain, as they will depend on the soil depth and the net balance between influx and efflux of material, but moving from Phase 1 to Phase 5 may take centuries.

Evidence supporting the degradation hypothesis (Figure 10-4).

- Soil erosion due to both wind and water mediated processes is several times more rapid in shrub-dominated ecosystems relative to grass dominated ecosystems (Abrahams et al., 1994; Wainwright et al., 2000; Li et al., 2007; Ravi et al., 2010; Turnbull et al., 2010a; Cunliffe et al., 2016d).
- In shrublands, erosional features such as soil pedestals and exhumed root balls indicate loss of the soil A horizon and lowering of the soil surface around plants during their lifespan (Abrahams et al., 1994, 1995; Gibbens and Lenz, 2001).
- As soil depth decreases, soil infiltration capacity also declines, increasing runoff generation and erosive potential. A positive feedback to this land degradation process can occur through the exhumation of pedogenic caliche horizons, which typically have lower permeability than the soil (Favis-Mortlock, 2013).
- IC concentrations in the near-surface soil generally increase across the grass-shrub ecotone (Figure 10-1, Chapter 7), which is consistent with the exhumation of previously covered carbonate horizon (Kieft et al., 1998; Buxbaum and Vanderbilt, 2007); but note that there is some suggestion that *L. tridentata* may also be more tolerant to high $CaCO_3$ concentrations than grasses, so correlation alone cannot not elucidate causation (Buxbaum and Vanderbilt, 2007).
- Hydrological connectivity increases across the grass-shrub ecotone, facilitating erosion by both water and wind mediated processes (Ravi et al., 2010; Turnbull et al., 2010a, 2010b; Puttock et al., 2013).
- Biogeochemical provenancing of OC in soils and eroded sediments (Turnbull, 2008; Puttock, 2013; Puttock et al., 2014) has found that:
    - In the shrub-dominated site, while SOC beneath shrubs is shrub-derived SOC in bare inter-shrub areas originated from grasses that were no longer present;
    - Erosion was incising into older soil horizons;

    - OC eroded from all plots predominantly originates from grass vegetation, and thus represents a loss of legacy OC from the shrub-dominated ecosystems.
- Erosional effluxes of essential plant nutrients, especially N and P, may accelerate with increased runoff and erosion (Turnbull et al., 2011), hindering plant productivity in periods when water limitations are alleviated.

It is possible to estimate a rate of surface lowering *at these spatial scales* (300 m^2) resulting from erosion during monsoonal rainfall events (Chapter 6) (Cunliffe et al., 2016d), using average number of rainstorm events per site and site specific bulk density (Table 10.1). These estimates are approximate, as they do not include fluxes resulting from precipitation events occurring outside of the monitored monsoon period or from aeolian processes, and the total monitoring period (four seasons) is short relative to the degree of climatic variability in these semi-arid landscapes (Wainwright, 2005; Petrie et al., 2014). Notwithstanding these limitations, the relative rates of surface lowering are highly instructive, increasing systematically across the grass-shrub ecotone resulting in a three-fold difference between the grass- and shrub-dominated end member sites.

Table 10.1. Estimated rates of surface lowering resulting from monsoonal storms.

Site	Grass	Grass-Shrub	Shrub-Grass	Shrub
Mean event yield [g]	684.1	1 508.1	1 580.7	2 425.9
Annual average sediment yield from monsoonal events [g yr^{-1}]*	3 146.8	6 937.3	7 271.0	11 159.1
Surface lowering [mm yr^{-1}]**	0.0078	0.0159	0.0188	0.0258

* Calculated using an annual average of 4.6 monitored rainstorm events.

** Converted from mass to volume using site specific bulk density (Appendix 1).

Following a meta-analysis of published literature, Burg *et al*. (2015) found that pedogenesis in arid regions is typically on the order of 0.02 to 0.001 mm yr^{-1}. Critically, one must consider the question: *Does the change in ecosystem structure and function associated with woody shrub encroachment accelerate pedogenesis in these environments?* The removal of overburden exposing regolith and bedrock

to sub-aerial weathering processes can accelerate the initial stages of pedogenesis. However, pedogenesis is a strongly bio-mediated processes, and the reduction in soil and vascular plants reduces inputs of humic acids which slows pedogenesis. Burg *et al*. (2015) suggest that the latter processes is more important, and thus that pedogenesis is likely to *reduce* following woody shrub encroachment. Even if the rate of pedogenesis remains the same, this is likely not sufficient to offset the accelerated soil losses.

It is necessary to also consider negative feedbacks limiting the degradation process described above. For example, size selective erosion of soils with high stone contents leads to armouring (e.g. desert pavements, section 6.5.1), which increases resilience to erosion (Rieke-Zapp et al., 2007). However, such armoured layers also impede infiltration, increasing infiltration-excess runoff generation (Yair and Lavee, 1976; Abrahams et al., 1988; Abrahams and Parsons, 1991). This greater runoff increases the erosive potential of overland flow and also reduces soil moisture availability for subsequent vegetative uptake. The efficacy of such armouring for reducing erosion is further compromised by the high erosive energies resulting from the high intensity rainfall events (Wainwright, 2005; Petrie et al., 2014), which are sufficient to detach and transport fairly coarse (>6 mm in diameter) clasts even just at the 30 × 10 m scales dominated by interrill erosion processes (Turnbull et al., 2010a). Therefore it is considered unlikely that the formation of armouring will significantly inhibit the overall degradation process. Recruitment of new plants is extremely limited on bare, resource-poor desert pavements (Abrahams et al., 1995; Moreno-de las Heras et al., 2016). Therefore, even if the soil resource is not completely lost from the landscape, ecosystem OC stocks in biomass and the soil will be reduced through reduced inputs from primary productivity.

In summary, present mechanistic understanding of the changes in ecosystem structure and function associated with woody shrub encroachment in these semi-arid landscapes, suggests that even if woody shrub encroachment causes a short-term *increase* in C uptake and storage by a terrestrial ecosystem, over longer timescales, degradation of the soil resource and reduction in water availability will lead to a *reduced* uptake and storage of C in these landscapes. This view is contrary to the widely promulgated hypothesis that that woody shrub encroachment in drylands increases ecosystem C storage in these landscapes (e.g. Pacala et al.,

2007), which I suggest does not sufficiently consider the long-term effects of the vegetation transition.

10.5. Discussion of Future Research Directions

The terrestrial C sink is a very important component of the global C cycle, but there is significant uncertainty over the current functioning and future trends of this component. Dryland ecosystems play a major, and oft underappreciated, role in the global C cycle, but are subject to widespread change, including woody shrub encroachment. Woody shrub encroachment is generally considered to increase C storage in the terrestrial ecosystem. However, as demonstrated through this thesis, this hypothesis is inconsistent with mechanistic understanding of degradation processes in semi-arid rangelands. In some environmental contexts, woody shrub encroachment increases ecosystem C stocks, while in others it appears to decrease it. Resolving this dichotomy requires better integration of process understanding across scales, which will require a combination of empirical and process-based numerical modelling approaches to develop mutually consistent understanding (Sankey et al., 2013; Müller et al., 2014a).

Future quantification of C stocks and fluxes should not assume that coarse (>2 mm) clasts contain no organic or inorganic C. Holistic monitoring approaches applied at consistent spatial-scales (where possible) would be extremely valuable for concomitant comparisons of various C flux pathways in these dynamic ecosystems. Such monitoring must include the transport of OC associated with the low density particles (<1 g cm^3), and should run for at least the medium term (>5 years) to better encapsulate processes in these temporally variable landscapes.

A key question pertains to the ultimate fate of eroded C. As described in section 10.3, significant advances are being made on this front by other workers. It is constructive to suggest that such integrated efforts should from the onset include different environmental contexts, to avoid the traditional over-focus on erosional C dynamics in temperate agro-ecosystems. Developing truly multi-scale understanding of the fate of eroded C must combine insights from empirical measurements of fluxes (Rhoton et al., 2006; Meixner et al., 2012; Cunliffe et al., 2016d), biogeochemical tracing techniques (Puttock et al., 2012b, 2014) and process-based numerical modelling approaches (Fierer and Gabet, 2002).

Arguably the most exciting and fruitful future research arising from this thesis is the potential application of the ground-breaking proximal remote sensing techniques to characterise ecosystem structure and associated C stocks with high precision and at fine grain developed in Chapter 8 (Puttock et al., 2015; Cunliffe et al., 2016a, 2016b). Techniques such as these will revolutionise the study of ecosystem dynamics in a range of environmental contexts (*sensu* Anderson and Gaston, 2013). Evidencing the transferability of these proximal remote sensing approaches, the author is involved in their use for quantifying the impacts of Eurasian beaver reintroductions on riparian ecosystem structure and function (Puttock et al., 2015, 2017; Brazier et al., 2016), and is already transferring these approaches to quantify climate-mediated vegetation change in the Canadian Arctic (Myers-Smith et al., 2011, 2015a, 2015b).

In the present theme of semi-arid C dynamics, drone-acquired survey of vegetation biomass and associated C stocks are an excellent tool for acquiring novel datasets with which to evaluate and refine dynamic global vegetation models (DGVMs). This potential application is described in detail in sections 3.3 and 8. DGVMs form an essential component to the Earth Surface Models (ESMs) used to simulate planetary-scale changes in climate (IPCC, 2013); however, significant uncertainty persists in the model representations of vegetation dynamics, contributing to uncertainty in predictions of future climate (Cox et al., 2000; Richardson et al., 2013; Friend et al., 2013; Ahlström et al., 2015; Le Quéré et al., 2014; Poulter et al., 2014; Murray-Tortarolo et al., 2016). Efforts to improve the empirical foundation of the DGVMs in dryland ecosystems are particularly important as, although these models perform worst in water-limited short sward ecosystems such as grasslands and shrublands (Murray-Tortarolo et al., 2016), DGVM predictions have recently been used to suggest that dryland ecosystems play a dominant role in controlling both the long-terms trends and most of the inter annual variability in the global terrestrial C sink (Poulter et al., 2014; Ahlström et al., 2015).

Taking these ideas forward, a proposal has been developed to acquire a time-series of RPAS-acquired biomass data at existing eddy covariance sites to evaluate the capacity of several DGVMs to represent various plant functional types (C3 and C4 grasses, shrubs, trees) across a gradient of aridity. The project team consists of Richard Brazier (PI), Stephen Sitch (CI), Karen Anderson (CI), Tim Hill (CI) and the author (Research-CI). A proposal for this project was submitted to the NERC as a standard grant in the Jan 2016 round. Although the proposal was not funded in that round, it received favourable reviews with a grade of 8/10, and a revised proposal will be resubmitted in Jan 2017.

11. Conclusions

- A substantial proportion of the soil organic and inorganic C stocks is associated with >2 mm clasts, consequently C associated with these coarse particles should be considered when undertaking inventories for C budgets in these dryland landscapes.

- There was a systematic increase in the average erosional yields of organic C across the grass-shrub ecotone, with a six-fold increase from the shrub-dominated site relative to the grass-dominated site. This was controlled by a three-fold increase in erosion rates and a three-fold increase in organic C enrichment rates across the grass-shrub ecotone. These erosional effluxes should be considered when comparing the C budgets of grass-dominated versus shrub-dominated ecosystems. Organic C enrichment was a significant and persistent phenomenon at hillslope scales and is important for understanding lateral transfers of C across terrestrial systems.

- There was a systematic increase in the average erosional yields of inorganic C across the grass-shrub ecotone, with a three-fold increase from the shrub-dominated site relative to the grass-dominated site, largely due to the accelerated erosion rates.

- Novel, inexpensive proximal remote sensing techniques were developed, using drone-acquired image data and structure-from-motion photogrammetry, which enable the efficient characterisation of ecosystem 3D structure at ultrafine grain (cm^2) over landscape extents (10's of ha). The information products generated using these techniques will revolutionise the study of terrestrial ecosystems. For example, spatially explicit data on aboveground biomass in heterogeneous and dynamic short-sward dryland ecosystems, may be used to evaluate models to test the role these systems play in the global biogeochemical cycling of C.

- To support experiments over spatio-temporal scales that cannot be observed, a process based numerical modelling approach was evaluated comprehensively against observations of hydrology and yields of sediment, organic carbon and inorganic carbon for a large assemblage of natural rainfall events. The model evaluation presented herein refined previous findings regarding the capabilities and shortcomings of the present model structure. The hydrological component often performs very well, but the sediment transport component requires further refinement, particularly with regards to the particle size distribution. The erosional redistribution of inorganic C can be reproduced well by the model structure employed herein, but simulating organic C redistribution will require further improvements to the representation of processes leading to organic C enrichment.

- The implications of woody shrub encroachment into former grasslands for ecosystem carbon storage differ between environmental contexts. Based on mechanistic understanding of degradation processes in semi-arid ecosystems, it is likely that even if woody shrub encroachment leads to a short-term gain in ecosystem C storage, over longer timescales degradation of the soil resource will lead to a reduced uptake and storage of C in these shrub-encroached semi-arid landscapes.

Understanding Structure and Function in Semiarid Ecosystems: Implications for Terrestrial Carbon Dynamics in Drylands

Submitted by Andrew Michael Cunliffe to the University of Exeter as a thesis for the degree of Doctor of Philosophy in Physical Geography, May 2016

Supervisors: Professor Richard E. Brazier and Dr Karen Anderson

Volume 2 of 2

12. References

Abrahams, A.D., Li, G., Parsons, A.J., 1996. Rill hydraulics on a semiarid hillslope, southern Arizona. Earth Surface Processes and Landforms 21, 35–47. doi:10.1002/(SICI)1096-9837(199601)21:1<35::AID-ESP539>3.0.CO;2-T

Abrahams, A.D., Parsons, A.J., 1991. Relation between infiltration and stone cover on a semiarid hillslope, southern Arizona. Journal of Hydrology 122, 49–59. doi:10.1016/0022-1694(91)90171-D

Abrahams, A.D., Parsons, A.J., Luk, S.-H., 1989. Distribution of depth of overland flow on desert hillslopes and its implications for modeling soil erosion. Journal of Hydrology 106, 177–184.

Abrahams, A.D., Parsons, A.J., Luk, S.-H., 1988. Hydrologic and sediment responses to simulated rainfall on desert hillslopes in southern Arizona. Catena 15, 103–117.

Abrahams, A.D., Parsons, A.J., Wainwright, J., 2003. Disposition of rainwater under creosotebush. Hydrological Processes 17, 2555–2566. doi:10.1002/hyp.1272

Abrahams, A.D., Parsons, A.J., Wainwright, J., 1995. Effects of vegetation change on interrill runoff and erosion, Walnut Gulch, southern Arizona. Geomorphology 13, 37–48.

Abrahams, A.D., Parsons, A.J., Wainwright, J., 1994. Resistance to overland flow on semiarid grassland and shrubland hillslopes, Walnut Gulch, southern Arizona. Journal of Hydrology 156, 431–446.

Adams, D.K., Comrie, A.C., 1997. The North American Monsoon. Bull. Amer. Meteor. Soc. 78, 2197–2213. doi:10.1175/1520-0477(1997)078<2197:TNAM>2.0.CO;2

Adams, J.M., 1993. Caliche carbonate and the carbon cycle. Nature 361, 213–214.

Adams, J.M., Piovesan, G., 2002. Uncertainties in the role of land vegetation in the carbon cycle. Chemosphere 49, 805–819.

Adams, J.M., Post, W.M., 1999. A preliminary estimate of changing calcrete carbon storage on land since the Last Glacial Maximum. Global and Planetary Change 20, 243–256. doi:10.1016/S0921-8181(99)00015-6

Adeel, Z., Safriel, U., Niemeijer, D., White, R., 2005. Ecosystems and Human Wellbeing: Desertification Synthesis, Millennium Ecosystem Assessment. World Resources Institute, Washington, D.C.

Adeline, K.R.M., Chen, M., Briottet, X., Pang, S.K., Paparoditis, N., 2013. Shadow detection in very high spatial resolution aerial images: A comparative study. ISPRS Journal of Photogrammetry and Remote Sensing 80, 21–38. doi:10.1016/j.isprsjprs.2013.02.003

Agisoft, 2015. Agisoft PhotoScan User Manual: Professional Edition, V 1.2.0. Agisoft.

Agisoft, 2014. Agisoft PhotoScan User Manual: Professional Edition, V 1.1.0. Agisoft.

Agnelli, A., Celi, L., Degl'Innocenti, A., Corti, G., Ugolini, F.C., 2000. Chemical and spectroscopic characterization of the humic substances from sandstone-derived rock fragments. Soil Science 165, 314–327.

Agnelli, A., Trumbore, S.E., Corti, G., Ugolini, F.C., 2002. The dynamics of organic matter in rock fragments in soil investigated by 14C dating and measurements of 13C. European Journal of Soil Science 53, 147–159. doi:10.1046/j.1365-2389.2002.00432.x

Aguiar, M.R., Paruelo, J.M., Sala, O.E., Lauenroth, W.K., 1996. Ecosystem responses to changes in plant functional type composition: an example from the Patagonian steppe. Journal of Vegetation Science 7, 381–390.

Ahlström, A., Raupach, M.R., Schurgers, G., Smith, B., Arneth, A., Jung, M., Reichstein, M., Canadell, J.G., Friedlingstein, P., Jain, A.K., Kato, E., Poulter, B., Sitch, S., Stocker, B.D., Viovy, N., Wang, Y.P., Wiltshire, A., Zaehle, S., Zeng, N., 2015. The dominant role of semi-arid ecosystems in the trend and variability of the land CO2 sink. Science 348, 895–899. doi:10.1126/science.aaa1668

Aide, M., Van Auken, O.W., 1985. Chihuahuan desert vegetation of limestone and basalt slopes in west Texas. The Southwestern Naturalist 533–542.

Ainsworth, E.A., Long, S.P., 2005. What have we learned from 15 years of free-air CO2 enrichment (FACE)? A meta-analytic review of the responses of photosynthesis, canopy properties and plant production to rising CO2. New Phytologist 165, 351–372. doi:10.1111/j.1469-8137.2004.01224.x

Akay, A.E., Oğuz, H., Karas, I.R., Aruga, K., 2008. Using LiDAR technology in forestry activities. Environ Monit Assess 151, 117–125. doi:10.1007/s10661-008-0254-1

Alberts, E.E., Moldenhauer, W.C., 1981. Nitrogen and phosphorus transported by eroded soil aggregates. Soil Science Society of America Journal 45, 391. doi:10.2136/sssaj1981.03615995004500020032x

Allen, A.P., Pockman, W.T., Restrepo, C., Milne, B.T., 2008. Allometry, growth and population regulation of the desert shrub Larrea tridentata. Functional Ecology 22, 197–204. doi:10.1111/j.1365-2435.2007.01376.x

Alonso-Zarza, A.M., Wright, V.P., 2010. Chapter 5 Calcretes, in: Tanner, A.M.A.-Z. and L.H. (Ed.), Developments in Sedimentology, Carbonates in Continental Settings: Facies, Environments, and Processes. Elsevier, pp. 225–267.

Ambrosia, V.C., Pelerson, D.L., Brass, I.A., 1983. Volume estimation techniques for pinyon pine/Utah juniper woodlands using Landsat data and ground information, in: Bell, J.E., Atterbury, T. (Eds.), Renewable Resource Inventories for Monitoring Changes and Trends. pp. 188–192.

Andariese, S.W., Covington, W.W., 1986. Biomass estimation for four common grass species in northern Arizona ponderosa pine. Journal of range management (USA).

Anderson, K., Bennie, J., Wetherelt, A., 2010. Laser scanning of fine scale pattern along a hydrological gradient in a peatland ecosystem. Landscape Ecology 25, 477–492. doi:10.1007/s10980-009-9408-y

Anderson, K., Gaston, K.J., 2013. Lightweight unmanned aerial vehicles (UAVs) will revolutionise spatial ecology. Frontiers in Ecology and Environment 11, 138–146. doi:10.1890/120150

Andrén, O., Kätterer, T., 1997. ICBM: the introductory carbon balance model for exploration of soil carbon balances. Ecological Applications 7, 1226–1236.

Ansley, R.J., Mirik, M., Surber, B.W., Park, S.C., 2012. Canopy area and aboveground mass of individual redberry juniper (Juniperus pinchotii) trees. Rangeland Ecology & Management 65, 189–195. doi:10.2111/REM-D-11-00112.1

Ansley, R.J., Pinchak, W.E., Ueckert, D.N., 1995. Changes in Redberry Juniper Distribution in Northwest Texas (1948 to 1982). Rangelands 17, 49–53.

Antonarakis, A.S., Saatchi, S.S., Chazdon, R.L., Moorcroft, P.R., 2011. Using Lidar and Radar measurements to constrain predictions of forest ecosystem structure and function. Ecological Applications 21, 1120–1137. doi:10.1890/10-0274.1

Archer, D., Kheshgi, H., Maier-Reimer, E., 1998. Dynamics of fossil fuel CO2 neutralization by marine CaCO3. Global Biogeochem. Cycles 12, 259–276. doi:10.1029/98GB00744

Archer, D., Maier-Reimer, E., 1994. Effect of deep-sea sedimentary calcite preservation on atmospheric CO2 concentration. Nature 367, 260–263. doi:10.1038/367260a0

Archer, S.R., 2010. Rangeland conservation and shrub encroachment: new perspectives on an old problem, in: du Toit. J, Kock, R., Deutsch, J. (Eds.), Wild Rangelands: Conserving Wildlife While Maintaining Livestock in Semi-Arid Ecosystems. Wiley-Blackwell, Oxford, pp. 53–97.

Archer, S.R., Boutton, T.W., Hibbard, K.A., 2001. Trees in grasslands: biogeochemical consequences of woody plant expansion, in: Schulze, E.-D., Harrison, S.P., Heimann, M., Holland, E.A., Lloyd, J., Prentice, I.C., Schimel, D.S. (Eds.), Global Biogeochemical Cycles in the Climate System. Academic Press, San Diego, pp. 115–130.

Archer, S.R., Schimel, D.S., Holland, E.A., 1995. Mechanisms of shrubland expansion: land use, climate or CO2? Climatic Change 29, 91–99. doi:10.1007/BF01091640

Ares, A., Fownes, J.H., 2000. Comparisons between generalized and specific tree biomass functions as applied to tropical ash (Fraxinus uhdei). New Forests 20, 277–286. doi:10.1023/A:1006766529550

Asner, G.P., 2009. Tropical forest carbon assessment: integrating satellite and airborne mapping approaches. Environ. Res. Lett. 4, 34009. doi:10.1088/1748-9326/4/3/034009

Asner, G.P., Archer, S.R., Hughes, R.F., Ansley, R.J., Wessman, C.A., 2003. Net changes in regional woody vegetation cover and carbon storage in Texas drylands, 1937–1999. Global Change Biology 9, 316–335. doi:10.1046/j.1365-2486.2003.00594.x

Asner, G.P., Clark, J.K., Mascaro, J., Galindo García, G.A., Chadwick, K.D., Navarrete Encinales, D.A., Paez-Acosta, G., Cabrera Montenegro, E., Kennedy-Bowdoin, T., Duque, Á., Balaji, A., von Hildebrand, P., Maatoug, L., Phillips Bernal, J.F., Yepes Quintero, A.P., Knapp, D.E., García Dávila, M.C., Jacobson, J., Ordóñez, M.F., 2012. High-resolution mapping of forest carbon stocks in the Colombian Amazon. Biogeosciences 9, 2683–2696. doi:10.5194/bg-9-2683-2012

Atkin, O.K., Bloomfield, K.J., Reich, P.B., Tjoelker, M.G., Asner, G.P., Bonal, D., Bönisch, G., Bradford, M.G., Cernusak, L.A., Cosio, E.G., Creek, D., Crous, K.Y., Domingues, T.F., Dukes, J.S., Egerton, J.J.G., Evans, J.R., Farquhar, G.D., Fyllas, N.M., Gauthier, P.P.G., Gloor, E., Gimeno, T.E., Griffin, K.L., Guerrieri, R., Heskel, M.A., Huntingford, C., Ishida, F.Y., Kattge, J., Lambers, H., Liddell, M.J., Lloyd, J., Lusk, C.H., Martin, R.E., Maksimov, A.P., Maximov, T.C., Malhi, Y., Medlyn, B.E., Meir, P., Mercado, L.M., Mirotchnick, N., Ng, D., Niinemets, Ü., O'Sullivan, O.S., Phillips, O.L., Poorter, L., Poot, P., Prentice, I.C., Salinas, N., Rowland, L.M., Ryan, M.G., Sitch, S., Slot, M., Smith, N.G., Turnbull, M.H., VanderWel, M.C., Valladares, F., Veneklaas, E.J., Weerasinghe, L.K., Wirth, C., Wright, I.J., Wythers, K.R., Xiang, J., Xiang, S., Zaragoza-Castells, J., 2015. Global variability in leaf respiration in relation to climate, plant functional types and leaf traits. New Phytol 206, 614–636. doi:10.1111/nph.13253

Aufdenkampe, A.K., Mayorga, E., Raymond, P.A., Melack, J.M., Doney, S.C., Alin, S.R., Aalto, R.E., Yoo, K., 2011. Riverine coupling of biogeochemical cycles

between land, oceans, and atmosphere. Frontiers in Ecology and the Environment 9, 53–60. doi:10.1890/100014
Austin, A.T., Yahdjian, L., Stark, J.M., Belnap, J., Porporato, A., Norton, U., Ravetta, D.A., Schaeffer, S.M., 2004. Water pulses and biogeochemical cycles in arid and semiarid ecosystems. Oecologia 141, 221–235.
Baccini, A., Laporte, N., Goetz, S.J., Sun, M., Dong, H., 2008. A first map of tropical Africa's above-ground biomass derived from satellite imagery. Environ. Res. Lett. 3, 45011. doi:10.1088/1748-9326/3/4/045011
Báez, S., Collins, S.L., 2008. Shrub invasion decreases diversity and alters community stability in northern Chihuahuan desert plant communities. PLoS One 3, e2332. doi:10.1371/journal.pone.0002332
Báez, S., Collins, S.L., Pockman, W.T., Johnson, J.E., Small, E.E., 2013. Effects of experimental rainfall manipulations on Chihuahuan Desert grassland and shrubland plant communities. Oecologia. doi:10.1007/s00442-012-2552-0
Báez, S., Fargione, J., Moore, D.I., Collins, S.L., Gosz, J.R., 2007. Atmospheric nitrogen deposition in the northern Chihuahuan desert: Temporal trends and potential consequences. Journal of Arid Environments 68, 640–651. doi:10.1016/j.jaridenv.2006.06.011
Bagnold, R.A., 1980. An empirical correlation of bedload transport rates in flumes and natural rivers. Proceedings of the Royal Society of London A: Mathematical, Physical and Engineering Sciences 372, 453–473. doi:10.1098/rspa.1980.0122
Baird, A.J., 2013. Soil and Hillslope Hydrology, in: Wainwright, J., Mulligan, M. (Eds.), Environmental Modelling: Finding Simplicity in Complexity. Wiley-Blackwell, pp. 165–182.
Baisden, W.T., Parfitt, R.L., Trustrum, N.A., 2002. Using nutrient balance to estimate net C balance in landslide-prone pastoral hill country: testing the "dynamic equilibrium" hypothesis in New Zealand soft rock landscapes. Presented at the 12th International Soil Conservation Organization Conference: Sustainable Utilization of Global Soil and Water Resources, Tsinghua University Press, Beijing, China, pp. 298–301.
Baldocchi, D.D., 2003. Assessing the eddy covariance technique for evaluating carbon dioxide exchange rates of ecosystems: past, present and future. Global Change Biology 9, 479–492. doi:10.1046/j.1365-2486.2003.00629.x
Baldock, J.A., Skjemstad, J.O., 2000. Role of the soil matrix and minerals in protecting natural organic materials against biological attack. Organic Geochemistry 31, 697–710. doi:10.1016/S0146-6380(00)00049-8
Balesdent, J., Besnard, E., Arrouays, D., Chenu, C., 1998. The dynamics of carbon in particle-size fractions of soil in a forest-cultivation sequence. Plant and Soil 201, 49–57. doi:10.1023/A:1004337314970
Balzarolo, M., Vicca, S., Nguy-Robertson, A.L., Bonal, D., Elbers, J.A., Fu, Y.H., Grünwald, T., Horemans, J.A., Papale, D., Peñuelas, J., Suyker, A., Veroustraete, F., 2016. Matching the phenology of Net Ecosystem Exchange and vegetation indices estimated with MODIS and FLUXNET in-situ observations. Remote Sensing of Environment 174, 290–300. doi:10.1016/j.rse.2015.12.017
Barbour, M.G., 1973. Desert dogma reexamined: root/shoot productivity and plant spacing. American Midland Naturalist 89, 41–57. doi:10.2307/2424134
Barbour, M.G., 1969. Patterns of genetic similarity between Larrea divaricata of North and South America. American Midland Naturalist 81, 54–67. doi:10.2307/2423651

Barbour, M.G., MacMahon, J.A., Bamberg, S.A., Ludwig, J.A., 1977. The structure and distribution of Larrea communities, in: Mabry, T.H., Hunziker, J.H., Difeo, D.R. (Eds.), Creosote Bush: Biology and Chemistry of Larrea in New World Deserts. Dowden, Hutchinson and Ross, Stroudverg, pp. 227–251.

Barger, N.N., Archer, S.R., Campbell, J.L., Huang, C., Morton, J.A., Knapp, A.K., 2011. Woody plant proliferation in North American drylands: a synthesis of impacts on ecosystem carbon balance. Journal of Geophysical Research 116, G00K07. doi:10.1029/2010JG00150

Barth, R.C., Klemmedson, J.O., 1978. Shrub-induced spatial patterns of dry matter, nitrogen, and organic carbon. Soil Science Society of America Journal 42, 804–809.

BassiriRad, H., Reynolds, J.F., Virginia, R.A., Brunelle, M.H., 1997. Growth and root NO3-and PO43-uptake capacity of three desert species in response to atmospheric CO2 enrichment. Functional Plant Biology 24, 353–358. doi:10.1071/PP96109

Batjes, N.H., 1998. Mitigation of atmospheric CO2 concentrations by increased carbon sequestration in the soil. Biology and Fertility of Soils 27, 230–235.

Batjes, N.H., 1996. Total carbon and nitrogen in the soils of the world. European Journal of Soil Science 47, 151–163.

Batjes, N.H., Sombroek, W.G., 1997. Possibilities for carbon sequestration in tropical and subtropical soils. Global Change Biology 3, 161–173.

Bauer, A., Black, A.L., 1981. Soil carbon, nitrogen, and bulk density comparisons in two cropland tillage systems after 25 years and in virgin grassland. Soil Science Society of America Journal 45, 1166–1170.

Beauchamp, E.G., Seech, A.G., 1990. Denitrification with different sizes of soil aggregates obtained from dry-sieving and from sieving with water. Biol Fertil Soils 10, 188–193. doi:10.1007/BF00336134

Beck, R.F., McNeely, R.P., Gibbens, R.P., 1999. Mesquite-Grassland Ecotones in the Chihuahuan Desert. USDA Forest Service Proceedings RMRS-P-11.

Belnap, J., 2006. The potential roles of biological soil crusts in hydrologic cycles. Hydrological Processes 20, 3159–3178. doi:10.1002/hyp.6325

Beniston, J.W., Shipitalo, M.J., Lal, R., Dayton, E.A., Hopkins, D.W., Jones, F., Joynes, A., Dungait, J. a. J., 2015. Carbon and macronutrient losses during accelerated erosion under different tillage and residue management. European Journal of Soil Science 66, 218–225. doi:10.1111/ejss.12205

Bergen, K.M., Goetz, S.J., Dubayah, R.O., Henebry, G.M., Hunsaker, C.T., Imhoff, M.L., Nelson, R.F., Parker, G.G., Radeloff, V.C., 2009. Remote sensing of vegetation 3-D structure for biodiversity and habitat: Review and implications for lidar and radar spaceborne missions. J. Geophys. Res. 114, G00E06. doi:10.1029/2008JG000883

Berhe, A.A., Harden, J.W., Torn, M.S., Harte, J., 2008. Linking soil organic matter dynamics and erosion-induced terrestrial carbon sequestration at different landform positions. Journal of Geophysical Research: Biogeosciences 113, G04039. doi:10.1029/2008jg000751

Berhe, A.A., Harte, J., Harden, J.W., Torn, M.S., 2007. The significance of the erosion-induced terrestrial carbon sink. BioScience 57, 337–346. doi:10.1641/B570408

Berner, L.T., Alexander, H.D., Loranty, M.M., Ganzlin, P., Michelle, M.C., Davydov, S.P., Goetz, S.J., 2015. Biomass allometry for alder, dwarf birch, and willow in boreal forest and tundra ecosystems of far northeastern Siberia and north-central Alaska. Forest Ecology and Management 337, 110–118. doi:10.1016/j.foreco.2014.10.027

Bestelmeyer, B.T., 2005. Does desertification diminish biodiversity? Enhancement of ant diversity by shrub invasion in south-western USA. Diversity and Distributions 11, 45–55.

Bestelmeyer, B.T., Okin, G.S., Duniway, M.C., Archer, S.R., Sayre, N.F., Williamson, J.C., Herrick, J.E., 2015. Desertification, land use, and the transformation of global drylands. Frontiers in Ecology and the Environment 13, 28–36. doi:10.1890/140162

Beuselinck, L., Steegen, A., Govers, G., Nachtergaele, J., Takken, I., Poesen, J., 2000. Characteristics of sediment deposits formed by intense rainfall events in small catchments in the Belgian Loam Belt. Geomorphology 32, 69–82. doi:10.1016/S0169-555X(99)00068-9

Beven, K.J., Brazier, R.E., 2011. Dealing with uncertainty in erosion model predictions, in: Morgan, R.P.C., Nearing, M.A. (Eds.), Handbook of Erosion Modelling. Wiley-Blackwell, Chichester, UK, pp. 52–80.

Bhark, E.W., 2002. Water Availability to Vegetation Across a Semiarid Shrubland and Grassland Ecotone, Sevilleta Wildlife Refuge, New Mexico. New Mexico Institue of Mining and Technology, Socorro, New Mexico.

Bhark, E.W., Small, E.E., 2003. Association between plant canopies and the spatial patterns of infiltration in shrubland and grassland of the Chihuahuan Desert, New Mexico. Ecosystems 6, 185–196. doi:10.1007/s10021-002-0210-9

Bianchi, T.S., 2011. The role of terrestrially derived organic carbon in the coastal ocean: A changing paradigm and the priming effect. PNAS 108, 19473–19481. doi:10.1073/pnas.1017982108

Bianchi, T.S., 2007. Biogeochemistry of Estuaries. Oxford University Press, USA.

Biedenbender, S.H., McClaran, M.P., Quade, J., Weltz, M.A., 2004. Landscape patterns of vegetation change indicated by soil carbon isotope composition. Geoderma 119, 69–83. doi:10.1016/S0016-7061(03)00234-9

Biggs, T.H., Quade, J., Webb, R.H., 2002. δ13C values of soil organic matter in semiarid grassland with mesquite (Prosopis) encroachment in southeastern Arizona. Geoderma 110, 109–130.

Bilotta, G.S., Brazier, R.E., 2008. Understanding the influence of suspended solids on water quality and aquatic biota. Water Research 42, 2849–2861.

Bird, S.B., Herrick, J.E., Wander, M.M., 2001. Exploiting heterogeneity of soil organic matter in rangelands: benefits for carbon sequestration, in: Follett, R.F., Kimble, J.M., Lal, R. (Eds.), The Potential of US Grazing Lands to Sequester Carbon and Mitigate the Greenhouse Effect. CRC-Lewis, Boca Raton, pp. 121–138.

Bird, S.B., Herrick, J.E., Wander, M.M., Wright, S.F., 2002. Spatial heterogeneity of aggregate stability and soil carbon in semi-arid rangeland. Environmental Pollution 116, 445–455.

Bisutti, I., Hilke, I., Raessler, M., 2004. Determination of total organic carbon – an overview of current methods. TrAC Trends in Analytical Chemistry 23, 716–726. doi:10.1016/j.trac.2004.09.003

Bisutti, I., Hilke, I., Schumacher, J., Raessler, M., 2007. A novel single-run dual temperature combustion (SRDTC) method for the determination of organic, in-organic and total carbon in soil samples. Talanta 71, 521–528. doi:10.1016/j.talanta.2006.04.022

Boardman, J., Parsons, A.J., Holland, R., Holmes, P.J., Washington, R., 2003. Development of badlands and gullies in the Sneeuberg, Great Karoo, South Africa. CATENA, Gully Erosion and Global Change 50, 165–184. doi:10.1016/S0341-8162(02)00144-3

Bochet, E., Poesen, J., Rubio, J.L., 2006. Runoff and soil loss under individual plants of a semi-arid Mediterranean shrubland: influence of plant morphology and rainfall intensity. Earth Surface Processes and Landforms 31, 536–549. doi:10.1002/esp.1351

Boix-Fayos, C., Martínez-Mena, M., Arnau-Rosalén, E., Calvo-Cases, A., Castillo, V., Albaladejo, J., 2006. Measuring soil erosion by field plots: Understanding the sources of variation. Earth-Science Reviews 78, 267–285. doi:10.1016/j.earscirev.2006.05.005

Bond, W.J., Midgley, G.F., Woodward, F.I., 2003. The importance of low atmospheric CO2 and fire in promoting the spread of grasslands and savannas. Global Change Biology 9, 973–982. doi:10.1046/j.1365-2486.2003.00577.x

Borges, A.V., 2011. Present day carbon dioxide fluxes in the coastal ocean and possible feedbacks under global change, in: Duarte, P., Santana-Casiano, J.M. (Eds.), Oceans and the Atmospheric Carbon Content. Springer, pp. 47–77.

Borken, W., Matzner, E., 2009. Reappraisal of drying and wetting effects on C and N mineralization and fluxes in soils. Global Change Biology 15, 808–824. doi:10.1111/j.1365-2486.2008.01681.x

Boutton, T.W., Archer, S.R., Midwood, A.J., Zitzer, S.F., Bol, R., 1998. δ13C values of soil organic carbon and their use in documenting vegetation change in a subtropical savanna ecosystem. Geoderma 82, 5–41. doi:10.1016/S0016-7061(97)00095-5

Bouwman, A.F., 1989. Modelling soil organic matter decomposition and rainfall erosion in two tropical soils after forest clearing for permanent agriculture. Land Degradation & Development 1, 125–140.

Bradford, J.B., Schlaepfer, D.R., Lauenroth, W.K., Burke, I.C., 2014. Shifts in plant functional types have time-dependent and regionally variable impacts on dryland ecosystem water balance. J Ecol 102, 1408–1418. doi:10.1111/1365-2745.12289

Bras, R.L., Tucker, G.E., Teles, V., 2003. Six myths about mathematical modeling in geomorphology, in: Wilcock, P.R., Iverson, R.M. (Eds.), Prediction in Geomorphology. American Geophysical Union, pp. 63–79.

Brazier, R.E., Beven, K.J., Freer, J., Rowan, J.S., 2000. Equifinality and uncertainty in physically based soil erosion models: application of the GLUE methodology to WEPP – the Water Erosion Prediction Project – for sites in the UK and USA. Earth Surface Processes and Landforms 25, 825–845. doi:10.1002/1096-9837(200008)25:8<825::AID-ESP101>3.0.CO;2-3

Brazier, R.E., Hutton, C., Parsons, A.J., Wainwright, J., 2011. Scaling soil erosion models in space and time, in: Morgan, R.P.C., Nearing, M.A. (Eds.), Handbook of Erosion Modelling. Wiley-Blackwell, Chichester, UK, pp. 98–116.

Brazier, R.E., Parsons, A.J., Wainwright, J., Powell, D.M., Schlesinger, W.H., 2007. Upscaling understanding of nitrogen dynamics associated with overland flow in a semi-arid environment. Biogeochemistry 82, 265–278. doi:10.1007/s10533-007-9070-x

Brazier, R.E., Puttock, A.K., Graham, H., Anderson, K., Cunliffe, A.M., Elliot, M., 2016. Quantifying the multiple, environmental benefits of reintroducing the Eurasian Beaver, in: Geophysical Research Abstracts. Presented at the European Geosciences Union - General Assembly, EGU, Vienna, Austria.

Brazier, R.E., Turnbull, L., Bol, R., Wainwright, J., 2013. Carbon loss by water erosion in drylands: implications from a study of vegetation change in the southwest USA. Hydrological Processes. doi:10.1002/hyp.9741

Brazier, R.E., Wainwright, J., Parsons, A.J., Powell, D.M., Simanton, R., Larsen, H., 2003. Monitoring and modelling runoff in semi-arid areas from the hillslope to the watershed scale. Presented at the First Interagency Conference on Research in the Watersheds, pp. 101–106.

Breecker, D.O., Sharp, Z.D., McFadden, L.D., 2009. Seasonal bias in the formation and stable isotopic composition of pedogenic carbonate in modern soils from central New Mexico, USA. Geological Society of America Bulletin 121, 630–640.

Briggs, J.M., Knapp, A.K., Blair, J.M., Heisler, J.L., Hoch, G.. A., Lett, M.S., McCarron, J.K., 2005. An ecosystem in transition: causes and consequences of the conversion of mesic grassland to shrubland. BioScience 55, 243–254. doi:10.1641/0006-3568(2005)055[0243:AEITCA]2.0.CO;2

Briggs, J.M., Knapp, A.K., Brock, B.L., 2002. Expansion of woody plants in tallgrass prairie: a fifteen-year study of fire and fire-grazing interactions. The American Midland Naturalist 147, 287–294.

Brisson, J., Reynolds, J.F., 1994. The effect of neighbors on root distribution in a creosotebush (Larrea tridentata) population. Ecology 75, 1693–1702. doi:10.2307/1939629

Brodie, C.R., Casford, J.S.L., Lloyd, J.M., Leng, M.J., Heaton, T.H.E., Kendrick, C.P., Yongqiang, Z., 2011a. Evidence for bias in C/N, δ13C and δ15N values of bulk organic matter, and on environmental interpretation, from a lake sedimentary sequence by pre-analysis acid treatment methods. Quaternary Science Reviews 30, 3076–3087. doi:10.1016/j.quascirev.2011.07.003

Brodie, C.R., Leng, M.J., Casford, J.S.L., Kendrick, C.P., Lloyd, J.M., Yongqiang, Z., Bird, M.I., 2011b. Evidence for bias in C and N concentrations and δ13C composition of terrestrial and aquatic organic materials due to pre-analysis acid preparation methods. Chemical Geology 282, 67–83. doi:10.1016/j.chemgeo.2011.01.007

Brown, J.H., Valone, T.J., Curtin, C.G., 1997. Reorganization of an arid ecosystem in response to recent climate change. Proceedings of the National Academy of Sciences 94, 9729–9733.

Brown, J.R., Angerer, J., Salley, S.W., Blaisdell, R., Stuth, J.W., 2010. Improving estimates of rangeland carbon sequestration potential in the US Southwest. Rangeland Ecology & Management 63, 147–154. doi:10.2111/08-089.1

Brown, J.R., Archer, S.R., 1999. Shrub invasion of grassland: recruitment is continuous and not regulated by herbaceous biomass or density. Ecology 80, 2385–2396. doi:10.1890/0012-9658(1999)080[2385:SIOGRI]2.0.CO;2

Brown, J.R., Archer, S.R., 1987. Woody plant seed dispersal and gap formation in a North American subtropical savanna woodland: The role of domestic herbivores. Vegetatio 73, 73– 80. doi:10.1007/BF00031854

Brown, K.D., 2004. Pharmaceutically active compounds in residential and hospital effluent, municipal wastewater, and the Rio Grande in Albuquerque, New Mexico (MSc). The University of New Mexico, Albuquerque, New Mexico.

Browning, D.M., Rango, A., Karl, J.W., Laney, C.M., Vivoni, E.R., Tweedie, C.E., 2015. Emerging technological and cultural shifts advancing drylands research and management. Frontiers in Ecology and the Environment 13, 52–60. doi:10.1890/140161

Bryan, R.B., 2000. Soil erodibility and processes of water erosion on hillslope. Geomorphology 32, 385–415. doi:10.1016/S0169-555X(99)00105-1

Bryson, M., Reid, A., Hung, C., Ramos, F.T., Sukkarieh, S., 2014. Cost-effective mapping using unmanned aerial vehicles in ecology monitoring applications, in: Khatib, O., Kumar, V., Sukhatme, G. (Eds.), Experimental Robotics, Springer Tracts in Advanced Robotics. Springer Berlin Heidelberg, pp. 509–523.

Buech, R.R., Rugg, D.J., 1989. Biomass relations of shrub components and their generality. Forest Ecology and Management 26, 257–264. doi:10.1016/0378-1127(89)90086-8

Buffington, L.C., Herbel, C.H., 1965. Vegetational changes on a semidesert grassland range from 1858 to 1963. Ecological Monographs 35, 139–164.

Burg, D., Malkinson, D., Katriel, G., Wittenberg, L., 2015. Modeling the dynamics of soil erosion and vegetative control — catastrophe and hysteresis. Theor Ecol 8, 67–79. doi:10.1007/s12080-014-0233-9

Burk, J.H., Dick-Peddie, W.A., 1973. Comparative production of Larrea Divaricata Cav. on three geomorphic surfaces in Southern New Mexico. Ecology 54, 1094–1102. doi:10.2307/1935575

Burnett, S.A., Hattey, J.A., Johnson, J.E., Swann, A.L., Moore, D.I., Collins, S.L., 2012. Effects of fire on belowground biomass in Chihuahuan desert grassland. Ecosphere 3.

Burrows, W.H., Henry, B.K., Back, P.V., Hoffmann, M.B., Tait, L.J., Anderson, E.R., Menke, N., Danaher, T., Carter, J.O., . McKeon, G.M., 2002. Growth and carbon stock change in eucalypt woodlands in northeast Australia: ecological and greenhouse sink implications. Global Change Biology 8, 769–784. doi:10.1046/j.1365-2486.2002.00515.x

Buxbaum, C.A.Z., Vanderbilt, K., 2007. Soil heterogeneity and the distribution of desert and steppe plant species across a desert-grassland ecotone. Journal of Arid Environments 69, 617–632.

Cable, D.R., 1975. Influence of precipitation on perennial grass production in the semidesert southwest. Ecology 981–986.

Cai, W.-J., 2003. Riverine inorganic carbon flux and rate of biological uptake in the Mississippi River plume. Geophysical Research Letters 30, 1032. doi:10.1029/2002GL016312

Cai, W.-J., Guo, X., Chen, C.-T.A., Dai, M., Zhang, L., Zhai, W., Lohrenz, S.E., Yin, K., Harrison, P.J., Wang, Y., 2008. A comparative overview of weathering intensity and HCO3- flux in the world's major rivers with emphasis on the Changjiang, Huanghe, Zhujiang (Pearl) and Mississippi Rivers. Continental Shelf Research 28, 1538–1549. doi:10.1016/j.csr.2007.10.014

Calders, K., Newnham, G., Burt, A., Murphy, S., Raumonen, P., Herold, M., Culvenor, D., Avitabile, V., Disney, M., Armston, J., Kaasalainen, M., 2015. Nondestructive estimates of above-ground biomass using terrestrial laser scanning. Methods Ecol Evol 6, 198–208. doi:10.1111/2041-210X.12301

Calvo-Cases, A., Boix-Fayos, C., Imeson, A.C., 2003. Runoff generation, sediment movement and soil water behaviour on calcareous (limestone) slopes of some Mediterranean environments in southeast Spain. Geomorphology, Long-term landscape development in southern Spain 50, 269–291. doi:10.1016/S0169-555X(02)00218-0

Cambardella, C.A., Elliott, E.T., 1994. Carbon and nitrogen dynamics of soil organic matter fractions from cultivated grassland soils. Soil Science Society of America Journal 58, 123–130.

Cammeraat, L.H., 2002. A review of two strongly contrasting geomorphological systems within the context of scale. Earth Surf. Process. Landforms 27, 1201–1222. doi:10.1002/esp.421

Canfield, R.H., 1939. The effect of intensity and frequency of clipping on density and yield of Black Grama and Tobosa Grass (Technical Bulletin No. No. 681). Department of Agriculture Forest Service.
Cao, M., Woodward, F.I., 1998. Net primary and ecosystem production and carbon stocks of terrestrial ecosystems and their responses to climate change. Global Change Biology 4, 185–198. doi:10.1046/j.1365-2486.1998.00125.x
Caracciolo, D., Istanbulluoglu, E., Noto, L.V., Collins, S.L., 2016. Mechanisms of shrub encroachment into Northern Chihuahuan Desert grasslands and impacts of climate change investigated using a cellular automata model. Advances in Water Resources 46–62. doi:10.1016/j.advwatres.2016.03.002
Carter, L.F., Porter, S.D., 1997. Trace-element accumulation by Hygrohypnum ochraceum in the upper Rio Grande Basin, Colorado and New Mexico, USA. Environmental Toxicology and Chemistry 16, 2521–2528. doi:10.1002/etc.5620161213
Castillo, V.M., Gómez-Plaza, A., Martínez-Mena, M., 2003. The role of antecedent soil water content in the runoff response of semiarid catchments: a simulation approach. Journal of Hydrology 284, 114–130. doi:10.1016/S0022-1694(03)00264-6
Cayan, D.R., Dettinger, M.D., Diaz, H.F., Graham, N.E., 1998. Decadal variability of precipitation over western North America. J. Climate 11, 3148–3166. doi:10.1175/1520-0442(1998)011<3148:DVOPOW>2.0.CO;2
CCSP, 2007. The First State of the Carbon Cycle Report (SOCCR): The North American Carbon Budget and Implications for the Global Carbon Cycle (A Report by the U.S. Climate Change Science Program and the Subcommittee on Global Change Research). National Oceanic and Atmospheric Administration, National Climatic Data Center, Asheville, NC, USA.
Cerdà, A., Brazier, R.E., Nearing, M., de Vente, J., 2013. Scales and erosion. Catena 102, 1–2. doi:10.1016/j.catena.2011.09.006
Chabot, D., Bird, D.M., 2015. Wildlife research and management methods in the 21st century: Where do unmanned aircraft fit in? J. Unmanned Veh. Sys. 1–19. doi:10.1139/juvs-2015-0021
Chabot, D., Craik, S.R., Bird, D.M., 2015. Population census of a large Common Tern colony with a small unmanned aircraft. PLoS ONE 10, e0122588. doi:10.1371/journal.pone.0122588
Chang, A., Jung, J., Kim, Y., 2015. Estimation of forest stand diameter class using airborne lidar and field data. Remote Sensing Letters 6, 419–428. doi:10.1080/2150704X.2015.1035770
Chang, A., Kim, Y., Kim, Y., Eo, Y., 2012. Estimation of individual tree biomass from airborne lidar data using tree height and crown diameter. Disaster Advances 5, 360–365.
Chaplot, V.A.M., Rumpel, C., Valentin, C., 2005. Water erosion impact on soil and carbon redistributions within uplands of Mekong River. Global Biogeochemical Cycles 19, GB4004. doi:10.1029/2005gb002493
Chaplot, V., Poesen, J., 2012. Sediment, soil organic carbon and runoff delivery at various spatial scales. Catena 88, 46–56. doi:10.1016/j.catena.2011.09.004
Chappell, A., Baldock, J., Sanderman, J., 2016. The global significance of omitting soil erosion from soil organic carbon cycling schemes. Nature Clim. Change 6, 187–191. doi:10.1038/nclimate2829
Charley, J.L., West, N.E., 1975. Plant-induced soil chemical patterns in some shrub-dominated semi-desert ecosystems of Utah. Journal of Ecology 63, 945–963. doi:10.2307/2258613

Chartier, M.P., Rostagno, C.M., Videla, L.S., 2013. Selective erosion of clay, organic carbon and total nitrogen in grazed semiarid rangelands of northeastern Patagonia, Argentina. Journal of Arid Environments 88, 43–49. doi:10.1016/j.jaridenv.2012.08.011

Chave, J., Condit, R., Aguilar, S., Hernandez, A., Lao, S., Perez, R., 2004. Error propagation and scaling for tropical forest biomass estimates. Philosophical Transactions of the Royal Society of London B: Biological Sciences 359, 409–420. doi:10.1098/rstb.2003.1425

Cheng, H.H., Kimble, J.M., 2001. Characterization of soil organic carbon pools, in: Lal, R., Kimble, J.M., Follett, R.F., Steward, B.A. (Eds.), Assessment Methods for Soil Carbon. pp. 117–129.

Chenu, C., Plante, A.F., 2006. Clay-sized organo-mineral complexes in a cultivation chronosequence: revisiting the concept of the "primary organo-mineral complex." European Journal of Soil Science 57, 596–607. doi:10.1111/j.1365-2389.2006.00834.x

Chew, R.M., Chew, A.E., 1965. The primary productivity of a desert-shrub (Larrea tridentata) community. Ecological Monographs 35, 355–375. doi:10.2307/1942146

Chichester, F.W., Chaison, R.F., 1992. Analysis of carbon in calcareous soils using a two temperature dry combustion infrared instrumental procedure. Soil Science 153, 237–241.

Chojnacky, D.C., 1985. Pinyon-Juniper Volume Equations for the Central Rocky Mountain States (Research Paper No. INT-339). U.S. Department of Agriculture, Forest Service, Intermt. Forest and Range Experimental Station, Ogden, Utah.

Chojnacky, D.C., Heath, L.S., Jenkins, J.C., 2014. Updated generalized biomass equations for North American tree species. Forestry 87, 129–151. doi:10.1093/forestry/cpt053

Chojnacky, D.C., Moisen, G., 1993. Converting wood volume to biomass for pinyon and juniper. (Research Note No. INT-411). U.S. Department of Agriculture, Forest Service, Intermountain Research Station.

Chopping, M.J., Martonchik, J., Rango, A., Peters, D.P.C., Su, L., Laliberte, A., 2005. Geometric-optical modeling of desert grassland canopy structure with MISR, in: Proceedings of the 9th International Symposium on Physical Measurements and Signatures in Remote Sensing (ISPMSRS 2005). Bejing, China, pp. 141–143.

Chopping, M.J., Rango, A., Havstad, K.M., Schiebe, F.R., Ritchie, J.C., Schmugge, T.J., French, A.N., Su, L., McKee, L., Davis, M.R., 2003. Canopy attributes of desert grassland and transition communities derived from multiangular airborne imagery. Remote Sensing of Environment 85, 339–354. doi:10.1016/S0034-4257(03)00012-9

Chopping, M.J., Snyder, C., Laliberte, A., Rango, A., Maxwell, C., 2004. Differences in grass-shrub transition zone canopy composition from CHRIS/Proba multi-angle data, in: Geoscience and Remote Sensing Symposium, 2004. IGARSS '04. Proceedings. 2004 IEEE International. Presented at the Geoscience and Remote Sensing Symposium, 2004. IGARSS '04. Proceedings. 2004 IEEE International, pp. 4746–4749 vol.7. doi:10.1109/IGARSS.2004.1370219

Chopping, M.J., Su, L., Laliberte, A., Rango, A., Peters, D.P.C., Kollikkathara, N., 2006. Mapping shrub abundance in desert grasslands using geometric-optical modeling and multi-angle remote sensing with CHRIS/Proba. Remote Sensing of Environment 104, 62–73. doi:10.1016/j.rse.2006.04.022

Christian, P.M., 2015. The suitability of very low cost unpiloted aircraft systems (UAS) for environmental science research (Thesis). San Francisco State University.

Ciais, P., Sabine, C., Bala, G., Bopp, L., Brovkin, V., Canadell, J., Chhabra, A., DeFries, R., Galloway, J., Heimann, M., Jones, C., Quere, C.L., Myneni, R.B., Piao, S., Thornton, P., 2013. Carbon and Other Biogeochemical Cycles, in: Stocker, T.F., Qin, D., Plattner, G.-K., Tignor, M., Allen, S.K., Boschung, J., Nauels, A., Xia, Y., Bex, V., Midgley, P.M. (Eds.), Climate Change 2013: The Physical Science Basis. Contribution of Working Group I to the Fifth Assessment Report of the Intergovernmental Panel on Climate Change. Cambridge University Press, Cambridge, United Kingdom, p. 106.

Clark, J.S., Grimm, E.C., Donovan, J.J., Fritz, S.C., Engstrom, D.R., Almendinger, J.E., 2002. Drought cycles and landscape responses to past aridity on prairies of the Northern Great Plains, USA. Ecology 83, 595–601. doi:10.2307/3071864

Cleary, M.B., Pendall, E., Ewers, B.E., 2008. Testing sagebrush allometric relationships across three fire chronosequences in Wyoming, USA. Journal of Arid Environments 72, 285–301. doi:10.1016/j.jaridenv.2007.07.013

Cleland, E.E., Collins, S.L., Dickson, T.L., Farrer, E.C., Gross, K.L., Gherardi, L.A., Hallett, L., Hobbs, R., Hsu, J.S.-T., Turnbull, L., Suding, K.N., 2013. Sensitivity of grassland plant community composition to spatial versus temporal variation in precipitation. Ecology 94, 1687–1696. doi:10.1890/12-1006.1

Clough, A., Skjemstad, J.O., 2000. Physical and chemical protection of soil organic carbon in three agricultural soils with different contents of calcium carbonate. Soil Res. 38, 1005–1016.

Cogle, A. l., Rao, K. p. c., Yule, D. f., Smith, G.., George, P. j., Srinivasan, S. t., Jangawad, L., 2002. Soil management for Alfisols in the semiarid tropics: erosion, enrichment ratios and runoff. Soil Use and Management 18, 10–17. doi:10.1111/j.1475-2743.2002.tb00044.x

Cohen, J., 1960. A coefficient of agreement for nominal scales. Educational and Psychological Measurement 20, 37–46. doi:10.1177/001316446002000104

Cole, J.J., Prairie, Y.T., Caraco, N.F., McDowell, W.H., Tranvik, L.J., Striegl, R.G., Duarte, C.M., Kortelainen, P., Downing, J.A., Middelburg, J.J., Melack, J., 2007. Plumbing the global carbon cycle: integrating inland waters into the terrestrial carbon budget. Ecosystems 10, 171–184.

Collins, S.L., Fargione, J.E., Crenshaw, C.L., Nonaka, E., Elliott, J.R., Xia, Y., Pockman, W.T., 2010. Rapid plant community responses during the summer monsoon to nighttime warming in a northern Chihuahuan Desert grassland. Journal of Arid Environments 74, 611–617. doi:10.1016/j.jaridenv.2009.10.005

Conant, R.T., Klopatek, J.M., Malin, R.C., Klopatek, C.C., 1998. Carbon pools and fluxes along an environmental gradient in northern Arizona. Biogeochemistry 43, 43–61.

Conen, F., Zimmermann, M., Leifeld, J., Seth, B., Alewell, C., 2008. Relative stability of soil carbon revealed by shifts in 15N and C:N ratio. Biogeosciences 5, 123–128.

Congalton, R.G., 1991. A review of assessing the accuracy of classifications of remotely sensed data. Remote Sensing of Environment 37, 35–46. doi:10.1016/0034-4257(91)90048-B

Connin, S.L., Virginia, R.A., Chamberlain, C.P., 1997a. Carbon isotopes reveal soil organic matter dynamics following arid land shrub expansion. Oecologia 110, 374–386.

Connin, S.L., Virginia, R.A., Chamberlain, C.P., Huenneke, L.F., Harrison, K., Schlesinger, W.H., 1997b. Dynamics of carbon storage in degraded arid land environments: a case study from the Jornada Experimental Range, New Mexico (USA), in: Squires, V.R., Glenn, E.P., Ayoub, A.T. (Eds.), Drylands and Global Change in the Twenty-First Century. University of Arizona Press, Arizona.

Cook, B.I., Seager, R., 2013. The response of the North American Monsoon to increased greenhouse gas forcing. J. Geophys. Res. Atmos. 118, 1690–1699. doi:10.1002/jgrd.50111

Cooper, J.R., Wainwright, J., Parsons, A.J., Onda, Y., Fukuwara, T., Obana, E., Kirchener, B., Long, E.J., Hargrave, G.H., 2012. A new approach for simulating the redistribution of soil particles by water erosion: a marker-in-cell model. Journal of Geophysical Research: Earth Surface. doi:10.1029/2012JF2499

Coppinger, K.D., Reiners, W.A., Burke, I.C., Olson, R.K., 1991. Net erosion on a sagebrush steppe landscape as determined by cesium-137 distribution. Soil Science Society of America Journal 55, 254–258.

Corkidi, L., Rowland, D.L., Johnson, N.C., Allen, E.B., 2002. Nitrogen fertilization alters the functioning of arbuscular mycorrhizas at two semiarid grasslands. Plant and Soil 240, 299–310. doi:10.1023/A:1015792204633

Cornelis, W.M., 2006. Hydroclimatology and wind erosion in arid and semi-arid environments, in: D'Odorico, P., Porporato, A. (Eds.), Dryland Ecohydrology. Springer, pp. 141–159.

Corti, G., Ugolini, F.C., Agnelli, A., Certini, G., Cuniglio, R., Berna, F., Fernández Sanjurjo, M.J., 2002. The soil skeleton, a forgotten pool of carbon and nitrogen in soil. European Journal of Soil Science 53, 283–298. doi:10.1046/j.1365-2389.2002.00442.x

Cox, P.M., Betts, R.A., Jones, C.D., Spall, S.A., Totterdell, I.J., 2000. Acceleration of global warming due to carbon-cycle feedbacks in a coupled climate model. Nature 408, 184–187.

Croft, H., Kuhn, N.J., Anderson, K., 2012. On the use of remote sensing techniques for monitoring spatio-temporal soil organic carbon dynamics in agricultural systems. Catena 94, 64–74. doi:10.1016/j.catena.2012.01.001

Cross, A.F., Schlesinger, W.H., 1999. Plant regulation of soil nutrient distribution in the northern Chihuahuan Desert. Plant Ecology 145, 11–25.

Cunliffe, A.M., Anderson, K., Brazier, R.E., 2013a. Soil organic carbon in semiarid rangelands. Presented at the British Society of Soil Science AGM, Lancaster.

Cunliffe, A.M., Baird, A.J., Holden, J., 2013b. Hydrological hotspots in blanket peatlands: Spatial variation in peat permeability around a natural soil pipe. Water Resources Research 49, 5342–5354. doi:10.1002/wrcr.20435

Cunliffe, A.M., Brazier, R., Anderson, K., 2016a. Drone-acquired structure-from-motion photogrammetry for high-precision measurements of biomass in semi-arid rangelands, in: Geophysical Research Abstracts. Presented at the European Geosciences Union General Assembly, EGU, Vienna, Austria.

Cunliffe, A.M., Brazier, R.E., Anderson, K., 2016b. Ultra-fine grain landscape-scale quantification of dryland vegetation structure with drone-acquired structure-from-motion photogrammetry. Remote Sensing of Environment 183, 129–143. doi:10.1016/j.rse.2016.05.019

Cunliffe, A.M., Brazier, R.E., Anderson, K., 2015. Drones in the desert: characterising biotic structure in semiarid rangelands via drone-acquired SfM. Presented at the Environmental UAV Conference, John Moores University, Liverpool, UK.

Cunliffe, A.M., Brazier, R.E., Vernon, I., 2014a. Are we overestimating organic carbon concentrations in soils containing inorganic carbon?, in: Geophysical Research Abstracts. Presented at the European Geosciences Union General Assembly, EGU, Vienna, Austria.

Cunliffe, A.M., Puttock, A.K., Anderson, K., Brazier, R.E., 2014b. The distribution and fluvial redistribution of soil organic carbon in semiarid rangelands, in: Geophysical Research Abstracts. Presented at the European Geosciences Union - General Assembly, EGU, Vienna, Austria.

Cunliffe, A.M., Puttock, A.K., Turnbull, L., Wainwright, J., Brazier, R.E., 2016c. Erosion-induced carbon fluxes from semiarid rangelands: implications of vegetation cover and enrichment dynamics for carbon inputs to aquatic systems, in: Geophysical Research Abstracts. Presented at the European Geosciences Union General Assembly, EGU, Vienna, Austria.

Cunliffe, A.M., Puttock, A.K., Turnbull, L., Wainwright, J., Brazier, R.E., 2016d. Dryland, calcareous soils store (and lose) significant quantities of near-surface organic carbon. Journal of Geophysical Research: Earth Surface. doi:10.1002/2015JF003628

Dahm, C.N., Moore, D.I., 1994. The El Nino/Souther Oscillation phenomenon and the Sevilleta long-term ecological research site, in: Greenland, D. (Ed.), El Nino and Long-Term Ecological Research (LTER) Sites. LTER Network office, University of Washington, Seattle.

Dalal, R.C., Mayer, R.J., 1986. Long term trends in fertility of soils under continuous cultivation and cereal cropping in southern Queensland. IV. Loss of organic carbon from different density functions. Soil Research 24, 301–309.

Dandois, J.P., Ellis, E.C., 2013. High spatial resolution three-dimensional mapping of vegetation spectral dynamics using computer vision. Remote Sensing of Environment 136, 259–276. doi:10.1016/j.rse.2013.04.005

Dandois, J.P., Ellis, E.C., 2010. Remote sensing of vegetation structure using computer vision. Remote Sensing 2, 1157–1176. doi:10.3390/rs2041157

Dandois, J.P., Olano, M., Ellis, E.C., 2015. Optimal altitude, overlap, and weather conditions for computer vision UAV estimates of forest structure. Remote Sensing 7, 13895–13920. doi:10.3390/rs71013895

Davies, A.B., Asner, G.P., 2014. Advances in animal ecology from 3D-LiDAR ecosystem mapping. Trends in Ecology & Evolution 29, 681–691. doi:10.1016/j.tree.2014.10.005

Dawson, J.J.C., Smith, P., 2007. Carbon losses from soil and its consequences for land-use management. Science of the Total Environment 382, 165–190. doi:10.1016/j.scitotenv.2007.03.023

De Baets, S., Meersmans, J., Vanacker, V., Quine, T.A., Van Oost, K., 2013. Spatial variability and change in soil organic carbon stocks in response to recovery following land abandonment and erosion in mountainous drylands. Soil Use and Management 29, 65–76. doi:10.1111/sum.12017

De Soyza, A.G., Whitford, W.G., Martinez-Meza, E., Van Zee, J.W., 1997. Variation in creosotebush (Larrea tridentata) canopy morphology in relation to habitat, soil fertility and associated annual plant communities. American Midland Naturalist 137, 13–26. doi:10.2307/2426751

De Zorzi, P., Barbizzi, S., Belli, M., Ciceri, G., Fajgelj, A., Moore, D., Sansone, U., Van Der Perk, M., 2005. Terminology in Soil Sampling. Pure Appl. Chem 77, 827–841. doi:10.1351/pac200577050827

Denman, K.L., Brasseur, G., Chidthaisong, A., Ciais, P., Cox, P.M., Dickinson, R.E., Hauglustaine, D., Heinze, C., Holland, E., Jacob, D., Lohmann, U., Ramachandran, S., da Silva Dias, P.L., Wofsy, S.C., Zhang, X., 2007. Couplings between changes in the climate system and biogeochemistry, in: Solomon, S., Qin, D., Manning, M., Chen, Z., Marquis, M., Averyt, K.B., Tignor, M., Miller, H.L. (Eds.), Climate Change 2007: The Physical Science Basis. Contribution of Working Group I to the Fourth Assessment Report of the Intergovernmental Panel on Climate Change. Cambridge University Press, Cambridge, United Kingdom.

Deser, C., Knutti, R., Solomon, S., Phillips, A.S., 2012. Communication of the role of natural variability in future North American climate. Nature Clim. Change 2, 775–779. doi:10.1038/nclimate1562

Ditmer, M.A., Vincent, J.B., Werden, L.K., Tanner, J.C., Laske, T.G., Iaizzo, P.A., Garshelis, D.L., Fieberg, J.R., 2015. Bears show a physiological but limited behavioral response to unmanned aerial vehicles. Current Biology 25, 2278–2283. doi:10.1016/j.cub.2015.07.024

D'Odorico, P., Porporato, A., 2006a. Ecohydrology of arid and semiarid ecosystems: an introduction, in: D'Odorico, P., Porporato, A. (Eds.), Dryland Ecohydrology. Springer, p. 10.

D'Odorico, P., Porporato, A., 2006b. Soil moisture dynamics in water-limited ecosystems, in: D'Odorico, P., Porporato, A. (Eds.), Dryland Ecohydrology. Springer, pp. 31–46.

Dodson, C., 2012. A Guide to Plants of the Northern Chihuahuan Desert. University of New Mexico Press, Albuquerque, New Mexico.

Doetterl, S., Six, J., Van Wesemael, B., Van Oost, K., 2012. Carbon cycling in eroding landscapes: geomorphic controls on soil organic C pool composition and C stabilization. Global Change Biology 18, 2218–2232. doi:10.1111/j.1365-2486.2012.02680.x

Dregne, H., Kassas, M., Rozanov, B., 1991. A new assessment of the world status of desertification. Desertification Control Bulletin 20, 6–18.

Duchaufour, P., 1976. Dynamics of organic matter in soils of temperate regions: Its action on pedogenesis. Geoderma 15, 31–40. doi:10.1016/0016-7061(76)90068-9

Dulava, S., Bean, W.T., Richmond, O.M.W., 2015. Applications of Unmanned Aircraft Systems (UAS) for Waterbird Surveys. Environmental Practice 17, 201–210. doi:10.1017/S1466046615000186

Dunford, R., Michel, K., Gagnage, M., Piégay, H., Trémelo, M.-L., 2009. Potential and constraints of unmanned aerial vehicle technology for the characterization of Mediterranean riparian forest. International Journal of Remote Sensing 30, 4915–4935. doi:10.1080/01431160903023025

Dungan, J.L., Perry, J.N., Dale, M.R.T., Legendre, P., Citron-Pousty, S., Fortin, M.-J., Jakomulska, A., Miriti, M., Rosenberg, M.S., 2002. A balanced view of scale in spatial statistical analysis. Ecography 25, 626–640. doi:10.1034/j.1600-0587.2002.250510.x

Egashira, K., Nakai, S., 1987. Size distribution and wet density of sediment eroded under simulated rainfall. Soil Science and Plant Nutrition 33, 347–354. doi:10.1080/00380768.1987.10557580

Ehleringer, J., 2001. Productivity of deserts, in: Roy, J., Saugier, B., Mooney, H. (Eds.), Terrestrial Global Productivity. Academic Press, San Diego, California, USA, pp. 345–362.

Eldridge, D.J., Bowker, M.A., Maestre, F.T., Roger, E., Reynolds, J.F., Whitford, W.G., 2011. Impacts of shrub encroachment on ecosystem structure and functioning: towards a global synthesis. Ecology Letters 14, 709–722. doi:10.1111/j.1461-0248.2011.01630.x

Eldridge, D.J., Maestre, F.T., Maltez-Mouro, S., Bowker, M.A., 2012. A global database of shrub encroachment effects on ecosystem structure and functioning. Ecology 93, 2499–2499. doi:10.1890/12-0749.1

Ellert, B.H., Janzen, H.H., McConkey, B.G., 2001. Measuring and comparing soil carbon storage, in: Lal, R., Kimble, J.M., Follett, R.F., Steward, B.A. (Eds.), Assessment Methods for Soil Carbon. pp. 131–146.

Elmendorf, S.C., Henry, G.H.R., Hollister, R.D., Björk, R.G., Boulanger-Lapointe, N., Cooper, E.J., Cornelissen, J.H.C., Day, T.A., Dorrepaal, E., Elumeeva, T.G., Gill, M., Gould, W.A., Harte, J., Hik, D.S., Hofgaard, A., Johnson, D.R., Johnstone, J.F., Jónsdóttir, I.S., Jorgenson, J.C., Klanderud, K., Klein, J.A., Koh, S., Kudo, G., Lara, M., Lévesque, E., Magnússon, B., May, J.L., Mercado-Dı´az, J.A., Michelsen, A., Molau, U., Myers-Smith, I.H., Oberbauer, S.F., Onipchenko, V.G., Rixen, C., Martin Schmidt, N., Shaver, G.R., Spasojevic, M.J., Þórhallsdóttir, Þ.E., Tolvanen, A., Troxler, T., Tweedie, C.E., Villareal, S., Wahren, C.-H., Walker, X., Webber, P.J., Welker, J.M., Wipf, S., 2012. Plot-scale evidence of tundra vegetation change and links to recent summer warming. Nature Clim. Change 2, 453–457. doi:10.1038/nclimate1465

Elmore, A.J., Mustard, J.F., Manning, S.J., Lobell, D.B., 2000. Quantifying vegetation change in semiarid environments: precision and accuracy of spectral mixture analysis and the normalized difference vegetation index. Remote Sensing of Environment 73, 87–102. doi:10.1016/S0034-4257(00)00100-0

Emmerich, W.E., 2003. Carbon dioxide fluxes in a semiarid environment with high carbonate soils. Agricultural and Forest Meteorology 116, 91–102.

Encinales, D.N., 2016. Improving estimates of CO2 emissions under REDD+ in the Colombian Amazon: Better understanding for climate change mitigation (Doctor of Philosophy). University of Exeter.

Engel, A., Abramson, L., Szlosek, J., Liu, Z., Stewart, G., Hirschberg, D., Lee, C., 2009a. Investigating the effect of ballasting by CaCO3 in Emiliania huxleyi, II: Decomposition of particulate organic matter. Deep Sea Research Part II: Topical Studies in Oceanography, MedFlux:Investigations of Particle Flux in the Twilight Zone 56, 1408–1419. doi:10.1016/j.dsr2.2008.11.028

Engel, A., Szlosek, J., Abramson, L., Liu, Z., Lee, C., 2009b. Investigating the effect of ballasting by CaCO3 in Emiliania huxleyi: I. Formation, settling velocities and physical properties of aggregates. Deep Sea Research Part II: Topical Studies in Oceanography, MedFlux:Investigations of Particle Flux in the Twilight Zone 56, 1396–1407. doi:10.1016/j.dsr2.2008.11.027

Enquist, B.J., 2002. Universal scaling in tree and vascular plant allometry: toward a general quantitative theory linking plant form and function from cells to ecosystems. Tree Physiol 22, 1045–1064. doi:10.1093/treephys/22.15-16.1045

Epron, D., Nouvellon, Y., Ryan, M.G., 2012. Introduction to the invited issue on carbon allocation of trees and forests. Tree Physiol 32, 639–643. doi:10.1093/treephys/tps055

Epstein, J.M., 2008. Why Model?
Erdody, T.L., Moskal, L.M., 2010. Fusion of LiDAR and imagery for estimating forest canopy fuels. Remote Sensing of Environment 114, 725–737. doi:10.1016/j.rse.2009.11.002
ESRI, 2016. ArcGIS Desktop Help. ESRI.
Eswaran, H., Reich, P.F., Kimble, J.M., Beinroth, F.H., Padmanabhan, E., Moncharoen, P., 2000. Global carbon sinks, in: Lal, R., Kimble, J.M., Eswaran, H., Stewart, B.A. (Eds.), Global Glimate Change and Pedogenic Carbonate. CRC Press, Boca Raton, FL., pp. 15–26.
Ewing, S.A., Southard, R.J., Macalady, J.L., Hartshorn, A.S., Johnson, M.J., 2007. Soil microbial fingerprints, carbon, and nitrogen in a Mojave Desert creosote-bush ecosystem. Soil Science Society of America Journal 71, 469–475.
FAA, 2013. Integration of Civil Unmanned Aircraft Systems (UAS) in the National Airspace System (NAS) Roadmap.
FAA, 2011. Fact Sheet: Unmanned Aircraft Systems (UAS).
FAA, 2010. FAA Safety Briefing: The Wings of Change.
FAA, 2007. Unmanned Aircraft Operations in the National Airspace System.
FAA, 2005. Unmanned Aircraft Systems Operations in the U.S. National Airspace System - Interim Operational Approval Guidance.
FAA, 1981. Model Aircraft Operating Standards.
Falster, D.S., Westoby, M., 2003. Leaf size and angle vary widely across species: what consequences for light interception? New Phytologist 158, 509–525. doi:10.1046/j.1469-8137.2003.00765.x
Fan, S., Gloor, M., Mahlman, J., Pacala, S.W., Sarmiento, J., Takahashi, T., Tans, P., 1998. A large terrestrial carbon sink in North America implied by atmospheric and oceanic carbon dioxide data and models. Science 282, 442–446.
Favis-Mortlock, D., 2013. Non-Linear Dynamics, Self-Organization and Cellular Automata Models, in: Wainwright, J., Mulligan, M. (Eds.), Environmental Modelling: Finding Simplicity in Complexity. Wiley-Blackwell, pp. 45–68.
Féret, J.-B., Asner, G.P., 2012. Semi-supervised methods to identify individual crowns of lowland tropical canopy species using imaging spectroscopy and LiDAR. Remote Sensing 4, 2457–2476. doi:10.3390/rs4082457
Fernández, J.M., Peltre, C., Craine, J.M., Plante, A.F., 2012. Improved characterization of soil organic matter by thermal analysis using CO2/H2O evolved gas analysis. Environ. Sci. Technol. 46, 8921–8927. doi:10.1021/es301375d
Ffolliott, P.F., Gottfried, G.J., 2002. Dynamics of a Pinyon-Juniper stand in Northern Arizona: A half-century history (Research Paper No. RMRS-RP-35). Department of Agriculture, Forest Service, Rocky Mountain Research Station, Fort Collins, CO, USA.
Field, J.P., Belnap, J., Breshears, D.D., Neff, J., Okin, G.S., Whicker, J.J., Painter, T.H., Ravi, S., Reheis, M.C., Reynolds, R., 2010. The ecology of dust. Frontiers in Ecology and the Environment 8, 423–430. doi:10.1890/090050
Field, J.P., Breshears, D.D., Whicker, J.J., 2009. Toward a more holistic perspective of soil erosion: Why aeolian research needs to explicitly consider fluvial processes and interactions. Aeolian Research 1, 9–17. doi:10.1016/j.aeolia.2009.04.002
Fierer, N.G., Gabet, E.J., 2002. Carbon and nitrogen losses by surface runoff following changes in vegetation. Journal of Environmental Quality 31, 1207–1213. doi:10.2134/jeq2002.1207

Finch, D.M., 2012. Climate Change in Grasslands, Shrublands and Deserts of the Interior American West: A Review and Needs Assessment. United States Department of Agriculture, Fort Collins.

Finkelstein, P.L., Sims, P.F., 2001. Sampling error in eddy correlation flux measurements. J. Geophys. Res. 106, 3503–3509. doi:10.1029/2000JD900731

Fisher, F.M., Zak, J.C., Cunningham, G.L., Whitford, W.G., 1988. Water and nitrogen effects on growth and allocation patterns of creosotebush in the Northern Chihuahuan Desert. Journal of Range Management 41, 387–391. doi:10.2307/3899572

Flores Cervantes, J.H., Istanbulluoglu, E., Vivoni, E.R., Holifield Collins, C.D., Bras, R.L., 2012. A geomorphic perspective on terrain-modulated organization of vegetation productivity: analysis in two semiarid grassland ecosystems in Southwestern United States. Ecohydrology. doi:10.1002/eco.1333

Follett, R.F., Kimble, J.M., Lal, R., 2001. The potential of US grazing lands to sequester carbon and mitigate the greenhouse effect, in: Follett, R.F., Kimble, J.M., Lal, R. (Eds.), The Potential of US Grazing Lands to Sequester Carbon and Mitigate the Greenhouse Effect. CRC-Lewis, Boca Raton, FL, USA., pp. 369–398.

Follett, R.F., Reed, D.A., 2010. Soil carbon sequestration in grazing lands: societal benefits and policy implications. Rangeland Ecology & Management 63, 4–15. doi:10.2111/08-225.1

Fontaine, S., Barot, S., Barre, P., Bdioui, N., Mary, B., Rumpel, C., 2007. Stability of organic carbon in deep soil layers controlled by fresh carbon supply. Nature 450, 277–280.

Fontaine, S., Mariotti, A., Abbadie, L., 2003. The priming effect of organic matter: a question of microbial competition? Soil Biology and Biochemistry 35, 837–843. doi:10.1016/S0038-0717(03)00123-8

Foster, B.L., Tilman, D., 2000. Dynamic and static views of succession: Testing the descriptive power of the chronosequence approach. Plant Ecology 146, 1–10. doi:10.1023/A:1009895103017

Frank, D.A., Pontes, A.W., McFarlane, K.J., 2012. Controls on soil organic carbon stocks and turnover among North American ecosystems. Ecosystems 15, 604–615. doi:10.1007/s10021-012-9534-2

Friedel, M.H., Laycock, W.A., Bastin, G.N., 2000. Assessing rangeland condition and trend, in: ’t Mannetje, L., Jones, R.M. (Eds.), Field and Laboratory Methods for Grassland and Animal Production Research. CABI Publishing, Ney York, NY, USA, pp. 227–262.

Friend, A.D., Lucht, W., Rademacher, T.T., Keribin, R., Betts, R., Cadule, P., Ciais, P., Clark, D.B., Dankers, R., Falloon, P.D., Ito, A., Kahana, R., Kleidon, A., Lomas, M.R., Nishina, K., Ostberg, S., Pavlick, R., Peylin, P., Schaphoff, S., Vuichard, N., Warszawski, L., Wiltshire, A., Woodward, F.I., 2013. Carbon residence time dominates uncertainty in terrestrial vegetation responses to future climate and atmospheric CO2. PNAS 111, 3280–3285. doi:10.1073/pnas.1222477110

Friggens, M.M., Warwell, M.V., Chambers, J.C., Kitchen, S.G., 2012. Modeling and predicting vegetation response of Western USA grasslands, shrublands, and deserts to climate change, in: Finch, D.M. (Ed.), Climate Change in Grasslands, Shrublands, and Deserts of the Interior American West: A Review and Needs Assesment.

Frolking, S., Palace, M.W., Clark, D.B., Chambers, J.Q., Shugart, H.H., Hurtt, G.C., 2009. Forest disturbance and recovery: A general review in the context of

spaceborne remote sensing of impacts on aboveground biomass and canopy structure. J. Geophys. Res. 114, G00E02. doi:10.1029/2008JG000911
Furbish, D.J., Childs, E.M., Haff, P.K., Schmeeckle, M.W., 2009. Rain splash of soil grains as a stochastic advection-dispersion process, with implications for desert plant-soil interactions and land-surface evolution. J. Geophys. Res. 114, F00A03. doi:10.1029/2009JF001265
Gabet, E.J., Fierer, N., Chadwick, O.A., 2005. Prediction of sediment-bound nutrient delivery from semi-arid California watersheds. Journal of Geophysical Research: Biogeosciences 110, G02001. doi:10.1029/2005jg000032
Galy, V., Bouchez, J., France-Lanord, C., 2007. Determination of total organic carbon content and δ13C in carbonate-rich detrital sediments. Geostandards and Geoanalytical Research 31, 199–207. doi:10.1111/j.1751-908X.2007.00864.x
Gao, Q., Reynolds, J.F., 2003. Historical shrub–grass transitions in the northern Chihuahuan Desert: modeling the effects of shifting rainfall seasonality and event size over a landscape gradient. Global Change Biology 9, 1475–1493. doi:10.1046/j.1365-2486.2003.00676.x
Garbrecht, J., Martz, L., 1994. Grid size dependency of parameters extracted from digital elevation models. Computers & Geosciences 20, 85–87. doi:10.1016/0098-3004(94)90098-1
Gaylord, M.L., Kolb, T.E., Pockman, W.T., Plaut, J.A., Yepez, E.A., Macalady, A.K., Pangle, R.E., McDowell, N.G., 2013. Drought predisposes piñon–juniper woodlands to insect attacks and mortality. New Phytologist.
Gentine, P., Guérin, M., Uriarte, M., McDowell, N.G., Pockman, W.T., 2015. An allometry-based model of the survival strategies of hydraulic failure and carbon starvation. Ecohydrol. n/a-n/a. doi:10.1002/eco.1654
Getzin, S., Nuske, R.S., Wiegand, K., 2014. Using unmanned aerial vehicles (UAV) to quantify spatial gap patterns in forests. Remote Sensing 6, 6988–7004. doi:10.3390/rs6086988
Getzin, S., Wiegand, K., Schöning, I., 2012. Assessing biodiversity in forests using very high-resolution images and unmanned aerial vehicles. Methods in Ecology and Evolution 3, 397–404. doi:10.1111/j.2041-210X.2011.00158.x
Ghadiri, H., Rose, C.W., 1991a. Sorbed chemical transport in overland flow: II. enrichment ratio variation with erosion processes. Journal of Environmental Quality 20, 634–641. doi:10.2134/jeq1991.00472425002000030021x
Ghadiri, H., Rose, C.W., 1991b. Sorbed chemical transport in overland flow: I. A nutrient and pesticide enrichment mechanism. Journal of Environmental Quality 20, 628–633.
Gholz, H.L., 1980. Structure and productivity of Juniperus occidentalis in central oregon. American Midland Naturalist 103, 251–261. doi:10.2307/2424623
Gibbens, R.P., Beck, R.F., McNeely, R.P., Herbel, C.H., 1992. Recent rates of Mesquite establishment in the northern Chihuahuan Desert. Journal of Range Management 45, 585–588. doi:10.2307/4002576
Gibbens, R.P., Lenz, J.M., 2001. Root systems of some Chihuahuan Desert plants. Journal of Arid Environments 49, 221–263.
Gibbens, R.P., McNeely, R.P., Havstad, K.M., Beck, R.F., Nolen, B., 2005. Vegetation change in the Jornada Basin from 1858 to 1998. Journal of Arid Environments 61, 651–668. doi:10.1016/j.jaridenv.2004.10.001
Gifford, R.M., Howden, M., 2001. Vegetation thickening in an ecological perspective: significance to national greenhouse gas inventories. Environmental Science & Policy 4, 59–72. doi:10.1016/S1462-9011(00)00109-X

Gile, L.H., 1970. Soils of the Rio Grande Valley Border in Southern New Mexico. Soil Science Society of America Journal 34, 465–472. doi:10.2136/sssaj1970.03615995003400030032x

Gile, L.H., Hawley, J.W., Grossman, R.B., 1981. Soils and Geomorphology in the Basin and Range Area of Southern New Mexico: Guidebook to the Desert Project. New Mexico Bureau of Mines and Mineral Resources, Socorro, NM, USA.

Gillan, J.K., Karl, J.W., Duniway, M., Elaksher, A., 2014. Modeling vegetation heights from high resolution stereo aerial photography: An application for broad-scale rangeland monitoring. Journal of Environmental Management 144, 226–235. doi:10.1016/j.jenvman.2014.05.028

Gillette, D.A., Pitchford, A.M., 2004. Sand flux in the northern Chihuahuan desert, New Mexico, USA, and the influence of mesquite-dominated landscapes. J. Geophys. Res. 109, F04003. doi:10.1029/2003JF000031

Gini, R., Pagliari, D., Passoni, D., Pinto, L., Sona, G., Dosso, P., 2013. UAV photogrammetry: block triangulation comparisons. ISPRS - International Archives of the Photogrammetry, Remote Sensing and Spatial Information Sciences XL-1/W2, 157–162. doi:10.5194/isprsarchives-XL-1-W2-157-2013

Gislason, S.R., Oelkers, E.H., Eiriksdottir, E.S., Kardjilov, M.I., Gisladottir, G., Sigfusson, B., Snorrason, A., Elefsen, S., Hardardottir, J., Torssander, P., 2009. Direct evidence of the feedback between climate and weathering. Earth and Planetary Science Letters 277, 213–222. doi:10.1016/j.epsl.2008.10.018

Glenn, E., Squires, V., Olsen, M., Frye, R., 1993. Potential for carbon sequestration in the drylands. Water Air Soil Pollut 70, 341–355. doi:10.1007/bf01105006

Glenn, E., Stafford Smith, M., Squires, V., 1998. On our failure to control desertification: implications for global change issues, and a research agenda for the future. Environmental Science & Policy 1, 71–78. doi:10.1016/S1462-9011(98)00007-0

Glenn, N.F., Spaete, L.P., Sankey, T.T., Derryberry, D.R., Hardegree, S.P., Mitchell, J.J., 2011. Errors in LiDAR-derived shrub height and crown area on sloped terrain. Journal of Arid Environments 75, 377–382. doi:10.1016/j.jaridenv.2010.11.005

Gobakken, T., Næsset, E., 2004. Estimation of diameter and basal area distributions in coniferous forest by means of airborne laser scanner data. Scandinavian Journal of Forest Research 19, 529–542. doi:10.1080/02827580410019454

Gocke, M., Pustovoytov, K., Kuzyakov, Y., 2011. Carbonate recrystallization in root-free soil and rhizosphere of Triticum aestivum and Lolium perenne estimated by 14C labeling. Biogeochemistry 103, 209–222. doi:10.1007/s10533-010-9456-z

Goebel, M.E., Perryman, W.L., Hinke, J.T., Krause, D.J., Hann, N.A., Gardner, S., LeRoi, D.J., 2015. A small unmanned aerial system for estimating abundance and size of Antarctic predators. Polar Biol 38, 619–630. doi:10.1007/s00300-014-1625-4

Goetz, S., Dubayah, R., 2011. Advances in remote sensing technology and implications for measuring and monitoring forest carbon stocks and change. Carbon Management 2, 231–244. doi:10.4155/cmt.11.18

Goetz, S., Steinberg, D., Dubayah, R., Blair, B., 2007. Laser remote sensing of canopy habitat heterogeneity as a predictor of bird species richness in an eastern temperate forest, USA. Remote Sensing of Environment 108, 254–263. doi:10.1016/j.rse.2006.11.016

Goldberg, D.E., Turner, R.M., 1986. Vegetation Change and Plant Demography in Permanent Plots in the Sonoran Desert. Ecology 67, 695–712. doi:10.2307/1937693
Goldstein, M., Seheult, A., Vernon, I., 2013. Assessing Model Adequacy, in: Wainwright, J., Mulligan, M. (Eds.), Environmental Modelling: Finding Simplicity in Complexity. Wiley-Blackwell, pp. 435–452.
Gomez, B., Baisden, W.T., Rogers, K.M., 2010. Variable composition of particle-bound organic carbon in steepland river systems. Journal of Geophysical Research: Earth Surface 115, F04006. doi:10.1029/2010jf001713
Gonçalves, J., Henriques, R., Alves, P., Sousa-Silva, R., Monteiro, A.T., Lomba, Â., Marcos, B., Honrado, J., 2015. Evaluating an unmanned aerial vehicle-based approach for assessing habitat extent and condition in fine-scale early successional mountain mosaics. Appl Veg Sci n/a-n/a. doi:10.1111/avsc.12204
Goodale, C.L., Davidson, E.A., 2002. Uncertain sinks in the shrubs. Nature 418, 593.
Goodman, A.M., Ennos, A.R., 1999. The effects of soil bulk density on the morphology and anchorage mechanics of the root systems of sunflower and maize. Ann Bot 83, 293–302. doi:10.1006/anbo.1998.0822
Goodman, A.M., Ennos, A.R., 1996. A comparative study of the response of the roots and shoots of sunflower and maize to mechanical stimulation. J. Exp. Bot. 47, 1499–1507. doi:10.1093/jxb/47.10.1499
Gosz, J.R., 1993. Ecotone hierarchies. Ecological Applications 3, 370–376.
Goudie, A.S., 1996. Organic agency in calcrete development. Journal of Arid Environments 32, 103–110. doi:10.1006/jare.1996.0010
Govers, G., Lobb, D.A., Quine, T.A., 1999. Tillage erosion and translocation: emergence of a new paradigm in soil erosion research. Soil & Tillage Research 51, 167–174.
Grand-Clement, E., Luscombe, D.J., Anderson, K., Gatis, N., Benaud, P., Brazier, R.E., 2014. Antecedent conditions control carbon loss and downstream water quality from shallow, damaged peatlands. Science of The Total Environment 493, 961–973. doi:10.1016/j.scitotenv.2014.06.091
Grayson, R.B., Moore, I.D., McMahon, T.A., 1992. Physically based hydrologic modeling: 2. Is the concept realistic? Water Resources Research 28, 2659. doi:10.1029/92WR01259
Greaves, H.E., Vierling, L.A., Eitel, J.U.H., Boelman, N.T., Magney, T.S., Prager, C.M., Griffin, K.L., 2015. Estimating aboveground biomass and leaf area of low-stature Arctic shrubs with terrestrial LiDAR. Remote Sensing of Envrionment 164, 26–35. doi:10.1016/j.rse.2015.02.023
Gregorich, E.G., 1996. Soil quality: a Canadian perspective, in: Ca, eron, Cornforth, I.S., McLaren, R.G., Beare, M.H., Basher, L.R., Metherell, A.K., Kerr, J.E. (Eds.), Soil Quality Indicators for Sustainable Agriculture in New Zealand: Proceedings of a Workshop. Lincoln University, Christchurch, New Zealand, pp. 40–52.
Gregorich, E.G., Greer, K.J., Anderson, D.W., Liang, B.C., 1998. Carbon distribution and losses: erosion and deposition effects. Soil and Tillage Research 47, 291–302.
Gregorich, E.G., Kachanoski, R.G., Voroney, R.P., 1989. Carbon mineralization in soil size fractions after various amounts of aggregate disruption. Journal of Soil Science 40, 649–659. doi:10.1111/j.1365-2389.1989.tb01306.x
Grier, C.C., Elliott, K.J., McCullough, D.G., 1992. Biomass distribution and productivity of Pinus edulis—Juniperus monosperma woodlands of north-

central Arizona. Forest Ecology and Management 50, 331–350. doi:10.1016/0378-1127(92)90346-B
Grimaldi, S., Nardi, F., Benedetto, F.D., Istanbulluoglu, E., Bras, R.L., 2007. A physically-based method for removing pits in digital elevation models. Advances in Water Resources, Recent Developments in Hydrologic Analysis 30, 2151–2158. doi:10.1016/j.advwatres.2006.11.016
Grover, H.D., Musick, H.B., 1990. Shrubland encroachment in southern New Mexico, USA: an analysis of desertification processes in the American Southwest. Climatic Change 17, 305–330.
Guevara, J.C., Gonnet, J.M., Estevez, O.R., 2002. Biomass estimation for native perennial grasses in the plain of Mendoza, Argentina. Journal of Arid Environments 50, 613–619. doi:10.1006/jare.2001.0915
Guibert, H., Fallavier, P., Roméro, J.-J., 1999. Carbon content in soil particle size and consequence on cation exchange capacity of alfisols. Commun. Soil Sci. Plant Anal. 30, 2521–2537. doi:10.1080/00103629909370392
Gutzler, D.S., Kann, D.M., Thornbrugh, C., 2002. Modulation of ENSO-based long-lead outlooks of southwestern US winter precipitation by the Pacific Decadal Oscillation. Weather and Forecasting 17, 1163–1172.
Gutzler, D.S., Robbins, T.O., 2011. Climate variability and projected change in the western United States: regional downscaling and drought statistics. Climate Dynamics 37, 835–849. doi:10.1007/s00382-010-0838-7
Haala, N., 2011. Multiray photogrammetry and dense image matching [WWW Document]. Universität Stuttgar; Institut für Photogrammetrie. URL http://www.ifp.uni-stuttgart.de/PhoWo/2011/presentations/190Haala.pdf (accessed 4.25.16).
Hackney, C., Clayton, 2015. Unmanned Aerial Vehicles (UAVs) and their application in geomorphic mapping, in: Geomorphological Techniques. British Society for Geomorphology, p. Chapter 2, Section 1.7.
Hairsine, P.B., Sander, G.C., 2009. Comment on “A transport-distance based approach to scaling erosion rates”: Parts 1, 2 and 3 by Wainwright et al. Earth Surface Processes and Landforms 34, 882–885. doi:10.1002/esp.1782
Halikia, I., Zoumpoulakis, L., Christodoulou, E., Prattis, D., 2001. Kinetic study of the thermal decomposition of calcium carbonate by isothermal methods of analysis. The European Journal of Mineral Processing and Environmental Protection 1, 89–102.
Han, L., Sun, K., Jin, J., Xing, B., 2016. Some concepts of soil organic carbon characteristics and mineral interaction from a review of literature. Soil Biology and Biochemistry 94, 107–121. doi:10.1016/j.soilbio.2015.11.023
Hansen, A., Rotella, J.J., 2000. Bird responses to forest fragmentation, in: Knight, R.L., Smith, F.W., Romme, W.H., Buskirk, S.W. (Eds.), Forest Fragmentation in the Southern Rockies. University Press of Boulder Colorado, Boulder, Colorado, USA.
Harden, J.W., Sharpe, J.M., Parton, W.J., Ojima, D.S., Fries, T.L., Huntington, T.G., Dabney, S.M., 1999. Dynamic replacement and loss of soil carbon on eroding cropland. Global Biogeochemical Cycles 13, 885–901. doi:10.1029/1999gb900061
Harman, C.J., Lohse, K.A., Troch, P.A., Sivapalan, M., 2014. Spatial patterns of vegetation, soils and microtopography from terrestrial laser scanning on two semi-arid hillslopes of contrasting lithology. Journal of Geophysical Research: Biogeosciences 119, 163–180. doi:10.1002/2013JG002507
Harris, D., Horwáth, W.R., van Kessel, C., 2001. Acid fumigation of soils to remove carbonates prior to total organic carbon or CARBON-13 isotopic analysis.

Soil Science Society of America Journal 65, 1853. doi:10.2136/sssaj2001.1853
Harrison, S.P., Kohfeld, K.E., Roelandt, C., Claquin, T., 2001. The role of dust in climate changes today, at the last glacial maximum and in the future. Earth-Science Reviews, Recent research on loess and palaeosols, pure and applied 54, 43–80. doi:10.1016/S0012-8252(01)00041-1
Hassan, M.A., Church, M., Ashworth, P.J., 1992. Virtual rate and mean distance of travel of individual clasts in gravel-bed channels. Earth Surf. Process. Landforms 17, 617–627. doi:10.1002/esp.3290170607
Hastings, J.R., Turner, R.M., 1965. The Changing Mile. University of Arizona Press, Tuscan, AZ.
Hellesen, T., Matikainen, L., 2013. An object-based approach for mapping shrub and tree cover on grassland habitats by use of LiDAR and CIR Orthoimages. Remote Sensing 5, 558–583. doi:10.3390/rs5020558
Henry, B.K., Danaher, T., McKeon, G.M., Burrows, W.H., 2002. A review of the potential role of greenhouse gas abatement in native vegetation management in Queensland's rangelands. Rangel. J. 24, 112–132.
Herrick, J.E., Van Zee, J.W., Havstad, K.M., Burkett, L., Whitford, W.G., 2005. Monitoring Manual for Grassland, Shrubland and Savanna Ecosystems. Volume I: Quick Start and Volume II: Design, Supplementary Methods and Interpretation. USDA-ARS Jornada Experimental Range, Las Cruces, NM, UAS.
Herweijer, C., Seager, R., Cook, E.R., 2006. North American droughts of the mid to late nineteenth century: a history, simulation and implication for Mediaeval drought. The Holocene 16, 159–171. doi:10.1191/0959683606hl917rp
Hessel, R., 2005. Effects of grid cell size and time step length on simulation results of the Limburg soil erosion model (LISEM). Hydrological Processes 19, 3037–3049. doi:10.1002/hyp.5815
Hewett, C.J.M., Wainwright, J., Parsons, A.J., Cooper, J.R., Kitchener, B.G.B., Hargrave, G., Long, E.J., Onda, Y., Patin, J., In Prep. Simulating changes in topography during storms in process-based soil erosion modelling.
Hibbard, K.A., Archer, S.R., Schimel, D.S., Valentine, D.W., 2001. Biogeochemical changes accompanying woody plant encroachment in a subtropical savanna. Ecology 82, 1999–2011. doi:10.1890/0012-9658(2001)082[1999:BCAWPE]2.0.CO;2
Hill, T.C., Williams, M., Bloom, A.A., Mitchard, E.T.A., Ryan, C.M., 2013. Are inventory based and remotely sensed above-ground biomass estimates consistent? PLoS ONE 8, e74170. doi:10.1371/journal.pone.0074170
Hirmas, D.R., Graham, R.C., 2011. Pedogenesis and soil-geomorphic relationships in an arid mountain range, Mojave Desert, California. Soil Science Society of America Journal 75, 192–206. doi:10.2136/sssaj2010.0152
Hochstrasser, T., Millington, J.D.A., Papanastasis, V.P., Parsons, A.J., Roggero, P.P., Brazier, R.E., Estrany, J., Farina, A., Puttock, A.K., 2014. The study of land degradation in drylands: state of the art, in: Müller, E.N., Wainwright, J., Parsons, A.J., Turnbull, L. (Eds.), Patterns of Land Degradation in Drylands: Understanding Self-Organising Ecogeomorphic Systems, 13-54. Springer, Dordrecht.
Holland, E.A., Parton, W.J., Detling, J.K., Coppock, D.L., 1992. Physiological responses of plant populations to herbivory and their consequences for ecosystem nutrient flow. The American Naturalist 140, 685–706.

Hollinger, D.Y., Richardson, A.D., 2005. Uncertainty in eddy covariance measurements and its application to physiological models. Tree Physiol 25, 873–885. doi:10.1093/treephys/25.7.873

Holmén, K., 2000. The Global Carbon Cycle, in: Jacobson, M.C., Charlson, R.J., Rodhe, H., Orians, G.H. (Eds.), Earth System Science: From Biogeochemical Cycles to Global Change, International Geophysics Series. Academic Press, London, pp. 282–321.

Hoogmoed, W.B., Stroosnijder, L., 1984. Crust formation on sandy soils in the Sahel I. Rainfall and infiltration. Soil and Tillage Research 4, 5–23. doi:10.1016/0167-1987(84)90013-8

Hooper, D.U., Johnson, L., 1999. Nitrogen limitation in dryland ecosystems: Responses to geographical and temporal variation in precipitation. Biogeochemistry 46, 247–293. doi:10.1007/BF01007582

Houghton, R.A., 2007. Balancing the global carbon budget. Annual Reviews of Earth and Planetary Science 35, 313–347. doi:10.1146/annurev.earth.35.031306.140057

Houghton, R.A., 2003a. Revised estimates of the annual net flux of carbon to the atmosphere from changes in land use and land management 1850–2000. Tellus B 55, 378–390. doi:10.1034/j.1600-0889.2003.01450.x

Houghton, R.A., 2003b. Why are estimates of the terrestrial carbon balance so different? Global Change Biology 9, 500–509.

Houghton, R.A., Hackler, J.L., Lawrence, K.T., 2000. Changes in terrestrial carbon storage in the United States. 2: The role of fire and fire management. Global Ecology and Biogeography 9, 145–170. doi:10.1046/j.1365-2699.2000.00164.x

Houghton, R.A., Hackler, J.L., Lawrence, K.T., 1999. The US carbon budget: contributions from land-use change. Science 285, 574–578.

Houghton, R.A., Hall, F., Goetz, S.J., 2009. Importance of biomass in the global carbon cycle. J. Geophys. Res. 114, G00E03. doi:10.1029/2009JG000935

House, J.I., Archer, S., Breshears, D.D., Scholes, R.J., NCEAS Tree–Grass Interactions Participants, 2003. Conundrums in mixed woody–herbaceous plant systems. Journal of Biogeography 30, 1763–1777. doi:10.1046/j.1365-2699.2003.00873.x

House, J.I., Hall, D.O., 2001. Productivity of Tropical Savannas and Grasslands, in: Roy, J., Saugier, B., Mooney, H. (Eds.), Terrestrial Global Productivity. Academic Press, San Diego, pp. 363–400.

Howes, D.A., Abrahams, A.D., 2003. Modeling runoff and runon in a desert shrubland ecosystem, Jornada Basin, New Mexico. Geomorphology 53, 45–73.

Hu, Y., Fister, W., Kuhn, N.J., 2013. Temporal variation of SOC enrichment from interrill erosion over prolonged rainfall simulations. Agriculture 3, 726–740. doi:10.3390/agriculture3040726

Hu, Y., Kuhn, N.J., 2016. Erosion-induced exposure of SOC to mineralization in aggregated sediment. CATENA 137, 517–525. doi:10.1016/j.catena.2015.10.024

Hu, Y., Kuhn, N.J., 2014. Aggregates reduce transport distance of soil organic carbon: are our balances correct? Biogeosciences Discuss. 11, 8829–8859. doi:10.5194/bgd-11-8829-2014

Huang, C., Asner, G.P., Martin, R.E., Barger, N.N., Neff, J.C., 2009. Multiscale analysis of tree cover and aboveground carbon stocks in pinyon–juniper woodlands. Ecological Applications 19, 668–681. doi:10.1890/07-2103.1

Huang, C.-Y., Marsh, S.E., McClaran, M.P., Archer, S.R., 2007. Postfire stand structure in a semiarid savanna: cross-scale challenges estimating biomass. Ecological Applications 17, 1899–1910. doi:10.1890/06-1968.1

Huenneke, L.F., Anderson, J.P., Remmenga, M., Schlesinger, W.H., 2002. Desertification alters patterns of aboveground net primary production in Chihuahuan ecosystems. Global Change Biology 8, 247–264.

Huenneke, L.F., Clason, D., Muldavin, E., 2001. Spatial heterogeneity in Chihuahuan Desert vegetation: implications for sampling methods in semi-arid ecosystems. Journal of Arid Environments 47, 257–270. doi:10.1006/jare.2000.0678

Huenneke, L.F., Schlesinger, W.H., 2006. Patterns of net primary production in Chihuahuan Desert ecosystems, in: Havstad, K.M., Huenneke, L.F., Schlesinger, W.H. (Eds.), Structure and Function of a Chihuahuan Desert Ecosystem. Oxford University Press, New York, pp. 232–246.

Hufkens, K., Bogaert, J., Dong, Q.H., Lu, L., Huang, C.L., Ma, M.G., Che, T., Li, X., Veroustraete, F., Ceulemans, R., 2008. Impacts and uncertainties of upscaling of remote-sensing data validation for a semi-arid woodland. Journal of Arid Environments 72, 1490–1505. doi:10.1016/j.jaridenv.2008.02.012

Hulet, A., Roundy, B.A., Petersen, S.L., Bunting, S.C., Jensen, R.R., Roundy, D.B., 2014. Utilizing national agriculture imagery program data to estimate tree cover and biomass of piñon and juniper woodlands. Rangeland Ecology & Management 67, 563–572. doi:10.2111/REM-D-13-00044.1

Humphrey, R.R., 1958. The desert grassland a history of vegetational change and an analysis of causes. Botanical Review 24, 193–252. doi:10.2307/4353584

Humphrey, R.R., Mehrhoff, L.A., 1958. Vegetation changes on a Southern Arizona grassland range. Ecology 39, 720–726. doi:10.2307/1931612

Hunziker, J.H., 1975. On the geographical origin of Larrea divaricata (Zygophyllaceae). Annals of the Missouri Botanical Garden 62, 497–500. doi:10.2307/2395211

Hutton, C.J., 2012. Chapter 5- Section 2: Modelling Geomorphic Systems: Numerical Modelling, in: Geomorphological Techniques. British Society for Geomorphology, p. 13.

Huxman, T.E., Snyder, K.A., Tissue, D., Leffler, A.J., Ogle, K., Pockman, W.T., Sandquist, D.R., Potts, D.L., Schwinning, S., 2004. Precipitation pulses and carbon fluxes in semiarid and arid ecosystems. Oecologia 141, 254–268. doi:10.1007/s00442-004-1682-4

Idso, S.B., 1992. Shrubland expansion in the American Southwest. Climatic Change 22, 85–86.

Idso, S.B., Quinn, J.A., 1983. Vegetational redistribution in Arizona and New Mexico in response to a doubling of the atmospheric CO2 concentration, Climatolgical Publication Sci. Laboratory of Climatology, Arizona State University, Tempe, AZ, USA.

IPCC, 2014. Climate Change 2014: Impacts, Adaptation, and Vulnerability. Contribution of Working Group III to the Fifth Assessment Report of the Intergovernmental Panel on Climate Change. Cambridge University Press, Cambridge, United Kingdom, p. 996.

IPCC, 2013. Climate Change 2013: The Physical Science Basis. Contribution of Working Group I to the Fifth Assessment Report of the Intergovernmental Panel on Climate Change, in: Stocker, T.F., Qin, D., Plattner, G.-K., Tignor, M.M.B., Allen, S.K., Boschung, J., Nauels, A., Xia, Y., Bex, V., Midgley, P. (Eds.), . Cambridge University Press, Cambridge, United Kingdom, p. 996.

IPCC, 2007. Climate Change 2007: The Physical Science Basis. Contribution of Working Group I to the Fourth Assessment Report of the Intergovernmental Panel on Climate Change, in: Solomon, S., Qin, D., Manning, M., Chen, Z., Marquis, M., Averyt, K.B., Tignor, M., Miller, H.L. (Eds.), . Cambridge University Press, Cambridge, United Kingdom, p. 996.

IPCC, 2001. Climate change 2001: The scientific basis. Volume 1 of the Third Assessment Report of the Intergovernmental Panel on Climate Change.

IPCC, 1995. IPCC Second Assessment Report: Climate Change 1995: The Science of Climate Change. IPCC, Cambridge UK.

IPCC, 1990. Climate Change 1990: Working Group I: Scientific Assessment of Climate Change. IPCC, Cambridge UK.

IUPAC, 2005. Nomenclature of Inorganic Chemistry: IUPAC Recomendations. Internaitonal Union of Pure and Applied Chemistry.

Jachner, S., van den Boogaart, G., Petzoldt, T., 2007. Statistical methods for the qualitative assessment of dynamic models with time delay (R Package qualV). Journal of Statistical Software 22, 1–30.

Jacinthe, P.-A., Lal, R., 2001. A mass balance approach to assess carbon dioxide evolution during erosional events. Land Degrad. Dev. 12, 329–339. doi:10.1002/ldr.454

Jacinthe, P.-A., Lal, R., Kimble, J.M., 2001. Assessing water erosion impacts on soil carbon pools and fluxes, in: Lal, R., Kimble, J.M., Follett, R.F., Stewart, B.A. (Eds.), Assessment Methods for Soil Carbon. Lewis Publishers, Boca Raton, FL, USA, pp. 427–449.

Jacinthe, P.-A., Lal, R., Owens, L.B., Hothem, D.L., 2004. Transport of labile carbon in runoff as affected by land use and rainfall characteristics. Soil and Tillage Research 77, 111–123. doi:10.1016/j.still.2003.11.004

Jackson, R.B., 2000. Belowground processes and global change. Ecological Applications 10, 397–398.

Jackson, R.B., Banner, J.L., Jobbágy, E.G., Pockman, W.T., Wall, D.H., 2002. Ecosystem carbon loss with woody plant invasion of grasslands. Nature 418, 623–626. doi:10.1038/nature00910

Jackson, R.B., Mooney, H.A., Schulze, E.-D., 1997. A global budget for fine root biomass, surface area, and nutrient contents. Proceedings of the National Academy of Sciences 94, 7362–7366.

Jackson, R.B., Schenk, H.J., Jobbágy, E.G., Canadell, J., Colello, G.D., Dickinson, R.E., Field, C.B., Friedlingstein, P., Heimann, M., Hibbard, K., 2000. Belowground consequences of vegetation change and their treatment in models. Ecological Applications 10, 470–483.

James, M.R., Robson, S., 2014. Mitigating systematic error in topographic models derived from UAV and ground-based image networks. Earth Surf. Process. Landforms 39, 1413–1420. doi:10.1002/esp.3609

James, M.R., Robson, S., 2012. Straightforward reconstruction of 3D surfaces and topography with a camera: Accuracy and geoscience application. Journal of Geophysical Research 117, F03017. doi:10.1029/2011JF002289

Jandl, R., Rodeghiero, M., Martinez, C., Cotrufo, M.F., Bampa, F., van Wesemael, B., Harrison, R.B., Guerrini, I.A., Richter Jr., D. deB, Rustad, L., Lorenz, K., Chabbi, A., Miglietta, F., 2014. Current status, uncertainty and future needs in soil organic carbon monitoring. Science of The Total Environment 468–469, 376–383. doi:10.1016/j.scitotenv.2013.08.026

Janzen, H.H., 2004. Carbon cycling in earth systems—a soil science perspective. Agriculture, ecosystems & environment 104, 399–417. doi:10.1016/j.agee.2004.01.040

Jarecki, M.K., Lal, R., James, R., 2005. Crop management effects on soil carbon sequestration on selected farmers' fields in northeastern Ohio. Soil and Tillage Research 81, 265–276. doi:10.1016/j.still.2004.09.013

Jenkins, J.C., Chojnacky, D.C., Heath, L.S., Birdsey, R.A., 2003. National-scale biomass estimators for United States tree species. Forest Science 49, 12–35.

Jin, K., Cornelis, W.M., Gabriels, D., Baert, M., Wu, H.J., Schiettecatte, W., Cai, D.X., De Neve, S., Jin, J.Y., Hartmann, R., Hofman, G., 2009. Residue cover and rainfall intensity effects on runoff soil organic carbon losses. CATENA 78, 81–86. doi:10.1016/j.catena.2009.03.001

Jin, K., Cornelis, W.M., Schiette, W., Lu, J.J., Buysse, T., Baert, G., Wu, H.J., Yao, Y., Cai, D.X., Jin, J.Y., De Neve, S., Hartmann, R., Gabriels, D., 2008. Redistribution and loss of soil organic carbon by overland flow under various soil management practices on the Chinese Loess Plateau. Soil Use and Management 24, 181–191. doi:10.1111/j.1475-2743.2008.00151.x

Jobbágy, E.G., Jackson, R.B., 2000. The vertical distribution of soil organic carbon and its relation to climate and vegetation. Ecological Applications 10, 423–436.

Jull, A.J.T., 2007. AMS Method.

Jung, K., Kaiser, S., Böhm, S., Nieschulze, J., Kalko, E.K.V., 2012. Moving in three dimensions: effects of structural complexity on occurrence and activity of insectivorous bats in managed forest stands. Journal of Applied Ecology 49, 523–531. doi:10.1111/j.1365-2664.2012.02116.x

Kaiser, A., Neugirg, F., Rock, G., Müller, C., Haas, F., Ries, J., Schmidt, J., 2014. Small-scale surface reconstruction and volume calculation of soil erosion in complex Moroccan gully morphology using Structure from Motion. Remote Sensing 6, 7050–7080. doi:10.3390/rs6087050

Kanda, M., Inagaki, A., Letzel, M.O., Raasch, S., Watanabe, T., 2004. LES Study of the Energy Imbalance Problem with Eddy Covariance Fluxes. Boundary-Layer Meteorology 110, 381–404. doi:10.1023/B:BOUN.0000007225.45548.7a

Kieft, T.L., White, C.S., Loftin, S.R., Aguilar, R., Craig, J.A., Skaar, D.A., 1998. Temporal dynamics in soil carbon and nitrogen resources at a grassland-shrubland ecotone. Ecology 79, 671–683.

Kimble, J.M., Grossman, R.B., Samson-Liebig, S.E., 2001. Methodology for sampling and preparation for soil carbon determinations, in: Lal, R., Kimble, J.M., Follett, R.F., Stewart, B.A. (Eds.), Assessment Methods for Soil Carbon. pp. 15–30.

Kimes, D.S., 1984. Modeling the directional reflectance from complete homogeneous vegetation canopies with various leaf-orientation distributions. J. Opt. Soc. Am. A, JOSAA 1, 725–737. doi:10.1364/JOSAA.1.000725

Kirkby, M.J., 2010. Distance, time and scale in soil erosion processes. Earth Surface Processes and Landforms 35, 1621–1623. doi:10.1002/esp.2063

Kirschbaum, M.U.F., 2000. Will changes in soil organic carbon act as a positive or negative feedback on global warming? Biogeochemistry 48, 21–51.

Klappa, C.F., 1980. Rhizoliths in terrestrial carbonates: classification, recognition, genesis and significance. Sedimentology 27, 613–629. doi:10.1111/j.1365-3091.1980.tb01651.x

Klopatek, J.M., Conant, R.T., Francis, J.M., Malin, R.A., Murphy, K.L., Klopatek, C.C., 1998. Implications of patterns of carbon pools and fluxes across a semiarid environmental gradient. Landscape and Urban Planning 39, 309–317. doi:10.1016/S0169-2046(97)00076-5

Knapp, A.K., Briggs, J.M., Collins, S.L., Archer, S.R., Bret-Harte, M.S., Ewers, B.E., Peters, D.P.C., Young, D.R., Shaver, G.R., Pendall, E., Cleary, M.B., 2008. Shrub encroachment in North American grasslands: shifts in growth form dominance rapidly alters control of ecosystem carbon inputs. Global Change Biology 14, 615–623. doi:10.1111/j.1365-2486.2007.01512.

Knapp, A.K., Hamerlynck, E.P., Ham, J.M., Owensby, C.E., 1996. Responses in stomatal conductance to elevated CO2 in 12 grassland species that differ in growth form. Plant Ecology 125, 31–41.

Köchy, M., Wilson, S.D., 2001. Nitrogen deposition and forest expansion in the Northern Great Plains. Journal of Ecology 89, 807–817. doi:10.2307/3072154

Kollongei, K.. J., Lorentz, S.. A., 2014. Connectivity influences on nutrient and sediment migration in the Wartburg catchment South Africa. Physics and Chemistry of the Earth, Parts A/B/C 67–69, 12–22. doi:10.1016/j.pce.2014.01.002

Komada, T., Anderson, M.R., Dorfmeier, C.L., 2008. Carbonate removal from coastal sediments for the determination of organic carbon and its isotopic signatures, δ13C and Δ14C: comparison of fumigation and direct acidification by hydrochloric acid. Limnology and Oceanography 6, 254–262.

Krämer, S., Miller, P.M., Eddleman, L.E., 1996. Root system morphology and development of seedling and juvenile Juniperus occidentalis. Forest Ecology and Management 86, 229–240. doi:10.1016/S0378-1127(96)03769-3

Krause, P., Boyle, D.P., Bäse, F., 2005. Comparison of different efficiency criteria for hydrological model assessment. Advances in Geosciences 5, 89–97. doi:10.5194/adgeo-5-89-2005

Krofcheck, D.J., Eitel, J.U.H., Vierling, L.A., Schulthess, U., Hilton, T.M., Dettweiler-Robinson, E., Pendleton, R., Litvak, M.E., 2014. Detecting mortality induced structural and functional changes in a piñon-juniper woodland using Landsat and RapidEye time series. Remote Sensing of Environment, Special Issue on 2012 ForestSAT 151, 102–113. doi:10.1016/j.rse.2013.11.009

Krofcheck, D.J., Lippitt, C.D., Loerch, A.C., Litvak, M.E., 2015. Repeat, low altitude measurements of vegetation status and biomass using manned aerial and UAS imagery in a Piñon-Juniper woodland (Invited). Presented at the AGU Fall Meeting, AGU, San Francisco.

Krueger, T., Freer, J., Quinton, J.N., Macleod, C.J.A., Bilotta, G.S., Brazier, R.E., Butler, P., Haygarth, P.M., 2010. Ensemble evaluation of hydrological model hypotheses. Water Resources Research 46, W07516. doi:10.1029/2009WR007845

Krull, E.S., Skjemstad, J.O., Burrows, W.H., Bray, S.G., Wynn, J.G., Bol, R., Spouncer, L., Harms, B., 2005. Recent vegetation changes in central Queensland, Australia: Evidence from δ13C and 14C analyses of soil organic matter. Geoderma 126, 241–259. doi:10.1016/j.geoderma.2004.09.012

Kuhn, N.J., 2007. Erodibility of soil and organic matter: independence of organic matter resistance to interrill erosion. Earth Surface Processes and Landforms 32, 794–802. doi:10.1002/esp.1486

Kuhn, N.J., Armstrong, E.K., 2012. Erosion of organic matter from sandy soils: Solving the mass balance. Catena 98, 87–95. doi:10.1016/j.catena.2012.05.014

Kuhn, N.J., Armstrong, E.K., Ling, A.C., Connolly, K.L., Heckrath, G., 2012. Interrill erosion of carbon and phosphorus from conventionally and organically farmed Devon silt soils. CATENA, Experiments in Earth surface process research 91, 94–103. doi:10.1016/j.catena.2010.10.002

Kuhn, N.J., Hoffmann, T., Schwanghart, W., Dotterweich, M., 2009. Agricultural soil erosion and global carbon cycle: controversy over? Earth Surface Processes and Landforms 34, 1033–1038. doi:10.1002/esp.1796

Kuzyakov, Y., 2010. Priming effects: Interactions between living and dead organic matter. Soil Biology and Biochemistry 42, 1363–1371. doi:10.1016/j.soilbio.2010.04.003

Lacoste, M., Viaud, V., Michot, D., Walter, C., 2015. Landscape-scale modelling of erosion processes and soil carbon dynamics under land-use and climate change in agroecosystems. Eur J Soil Sci n/a-n/a. doi:10.1111/ejss.12267

Ladwig, L.M., Collins, S.L., Swann, A.L., Xia, Y., Allen, M.F., Allen, E.B., 2012. Above- and belowground responses to nitrogen addition in a Chihuahuan Desert grassland. Oecologia 169, 177–185. doi:10.1007/s00442-011-2173-z

Lal, R., 2008. Carbon sequestration. Philosophical Transactions of the Royal Society B: Biological Sciences 363, 815–830.

Lal, R., 2005. Soil erosion and carbon dynamics. Soil and Tillage Research 81, 137–142. doi:10.1016/j.still.2004.09.002

Lal, R., 2004a. Soil carbon sequestration impacts on global climate change and food security. Science 304, 1623–1627. doi:10.1126/science.1097396

Lal, R., 2004b. Soil carbon sequestration to mitigate climate change. Geoderma 123, 1–22.

Lal, R., 2004c. Carbon sequestration in dryland ecosystems. Environmental Management 33, 528–544. doi:10.1007/s00267-003-9110-9

Lal, R., 2003. Soil erosion and the global carbon budget. Environment International 29, 437–450. doi:10.1016/S0160-4120(02)00192-7

Lal, R., 2001a. Soil degradation by erosion. Land Degradation & Development 12, 519–539. doi:10.1002/ldr.472

Lal, R., 2001b. Fate of eroded soil carbon: emission or sequestration, in: Lal, R. (Ed.), Soil Carbon Sequestration and the Greenhouse Effect. Soil Science Society of America Special Publication, Madison, WI., pp. 173–181.

Lal, R., 2001c. Potential of desertification control to sequester carbon and mitigate the greenhouse effect. Climatic Change 51, 35–72.

Lal, R., 2001d. Soil erosion and carbon dynamics on grazing land, in: The Potential of US Grazing Lands to Sequester Carbon and Mitigate the Greenhouse Effect. Lewis Publishers, Boca Raton, FL, USA, pp. 231–247.

Lal, R., 1999. Soil management and restoration for C sequestration to mitigate the accelerated greenhouse effect. Progress in Environmental Science 1, 307–326.

Lal, R., 1976. Soil erosion problems on an alfisol in western Nigeria and their control. International Institute of Tropical Agriculture, Ibadan, Nigeria.

Lal, R., Follett, R.F., Kimble, J.M., 2001a. Research and development priorities, in: Follett, R.F., Kimble, J.M., Lal, R. (Eds.), The Potential of US Grazing Lands to Sequester Carbon and Mitigate the Greenhouse Effect. Lewis Publishers, Boca Raton, FL, USA, pp. 231–238.

Lal, R., Follett, R.F., Stewart, B.A., Kimble, J.M., 2007. Soil carbon sequestration to mitigate climate change and advance food security. Soil Science 172, 943–956.

Lal, R., Griffin, M., Apt, J., Lave, L., Morgan, M.G., 2004a. Managing soil carbon. Science 304, 393–393.

Lal, R., Griffin, M., Apt, J., Lave, L., Morgan, M.G., 2004b. Response to Comments on“ Managing Soil Carbon.” Science 305, 1567–1567. doi:10.1126/science.1101271

Lal, R., Hassan, H.M., Dumanski, J., 1999. Desertification control to sequester carbon and mitigate the greenhouse effect, in: Rosenberg, N.J., Izaurralde, R.C., Malone, E.L. (Eds.), Carbon Sequestration in Soils: Science, Monitoring and Beyond. Battelle Press, Columbus, OH. USA, pp. 83–137.

Lal, R., Kimble, J.M., 2001. Importance of soil bulk density and methods of its importance, in: Lal, R., Kimble, J.M., Follett, R.F., Stewart, B.A. (Eds.), Assessment Methods for Soil Carbon. pp. 31–44.

Lal, R., Kimble, J.M., Follett, R.F., 2001b. Methodological challenges toward balancing soil C pools and fluxes, in: Lal, R., Kimble, J.M., Follett, R.F., Stewart, B.A. (Eds.), Assessment Methods for Soil Carbon. Lewis Publishers, Boca Raton, FL, USA, pp. 659–666.

Lal, R., Kimble, J.M., Follett, R.F., Cole, C.V., 1998. The potential of U.S. Cropland to Sequester Carbon and Mitigate the Greenhouse Effect. Ann Arbor Press, Chelsea, MI, USA.

Lal, R., Pimentel, D., 2008. Soil erosion: A carbon sink or source? Science 319, 1040–1042. doi:10.1126/science.319.5866.1040

Laliberte, A.S., Rango, A., 2011. Unmanned aircraft systems (UAS) for vegetation mapping: very high resolution multispectral imagery and terrain extraction, in: American Society for Photogrammetry and Remote Sensing Annual Meeting, May 1-5, 2011. Milwaukee, Wisconsin, USA.

Laliberte, A.S., Rango, A., 2009. UAS-derived imagery and terrain models for rangeland mapping and monitoring. Presented at the Unmanned Vehicle Systems (UVS) Canada Conference, Victoria, BC, Canada.

Laliberte, A.S., Rango, A., Havstad, K.M., Paris, J.F., Beck, R.F., McNeely, R., Gonzalez, A.L., 2004. Object-oriented image analysis for mapping shrub encroachment from 1937 to 2003 in southern New Mexico. Remote Sensing of Environment 93, 198–210.

Lambert, M.-C., Ung, C.-H., Raulier, F., 2005. Canadian national tree aboveground biomass equations. Can. J. For. Res. 35, 1996–2018. doi:10.1139/x05-112

Lamlom, S.H., Savidge, R.A., 2003. A reassessment of carbon content in wood: variation within and between 41 North American species. Biomass and Bioenergy 25, 381–388. doi:10.1016/S0961-9534(03)00033-3

Landis, J.R., Koch, G.G., 1977. A One-Way components of variance model for categorical data. Biometrics 33, 671–679. doi:10.2307/2529465

Lane, L.J., Kidwell, M.R., 2003. Hydrology and soil erosion. USDA Forest Service Proceedings RMRS-P-30.

Laport, R.G., Minckley, R.L., Ramsey, J., 2012. Phylogeny and Cytogeography of the North American Creosote Bush (Larrea tridentata, Zygophyllaceae). Systematic Botany 37, 153–164. doi:10.1600/036364412X616738

Larney, F.J., Bullock, M.S., Janzen, H.H., Ellert, B.H., Olson, E.C.S., 1998. Wind erosion effects on nutrient redistribution and soil productivity. Journal of Soil and Water Conservation 53, 133–140.

Latif, M., Barnett, T.P., 1996. Decadal climate variability over the North Pacific and North America: dynamics and predictability. J. Climate 9, 2407–2423. doi:10.1175/1520-0442(1996)009<2407:DCVOTN>2.0.CO;2

Le Quéré, C., 2010. Trends in the land and ocean carbon uptake. Current Opinion in Environmental Sustainability 2, 219–224.

Le Quéré, C., Moriarty, R., Andrew, R.M., Peters, G.P., Ciais, P., Friedlingstein, P., Jones, S.D., Sitch, S., Tans, P., Arneth, A., Boden, T.A., Bopp, L., Bozec, Y., Canadell, J.G., Chevallier, F., Cosca, C.E., Harris, I., Hoppema, M., Houghton, R.A., House, J.I., Jain, A., Johannessen, T., Kato, E., Keeling, R.F., Kitidis, V., Klein Goldewijk, K., Koven, C., Landa, C.S., Landschützer,

P., Lenton, A., Lima, I.D., Marland, G., Mathis, J.T., Metzl, N., Nojiri, Y., Olsen, A., Ono, T., Peters, W., Pfeil, B., Poulter, B., Raupach, M.R., Regnier, P., Rödenbeck, C., Saito, S., Salisbury, J.E., Schuster, U., Schwinger, J., Séférian, R., Segschneider, J., Steinhoff, T., Stocker, B.D., Sutton, A.J., Takahashi, T., Tilbrook, B., van der Werf, G.R., Viovy, N., Wang, Y.-P., Wanninkhof, R., Wiltshire, A., Zeng, N., 2014. Global carbon budget 2014. Earth Syst. Sci. Data Discuss. 7, 521–610. doi:10.5194/essdd-7-521-2014

Lee, J.J., Phillips, D.L., Dodson, R.F., 1996. Sensitivity of the US corn belt to climate change and elevated CO2: II. Soil erosion and organic carbon. Agricultural systems 52, 503–521. doi:10.1016/S0308-521X(96)00015-7

Lefsky, M.A., Cohen, W.B., Parker, G.G., Harding, D.J., 2002. LiDAR remote sensing for ecosystem studies: LiDAR, an emerging remote sensing technology that directly measures the three-dimensional distribution of plant canopies, can accurately estimate vegetation structural attributes and should be of particular interest to forest, landscape, and global ecologists. BioScience 52, 19–30. doi:10.1641/0006-3568(2002)052[0019:LRSFES]2.0.CO;2

Legates, D.R., McCabe, G.J., 1999. Evaluating the use of "goodness-of-fit" Measures in hydrologic and hydroclimatic model validation. Water Resour. Res. 35, 233–241. doi:10.1029/1998WR900018

León, R.J.C., Aguiar, M.R., 1985. El deterioro por uso pasturil en estepas herbáceas patagónicas. Phytocoenologia 13, 181–196.

Lett, M.S., Knapp, A.K., Briggs, J.M., Blair, J.M., 2004. Influence of shrub encroachment on aboveground net primary productivity and carbon and nitrogen pools in a mesic grassland. Canadian Journal of Botany 82, 1363–1370.

Leys, J. (New S.W.C. and L.M., McTainsh, G. (Griffith U., 1994. Soil loss and nutrient decline by wind erosion - cause for concern [Mallee, New South Wales]. Australian Journal of Soil and Water Conservation (Australia).

Li, A., Glenn, N.F., Olsoy, P.J., Mitchell, J.J., Shrestha, R., 2015. Aboveground biomass estimates of sagebrush using terrestrial and airborne LiDAR data in a dryland ecosystem. Agricultural and Forest Meteorology 213, 138–147. doi:10.1016/j.agrformet.2015.06.005

Li, J., Okin, G.S., Alvarez, L.J., Epstein, H.E., 2008. Effects of wind erosion on the spatial heterogeneity of soil nutrients in two desert grassland communities. Biogeochemistry 88, 73–88.

Li, J., Okin, G.S., Alvarez, L.J., Epstein, H.E., 2007. Quantitative effects of vegetation cover on wind erosion and soil nutrient loss in a desert grassland of southern New Mexico, USA. Biogeochemistry 85, 317–332. doi:10.1007/s10533-007-9142-y

Liao, J.D., Boutton, T.W., Jastrow, J.D., 2006a. Storage and dynamics of carbon and nitrogen in soil physical fractions following woody plant invasion of grassland. Soil Biology and Biochemistry 38, 3184–3196.

Liao, J.D., Boutton, T.W., Jastrow, J.D., 2006b. Organic matter turnover in soil physical fractions following woody plant invasion of grassland: Evidence from natural 13C and 15N. Soil Biology and Biochemistry 38, 3197–3210. doi:10.1016/j.soilbio.2006.04.004

Lieth, H., 1975. Primary production of the major vegetation units of the world, in: Lieth, H., Whittaker, R.H. (Eds.), Primary Productivity of the Biosphere, Ecological Studies. Springer Berlin Heidelberg, pp. 203–215.

Lin, L.I.-K., 2000. A note on the concordance correlation coefficient. Biometrics 56, 324–325. doi:10.1111/j.0006-341X.2000.00324.x

Lin, L.I.-K., 1992. Assay validation using the concordance correlation coefficient. Biometrics 48, 599–604. doi:10.2307/2532314
Lin, L.I.-K., 1989. A concordance correlation coefficient to evaluate reproducibility. Biometrics 45, 255–268. doi:10.2307/2532051
Lin, L.I.-K., Hedayat, A.S., Wu, W., 2012. Statistical Tools for Measuring Agreement. Springer, New York, NY, USA.
Linchant, J., Lisein, J., Semeki, J., Lejeune, P., Vermeulen, C., 2015. Are unmanned aircraft systems (UASs) the future of wildlife monitoring? A review of accomplishments and challenges. Mammal Review 45, 239–252. doi:10.1111/mam.12046
Lipiec, J., Siczek, A., Sochan, A., Bieganowski, A., 2016. Effect of sand grain shape on root and shoot growth of wheat seedlings. Geoderma 265, 1–5. doi:10.1016/j.geoderma.2015.10.022
Lisein, J., Pierrot-Deseilligny, M., Bonnet, S., Lejeune, P., 2013. A photogrammetric workflow for the creation of a forest canopy height model from small unmanned aerial system imagery. Forests 4, 922–944. doi:10.3390/f4040922
Lister, D., 2007. Small-Scale Erosion-Driven Nutrient Dynamics in Different Vegetation Communities in Jornada, New Mexico: Implications for Land Degradation. University of Bristol.
Lister, D., Michaelides, K., Wadham, J.L., Wainwright, J., Parsons, A.J., 2007. Erosion-driven nutrient dynamics in different vegetation communities in Jornada, New Mexico: implications for land degradation, in: Geophysical Research Abstracts.
Liu, S., Bliss, N., Sundquist, E., Huntington, T.G., 2003. Modeling carbon dynamics in vegetation and soil under the impact of soil erosion and deposition. Global Biogeochemical Cycles 17, 1074. doi:10.1029/2002GB002010
Liu, Y.Y., Evans, J.P., McCabe, M.F., de Jeu, R.A.M., van Dijk, A.I.J.M., Dolman, A.J., Saizen, I., 2013a. Changing climate and overgrazing are decimating Mongolian Steppes. PLoS ONE 8, e57599. doi:10.1371/journal.pone.0057599
Liu, Y.Y., van Dijk, A.I.J.M., McCabe, M.F., Evans, J.P., de Jeu, R.A.M., 2013b. Global vegetation biomass change (1988–2008) and attribution to environmental and human drivers. Global Ecology and Biogeography 22, 692–705. doi:10.1111/geb.12024
Liu, Z., Dreybrodt, W., Wang, H., 2010. A new direction in effective accounting for the atmospheric CO2 budget: Considering the combined action of carbonate dissolution, the global water cycle and photosynthetic uptake of DIC by aquatic organisms. Earth-Science Reviews 99, 162–172. doi:10.1016/j.earscirev.2010.03.001
Loague, K., 1992. Soil water content at R-5. Part 1. Spatial and temporal variability. Journal of Hydrology 139, 233–251. doi:10.1016/0022-1694(92)90204-9
Loch, R., Donnollan, T., 1983. Field rainfall simulator studies on two clay soils of the Darling Downs, Queensland. II. Aggregate Breakdpwn, sediment properties and soil erodibility. Soil Res. 21, 47–58.
Long, E.J., Hargrave, G.K., Cooper, J.R., Kitchener, B.G.B., Parsons, A.J., Hewett, C.J.M., Wainwright, J., 2014. Experimental investigation into the impact of a liquid droplet onto a granular bed using three-dimensional, time-resolved, particle tracking. Phys. Rev. E 89, 32201. doi:10.1103/PhysRevE.89.032201
Lopez-Sangil, L., Rovira, P., 2013. Sequential chemical extractions of the mineral-associated soil organic matter: An integrated approach for the fractionation

of organo-mineral complexes. Soil Biology and Biochemistry 62, 57–67. doi:10.1016/j.soilbio.2013.03.004
Lowe, D.G., 2004. Distinctive image features from scale-invariant keypoints. International Journal of Computer Vision 60, 91–110.
Ludwig, J.A., 1977. Distributional adaptations of root systems in desert environments, in: Marshall, J.K. (Ed.), The Belowground Ecosystem: A Synthesis of Plant-Associated Processes. Colorado State University, Fort Collins, pp. 85–90.
Ludwig, J.A., Reynolds, J.F., Whitson, P.D., 1975. Size-biomass relationships of several Chihuahuan desert shrubs. American Midland Naturalist 94, 451–461.
Ludwig, W., Amiotte-Suchet, P., Munhoven, G., Probst, J.-L., 1998. Atmospheric CO2 consumption by continental erosion: present-day controls and implications for the last glacial maximum. Global and Planetary Change 16, 107–120.
Lufafa, A., Diédhiou, I., Ndiaye, N.A.S., Séné, M., Kizito, F., Dick, R.P., Noller, J.S., 2009. Allometric relationships and peak-season community biomass stocks of native shrubs in Senegal's Peanut Basin. Journal of Arid Environments 73, 260–266. doi:10.1016/j.jaridenv.2008.09.020
Luk, S.-H., Abrahams, A.D., Parsons, A.J., 1993. Sediment sources and sediment transport by rill flow and interrill flow on a semi-arid piedmont slope, southern Arizona. Catena 20, 93–111.
Luk, S.-H., Cai, Q.G., 1990. Laboratory experiments on crust development and rainsplash erosion of loess soils, China. Catena 17, 261–276.
Lukasewycz, M.T., Burkhard, L.P., 2005. Complete elimination of carbonates: A critical step in the accurate measurement of organic and black carbon in sediments. Environmental Toxicology and Chemistry 24, 2218–2221. doi:10.1897/04-653R.1
Luscombe, D.J., Brazier, R.E., Gatis, N., Wetherelt, A., Grand-Clement, E., Anderson, K., 2014. What does airborne LiDAR really measure in upland ecosystems? Ecohydrology 8, 584–594. doi:10.1002/eco.1527
Mackenzie, F.T., Lerman, A., Andersson, A.J., 2004. Past and present of sediment and carbon biogeochemical cycling models. Biogeosciences Discussions 1, 27–85.
Maestre, F.T., Bautista, S., Cortina, J., 2003. Positive, negative, and net effects in grass-shrub interactions in Mediterranean semiarid grasslands. Ecology 84, 3186–3197.
Maestre, F.T., Bowker, M.A., Puche, M.D., Belén Hinojosa, M., Martínez, I., García-Palacios, P., Castillo, A.P., Soliveres, S., Luzuriaga, A.L., Sánchez, A.M., 2009. Shrub encroachment can reverse desertification in semi-arid Mediterranean grasslands. Ecology letters 12, 930–941. doi:10.1111/j.1461-0248.2009.01352.x
Maestre, F.T., Reynolds, J., Huber-Sannwald, E., Herrick, J.E., Stafford-Smith, M., 2006. Understanding global desertification: biophysical and socioeconomic dimensions of hydrology, in: D'Odorico, P., Porporato, A. (Eds.), Dryland Ecohydrology. Springer, pp. 315–332.
Maharaj, S., Barton, C.D., Karathanasis, T.A.D., Rowe, H.D., Rimmer, S.M., 2007. Distinguishing "new" from "old" organic carbon in reclaimed coal mine sites using thermogravimetry II field validation. Soil Science 172, 302–312. doi:10.1097/SS.0b013e3180314702

Making Landings Safer [WWW Document], 2011. . Royal Air Force. URL http://www.raf.mod.uk/news/archive.cfm?storyid=DFF79349-5056-A318-A8DBA7DB432A0454

Malam Issa, O., Bissonnais, Y.L., Planchon, O., Favis-Mortlock, D.T., Silvera, N., Wainwright, J., 2006. Soil detachment and transport on field- and laboratory-scale interrill areas: erosion processes and the size-selectivity of eroded sediment. Earth Surface Processes and Landforms 31, 929–939. doi:10.1002/esp.1303

Mancini, F., Dubbini, M., Gattelli, M., Stecchi, F., Fabbri, S., Gabbianelli, G., 2013. Using unmanned aerial vehicles (UAV) for high-resolution reconstruction of topography: the structure from motion approach on coastal environments. Remote Sensing 5, 6880–6898. doi:10.3390/rs5126880

Manies, K.L., Harden, J.W., Kramer, L., Parton, W.J., 2001. Carbon dynamics within agricultural and native sites in the loess region of western Iowa. Global Change Biology 7, 545–555. doi:10.1046/j.1354-1013.2001.00427.x

Mariappan, S., 2016. Soil redistribution impacts on the spatial variation of nutrients, net carbon exchange with the atmosphere and soil respiration rates in highly eroding agricultural fields from the foothills of the Indian Himalaya (PhD Thesis). University of Exeter, Exeter, UK.

Mariappan, S., Cunliffe, A.M., Hartley, I., Dungait, J.A.J., Quine, T.A., In Prep. Erosion-induced redistribution of soil carbon and nutrients in agricultural landscapes of the Himalayan region. Geomorphology.

Marion, G.M., 1989. Correlation between long-term pedogenic CaCO3 formation rate and modern precipitation in deserts of the American Southwest. Quaternary Research 32, 291–295. doi:10.1016/0033-5894(89)90095-1

Marion, G.M., Schlesinger, W.H., Fonteyn, P.J., 1990. Spatial variability of CaCO3 solubility in a Chihuahuan desert soil. Arid Land Research and Management 4, 181–191. doi:10.1080/15324989009381247

Marshall, J.K. (Ed.), 1977. The Belowground Ecosystem: A Synthesis of Plant-associated Processes, Range Science Department Science Series. Colorado State University, Fort Collins,.

Martinez, C., Hancock, G.R., Kalma, J.D., 2010. Relationships between 137Cs and soil organic carbon (SOC) in cultivated and never-cultivated soils: An Australian example. Geoderma 158, 137–147. doi:10.1016/j.geoderma.2010.04.019

Martinez-Mena, M., Castillo, V., Albaladejo, J., 2001. Hydrological and erosional response to natural rainfall in a semi-arid area of south-east Spain. Hydrological Processes 15, 557–571. doi:10.1002/hyp.146

Martinez-Mena, M., López, J., Almagro, M., Albaladejo, J., Castillo, V., Ortiz, R., Boix-Fayos, C., 2012. Organic carbon enrichment in sediments: Effects of rainfall characteristics under different land uses in a Mediterranean area. Catena 94, 36–42. doi:10.1016/j.catena.2011.02.005

Martinez-Mena, M., Rogel, J.A., Albaladejo, J., Castillo, V., 1999. Influence of vegetal cover on sediment particle size distribution in natural rainfall conditions in a semiarid environment. Catena 38, 175–190.

Martinez-Meza, E., Whitford, W.G., 1996. Stemflow, throughfall and channelization of stemflow by roots in three Chihuahuan desert shrubs. Journal of Arid Environments 32, 271–287.

Marzaioli, F., Lubritto, C., Galdo, I.D., D'Onofrio, A., Cotrufo, M.F., Terrasi, F., 2010. Comparison of different soil organic matter fractionation methodologies: Evidences from ultrasensitive 14C measurements. Nuclear Instruments and

Methods in Physics Research Section B: Beam Interactions with Materials and Atoms 268, 1062–1066. doi:10.1016/j.nimb.2009.10.098
Masubelele, M.L., Hoffman, M.T., Bond, W.J., 2015. Biome stability and long-term vegetation change in the semi-arid, south-eastern interior of South Africa: A synthesis of repeat photo-monitoring studies. South African Journal of Botany. doi:10.1016/j.sajb.2015.06.001
Mata-González, R., Sosebee, R.E., Wan, C., 2002. Shoot and root biomass of desert grasses as affected by biosolids application. Journal of Arid Environments 50, 477–488. doi:10.1006/jare.2001.0897
Mayeux, H., 2001. Foreword, in: Follett, R.F., Kimble, J.M., Lal, R. (Eds.), The Potential of U.S. Grazing Lands to Sequester Carbon and Mitigate the Greenhouse Effect. Lewis Publishers, Boca Raton, FL, USA, pp. XXV–XXIX.
Mayeux, H.S., Johnson, H.B., Polley, H.W., 1991. Global change and vegetation dynamics, in: James, L.F., Evans, J.O., Ralphs, M.H., Singler, B.J. (Eds.), Noxious Range Weeds. Westview Press, Boulder, CO, pp. 62–74.
Mayor, Á.G., Bautista, S., Small, E.E., Dixon, M., Bellot, J., 2008. Measurement of the connectivity of runoff source areas as determined by vegetation pattern and topography: A tool for assessing potential water and soil losses in drylands. Water Resources Research 44, W10423. doi:10.1029/2007wr006367
McAuliffe, J.R., 1994. Landscape evolution, soil formation, and ecological patterns and processes in Sonoran Desert bajadas. Ecological Monographs 64, 112–148. doi:10.2307/2937038
McBride, G.B., 2005. A proposal for strength-of-agreement criteria for Lin's Concordance Correlation Coefficient (No. NIWA Client Report: HAM2005-062).
McCall, P.L., Robbins, J.A., Matisoff, G., 1984. Geochronology of recent deposits 137Cs and 210Pb transport and geochronologies in urbanized reservoirs with rapidly increasing sedimentation rates. Chemical Geology 44, 33–65. doi:10.1016/0009-2541(84)90066-4
McCarty, G.W., Ritchie, J.C., 2002. Impact of soil movement on carbon sequestration in agricultural ecosystems. Environmental Pollution 116, 423–430. doi:10.1016/S0269-7491(01)00219-6
McClaran, M.P., Moore-Kucera, J., Martens, D.A., van Haren, J., Marsh, S.E., 2008. Soil carbon and nitrogen in relation to shrub size and death in a semi-arid grassland. Geoderma 145, 60–68. doi:10.1016/j.geoderma.2008.02.006
McCraw, D.J., 1985. A phytogeographic history of Larrea in southwestern New Mexico illustrating the historical expansion of the Chihuahuan Desert. Albuquerque, NM, US, University of New Mexico.
McGlynn, I.O., Okin, G.S., 2006. Characterization of shrub distribution using high spatial resolution remote sensing: Ecosystem implications for a former Chihuahuan Desert grassland. Remote Sensing of Environment 101, 554–566. doi:10.1016/j.rse.2006.01.016
McGuire, A.D., Sitch, S., Clein, J.S., Dargaville, R., Esser, G., Foley, J.A., Heimann, M., Joos, F., Kaplan, J., Kicklighter, D.W., Meier, R.A., Melillo, J.M., Moore III, B., Prentice, I.C., Ramankutty, N., Reichenau, T., Schloss, A., 2001. Carbon balance of the terrestrial biosphere in the twentieth century: Analyses of C02, climate and land use effects with four process-based ecosystem models. Global Biogeochemical Cycles 15, 183–206.
McGwire, K.C., Weltz, M.A., Finzel, J.A., Morris, C.E., Fenstermaker, L.F., McGraw, D.S., 2013. Multiscale assessment of green leaf cover in a semi-arid

rangeland with a small unmanned aerial vehicle. International Journal of Remote Sensing 34, 1615–1632. doi:10.1080/01431161.2012.723836
McKinley, D.C., Blair, J.M., 2008. Woody plant encroachment by Juniperus virginiana in a mesic native grassland promotes rapid carbon and nitrogen accrual. Ecosystems 11, 454–468.
McNeil, B.E., Pisek, J., Lepisk, H., Flamenco, E.A., 2016. Measuring leaf angle distribution in broadleaf canopies using UAVs. Agricultural and Forest Meteorology 218–219, 204–208. doi:10.1016/j.agrformet.2015.12.058
McShane, G., James, M.R., Quinton, J., Anderson, K., DeBell, L., Evans, M., Farrow, L., Glendell, M., Jones, L., Kirkham, M., Lark, M., Rawlins, B., Rickson, J., Quine, T., Wetherelt, A., Brazier, R., 2014. Comparing and combining terrestrial laser scanning with ground-and UAV-based imaging for national-level assessment of soil erosion. Presented at the EGU General Assembly Conference Abstracts, p. 7709.
Mearns, L.O., Arritt, R., Biner, S., Bukovsky, M.S., McGinnis, S., Sain, S., Caya, D., Correia, J., Flory, D., Gutowski, W., Takle, E.S., Jones, R., Leung, R., Moufouma-Okia, W., McDaniel, L., Nunes, A.M.B., Qian, Y., Roads, J., Sloan, L., Snyder, M., 2012. The North American regional climate change assessment program: overview of Phase I Results. Bull. Amer. Meteor. Soc. 93, 1337–1362. doi:10.1175/BAMS-D-11-00223.1
Meersmans, J., Van Wesemael, B., Van Molle, M., 2009. Determining soil organic carbon for agricultural soils: a comparison between the Walkley & Black and the dry combustion methods (north Belgium). Soil Use and Management 25, 346–353. doi:10.1111/j.1475-2743.2009.00242.x
Meeuwig, R.O., 1979. Growth characteristics of pinyon-juniper stands in the western Great Basin (No. INT-238). USDA For. Serv. Res. Pap., Intermt. Forest and Range Experimental Station, Ogden, Utah.
Meeuwig, R.O., Cooper, S.V., 1981. Stand Estimates of Biomass and Growth on Pinyon-juniper Woodlands in Nevada. U.S. Department of Agriculture, Forest Service, Intermountain Forest and Range Experiment Station.
Meixner, T., Brooks, P.D., Hogan, J., Soto, C., Simpson, S., 2012. Carbon and nitrogen export from semiarid uplands to perennial rivers: connections and missing links, San Pedro River, Arizona, USA. Geography Compass 6, 546–559.
Melillo, J.M., Prentice, I.C., Farquhar, G.D., Schulze, E.D., Sala, O.E., 1996. Terrestrial biotic responses to environmental change and feedbacks to climate, in: Houghton, R.A., Jenkins, G.J., Ephraums, J.J. (Eds.), Climate Change 1995: The Science of Climate Change. Cambridge University Press, Cambridge, United Kingdom and New York, NY, USA, pp. 443–481.
Merritt, W.S., Letcher, R.A., Jakeman, A.J., 2003. A review of erosion and sediment transport models. Environmental Modelling & Software 18, 761–799.
Merz, B., Plate, E.J., 1997. An analysis of the effects of spatial variability of soil and soil moisture on runoff. Water Resour. Res. 33, 2909–2922. doi:10.1029/97WR02204
Metz, B., Davidson, O.R., Bosch, P.R., Dave, R., Meyer, L.A., 2007. Contribution of Working Group III to the Fourth Assessment Report of the Intergovernmental Panel on Climate Change, 2007, IPCC assesment reports. Cambridge University Press, Cambridge, United Kingdom.
Meyer, H., Lehnert, L.W., Wang, Y., Reudenbach, C., Nauss, T., Bendic, J., 2016. Mapping vegetation cover and biomass on the Qinghai-Tibet-Plateau using hyperspectral measurements and multispectral satellite images. Presented

at the European Geosciences Union - General Assembly, EGU, Vienna, Austria, p. EGU2016-2710.
Meyer, S.E., 2012. Restoring and managing cold desert shrublands for climate change mitigation, in: Finch, D.M. (Ed.), Climate Change in Grasslands, Shrublands, and Deserts of the Interior American West. U.S. Department of Agriculture, Forest Service, Rocky Mountain Research Station., Fort Collins, CO, pp. 21–34.
Michaelides, K., Lister, D., Wainwright, J., Parsons, A.J., 2012. Linking runoff and erosion dynamics to nutrient fluxes in a degrading dryland landscape. Journal of Geophysical Research: Biogeosciences 117, n/a–n/a. doi:10.1029/2012JG002071
Michaelides, K., Lister, D., Wainwright, J., Parsons, A.J., 2009. Vegetation controls on small-scale runoff and erosion dynamics in a degrading dryland environment. Hydrological Processes 23, 1617–1630. doi:10.1002/hyp.7293
Michaelides, K., Martin, G.J., 2012. Sediment transport by runoff on debris-mantled dryland hillslopes. Journal of Geophysical Research: Earth Surface 117, n/a–n/a. doi:10.1029/2012JF002415
Michaelides, K., Wainwright, J., 2008. Internal testing of a numerical model of hillslope–channel coupling using laboratory flume experiments. Hydrol. Process. 22, 2274–2291. doi:10.1002/hyp.6823
Michaelides, K., Wainwright, J., 2002. Modelling the effects of hillslope–channel coupling on catchment hydrological response. Earth Surface Processes and Landforms 27, 1441–1457.
Michaelides, K., Wilson, M.D., 2007. Uncertainty in predicted runoff due to patterns of spatially variable infiltration. Water Resources Research 43, n/a-n/a. doi:10.1029/2006WR005039
Michaud, J., Sorooshian, S., 1994. Comparison of simple versus complex distributed runoff models on a midsized semiarid watershed. Water Resour. Res. 30, 593–605. doi:10.1029/93WR03218
Midwood, A.J., Boutton, T.W., 1998. Soil carbonate decomposition by acid has little effect on δ13C of organic matter. Soil Biology and Biochemistry 30, 1301–1307. doi:10.1016/S0038-0717(98)00030-3
Miller, E.L., Meeuwig, R.O., Budy, J.D., 1981. Biomass of Singleleaf Pinyon and Utah Juniper (No. Research Paper INT-273). United States Department of Agriculture, Forest Service, Intermountain Forest and Range Experimental Station.
Miller, P.M., Eddleman, L.E., Kramer, S., 1990. Allocation patterns of carbon and minerals in juvenile and small-adult Juniperus occidentalis. Forest Science 36, 734–747.
Miller, S.N., Kepner, W.G., Mehaffey, M.H., Hernandez, M., Miller, R.C., Goodrich, D.C., Devonald, K.K., Heggem, D.T., Miller, W.P., 2007. Integrating landscape assessment and hydrologic modeling for land cover change analysis. JAWRA Journal of the American Water Resources Association 38, 915–929.
Milne, B.T., Moore, D.I., Betancourt, J.L., Parks, J.A., Swetnam, T.W., Parmenter, R.R., Pockman, W.T., 2003. Multidecadal drought cycles in south-central New Mexico: patterns and consequences, in: Greenland, D., Goodin, D., Smith, R. (Eds.), Climate Variability and Ecosystem Response at Long Term Ecological Research (LTER) Sites. Oxford University Press, New York, New York, USA, pp. 286–307.
Mirik, M., Chaudhuri, S., Surber, B., Ale, S., Ansley, R.J., 2013a. Evaluating biomass of Juniper Trees (Juniperus pinchotii) from imagery-derived canopy

area using the support vector machine classifier. Advances in Remote Sensing 2, 181–192. doi:10.4236/ars.2013.22021

Mirik, M., Chaudhuri, S., Surber, B., Ale, S., Ansley, R.J., 2013b. Detection of two intermixed invasive woody species using colour infrared aerial imagery and the support vector machine classifier. Journal of Applied Remote Sensing 7. doi:10.1117/1.JRS.7.073588

Mitchell, H.F., Lakshminarayan, P.G., Otake, T., Babcock, B.A., 1998. The impact of soil conservation policies on carbon sequestration in agricultural soils of the central United States, in: Lal, R., Kimble, J.M., Follett, R.F., Stewart, B.A. (Eds.), Management of Carbon Sequestration in Soil. CRC Press, Boca Raton, FL, USA.

Mitchell, J.J., Glenn, N.F., Sankey, T.T., Derryberry, D.R., Anderson, M.O., Hruska, R.C., 2011. Small-footprint LiDAR estimations of sagebrush canopy characteristics. Photogrammetric Engineering & Remote Sensing 77, 521–530. doi:10.14358/PERS.77.5.521

Mokany, K., Raison, R.J., Prokushkin, A.S., 2006. Critical analysis of root : shoot ratios in terrestrial biomes. Global Change Biology 12, 84–96. doi:10.1111/j.1365-2486.2005.001043.x

Monger, H.C., Gallegos, R.A., 2000. Biotic and abiotic processes and rates of pedogenic carbonate accumulation in the southwestern United States - relationship to atmospheric CO2 sequestration, in: Lal, R., Kimble, J.M., Eswaran, H., Stewart, B.A. (Eds.), Global Climate Change and Pedogenic Carbonates. CRC Press, Boca Raton, FL, pp. 273–289.

Mooney, H.A., Drake, B.G., Luxmoore, R.J., Oechel, W.C., Pitelka, L.F., 1991. Predicting ecosystem responses to elevated CO2 concentrations. BioScience 96–104.

Moore, D.C., Singer, M.J., 1990. Crust formation effects on soil erosion processes. Soil Science Society of America Journal 54, 1117–1123. doi:10.2136/sssaj1990.03615995005400040033x

Moore, D.I., 2015. Core Research Site Web Seasonal Biomass and Seasonal and Annual NPP Data for the Net Primary Production Study at the Sevilleta National Wildlife Refuge, New Mexico (1999-2014). Albuquerque, NM: Sevilleta Long Term Ecological Research Site Database: SEV182. http://sev.lternet.edu/data/sev-182.

Mora, J.L., Guerra, J.A., Armas, C.M., Rodríguez-Rodríguez, A., Arbelo, C.D., Notario, J.S., 2007. Mineralization rate of eroded organic C in Andosols of the Canary Islands. Science of the total environment 378, 143–146. doi:10.1016/j.scitotenv.2007.01.040

Moreland, E.E., Cameron, M.F., Angliss, R.P., Boveng, P.L., 2015. Evaluation of a ship-based unoccupied aircraft system (UAS) for surveys of spotted and ribbon seals in the Bering Sea pack ice. J. Unmanned Veh. Sys. 3, 114–122. doi:10.1139/juvs-2015-0012

Moreno de las Heras, M., Diaz-Sierra, R., Turnbull, L., Wainwright, J., 2015. Assessing vegetation structure and ANPP dynamics in a grassland-shrubland Chihuahuan ecotone using NDVI-rainfall relationships. Biogeosciences Discuss. 12, 51–92. doi:10.5194/bgd-12-51-2015

Moreno-de las Heras, M., Turnbull, L., Wainwright, J., 2016. Seed-bank structure and plant-recruitment conditions regulate the dynamics of a grassland-shrubland Chihuahuan ecotone. Ecology n/a-n/a. doi:10.1002/ecy.1446

Morgan, R.P.C., Quinton, J.N., 2001. Erosion Modeling, in: Doe III, W.W., Harmon, R.S. (Eds.), Landscape Erosion and Evolution Modeling. Kluwer Academic I Plenum Publishers, pp. 122–139.

Muldavin, E.H., Moore, D.I., Collins, S.L., Wetherill, K.R., Lightfoot, D.C., 2008. Aboveground net primary production dynamics in a northern Chihuahuan Desert ecosystem. Oecologia 155, 123–132.
Müller, E.N., 2004. Scaling approaches to the modelling of water, sediment and nutrient fluxes within semi-arid landscapes, Jornada Basin, New Mexico. King's College London.
Müller, E.N., Francke, T., Batalla, R.J., Bronstert, A., 2009. Modelling the effects of land-use change on runoff and sediment yield for a meso-scale catchment in the Southern Pyrenees. Catena 79, 288–296. doi:10.1016/j.catena.2009.06.007
Müller, E.N., Tietjen, B., Turnbull, L., 2013. Modelling ecogeomorphological feedback mechanisms for the analysis of land degradation patterns of a semi-arid shrubland-grassland transition zone. Presented at the EGU General Assembly, p. 1.
Müller, E.N., Tietjen, B., Turnbull, L., Wainwright, J., In Review. Ecohydrological modelling of land degradation in drylands: feedbacks between water, erosion, vegetation and soil. Journal of Geophysical Research – Biogeosciences.
Müller, E.N., Wainwright, J., Parsons, A.J., 2008. Spatial variability of soil and nutrient characteristics of semi-arid grasslands and shrublands, Jornada Basin, New Mexico. Ecohydrology 1, 3–12. doi:10.1002/eco.1
Müller, E.N., Wainwright, J., Parsons, A.J., 2007a. The stability of vegetation boundaries and the propagation of desertification in the American Southwest: A modelling approach. Ecological Modelling 208, 91–101. doi:10.1016/j.ecolmodel.2007.04.010
Müller, E.N., Wainwright, J., Parsons, A.J., 2007b. Impact of connectivity on the modeling of overland flow within semiarid shrubland environments. Water Resources Research 43. doi:10.1029/2006WR005006
Müller, E.N., Wainwright, J., Parsons, A.J., Turnbull, L. (Eds.), 2014a. Patterns of Land Degradation in Drylands: Understanding Self-Organising Ecogeomorphic Systems. Springer, Dordrecht.
Müller, E.N., Wainwright, J., Parsons, A.J., Turnbull, L., Millington, J.D.A., Papanastasis, V., 2014b. Land degradation in drylands: Reevaluating pattern-process interrelationships and the role of ecogeomorphology, in: Müller, E.N., Wainwright, J., Parsons, A.J., Turnbull, L. (Eds.), Patterns of Land Degradation in Drylands: Understanding Self-Organising Ecogeomorphic Systems, 367-383. Springer, Dordrecht.
Mundt, J.T., Streutker, D.R., Glenn, N.F., 2006. Mapping sagebrush distribution using fusion of hyperspectral and lidar classifications. Photogrammetric Engineering and Remote Sensing 72, 47–54.
Murray-Tortarolo, G., Friedlingstein, P., Sitch, S., Jaramillo, V.J., Murguia-Flores, F., Anav, A., Liu, Y., Arenth, A., Arvanitis, A., Harper, A., Jain, A., Kato, E., Koven, C., Poulter, B., Stocker, B.D., Wiltshire, A., Zaehle, S., Zeng, N., 2016. The carbon cycle in Mexico: past, present and future of C stocks and fluxes. Biogeosciences 13, 223–238. doi:10.5194/bg-13-223-2016
Mutema, M., Chaplot, V., Jewitt, G., Chivenge, P., Blöschl, G., 2015. Annual water, sediment, nutrient, and organic carbon fluxes in river basins: A global meta-analysis as a function of scale. Water Resources Research. doi:10.1002/2014WR016668
Muukkonen, P., Heiskanen, J., 2007. Biomass estimation over a large area based on standwise forest inventory data and ASTER and MODIS satellite data: A

possibility to verify carbon inventories. Remote Sensing of Environment 107, 617–624. doi:10.1016/j.rse.2006.10.011

Myers-Smith, I.H., Elmendorf, S.C., Beck, P.S.A., Wilmking, M., Hallinger, M., Blok, D., Tape, K.D., Rayback, S.A., Macias-Fauria, M., Forbes, B.C., Speed, J.D.M., Boulanger-Lapointe, N., Rixen, C., Lévesque, E., Schmidt, N.M., Baittinger, C., Trant, A.J., Hermanutz, L., Collier, L.S., Dawes, M.A., Lantz, T.C., Weijers, S., Jørgensen, R.H., Buchwal, A., Buras, A., Naito, A.T., Ravolainen, V., Schaepman-Strub, G., Wheeler, J.A., Wipf, S., Guay, K.C., Hik, D.S., Vellend, M., 2015a. Climate sensitivity of shrub growth across the tundra biome. Nature Clim. Change 5, 887–891. doi:10.1038/nclimate2697

Myers-Smith, I.H., Forbes, B.C., Wilmking, M., Hallinger, M., Lantz, T., Blok, D., Tape, K.D., Macias-Fauria, M., Sass-Klaassen, U., Lévesque, E., Boudreau, S., Ropars, P., Luise Hermanutz, Trant, A., Collier, L.S., Weijers, S., Rozema, J., Rayback, S.A., Schmidt, N.M., Schaepman-Strub, G., Wipf, S., Rixen, C., Ménard, C.B., Susanna Venn, Goetz, S., Andreu-Hayles, L., Elmendorf, S., Ravolainen, V., Welker, J., Paul Grogan, Epstein, H.E., Hik, D.S., 2011. Shrub expansion in tundra ecosystems: dynamics, impacts and research priorities. Environ. Res. Lett. 6, 45509. doi:10.1088/1748-9326/6/4/045509

Myers-Smith, I.H., Hallinger, M., Blok, D., Sass-Klaassen, U., Rayback, S.A., Weijers, S., J. Trant, A., Tape, K.D., Naito, A.T., Wipf, S., Rixen, C., Dawes, M.A., A. Wheeler, J., Buchwal, A., Baittinger, C., Macias-Fauria, M., Forbes, B.C., Lévesque, E., Boulanger-Lapointe, N., Beil, I., Ravolainen, V., Wilmking, M., 2015b. Methods for measuring arctic and alpine shrub growth: A review. Earth-Science Reviews 140, 1–13. doi:10.1016/j.earscirev.2014.10.004

Nadeu, E., Berhe, A.A., de Vente, J., Boix-Fayos, C., 2012. Erosion, deposition and replacement of soil organic carbon in Mediterranean catchments: a geomorphological, isotopic and land use change approach. Biogeosciences 9, 1099–1111. doi:10.5194/bg-9-1099-2012

Nadeu, E., Boix-Fayos, C., de Vente, J., López, J., Martínez Mena, M., 2010. Organic carbon mobilization by different erosive processes in the slope-channel connection. Pirineos 165, 157–177.

Nadeu, E., de Vente, J., Martínez-Mena, M., Boix-Fayos, C., 2011. Exploring particle size distribution and organic carbon pools mobilized by different erosion processes at the catchment scale. J Soils Sediments 11, 667–678. doi:10.1007/s11368-011-0348-1

Nafus, A.M., McClaran, M.P., Archer, S.R., Throop, H.L., 2009. Multispecies allometric models predict grass biomass in semidesert rangeland. Rangeland Ecology & Management 62, 68–72.

Nash, D.J., McLaren, S.J., 2003. Kalahari valley calcretes: their nature, origins, and environmental significance. Quaternary International 111, 3–22. doi:10.1016/S1040-6182(03)00011-9

Nash, J.E., Sutcliffe, J.V., 1970. River flow forecasting through conceptual models part I—A discussion of principles. Journal of Hydrology 10, 282–290.

Nearing, M.A., Hairsine, P.B., 2011. The future of soil erosion modelling, in: Morgan, R.P.C., Nearing, M.A. (Eds.), Handbook of Erosion Modelling. Wiley-Blackwell, Chichister, UK, pp. 389–397.

Nearing, M.A., Nichols, M.H., Stone, J.J., Renard, K.G., Simanton, J.R., 2007. Sediment yields from unit-source semiarid watersheds at Walnut Gulch. Water Resources Research 43, W06426.

Neave, M., Abrahams, A.D., 2002. Vegetation influences on water yields from grassland and shrubland ecosystems in the Chihuahuan Desert. Earth Surface Processes and Landforms 27, 1011–1020. doi:10.1002/esp.389

Neilson, R.P., 1986. High-resolution climatic analysis and southwest biogeography [Bouteloua eriopoda; Larrea tridentata; prosopis glandulosa]. Science (Washington, DC);(United States) 232.

Neilson, R.P., Lenihan, J.M., Bachelet, D., Drapek, R.J., 2005. Climate change implications for sagebrush ecosystems. Presented at the Transactions of the 70th North American Wildlife and Natural Resources Conference, Wildlife Management Institution Publications Department, pp. 145–159.

Nelson, E.W., 1934. The influence of precipitation and grazing upon black grama grass range (Technical Bulletin No. No. 409). US Department of Agriculture Forest Service.

Nelson, P.N., Dictor, M.C., Soulas, G., 1994. Availability of organic carbon in soluble and particle-size fractions from a soil profile. Soil Biology and Biochemistry 26, 1549–1555. doi:10.1016/0038-0717(94)90097-3

Neufeld, H.S., Meinzer, F.C., Wisdom, C.S., Sharifi, M.R., Rundel, P.W., Neufeld, M.S., Goldring, Y., Cunningham, G.L., 1988. Canopy architecture of Larrea tridentata (DC.) Cov., a desert shrub: foliage orientation and direct beam radiation interception. Oecologia 75, 54–60. doi:10.1007/BF00378813

Norris, M.D., Blair, J.M., Johnson, L.C., McKane, R.B., 2001. Assessing changes in biomass, productivity, and C and N stores following Juniperus virginiana forest expansion into tallgrass prairie. Canadian Journal of Forest Research 31, 1940–1946.

Northup, B.K., Zitzer, S.F., Archer, S., McMurtry, C.R., Boutton, T.W., 2005. Above-ground biomass and carbon and nitrogen content of woody species in a subtropical thornscrub parkland. Journal of Arid Environments 62, 23–43. doi:10.1016/j.jaridenv.2004.09.019

Nouvellon, Y., Moran, M.S., Seen, D.L., Bryant, R., Rambal, S., Ni, W., Bégué, A., Chehbouni, A., Emmerich, W.E., Heilman, P., Qi, J., 2001. Coupling a grassland ecosystem model with Landsat imagery for a 10-year simulation of carbon and water budgets. Remote Sensing of Environment 78, 131–149.

Nouwakpo, S.K., Weltz, M.A., McGwire, K., 2015. Assessing the performance of structure-from-motion photogrammetry and terrestrial LiDAR for reconstructing soil surface microtopography of naturally vegetated plots. Earth Surf. Process. Landforms 41, 308–322. doi:10.1002/esp.3787

Nowak, R.S., Moore, D.J., Tausch, R.J., 1999. Ecophysiological patterns of pinyon and juniper (No. RMRS-P-9). USDA Forest Service Proceedings.

NPS, 2014. USA National Park Service [WWW Document]. US National Park Service: Zion. URL http://www.nps.gov/zion/learn/news/droneharassesbhs.htm (accessed 9.22.15).

Nunes, J.P., Nearing, M.A., 2011. Modelling impacts of climate change: case studies using the new generation of erosion models, in: Morgan, R.P.C., Nearing, M.A. (Eds.), Handbook of Erosion Modelling. Wiley-Blackwell, Chichister, UK, pp. 289–312.

Ogrinc, N., Lojen, S., Faganeli, J., 2002. A mass balance of carbon stable isotopes in an organic-rich methane-producing lacustrine sediment (Lake Bled, Slovenia). Global and Planetary Change, The global carbon cycle and its changes over glacial-interglacial cycles 33, 57–72. doi:10.1016/S0921-8181(02)00061-9

Oh, N.-H., Raymond, P.A., 2006. Contribution of agricultural liming to riverine bicarbonate export and CO2 sequestration in the Ohio River basin. Global Biogeochemical Cycles 20, n/a-n/a. doi:10.1029/2005gb002565
Okin, G.S., Mahowald, N., Chadwick, O.A., Artaxo, P., 2004. Impact of desert dust on the biogeochemistry of phosphorus in terrestrial ecosystems. Global Biogeochemical Cycles 18. doi:10.1029/2003GB002145
Olk, D.C., Cassman, K.G., Fan, T.W.M., 1995. Characterization of two humic acid fractions from a calcareous vermiculitic soil: implications for the humification process. Geoderma 65, 195–208. doi:10.1016/0016-7061(95)94048-9
Olsoy, P.J., 2013. Discrimination of Sargebrush aboveground biomass using terrestrial laser scanning (TLS) (MSc). Idaho State University.
Olsoy, P.J., Glenn, N.F., Clark, P.E., Derryberry, D.R., 2014. Aboveground total and green biomass of dryland shrub derived from terrestrial laser scanning. ISPRS Journal of Photogrammetry and Remote Sensing 88, 166–173. doi:10.1016/j.isprsjprs.2013.12.006
Oren, R., Hsieh, C.-I., Stoy, P., Albertson, J., Mccarthy, H.R., Harrell, P., Katul, G.G., 2006. Estimating the uncertainty in annual net ecosystem carbon exchange: spatial variation in turbulent fluxes and sampling errors in eddy-covariance measurements. Global Change Biology 12, 883–896. doi:10.1111/j.1365-2486.2006.01131.x
Óskarsson, H., Arnalds, Ó., Gudmundsson, J., Gudbergsson, G., 2004. Organic carbon in Icelandic Andosols: geographical variation and impact of erosion. Catena 56, 225–238. doi:10.1016/j.catena.2003.10.013
Owe, M., de Jeu, R., Walker, J., 2001. A methodology for surface soil moisture and vegetation optical depth retrieval using the microwave polarization difference index. IEEE Transactions on Geoscience and Remote Sensing 39, 1643–1654. doi:10.1109/36.942542
Owens, L.B., Malone, R.W., Hothem, D.L., Starr, G.C., Lal, R., 2002. Sediment carbon concentration and transport from small watersheds under various conservation tillage practices. Soil and Tillage Research 67, 65–73. doi:10.1016/S0167-1987(02)00031-4
Owen-Smith, R.N., 1992. Megaherbivores: the influence of very large body size on ecology. Cambridge University Press.
Oyonarte, C., Pérez-Pujalte, A., Delgado, G., Delgado, R., Almendros, G., 1994. Factors affecting soil organic matter turnover in a Mediterranean ecosystems from Sierra de Gador (Spain): An analytical approach. Communications in Soil Science and Plant Analysis 25, 1929–1945. doi:10.1080/00103629409369164
Pacala, S., Birdsey, R.A., Bridgham, S.D., Conant, R.T., Davis, K., Hales, B., Houghton, R.A., Jenkins, J.C., Johnston, M., Marland, G., Paustian, K., Caspersen, J., Socolow, R., Tol, R.S., 2007. The North American carbon budget past and present, in: King, A.W., Dilling, L., Zimmerman, G.P., Fairman, D.M., Houghton, R.A., Marland, G., Rose, A.Z., Wilbanks, T.J. (Eds.), The First State of the Carbon Cycle Report (SOCCR): The North American Carbon Budget and Implications for the Global Carbon Cycle. National Oceanic and Atmospheric Administration, National Climatic Data Center, Asheville, NC, USA, pp. 29–36, 167–170.
Pacala, S.W., Hurtt, G.C., Baker, D., Peylin, P., Houghton, R.A., Birdsey, R.A., Heath, L., Sundquist, E.T., Stallard, R.F., Ciais, P., Moorcroft, P., Caspersen, J.P., Shevliakova, E., Moore, B., Kohlmaier, G., Holland, E., Gloor, M., Harmon, M.E., Fan, S.-M., Sarmiento, J.L., Goodale, C.L., Schimel, D.S.,

Field, C.B., 2001. Consistent land-and atmosphere-based US carbon sink estimates. Science 292, 2316–2320. doi:10.1126/science.1057320
Padilla, F.M., Miranda, J.D., Jorquera, M.J., Pugnaire, F.I., 2009. Variability in amount and frequency of water supply affects roots but not growth of arid shrubs. Plant Ecology 204, 261–270.
Palis, R.G., Ghadiri, H., Rose, C.W., Saffigna, P.G., 1997. Soil erosion and nutrient loss. III. Changes in the enrichment ratio of total nitrogen and organic carbon under rainfall detachment and entrainment. Australian Journal of Soil Research 35, 891–905.
Palis, R.G., Okwach, G., Rose, C.W., Saffigna, P.G., 1990a. Soil erosion processes and nutrient loss. I. The interpretation of enrichment ratio and nitrogen loss in runoff sediment. Soil Research 28, 623–639. doi:10.1071/SR9900623
Palis, R.G., Okwach, G., Rose, C.W., Saffigna, P.G., 1990b. Soil erosion processes and nutrient loss. II. The effect of surface contact cover and erosion processes on enrichment ratio and nitrogen loss in eroded sediment. Australian Journal of Soil Research 28, 641–658.
Pangle, R.E., Limousin, J.-M., Plaut, J.A., Yepez, E.A., Hudson, P.J., Boutz, A.L., Gehres, N., Pockman, W.T., McDowell, N.G., 2015. Prolonged experimental drought reduces plant hydraulic conductance and transpiration and increases mortality in a piñon–juniper woodland. Ecol Evol 5, 1618–1638. doi:10.1002/ece3.1422
Parsons, A.J., Abrahams, A.D. (Eds.), 1992. Overland Flow Hydraulics and Erosion Mechanics. UCL Press, London.
Parsons, A.J., Abrahams, A.D., Luk, S.-H., 1991. Size characteristics of sediment in interrill overland flow on a semiarid hillslope, southern Arizona. Earth Surface Processes and Landforms 16, 143–152. doi:10.1002/esp.3290160205
Parsons, A.J., Abrahams, A.D., Luk, S.-H., 1990. Hydraulics of interrill overland flow on a semi-arid hillslope, southern Arizona. Journal of Hydrology 117, 255–273. doi:10.1016/0022-1694(90)90096-G
Parsons, A.J., Abrahams, A.D., Simanton, J.R., 1992. Microtopography and soil-surface materials on semi-arid piedmont hillslopes, southern Arizona. Journal of Arid Environments 22, 107–115.
Parsons, A.J., Abrahams, A.D., Wainwright, J., 1996. Responses of interrill runoff and erosion rates to vegetation change in southern Arizona. Geomorphology 14, 311–317. doi:10.1016/0169-555X(95)00044-6
Parsons, A.J., Abrahams, A.D., Wainwright, J., 1994. Rainsplash and erosion rates in an interrill area on semi-arid grassland, southern Arizona. Catena 22, 215–226. doi:10.1016/0341-8162(94)90003-5
Parsons, A.J., Brazier, R.E., Wainwright, J., Powell, D.M., 2006. Scale relationships in hillslope runoff and erosion. Earth Surface Processes and Landforms 31, 1384–1393. doi:10.1002/esp.1345
Parsons, A.J., Stone, P.M., 2006. Effects of intra-storm variations in rainfall intensity on interrill runoff and erosion. CATENA 67, 68–78. doi:10.1016/j.catena.2006.03.002
Parsons, A.J., Wainwright, J., Abrahams, A.D., Simanton, J.R., 1997. Distributed dynamic modelling of interrill overland flow. Hydrological Processes 11, 1833–1859. doi:10.1002/(SICI)1099-1085(199711)11:14<1833::AID-HYP499>3.0.CO;2-7
Parsons, A.J., Wainwright, J., Mark Powell, D., Kaduk, J., Brazier, R.E., 2004. A conceptual model for determining soil erosion by water. Earth Surface Processes and Landforms 29, 1293–1302. doi:10.1002/esp.1096

Paulsen, H.A., Ares, F.N., 1962. Grazing values and management of Black Grama and Tobosa Grasslands and associated shrub ranges of the Southwest (Technical Bulletin No. No. 1270). US Department of Agriculture Forest Service.

Peters, D.P.C., 2002. Plant species dominance at a grassland–shrubland ecotone: an individual-based gap dynamics model of herbaceous and woody species. Ecological Modelling 152, 5–32.

Peters, D.P.C., Bestelmeyer, B.T., Herrick, J.E., Fredrickson, E.L., Monger, H.C., Havstad, K.M., 2006a. Disentangling complex landscapes: new insights into arid and semiarid system dynamics. BioScience 56, 491–501. doi:10.1641/0006-3568(2006)56[491:DCLNII]2.0.CO;2

Peters, D.P.C., Herrick, J.E., Monger, H.C., Huang, H., 2010. Soil-vegetation-climate interactions in arid landscapes: Effects of the North American monsoon on grass recruitment. Journal of Arid Environments 74, 618–623.

Peters, D.P.C., Mariotto, I., Havstad, K.M., Murray, L.W., 2006b. Spatial variation in remnant grasses after a grassland-to-shrubland state change: implications for restoration. Rangeland Ecology & Management 59, 343–350. doi:10.2111/05-202R1.1

Peters, D.P.C., Yao, J., Sala, O.E., Anderson, J.P., 2012. Directional climate change and potential reversal of desertification in arid and semiarid ecosystems. Global Change Biology 18, 151–163. doi:10.1111/j.1365-2486.2011.02498.x

Petrie, M.D., Collins, S.L., Gutzler, D.S., Moore, D.M., 2014. Regional trends and local variability in monsoon precipitation in the northern Chihuahuan Desert, USA. Journal of Arid Environments 103, 63–70. doi:10.1016/j.jaridenv.2014.01.005

Petrie, M.D., Collins, S.L., Swann, A.M., McCall, P.L., Litvak, M.E., 2015. Grassland to shrubland state transitions enhance carbon sequestration in the northern Chihuahuan Desert. Glob Change Biol 21, 1226–1235. doi:10.1111/gcb.12743

Pidgeon, A.M., Mathews, N.E., Benoit, R., Nordheim, E.V., 2001. Response of avian communities to historic habitat change in the northern Chihuahuan Desert. Conservation Biology 15, 1772–1789. doi:10.1046/j.1523-1739.2001.00073.x

Pieper, R.D., 1990. Overstory-understory relations in Pinyon-Juniper woodlands in New Mexico. Journal of Range Management 43, 413–415. doi:10.2307/3899002

Planchon, O., Darboux, F., 2001. A fast, simple and versatile algorithm to fill the depressions of digital elevation models. Catena 46, 159–176.

Plante, A., 2013. Distribution of radiocarbon ages in soil organic matter by thermal fractionation. Radiocarbon 55. doi:10.2458/azu_js_rc.55.16310

Plaut, J.A., Wadsworth, W.D., Pangle, R., Yepez, E.A., McDowell, N.G., Pockman, W.T., 2013. Reduced transpiration response to precipitation pulses precedes mortality in a piñon–juniper woodland subject to prolonged drought. New Phytol 200, 375–387. doi:10.1111/nph.12392

Poesen, J.W., Boardman, J., Wilcox, B., Valentin, C., 1996. Water erosion monitoring and experimentation for global change studies. Journal of Soil and Water Conservation 51, 386–390.

Polyakov, V.O., Lal, R., 2004a. Soil erosion and carbon dynamics under simulated rainfall. Soil Science 169, 590–599.

Polyakov, V.O., Lal, R., 2004b. Modeling soil organic matter dynamics as affected by soil water erosion. Environment International 30, 547–556. doi:10.1016/j.envint.2003.10.011

Polyakov, V.O., Nearing, M.A., Stone, J.J., Holifield Collins, C.D., Nichols, M.H., 2016. Quantifying decadal-scale erosion rates and their short-term variability on ecological sites in a semi-arid environment. CATENA 137, 501–507. doi:10.1016/j.catena.2015.10.023

Pomeroy, P., O'Connor, L., Davies, P., 2015. Assessing use of and reaction to unmanned aerial systems in gray and harbor seals during breeding and molt in the UK. J. Unmanned Veh. Sys. 3, 102–113. doi:10.1139/juvs-2015-0013

Popescu, S.C., Wynne, R.H., Nelson, R.F., 2003. Measuring individual tree crown diameter with lidar and assessing its influence on estimating forest volume and biomass. Canadian Journal of Remote Sensing 29, 564–577. doi:10.5589/m03-027

Popper, K.R., 1959. The Logic of Scientific Discovery. Hutchinson, London.

Post, W.M., Izaurralde, R.C., Mann, L.K., Bliss, N., 2001. Monitoring and verifying changes of organic carbon in soil, in: Rosenberg, N.J., Izaurralde, R.C. (Eds.), Storing Carbon in Agricultural Soils: A Multi-Purpose Environmental Strategy. Springer Netherlands, pp. 73–99.

Poulter, B., Frank, D., Ciais, P., Myneni, R.B., Andela, N., Bi, J., Broquet, G., Canadell, J.G., Chevallier, F., Liu, Y.Y., Running, S.W., Sitch, S., van der Werf, G.R., 2014. Contribution of semi-arid ecosystems to interannual variability of the global carbon cycle. Nature 509, 600–603. doi:10.1038/nature13376

Pregitzer, K.S., DeForest, J.L., Burton, A.J., Allen, M.F., Ruess, R.W., Hendrick, R.L., 2002. Fine root architecture of nine North American trees. Ecological Monographs 72, 293–309. doi:10.1890/0012-9615(2002)072[0293:FRAONN]2.0.CO;2

Proffitt, A., Rose, C., 1991. Soil erosion processes.II. Settling velocity characteristics of eroded sediment. Soil Res. 29, 685–695.

Puigdefábregas, J., Sole, A., Gutierrez, L., Del Barrio, G., Boer, M., 1999. Scales and processes of water and sediment redistribution in drylands: results from the Rambla Honda field site in Southeast Spain. Earth-Science Reviews 48, 39–70. doi:10.1016/S0012-8252(99)00046-X

Puliti, S., Ørka, H.O., Gobakken, T., Næsset, E., 2015. Inventory of small forest areas using an unmanned aerial system. Remote Sensing 7, 9632–9654. doi:10.3390/rs70809632

Puttock, A., 2013. Vegetation Change and Water, Sediment and Carbon Dynamics in Semi-Arid Environments. University of Exeter.

Puttock, A., Brazier, R.E., Dungait, J.A.J., Bol, R., Macleod, C.J.A., 2012a. Developing an understanding of vegetation change and fluvial carbon fluxes in semi-arid environments. Presented at the EGU General Assembly Conference Abstracts, p. 366.

Puttock, A., Dungait, J.A.J., Bol, R., Dixon, E.R., Macleod, C.J.A., Brazier, R.E., 2012b. Stable carbon isotope analysis of fluvial sediment fluxes over two contrasting C4-C3 semi-arid vegetation transitions. Rapid Communications in Mass Spectrometry 26, 2386–2392. doi:10.1002/rcm.6257

Puttock, A., Dungait, J.A.J., Macleod, C.J.A., Bol, R., Brazier, R.E., 2014. Woody plant encroachment accelerates erosion of previously stable organic carbon from dryland soils. J. Geophys. Res. Biogeosci. 2014JG002635. doi:10.1002/2014JG002635

Puttock, A., Macleod, C.J.A., Bol, R., Dungait, J.A.J., Brazier, R.E., 2013. Changes in ecosystem structure, function and hydrological connectivity in semi-arid grass to woody vegetation transitions. Earth Surface Processes and Landforms 38, 1602–1611. doi:10.1002/esp.3455

Puttock, A.K., Cunliffe, A.M., Anderson, K., Brazier, R.E., 2015. Monitoring the impact of Eurasian beaver reintroduction on ecosystem structure using aerial photography collected from a multi-rotor drone. Journal of Unmanned Vehicle Systems 3, 123–130. doi:10.1139/juvs-2015-0005

Puttock, A.K., Graham, H., Cunliffe, A.M., Elliott, M., Brazier, R.E., 2017. Eurasian beaver activity increases water storage, attenuates flow and mitigates diffuse pollution from intensively-managed grasslands. Science of the Total Environment 576, 430–443. doi:10.1016/j.scitotenv.2016.10.122

Quan, J., Barton, D., Conroy, C., Ashley, C., 1994. A preliminary assessment of the economic impact of desertification in Namibia. Directorate of Environmental Affairs, Ministry of Environment and Tourism.

Quilter, M.C., Anderson, V.J., 2001. A proposed method for determining shrub utilization using (LA/LS) imagery. Journal of Range Management 54, 378–381. doi:10.2307/4003106

Quine, T.A., Van Oost, K., 2007. Quantifying carbon sequestration as a result of soil erosion and deposition: Retrospective assessment using caesium-137 and carbon inventories. Global Change Biology 13, 2610–2625. doi:10.1111/j.1365-2486.2007.01457.x

Quinton, J., Davies, J., Tipping, E., 2014. Modelling soil carbon movement by erosion over large scales and long time periods. Presented at the European Geophysical Union - General Assembly, EGU, Vienna, Austria, p. EGU2014-2082.

Quinton, J.N., 1997. Reducing predictive uncertainty in model simulations: a comparison of two methods using the European Soil Erosion Model (EUROSEM). Catena 30, 101–117.

Quinton, J.N., Catt, J.A., Wood, G.A., Steer, J., 2006. Soil carbon losses by water erosion: Experimentation and modeling at field and national scales in the UK. Agriculture, ecosystems & environment 112, 87–102. doi:10.1016/j.agee.2005.07.005

Quinton, J.N., Govers, G., Van Oost, K., Bardgett, R.D., 2010. The impact of agricultural soil erosion on biogeochemical cycling. Nature Geosci 3, 311–314. doi:10.1038/ngeo838

Quiroga, A.R., Buschiazzo, D.E., Peinemann, N., 1998. Management discriminant properties in semiarid soils. Soil Science 163, 591–597.

Quiroga, A.R., Buschiazzo, D.E., Peinemann, N., 1996. Soil organic matter particle size fractions in soils of the semiarid Argentinian Pampas. Soil Science 161, 104–108.

Rabenhorst, M.C., 1988. Determination of organic and carbonate carbon in calcareous soils using dry combustion. Soil Science Society of America Journal 52, 965–968. doi:10.2136/sssaj1988.03615995005200040012x

R Core Team, 2015. R: A language and environment for statistical computing. R Foundation for Statistical Computing, Vienna, Austria.

Ramnarine, R., Voroney, R.P., Wagner-Riddle, C., Dunfield, K.E., 2011. Carbonate removal by acid fumigation for measuring the δ13C of soil organic carbon. Can. J. Soil. Sci. 91, 247–250. doi:10.4141/cjss10066

Rango, A., Chopping, M.J., Ritchie, J., Havstad, K.M., Kustas, W., Schmugge, T., 2000. Morphological characteristics of shrub coppice dunes in desert grasslands of southern New Mexico derived from scanning LiDAR. Remote Sensing of Environment 74, 26–44. doi:10.1016/S0034-4257(00)00084-5

Rango, A., Huenneke, L.F., Buonopane, M., Herrick, J.E., Havstad, K.M., 2005. Using historic data to assess effectiveness of shrub removal in southern New

Mexico. Journal of Arid Environments 62, 75–91. doi:10.1016/j.jaridenv.2004.11.001
Rango, A., Laliberte, A., Herrick, J.E., Winters, C., Havstad, K., Steele, C., Browning, D., 2009. Unmanned aerial vehicle-based remote sensing for rangeland assessment, monitoring, and management. Journal of Applied Remote Sensing 3, 33542-33542–15.
Rango, A., Laliberte, A., Steele, C., Herrick, J.E., Bestelmeyer, B., Schmugge, T., Roanhorse, A., Jenkins, V., 2006. Using unmanned aerial vehicles for rangelands: current applications and future potentials. Environmental Practice 8, 159–168. doi:10.1017/S1466046606060224
Rango, A., Vivoni, E.R., Anderson, C.A., Pierini, N.A., Schreiner-McGraw, A., Saripalli, S., Slaughter, A., Laliberte, A.S., 2014. Application of high-resolution images from unmanned aircraft systems for watershed and rangeland science, in: Lakshmi, V., Alsdorf, D., Anderson, R., Biancamaria, S., Cosh, M., Entin, J., Huffman, G., Kustas, W., Oevelen, P. van, Painter, T., Parajka, J., Rodell, tthew, Rüdiger, C. (Eds.), Remote Sensing of the Terrestrial Water Cycle. John Wiley & Sons, Inc, pp. 451–461.
Ratajczak, Z., Nippert, J.B., Briggs, J.M., Blair, J.M., 2014. Fire dynamics distinguish grasslands, shrublands and woodlands as alternative attractors in the Central Great Plains of North America. J Ecol 102, 1374–1385. doi:10.1111/1365-2745.12311
Ratajczak, Z., Nippert, J.B., Collins, S.L., 2012. Woody encroachment decreases diversity across North American grasslands and savannas. Ecology 93, 697–703.
Ratcliffe, N., Guihen, D., Robst, J., Crofts, S., Stanworth, A., Enderlein, P., 2015. A protocol for the aerial survey of penguin colonies using UAVs. J. Unmanned Veh. Sys. doi:10.1139/juvs-2015-0006
Ravi, S., Breshears, D.D., Huxman, T.E., D'Odorico, P., 2010. Land degradation in drylands: Interactions among hydrologic–aeolian erosion and vegetation dynamics. Geomorphology 116, 236–245. doi:10.1016/j.geomorph.2009.11.023
Ravi, S., D'Odorico, P., Zobeck, T.M., Over, T.M., Collins, S.L., 2007. Feedbacks between fires and wind erosion in heterogeneous arid lands. Journal of Geophysical Research: Biogeosciences 112, n/a–n/a. doi:10.1029/2007JG000474
Rawling, G.C., 2005. Geology and hydrologic setting of springs and seeps on the Sevilleta National Wildlife Refuge (Open-file Report No. 495). New Mexico Bureau of Geology and Mineral Resources, New Mexico Tech, Socorro, New Mexico.
Raymond, P.A., Cole, J.J., 2003. Increase in the export of alkalinity from North America's largest river. Science 301, 88–91. doi:10.1126/science.1083788
Raymond, P.A., Oh, N.-H., Turner, R.E., Broussard, W., 2008. Anthropogenically enhanced fluxes of water and carbon from the Mississippi River. Nature 451, 449–452. doi:10.1038/nature06505
Reheis, M.C., Goodmacher, J.C., Harden, J.W., McFadden, L.D., Rockwell, T.K., Shroba, R.R., Sowers, J.M., Taylor, E.M., 1995. Quaternary soils and dust deposition in southern Nevada and California. Geological Society of America Bulletin 107, 1003–1022. doi:10.1130/0016-7606(1995)107<1003:qsaddi>2.3.co;2
Rehfeldt, G.E., Crookston, N.L., Warwell, M.V., Evans, J.S., 2006. Empirical analyses of plant-climate relationships for the western United States. International Journal of Plant Sciences 167, 1123–1150. doi:10.1086/507711

Remondino, F., Spera, M.G., Nocerino, E., Menna, F., Nex, F., 2014. State of the art in high density image matching. Photogram Rec 29, 144–166. doi:10.1111/phor.12063

Renwick, W.H., Smith, S.V., Sleezer, R.O., Buddemeier, R.W., 2004. Comment on" Managing Soil Carbon"(II). Science 305, 1567–1567.

Reynolds, H., 1950. Relation of Merriam kangaroo rats to range vegetation in Southern Arizona. Ecology 31, 456–463. doi:10.2307/1931498

Reynolds, J.F., Kemp, P.R., Tenhunen, J.D., 2000. Effects of long-term rainfall variability on evapotranspiration and soil water distribution in the Chihuahuan Desert: a modeling analysis. Plant Ecology 150, 145–159.

Reynolds, J.F., Smith, D.M.S., Lambin, E.F., Turner II, B.L., Mortimore, M., Batterbury, S.P.J., Downing, T.E., Dowlatabadi, H., Fernández, R.J., Herrick, J.E., Huber-Sannwald, E., Jiang, H., Leemans, R., Lynam, T., Maestre, F.T., Ayarza, M., Walker, B., 2007. Global desertification: building a science for dryland development. Science 316, 847–851. doi:10.1126/science.1131634

Rhoton, F.E., Emmerich, W.E., Goodrich, D.C., Miller, S.N., McChesney, D.S., 2006. Soil geomorphological characteristics of a semiarid watershed: influence on carbon distribution and transport. Soil Science Society of America Journal 70, 1532–1540. doi:10.2136/sssaj2005.0239

Richardson, A.D., Keenan, T.F., Migliavacca, M., Ryu, Y., Sonnentag, O., Toomey, M., 2013. Climate change, phenology, and phenological control of vegetation feedbacks to the climate system. Agricultural and Forest Meteorology 169, 156–173. doi:10.1016/j.agrformet.2012.09.012

Richter, D.D., Barbbar, L.I., Huston, M.A., Jaeger, M., 1990. Effects of annual tillage on organic carbon in a fine textured Udalf: the importance of root dynamics to soil carbon storage. Soil Science 149.

Ridolfi, L., Laio, F., D'Odorico, P., 2008. Fertility island formation and evolution in dryland ecosystems. Ecology and Society 13, 13.

Rieke-Zapp, D., Poesen, J., Nearing, M.A., 2007. Effects of rock fragments incorporated in the soil matrix on concentrated flow hydraulics and erosion. Earth Surface Processes and Landforms 32, 1063–1076. doi:10.1002/esp.1469

Rietkerk, M., Ketner, P., Stroosnijder, L., Prins, H.H., 1996. Sahelian rangeland development; a catastrophe? Journal of Range Management 512–519.

Rios-Arana, J.V., Walsh, E.J., Gardea-Torresdey, J.L., 2004. Assessment of arsenic and heavy metal concentrations in water and sediments of the Rio Grande at El Paso–Juarez metroplex region. Environment International 29, 957–971. doi:10.1016/S0160-4120(03)00080-1

Ritchie, J.C., 1989. Carbon content of small reservoirs. Journal of the American Water Resources Association 25, 301–308. doi:10.1111/j.1752-1688.1989.tb03065.x

Robertson, G.P., Paul, E.A., 2000. Decomposition and soil organic matter dynamics, in: Sala, O.E., Jackson, R.B., Mooney, H.A., Howarth, R.W. (Eds.), Methods in Ecosystem Science. Springer, New York, NY, USA, pp. 104–116.

Robinson, D., 2004. Scaling the depths: below-ground allocation in plants, forests and biomes. Functional Ecology 18, 290–295. doi:10.1111/j.0269-8463.2004.00849.x

Roderick, M.L., Chewings, V.H., Smith, R.C.G., 2000. Remote sensing in vegetation and animal studies, in: 't Mannetje, L., Jones, R.M. (Eds.), Field and Laboratory Methods for Grassland and Animal Production Research. CABI Publishing, Ney York, NY, USA, pp. 205–226.

Rodgers, S.J., 1968. Evaluation of the dust cloud generated by helicopter rotor downwash. MSA RESEARCH CORP EVANS CITY PA.

Rojas, R., Velleux, M., Julien, P.Y., Johnson, B.E., 2008. Grid scale effects on watershed soil erosion models. Journal of Hydrologic Engineering 13, 793–802.

Ropelewski, C.F., Halpert, M.S., 1986. North American precipitation and temperature patterns associated with the El Niño/Southern Oscillation (ENSO). Mon. Wea. Rev. 114, 2352–2362. doi:10.1175/1520-0493(1986)114<2352:NAPATP>2.0.CO;2

Rozas, V., DeSoto, L., Olano, J.M., 2009. Sex-specific, age-dependent sensitivity of tree-ring growth to climate in the dioecious tree Juniperus thurifera. New Phytologist 182, 687–697. doi:10.1111/j.1469-8137.2009.02770.x

Rumpel, C., Chaplot, V., Planchon, O., Bernadou, J., Valentin, C., Mariotti, A., 2006. Preferential erosion of black carbon on steep slopes with slash and burn agriculture. Catena 65, 30–40.

Rutledge, S., Campbell, D.I., Baldocchi, D., Schipper, L.A., 2010. Photodegradation leads to increased carbon dioxide losses from terrestrial organic matter. Global Change Biology 16, 3065–3074. doi:10.1111/j.1365-2486.2009.02149.x

Safriel, U., Adeel, Z., Niemeijer, D., Puigdefabregas, J., White, R., Lal, R., Winslow, M., Ziedler, J., Prince, S., Archer, E., King, C., Shapiro, B., Wessels, K., Nielsen, T., Portnov, B., Reshef, I., Thonell, J., Lachman, E., McNab, D., 2005. Dryland Systems, in: Ecosystems and Human Well-Being: Current State and Trends. pp. 623–662.

Sainju, U.M., Terrill, T.H., Gelaye, S., Singh, B.P., 2003. Soil aggregation and carbon and nitrogen pools under rhizoma peanut and perennial weeds. Soil Science Society of America Journal 67, 146–155. doi:10.2136/sssaj2003.1460

Sainju, U.M., Whitehead, W.F., Singh, B.P., 2011. Cover crops and nitrogen fertilization effects on soil aggregation and carbon and nitrogen pools. Canadian Journal of Soil Science. doi:10.4141/S02-056

Sala, O.E., Maestre, F.T., 2014. Grass–woodland transitions: determinants and consequences for ecosystem functioning and provisioning of services. J Ecol 102, 1357–1362. doi:10.1111/1365-2745.12326

Sankey, J.B., Munson, S.M., Webb, R.H., Wallace, C.S.A., Duran, C.M., 2015. Remote sensing of Sonoran Desert vegetation structure and phenology with ground-based LiDAR. Remote Sensing 7, 342–359. doi:10.3390/rs70100342

Sankey, J.B., Ravi, S., Wallace, C.S.A., Webb, R.H., Huxman, T.E., 2012. Quantifying soil surface change in degraded drylands: Shrub encroachment and effects of fire and vegetation removal in a desert grassland. Journal of Geophysical Research 117, G02025. doi:10.1029/2012JG002002

Sankey, T., Shrestha, R., Sankey, J.B., Hardegree, S., Strand, E., 2013. Lidar-derived estimate and uncertainty of carbon sink in successional phases of woody encroachment. J. Geophys. Res. Biogeosci. 118, 1144–1155. doi:10.1002/jgrg.20088

Sankey, T.T., Bond, P., 2011. LiDAR-based classification of sagebrush community types. Rangeland Ecology & Management 64, 92–98. doi:10.2111/REM-D-10-00019.1

Sardà-Palomera, F., Bota, G., Viñolo, C., Pallarés, O., Sazatornil, V., Brotons, L., Gomáriz, S., Sardà, F., 2012. Fine-scale bird monitoring from light unmanned aircraft systems. Ibis 154, 177–183. doi:10.1111/j.1474-919X.2011.01177.x

Schade, J.D., Hobbie, S.E., 2005. Spatial and temporal variation in islands of fertility in the Sonoran Desert. Biogeochemistry 73, 541–553. doi:10.1007/s10533-004-1718-1
Schaefer, D., Steinberger, Y., Whitford, W.G., 1985. The failure of nitrogen and lignin control of decomposition in a North American desert. Oecologia 65, 382–386. doi:10.1007/BF00378913
Schenk, H.J., Jackson, R.B., 2002. Rooting depths, lateral root spreads and below-ground/above-ground allometries of plants in water-limited ecosystems. Journal of Ecology 90, 480–494. doi:10.1046/j.1365-2745.2002.00682.x
Schiettecatte, W., Gabriels, D., Cornelis, W.M., Hofman, G., 2008a. Enrichment of organic carbon in sediment transport by interrill and rill erosion processes. Soil Science Society of America Journal 72, 50–55. doi:10.2136/sssaj2007.0201
Schiettecatte, W., Gabriels, D., Cornelis, W.M., Hofman, G., 2008b. Impact of deposition on the enrichment of organic carbon in eroded sediment. Catena 72, 340–347. doi:10.1016/j.catena.2007.07.001
Schiffman, R., 2014. Drones flying high as new tool for field biologists. Science 344, 459–459. doi:10.1126/science.344.6183.459
Schimel, D.S., House, J.I., Hibbard, K.A., Bousquet, P., Ciais, P., Peylin, P., Braswell, B.H., Apps, M.J., Baker, D., Bondeau, A., Canadell, J.G., Ghurkina, G., Cramer, W., Denning, A.S., Field, C.B., Friedlingstein, P., Goondale, C., Heimann, M., Houghton, R.A., Melillo, J.M., Moore III, B., Murdiyarso, D., Noble, I., Pacala, S.W., Prentice, I.C., Raupach, M.R., Rayner, P.J., Scholes, R.J., Steffen, W.L., Wirth, C., 2001. Recent patterns and mechanisms of carbon exchange by terrestrial ecosystems. Nature 414, 169–172.
Schimel, D.S., Kelly, E.F., Yonker, C., Aguilar, R., Heil, R., 1985. Effects of errosional processes on nutrient cycling in semiarid landscapes, in: Caldwell, D.E., Brierley, J.A., Brierley, C.L. (Eds.), Planetary Ecology. Van Nostrand Reinhold, New York, NY, pp. 571–580.
Schindler, D.W., 1999. The mysterious missing sink. Nature 398, 105–106.
Schlesinger, W.H., 2016. An evaluation of abiotic carbon sinks in deserts. Global Change Biology. doi:10.1111/gcb.13336
Schlesinger, W.H., 1997. Biogeochemistry: An Analysis of Global Change, 2nd ed. Academic Press, San Diego, CA, USA.
Schlesinger, W.H., 1995. Soil respiration and changes in soil carbon stocks, in: Woodwell, G.M., Mackenzie, G.M. (Eds.), Biotic Feedbacks in the Global Climatic System: Will Warming Feed the Warming? Oxford University Press, Ney York, NY. USA, pp. 159–168.
Schlesinger, W.H., 1985. The formation of caliche in soils of the Mojave Desert, California. Geochimica et Cosmochimica Acta 49, 57–66.
Schlesinger, W.H., 1982. Carbon storage in the calice of arid soils: a case study from Arizona. Carbon 133.
Schlesinger, W.H., Abrahams, A.D., Parsons, A.J., Wainwright, J., 1999. Nutrient losses in runoff from grassland and shrubland habitats in Southern New Mexico: I. Rainfall simulation experiments. Biogeochemistry 45, 21–34. doi:10.1007/BF00992871
Schlesinger, W.H., Bernhardt, E.S., 2013a. Chapter 6 - The Biosphere: Biogeochemical Cycling on Land, in: Bernhardt, W.H.S.S. (Ed.), Biogeochemistry (Third Edition). Academic Press, Boston, pp. 173–231.
Schlesinger, W.H., Bernhardt, E.S., 2013b. Chapter 5 - The Biosphere: The Carbon Cycle of Terrestrial Ecosystems, in: Bernhardt, W.H.S.S. (Ed.), Biogeochemistry (Third Edition). Academic Press, Boston, pp. 135–172.

Schlesinger, W.H., Pilmanis, A.M., 1998. Plant-soil interactions in deserts. Biogeochemistry 42, 169–187. doi:10.1023/A:1005939924434
Schlesinger, W.H., Raikes, J.A., Hartley, A.E., Cross, A.F., 1996. On the spatial pattern of soil nutrients in desert ecosystems. Ecology 77, 364–374. doi:10.2307/2265615
Schlesinger, W.H., Reynolds, J.F., Cunningham, G.L., Huenneke, L.F., Jarrell, W.M., Virginia, R.A., Whitford, W.G., 1990. Biological feedbacks in global desertification. Science 247, 1043–1048. doi:10.1126/science.247.4946.1043
Schlesinger, W.H., Tartowski, S.L., Schhmidt, S.M., 2006. Nutrient cycling within an arid ecosystem, in: Havstad, K.M., Huenneke, L.F., Schlesinger, W.H. (Eds.), Structure and Function of a Chihuahuan Desert Ecosystem. Oxford University Press, New York, pp. 133–149.
Schlesinger, W.H., Ward, T.J., Anderson, J.P., 2000. Nutrient losses in runoff from grasslandand shrubland habitats in southern New Mexico: II. Field plots. Biogeochemistry 49, 69–86. doi:10.1023/A:1006246126915
Schubert, S.D., Suarez, M.J., Pegion, P.J., Koster, R.D., Bacmeister, J.T., 2010. Causes of Long-Term Drought in the U.S. Great Plains. Journal of Climate 17, 485–503. doi:10.1175/1520-0442(2004)017<0485:COLDIT>2.0.CO;2
Schubert, S.D., Suarez, M.J., Pegion, P.J., Koster, R.D., Bacmeister, J.T., 2004. On the cause of the 1930s Dust Bowl. Science 303, 1855–1859. doi:10.1126/science.1095048
Schumacher, B.A., 2002. Methods for the determination of total organic carbon (TOC) in soils and sediments. U. S. Environmental Protection Agency, Las Vegas, NV, USA.
Schwendenmann, L., Pendall, E., 2006. Effects of forest conversion into grassland on soil aggregate structure and carbon storage in Panama: evidence from soil carbon fractionation and stable isotopes. Plant and Soil 288, 217–232.
Schwinning, S., Starr, B.I., Ehleringer, J., 2005. Summer and winter drought in a cold desert ecosystem (Colorado Plateau) part I: effects on soil water and plant water uptake. Journal of Arid Environments 60, 547–566.
Scoging, H.M., 1992. Modelling overland-flow hydrology for dynamic hydraulics, in: Parsons, A.J., Abrahams, A.D. (Eds.), Overland Flow Hydraulics and Erosion Mechanics. UCL Press, London, pp. 81–94.
Scoging, H.M., Parsons, A.J., Abrahams, A.D., 1992. Application of a dynamics overland flow model to a semi-arid hillslope, Walnut Gulch, Arizona, in: Parsons, A.J., Abrahams, A.D. (Eds.), Overland Flow Hydraulics and Erosion Mechanics. UCL Press, London, pp. 96–135.
Scott, M.R., Slater, P.F., 1987. Transport of plutonium by the Mississippi River System and Other Rivers in the Souther United States, in: Pinder III, J.E., Alberts, J.J., McLeod, K.W., Schreckhise, R.G. (Eds.), Environmnetal Research on Actinide Elements. US Department of Energy, pp. 229–318.
Scott, R.L., Biederman, J.A., Hamerlynck, E.P., Barron-Gafford, G.A., 2016. The carbon balance pivot point of southwestern U.S. semiarid ecosystems: Insights from the 21st century drought. Journal of Geophysical Research: Biogeosciences. doi:10.1002/2015JG003181
Scott, R.L., Jenerette, G.D., Potts, D.L., Huxman, T.E., 2009. Effects of seasonal drought on net carbon dioxide exchange from a woody-plant-encroached semiarid grassland. Journal of Geophysical Research 114, G04004. doi:10.1029/2008JG000900

Scurlock, J.M.O., Johnson, K., Olson, R.J., 2002. Estimating net primary productivity from grassland biomass dynamics measurements. Global Change Biology 8, 736–753. doi:10.1046/j.1365-2486.2002.00512.x

Seager, R., Kushnir, Y., Herweijer, C., Naik, N., Velez, J., 2005. Modeling of tropical forcing of persistent droughts and pluvials over Western North America: 1856–2000. J. Climate 18, 4065–4088. doi:10.1175/JCLI3522.1

Seager, R., Ting, M., Held, I., Kushnir, Y., Lu, J., Vecchi, G., Huang, H.P., Harnik, N., Leetmaa, A., Lau, N.C., 2007. Model projections of an imminent transition to a more arid climate in southwestern North America. Science 316, 1181–1184. doi:10.1126/science.1139601

Seager, R., Ting, M., Li, C., Naik, N., Cook, B., Nakamura, J., Liu, H., 2013. Projections of declining surface-water availability for the southwestern United States. Nature Clim. Change 3, 482–486. doi:10.1038/nclimate1787

Seager, R., Vecchi, G.A., 2010. Greenhouse warming and the 21st century hydroclimate of southwestern North America. PNAS 107, 21277–21282. doi:10.1073/pnas.0910856107

Serna-Pérez, A., Monger, H.C., Herrick, J.E., Murray, L., 2006. Carbon dioxide emissions from exhumed petrocalcic horizons. Soil Science Society of America Journal 70, 795–805. doi:10.2136/sssaj2005.0099

Shafer, S.L., Bartlein, P.J., Thompson, R.S., 2001. Potential changes in the distribution of western North America tree and shrub taxa under future climate scenarios. Ecosystems 4, 200–215.

Shahbazi, M., Sohn, G., Théau, J., Menard, P., 2015. Development and evaluation of a UAV-photogrammetry system for precise 3D environmental modeling. Sensors 15, 27493–27524. doi:10.3390/s151127493

Sharpley, A.N., 1985. The selective erosion of plant nutrients in runoff. Soil Science Society of America Journal 49, 1527–1534. doi:10.2136/sssaj1985.03615995004900060039x

Sigman, D.M., Boyle, E.A., 2000. Glacial/interglacial variations in atmospheric carbon dioxide. Nature 407, 859–869.

Sims, P.L., Singh, J.S., 1978. The structure and function of ten western North American grasslands: III. net primary production, turnover and efficiencies of energy capture and water use. Journal of Ecology 66, 573–597. doi:10.2307/2259152

Sims, P.L., Singh, J.S., Lauenroth, W.K., 1978. The structure and function of ten Western North American grasslands: I. abiotic and vegetational characteristics. Journal of Ecology 66, 251–285. doi:10.2307/2259192

Singh, S.P., 1964. Cover, biomass, and root-shoot habit of Larrea divaricata on a selected site in southern New Mexico (MSc). New Mexico State University, Las Cruces, New Mexico, USA.

Singh, T., 1986. Generalizing biomass equations for the boreal forest region of west-central Canada. Forest Ecology and Management 17, 97–107. doi:10.1016/0378-1127(86)90102-7

Singh, V.P., 2001. Kinematic wave modelling in water resources: a historical perspective. Hydrol. Process. 15, 671–706. doi:10.1002/hyp.99

Singh, V.P., 1996. Kinematic Wave Modelling in Water Resources. Wiley, Chichester, UK.

Sitch, S., Huntingford, C., Gedney, N., Levy, P.E., Lomas, M.R., Piao, S.L., Betts, R., Ciais, P., Cox, P.M., Friedlingstein, P., 2008. Evaluation of the terrestrial carbon cycle, future plant geography and climate-carbon cycle feedbacks using five Dynamic Global Vegetation Models (DGVMs). Global Change Biology 14, 2015–2039. doi:10.1111/j.1365-2486.2008.01626.x

Six, J., Callewaert, P., Lenders, S., De Gryze, S., Morris, S.J., Gregorich, E.G., Paul, E.A., Paustian, K., 2002. Measuring and understanding carbon storage in afforested soils by physical fractionation. Soil Science Society of America Journal 66, 1981–1987.

Slattery, M.C., Burt, T.P., 1997. Particle size characteristics of suspended sediment in hillslope runoff and stream flow. Earth Surface Processes and Landforms 22, 705–719. doi:10.1002/(sici)1096-9837(199708)22:8<705::aid-esp739>3.0.co;2-6

Smith, C.E., Sykora-Bodie, S.T., Bloodworth, B., Pack, S.M., Spradlin, T.R., LeBoeuf, N.R., 2016. Assessment of known impacts of unmanned aerial systems (UAS) on marine mammals: data gaps and recommendations for researchers in the United States. J. Unmanned Veh. Sys. 1–14. doi:10.1139/juvs-2015-0017

Smith, G., Holechek, J.L., Cardenas, M., 1996. Wildlife numbers on excellent and good condition Chihuahuan Desert rangelands: an observation. Journal of Range Management 49, 489–493. doi:10.2307/4002287

Smith, J.L., Halvorson, J.J., Bolton, H., 1994. Spatial relationships of soil microbial biomass and C and N mineralization in a semi-arid shrub-steppe ecosystem. Soil Biology and Biochemistry 26, 1151–1159. doi:10.1016/0038-0717(94)90137-6

Smith, M.W., Vericat, D., 2015. From experimental plots to experimental landscapes: topography, erosion and deposition in sub-humid badlands from Structure-from-Motion photogrammetry. Earth Surf. Process. Landforms n/a-n/a. doi:10.1002/esp.3747

Smith, P., 2004. How long before a change in soil organic carbon can be detected? Global Change Biology 10, 1878–1883. doi:10.1111/j.1365-2486.2004.00854.x

Smith, R.E., Parlange, J.-Y., 1978. A parameter-efficient hydrologic infiltration model. Water Resources Research 14, 533–538. doi:10.1029/WR014i003p00533

Smith, R.E., Quinton, J., Goodrich, D.C., Nearing, M.A., 2010. Soil-erosion models: where do we really stand? Earth Surface Processes and Landforms 35, 1344–1348. doi:10.1002/esp.1985

Smith, S.D., Huxman, T.E., Zitzer, S.F., Charlet, T.N., Housman, D.C., Coleman, J.S., Fenstermaker, L.K., Seemann, J.R., Nowak, R.S., 2000. Elevated CO2 increases productivity and invasive species success in an arid ecosystem. Nature 408, 79–81. doi:10.1038/35040544

Smith, S.V., Renwick, W.H., Buddemeier, R.W., Crossland, C.J., 2001. Budgets of soil erosion and deposition for sediments and sedimentary organic carbon across the conterminous United States. Global Biogeochemical Cycles 15, 697–707.

Smith, W.B., Brand, G.J., 1983. Allometric Biomass Equations for 98 Species of Herbs, Shrubs and Small Trees (Research Note No. Research Note NC-299). U.S. Dept. of Agriculture, Forest Service, North Central Forest Experiment Station, St. Paul, MN, USA.

Snavely, N., Seitz, S.M., Szeliski, R., 2008. Modeling the World from Internet Photo Collections. Int J Comput Vis 80, 189–210. doi:10.1007/s11263-007-0107-3

Soliveres, S., García-Palacios, P., Maestre, F.T., Escudero, A., Valladares, F., 2013. Changes in rainfall amount and frequency do not affect the outcome of the interaction between the shrub Retama sphaerocarpa and its neighbouring grasses in two semiarid communities. Journal of Arid Environments 91, 104–112. doi:10.1016/j.jaridenv.2012.12.011

Sollins, P., Homann, P., Caldwell, B.A., 1996. Stabilization and destabilization of soil organic matter: mechanisms and controls. Geoderma 74, 65–105. doi:10.1016/S0016-7061(96)00036-5

Sombroek, W.G., Nachtergaele, F.O., Hevel, A., 1993. Amounts, dynamics and sequestering of carbon in tropical and subtropical soils. Ambio 22, 417–426.

Sona, G., Pinto, L., Pagliari, D., Passoni, D., Gini, R., 2014. Experimental analysis of different software packages for orientation and digital surface modelling from UAV images. Earth Sci Inform 7, 97–107. doi:10.1007/s12145-013-0142-2

Soulard, C.E., Esque, T.C., Bedford, D.R., Bond, S., 2013. The role of fire on soil mounds and surface roughness in the Mojave Desert. Earth Surf. Process. Landforms 38, 111–121. doi:10.1002/esp.3264

Sponseller, R.A., 2007. Precipitation pulses and soil CO2 flux in a Sonoran Desert ecosystem. Global Change Biology 13, 426–436. doi:10.1111/j.1365-2486.2006.01307.x

Stallard, R.F., 1998. Terrestrial sedimentation and the carbon cycle: coupling weathering and erosion to carbon burial. Global Biogeochemical Cycles 12, 231–257.

Starks, P.J., Venuto, B.C., Eckroat, J.A., Lucas, T., 2011. Measuring Eastern Redcedar (Juniperus virginiana L.) mass with the use of satellite imagery. Rangeland Ecology & Management 64, 178–186. doi:10.2111/REM-D-10-00057.1

Starr, G.C., Lal, R., Kimble, J.M., Owens, L., 2001. Assessing the impact of erosion on soil organic carbon pools and fluxes, in: Lal, R., Kimble, J.M., Follett, R.F., Stewart, B.A. (Eds.), Assessment Methods for Soil Carbon. pp. 417–426.

Starr, G.C., Lal, R., Malone, R., Hothem, D., Owens, L., Kimble, J., 2000. Modeling soil carbon transported by water erosion processes. Land Degradation & Development 11, 83–91.

Steichen, T., Cox, N., 2002. A note on the concordance correlation coefficient. Stata Journal 2, 183–189.

Sterk, G., Herrmann, L., Bationo, A., 1996. Wind-blown nutrient transport and soil productivity changes in southwest Niger. Land Degrad. Dev. 7, 325–335. doi:10.1002/(SICI)1099-145X(199612)7:4<325::AID-LDR237>3.0.CO;2-Q

Stevenson, B.A., Verburg, P.S.J., 2006. Effluxed CO2-13C from sterilized and unsterilized treatments of a calcareous soil. Soil Biology and Biochemistry 38, 1727–1733. doi:10.1016/j.soilbio.2005.11.028

Stewart, J., Parsons, A.J., Wainwright, J., Okin, G.S., Bestelmeyer, B., Fredrickson, E.L., Schlesinger, W.H., 2014. Modelling emergent patterns of dynamic desert ecosystems. Ecological Monographs 84, 373–410. doi:10.1890/12-1253.1

Stone, R., 2008. Have desert researchers discovered a hidden loop in the carbon cycle? Science 320, 1409–1410. doi:10.1126/science.320.5882.1409

Strand, E.K., Vierling, L.A., Smith, A.M.S., Bunting, S.C., 2008. Net changes in aboveground woody carbon stock in western juniper woodlands, 1946–1998. Journal of Geophysical Research: Biogeosciences 113. doi:10.1029/2007JG000544

Streutker, D.R., Glenn, N.F., 2006. LiDAR measurement of sagebrush steppe vegetation heights. Remote Sensing of Environment 102, 135–145. doi:10.1016/j.rse.2006.02.011

Stringer, L.C., Dougill, A.J., Thomas, A.D., Spracklen, D.V., Chesterman, S., Speranza, C.I., Rueff, H., Riddell, M., Williams, M., Beedy, T., Abson, D.J., Klintenberg, P., Syampungani, S., Powell, P., Palmer, A.R., Seely, M.K.,

Mkwambisi, D.D., Falcao, M., Sitoe, A., Ross, S., Kopolo, G., 2012. Challenges and opportunities in linking carbon sequestration, livelihoods and ecosystem service provision in drylands. Environmental Science & Policy 19–20, 121–135. doi:10.1016/j.envsci.2012.02.004

Stursova, M., Crenshaw, C.L., Sinsabaugh, R.L., 2006. Microbial responses to long-term N deposition in a semiarid grassland. Microbial Ecology 51, 90–98. doi:10.1007/s00248-005-516-y

Sutfin, N.A., Wohl, E.E., Dwire, K.A., 2015. Banking carbon: A review of organic carbon storage and physical factors influencing retention in floodplains and riparian ecosystems. Earth Surf. Process. Landforms n/a-n/a. doi:10.1002/esp.3857

Swetnam, T.W., Betancourt, J.L., 1998. Mesoscale disturbance and ecological response to decadal climatic variability in the American Southwest. Journal of Climate 11, 3128–3147.

't Mannetje, L., 2000. Measuring biomass of grassland vegetation, in: 't Mannetje, L., Jones, R.M. (Eds.), Field and Laboratory Methods for Grassland and Animal Production Research. CABI Publishing, Ney York, NY, USA, pp. 151–178.

Tatard, L., Planchon, O., Wainwright, J., Nord, G., Favis-Mortlock, D.T., Silvera, N., Ribolzi, O., Esteves, M., Huang, C.H., 2008. Measurement and modelling of high-resolution flow-velocity data under simulated rainfall on a low-slope sandy soil. Journal of Hydrology 348, 1–12. doi:10.1016/j.jhydrol.2007.07.016

Taube, S.R., Furbish, D.J., 2010. Effects of moisture and grain size on the mechanisms of rainsplash transport. AGU Fall Meeting Abstracts 1, 689.

Taylor, J.R., 1997. An introduction to error analysis: the study of uncertanties in physical measurements. University Science Books, Sausalito, CA, USA.

Thomas, A.D., Dougill, A.J., Elliott, D., Mairs, H., 2014. Carbon storage and CO2 efflux from in salt pan sediments on Ntwetwe Pan, Makgadikgadi Basin, Botswana. Geoderma 219–220, 72–81. doi:10.1016/j.geoderma.2013.12.028

Thomas, R.Q., Hurtt, G.C., Dubayah, R., Schilz, M.H., 2008. Using lidar data and a height-structured ecosystem model to estimate forest carbon stocks and fluxes over mountainous terrain. Canadian Journal of Remote Sensing 34, S351–S363. doi:10.5589/m08-036

Thomas, S.C., Martin, A.R., 2012. Carbon content of tree tissues: a synthesis. Forests 3, 332–352. doi:10.3390/f3020332

Thomey, M.L., Ford, P.L., Reeves, M.C., Finch, D.M., Litvak, M.E., Collins, S.L., 2014. Climate change impacts on future carbon stores and management of warm deserts of the United States. Rangelands 36, 16–24. doi:10.2111/RANGELANDS-D-13-00045.1

Throop, H.L., Archer, S.R., Monger, H.C., Waltman, S., 2012a. When bulk density methods matter: Implications for estimating soil organic carbon pools in rocky soils. Journal of Arid Environments 77, 66–71. doi:10.1016/j.jaridenv.2011.08.020

Throop, H.L., Reichmann, L.G., Sala, O.E., Archer, S.R., 2012b. Response of dominant grass and shrub species to water manipulation: an ecophysiological basis for shrub invasion in a Chihuahuan Desert Grassland. Oecologia 1–11. doi:10.1007/s00442-011-2217-4

Tietema, T., 1993. Biomass determination of fuelwood trees and bushes of Botswana, Southern Africa. Forest Ecology and Management 60, 257–269. doi:10.1016/0378-1127(93)90083-Y

Tietjen, B., Jeltsch, F., Zehe, E., Classen, N., Groengroeft, A., Schiffers, K., Oldeland, J., 2009. Effects of climate change on the coupled dynamics of water and vegetation in drylands. Ecohydrology n/a-n/a. doi:10.1002/eco.70

Tilly, N., Aasen, H., Bareth, G., 2015a. Fusion of plant height and vegetation indices for the estimation of barley biomass. Remote Sensing 7, 11449–11480. doi:10.3390/rs70911449

Tilly, N., Hoffmeister, D., Cao, Q., Lenz-Wiedemann, V., Miao, Y., Bareth, G., 2015b. Transferability of models for estimating paddy rice biomass from spatial plant height data. Agriculture 5, 538–560. doi:10.3390/agriculture5030538

Titus, J.H., Nowak, R.S., Smith, S.D., 2002. Soil resource heterogeneity in the Mojave Desert. Journal of Arid Environments 52, 269–292. doi:10.1006/jare.2002.1010

Tonkin, T.N., Midgley, N.G., Graham, D.J., Labadz, J.C., 2014. The potential of small unmanned aircraft systems and structure-from-motion for topographic surveys: A test of emerging integrated approaches at Cwm Idwal, North Wales. Geomorphology 226, 35–43. doi:10.1016/j.geomorph.2014.07.021

Torn, M.S., Lapenis, A.G., Timofeev, A., Fischer, M.L., Babikov, B.V., Harden, J.W., 2002. Organic carbon and carbon isotopes in modern and 100-year-old-soil archives of the Russian steppe. Global Change Biology 8, 941–953. doi:10.1046/j.1365-2486.2002.00477.x

Torn, M.S., Trumbore, S.E., Chadwick, O.A., Vitousek, P.M., Hendricks, D.M., 1997. Mineral control of soil organic carbon storage and turnover. Nature 389, 170–173.

Tromble, J.M., Renard, K.G., Thatcher, A.P., 1974. Infiltration for three rangeland soil-vegetation complexes. Journal of Range Management 27, 318–321. doi:10.2307/3896834

Truman, C.C., Strickland, T.C., Potter, T.L., Franklin, D.H., Bosch, D.D., Bednarz, C.W., 2007. Variable rainfall intensity and tillage effects on runoff, sediment, and carbon losses from a loamy sand under simulated rainfall. Journal of Environmental Quality 36, 1495–1502. doi:10.2134/jeq2006.0018

Tuominen, S., Balazs, A., Saari, H., Pölönen, I., Sarkeala, J., Viitala, R., 2015. Unmanned aerial system imagery and photogrammetric canopy height data in area-based estimation of forest variables. doi:10.14214/sf.1348

Turnbull, L., 2008. Ecohydrological interactions across a semi-arid grassland to shrubland transition. University of Sheffield, Sheffield, UK.

Turnbull, L., Brazier, R.E., Wainwright, J., Dixon, L., Bol, R., 2008a. Use of carbon isotope analysis to understand semi-arid erosion dynamics and long-term semi-arid land degradation. Rapid Communications in Mass Spectrometry 22, 1697–1702.

Turnbull, L., Hochstasser, T., Wieczorek, M., Baas, A., Wainwright, J., Scarsoglio, S., Tietjen, B., Jeltsch, F., Müller, E.N., 2014a. Approaches to modelling ecogeomorphic systems, in: Müller, E.N., Wainwright, J., Parsons, A.J., Turnbull, L. (Eds.), Patterns of Land Degradation in Drylands: Understanding Self-Organising Ecogeomorphic Systems. Springer, pp. 171–209.

Turnbull, L., Müller, E.N., Tietjen, B., Wainwright, J., 2014b. Modelling ecogeomorphic feedbacks: investigating mechanisms of land degradation in semi-arid grassland and shrubland. Presented at the EGU General Assembly, EGU, Vienna, Austria.

Turnbull, L., Parsons, A.J., Wainwright, J., Anderson, J.P., 2013. Runoff responses to long-term rainfall variability in a shrub-dominated catchment. Journal of Arid Environments 91, 88–94. doi:10.1016/j.jaridenv.2012.12.002

Turnbull, L., Wainwright, J., Brazier, R.E., 2011. Nitrogen and phosphorus dynamics during runoff events over a transition from grassland to shrubland in the south-western United States. Hydrological Processes 25, 1–17. doi:10.1002/hyp.7806

Turnbull, L., Wainwright, J., Brazier, R.E., 2010a. Changes in hydrology and erosion over a transition from grassland to shrubland. Hydrological Processes 24, 393–414. doi:10.1002/hyp.7491

Turnbull, L., Wainwright, J., Brazier, R.E., 2010b. Hydrology, erosion and nutrient transfers over a transition from semi-arid grassland to shrubland in the South-Western USA: A modelling assessment. Journal of Hydrology 388, 258–272. doi:10.1016/j.jhydrol.2010.05.005

Turnbull, L., Wainwright, J., Brazier, R.E., 2008b. A conceptual framework for understanding semi-arid land degradation: Ecohydrological interactions across multiple-space and time scales. Ecohydrology 1, 23–34. doi:10.1002/eco.4

Turnbull, L., Wainwright, J., Brazier, R.E., Bol, R., 2010c. Biotic and abiotic changes in ecosystem structure over a shrub-encroachment gradient in the Southwestern USA. Ecosystems 13, 1239–1255. doi:10.1007/s10021-010-9384-8

Turnbull, L., Wilcox, B.P., Belnap, J., Ravi, S., D'Odorico, P., Childers, D., Gwenzi, W., Okin, G.S., Wainwright, J., Caylor, K.K., 2012. Understanding the role of ecohydrological feedbacks in ecosystem state change in drylands. Ecohydrology 5, 174–183. doi:10.1002/eco.265

Turner, D., Lucieer, A., Wallace, L., 2014. Direct georeferencing of ultrahigh-resolution UAV imagery. IEEE Transactions on Geoscience and Remote Sensing 52, 2738–2745. doi:10.1109/TGRS.2013.2265295

Turner, I.L., Harley, M.D., Drummond, C.D., 2016. UAVs for coastal surveying. Coastal Engineering 114, 19–24. doi:10.1016/j.coastaleng.2016.03.011

Twine, T.E., Kustas, W.P., Norman, J.M., Cook, D.R., Houser, P.R., Meyers, T.P., Prueger, J.H., Starks, P.J., Wesely, M.L., 2000. Correcting eddy-covariance flux underestimates over a grassland. Agricultural and Forest Meteorology 103, 279–300. doi:10.1016/S0168-1923(00)00123-4

Ugolini, F.C., Corti, G., Agnelli, A., Piccardi, F., 1996. Mineralogical, physical, and chemical properties of rock fragments. Soil Science, Soil Science 161, 521–542.

UNCCD, 2000. United Nations Convention to Combat Desertification.

Van Auken, O.W., 2009. Causes and consequences of woody plant encroachment into western North American grasslands. Journal of Environmental Management 90, 2931–2942. doi:10.1016/j.jenvman.2009.04.023

Van Auken, O.W., 2000. Shrub invasions of North American semiarid grasslands. Annual Review of Ecology and Systematics 197–215. doi:10.1146/annurev.ecolsys.31.1.197

Van Oost, K., Govers, G., Quine, T.A., Heckrath, G., 2004. Comment on "Managing soil carbon"(I). Science 305, 1567–1567.

Van Oost, K., Govers, G., Quine, T.A., Heckrath, G., Olesen, J.E., De Gryze, S., Merckx, R., 2005. Landscape-scale modeling of carbon cycling under the impact of soil redistribution: The role of tillage erosion. Global Biogeochemical Cycles 19, GB4014. doi:10.1029/2005GB002471

Van Oost, K., Quine, T.A., Govers, G., De Gryze, S., Six, J., Harden, J.W., Ritchie, J.C., McCarty, G.W., Heckrath, G., Kosmas, C., 2007. The impact of agricultural soil erosion on the global carbon cycle. Science 318, 626–629. doi:10.1126/science.1145724

Van Oost, K., Six, J., Govers, G., Quine, T.A., De Gryze, S., 2008. Reply to letter on “Soil Erosion: A carbon sink or source?” by R. Lal and D. Pimentel. Science 319, 1041–1042.

Vanderbilt, K.L., White, C.S., Hopkins, O., Craig, J.A., 2008. Aboveground decomposition in arid environments: Results of a long-term study in central New Mexico. Journal of Arid Environments 72, 696–709. doi:10.1016/j.jaridenv.2007.10.010

Vas, E., Lescroël, A., Duriez, O., Boguszewski, G., Grémillet, D., 2015. Approaching birds with drones: first experiments and ethical guidelines. Biology Letters 11. doi:10.1098/rsbl.2014.0754

Verhoeven, G., 2011. Taking computer vision aloft – archaeological three-dimensional reconstructions from aerial photographs with PhotoScan. Archaeol. Prospect. 18, 67–73. doi:10.1002/arp.399

Vet, R., Artz, R.S., Carou, S., Shaw, M., Ro, C.-U., Aas, W., Baker, A., Bowersox, V.C., Dentener, F., Galy-Lacaux, C., Hou, A., Pienaar, J.J., Gillett, R., Forti, M.C., Gromov, S., Hara, H., Khodzher, T., Mahowald, N.M., Nickovic, S., Rao, P.S.P., Reid, N.W., 2014. A global assessment of precipitation chemistry and deposition of sulfur, nitrogen, sea salt, base cations, organic acids, acidity and pH, and phosphorus. Atmospheric Environment, A global assessment of precipitation chemistry and deposition of sulfur, nitrogen, sea salt, base cations, organic acids, acidity and pH, and phosphorus 93, 3–100. doi:10.1016/j.atmosenv.2013.10.060

Viaud, V., Angers, D.A., Parnaudeau, V., Morvan, T., Aubry, S.M., 2011. Response of organic matter to reduced tillage and animal manure in a temperate loamy soil. Soil Use and Management 27, 84–93. doi:10.1111/j.1475-2743.2010.00314.x

Vierling, K.T., Vierling, L.A., Gould, W.A., Martinuzzi, S., Clawges, R.M., 2008. Lidar: shedding new light on habitat characterization and modeling. Frontiers in Ecology and the Environment 6, 90–98. doi:10.1890/070001

Vierling, L.A., Xu, Y., Eitel, J.U.H., Oldow, J.S., 2013. Shrub characterization using terrestrial laser scanning and implications for airborne LiDAR assessment. Canadian Journal of Remote Sensing 38, 709–722. doi:10.5589/m12-057

von Lützow, M., Kögel-Knabner, I., Ekschmitt, K., Flessa, H., Guggenberger, G., Matzner, E., Marschner, B., 2007. SOM fractionation methods: Relevance to functional pools and to stabilization mechanisms. Soil Biology and Biochemistry 39, 2183–2207. doi:10.1016/j.soilbio.2007.03.007

Voroney, R.P., Van Veen, J.A., Paul, E.A., 1981. Organic C dynamics in grassland soils. 2. Model validation and simulation of the long-term effects of cultivation and rainfall erosion. Canadian Journal of Soil Science 61, 211–224.

Vuong, T.X., Heitkamp, F., Jungkunst, H.F., Reimer, A., Gerold, G., 2013. Simultaneous measurement of soil organic and inorganic carbon: evaluation of a thermal gradient analysis. J Soils Sediments 13, 1133–1140. doi:10.1007/s11368-013-0715-1

Wadcock, A.J., Ewing, L.A., Solis, E., Potsdam, M., Rajagopalan, G., 2008. Rotorcraft downwash flow field study to understand the aerodynamics of helicopter brownout. NATIONAL AERONAUTICS AND SPACE ADMINISTRATION MOFFETT FIELD CA AMES RESEARCH CENTER.

Wainwright, J., 2016. MAHLERAN Manual (MAHLERAN v1.01.7 Manual v1).

Wainwright, J., 2005. Climate and climatological variations in the Jornada Experimental Range and neighbouring areas of the US Southwest. Advances in Environmental Monitoring and Modelling 2.

Wainwright, J., 1996. Hillslope response to extreme storm events: the example of the Vaison-la-Romaine event, in: Anderson, M.G., Brooks, S.M. (Eds.), Advances in Hillslope Processes. John Wiley and Sons, Chichester, UK, pp. 997–1026.

Wainwright, J., Mulligan, M., 2013a. Introduction, in: Wainwright, J., Mulligan, M. (Eds.), Environmental Modelling: Finding Simplicity in Complexity. Wiley-Blackwell, pp. 3–6.

Wainwright, J., Mulligan, M. (Eds.), 2013b. Environmental Modelling: Finding Simplicity in Complexity, 2nd ed. Wiley-Blackwell.

Wainwright, J., Parsons, A.J., 2002. The effect of temporal variations in rainfall on scale dependency in runoff coefficients. Water Resources Research 38, 1271.

Wainwright, J., Parsons, A.J., Abrahams, A.D., 2000. Plot-scale studies of vegetation, overland flow and erosion interactions: case studies from Arizona and New Mexico. Hydrological Processes 14, 2921–2943.

Wainwright, J., Parsons, A.J., Abrahams, A.D., 1999a. Rainfall energy under creosotebush. Journal of Arid Environments 43, 111–120.

Wainwright, J., Parsons, A.J., Abrahams, A.D., 1999b. Field and computer simulation experiments on the formation of desert pavement. Earth Surface Processes and Landforms 24, 1025–1037.

Wainwright, J., Parsons, A.J., Abrahams, A.D., 1995. A simulation study of the role of raindrop erosion in the formation of desert pavements. Earth Surface Processes and Landforms 20, 277–291.

Wainwright, J., Parsons, A.J., Müller, E.N., Brazier, R.E., Powell, D.M., Fenti, B., 2008a. A transport-distance approach to scaling erosion rates: 2. Sensitivity and evaluation of Mahleran. Earth Surface Processes and Landforms 33, 962–984. doi:10.1002/esp.1623

Wainwright, J., Parsons, A.J., Müller, E.N., Brazier, R.E., Powell, D.M., Fenti, B., 2008b. A transport-distance approach to scaling erosion rates: 3. Evaluating scaling characteristics of Mahleran. Earth Surface Processes and Landforms 33, 1113–1128. doi:10.1002/esp.1622

Wainwright, J., Parsons, A.J., Müller, E.N., Brazier, R.E., Powell, D.M., Fenti, B., 2008c. A transport-distance approach to scaling erosion rates: 1. Background and model development. Earth Surface Processes and Landforms 33, 813–826. doi:10.1002/esp.1624

Wainwright, J., Parsons, A.J., Müller, E.N., Brazier, R.E., Powell, M.D., 2010. Standing proud: a response to “Soil-erosion models: where do we really stand?” by Smith et al. Earth Surface Processes and Landforms 35, 1349–1356. doi:10.1002/esp.2047

Wainwright, J., Parsons, A.J., Powell, D.M., Brazier, R.E., 2001. A new conceptual framework for understanding and predicting erosion by water from hillslopes and catchments, in: Ascough, J.C., Flanagan, D.C. (Eds.), . Presented at the Soil Erosion Research for the 21st Century: Proceedings of the International Symposium, American Society of Agricultrual Engineers, pp. 607–610.

Wainwright, J., Parsons, A.J., Schlesinger, W.H., Abrahams, A.D., 2002. Hydrology–vegetation interactions in areas of discontinuous flow on a semi-arid bajada, southern New Mexico. Journal of Arid Environments 51, 319–338.

Walker, L.R., Wardle, D.A., Bardgett, R.D., Clarkson, B.D., 2010. The use of chronosequences in studies of ecological succession and soil development. Journal of Ecology 98, 725–736. doi:10.1111/j.1365-2745.2010.01664.x

Wallace, A., Bamberg, S.A., Cha, J.W., 1974. Quantitative studies of roots of perennial plants in the Mojave Desert. Ecology 55, 1160–1162. doi:10.2307/1940368
Walling, D.E., 1999. Linking land use, erosion and sediment yields in river basins. Hydrobiologia 410, 223–240. doi:10.1023/A:1003825813091
Walling, D.E., 1988. Erosion and sediment yield research — Some recent perspectives. Journal of Hydrology 100, 113–141. doi:10.1016/0022-1694(88)90183-7
Walling, D.E., Fang, D., 2003. Recent trends in the suspended sediment loads of the world's rivers. Global and Planetary Change, The supply of flux of sediment along hydrological pathways: Anthropogenic influences at the global scale 39, 111–126. doi:10.1016/S0921-8181(03)00020-1
Walthert, L., Graf, U., Kammer, A., Luster, J., Pezzotta, D., Zimmermann, S., Hagedorn, F., 2010. Determination of organic and inorganic carbon, δ13C, and nitrogen in soils containing carbonates after acid fumigation with HCl. Z. Pflanzenernähr. Bodenk. 173, 207–216. doi:10.1002/jpln.200900158
Wan, Y., El-Swaify, S.A., 1998. Sediment enrichment mechanisms of organic carbon and phosphorus in a well-aggregated oxisol. Journal of Environmental Quality 27, 132–138. doi:10.2134/jeq1998.00472425002700010019x
Wan, Y., El-Swaify, S.A., 1997. Flow-induced transport and enrichment of erosional sediment from a well-aggregated and uniformly-textured Oxisol. Geoderma 75, 251–265. doi:10.1016/S0016-7061(96)00093-6
Wang, C., Glenn, N.F., 2008. A linear regression method for tree canopy height estimation using airborne lidar data. Canadian Journal of Remote Sensing 34, S217–S227. doi:10.5589/m08-043
Wang, L., Liu, H., 2006. An efficient method for identifying and filling surface depressions in digital elevation models for hydrologic analysis and modelling. International Journal of Geographical Information Science 20, 193–213. doi:10.1080/13658810500433453
Wang, L., Manzoni, S., Ravi, S., Riveros-Iregui, D., Caylor, K., 2015. Dynamic interactions of ecohydrological and biogeochemical processes in water-limited systems. Ecosphere 6, art133. doi:10.1890/ES15-00122.1
Wang, X., Cammeraat, E.L.H., Cerli, C., Kalbitz, K., 2014a. Soil aggregation and the stabilization of organic carbon as affected by erosion and deposition. Soil Biology and Biochemistry 72, 55–65. doi:10.1016/j.soilbio.2014.01.018
Wang, X., Cammeraat, E.L.H., Díaz, L., Kalbitz, K., 2014b. Mineralization of eroded organic carbon transported from a loess soil into water. Soil Science Society of America 78, 1360–1367. doi:10.2136/sssaj2013.10.0443
Wang, X., Cammeraat, E.L.H., Romeijn, P., Kalbitz, K., 2014c. Soil organic carbon redistribution by water erosion – the role of CO2 emissions for the carbon budget. PLoS ONE 9. doi:10.1371/journal.pone.0096299
Wang, X., Cammeraat, L.H., Wang, Z., Zhou, J., Govers, G., Kalbitz, K., 2013. Stability of organic matter in soils of the Belgian Loess Belt upon erosion and deposition. European Journal of Soil Science 64, 219–228. doi:10.1111/ejss.12018
Wang, X., Wang, J., Xu, M., Zhang, W., Fan, T., Zhang, J., 2015. Carbon accumulation in arid croplands of northwest China: pedogenic carbonate exceeding organic carbon. Scientific Reports 5, 11439. doi:10.1038/srep11439

Wang, X., Wang, J., Zhang, J., 2012. Comparisons of three methods for organic and inorganic carbon in calcareous soils of Northwestern China. PLoS ONE 7, e44334. doi:10.1371/journal.pone.0044334
Wang, X.J., Xu, M.G., Wang, J.P., Zhang, W.J., Yang, X.Y., Huang, S.M., Liu, H., 2014. Fertilization enhancing carbon sequestration as carbonate in arid cropland: assessments of long-term experiments in northern China. Plant Soil 380, 89–100. doi:10.1007/s11104-014-2077-x
Wang, Z., Govers, G., Oost, K.V., Clymans, W., den Putte, A.V., Merckx, R., 2013. Soil organic carbon mobilization by interrill erosion: Insights from size fractions. Journal of Geophysical Research: Earth Surface 118, 348–360. doi:10.1029/2012jf002430
Wang, Z., Govers, G., Steegen, A., Clymans, W., Van den Putte, A., Langhans, C., Merckx, R., Van Oost, K., 2010. Catchment-scale carbon redistribution and delivery by water erosion in an intensively cultivated area. Geomorphology 124, 65–74. doi:10.1016/j.geomorph.2010.08.010
Ward, D., 2010. A resource ratio model of the effects of changes in CO2 on woody plant invasion. Plant Ecology 209, 147–152. doi:10.1007/s11258-010-9731-z
Wardley, N.W., Milton, E.J., Hill, C.T., 1987. Remote sensing of structurally complex semi-natural vegetation— an example from heathland. International Journal of Remote Sensing. doi:10.1080/01431168708948613
Warne, R.W., Pershall, A.D., Wolf, B.O., 2010. Linking precipitation and C3–C4 plant production to resource dynamics in higher-trophic-level consumers. Ecology 91, 1628–1638. doi:10.1890/08-1471.1
Went, F.W., Westergaard, M., 1949. Ecology of Desert Plants. III. Development of Plants in the Death Valley National Monument, California. Ecology 30, 26–38. doi:10.2307/1932275
Wester, T., Wasklewicz, T., Staley, D., 2014. Functional and structural connectivity within a recently burned drainage basin. Geomorphology 206, 362–373. doi:10.1016/j.geomorph.2013.10.011
Westoby, M.J., Brasington, J., Glasser, N.F., Hambrey, M.J., Reynolds, J.M., 2012. “structure-from-motion” photogrammetry: A low-cost, effective tool for geoscience applications. Geomorphology 179, 300–314. doi:10.1016/j.geomorph.2012.08.021
White, M.A., De BEURS, K.M., Didan, K., Inouye, D.W., Richardson, A.D., Jensen, O.P., O’keefe, J., Zhang, G., Nemani, R.R., Van LEEUWEN, W.J.D., Brown, J.F., De WIT, A., Schaepman, M., Lin, X., Dettinger, M., Bailey, A.S., Kimball, J., Schwartz, M.D., Baldocchi, D.D., Lee, J.T., Lauenroth, W.K., 2009. Intercomparison, interpretation, and assessment of spring phenology in North America estimated from remote sensing for 1982–2006. Global Change Biology 15, 2335–2359. doi:10.1111/j.1365-2486.2009.01910.x
Whitford, W.G., 1997. Desertification and animal biodiversity in the desert grasslands of North America. Journal of Arid Environments 37, 709–720.
Whitford, W.G., Martinez Meza, E., DeSoyza, A., 1995. Morphological variation in creosotebush, Larrea tridentata: effects on ecosystem properties, in: Barrow, J.R., Durant, E., Sosebee, R.E., Tausch, R.J. (Eds.), . Presented at the Proceedings of the Symposium on Shrubland Ecosystem Dynamics in a Changing Climate, U.S. Department of Agriculture, Forest Service Intermountain Research Station., pp. 195–198.
Wiesmeier, M., Munro, S., Barthold, F., Steffens, M., Schad, P., Kögel-Knabner, I., 2015. Carbon storage capacity of semi-arid grassland soils and sequestration

potentials in Northern China. Glob Change Biol n/a-n/a. doi:10.1111/gcb.12957
Wilcox, B.P., 2010. Transformative ecosystem change and ecohydrology: ushering in a new era for watershed management. Ecohydrol. 3, 126–130. doi:10.1002/eco.104
Williams, R.D., Brasington, J., Vericat, D., Hicks, D.M., 2013. Hyperscale terrain modelling of braided rivers: fusing mobile terrestrial laser scanning and optical bathymetric mapping. Earth Surface Processes and Landforms n/a–n/a. doi:10.1002/esp.3437
Willmott, C.J., 1981. On the validation of models. Physical Geography 2, 184–194. doi:10.1080/02723646.1981.10642213
Willmott, C.J., Matsuura, K., 2005. Advantages of the mean absolute error (MAE) over the root mean square error (RMSE) in assessing average model performance. Climate Research 30, 79–82.
Wilson, A.M., Silander, J.A., Gelfand, A., Glenn, J.H., 2011. Scaling up: linking field data and remote sensing with a hierarchical model. International Journal of Geographical Information Science 25, 509–521. doi:10.1080/13658816.2010.522779
Wilson, B.F., 1995. Shrub stems: form and functions, in: Gartner, B.L. (Ed.), Plant Stems: Physiology and Functional Morphology. Academic Press, San Diego, California, USA, pp. 91–104.
Wolfe, D.W., Erickson, J.D., 1993. Carbon dioxide effects on plants: uncertainties and implications for modeling crop responses to climate change, in: Kaiser, H., Drennen, T. (Eds.), Agricultrual Dimensions of Global Climate Change. St. Lucie Press, Delray Beach, FL, USA, pp. 153–178.
Wolkovich, E.M., Lipson, D.A., Virginia, R.A., Cottingham, K.L., Bolger, D.T., 2009. Grass invasion causes rapid increases in ecosystem carbon and nitrogen storage in a semiarid shrubland. Global Change Biology 16, 1351–1365.
Woodget, A.S., Carbonneau, P.E., Visser, F., Maddock, I.P., 2015. Quantifying submerged fluvial topography using hyperspatial resolution UAS imagery and structure from motion photogrammetry. Earth Surf. Process. Landforms 40, 47–64. doi:10.1002/esp.3613
Wright, V.P., Platt, N.H., Marriott, S.B., Beck, V.H., 1995. A classification of rhizogenic (root-formed) calcretes, with examples from the Upper Jurassic-Lower Cretaceous of Spain and Upper Cretaceous of southern France. Sedimentary Geology 100, 143–158. doi:10.1016/0037-0738(95)00105-0
Wu, H., Guo, Z., Gao, Q., Peng, C., 2009. Distribution of soil inorganic carbon storage and its changes due to agricultural land use activity in China. Agriculture, ecosystems & environment 129, 413–421. doi:10.1016/j.agee.2008.10.020
Wullstein, L.H., Pratt, S.A., 1981. Scanning electron microscopy of Rhizosheaths of Oryzopsis hymenoides. American Journal of Botany 68, 408–419. doi:10.2307/2442778
Xie, J., Li, Y., Zhai, C., Li, C., Lan, Z., 2009. CO2 absorption by alkaline soils and its implication to the global carbon cycle. Environmental Geology 56, 953–961. doi:10.1007/s00254-008-1197-0
Yair, A., Lavee, H., 1976. Runoff generative process and runoff yield from arid talus mantled slopes. Earth Surface Processes 1, 235–247. doi:10.1002/esp.3290010305
Yair, A., Raz-Yassif, N., 2004. Hydrological processes in a small arid catchment: scale effects of rainfall and slope length. Geomorphology 61, 155–169.

Yang, T.W., 1970. Major Chromosome Races of Larrea divaricata in North America. Journal of the Arizona Academy of Science 6, 41–45. doi:10.2307/40022846
Yang, T.W., Lowe, C.H., 1968. Chromoseome variation in ecotypes of Larrea divaricata in the North American Desert. Madroño 19, 161–164.
Yao, J., Peters, D.P.C., Havstad, K.M., Gibbens, R.P., Herrick, J.E., 2006. Multi-scale factors and long-term responses of Chihuahuan Desert grasses to drought. Landscape Ecology 21, 1217–1231. doi:10.1007/s10980-006-0025-8
Yao, T., Yang, X., Zhao, F., Wang, Z., Zhang, Q., Jupp, D., Lovell, J., Culvenor, D., Newnham, G., Ni-Meister, W., Schaaf, C., Woodcock, C., Wang, J., Li, X., Strahler, A., 2011. Measuring forest structure and biomass in New England forest stands using Echidna ground-based lidar. Remote Sensing of Environment 115, 2965–2974. doi:10.1016/j.rse.2010.03.019
Yin, Z.-Y., Wang, X., 1999. A cross-scale comparison of drainage basin characteristics derived from digital elevation models. Earth Surface Processes and Landforms.
Yoo, K., Amundson, R., Heimsath, A.M., Dietrich, W.E., 2005. Erosion of upland hillslope soil organic carbon: Coupling field measurements with a sediment transport model. Global Biogeochemical Cycles 19, GB3003. doi:10.1029/2004GB002271
York, J.C., Dick-Peddie, W.A., 1969. Vegetation changes in southern New Mexico during the past 100 years, in: W.G., M., Goldman, B.J. (Eds.), Arid Lands in Perspective. University of Arizona Press, Tucson, AZ, USA, pp. 157–166.
Young, P.C., Leedal, D., 2013. Data-Based Mechanistic Modelling and the Emulation of Large Environmental System Models, in: Wainwright, J., Mulligan, M. (Eds.), Environmental Modelling: Finding Simplicity in Complexity. Wiley-Blackwell, pp. 111–132.
Zahawi, R.A., Dandois, J.P., Holl, K.D., Nadwodny, D., Reid, J.L., Ellis, E.C., 2015. Using lightweight unmanned aerial vehicles to monitor tropical forest recovery. Biological Conservation 186, 287–295. doi:10.1016/j.biocon.2015.03.031
Zambrano-Bigiarini, M., 2014. hydroGOF: Goodness-of-fit functions for comparison of simulated and observed hydrological time series.
Zar, J.H., 2010. Biostatistical Analysis, 5th ed. Pearson Prentice Hall, Upper Saddle River, NJ.
Zeebe, R.E., 2012. History of seawater carbonate chemistry, atmospheric CO2, and ocean acidification. Annual Review of Earth and Planetary Sciences 40, 141–165. doi:10.1146/annurev-earth-042711-105521
Zeebe, R.E., Wolf-Gladrow, D., 2001. CO2 in Seawater: Equilibrium, Kinetics, Isotopes. Elsevier, Amsterdam.
Zhang, J.H., Li, F.C., 2013. Soil redistribution and organic carbon accumulation under long-term (29 years) upslope tillage systems. Soil Use and Management 29, 365–373. doi:10.1111/sum.12040
Zhang, W., Montgomery, D.R., 1994. Digital elevation model grid size, landscape representation, and hydrologic simulations. Water Resources Research 30, 1019–1028. doi:10.1029/93WR03553
Zhang, X., Drake, N.A., Wainwright, J., Mulligan, M., 1999. Comparison of slope estimates from low resolution DEMs: scaling issues and a fractal method for their solution. Earth Surface Processes and Landforms 24, 763–779. doi:10.1002/(SICI)1096-9837(199908)24:9<763::AID-ESP9>3.0.CO;2-J
Zhang, X., Friedl, M.A., Schaaf, C.B., Strahler, A.H., Hodges, J.C.F., Gao, F., Reed, B.C., Huete, A., 2003. Monitoring vegetation phenology using MODIS.

Remote Sensing of Environment 84, 471–475. doi:10.1016/S0034-4257(02)00135-9
Zhang, X., Kondragunta, S., 2006. Estimating forest biomass in the USA using generalized allometric models and MODIS land products. Geophys. Res. Lett. 33, L09402. doi:10.1029/2006GL025879
Zhao, K., Popescu, S., 2009. Lidar-based mapping of leaf area index and its use for validating GLOBCARBON satellite LAI product in a temperate forest of the southern USA. Remote Sensing of Environment 113, 1628–1645. doi:10.1016/j.rse.2009.03.006
Zhao, K., Popescu, S., Nelson, R., 2009. Lidar remote sensing of forest biomass: A scale-invariant estimation approach using airborne lasers. Remote Sensing of Environment 113, 182–196. doi:10.1016/j.rse.2008.09.009
Zhu, D., Ren, Q., Xuan, Y., Chen, Y., Cluckie, I.D., 2013. An effective depression filling algorithm for DEM-based 2-D surface flow modelling. Hydrol. Earth Syst. Sci. 17, 495–505. doi:10.5194/hess-17-495-2013
Zhu, Z., Reed, B.C., 2012. Baseline and Projected Future Carbon Storage and Greenhouse-Gas Fluxes in Ecosystems of the Western United States (Professional Paper No. NO 1797). U.S. Department of the Interior, U.S. Geological Survey.
Ziadat, F.M., Taimeh, A.Y., 2013. Effect of rainfall intensity, slope, land use and antecedent soil moisture on soil erosion in an arid environment. Land Degrad. Develop. 24, 582–590. doi:10.1002/ldr.2239
Zimmermann, M., Leifeld, J., Schmidt, M.W.I., Smith, P., Fuhrer, J., 2006. Measured soil organic matter fractions can be related to pools in the RothC model. European Journal of Soil Science 58, 658–667. doi:10.1111/j.1365-2389.2006.00855.x
Zobeck, T.M., Fryrear, D.W., 1986. Chemical and physical characteristics of windblown sediment: II. Chemical characteristics and total soil and nutrient discharge. Transactions of the ASAE 29.
Zobeck, T.M., Fryrear, D.W., Pettit, R.D., 1989. Management effects on wind-eroded sediment and plant nutrients. Journal of Soil and Water Conservation 44, 160–163.

13. Appendices

13.1. Appendix 1: Soil Bulk Densities

Table 13.1. Soil bulk densities, inclusive of stones. (Standard Error)

Site	Grass	Grass-Shrub	Shrub-Grass	Shrub
Microsite				
Bare	1.40 (0.03)	1.45 (0.03)	1.49 (0.05)	1.44 (0.02)
Grass	1.28 (0.03)	1.47 (0.04)	1.25 (0.08)	NA
Shrub	NA	1.29 (0.04)	1.11 (0.09)	1.45 (0.02)
Aerially-weighted	**1.34 (0.04)**	**1.45 (0.06)**	**1.29 (0.13)**	**1.44 (0.02)**

13.2. Appendix 2: Thermograms from Multi-Temperature C Determinations

Thermograms of evolved CO_2 for all 13 thermal gradient determinations of OC and IC content. Thermograms are presented here for their shapes. Samples were either untreated ('Control'), or acid-washed ('AW'); '(R)' denotes analysis of replicate aliquots (i.e. 'Control(R)' or 'AW(R)'). Y-axes are in arbitrary units which were converted to concentrations using calibration standards for each sample.

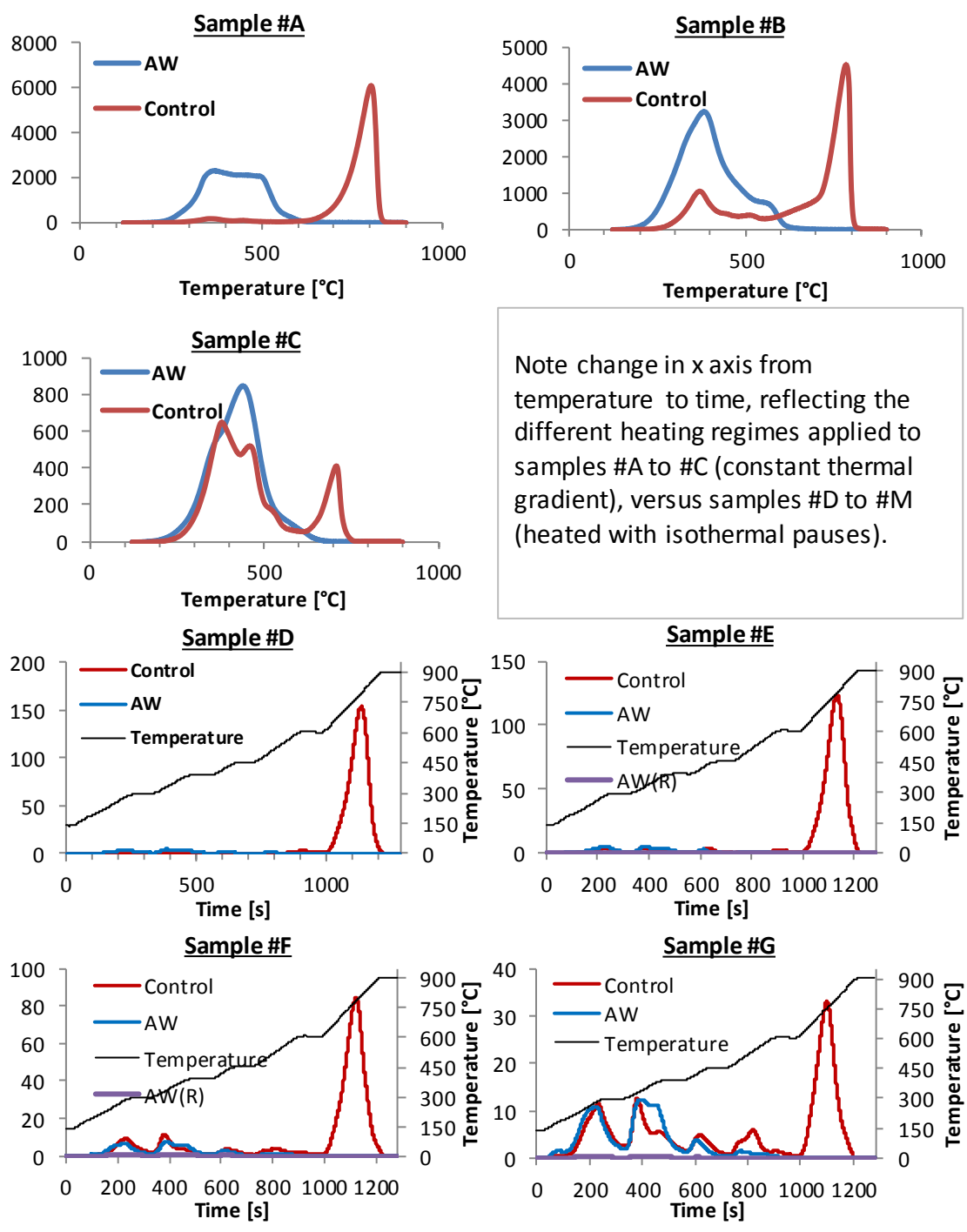

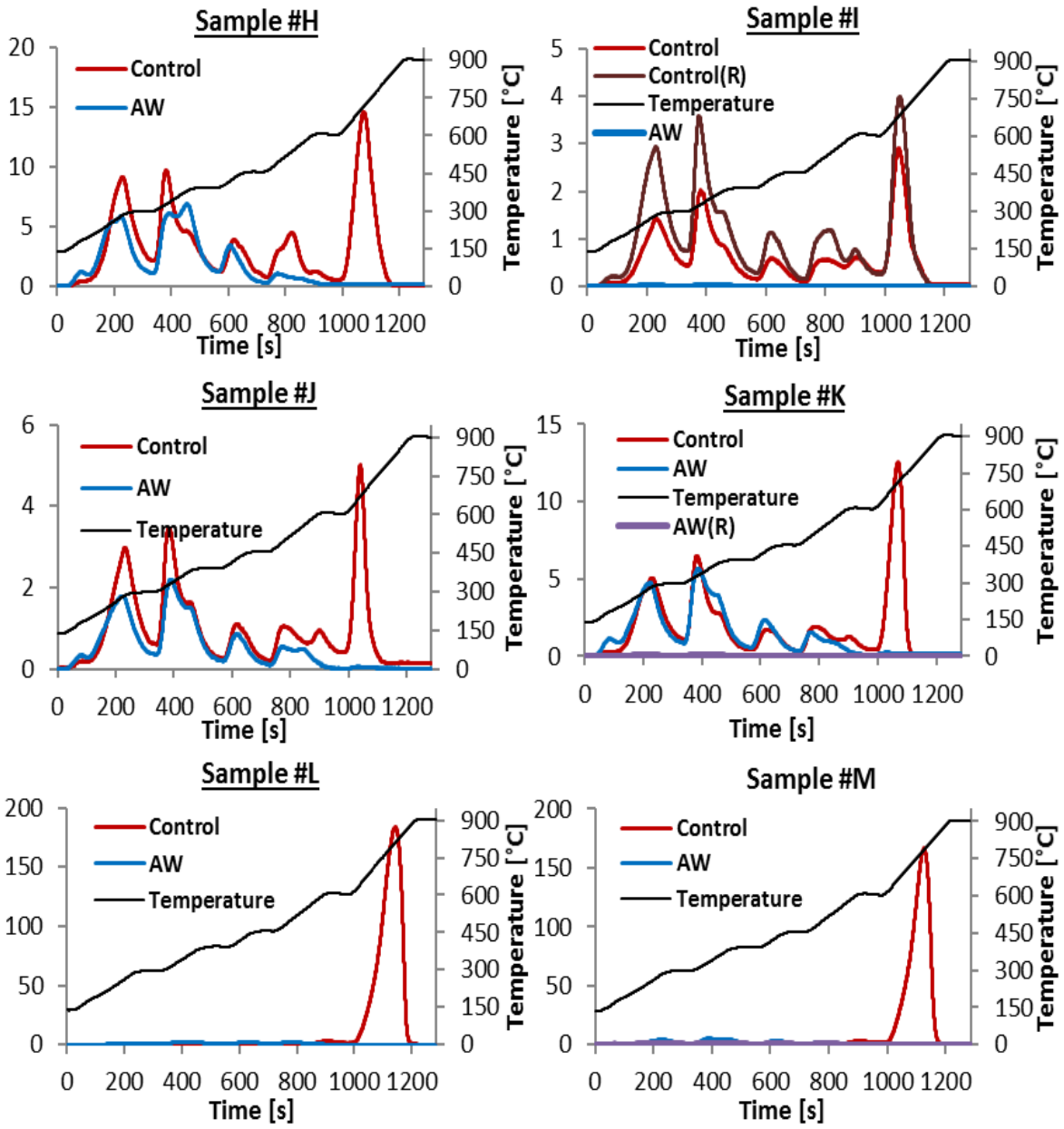
Sample #H
Control
AW
Time [s]
Temperature [°C]
Sample #I
Control
Control(R)
Temperature
AW
Time [s]
Temperature [°C]
Sample #J
Control
AW
Temperature
Time [s]
Temperature [°C]
Sample #K
Control
AW
Temperature
AW(R)
Time [s]
Temperature [°C]
Sample #L
Control
AW
Temperature
Time [s]
Temperature [°C]
Sample #M
Control
AW
Temperature
Time [s]
Temperature [°C]

13.3. Appendix 3: Hydrograph Scaling for Rainstorm Events

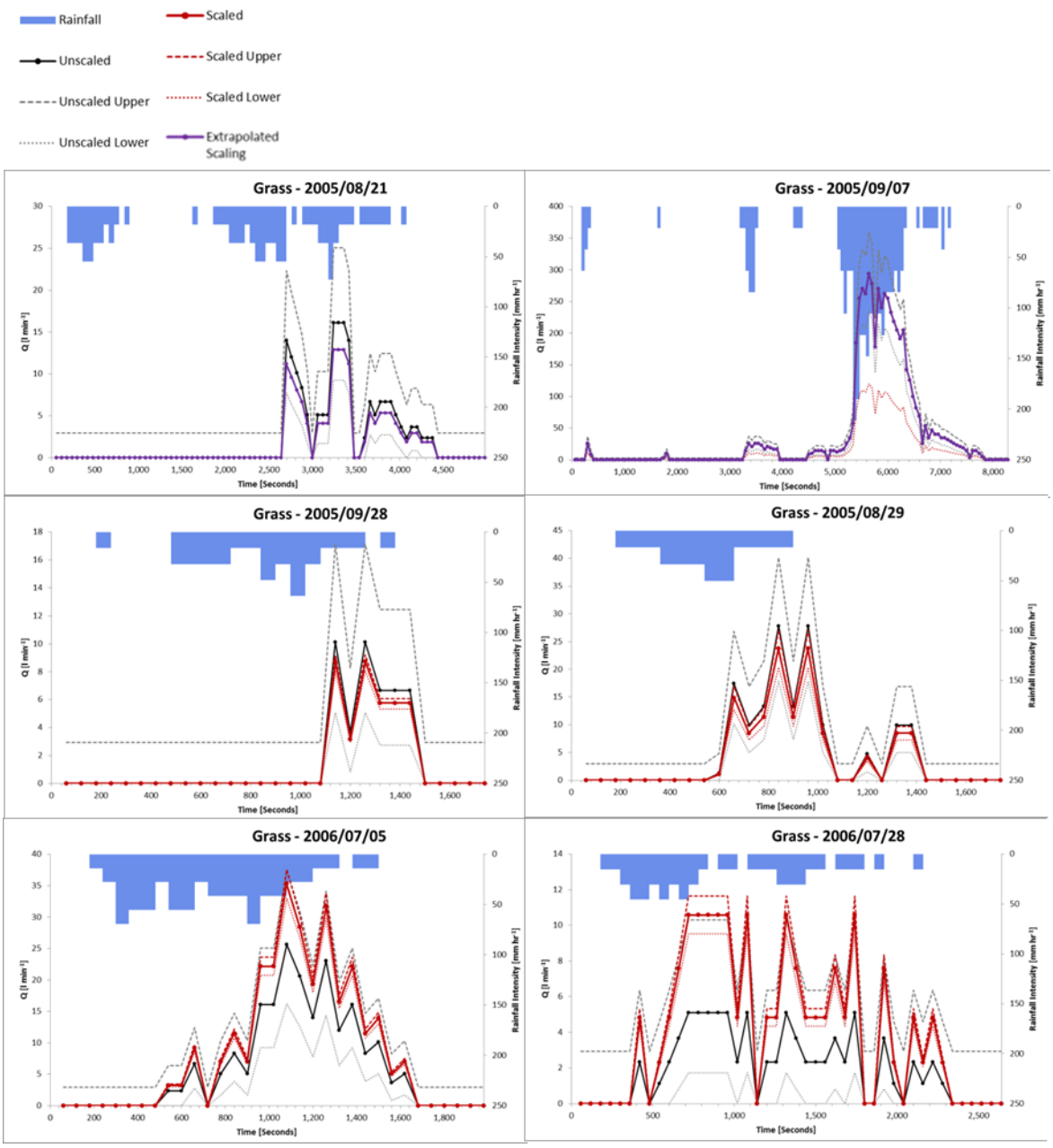

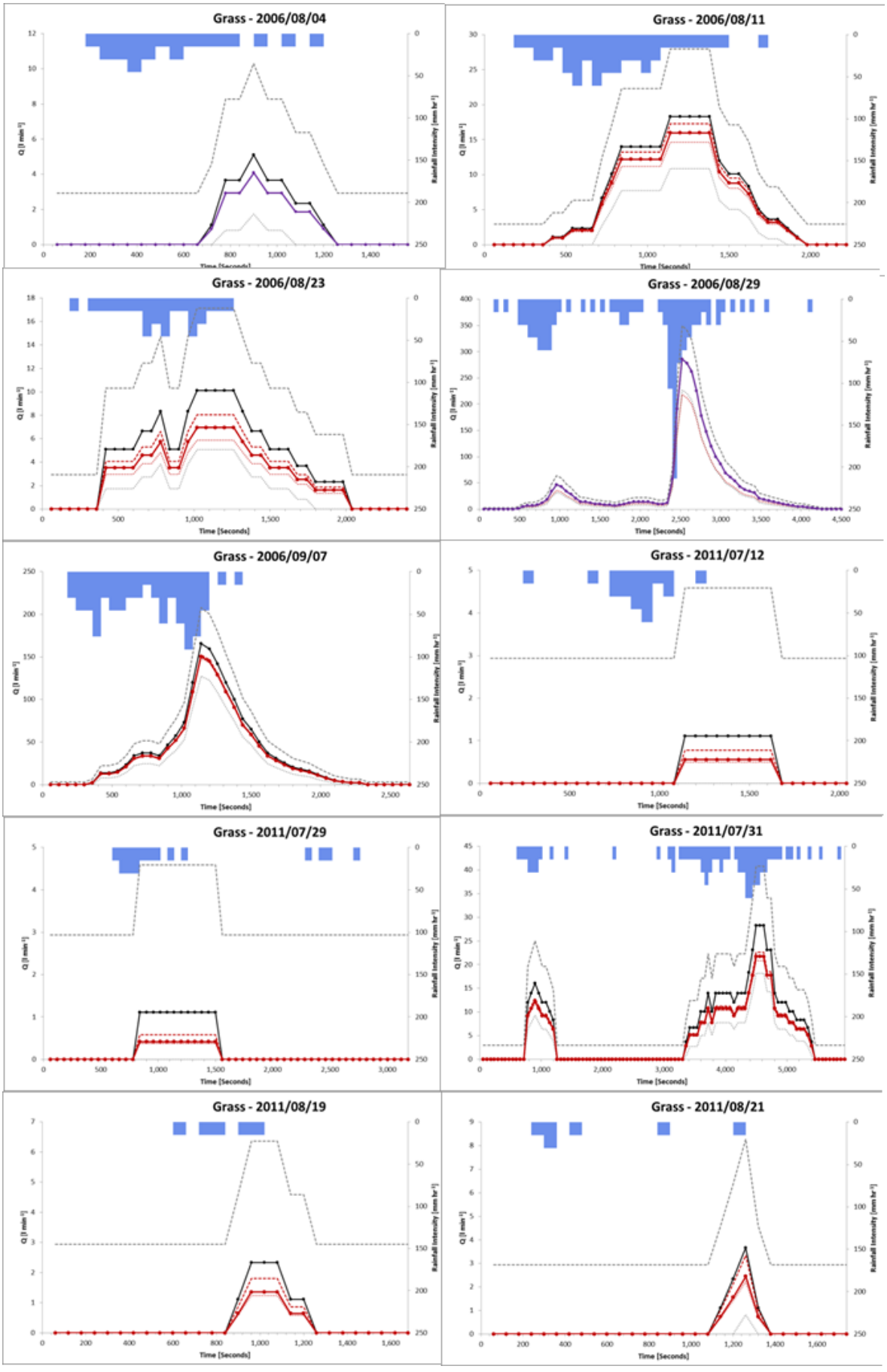
Grass - 2006/08/04
Grass - 2006/08/11
Grass - 2006/08/23
Grass - 2006/08/29
Grass - 2006/09/07
Grass - 2011/07/12
Grass - 2011/07/29
Grass - 2011/07/31
Grass - 2011/08/19
Grass - 2011/08/21
Time [Seconds]
Rainfall Intensity [mm hr⁻¹]

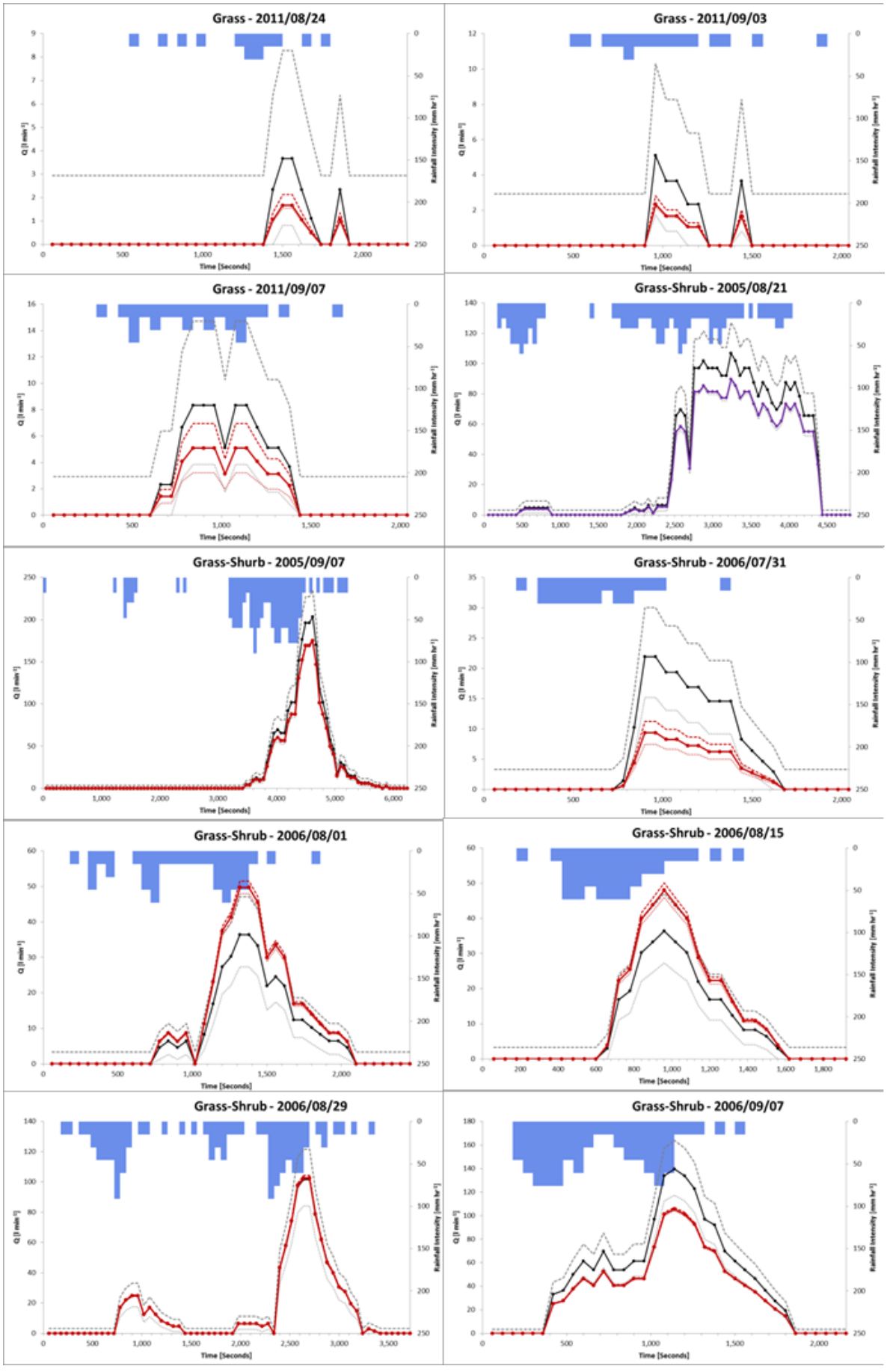
Grass - 2011/08/24
Grass - 2011/09/03
Grass - 2011/09/07
Grass-Shrub - 2005/08/21
Grass-Shurb - 2005/09/07
Grass-Shrub - 2006/07/31
Grass-Shrub - 2006/08/01
Grass-Shrub - 2006/08/15
Grass-Shrub - 2006/08/29
Grass-Shrub - 2006/09/07
Time [Seconds]
Rainfall Intensity [mm hr⁻¹]

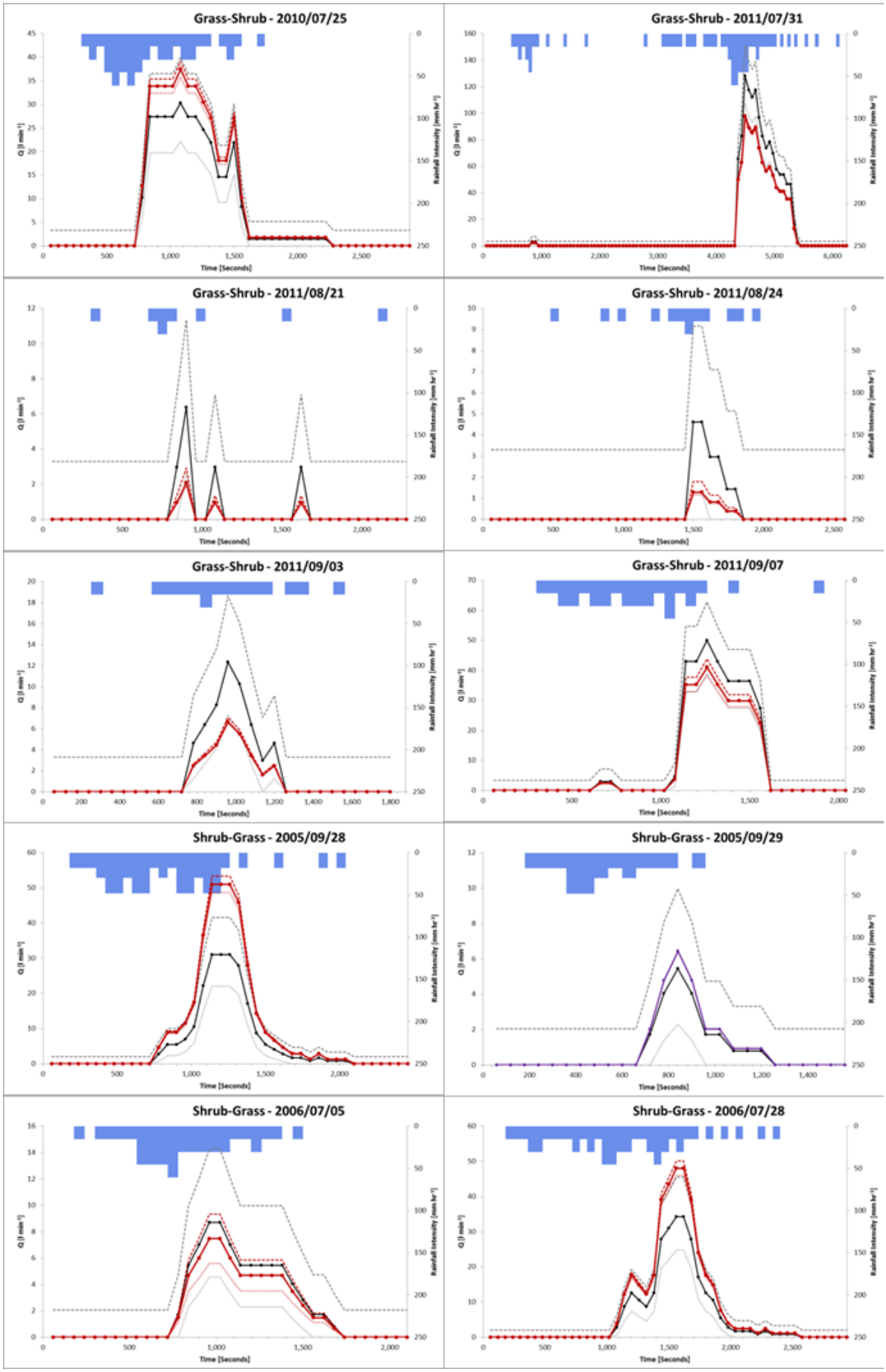
Grass-Shrub - 2010/07/25
Grass-Shrub - 2011/07/31
Grass-Shrub - 2011/08/21
Grass-Shrub - 2011/08/24
Grass-Shrub - 2011/09/03
Grass-Shrub - 2011/09/07
Shrub-Grass - 2005/09/28
Shrub-Grass - 2005/09/29
Shrub-Grass - 2006/07/05
Shrub-Grass - 2006/07/28
Time [Seconds]
Rainfall Intensity [mm hr⁻¹]

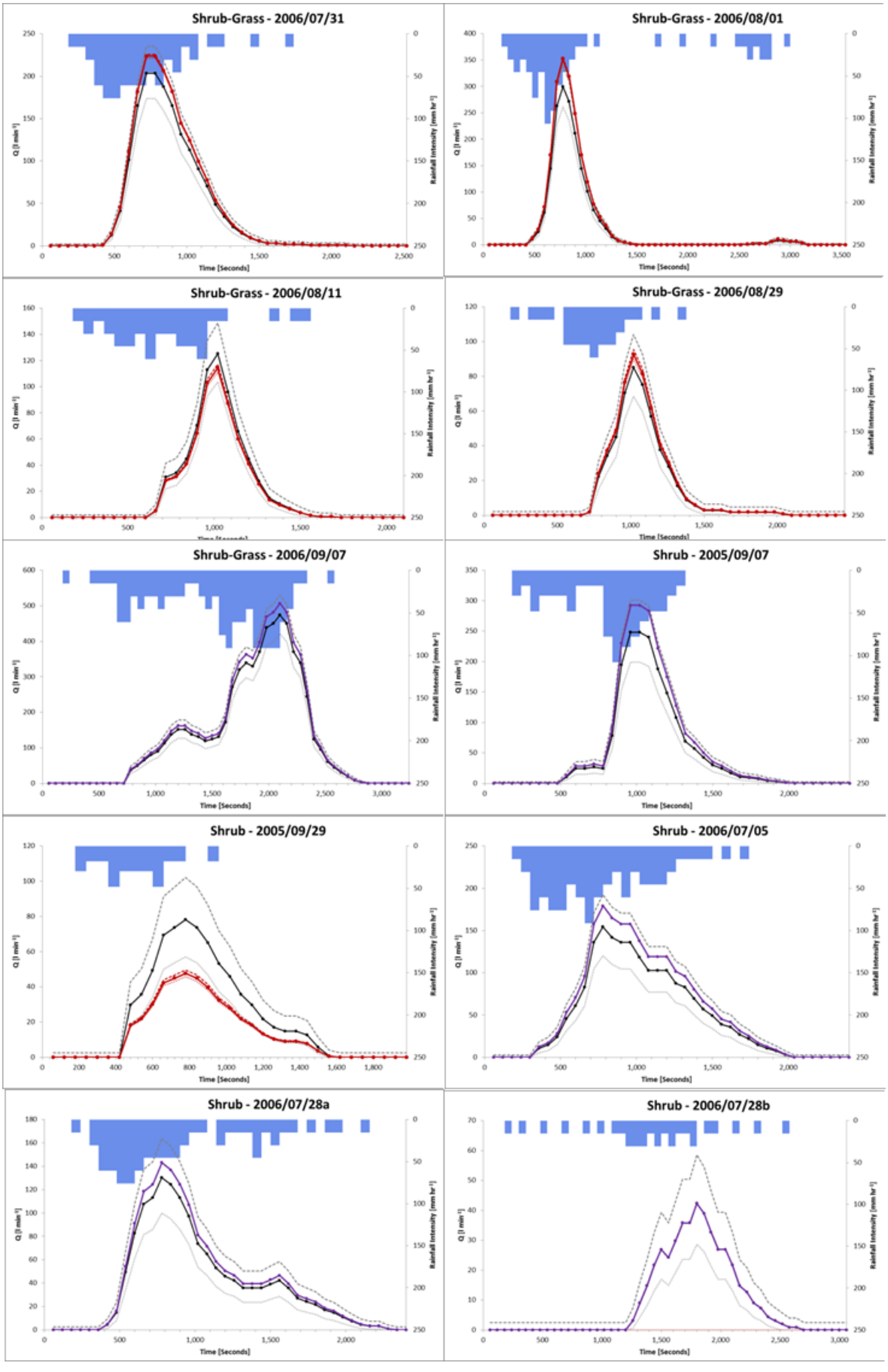
Shrub-Grass - 2006/07/31
Shrub-Grass - 2006/08/01
Shrub-Grass - 2006/08/11
Shrub-Grass - 2006/08/29
Shrub-Grass - 2006/09/07
Shrub - 2005/09/07
Shrub - 2005/09/29
Shrub - 2006/07/05
Shrub - 2006/07/28a
Shrub - 2006/07/28b
Time [Seconds]
Rainfall Intensity [mm hr⁻¹]

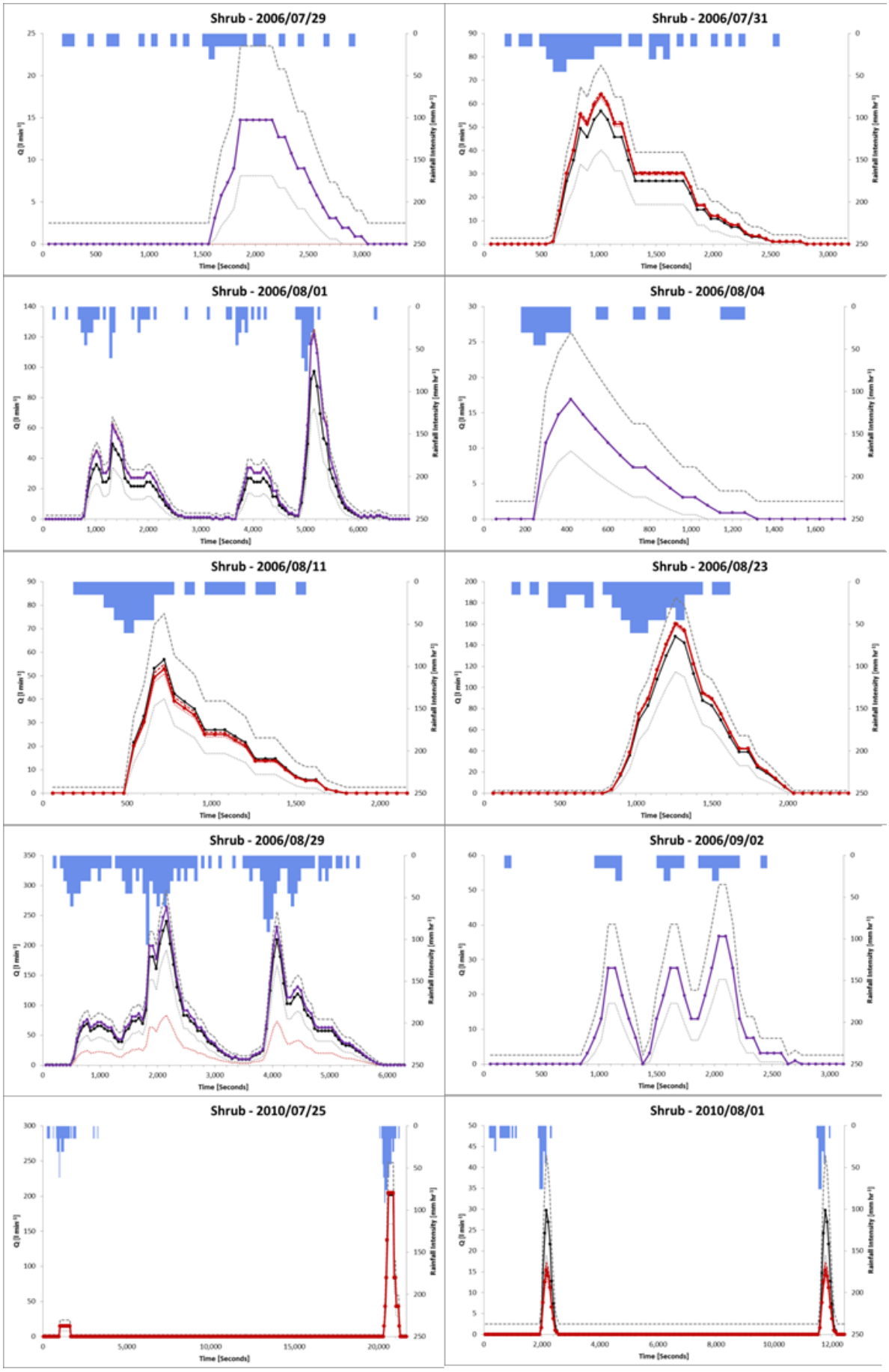
Shrub - 2006/07/29
Shrub - 2006/07/31
Shrub - 2006/08/01
Shrub - 2006/08/04
Shrub - 2006/08/11
Shrub - 2006/08/23
Shrub - 2006/08/29
Shrub - 2006/09/02
Shrub - 2010/07/25
Shrub - 2010/08/01
Time [Seconds]
Rainfall Intensity [mm hr⁻¹]

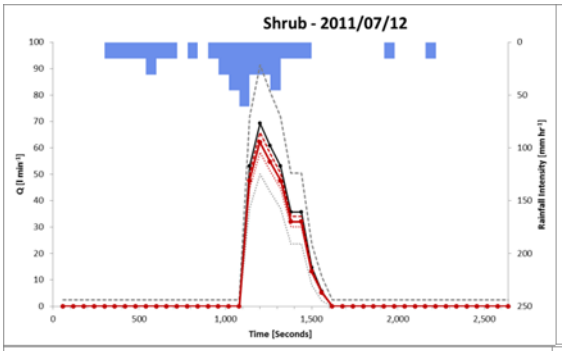
Shrub - 2011/07/12
Q [l min⁻¹]
Rainfall Intensity [mm hr⁻¹]
Time [Seconds]

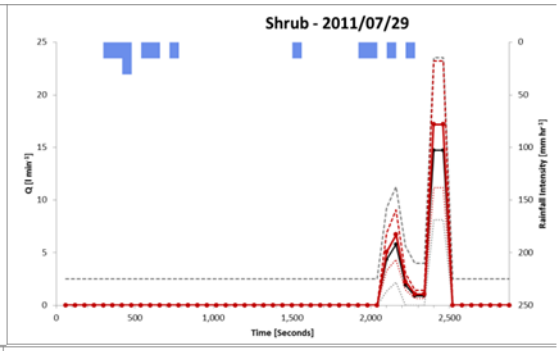
Shrub - 2011/07/29
Q [l min⁻¹]
Rainfall Intensity [mm hr⁻¹]
Time [Seconds]

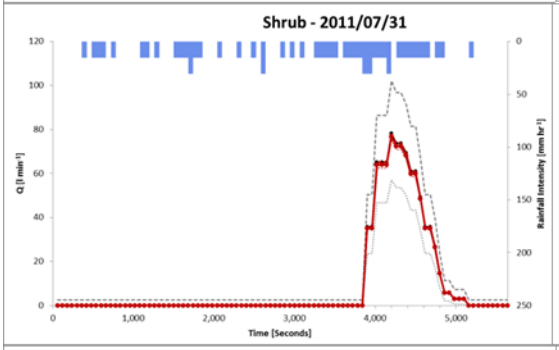
Shrub - 2011/07/31
Q [l min⁻¹]
Rainfall Intensity [mm hr⁻¹]
Time [Seconds]

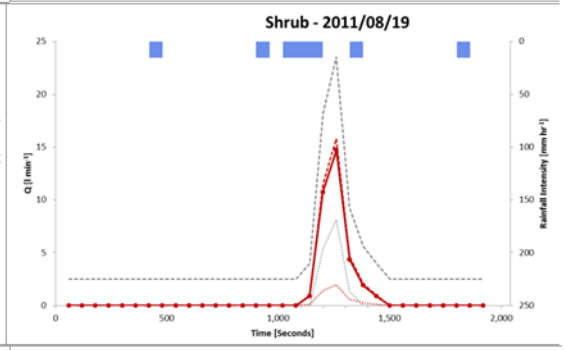
Shrub - 2011/08/19
Q [l min⁻¹]
Rainfall Intensity [mm hr⁻¹]
Time [Seconds]

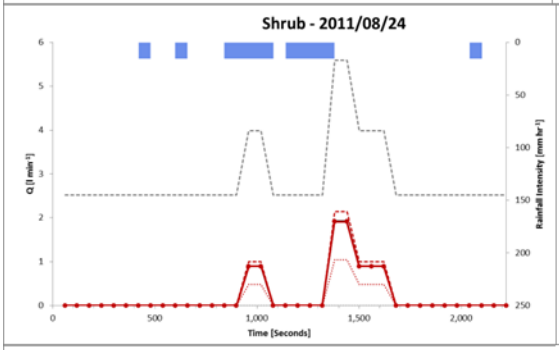
Shrub - 2011/08/24
Q [l min⁻¹]
Rainfall Intensity [mm hr⁻¹]
Time [Seconds]

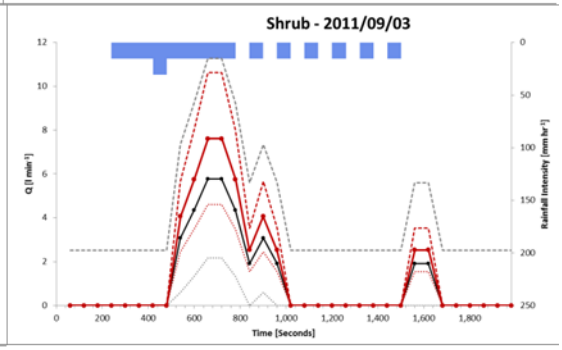
Shrub - 2011/09/03
Q [l min⁻¹]
Rainfall Intensity [mm hr⁻¹]
Time [Seconds]

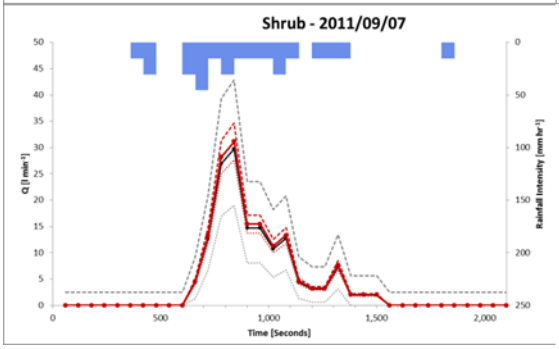
Shrub - 2011/09/07
Q [l min⁻¹]
Rainfall Intensity [mm hr⁻¹]
Time [Seconds]

13.4. Appendix 3: Digital Maps

Full page figures of all digital maps for all seven AOIs, including Orthomosaic true colour image, digital surface model (DSM), digital terrain model (DTM), canopy height model (CHM), classification of surface cover as bare or vegetated, and classification of surface cover between bare, grass and woody classes.

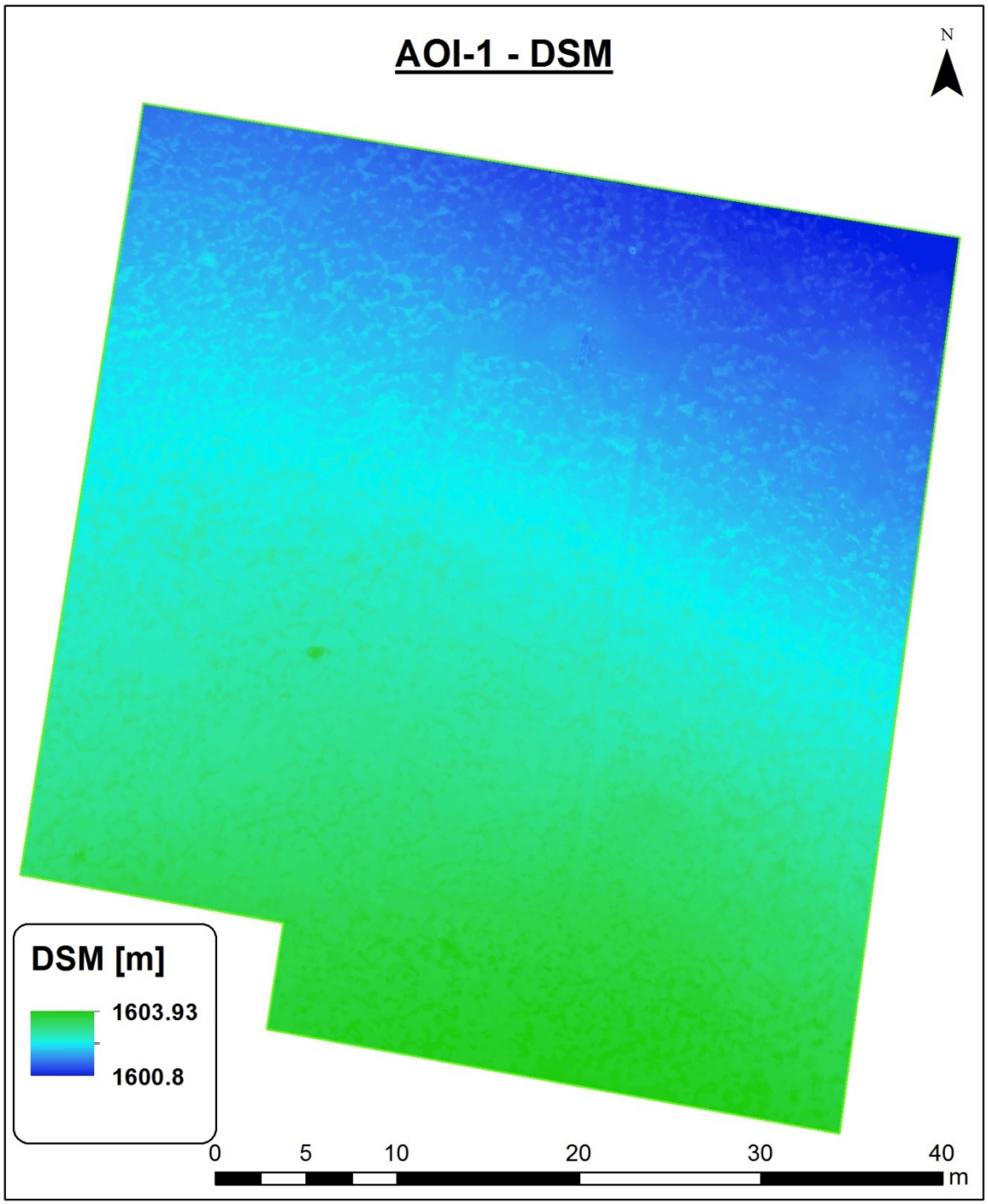
AOI-1 - DSM
N
DSM [m]
1603.93
1600.8
0
5
10
20
30
40
m

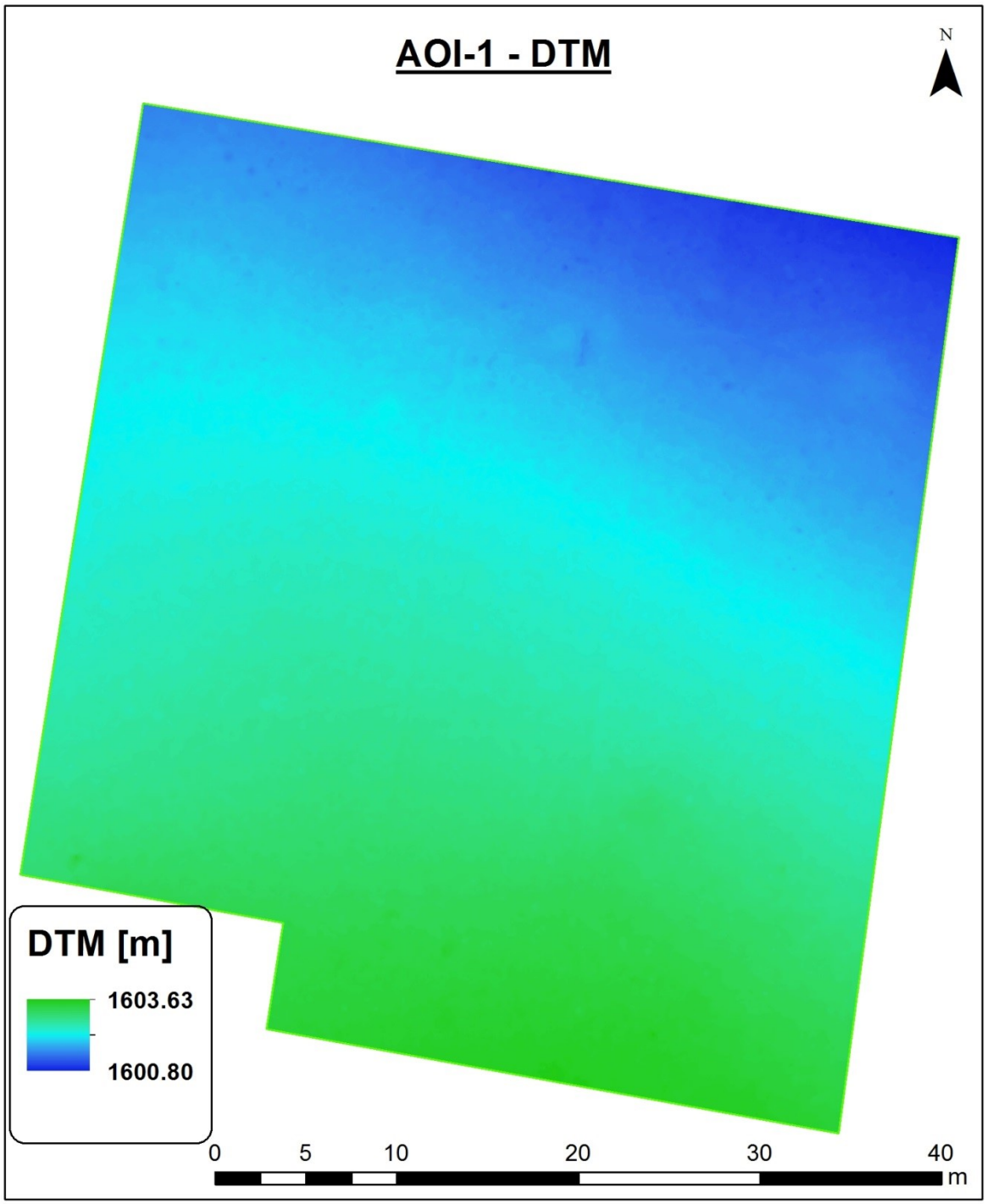
AOI-1 - DTM
N
DTM [m]
1603.63
1600.80
0
5
10
20
30
40
m

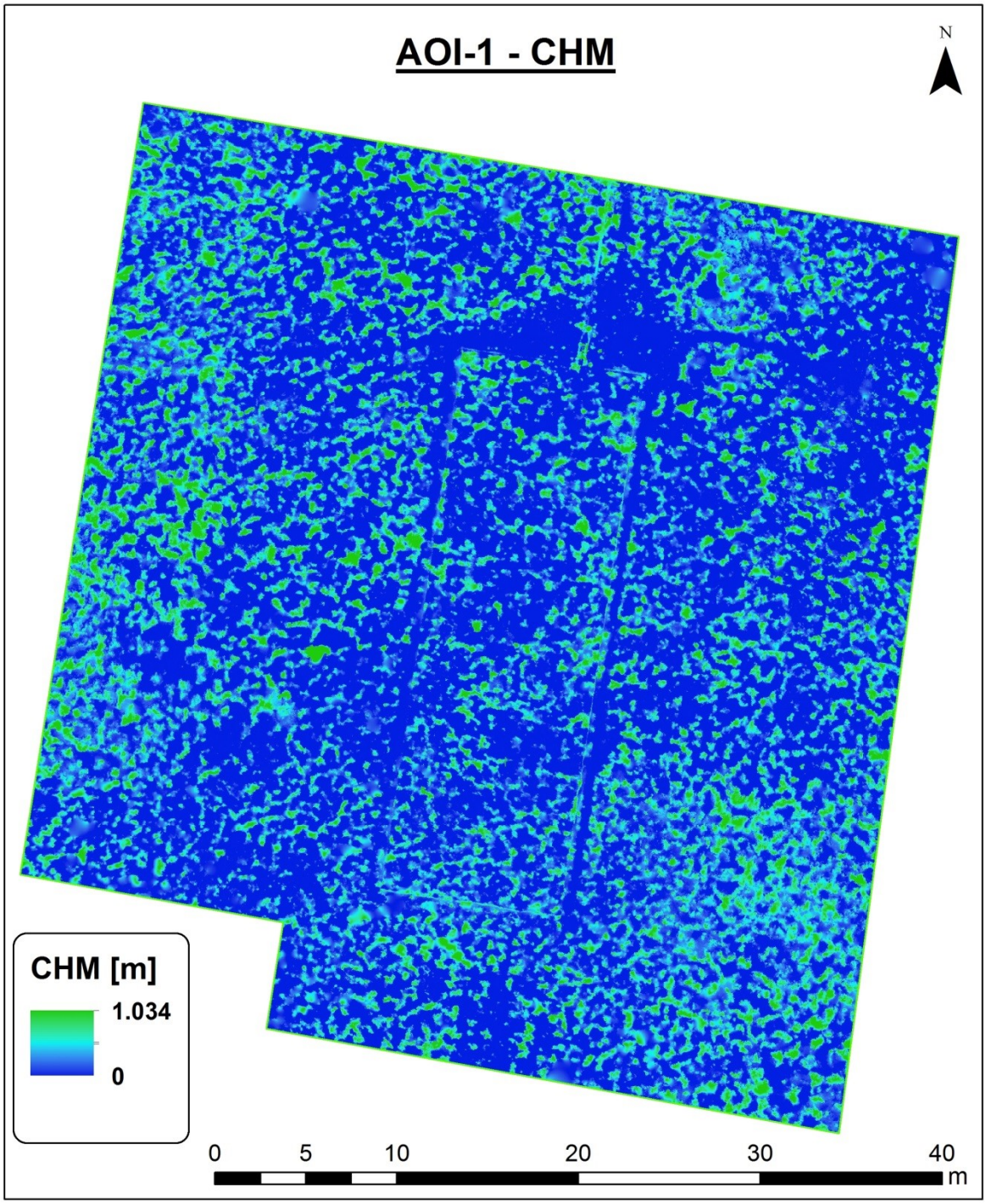
AOI-1 - CHM
N
CHM [m]
1.034
0
0
5
10
20
30
40
m

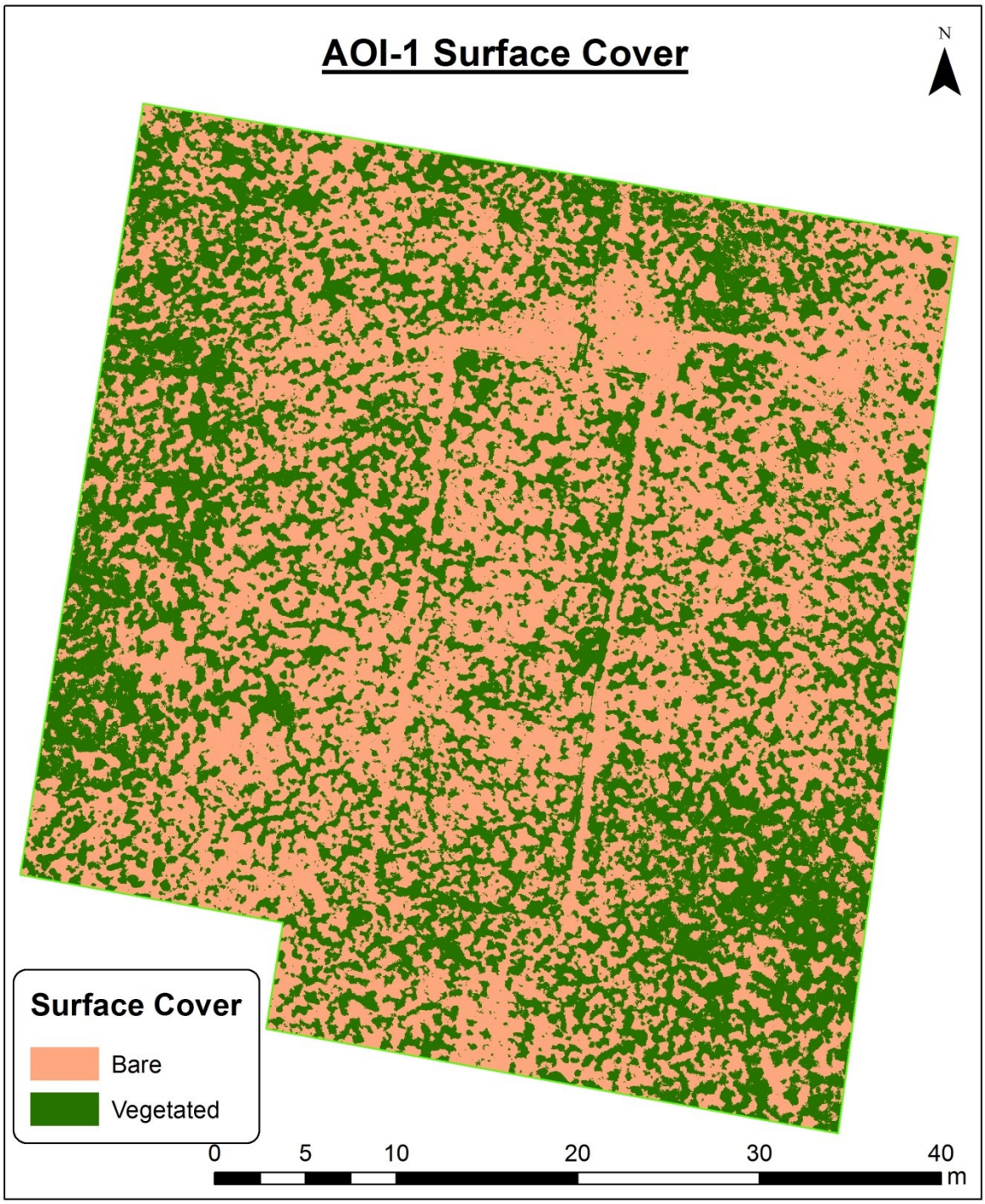
AOI-1 Surface Cover
N
Surface Cover
Bare
Vegetated
0
5
10
20
30
40
m

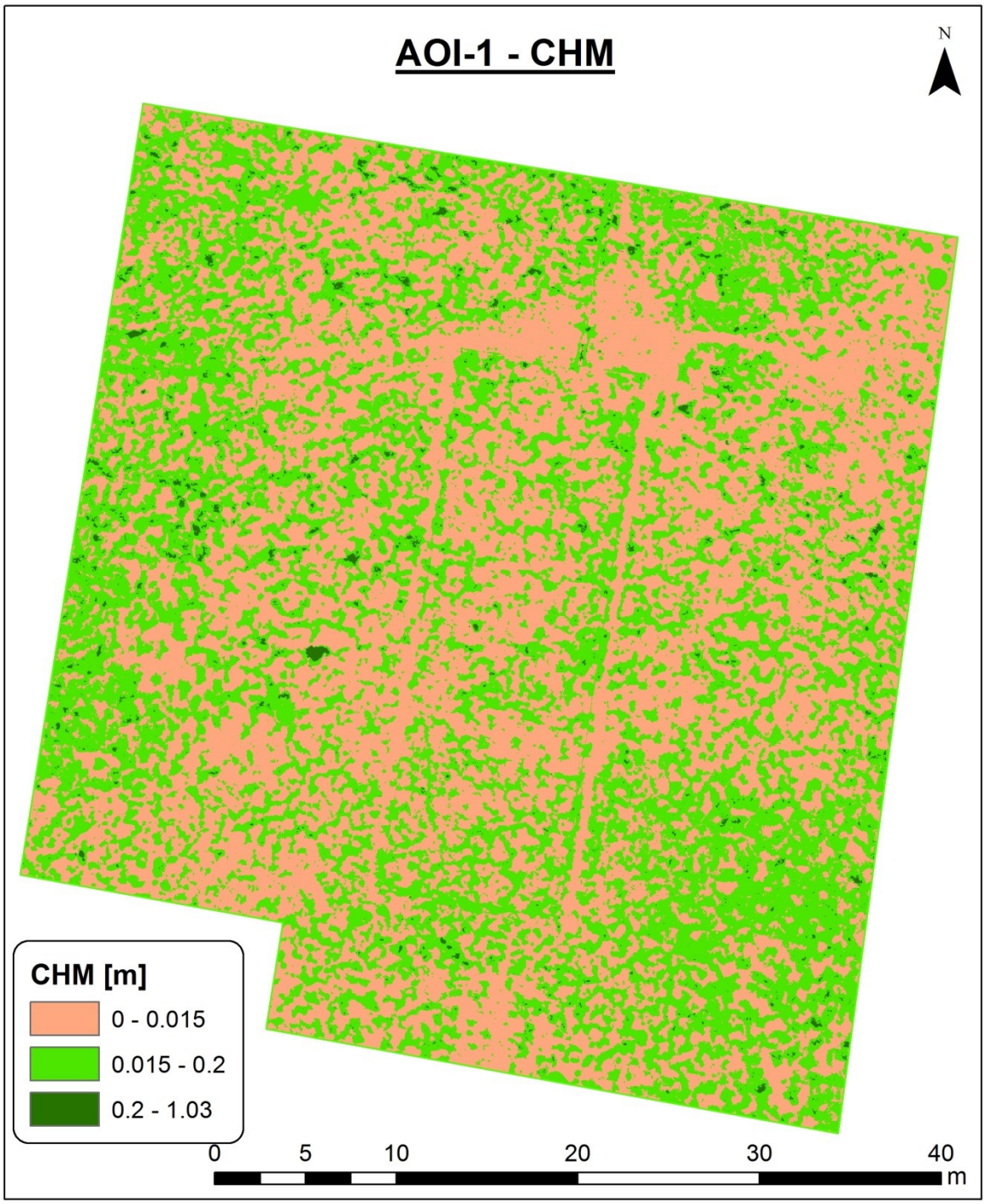
AOI-1 - CHM
N
CHM [m]
0 - 0.015
0.015 - 0.2
0.2 - 1.03
0
5
10
20
30
40
m

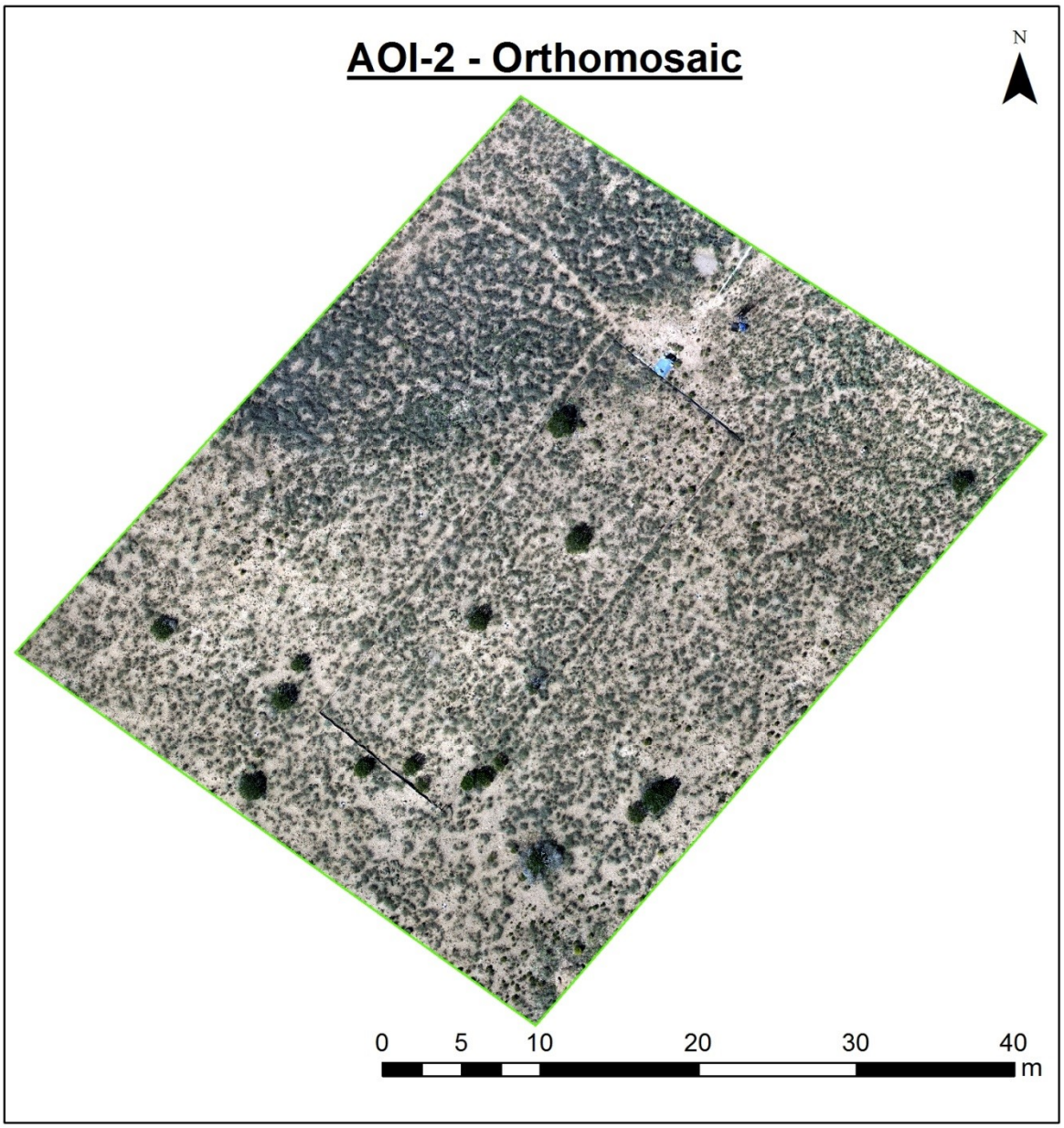
AOI-2 - Orthomosaic
N
0
5
10
20
30
40
m

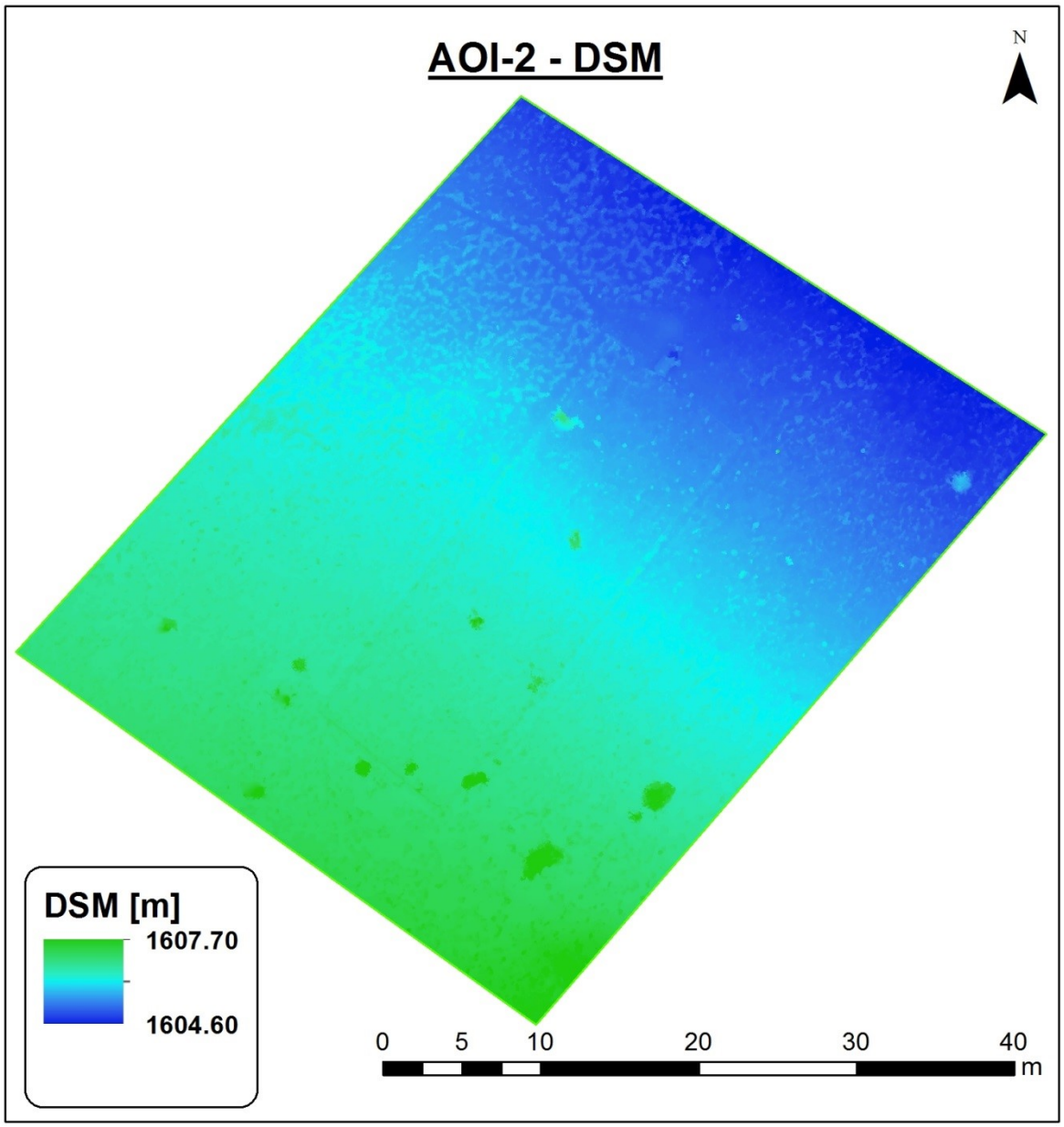
AOI-2 - DSM
N
DSM [m]
1607.70
1604.60
0
5
10
20
30
40
m

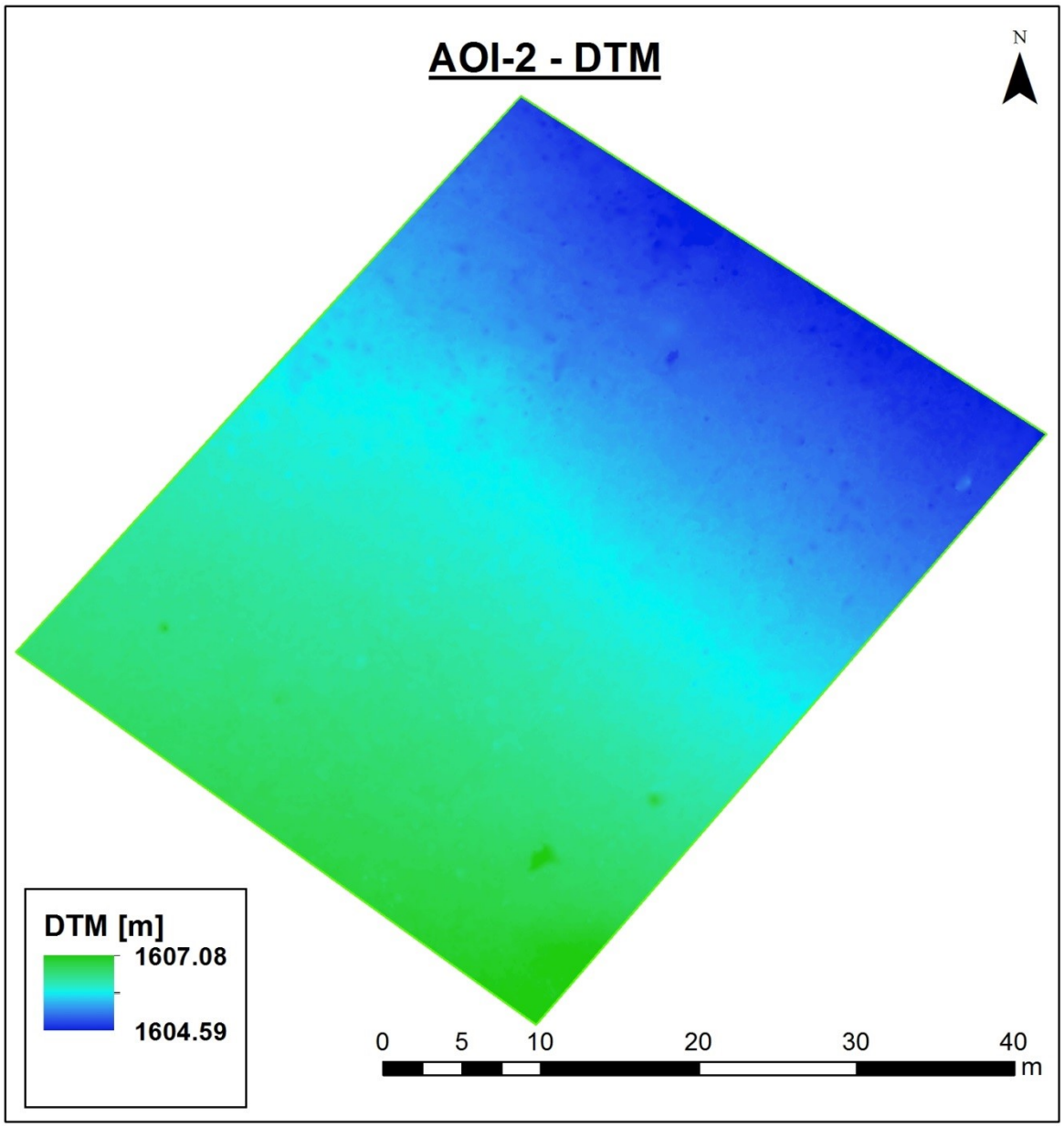
AOI-2 - DTM
N
DTM [m]
1607.08
1604.59
0
5
10
20
30
40
m

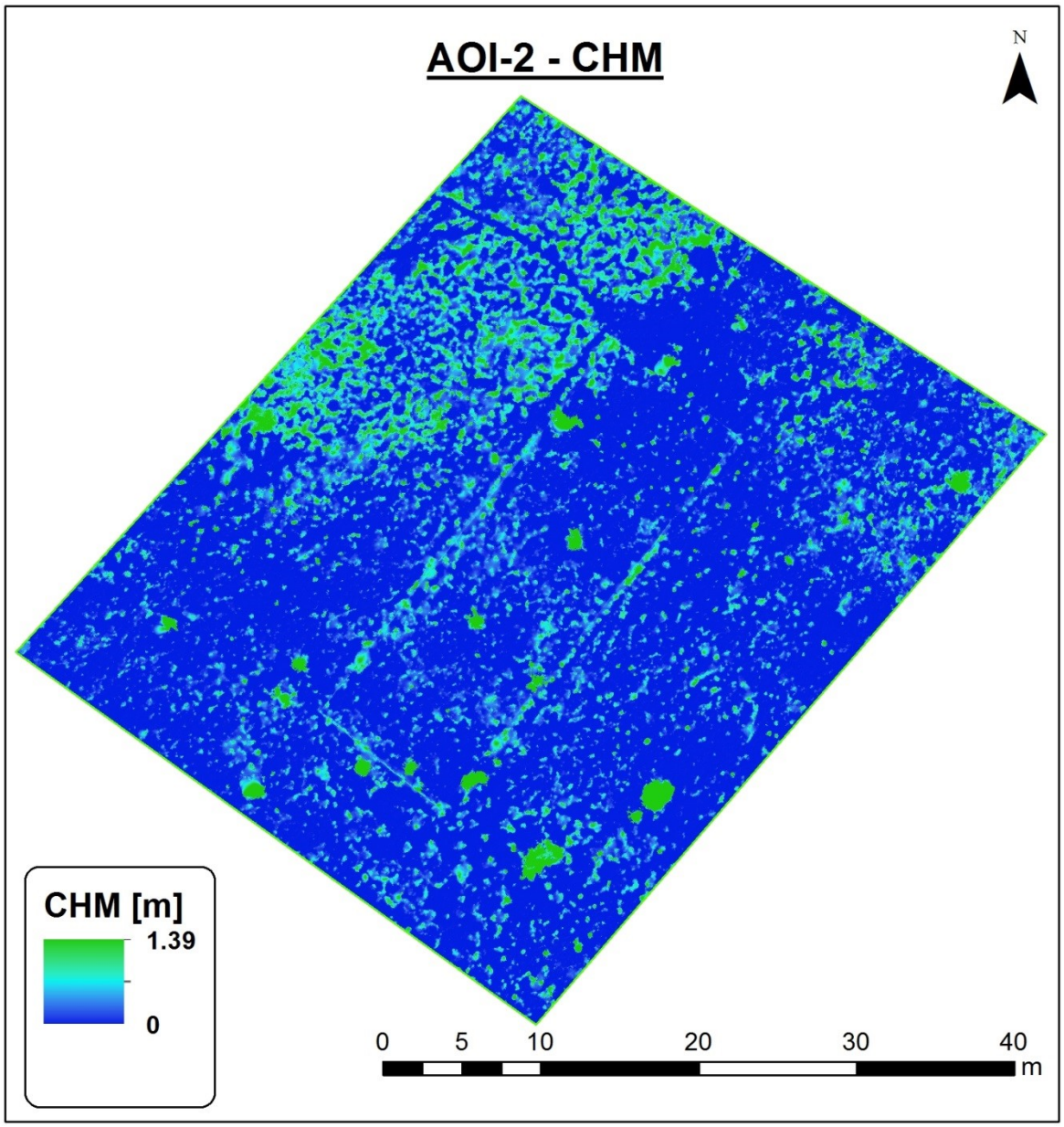
AOI-2 - CHM
N
CHM [m]
1.39
0
0
5
10
20
30
40
m

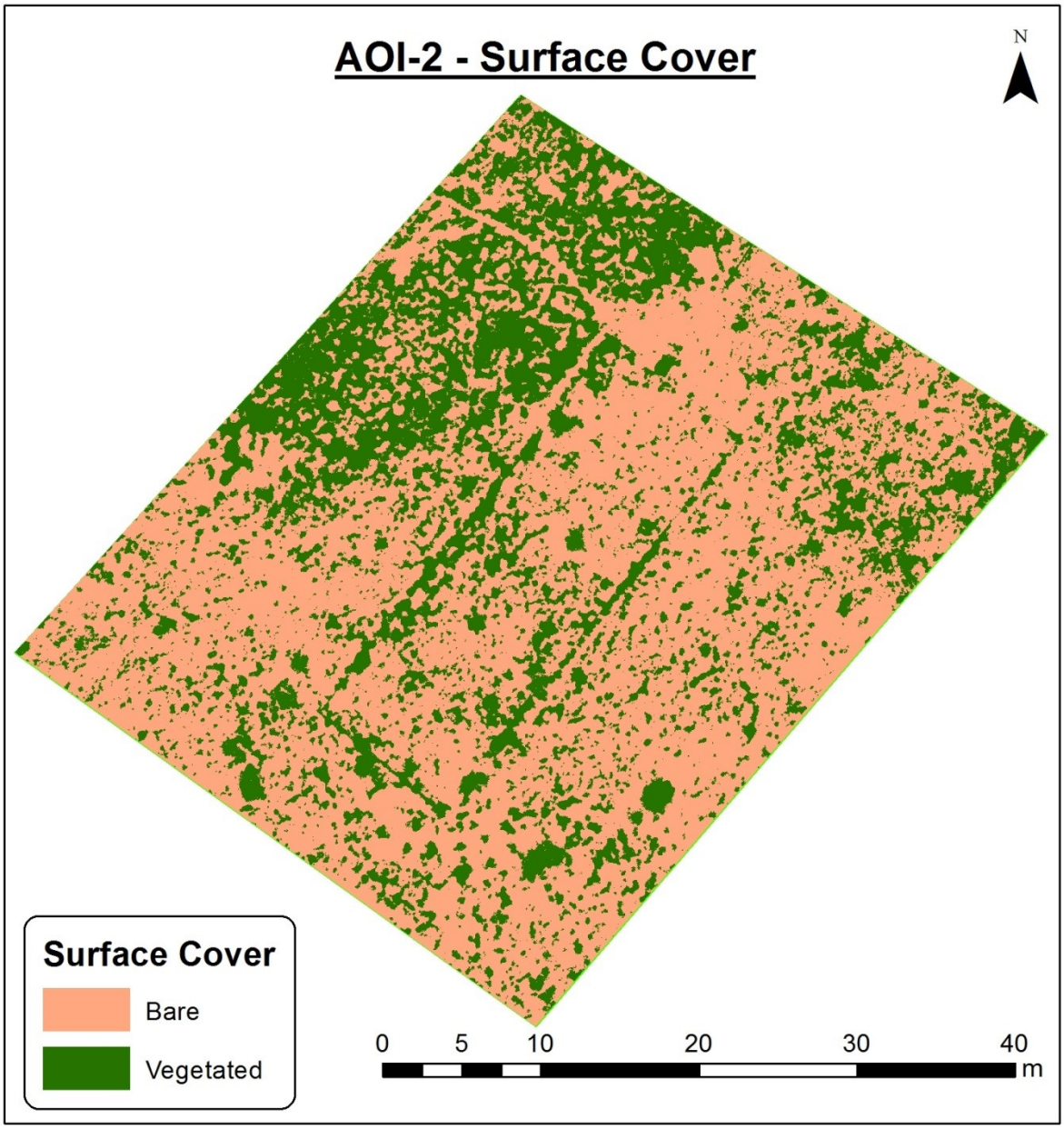
AOI-2 - Surface Cover
N
Surface Cover
Bare
Vegetated
0
5
10
20
30
40
m

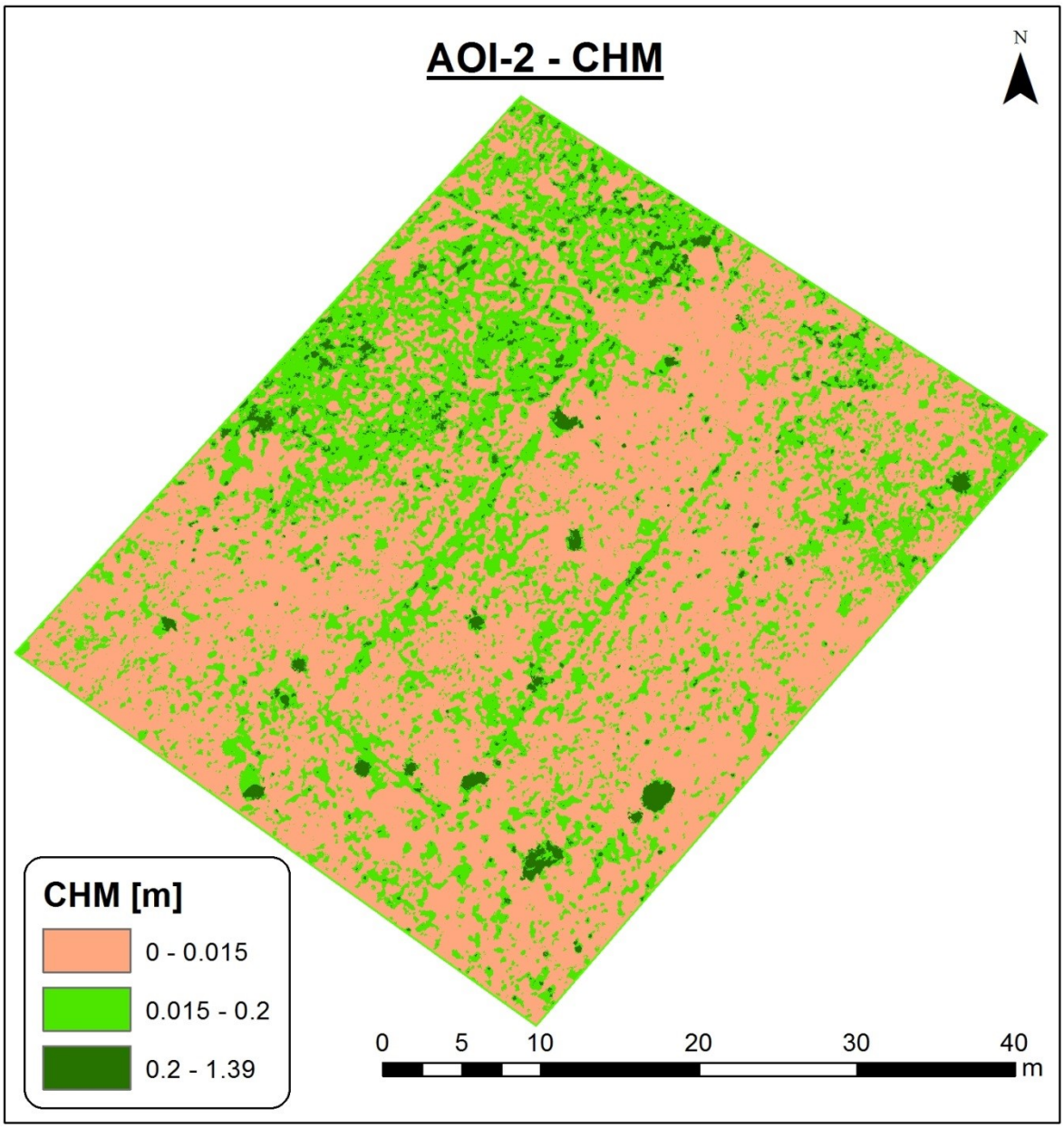
AOI-2 - CHM
N
CHM [m]
0 - 0.015
0.015 - 0.2
0.2 - 1.39
0
5
10
20
30
40
m

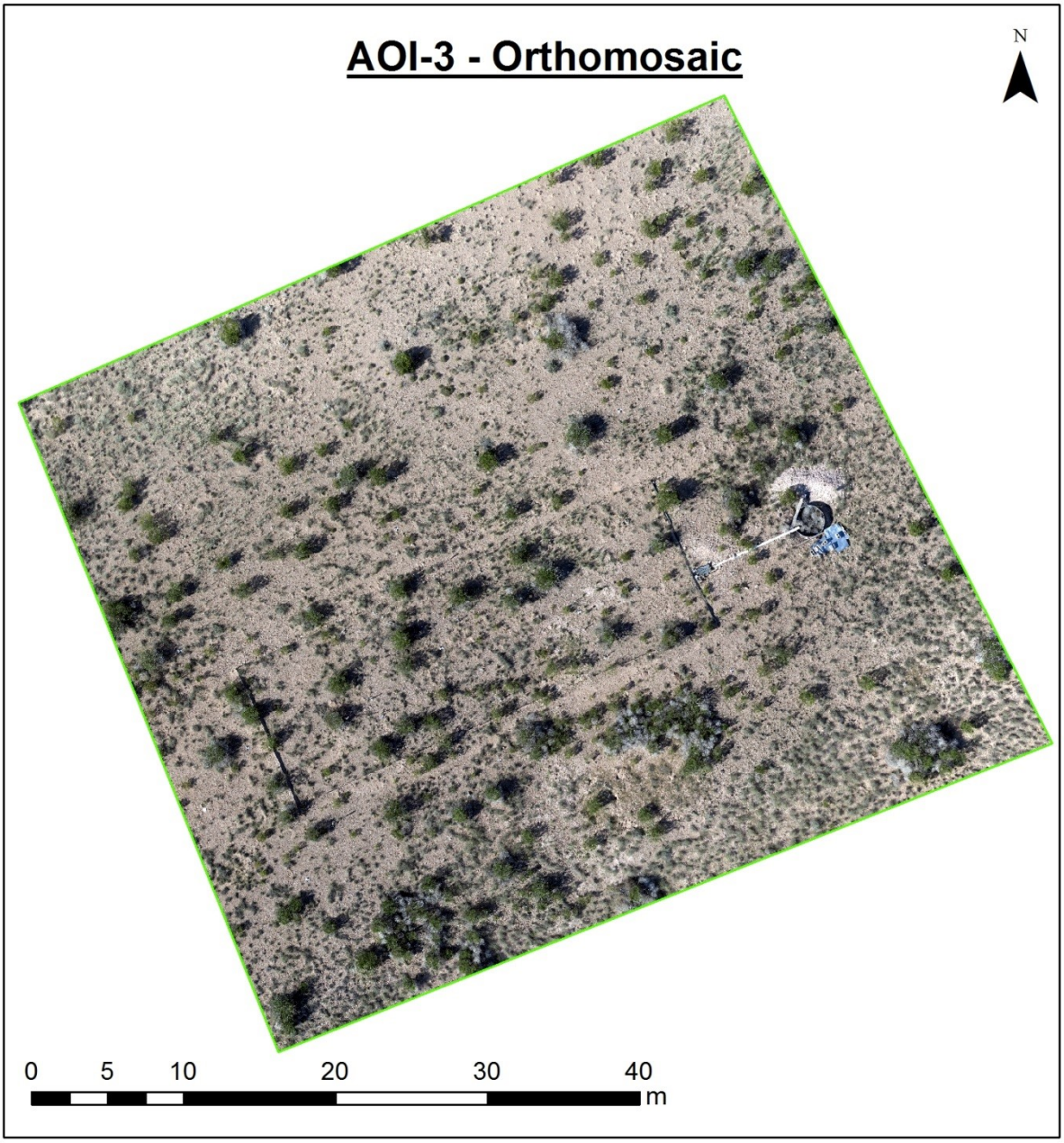
AOI-3 - Orthomosaic
N
0
5
10
20
30
40
m

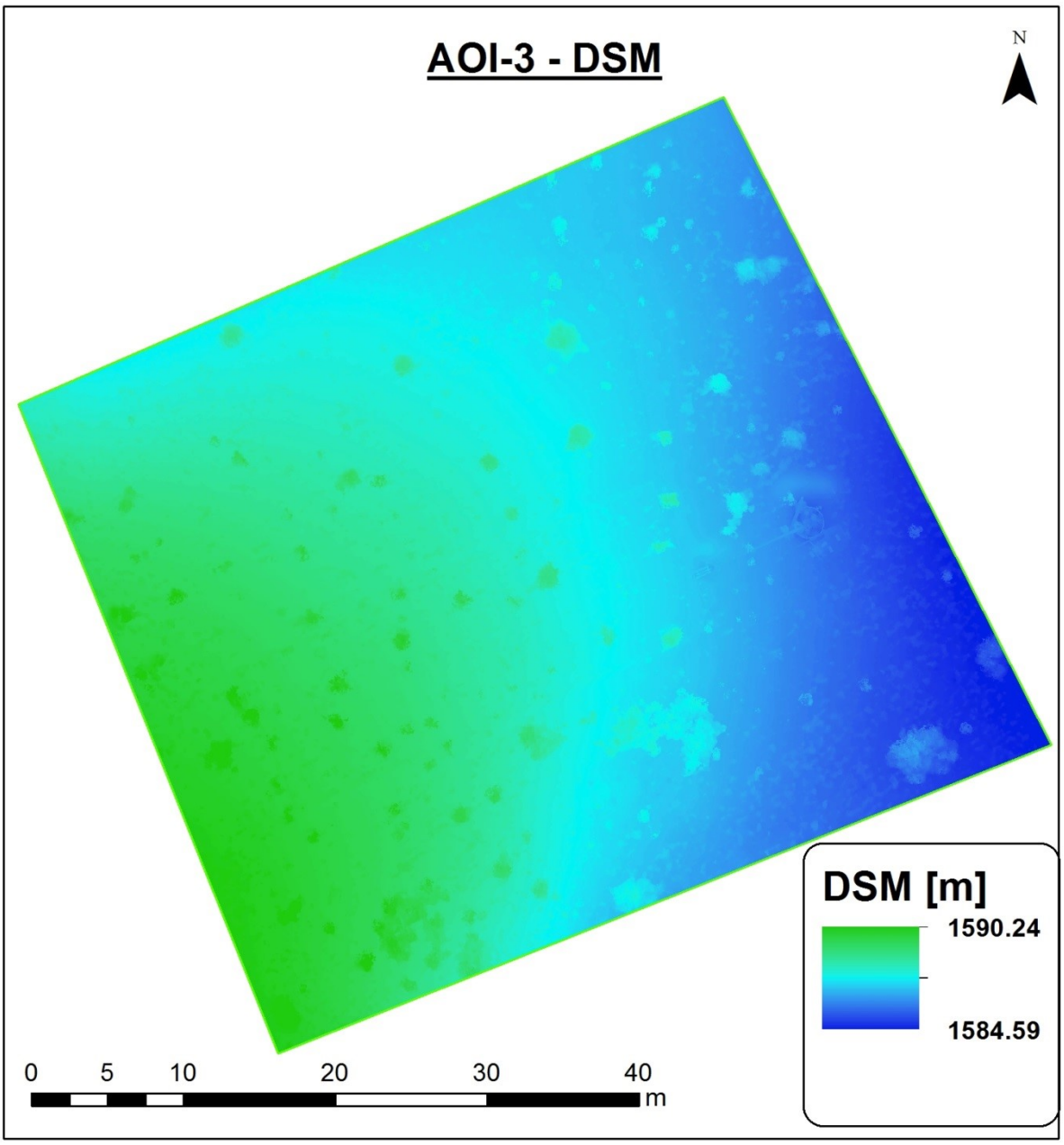
AOI-3 - DSM
N
DSM [m]
1590.24
1584.59
0
5
10
20
30
40
m

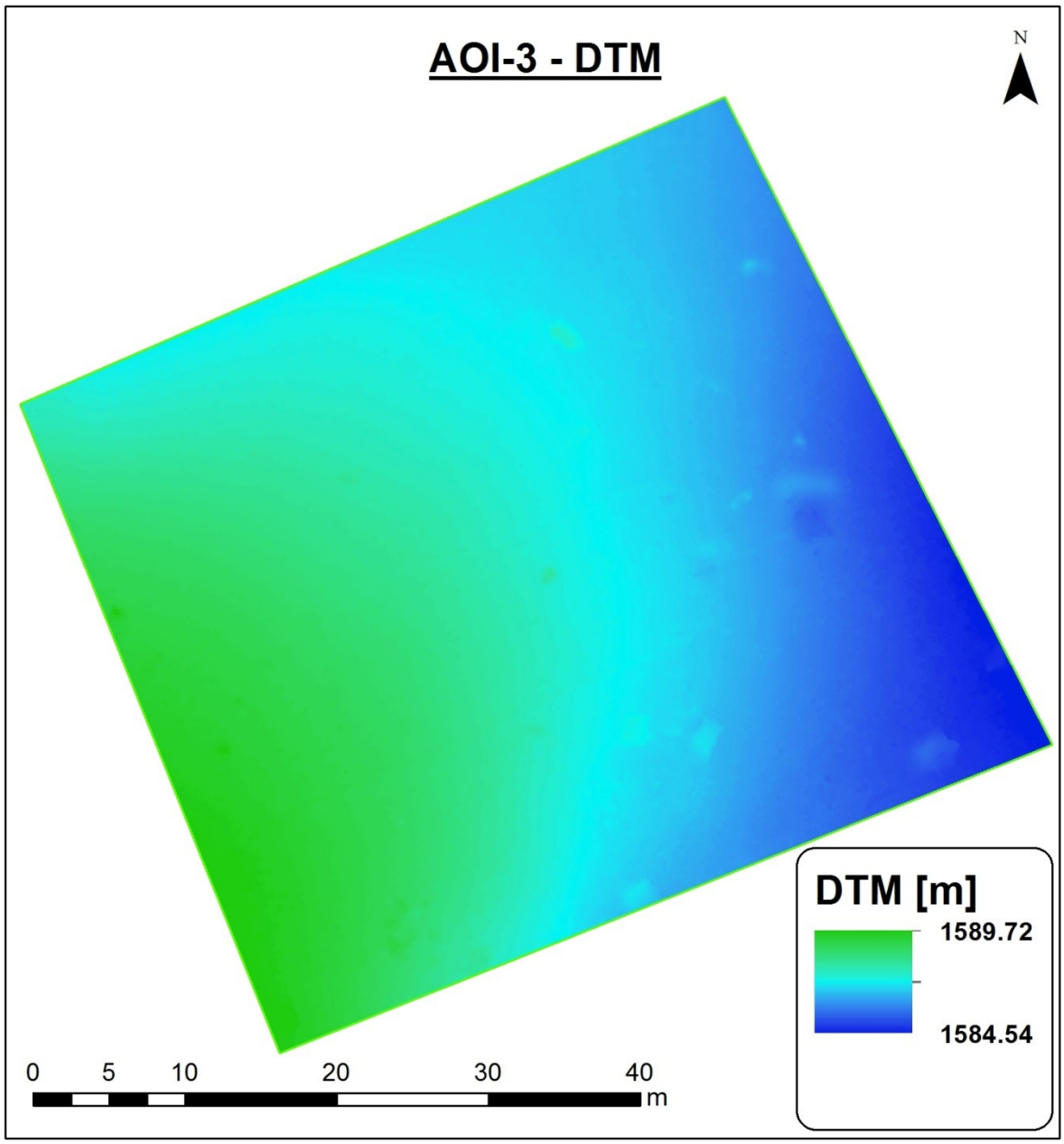
AOI-3 - DTM
N
DTM [m]
1589.72
1584.54
0
5
10
20
30
40
m

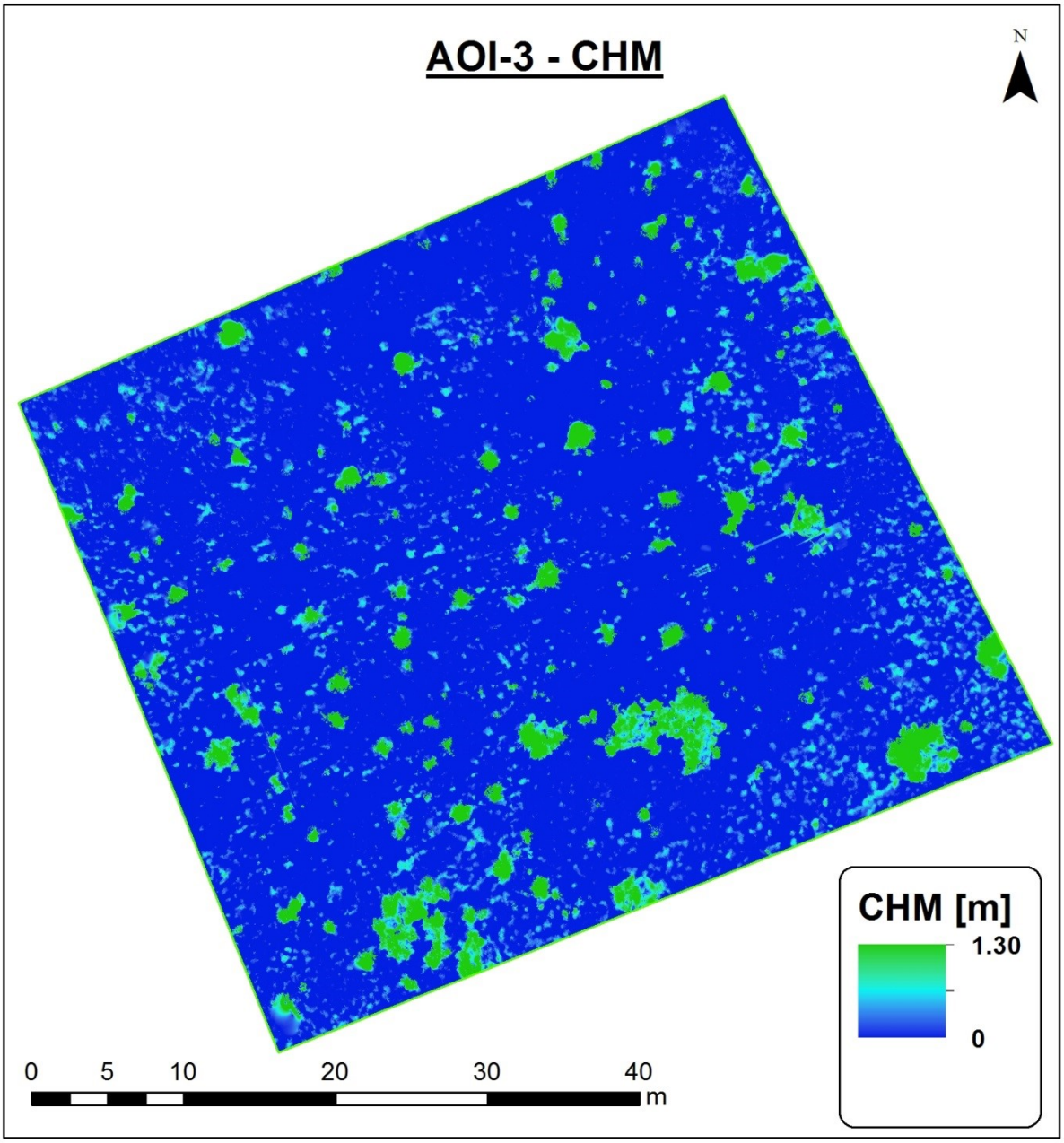
AOI-3 - CHM
N
CHM [m]
1.30
0
0
5
10
20
30
40
m

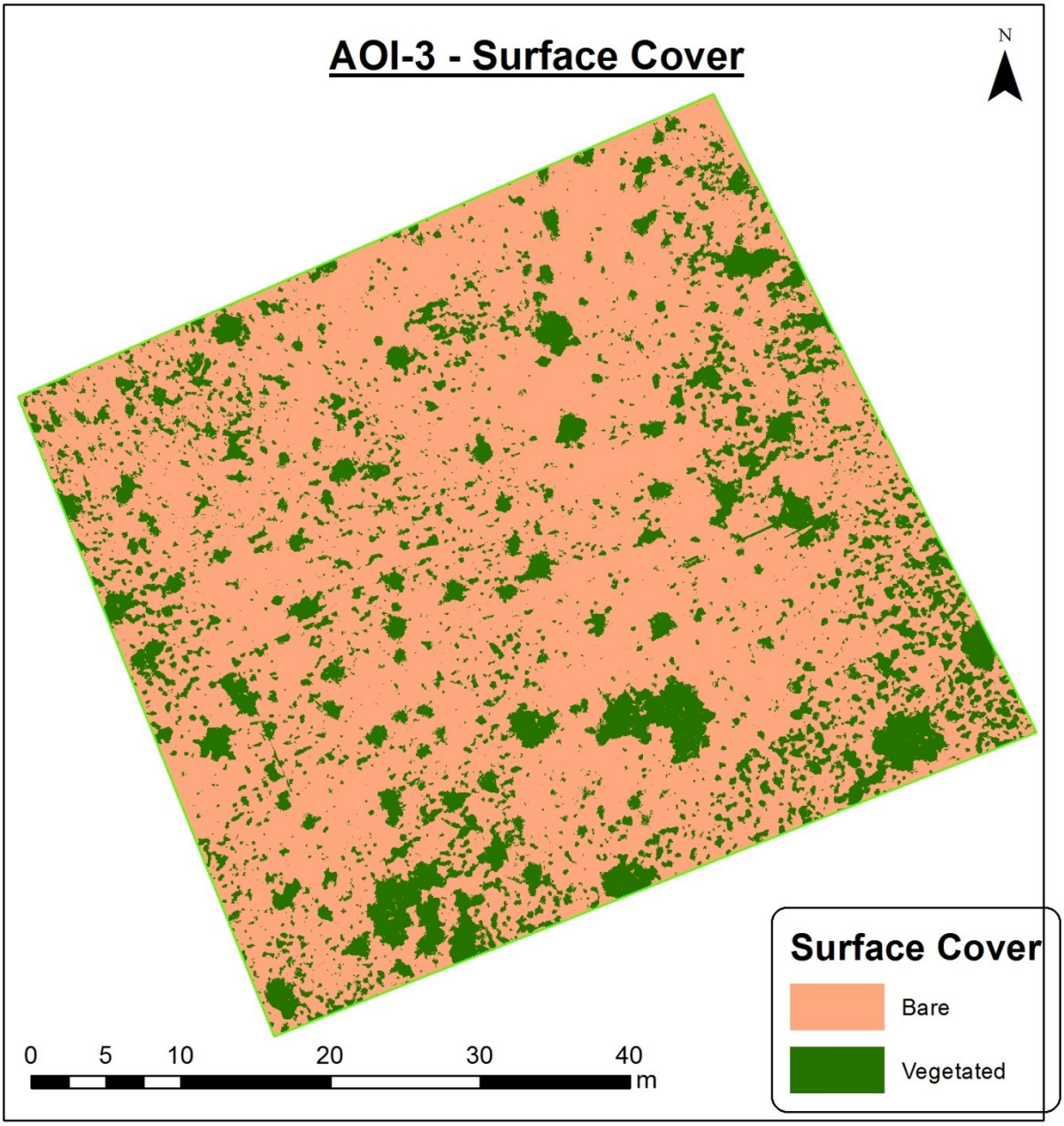
AOI-3 - Surface Cover
N
0
5
10
20
30
40
m
Surface Cover
Bare
Vegetated

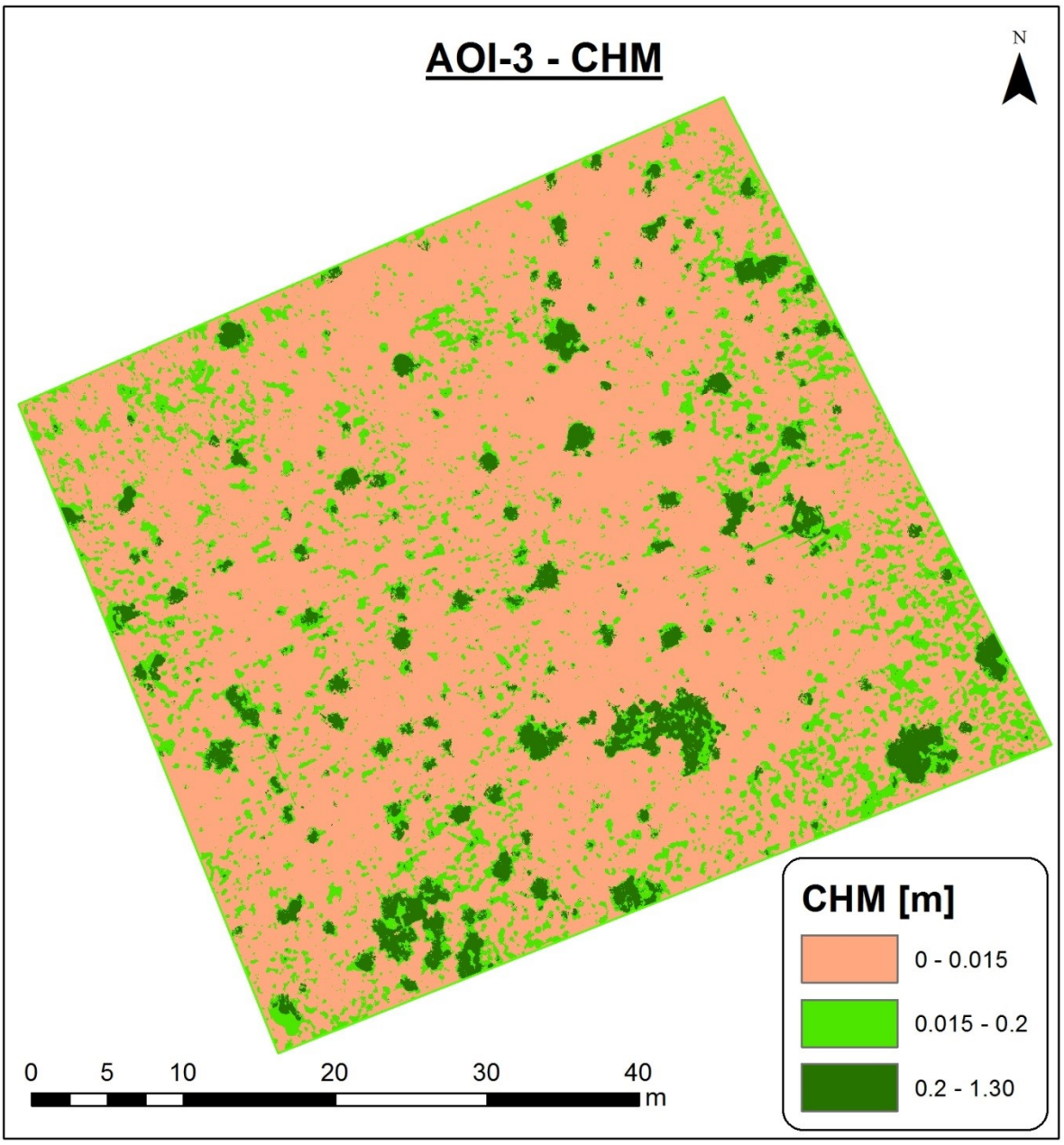
AOI-3 - CHM
N
CHM [m]
0 - 0.015
0.015 - 0.2
0.2 - 1.30
0
5
10
20
30
40
m

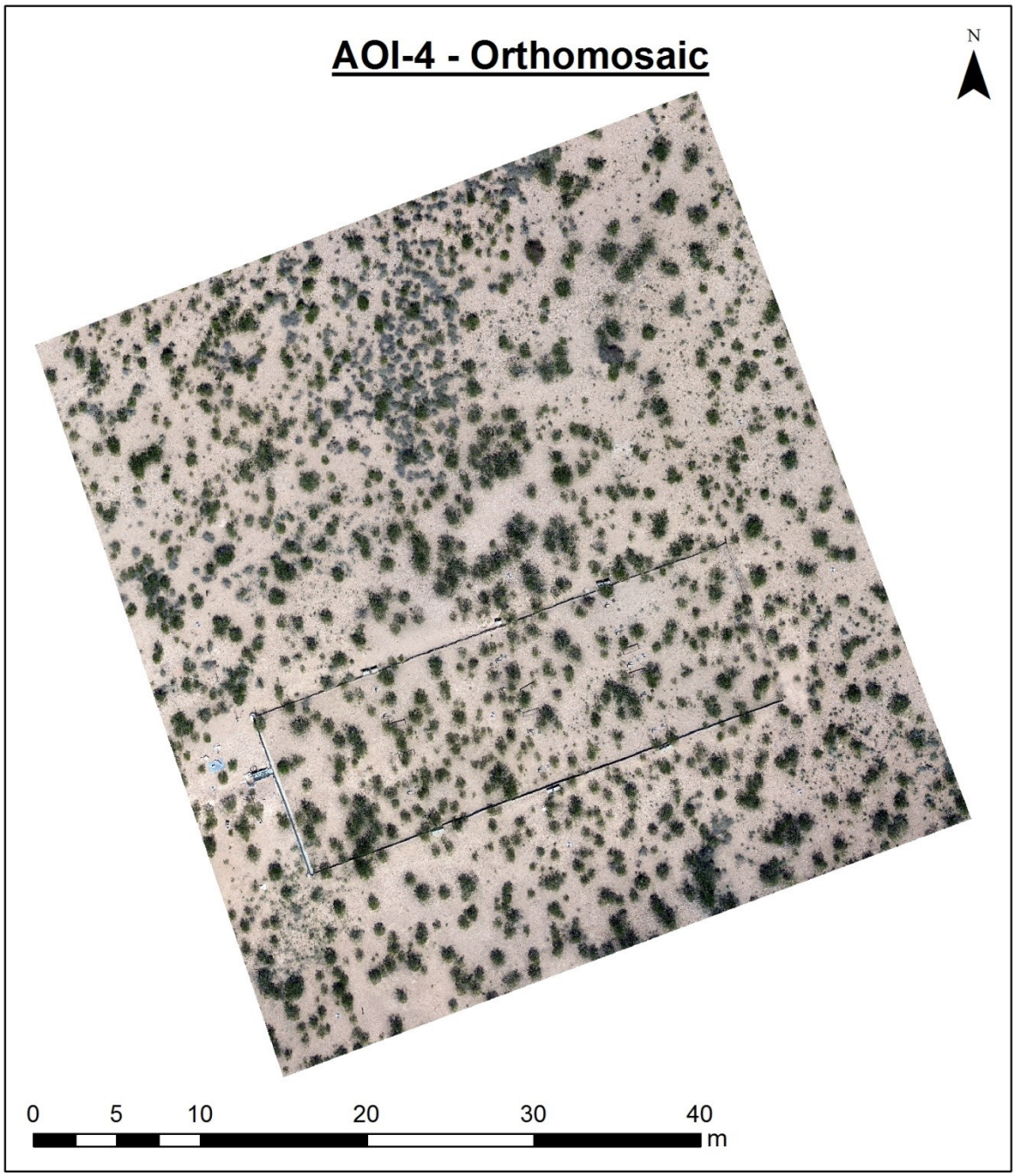
AOI-4 - Orthomosaic
N
0
5
10
20
30
40
m

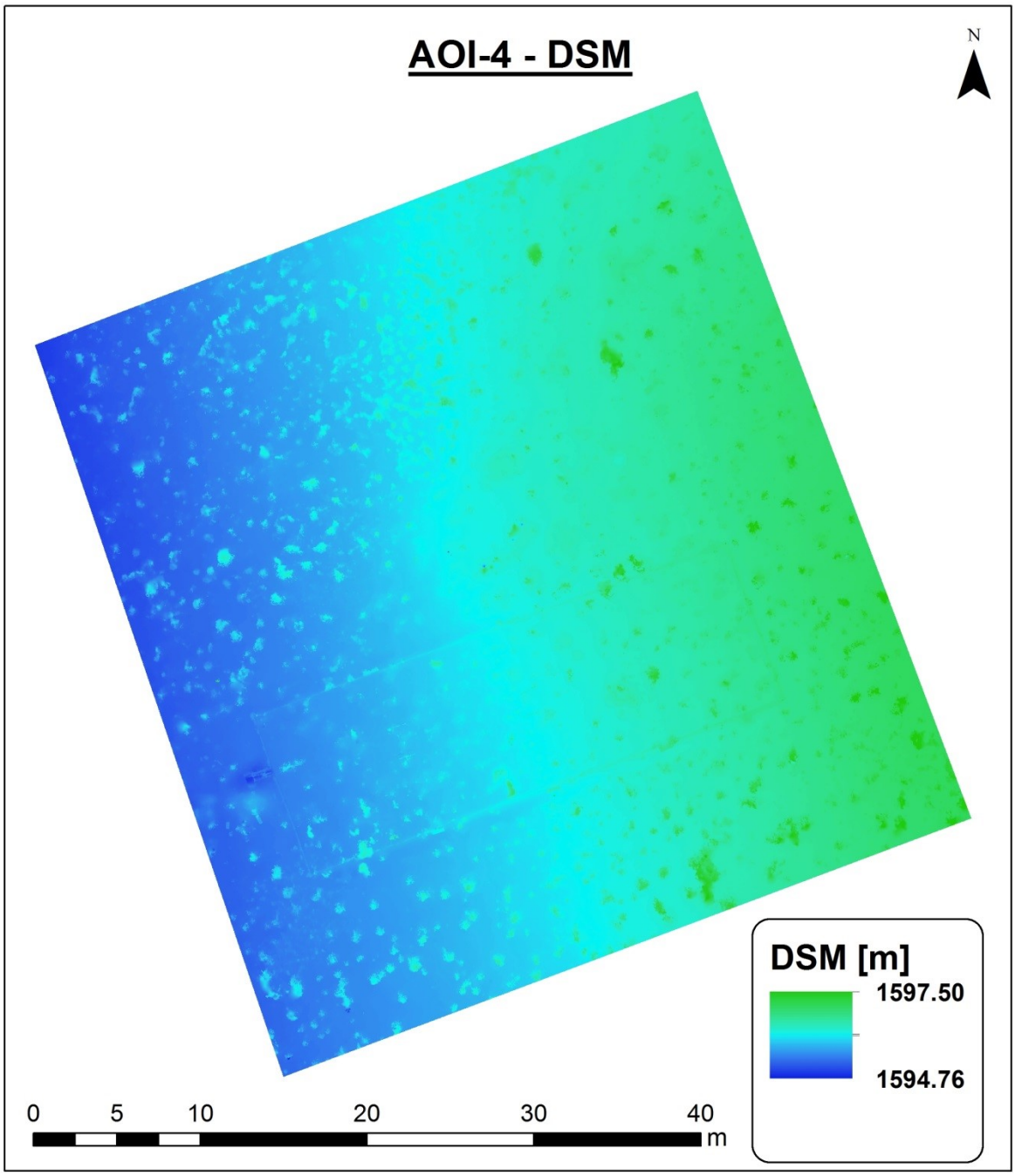
AOI-4 - DSM
N
DSM [m]
1597.50
1594.76
0
5
10
20
30
40
m

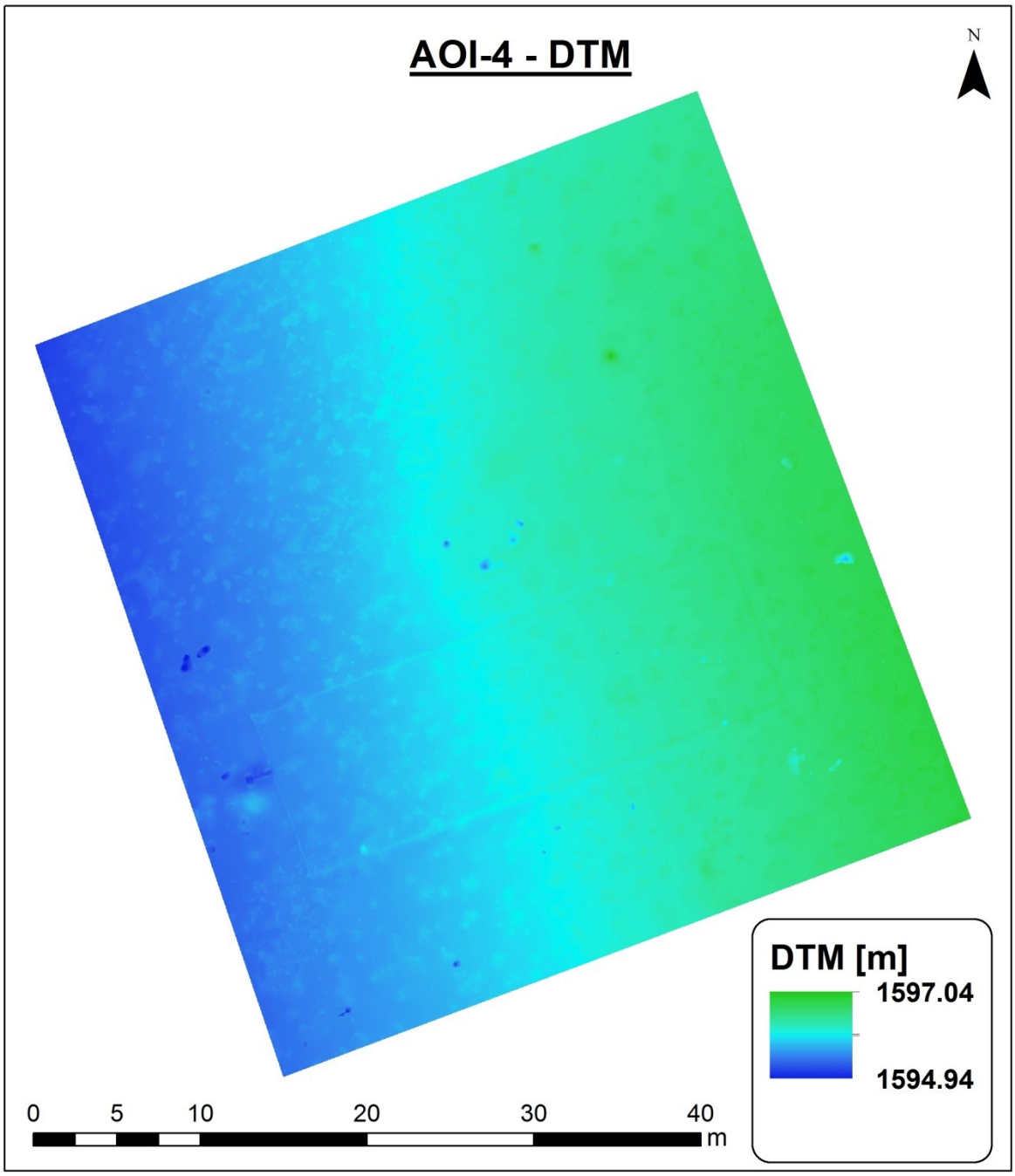
AOI-4 - DTM
N
DTM [m]
1597.04
1594.94
0
5
10
20
30
40
m

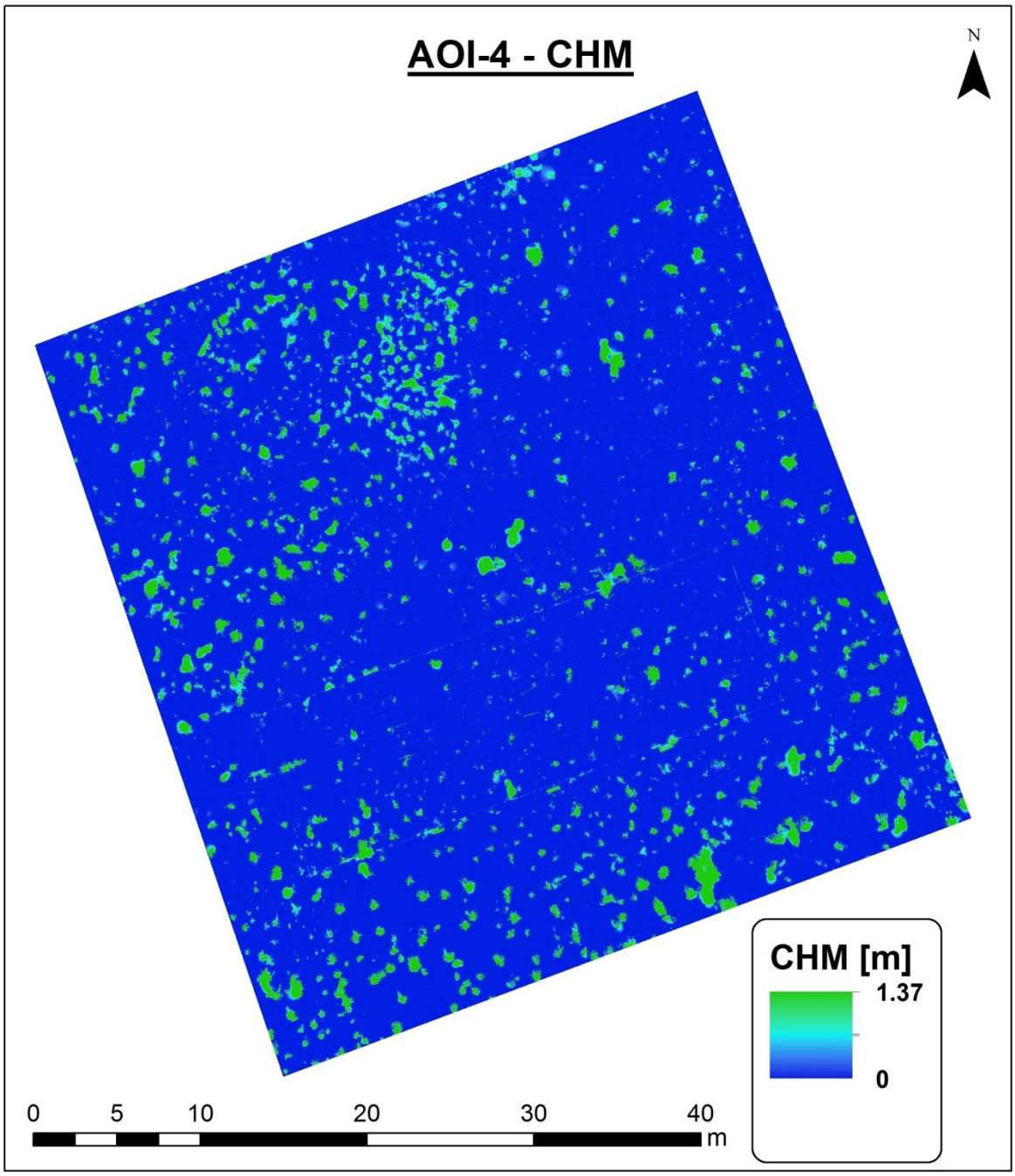
AOI-4 - CHM
N
CHM [m]
1.37
0
0
5
10
20
30
40
m

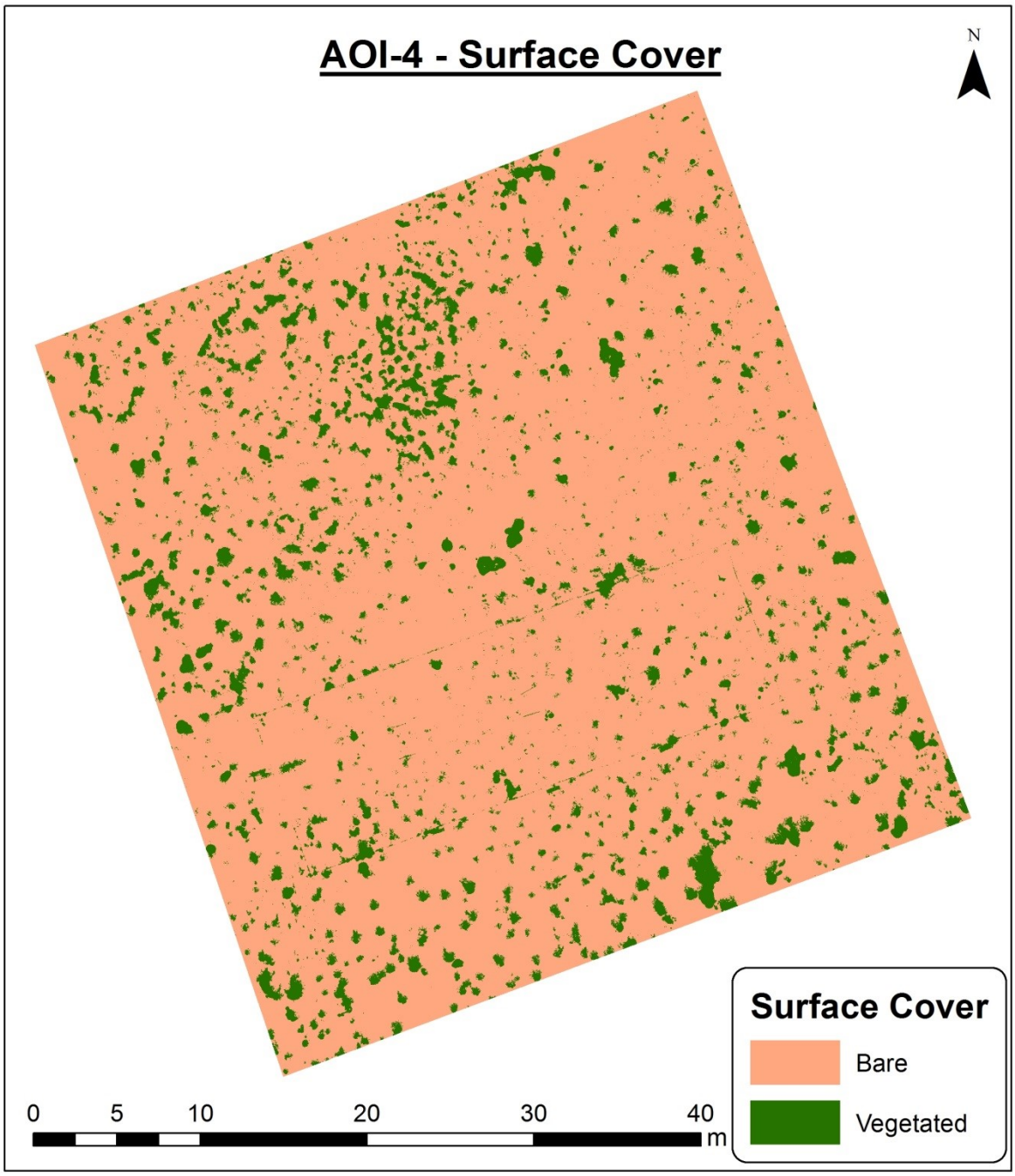
AOI-4 - Surface Cover
N
Surface Cover
Bare
Vegetated
0
5
10
20
30
40
m

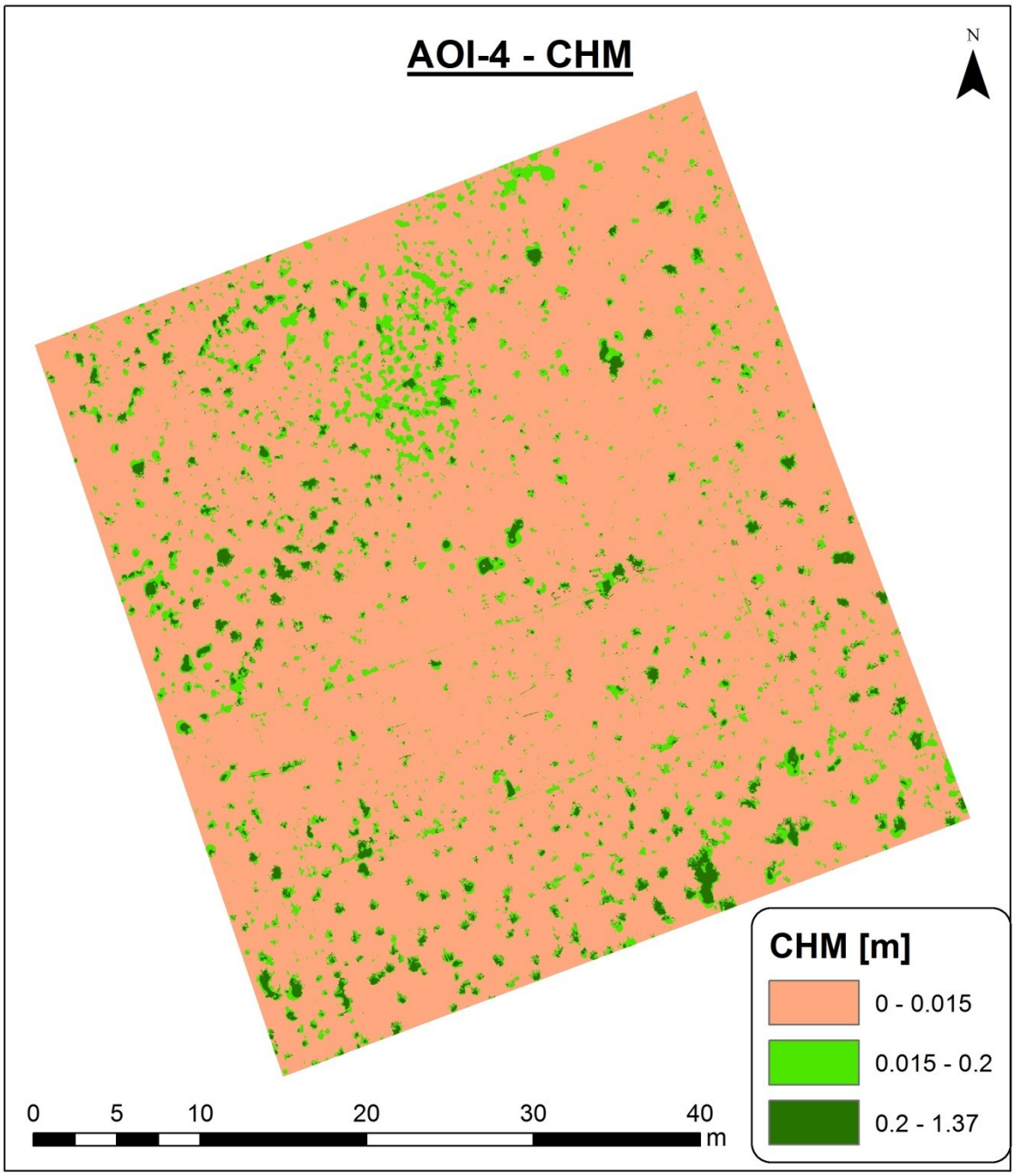
AOI-4 - CHM
N
CHM [m]
0 - 0.015
0.015 - 0.2
0.2 - 1.37
0
5
10
20
30
40
m

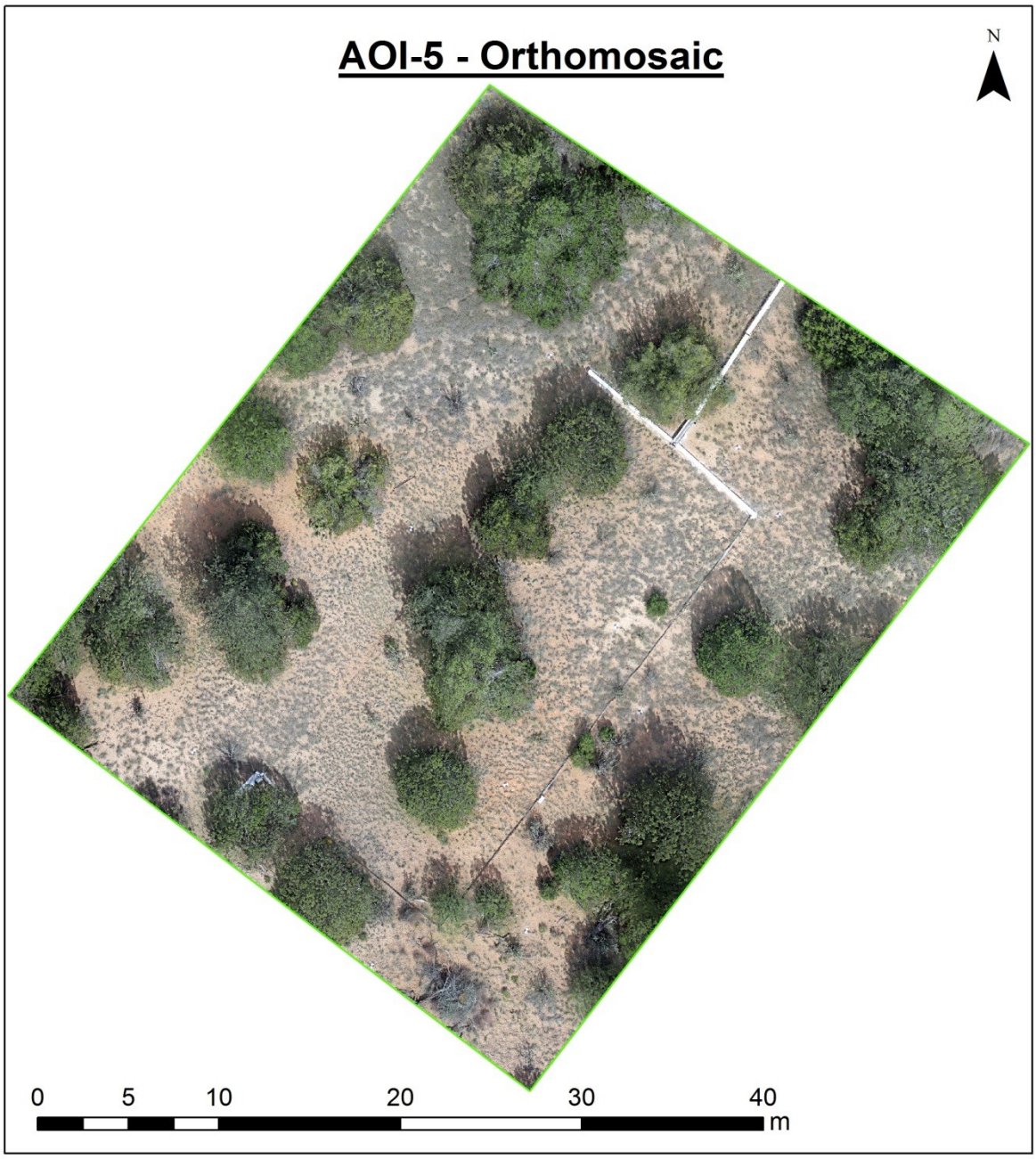
AOI-5 - Orthomosaic
N
0
5
10
20
30
40
m

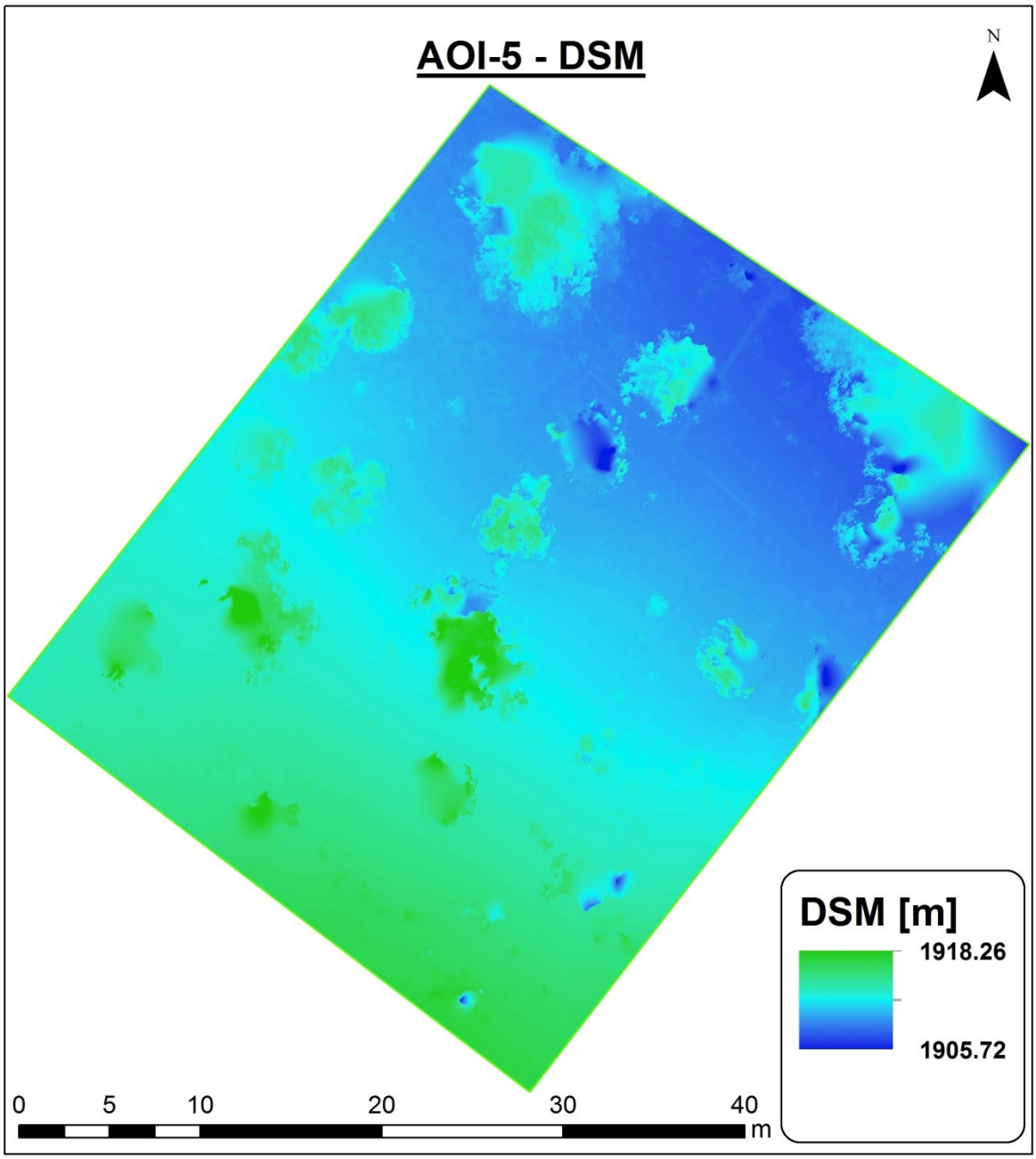
AOI-5 - DSM
N
DSM [m]
1918.26
1905.72
0
5
10
20
30
40
m

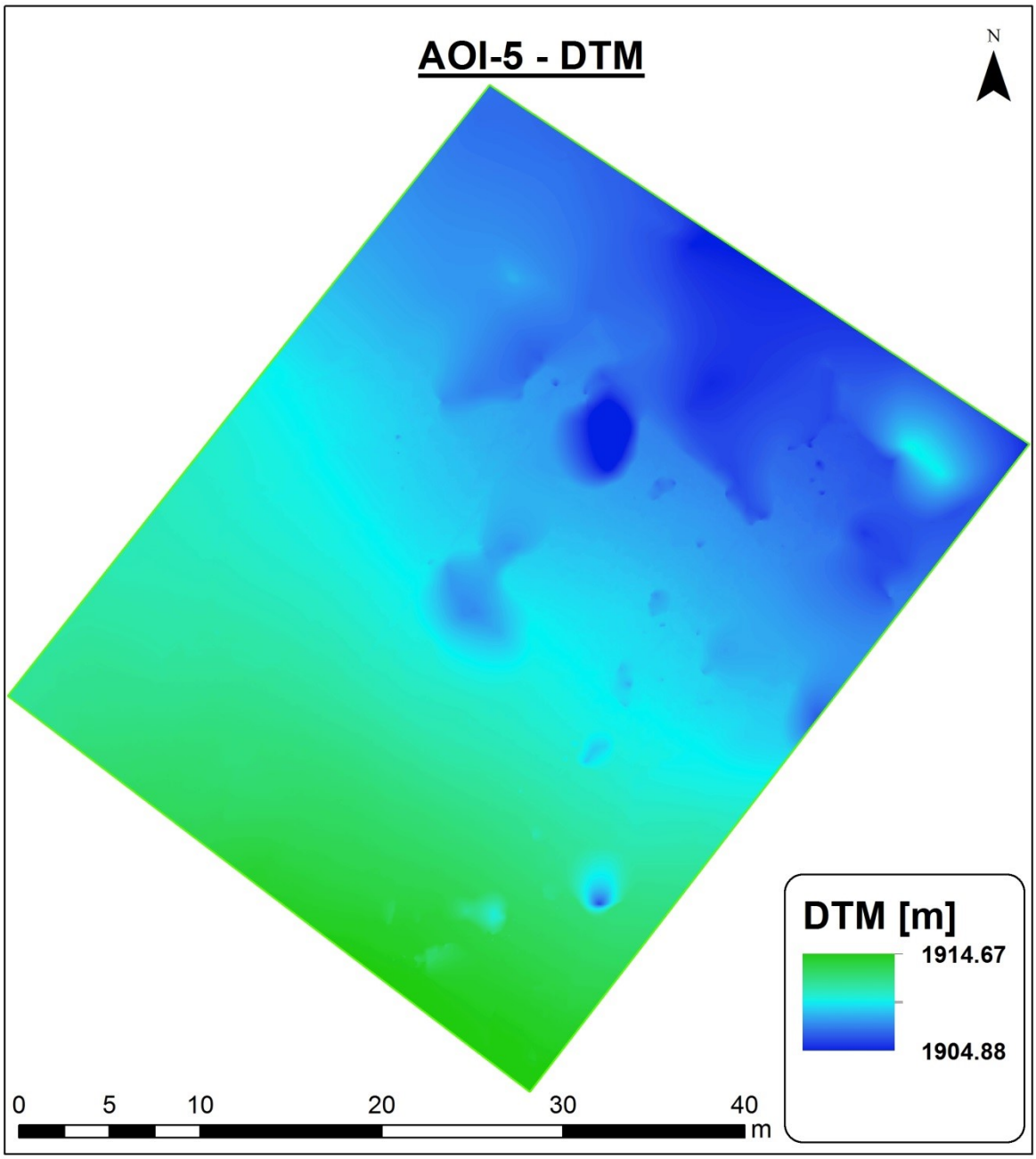
AOI-5 - DTM
N
DTM [m]
1914.67
1904.88
0
5
10
20
30
40
m

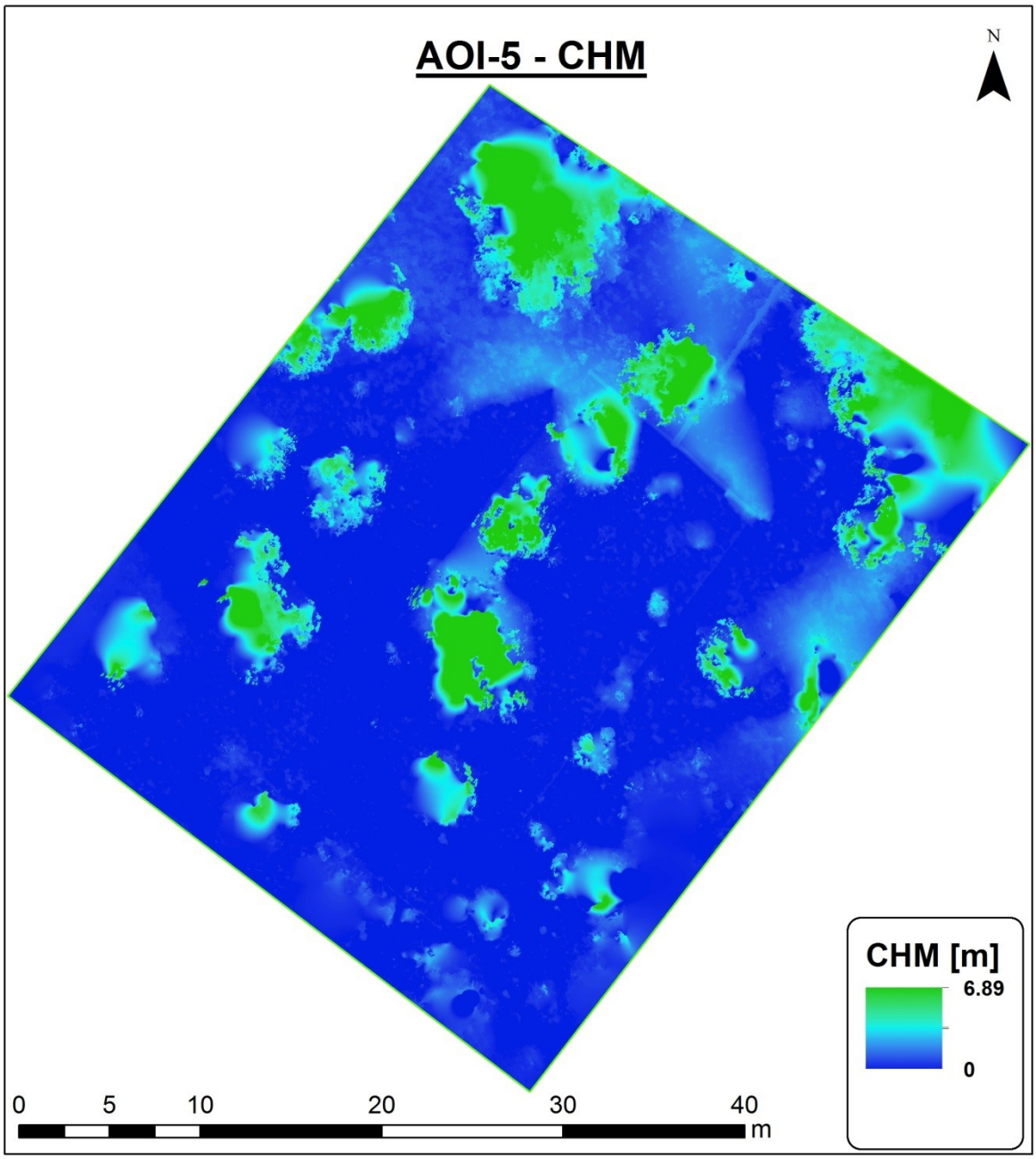
AOI-5 - CHM
N
CHM [m]
6.89
0
0
5
10
20
30
40
m

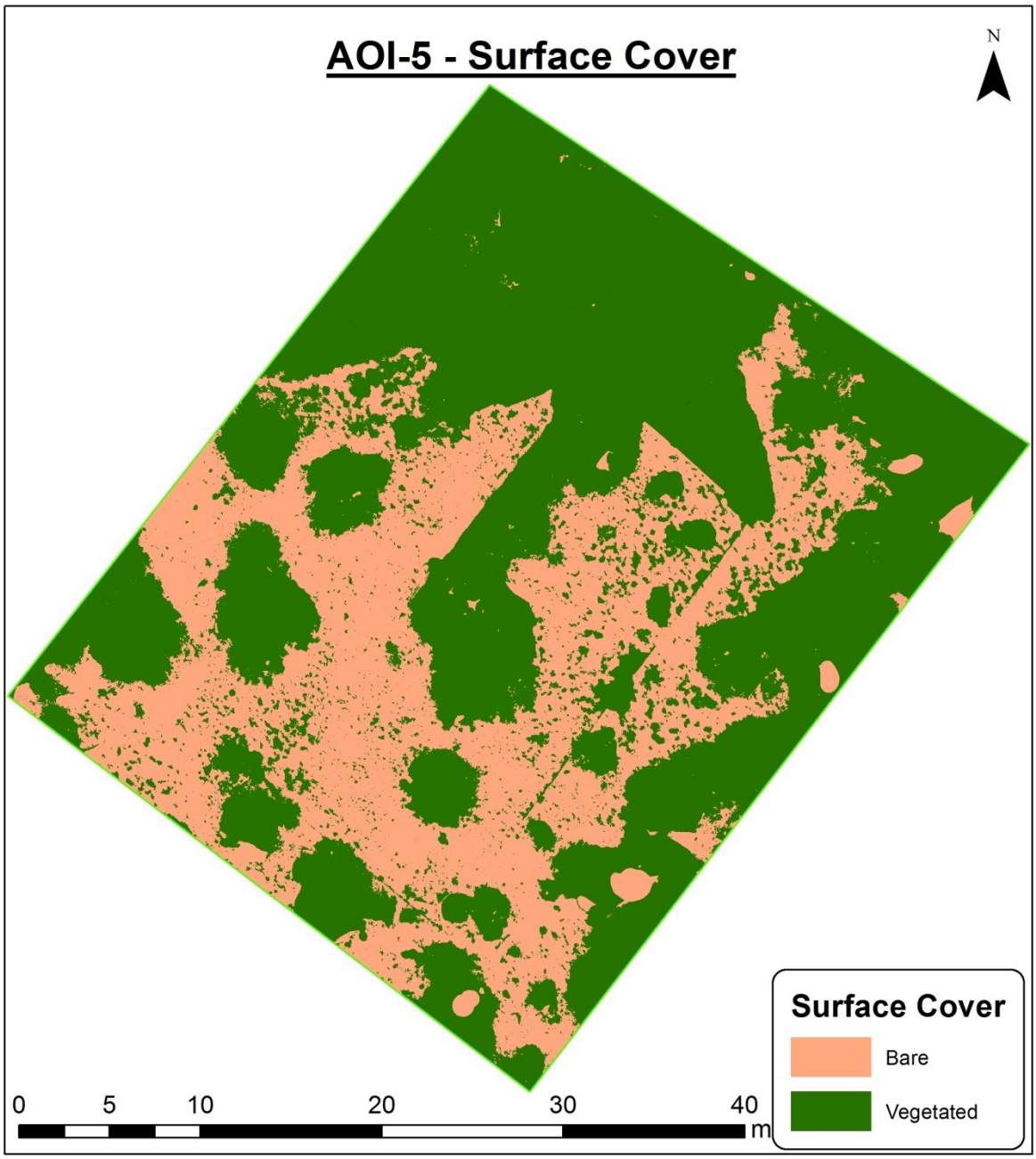
AOI-5 - Surface Cover
N
Surface Cover
Bare
Vegetated
0
5
10
20
30
40
m

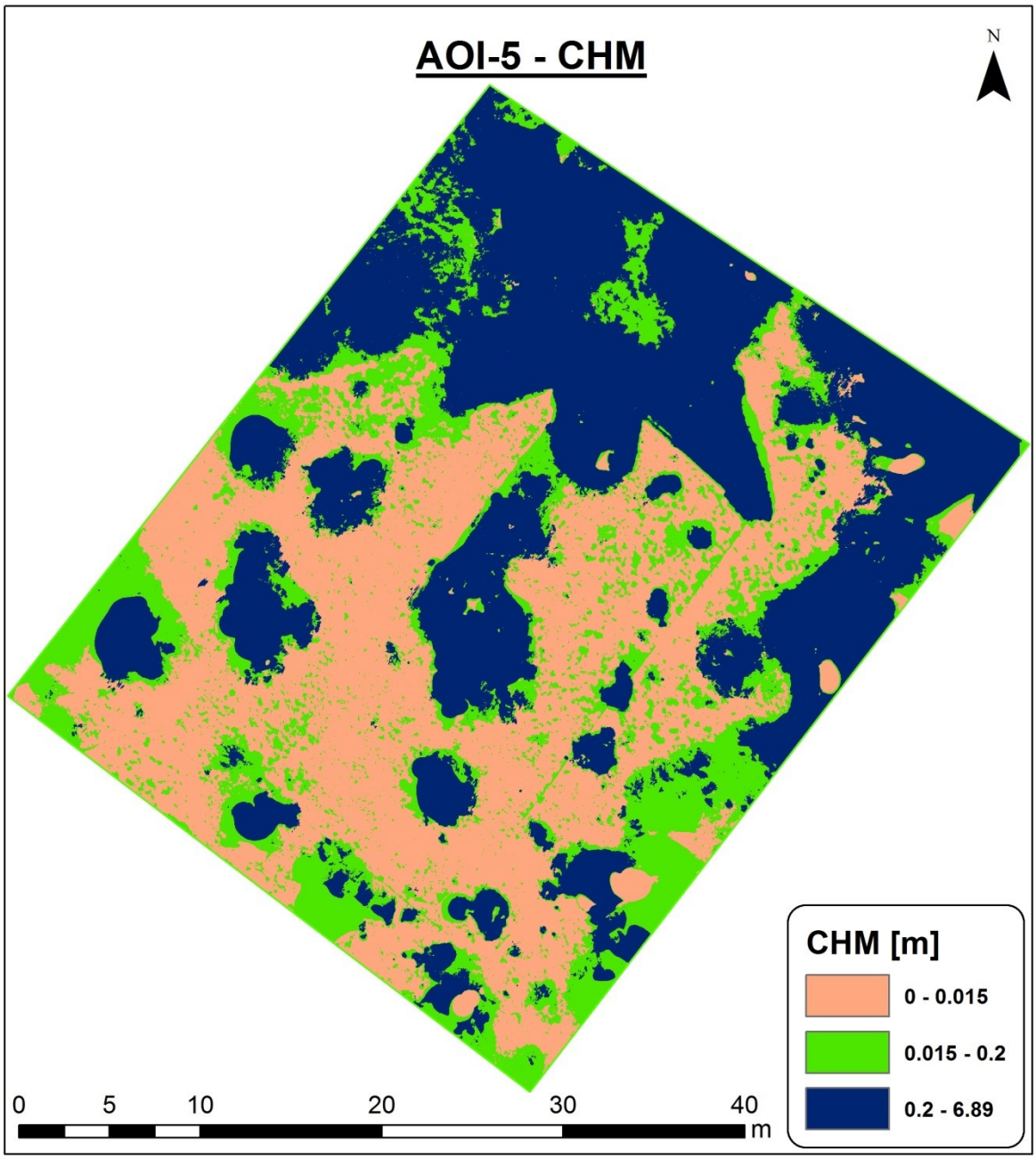
AOI-5 - CHM
N
CHM [m]
0 - 0.015
0.015 - 0.2
0.2 - 6.89
0
5
10
20
30
40
m

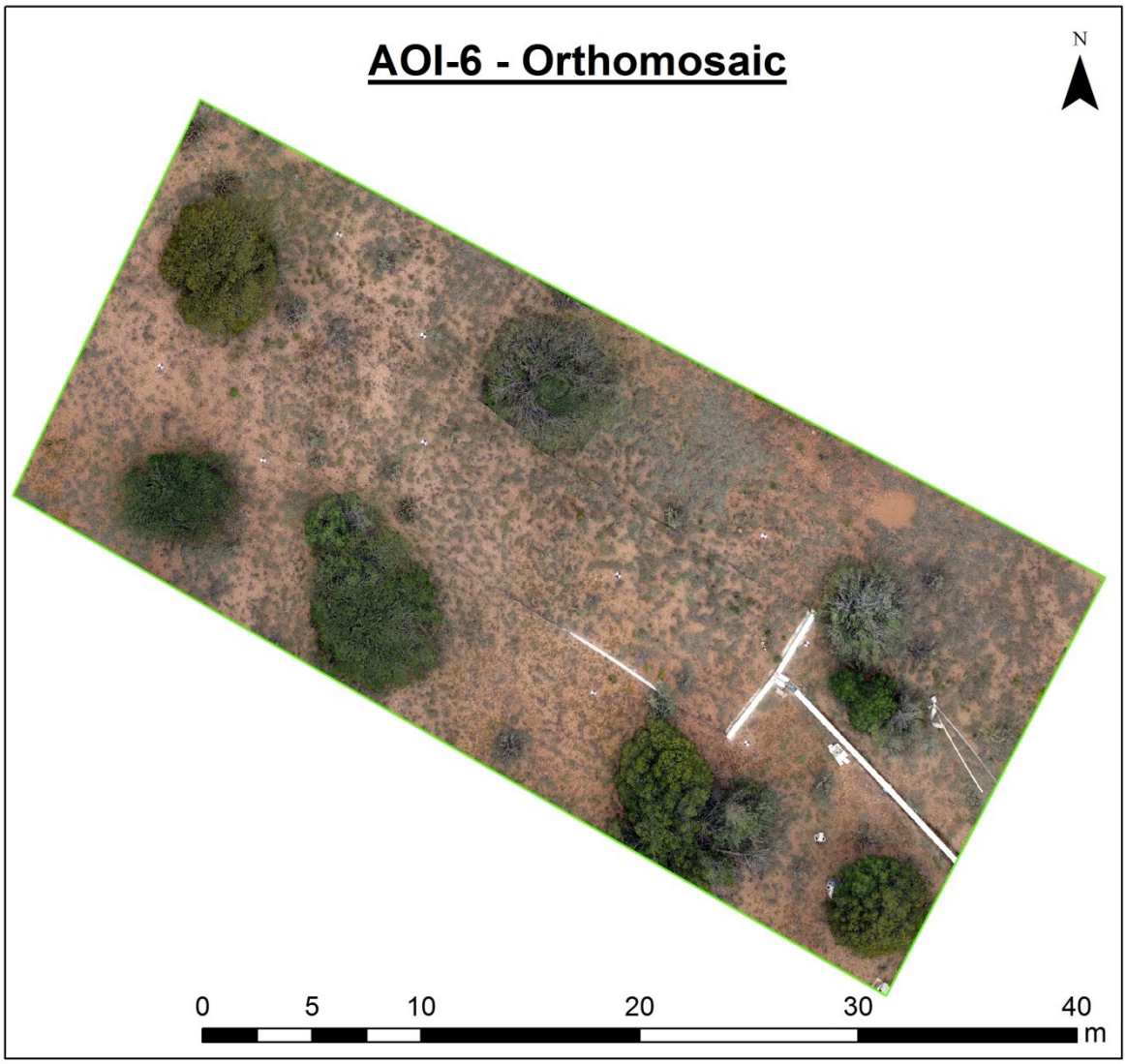
AOI-6 - Orthomosaic
N
0
5
10
20
30
40
m

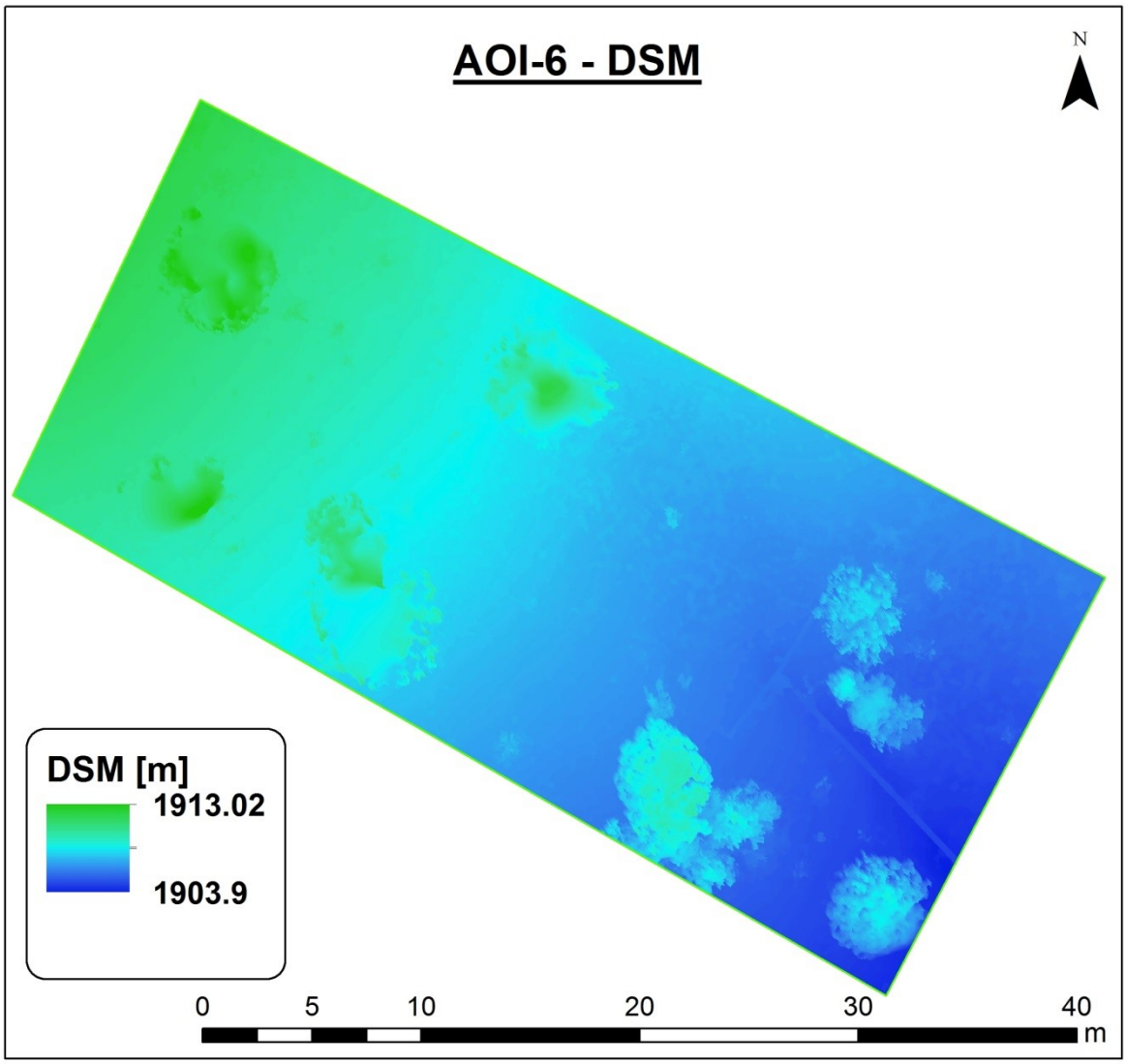
AOI-6 - DSM
N
DSM [m]
1913.02
1903.9
0
5
10
20
30
40
m

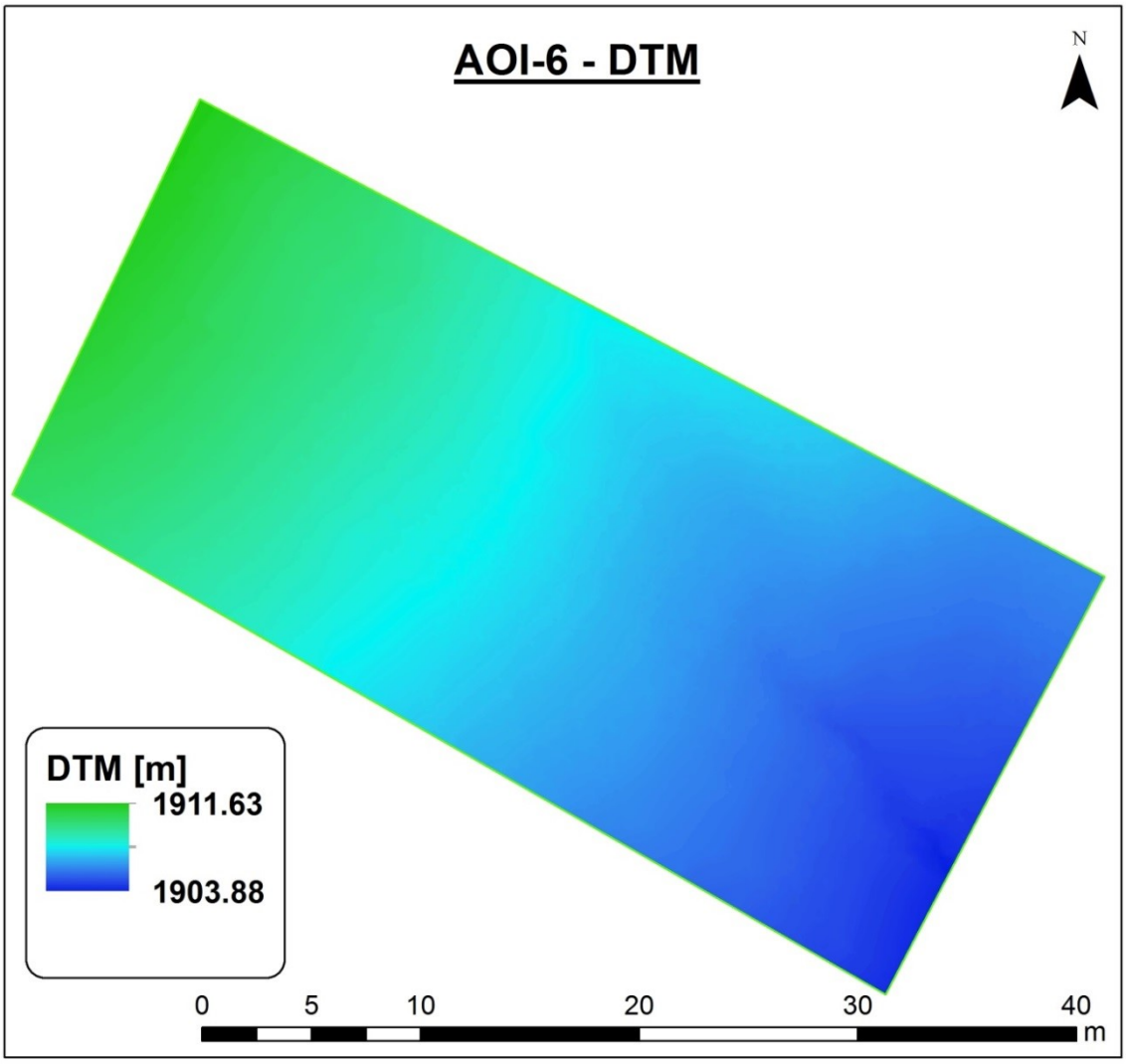
AOI-6 - DTM
N
DTM [m]
1911.63
1903.88
0
5
10
20
30
40
m

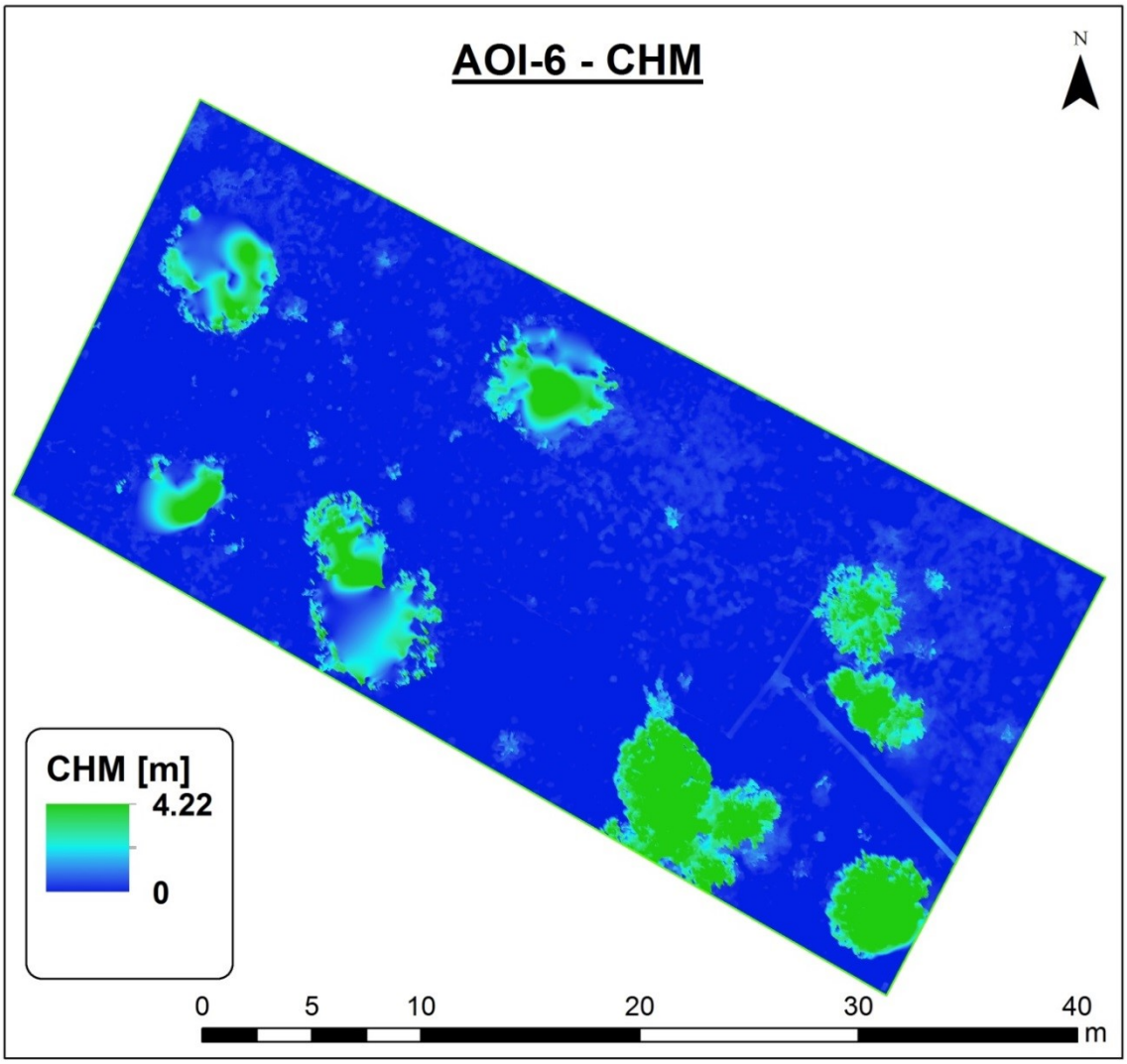
AOI-6 - CHM
N
CHM [m]
4.22
0
0
5
10
20
30
40
m

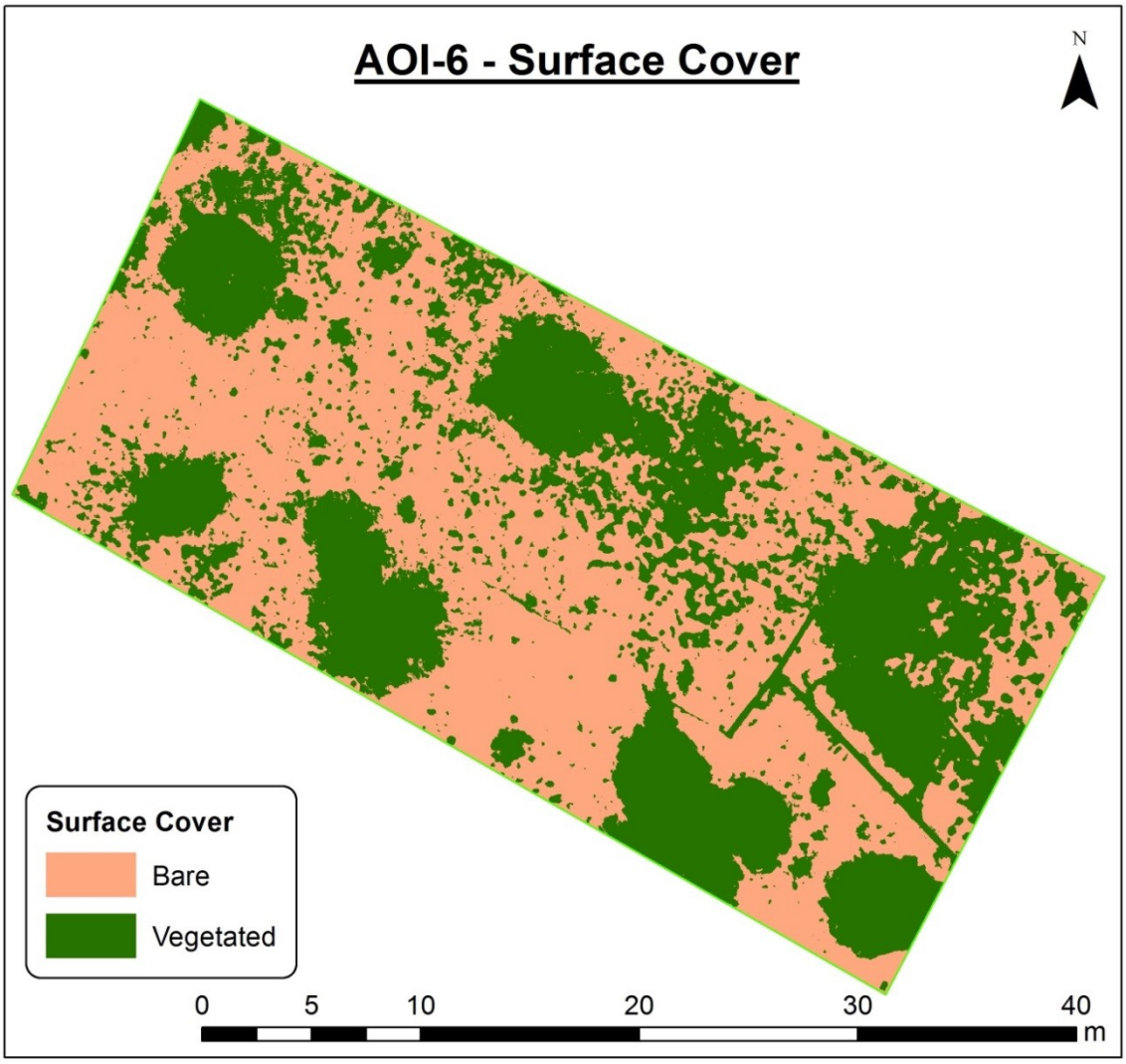
AOI-6 - Surface Cover
N
Surface Cover
Bare
Vegetated
0
5
10
20
30
40
m

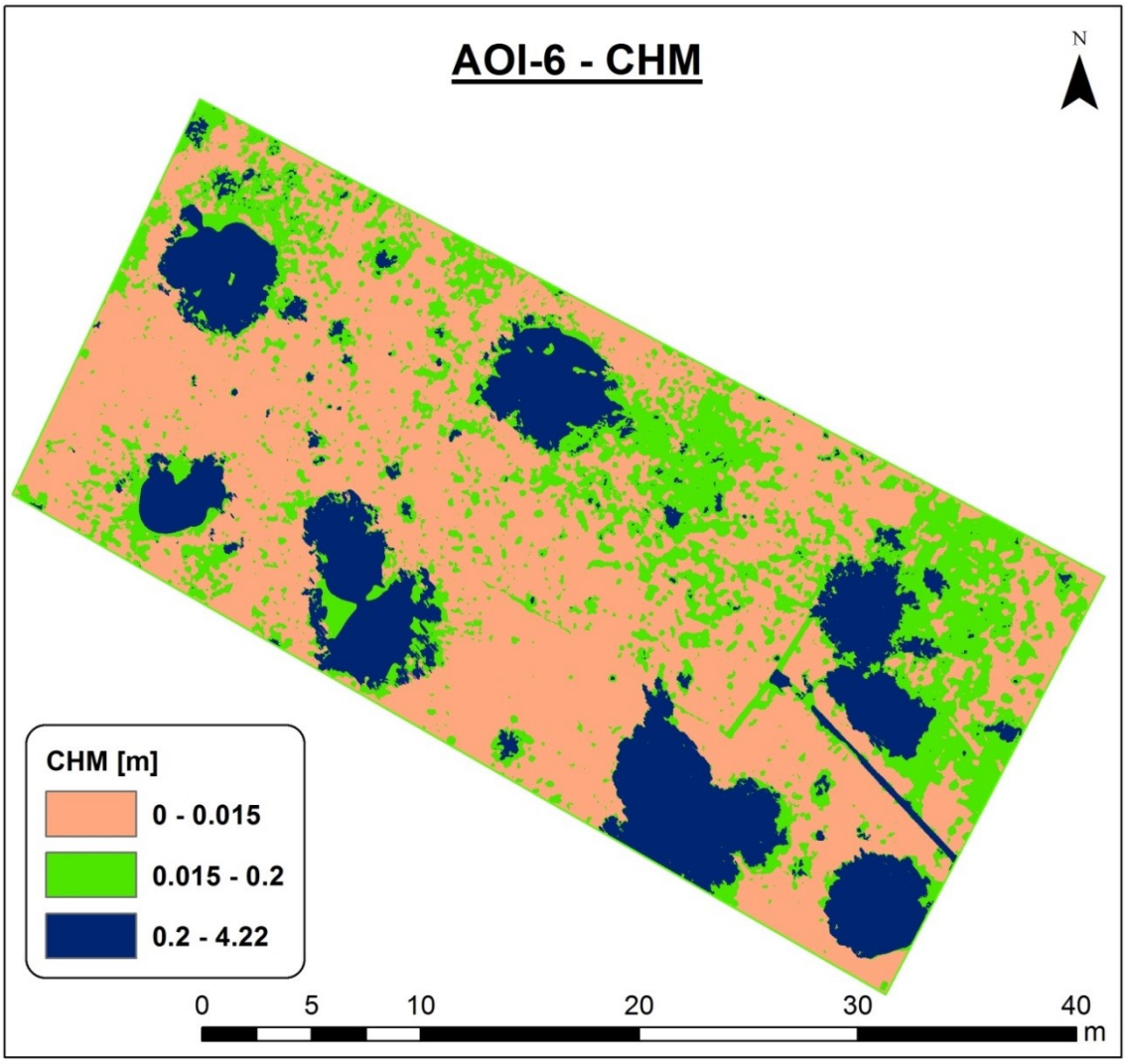
AOI-6 - CHM
N
CHM [m]
0 - 0.015
0.015 - 0.2
0.2 - 4.22
0
5
10
20
30
40
m

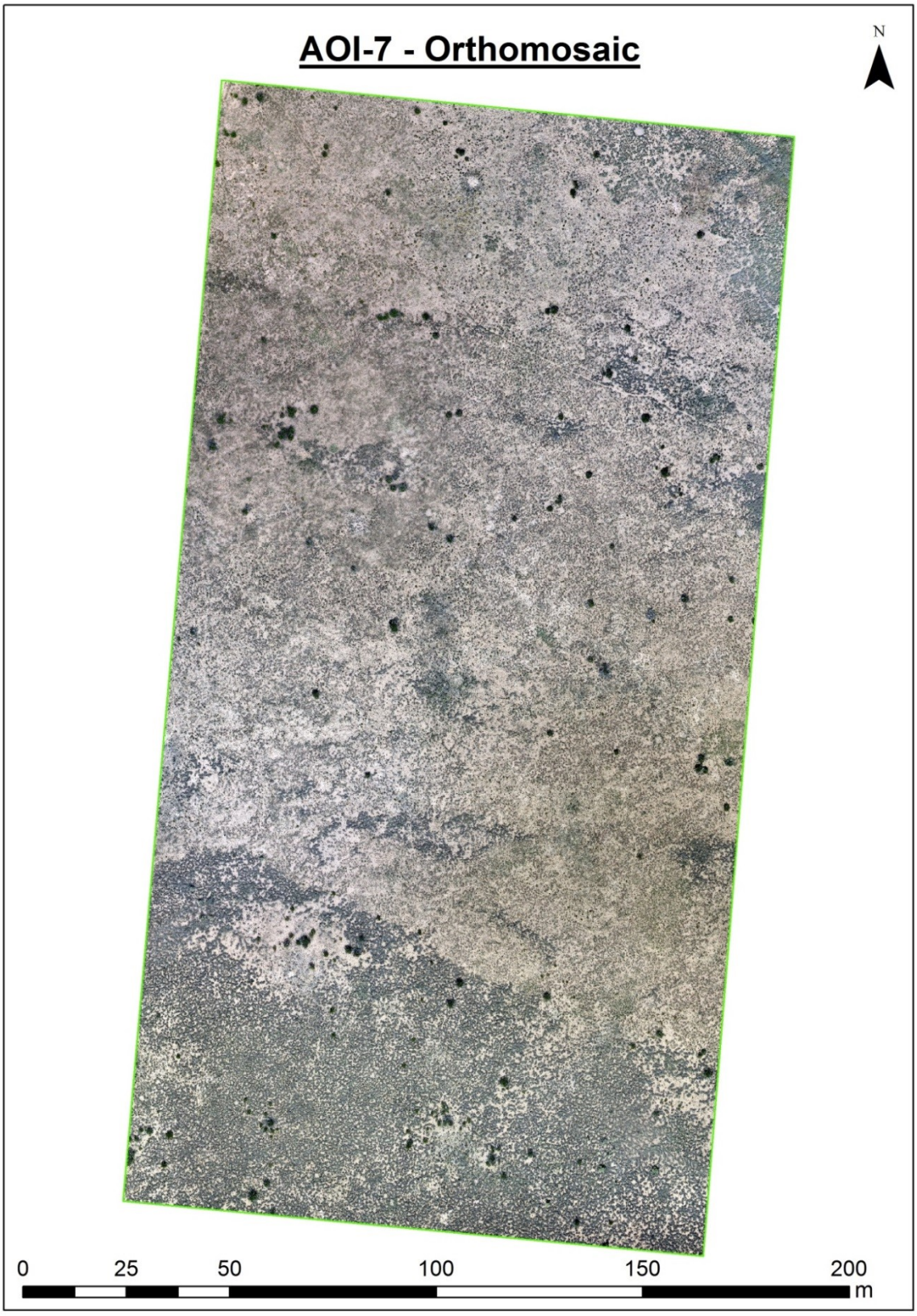
AOI-7 - Orthomosaic
N
0
25
50
100
150
200
m

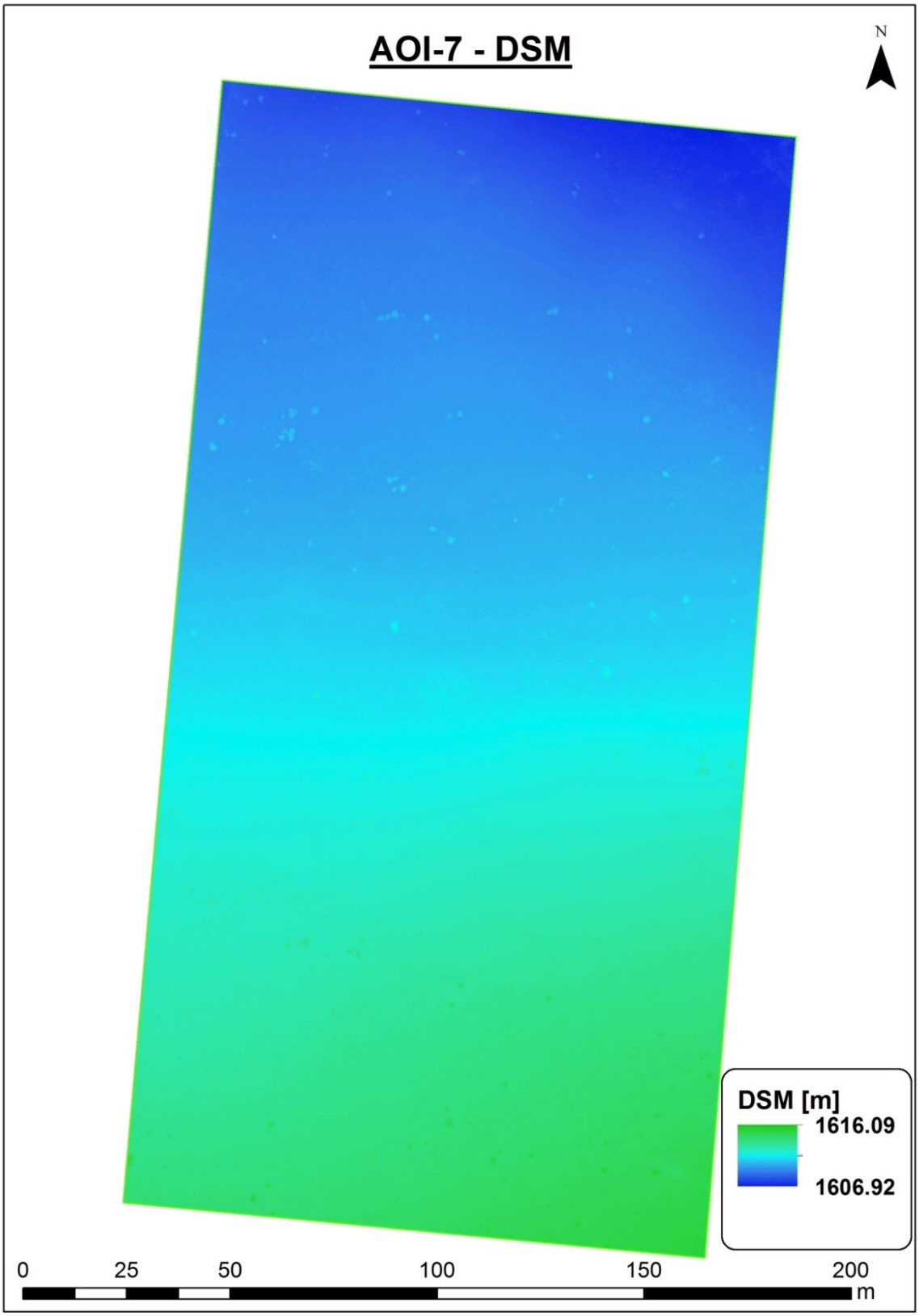
AOI-7 - DSM
N
DSM [m]
1616.09
1606.92
0
25
50
100
150
200
m

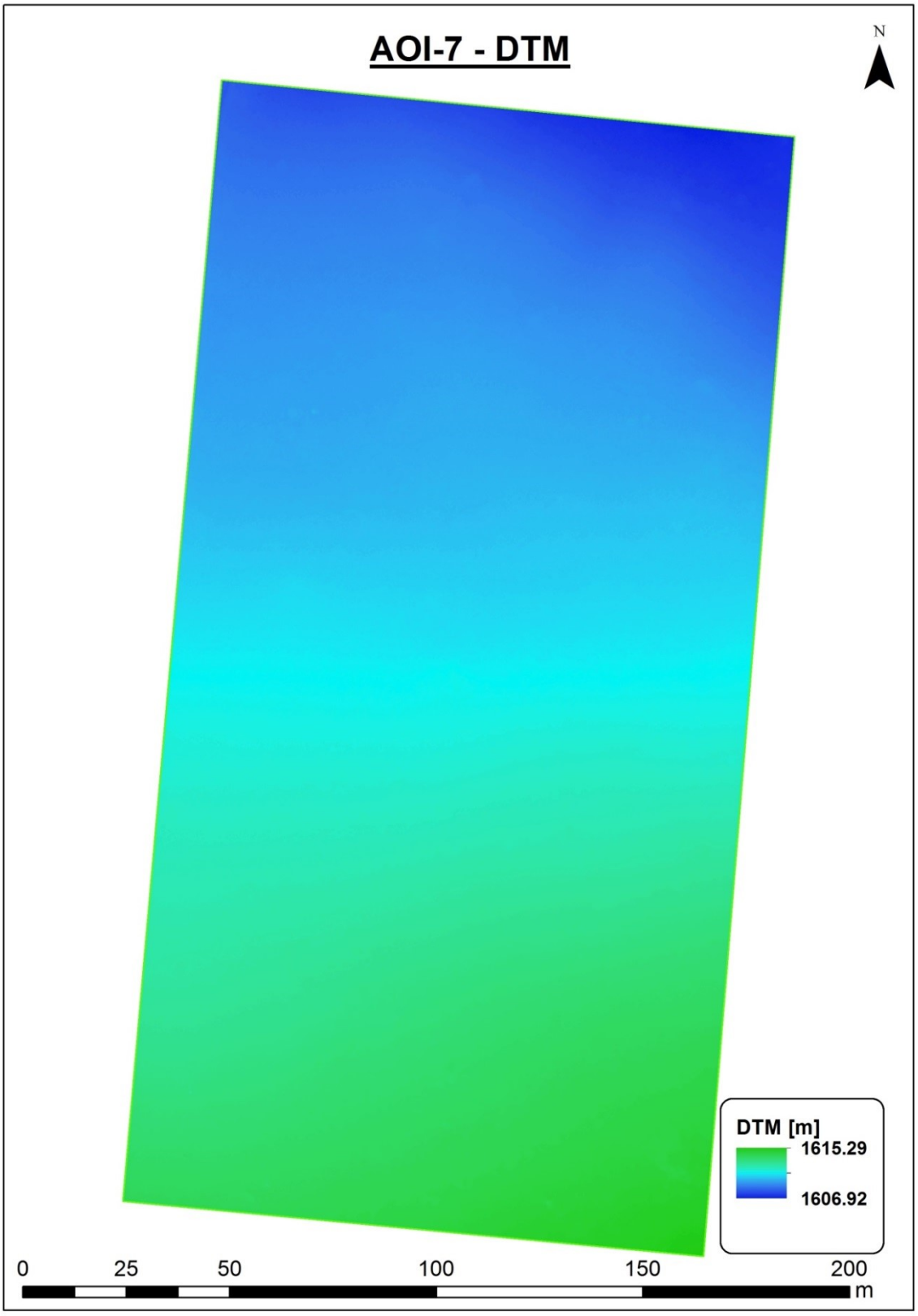
AOI-7 - DTM
N
DTM [m]
1615.29
1606.92
0
25
50
100
150
200
m

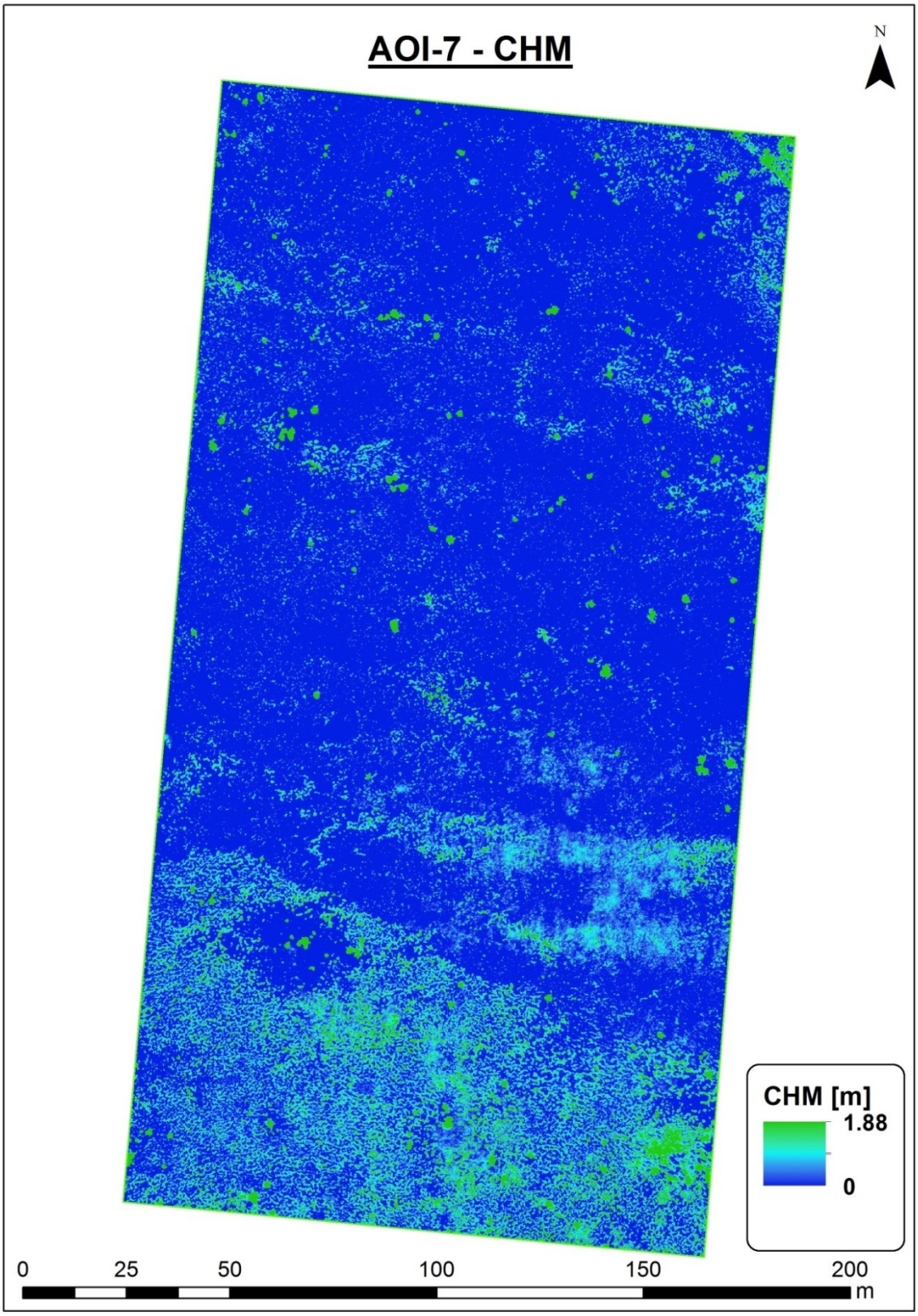
AOI-7 - CHM
N
CHM [m]
1.88
0
0
25
50
100
150
200
m

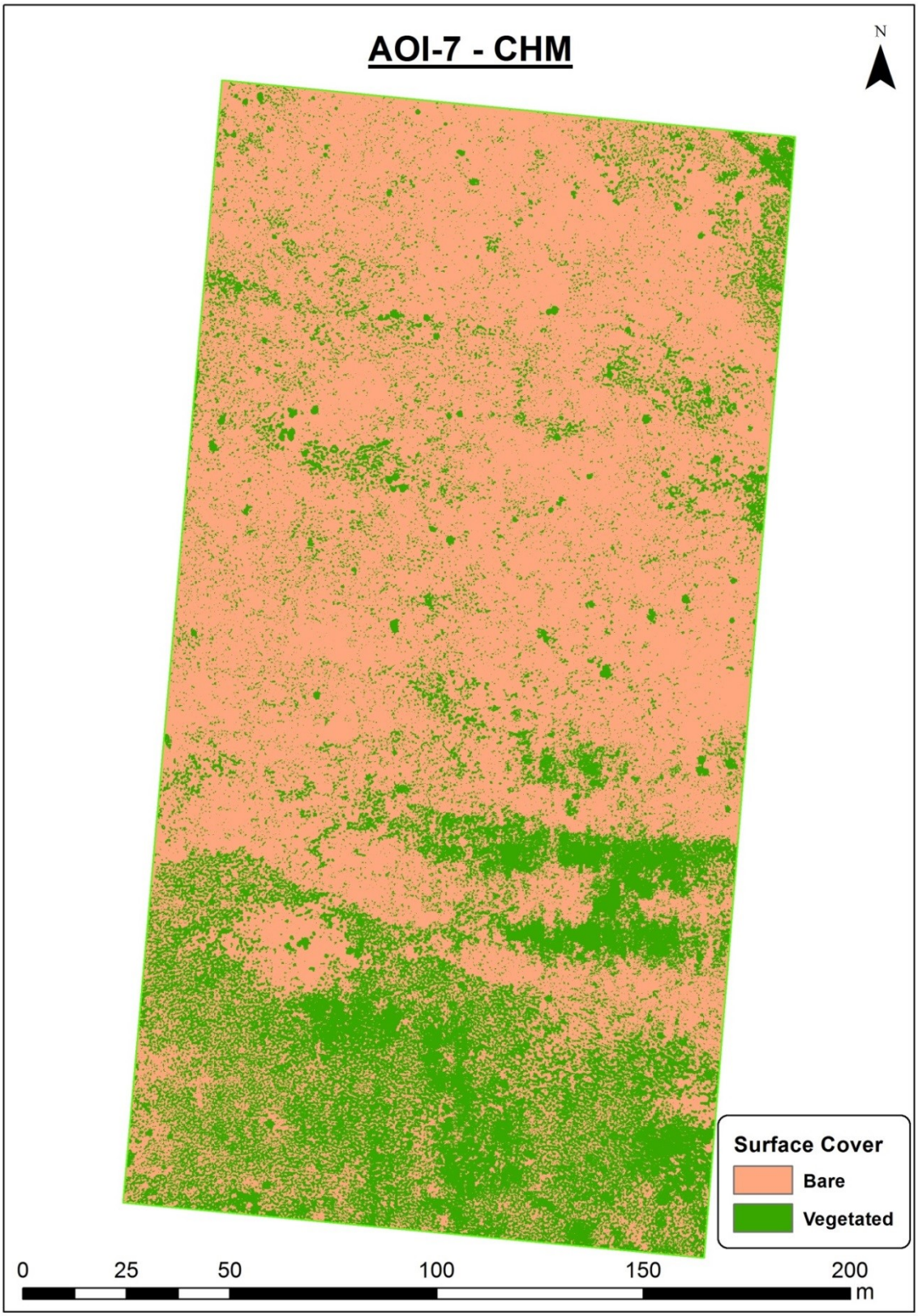
AOI-7 - CHM
N
Surface Cover
Bare
Vegetated
0
25
50
100
150
200
m

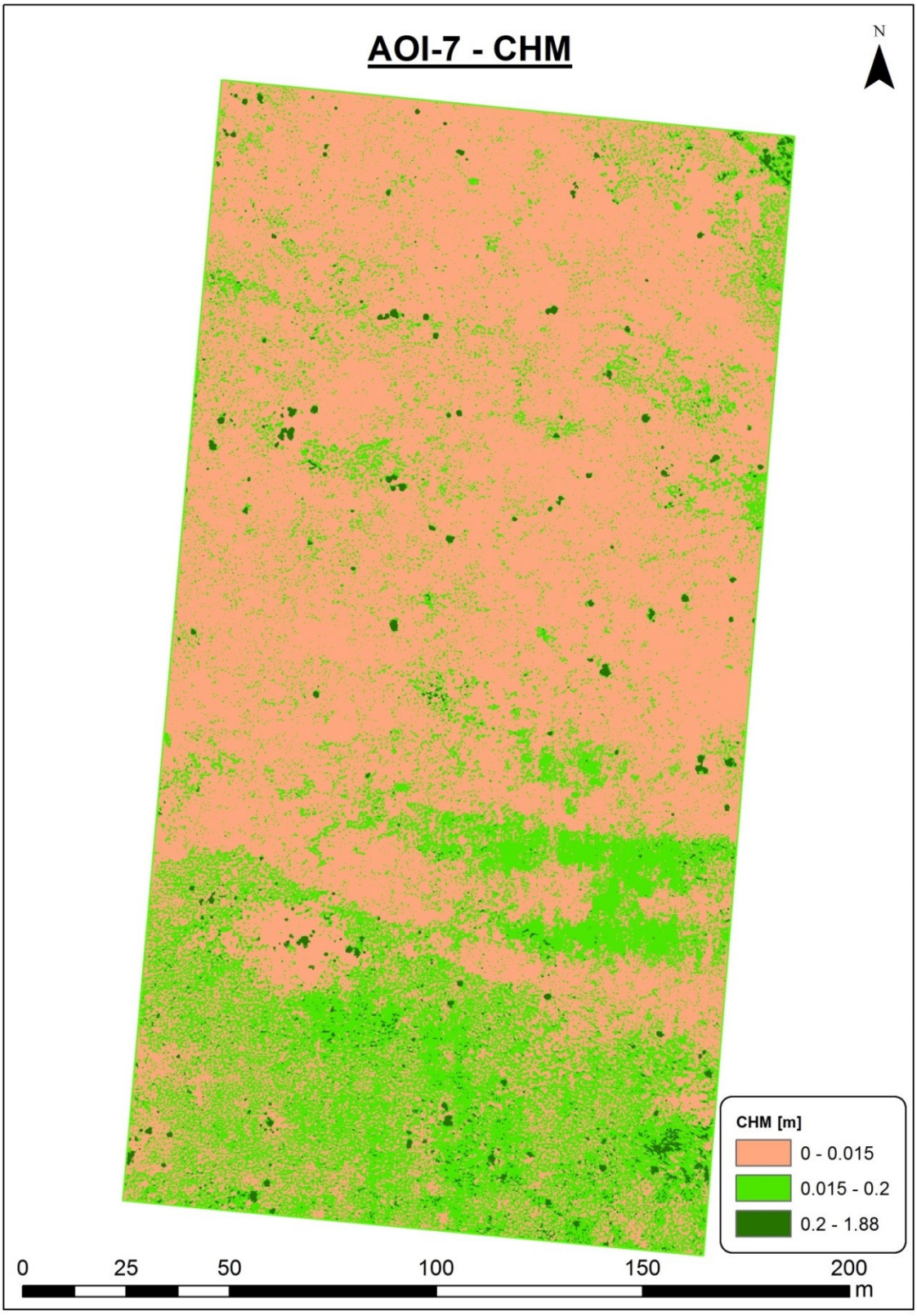
AOI-7 - CHM
N
CHM [m]
0 - 0.015
0.015 - 0.2
0.2 - 1.88
0
25
50
100
150
200
m

13.5. Appendix 4: Comparative Simulated and Observed Hydrographs

Comparative observed and modelled hydrographs for all runoff events. The blue bars indicate rainfall inputs, the red line shows the simulated hydrograph, the black line shows the observed hydrograph, and the grey shading indicates the uncertainty band around the observed hydrographs. Figures are stratified by site and ordered by magnitude of observed Q (largest to smallest).

Grass Site

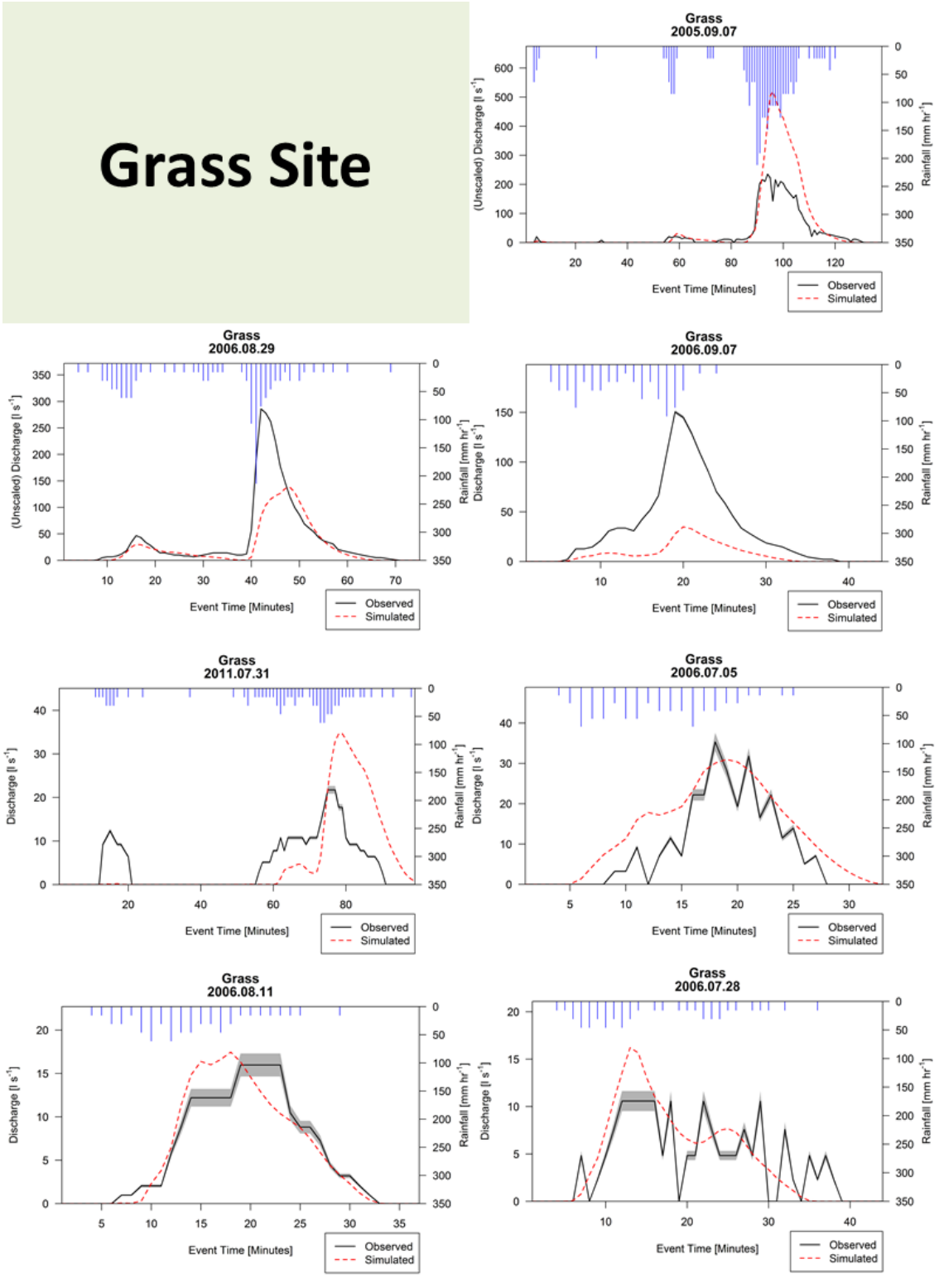

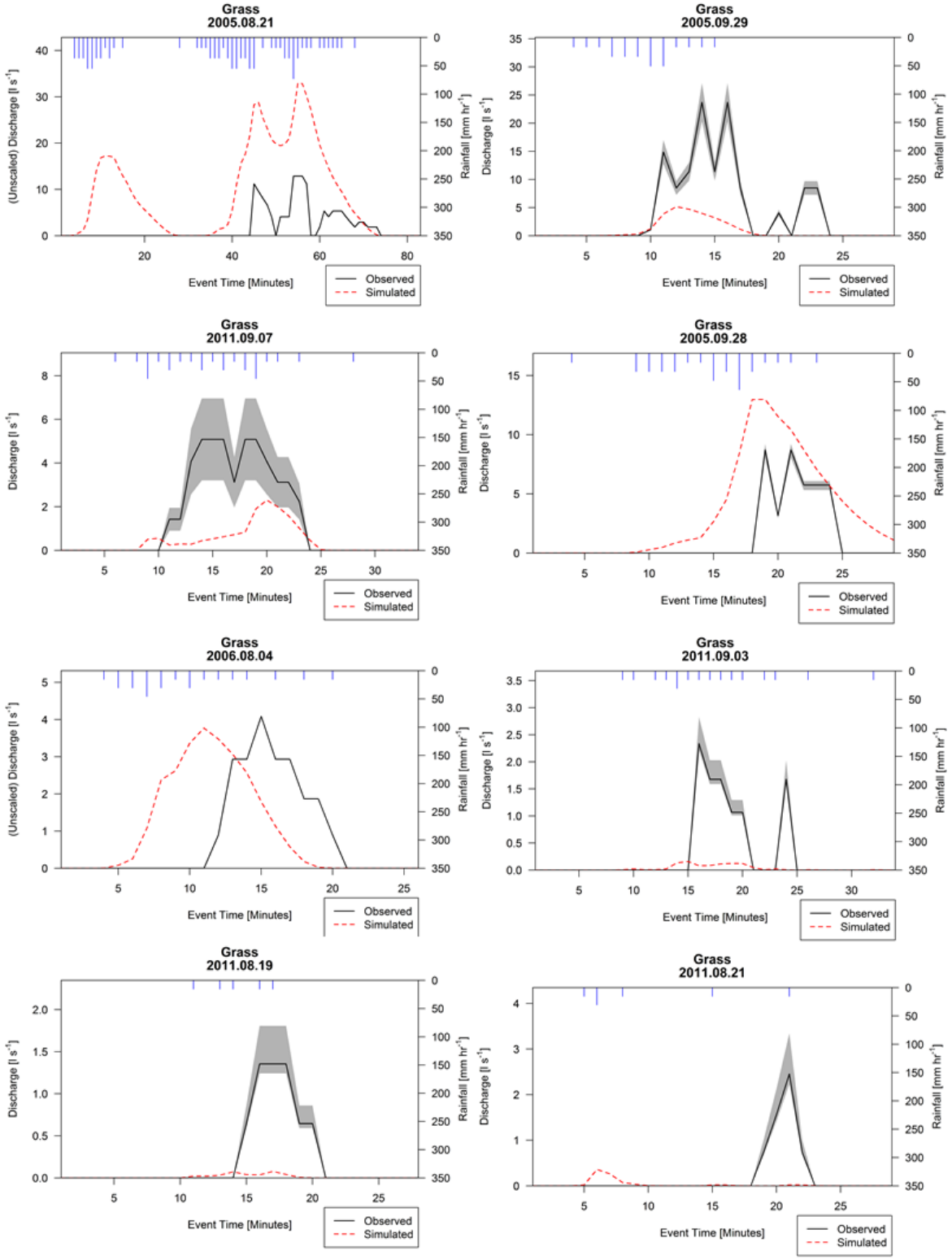
Grass
2005.08.21
(Unscaled) Discharge [l s⁻¹]
Rainfall [mm hr⁻¹]
Event Time [Minutes]
Observed
Simulated
Grass
2005.09.29
Discharge [l s⁻¹]
Rainfall [mm hr⁻¹]
Event Time [Minutes]
Observed
Simulated
Grass
2011.09.07
Discharge [l s⁻¹]
Rainfall [mm hr⁻¹]
Event Time [Minutes]
Observed
Simulated
Grass
2005.09.28
Discharge [l s⁻¹]
Rainfall [mm hr⁻¹]
Event Time [Minutes]
Observed
Simulated
Grass
2006.08.04
(Unscaled) Discharge [l s⁻¹]
Rainfall [mm hr⁻¹]
Event Time [Minutes]
Observed
Simulated
Grass
2011.09.03
Discharge [l s⁻¹]
Rainfall [mm hr⁻¹]
Event Time [Minutes]
Observed
Simulated
Grass
2011.08.19
Discharge [l s⁻¹]
Rainfall [mm hr⁻¹]
Event Time [Minutes]
Observed
Simulated
Grass
2011.08.21
Discharge [l s⁻¹]
Rainfall [mm hr⁻¹]
Event Time [Minutes]
Observed
Simulated

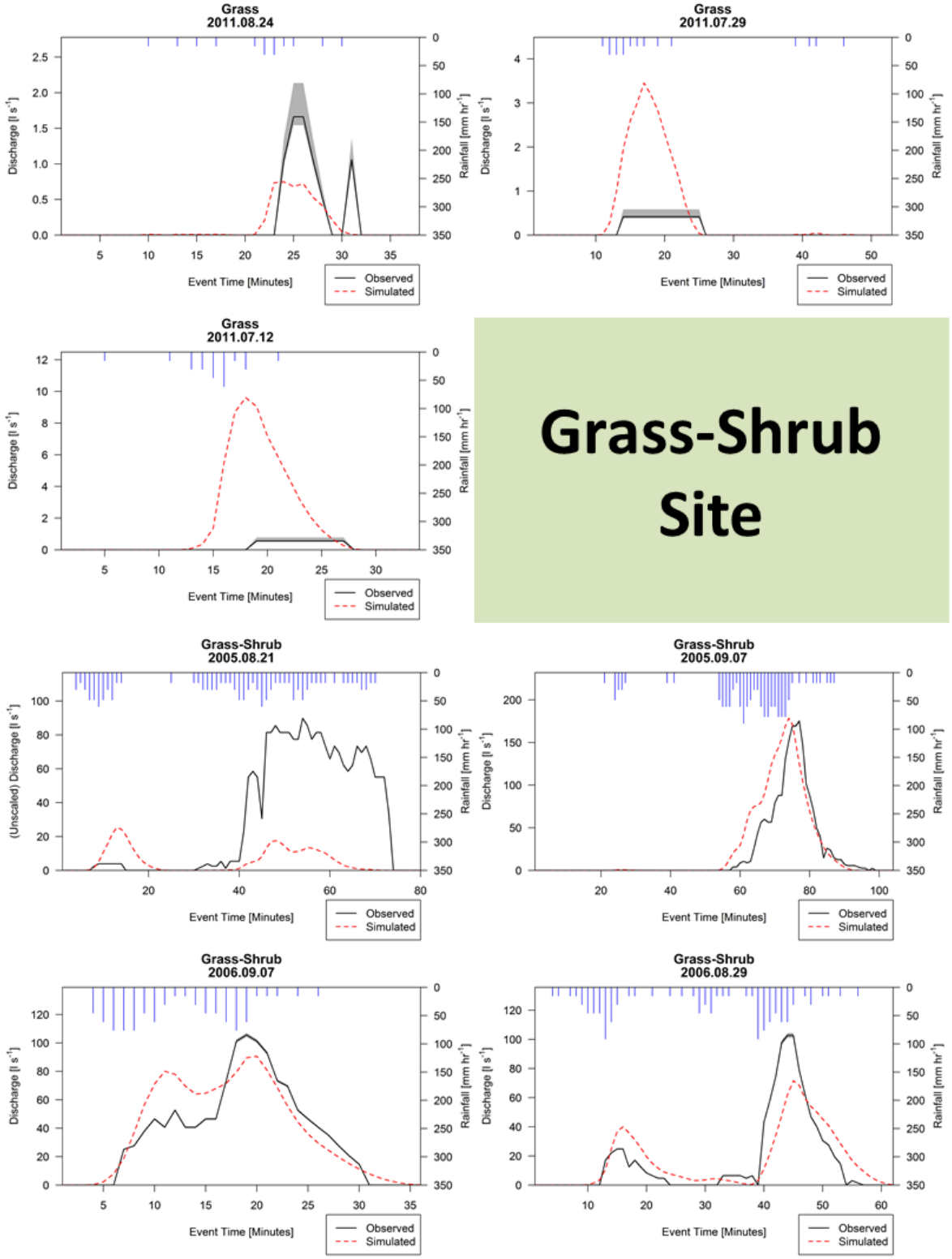
Grass
2011.08.24
Discharge [l s-1]
Rainfall [mm hr-1]
Event Time [Minutes]
Observed
Simulated
Grass
2011.07.29
Discharge [l s-1]
Rainfall [mm hr-1]
Event Time [Minutes]
Observed
Simulated
Grass
2011.07.12
Discharge [l s-1]
Rainfall [mm hr-1]
Event Time [Minutes]
Observed
Simulated
Grass-Shrub Site
Grass-Shrub
2005.08.21
(Unscaled) Discharge [l s-1]
Rainfall [mm hr-1]
Event Time [Minutes]
Observed
Simulated
Grass-Shrub
2005.09.07
Discharge [l s-1]
Rainfall [mm hr-1]
Event Time [Minutes]
Observed
Simulated
Grass-Shrub
2006.09.07
Discharge [l s-1]
Rainfall [mm hr-1]
Event Time [Minutes]
Observed
Simulated
Grass-Shrub
2006.08.29
Discharge [l s-1]
Rainfall [mm hr-1]
Event Time [Minutes]
Observed
Simulated

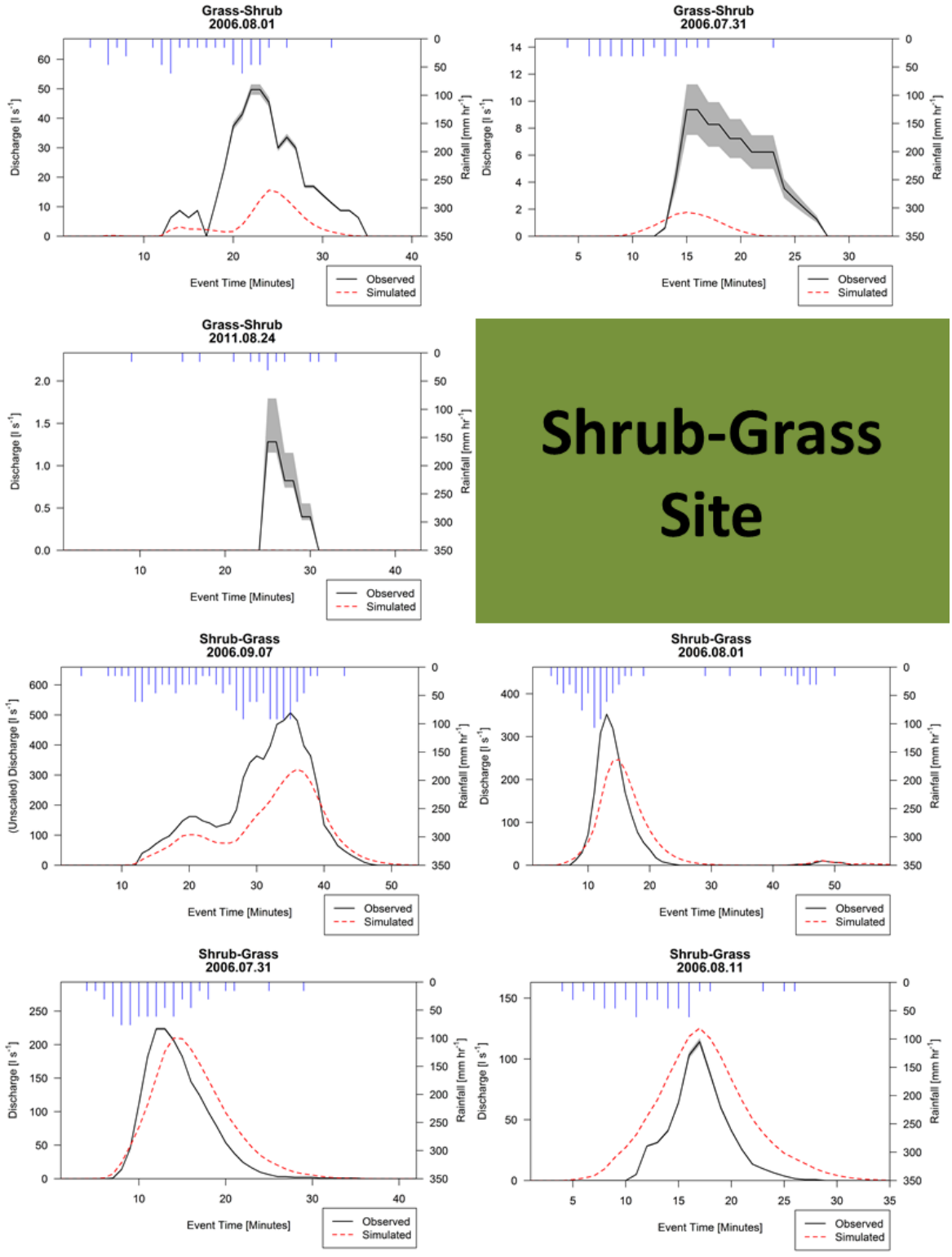
Grass-Shrub
2006.08.01
Discharge [l s⁻¹]
Rainfall [mm hr⁻¹]
Event Time [Minutes]
Observed
Simulated
Grass-Shrub
2006.07.31
Grass-Shrub
2011.08.24
Shrub-Grass
Site
Shrub-Grass
2006.09.07
(Unscaled) Discharge [l s⁻¹]
Shrub-Grass
2006.08.01
Shrub-Grass
2006.07.31
Shrub-Grass
2006.08.11

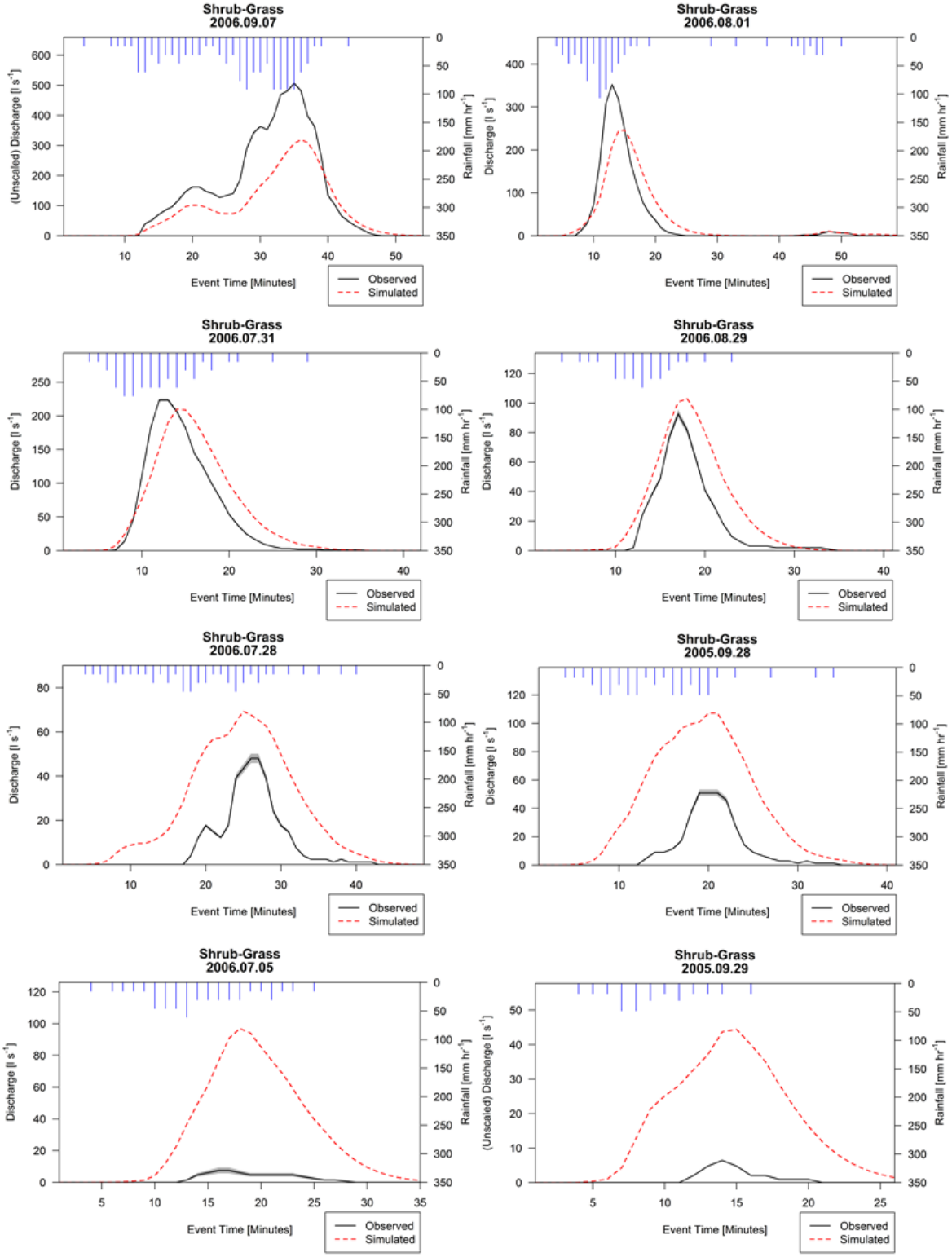
Shrub-Grass
2006.09.07
(Unscaled) Discharge [l s-1]
Rainfall [mm hr-1]
Event Time [Minutes]
Observed
Simulated
Shrub-Grass
2006.08.01
Discharge [l s-1]
Rainfall [mm hr-1]
Event Time [Minutes]
Observed
Simulated
Shrub-Grass
2006.07.31
Discharge [l s-1]
Rainfall [mm hr-1]
Event Time [Minutes]
Observed
Simulated
Shrub-Grass
2006.08.29
Discharge [l s-1]
Rainfall [mm hr-1]
Event Time [Minutes]
Observed
Simulated
Shrub-Grass
2006.07.28
Discharge [l s-1]
Rainfall [mm hr-1]
Event Time [Minutes]
Observed
Simulated
Shrub-Grass
2005.09.28
Discharge [l s-1]
Rainfall [mm hr-1]
Event Time [Minutes]
Observed
Simulated
Shrub-Grass
2006.07.05
Discharge [l s-1]
Rainfall [mm hr-1]
Event Time [Minutes]
Observed
Simulated
Shrub-Grass
2005.09.29
(Unscaled) Discharge [l s-1]
Rainfall [mm hr-1]
Event Time [Minutes]
Observed
Simulated

Shrub Site

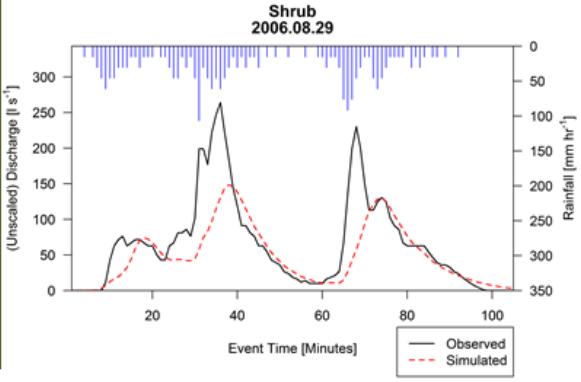
Shrub
2006.08.29
(Unscaled) Discharge [l s⁻¹]
Rainfall [mm hr⁻¹]
Event Time [Minutes]
Observed
Simulated

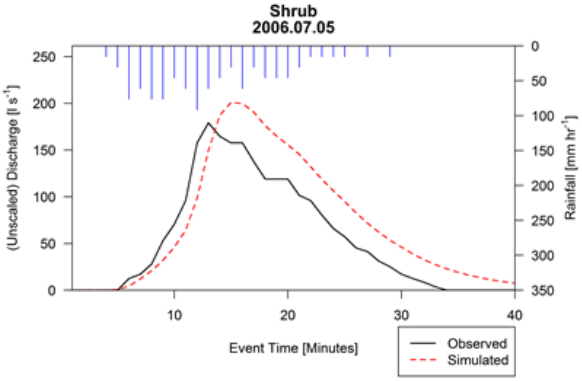
Shrub
2006.07.05
(Unscaled) Discharge [l s⁻¹]
Rainfall [mm hr⁻¹]
Event Time [Minutes]
Observed
Simulated

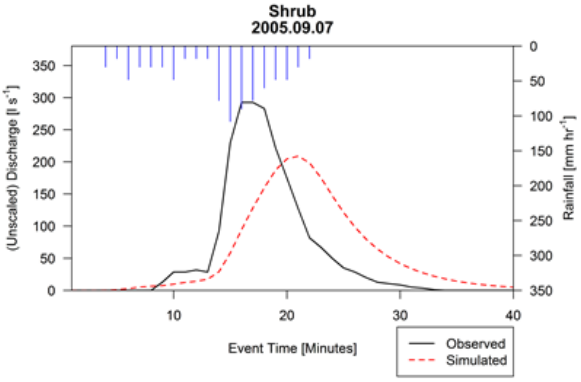
Shrub
2005.09.07
(Unscaled) Discharge [l s⁻¹]
Rainfall [mm hr⁻¹]
Event Time [Minutes]
Observed
Simulated

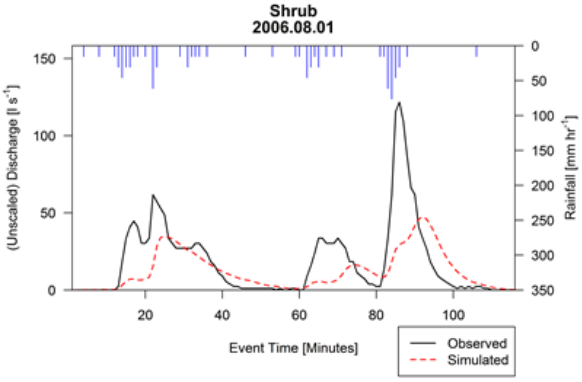
Shrub
2006.08.01
(Unscaled) Discharge [l s⁻¹]
Rainfall [mm hr⁻¹]
Event Time [Minutes]
Observed
Simulated

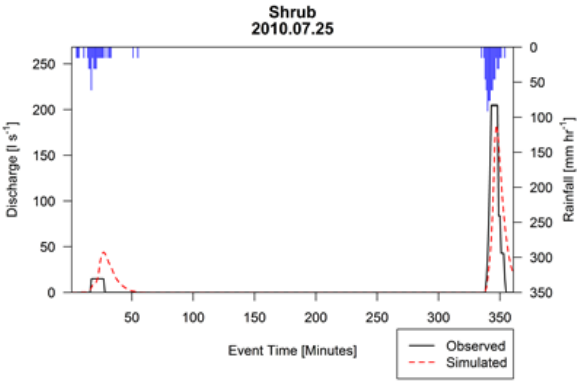
Shrub
2010.07.25
Discharge [l s⁻¹]
Rainfall [mm hr⁻¹]
Event Time [Minutes]
Observed
Simulated

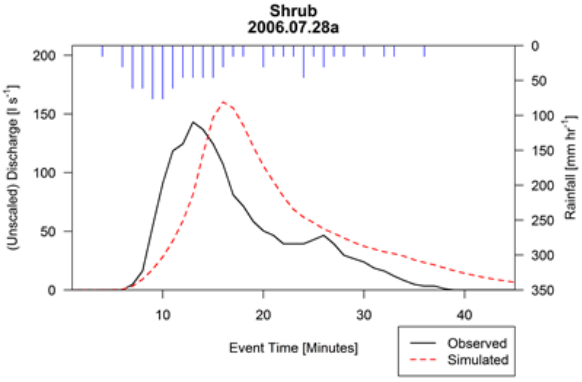
Shrub
2006.07.28a
(Unscaled) Discharge [l s⁻¹]
Rainfall [mm hr⁻¹]
Event Time [Minutes]
Observed
Simulated

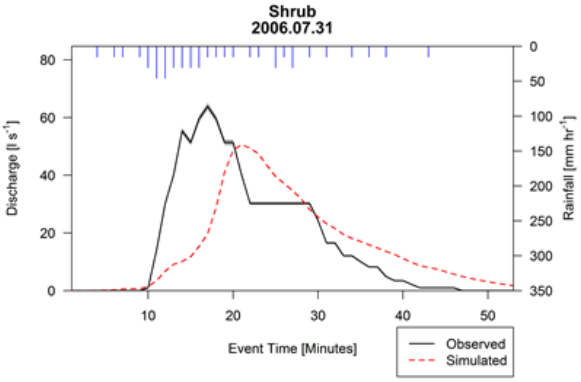
Shrub
2006.07.31
Discharge [l s⁻¹]
Rainfall [mm hr⁻¹]
Event Time [Minutes]
Observed
Simulated

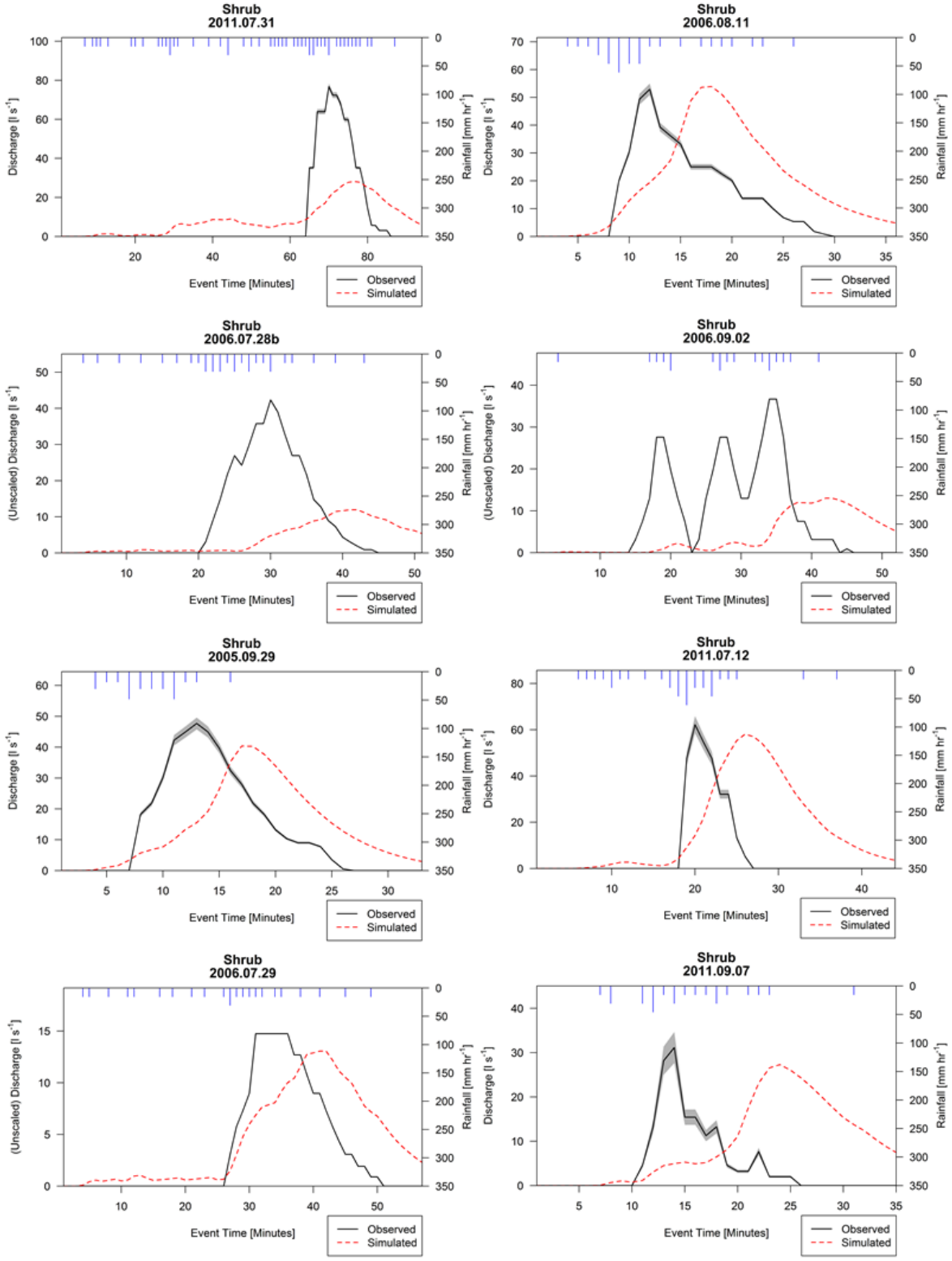
Shrub
2011.07.31
Shrub
2006.08.11
Shrub
2006.07.28b
Shrub
2006.09.02
Shrub
2005.09.29
Shrub
2011.07.12
Shrub
2006.07.29
Shrub
2011.09.07
Discharge [l s⁻¹]
(Unscaled) Discharge [l s⁻¹]
Rainfall [mm hr⁻¹]
Event Time [Minutes]
Observed
Simulated

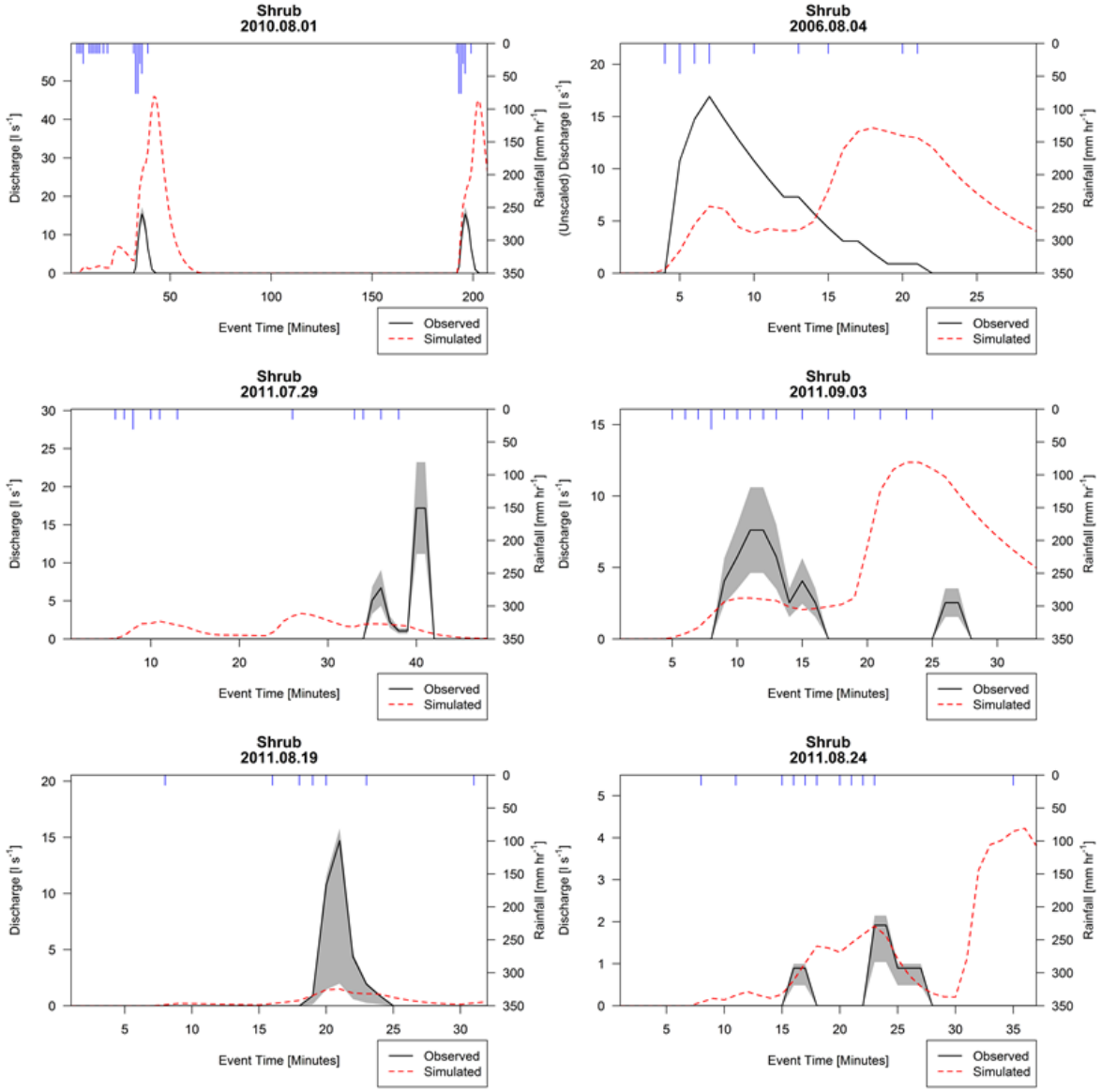
Shrub
2010.08.01
Discharge [l s-1]
Rainfall [mm hr-1]
Event Time [Minutes]
Observed
Simulated
Shrub
2006.08.04
(Unscaled) Discharge [l s-1]
Rainfall [mm hr-1]
Event Time [Minutes]
Observed
Simulated
Shrub
2011.07.29
Discharge [l s-1]
Rainfall [mm hr-1]
Event Time [Minutes]
Observed
Simulated
Shrub
2011.09.03
Discharge [l s-1]
Rainfall [mm hr-1]
Event Time [Minutes]
Observed
Simulated
Shrub
2011.08.19
Discharge [l s-1]
Rainfall [mm hr-1]
Event Time [Minutes]
Observed
Simulated
Shrub
2011.08.24
Discharge [l s-1]
Rainfall [mm hr-1]
Event Time [Minutes]
Observed
Simulated

13.6. Appendix 5: Tabular Summary of Hydrological Modelling Results

Summary of observed and modelled hydrology for runoff events across the four sites. An asterisk in the goodness-of-fit (GoF) column indicates events where equipment failures prevented monitoring of hydrographs. Site mean (and median) GoF values are in bold.

Date	Total discharge [l]			Peak Discharge [l min-1]			Goodness-of-Fit			
	Observed		Modelled	Observed		Modelled	RMSE [l min-1]	NSE	Index of Agreement	Spearman CC
Grass										
2005/08/21	149.3	*	761.4	12.9	*	33.2	10.84	-0.20	0.55	0.56
2005/09/07	4287.7	*	7693.6	235.2	*	525.2	76.27	0.64	0.79	0.85
2005/09/28	37.9	(35-40)	103.8	8.7	(8.1-9.2)	13.0	3.81	0.20	0.68	0.63
2005/09/29	124.1	(106.4-141.9)	26.3	23.7	(20.3-27.1)	5.2	6.72	-16.74	0.40	0.64
2006/07/05	276.6	(258.9-294.4)	419.2	35.3	(33.1-37.6)	31.6	6.43	0.64	0.76	0.90
2006/07/28	177.3	(159.6-195.1)	197.9	10.6	(9.52-11.6)	16.2	3.06	0.59	0.70	0.76
2006/08/04	21.3	*	26.4	4.1	*	3.8	1.61	-0.48	0.54	0.42
2006/08/11	212.8	(195.07-230.5)	218.8	16.0	(14.7-17.3)	17.7	2.06	0.90	0.88	0.95
2006/08/29	2861.9		1899.5	286.0		140.2	42.43	-0.16	0.74	0.93
2006/09/07	1425.8	(1408.02-1443.5)	332.5	150.5	(148.6-152.3)	35.3	40.50	-16.68	0.33	0.96
2010/07/25	451.4	(433.67-469.1)	1.0	*	*	0.4	*	*	*	*
2011/07/12	5.0	(4.5-7)	60.3	0.6	(0.5-0.8)	9.6	3.30	-0.24	0.59	0.60
2011/07/29	5.0	(4.5-7)	24.9	0.4	(0.4-0.6)	3.5	0.91	0.12	0.64	0.71
2011/07/31	436.6	(418.87-454.3)	539.6	21.7	(20.9-22.6)	35.2	8.08	0.37	0.61	0.72
2011/08/19	6.0	(5.5-8)	0.3	1.4	(1.2-1.8)	0.1	0.47	-479.97	0.11	0.62
2011/08/21	5.5	(5-7.5)	0.9	2.5	(2.2-3.3)	0.4	0.58	-51.40	0.15	0.07
2011/08/24	5.0	(6.5-7)	4.4	1.7	(1.5-2.1)	0.7	0.32	-0.86	0.69	0.58
2011/09/03	9.5	(9-11.5)	1.0	2.3	(2.2-2.8)	0.2	0.66	-195.51	0.17	0.49
2011/09/07	48.0	(30.27-65.7)	14.3	5.1	(3.2-7)	2.3	1.90	-8.06	0.45	0.75
							11.66 (3.18)	**-42.60 (-0.22)**	**0.54 (0.60)**	**0.67 (0.68)**

Grass-Shrub										
2005/08/21	2291.8	*	411.7	89.9	*	25.2	40.02	-34.03	0.23	0.62
2005/09/07	2033.2	(2015.5-2050.9)	2547.2	175.2	(173.7-176.7)	178.4	19.49	0.82	0.95	0.83
2006/07/31	82.9	(66.34-99.5)	11.6	9.4	(7.5-11.2)	1.8	3.65	-41.07	0.30	0.62
2006/08/01	464.4	(447.8-480.9)	109.8	49.7	(48.0-51.5)	15.6	14.97	-11.34	0.50	0.86
2006/08/11	149.3	(165.8-132.7)	214.7	*	*	17.5	*	*	*	*
2006/08/29	995.1	(978.5-1011.6)	1025.7	102.7	(101.0-104.4)	71.6	14.56	0.46	0.90	0.80
2006/09/07	1260.4	(1243.8-1277)	1352.6	105.6	(104.3-107)	90.6	14.29	0.80	0.95	0.92
2011/08/24	5.0	(4.0-7.0)	0.0	1.3	(1.2-1.8)	0.0	0.34	-8839904.0	0.00	0.50
							15.33	**-1262855.4**	**0.55**	**0.74**
							(14.56)	**(-11.34)**	**(0.50)**	**(0.80)**
Shrub-Grass										
2005/09/28	363.1	(346.6-379.6)	1461.5	51.0	(48.7-53.3)	107.3	38.01	0.02	0.66	0.87
2005/09/29	24.8	*	425.5	6.4	*	44.4	20.77	-0.85	0.51	0.80
2006/07/05	66.0	(49.5-82.5)	1039.2	7.5	(5.6-9.3)	96.9	41.13	-0.59	0.50	0.90
2006/07/28	379.6	(368.1-396.1)	1084.9	48.1	(46-50.1)	69.3	19.79	0.30	0.77	0.84
2006/07/31	1798.9	(1782.4-1815.4)	2078.6	223.6	(221.5-225.6)	209.7	26.90	0.84	0.96	0.97
2006/08/01	2047.7	(2029.9-2063.4)	2062.9	352.4	(349.3-355.4)	246.5	36.78	0.69	0.94	0.82
2006/08/11	637.0	(620.5-653.5)	1217.7	114.2	(111.3-117.2)	125.4	22.47	0.69	0.91	0.92
2006/08/29	551.2	(534.7-567.7)	886.4	92.6	(89.9-95.4)	103.0	14.01	0.81	0.94	0.92
2006/09/07	6935.0	*	4489.2	506.9	*	319.1	85.27	0.18	0.89	0.96
							33.90	**0.23**	**0.78**	**0.89**
							(26.90)	**(0.30)**	**(0.89)**	**(0.90)**

Shrub										
2005/09/07	2168.8	*	2282.6	292.6	*	208.9	69.29	0.17	0.79	0.85
2005/09/28	141.9	(124.1-159.6)	614.3	*	*	*	*	*	*	*
2005/09/29	443.3	(425.6-461.1)	465.4	47.7	(45.8-49.6)	40.4	15.35	-0.09	0.71	0.71
2006/07/05	2175.1	*	2816.4	179.2	*	201.2	41.13	-0.59	0.50	0.90
2006/07/28a	1623.0	*	2062.7	143.1	*	160.2	37.41	0.48	0.83	0.88
2006/07/28b	445.3	*	207.1	42.3	*	12.0	13.87	-7.35	0.28	0.43
2006/07/29	196.9	*	255.4	14.7	*	13.1	3.97	0.39	0.84	0.82
2006/07/31	886.7	(868.9-904.4)	822.3	63.9	(62.6-65.2)	50.6	14.93	0.25	0.82	0.84
2006/08/01	2111.1	*	1420.7	121.7	*	47.5	19.79	-0.96	0.70	0.78
2006/08/04	125.1	*	192.3	16.9	*	13.9	8.67	-2.04	0.35	0.02
2006/08/11	450.4	(432.7-468.2)	689.2	52.9	(50.8-55.0)	53.9	18.90	0.05	0.68	0.79
2006/08/29	6862.3	*	5160.3	264.0	*	148.5	42.77	0.16	0.83	0.87
2006/09/02	445.1	*	210.0	36.7	*	13.0	13.07	-4.78	0.27	0.26
2010/07/25	1981.6	(1963.9-1999.3)	2463.0	204.6	(202.7-206.4)	183.3	17.32	0.62	0.90	0.44
2010/08/01	148.3	(130.6-166)	1085.0	15.4	(13.6-17.3)	46.0	13.21	-0.03	0.43	0.46
2011/07/12	294.7	(277-312.4)	732.5	62.2	(58.4-65.9)	58.1	26.47	-0.47	0.55	0.46
2011/07/29	50.5	(32.2-68.2)	58.2	17.2	(11.2-23.2)	3.4	3.71	-11.59	0.19	0.17
2011/07/31	851.5	(833.8-869.2)	808.1	76.8	(75.2-78.4)	28.0	15.77	-1.93	0.70	0.71
2011/08/19	33.5	(4.5-36)	12.0	14.7	(2-15.8)	1.5	2.91	-37.08	0.34	0.68
2011/08/24	8.3	(4.5-9.3)	41.5	1.9	(1-2.2)	4.2	1.99	-0.65	0.46	0.18
2011/09/03	45.0	(27.3-62.7)	158.8	7.6	(4.6-10.6)	12.4	7.12	-1.25	0.41	-0.09
2011/09/07	157.2	(139.5-174.9)	330.1	31.1	(27.6-34.6)	27.3	15.22	-1.18	0.38	0.17
							19.18 (15.22)	**-3.23 (-0.59)**	**0.57 (0.55)**	**0.54 (0.68)**

13.7. Appendix 6: Tabular Summary of Erosion Modelling Results

Summary of observed and modelled erosion yield and particle size distribution for runoff events across the four sites. Only events which were both observed for sediment yield and simulated are included here.

Date	Hydrological		Sediment Yield [Kg]		Proportions by model sediment size class											
					Observed						Simulated					
	Q_Obs [l]	GoF-NSE	Observed	Simulated	1	2	3	4	5	6	1	2	3	4	5	6
Grass																
2005-08-21	149.3	-0.197	**1.83**	**0.21**	0.31	0.51	0.08	0.09	0.02	0.00	0.45	0.55	0.00	0.00	0.00	0.00
2005-09-07	4287.7	0.636	**4.11**	**46.91**	0.53	0.40	0.04	0.03	0.00	0.00	0.21	0.78	0.01	0.00	0.00	0.00
2005-09-29	124.1	-16.743	**0.00**	**0.00**							0.79	0.21	0.00	0.00	0.00	0.00
2006-07-05	276.6	0.639	**0.87**	**0.22**	0.43	0.44	0.05	0.04	0.04	0.00	0.42	0.57	0.00	0.00	0.00	0.00
2006-07-28	177.3	0.593	**0.20**	**0.02**	0.29	0.60	0.08	0.02	0.00	0.00	0.63	0.37	0.00	0.00	0.00	0.00
2006-08-04	21.3	-0.477	**0.10**	**0.00**	0.17	0.50	0.11	0.10	0.12	0.00	0.91	0.09	0.00	0.00	0.00	0.00
2006-08-11	212.8	0.895	**0.36**	**0.10**	0.29	0.57	0.09	0.03	0.01	0.00	0.51	0.49	0.00	0.00	0.00	0.00
2006-08-29	2861.9	-0.159	**2.05**	**12.03**	0.60	0.34	0.03	0.03	0.01	0.00	0.22	0.77	0.01	0.00	0.00	0.00
2006-09-07	1425.8	-16.681	**0.86**	**0.40**	0.50	0.41	0.05	0.03	0.01	0.00	0.31	0.69	0.01	0.00	0.00	0.00
2010-07-12	#N/A	#N/A	**0.05**	**0.02**	0.28	0.67	0.03	0.01	0.01	0.00	0.62	0.38	0.00	0.00	0.00	0.00
2010-07-25	451.4	#N/A	**0.39**	**0.00**	0.47	0.42	0.05	0.03	0.03	0.00	0.79	0.21	0.00	0.00	0.00	0.00
2011-07-12	5.0															
2011-07-29	5.0	0.116	**0.04**	**0.00**	0.28	0.65	0.02	0.01	0.04	0.00	0.97	0.03	0.00	0.00	0.00	0.00
2011-07-31	436.6	0.368	**1.01**	**0.16**	0.38	0.51	0.03	0.02	0.06	0.00	0.48	0.52	0.00	0.00	0.00	0.00
2011-08-19	6.0	-479.972	**0.07**	**0.00**	0.26	0.61	0.05	0.03	0.05	0.00	0.06	0.89	0.05	0.00	0.00	0.00
2011-08-21	5.5	-51.397	**0.07**	**0.00**	0.24	0.65	0.03	0.03	0.05	0.00	0.76	0.24	0.00	0.00	0.00	0.00
2011-08-24	6.5	-0.861	**0.12**	**0.00**	0.32	0.59	0.06	0.02	0.01	0.00	0.71	0.29	0.00	0.00	0.00	0.00
2011-09-03	9.5	-195.506	**0.11**	**0.00**	0.32	0.56	0.02	0.04	0.06	0.00	0.68	0.31	0.00	0.00	0.00	0.00
2011-09-07	48.0	-8.057	**0.25**	**0.00**	0.29	0.57	0.06	0.02	0.07	0.00	0.96	0.04	0.00	0.00	0.00	0.00
Grass-Shrub																
2005-09-07	2033.2	0.824	**6.25**	**2.42**	0.46	0.42	0.07	0.05	0.00	0.00	0.38	0.61	0.01	0.00	0.00	0.00
2006-08-11	149.3	#N/A	**0.53**	**0.14**	0.32	0.49	0.11	0.07	0.00	0.00	0.46	0.54	0.00	0.00	0.00	0.00

2006-08-29	995.1	0.457	**1.26**	**1.12**	0.46	0.42	0.06	0.06	0.00	0.00	0.35	0.64	0.00	0.00	0.00	0.00
2006-09-07	1260.4	0.801	**1.12**	**1.35**	0.39	0.49	0.07	0.05	0.01	0.00	0.35	0.64	0.00	0.00	0.00	0.00
2011-08-24	5.0	-8839904	**0.10**	**0.00**	0.23	0.64	0.05	0.02	0.05	0.00	0.16	0.07	0.00	0.00	0.78	0.00
Shrub-Grass																
2006-07-28	379.6	0.299	**#N/A**	**0.19**							0.44	0.56	0.00	0.00	0.00	0.00
2006-07-31	1798.9	0.843	**#N/A**	**3.12**							0.31	0.69	0.00	0.00	0.00	0.00
2006-08-01	2047.7	0.687	**#N/A**	**3.94**							0.31	0.68	0.01	0.00	0.00	0.00
Combi 2006/07/28, 2006/07/31, 2006/08/01			**4.77**	**7.26**	0.63	0.27	0.03	0.03	0.05	0.00	0.31	0.68	0.01	0.00	0.00	0.00
2006-08-11	637.0	0.687	**0.91**	**0.37**	0.53	0.33	0.05	0.05	0.05	0.00	0.34	0.65	0.00	0.00	0.00	0.00
2006-08-29	551.2	0.809	**0.71**	**0.28**	0.37	0.35	0.11	0.07	0.10	0.00	0.39	0.61	0.00	0.00	0.00	0.00
2006-09-07	6935.0	0.183	**6.18**	**6.55**	0.51	0.41	0.03	0.03	0.02	0.00	0.32	0.67	0.01	0.00	0.00	0.00
Shrub																
2005-09-07	2168.8	0.172	**10.83**	**3.15**	0.63	0.25	0.03	0.06	0.03	0.00	0.36	0.63	0.01	0.00	0.00	0.00
2006-07-05	2175.1	-0.588	**5.84**	**0.52**	0.42	0.44	0.06	0.05	0.03	0.00	0.38	0.61	0.00	0.00	0.00	0.00
2006/07/28a	1623.0	0.478		**2.15**							0.43	0.57	0.01	0.00	0.00	0.00
2006/07/28b	445.3	-7.352		**0.00**							1.00	0.00	0.00	0.00	0.00	0.00
2006-07-29	196.9	0.385		**0.00**							1.00	0.00	0.00	0.00	0.00	0.00
Combi 2006/07/28a, 2006/07/28b, 2006/07/29			**4.80**	**2.15**	0.52	0.32	0.07	0.07	0.02	0.00	0.43	0.57	0.01	0.00	0.00	0.00
2006-07-31	886.7	0.253									0.78	0.22	0.00	0.00	0.00	0.00
2006-08-01	2111.1	-0.96									0.51	0.48	0.00	0.00	0.00	0.00
2006-08-04	125.1	-2.039									0.88	0.11	0.00	0.00	0.00	0.00
Combi 2006/07/31, 2006/08/01, 2006/08/04			**3.64**	**0.37**	0.41	0.32	0.31	0.11	0.03	0.00	0.58	0.42	0.00	0.00	0.00	0.00
2006-08-11	450.4	0.052	**0.81**	**0.11**	0.38	0.40	0.09	0.09	0.04	0.00	0.65	0.35	0.00	0.00	0.00	0.00
2010-07-25	1981.6	0.617	**4.03**	**2.31**	0.50	0.25	0.10	0.07	0.09	0.00	0.42	0.57	0.01	0.00	0.00	0.00
2010-08-01	148.3	-0.029	**0.54**	**0.42**	0.29	0.49	0.07	0.06	0.09	0.00	0.43	0.57	0.00	0.00	0.00	0.00
2011-07-12	294.7	-0.467	**0.41**	**0.09**	0.36	0.42	0.10	0.07	0.05	0.00	0.65	0.34	0.00	0.00	0.00	0.00
2011-07-29	50.5	-11.59	**0.13**	**0.00**	0.30	0.50	0.08	0.06	0.06	0.00	0.97	0.03	0.00	0.00	0.00	0.00
2011-07-31	851.5	-1.927	**2.75**	**0.02**	0.42	0.34	0.10	0.08	0.07	0.00	0.79	0.21	0.00	0.00	0.00	0.00
2011-08-19	33.5	-37.075	**0.12**	**0.00**	0.38	0.40	0.08	0.07	0.08	0.00	0.15	0.84	0.00	0.00	0.00	0.00
2011-08-24	8.3	-0.651	**0.32**	**0.00**	0.24	0.61	0.06	0.03	0.05	0.00	0.13	0.86	0.00	0.00	0.00	0.00
2011-09-03	45.0	-1.246	**0.50**	**0.00**	0.28	0.55	0.06	0.04	0.07	0.00	0.98	0.02	0.00	0.00	0.00	0.00
2011-09-07	157.2	-1.183	**0.57**	**0.01**	0.34	0.51	0.04	0.07	0.03	0.00	0.94	0.06	0.00	0.00	0.00	0.00

13.8. Appendix 7: Published Article: ‘Dryland, calcareous soils store (and lose) significant quantities of near-surface organic carbon’

Material removed due to 3rd party copyright restrictions

Material removed due to 3rd party copyright restrictions

Material removed due to 3rd party copyright restrictions

Material removed due to 3rd party copyright restrictions

Material removed due to 3rd party copyright restrictions

Material removed due to 3rd party copyright restrictions

Material removed due to 3rd party copyright restrictions

Material removed due to 3rd party copyright restrictions

Material removed due to 3rd party copyright restrictions

Material removed due to 3rd party copyright restrictions

Material removed due to 3rd party copyright restrictions

Material removed due to 3rd party copyright restrictions

Material removed due to 3rd party copyright restrictions

Material removed due to 3rd party copyright restrictions

Material removed due to 3rd party copyright restrictions

Material removed due to 3rd party copyright restrictions

Material removed due to 3rd party copyright restrictions

Material removed due to 3rd party copyright restrictions

Material removed due to 3rd party copyright restrictions

13.9. Appendix 8: Published Article: ‘Ultra-fine grain landscape-scale quantification of dryland vegetation structure with drone-acquired structure-from-motion photogrammetry’

Material removed due to 3rd party copyright restrictions

Material removed due to 3rd party copyright restrictions

Material removed due to 3rd party copyright restrictions

Material removed due to 3rd party copyright restrictions

Material removed due to 3rd party copyright restrictions

Material removed due to 3rd party copyright restrictions

Material removed due to 3rd party copyright restrictions

Material removed due to 3rd party copyright restrictions

Material removed due to 3rd party copyright restrictions

Material removed due to 3rd party copyright restrictions

Material removed due to 3rd party copyright restrictions

Material removed due to 3rd party copyright restrictions

Material removed due to 3rd party copyright restrictions

Material removed due to 3rd party copyright restrictions

Material removed due to 3rd party copyright restrictions

13.10. Appendix 9: Published Article: ‘Aerial photography collected with a multirotor drone reveal impact of Eurasian beaver reintroduction on ecosystem structure’

Material removed due to 3rd party copyright restrictions

Material removed due to 3rd party copyright restrictions

Material removed due to 3rd party copyright restrictions

Material removed due to 3rd party copyright restrictions

Material removed due to 3rd party copyright restrictions

Material removed due to 3rd party copyright restrictions

Material removed due to 3rd party copyright restrictions